TECHNICAL DIGEST

1 9 9 6

ADVANCED SOLID-STATE LASERS

JANUARY 31–FEBRUARY 2, 1996

SAN FRANCISCO, CALIFORNIA

SPONSORED BY

OPTICAL SOCIETY OF AMERICA

COSPONSORED BY

IEEE/LASERS AND ELECTRO-OPTICS SOCIETY

REPORT DOCUMENTATION PAGE

Form Approved
OMB No. 0704-0188

1. AGENCY USE ONLY (Leave blank)	2. REPORT DATE	3. REPORT TYPE AND DATES COVERED
		FINAL REPORT - 17 Jan 96 - 16 Jan 97

4. TITLE AND SUBTITLE
Organization of the 1996 Advanced Solid-State Lasers Topical Meeting

5. FUNDING NUMBERS
1651/01

2301/CS

6. AUTHOR(S)
Dr Hennage

7. PERFORMING ORGANIZATION NAME(S) AND ADDRESS(ES)
Optical Society of America
2010 Massachusetts Ave NW
Washington, DC 20036

8. PERFORMING ORGANIZATION
AFOSR-TR-96

0565

9. SPONSORING / MONITORING AGENCY NAME(S) AND ADDRESS(ES)
AFOSR/NE
110 Duncan Avenue Suite B115
Bolling AFB DC 20332-0001

AGENCY REPORT NUMBER
F49620-96-1-0041

11. SUPPLEMENTARY NOTES

12a. DISTRIBUTION / AVAILABILITY STATEMENT
APPROVED FOR PUBLIC RELEASE: DISTRIBUTION UNLIMITED

12b. DISTRIBUTION CODE

13. ABSTRACT *(Maximum 200 words)*

The 1996 Advanced Solid State Lasers Topical Meeting was held in San Francisco on 31 January to 3 February 1996.

14. SUBJECT TERMS

15. NUMBER OF PAGES

16. PRICE CODE

17. SECURITY CLASSIFICATION OF REPORT	18. SECURITY CLASSIFICATION OF THIS PAGE	19. SECURITY CLASSIFICATION OF ABSTRACT	20. LIMITATION OF ABSTRACT
UNCLASSIFIED	UNCLASSIFIED	UNCLASSIFIED	

TECHNICAL DIGEST
1996

Summaries of the papers presented at the topical meeting

ADVANCED SOLID-STATE LASERS

JANUARY 31– FEBRUARY 2, 1996
SAN FRANCISCO, CALIFORNIA

SPONSORED BY
OPTICAL SOCIETY OF AMERICA

COSPONSORED BY
IEEE/LASERS AND ELECTRO-OPTICS SOCIETY

PARTIALLY SUPPORTED BY
NATIONAL AERONAUTICS AND SPACE ADMINISTRATION

Optical Society of America
2010 Massachusetts Avenue NW
Washington DC 20036-1023

Articles in this publication may be cited in other publications. To facilitate access to the original publication source, the following form for the citation is suggested:

Name of Author(s), "Title of Paper," in *Advanced Solid-State Lasers*, 1996 Technical Digest (Optical Society of America, Washington DC, 1996), pp. xx-xx.

Optical Society of America

ISBN

Conference Edition	1-55752-418-1
1996 Technical Digest Series	1-55752-417-3

Library of Congress Catalog Card Number

Conference Edition	95-72738

Printed in the U.S.A.

Contents

ADVANCED SOLID-STATE LASERS
TECHNICAL PROGRAM COMMITTEE

Stephen Payne, *General Chair*
Lawrence Livermore National Laboratory

Clifford R. Pollock, *Program Chair*
Cornell University

Douglas Anthon
ATx-Telecom Systems

Norman P. Barnes
NASA Langley Research Center

Walter R. Bosenberg
Lightwave Electronics Corporation

Bruce H. Chai
University of Central Florida/CREOL

Christopher M. Clayton
Phillips Laboratory

Martin M. Fejer
Stanford University

Paul French
Imperial College of Science & Technology , UK

Hagop Injeyan
TRW

Richard Moncorgé
University of Lyon, France

Dave Nabors
Coherent Laser Group

Michio Oka
Sony Corporation, Japan

Joe Pinto
U.S. Naval Research Laboratory

C. Ward Trussell
U.S. Night Vision and Electronic Sensors Directorate

Richard Wallenstein
Kaiserslautern Unversity, Germany

TUESDAY
JANUARY 30, 1996

GARDEN ROOM

6:00pm–8:00pm
Registration

WEDNESDAY
JANUARY 31, 1996

GARDEN ROOM

7:00am–6:00pm
Registration

GOLD ROOM

8:00am–8:15pm
Opening Remarks
Stephen Payne, *Lawrence Livermore National Laboratory, General Chair*

8:15am–8:45am
WA • Plenary I
Stephen Payne, *Lawrence Livermore National Laboratory, Presider*

8:15am (Invited)
WA1 • Novel uses of lasers in medicine, Kenton Gregory, *Oregon Medical Laser Center.* This presentation will include a summary of some current medical uses of lasers. **(p. 2)**

8:45am–9:45am
WB • Ultraviolet/Blue Lasers
Michio Oka, *Sony Corporation, Japan, Presider*

8:45am (Invited)
WB1 • Highly efficient cw blue light generation via first-order quasi-phase-matched frequency-doubling of a diode-pumped 946 nm Nd:YAG laser, V. Pruneri, R. Koch, P. G. Kazansky, W. A. Clarkson, P. St. J. Russell, D. C. Hanna, *Univ. Southampton, UK.* 49 mW of cw blue light have been generated by first-order quasi-phase-matched frequency doubling of a high-power, diode-pumped 946 nm Nd:YAG laser. **(p. 4)**

9:00am
WB2 • Efficient ultraviolet Ce:LiSAF laser using anti-solarant pump beam, A. J. Bayramian, C. D. Marshall, S. A. Payne, *Lawrence Livermore National Laboratory;* G. J. Quarles, V. Castillo, *Lightning Optical Corp.* The introduction of a 532-nm Nd:YAG beam can increase the efficiency of an ultraviolet Ce:LiSAF laser by 1.4× by bleaching the 266 nm pump-induced color centers. **(p. 7)**

9:15am
WB3 • High-efficiency UV light generation by CLBO, Y. Mori, M. Inagaki, S. Nakajima, A. Taguchi, A. Miyamoto, W. L. Zhou, T. Sasaki, S. Nakai, *Osaka Univ., Japan.* We report the demonstration of more than 10% 5 HG efficiency from fundamental and 49% 4 HG efficiency from second harmonic of Nd:YAG laser realized in CLBO. **(p. 10)**

9:30am
WB4 • CW 355 nm generation by doubly resonant sum-frequency mixing in an external resonator, Yushi Kaneda, Shigeo Kubota, *Sony Research Center, Japan.* 220 mW of cw ultraviolet output at 355 nm is obtained based on doubly resonant sum frequency mixing between 1064 nm and 532 nm in an external resonator. **(p. 13)**

TERRACE ROOM

9:45am–10:45am
WC • IR Lasers I Poster Session/Coffee Break and Exhibits

WC1 • Miniature Nd:YAG ring lasers with high single-frequency output power at 946 nm, I. Freitag, R. Henking, F. von Alvensleben, A. Tünnermann, *Laser Zentrum Hannover e.V., Germany.* Efficient room-temperature operation at the 946 nm quasi-three-level transition is reported for diode-pumped Nd:YAG ring lasers with 800 mW cw single-frequency output power. **(p. 18)**

WC2 • Experimental and theoretical investigations on the intensity noise properties of injection-locked lasers, I. Freitag, A. Tünnermann, H. Welling, *Laser Zentrum Hannover e.V., Germany;* C. C. Harb, D. E. McClelland, H.-A. Bachor, *The Australian National Univ.;* T. C. Ralph, *Univ. Auckland, New Zealand.* Experimental investigations on intensity noise in injection-locked, solid-state lasers are presented. An analytical quantum mechanical theory predicts the measured behavior qualitatively and quantitatively. **(p. 21)**

WC3 • Spectroscopic properties and laser oscillation of Yb/Er:$Ca_2Al_2SiO_7$ in the 1.6 μm eye-safe range, B. Simondi-Teisseire, B. Viana, A. M. Lejus, D. Vivien, *Laboratorie de Chimie Appliquée de L'Etat Solide, France;* C. Borel, R. Templier, C. Wyon, *CEA–LETI, France.* Spectroscopy, rate equation modelization of the Yb→Er energy transfer, and laser oscillation in the eye safe window are presented in the disordered Yb/Er:$Ca_2Al_2SiO_7$ (CAS). **(p. 24)**

WC4 • High energy diode side-pumped Cr:LiSAF laser, Christyl C. Johnson, Donald J. Reichle, Norman P. Barnes, *NASA Langley Research Center;* Gregory J. Quarles, *Lightning Optical Corp.* A diode side-pumped Cr:LiSAF laser with a 30 mJ normal mode output energy and an optical-to-optical efficiency of 17% are discussed. **(p. 27)**

WC5 • Lasing in diode-pumped thulium and thulium, holmium-doped YAP, I. F. Elder, M. J. P. Payne, *Defence Research Agency, UK.* The comparison between room temperature lasing in thulium and thulium, holmium-doped YAP crystals pumped by a single 3 W laser diode is discussed. **(p. 30)**

WC6 • Efficient pyrromethene-doped xerogels for tunable solid-state lasers, Mohammed Faloss, Michael Canva, Patrick Georges, Alain Brun, *Institut d'Optique Théorique et Appliquée, France;* Frédéric Chaput, Jean-Pierre Boilot, *École Polytechnique, France.* We report on improved pyrromethene-doped xerogels for tunable solid-state dye laser in the visible that yield to 80% slope efficiency and a lifetime of several hundreds of thousands pulses. **(p. 33)**

WC7 • High average power scaling of a compact, Q-switched, diode-pumped, Nd:YAG laser, J. L. Dallas, R. S. Afzal, *NASA Goddard Space Flight Center.* Scaling an altimeter laser to high repetition rates is investigated. We acquired 2.4 mJ at 975 Hz. Induced thermal effects and performance limits are identified. **(p. 36)**

WC8 • Enhanced performance flashlamp-pumped Ti:sapphire laser with phase conjugate resonator, N. W. Hopps, M. R. Dickinson, T. A. King, *Univ. Manchester, UK.* A flashlamp-pumped titanium:sapphire laser, incorporating a self-starting stimulated Brillouin scattering phase-conjugate resonator is presented. Lower divergence, better beam quality, and narrower linewidth are demonstrated. **(p. 39)**

WC9 • Slope efficiency and gain measurement of highly Cr^{4+}-doped forsterite, Takashi Fujii, Masahiro Nagano, Koshichi Nemoto, *Central Research Institute of Electric Power Industry, Japan.* High slope efficiency of 25% is obtained in highly Cr^{4+}-doped forsterite laser oscillation. One pass gain was measured by pump-and-probe technique. **(p. 42)**

WC10 • Passive Q-switching of the erbium-glass laser using Er^{3+}:CaF_2, Marly B. Camargo, Robert D. Stultz, Milton Birnbaum, *Univ. Southern California.* The advantages of passive *Q*-switching with Er^{3+}:CaF_2, as well as a phenomenological model of the $^4I_{13/2}$ fluorescence decay, are presented. **(p. 45)**

WC11 • Efficient single-transverse-mode laser-diode side-pumped thulium and holmium lasers: Modeling and experiment, Gunnar Rustad, Harald Hovland, Knut Stenersen, *Norwegian Defence Research Establishment.* Efficient Tm and Ho lasers employing a novel multi-pass side-pumping geometry are described. Simulations accounting for upconversion and ground-state depletion show reasonable agreement with the experiments. **(p. 48)**

WC12 • Simultaneous lasing of Nd^{3+}:$Sr_5(PO_4)_3F$ at 1.059 μm and 1.328 μm, X. X. Zhang, *Melles Griot;* M. Bass, B. H. T. Chai, *CREOL;* P. J. Johnson, J. C. Oles, *Lightning Optical Corp.;* L. K. Cheng, *E. I. duPont de Nemours & Co.* Simultaneous lasing at 1.059 μm and 1.328 μm has been demonstrated in Nd^{3+}-doped strontium fluorapatite, $Sr_5(PO_4)_3F$ or S-FAP, in lamp-pumped operation. More than 1 J of pulsed output energy has been achieved at each laser line. **(p. 51)**

WC13 • Comparison of spectroscopic and laser properties of Cr^{4+}:$Y_xLu_{3-x}Al_5O_{12}$ crystals, A. I. Zagumennyi, Yu. D. Zavartsev, P. A. Studenikin, V. I. Vlasov, V. A. Kozlov, I. A. Shcherbakov, A. F. Umyskov, *General Physics Institute, Moscow.* We present a spectroscopic investigation of the Cr^{4+}:$Y_xLu_{3-x}Al_5O_{12}$, a new laser material for the near-infrared region. We demonstrate simple diode side-pumped *Q*-switched Nd:$GdVO_4$ laser. **(p. 54)**

WC14 • Novel geometries for copper-vapor-laser-pumped Ti:sapphire lasers, W. J. Wadsworth, D. W. Coutts, C. E. Webb, *Univ. Oxford, UK.* We report a 6.2 kHz pulsed Ti:sapphire laser producing over 4 W average power, transversely pumped by a copper vapor laser. Damage-free power scaling is expected. **(p. 57)**

WC15 • Laser operation and spectroscopy of Cr^{3+}:Yb^{3+}:Ln^{3+}:YSGG, Yu. D. Zavartsev, A. A. Zagumennyi, V. V. Osiko, P. A. Studenikin, I. A. Shcherbakov, A. F. Umyskov, *General Physics Institute, Moscow.* Spectroscopic examinations and laser properties of the co-doped Cr^{3+}:Yb^{3+}-Ln^{3+}:YSGG systems (where Ln^{3+} are Ho^{3+}, Tm^{3+}, Er^{3+} ions) are discussed. **(p. 60)**

WC16 • Narrow band volume holographic 532-nm optical filter, Michael A. Krainak, Robert S. Afzal, *NASA Goddard Space Flight Center;* Anthony W. Yu, *Hughes STX Corp.;* Koichi Sayano, *Accuwave Inc.* We describe a narrow band (16 pm FWHM), passive, holographic 532-nm optical filter for use with frequency stabilized doubled Nd:YAG lasers. **(p. 63)**

GOLD ROOM

10:45am–12:30pm

WD • Parametric Oscillators

David Nabors, *Coherent Laser Group, Presider*

10:45am (Invited)

WD1 • High-power, high-repetition-rate optical parametric oscillator based on periodically poled $LiNbO_3$, W. R. Bosenberg, A. Drobshoff, *Lightwave Electronics Corp.;* L. E. Myers, *USAF Wright Laboratory.* We report a high-power (2 W at 1.54 μm, 0.6 W at 3.5 μm), high repetition rate (5–30 kHz) optical parametric oscillator based on periodically poled lithium niobate tunable over 3–5 μm. **(p. 68)**

11:00am

WD2 • Synchronous pumping of a periodically poled lithium niobate optical parametric oscillator, T. P. Grayson, L. E. Myers, *USAF Wright Laboratory;* M. D. Nelson, Vince Dominic, *Univ. Dayton.* We demonstrate the first synchronously pumped operation of an OPO using periodically poled lithium niobate as the nonlinear medium. Depletion efficiencies up to 83% are observed at 1.53 μm. Efficiency and wavelength tuning measurements are presented. **(p. 71)**

11:15am

WD3 • Effect of cavity design on optical parametric oscillator performance, William A. Neuman, Stephan P. Velsko, *Lawrence Livermore National Laboratory.* The effect of resonator cavity design on parametric oscillator performance is investigated theoretically. Certain unstable resonators produce energy conversion and beam quality superior to that of traditional resonators. **(p. 74)**

11:30am

WD4 • Continuous-wave mode-locked operation of a picosecond $AgGaSe_2$ optical parametric oscillator in the mid infrared, Chr. Grässer, S. Marzenell, R. Beigang, R. Wallenstein, *Univ. Kaiserslautern, Germany.* Operation of a picosecond cw mode-locked $AgGaSe_2$ OPO pumped by the 1.55 μm signal radiation of a KTP-OPO is reported. The OPO is tunable from 2 μm to 7 μm with average output powers of up to 500 mW. **(p. 77)**

11:45am
WD5 • Improved OPO brightness with a GRM non-confocal unstable resonator, Suresh Chandra, Toomas H. Allik, *Science Applications International Corp.;* J. Andrew Hutchinson, *US Army CECOM;* Mark S. Bowers, *Aculight Corp.* The use of a gradient reflectivity mirror is shown to improve the brightness of a 355 nm-pumped BBO, OPO over that of a plano–parallel resonator. **(p. 80)**

12:00m
WD6 • A KTA OPO pumped by a Q-switched injection-seeded Nd:YAG laser, T. Chuang, Jeffrey Kasinski, Horacio R. Verdún, *Fibertek, Inc.* We demonstrate a KTA OPO ($\theta = 90°$, $\phi = 15°$) pumped by a diode-pumped, *Q*-switched and injection-seeded Nd:YAG laser. The wavelength of the OPO was 1.5322 μm. The conversion efficiency was as high as 49%. **(p. 83)**

12:15pm
WD7 • Synchronous pumping of an optical parametric oscillator (OPO) using an amplified quasi-cw pump envelope, S. D. Butterworth, W. A. Clarkson, N. Moore, G. J. Friel, D. C. Hanna, *Univ. Southampton, UK.* A long pulse envelope, sliced from a cw mode-locked laser and then amplified, provides a versatile pump source; synchronous pumping of an OPO is demonstrated. **(p. 86)**

12:30pm–1:30pm
Lunch Break

GOLD ROOM

1:30pm–3:15pm
WE • Short Pulse Lasers I
Paul French, *Imperial College of Science and Technology, UK, Presider*

1:30pm
WE1 • Saturable Bragg reflector mode-locking of Cr^{4+}:YAG laser pumped by a diode-pumped Nd:YVO_4 laser, B. C. Collings, K. Bergman, *Princeton Univ.;* S. Tsuda, W. H. Knox, J. B. Stark, J. E. Cunningham, W. Y. Jan, R. Pathak, *AT&T Bell Laboratories.* We discuss saturable Bragg reflector mode-locking at 1540 nm in a Cr^{4+}:YAG laser pumped by a high power Nd:YVO_4 laser, and we compare with Kerr-lens mode-locking. **(p. 90)**

1:45pm
WE2 • An efficient diode-based Ti:sapphire ultrafast laser, Murray K. Reed, Michael K. Steiner–Shepard, Daniel K. Negus, *Coherent Inc.* 170 mW of 50-fs pulses and 30 mW of SHG is generated by a Ti:sapphire ultrafast laser pumped with a diode-laser-pumped intracavity-doubled Nd:YAG ring laser. **(p. 93)**

2:00pm
WE3 • All-solid-state diode-pumped tunable femtosecond Cr:LiSAF regenerative oscillator/amplifier, R. Mellish, R. Jones, N. P. Barry, S. C. W. Hyde, P. M. W. French, J. R. Taylor, *Imperial College, UK;* C. J. van der Poel, A. Valster, *Philips Optoelectronics Centre, The Netherlands.* An all-solid-state, diode-pumped, tunable femtosecond Cr:LiSAF KLM oscillator and 25 kHz microjoule regenerative amplifier is reported. The oscillator delivers pulses as short as 25 fs. **(p. 95)**

2:15pm
WE4 • Self-starting diode-pumped femtosecond Cr:LiSAF laser, Franck Falcoz, François Balembois, Patrick Georges, Gérard Roger, Alain Brun, *Institut d'Optique Théorique et Appliquée, France.* We report on an all-optical, solid-state self-starting Kerr lens mode-locked diode-pumped Cr:LiSAF laser that produces 55 fs pulses at 850 nm. **(p. 98)**

2:30pm
WE5 • Self-starting femtosecond diode-pumped Cr:LiSGAF laser, V. P. Yanovsky, F. W. Wise, *Cornell Univ.* A self-starting mode-locked and diode-pumped Cr:LiSGAF laser with a saturable mirror produces 100-fs pulses with 40 mW average power. **(p. 101)**

2:45pm
WE6 • 47 fs pulse generation from a prismless self-mode-locked Cr:LiSGaF laser, I. T. Sorokina, E. Sorokin, E. Wintner, *Technical Univ. Vienna, Austria;* A. Cassanho, *Lightning Optical Corp.;* H. P. Jenssen, *CREOL;* R. Szipöcs, *Research Institute for Solid State Physics, Hungary.* We report the generation of nearly bandwidth-limited 47 fs pulses from a self-mode-locked Cr:LiSrGaF laser, using Gires–Tournois interferometer structured dielectric mirrors for dispersion control. **(p. 104)**

3:00pm
WE7 • Infrared femtosecond pulse generation with a 250 kHz Ti:sapphire-pumped β-BaB_2O_4 optical parametric amplifier, Murray K. Reed, Michael K. Steiner–Shepard, *Coherent Inc.* A 250-kHz, 100-fs, Ti:sapphire regenerative amplifier system pumping a Type-II BBO OPA generates 0.5 μJ with continuous tuning from 1.1 μm to beyond 2.5 μm. **(p. 107)**

TERRACE ROOM

3:15pm–4:15pm
WF, Nonlinear Frequency Conversion Poster Session/ Refreshment Break and Exhibits

WF1 • Raman spectroscopic and nonlinear optical properties of barium nitrate crystal, P. G. Zverev, T. T. Basiev, *General Physics Institute, Moscow;* W. Jia, H. Liu, *Univ. Puerto Rico.* The temperature effect on spectral parameters of Raman modes, resulting in the change of SRS gain, is reported in barium nitrate crystal. The self-focusing of laser radiation in the Raman crystal has been investigated using the Z-scan technique. **(p. 112)**

WF2 • High power nonlinear generation of UV, Waverly Marsh, Dale Richter, James Barnes, *NASA.* To perform remote sensing of ozone accurately, one needs a high power source of UV light. We describe a solid-state nonlinear frequency conversion technique to generate high powers of UV light reliably. **(p. 114)**

WF3 • Phase-matched second-harmonic generation in ion-implanted $KNbO_3$ channel waveguides, D. Fluck, P. Günter, *Swiss Federal Institute of Technology;* St. Bauer, Ch. Buchal, *Forschungszentrum (KFA) Jülich, Germany.* Up to 1.3 mW blue light at 441 nm is generated in a 5.8-mm-long $KNbO_3$ channel waveguide for an incident fundamental power of 200 mW. **(p. 117)**

WF4 • Quasi-phase matching achieved in $LiTaO_3$ thin films grown on sapphire by rf magnetron sputtering, Florence Armani-Leplingard, John J. Kingston, David K. Fork, *Xerox Palo Alto Research Center.* We achieve quasi-phase matching in a $LiTaO_3$ thin film planar waveguide grown on sapphire using proton exchange to periodically deaden the nonlinearity of the crystal. **(p. 120)**

WF5 • Efficient tunable intracavity OPO in the mid IR, A. Englander, R. Lavi, R. Lallouz, *Soreq NRC, Israel.* Efficient intracavity optical parametric oscillation is demonstrated by use of different crystals placed inside the resonator of a diode side-pumped *Q*-switched Nd:YAG laser. Conversion efficiency from diode light to idler is 1.15%. A tuning range from 3.2–4.5 μm is achieved. **(p. 123)**

WF6 • Ultraviolet tunable Cr:LiSAF laser system for detection of chemical and biological agents, Eric Park, James Gorda, Martin Richardson, *CREOL;* Jay Fox, *US Army CECOM;* Cynthia Swim, *US Army CBDCOM.* We describe the design and construction of a MOPA configuration Cr:LiSAF based laser system utilizing frequency tripling to generate tunable radiation in the ultraviolet region. **(p. 126)**

WF7 • Application of laser and related materials to demonstrate large nonlinear optical effects and diffraction efficiency, Ian McMichael, Tallis Y. Chang, *Rockwell International Science Center;* Mikhail Noginov, *Alabama A&M Univ.;* Harry Tuller, *MIT.* Long metastable lifetimes in laser and related materials combined with a large index change makes possible large nonlinear optical effects using cw lasers. **(p. 128)**

WF8 • Synthesis and study of nonlinear single crystals $CeSc_3(BO_3)_4$, V. A. Lebedev, V. F. Pisarenko, Yu. M. Chuev, *Kuban State Univ., Russia.* Conditions of the crystalization of $LnSc_3(BO_3)_4$ (Ln = La,Ce,Gd, Nd, Yb, Er) systems in trigonal (R32) or monoclinic (C2/c) modification and spectral-luminescent characteristics Cr^{3+}, Nd^{3+}, Yb^{3+}, Er^{3+} in these crystals were studied. **(p. 131)**

WF9 • Modification of the optical transmission of flux-grown $KTiOPO_4$ crystal by growth in nitrogen ambient, Akio Miyamoto, Yusuke Mori, Takatomo Sasaki, Sadao Nakai, *Osaka Univ., Japan.* Optical transmission in the range below 550 nm of KTP crystal are improved by growing in nitrogen ambient. Strong relationship between optical absorption and Pt concentration are revealed. **(p. 132)**

WF10 • A 10 mW frequency-doubled diode laser at 491 nm, D. Fluck, T. Pliska, P. Günter, *Swiss Federal Institute of Technology.* 10 mW continuous-wave 491 nm light is generated by direct frequency doubling a master-oscillator power-amplifier laser diode in a 17-mm-long $KNbO_3$ crystal. **(p. 135)**

WF11 • Semi-analytical model of the pulsed optical parametric oscillator: Comparison with experiment, T. Debuisschert, J. Raffy, J. P. Pocholle, *Laboratoire Central de Recherches, France.* A model of the pulsed OPO is proposed. Nonlinear equations are solved analytically, wave-front structures are computed, and good agreement with the experiment is found. **(p. 138)**

WF12 • Analysis of incoherence effect of single-mode pump on second-harmonic generation, W.-L. Zhou, Y. Mori, T. Sasaki, S. Nakai, *Osaka Univ., Japan.* The incoherence effect on SHG of a single-mode pump is analyzed. A factor that demonstrates this effect is deduced as a function of the ratio of crystal length and pump coherence length. The value of this factor is above unity with a maximum of 1.253 when the crystal length is smaller than the pump coherence length, indicating an enhancement effect of single-mode pump on SHG. **(p. 141)**

WF13 • A diode-array-pumped continuous wave blue microchip laser, David G. Matthews, Neil MacKinnon, Richard S. Conroy, Bruce D. Sinclair, *Univ. St. Andrews, UK.* A diode-pumped Nd:YAG/$KNbO_3$ composite material microchip laser generates 1 mW of blue (473 nm) cw radiation near room temperature. Over 9 mW is produced Ti:sapphire-pumped. **(p. 144)**

WF14 • Intracavity, frequency-doubled, miniaturized Nd:$YAlO_3$ blue laser at 465 nm, Joseph H. Zarrabi, Paul Gavrilovic, Shobha Singh, *Polaroid Corp.* We have demonstrated a blue laser at 465 nm by intracavity frequency doubling of 930 nm transition in neodymium-doped crystal of yttrium orthoaluminate (Nd:$YAlO_3$). The compact plano-plano laser cavity comprising a 1.2-mm-thick Nd:$YAlO_3$ crystal and a 1.3 mm potassium niobate ($KNbO_3$) crystal generated more than 15 mW of blue power when pumped by a Ti:sapphire laser. **(p. 147)**

WF15 • Infrared to visible nonlinear up-and-down conversion processes using $AgGaS_2$ crystals, J.-J. Zondy, D. Touahri, O. Acef, *Bureau National de Métrologie/Observatoire de Paris, France.* Second-harmonic generation of a KCl:Li color center laser, upconversion of a near-IR diode laser by a CO_2 laser, and noncritical optical parametric amplification are reported by use of silver thiogallate. **(p. 150)**

WF16 • Visible picosecond pulse generation in a frequency-doubled optical parametric oscillator based on LiB_3O_5, S. French, M. Ebrahimzadeh, A. Miller, *Univ. St. Andrews, UK.* We report efficient generation of 870 fs pulses with average powers of 70 mW in the wavelength range 584–771 nm by externally frequency doubling a LiB_3O_5 optical parametric oscillator. **(p. 154)**

WF17 • Temperature (–32°C to +90°C) performance of a 20-Hz potassium titanyl phosphate optical parametric oscillator, Robert D. Stultz, Michael E. Ehritz, *Hughes Electro-Optical Systems.* The reliable performance of a 1.5 μm potassium titanyl phosphate optical parametric oscillator has been demonstrated over a temperature range of greater than 120°C. **(p. 156)**

WF18 • A single-mode grazing incidence BBO-OPO with a large scanning range, J. M. Boon-Engering, E. A. J. M. Bente, W. Hogervorst, *Laser Centre Vrije Univ., The Netherlands;* W. E. van der Veer, *Nederlands Centrum voor Laser Research, The Netherlands.* A single-mode BBO-OPO with a grazing incidence cavity scanning over 5 cm^{-1} is described. Stabilization scheme and some experimental results are presented. **(p. 159)**

WF19 • LD-pumped Nd:YAG green laser system, Yoichiro Maruyama, Masaki Ohba, Masaaki Kato, Takashi Arisawa, *Japan Atomic Energy Research Institute, Japan.* The average power of 19 W at 532 nm is generated efficiently by use of an LD-pumped zig-zag slab Nd:YAG laser MOPA system operated at the PRF of 1 kHz. **(p. 162)**

GOLD ROOM

4:15pm–6:00pm
WG • Near Infrared Lasers
Joseph F. Pinto, *US Naval Research Laboratory, Presider*

4:15pm
WG1 • 1-W continuous-wave diode-pumped Cr:LiSAF laser, D. Kopf, U. Keller, *Swiss Federal Institute of Technology;* R. J. Beach, M. A. Emanuel, *Lawrence Livermore National Laboratory.* We demonstrate a Cr:LiSAF laser with 1 W pure (not quasi) cw average output power. The Cr:LiSAF is pumped with a high-power 1 cm wide diode-laser array mode-matched to an asymmetric lasing mode. **(p. 166)**

4:30pm
WG2 • Efficient, single-mode, 1.5 mJ, passively Q-switched diode-pumped Nd:YAG laser, Robert S. Afzal, *NASA Goddard Space Flight Center;* John J. Zayhowski, T. Y. Fan, *MIT Lincoln Laboratory.* We demonstate an efficient, compact, 1.5 mJ, 3.9 ns, passively *Q*-switched, single mode, diode-pumped Nd:YAG laser using Cr^{4+}:YAG as a saturable absorber. **(p. 169)**

4:45pm
WG3 • CW-diode-pumped Nd:$GdVO_4$-laser passively Q-switched with Cr^{4+}:YAG as saturable absorber, I. V. Klimov, V. B. Tsvetkov, I. A. Shcherbakov, *Russian Academy of Sciences;* J. Bartschke, K.-J. Boller, R. Wallenstein, *Univ. Kaiserslautern, Germany.* We describe the influence of the polarization-dependent saturated absorption in a Cr^{4+}:YAG crystal on the output parameters of a diode-laser-pumped passively *Q*-switched Nd:$GdVO_4$ laser. Rotation of the Cr^{4+}:YAG crystal changes the pulse length from 30 ns to 170 ns, while the pulse repetition rate varies from 40 kHz to 300 kHz. **(p. 172)**

5:00pm
WG4 • Laser performance of a new ytterbium-doped phosphate laser glass, U. Griebner, R. Koch, H. Schönnagel, *Max-Born-Institut, Germany;* S. Jiang, M. J. Myers, D. Rhonehouse, S. J. Hamlin, *Kigre Inc.;* W. A. Clarkson, D. C. Hanna, *Univ. Southampton, UK.* Laser action of a new Yb^{3+}-doped phosphate glass with an output power of 250 mW and a slope efficiency of 43% is demonstrated by pumping with a cw-diode-pumped Nd:YAG laser operating at 946 nm. **(p. 175)**

5:15pm
WG5 • Diode-pumped continuous-wave Yb laser in fluoride phosphate glasses, T. Danger, E. Mix, E. Heumann, G. Huber, *Univ. Hamburg, Germany;* D. Ehrt, W. Seeber, *Univ. Jena, Germany.* Diode-pumped tunable cw laser action of Yb-doped glasses is demonstrated at room temperature. The maximum output power and slope efficiency is 239 mW and 69%, respectively. **(p. 178)**

5:30pm
WG6 • Performance of a Q-switched Yb:$Sr_5(PO_4)_3$ laser, Camile Bibeau, Raymond J. Beach, Stephen A. Payne, *Lawrence Livermore National Laboratory.* We report on the performance of a *Q*-switched Yb:S-FAP laser using an end-pumped cavity geometry with a lens duct for irradiance conditioning of the diode pump light. **(p. 181)**

5:45pm
WG7 • Room temperature upconversion-pumped cw Yb,Er:$YLiF_4$-laser at 1.234 μm, E. Heumann, P. Möbert, G. Huber, *Univ. Hamburg, Germany;* B. H. T. Chai, *CREOL.* We report room temperature upconversion-pumped continuous wave laser emission of Yb(5%),Er(1%):$YLiF_4$ at 1.234 μm excited by a Ti:sapphire laser and laser diodes at 960 nm and 968 nm, respectively. An output power of up to 160 mW is obtained with output coupling of 1%. **(p. 184)**

6:00pm–8:00pm
Free Time

GARDEN ROOM

7:30pm–9:00pm
Registration

GOLD ROOM

8:00pm–10:00pm
Postdeadline Paper Session
Walter Bosenberg, *Lightwave Electronics Corporation, Presider*

GARDEN ROOM

7:15am-12:30pm
Registration

GOLD ROOM

8:00am–8:30am
ThA • Plenary II
Clifford Pollock, *Cornell University, Presider*

8:00am (Invited)
ThA1 • Lasers for material processing in advanced manufacturing applications, A. C. Tam, *IBM Almaden Research Center.* New techniques for laser material processing have been developed using laser sources from the ultraviolet to the infrared. Practical applications in "hi-tech" industry are described. **(p. 188)**

8:30am–9:00am
ThB • Plenary III
Clifford Pollock, *Cornell University, Presider*

8:30am (Invited)
ThB1 • Military and dual use applications in the next decade, Rudolf G. Buser, *CECOM RDEC.* Sensing devices for military and related applications as well as forward working dual use concepts are discussed. As baseline present/near-term sensor requirements are analyzed, existing limitations due to physics and technology principals established, and possible pathways to solutions indicated. **(p. 192)**

9:00am–9:45am
ThC • High Power Lasers
Christopher Clayton, *Phillips Laboratory, Presider*

9:00am (Invited)
ThC1 • 69 W average power Yb:YAG laser, Hans Brueselbach, David S. Sumida, *Hughes Research Laboratories.* We report, we believe, the highest-to-date average power (69 W), quasi-cw power (150 W), and pulse energy (173 mJ at 400 Hz) from an InGaAs-diode-pumped Yb:YAG laser. **(p. 194)**

9:15am
ThC2 • High-power near-diffraction-limited and single-frequency operation of Yb:YAG thin disc laser, A. Voss, C. Stewen, M. Karszewski, A. Giesen, *Univ. Stuttgart, Germany;* U. Brauch, *Deutsche Forschungsanstalt für Luft- und Raumfahrt, Germany.* With a Yb:YAG thin-disc laser 57 W with η_{opt} = 38% and M^2 = 2 as well as 14 W single frequency with η_{opt} = 30% and M^2 = 1.02 are demonstrated. **(p. 197)**

9:30am
ThC3 • High power operation of Nd:YAG rod lasers pumped by fiber-coupled diode lasers, D. Golla, M. Bode, S. Knoke, W. Schöne, F. von Alvensleben, A. Tünnermann, *Laser Zentrum Hannover e.V., Germany.* Laser performance of cw Nd:YAG rod lasers at output powers of several 100 W are demonstrated. Optical-to-optical efficiencies of more than 40% are achieved. **(p. 200)**

TERRACE ROOM

9:45am–10:45am
ThD • Novel Architectures Poster Session/Coffee Break and Exhibits

ThD1 • High-resolution Doppler lidar employing a diode-pumped injection-seeded Tm:Lu,YAG transmitter, Christian J. Grund, *NOAA.* System design and demonstration of simultaneous 30 m range resolution and 5 cm/s velocity resolution in the marine boundary layer while operating from a ship are discussed. **(p. 204)**

ThD2 • Dual-rod Cr:LiSAF oscillator/amplifier for remote sensing applications, James W. Early, Charles Lester, Nigel J. Cockroft, *Los Alamos National Laboratory;* Christyl Johnson, Donald Reichle, *NASA Langley Research Center;* David W. Mordaunt, *Stratonics Inc.* Evaluations of dual-rod Cr:LiSAF oscillator and amplifier configurations are reported with improved gain and average power output of 16 W. **(p. 207)**

ThD3 • Yb^{3+},Er^{3+} co-doped materials for planar optical waveguide amplifiers, Markus P. Hehlen, Timothy R. Gosnell, Nigel J. Cockroft, *Los Alamos National Laboratory;* Allan J. Bruce, W. H. Grodkiewicz, Gerry Nykolak, Joseph Shmulovich, Ruby Ghosh, M. R. X. Barros, *AT&T Bell Laboratories.* The results of a spectroscopic characterization of an extensive series of Yb^{3+},Er^{3+} co-doped glasses for planar optical waveguide amplifiers are presented. **(p. 210)**

ThD4 • Far-infrared p-Ge laser: Temperature-dependent laser dynamics, Kijun Park, Robert E. Peale, Henry Weidner, Jin J. Kim, *CREOL.* A p-Ge sub-mm laser in **E⊥B** fields with Faraday and Voigt geometry using superconducting or permanent magnets reveals new temperature-dependent laser pulse dynamics. **(p. 213)**

ThD5 • Phase conjugator of the light beams based on Nd:YAG rod with the reciprocal feedback, O. L. Antipov, S. I. Belyaev, A. S. Kuzhelev, *Russian Academy of Science.* Self-pumped phase conjugation of the light beam in an inverted Nd:YAG rod with the reciprocal feedback loop is studied. The effect is caused by the simultaneous scattering of light waves by the refractive index grating of the inverted laser crystal. **(p. 216)**

ThD6 • Fundamental studies of a pulsed high gain Nd:YVO_4 amplifier, P. Dekker, J. M. Dawes, J. A. Piper, *Macquarie Univ., Australia.* We report temporal and spatial studies of the gain and ASE, and performance of a transversely diode-pumped Nd:YVO_4 amplifier, by use of an end-pumped Nd:YVO_4 oscillator. **(p. 218)**

ThD7 • Conductively cooled diode-pumped slab laser, A. D. Hays, N. Martin, R. Burnham, *Fibertek Inc.* A conductively cooled diode-pumped laser oscillator produces 20 mJ at 1.064 μm at a repetition rate of 50 Hz. Beam quality and pulse-length are 1.41 mm-mrad and 5 nsec FWHM. The oscillator serves as the first stage of a space-based laser altimeter transmitter. **(p. 221)**

ThD8 • Tb^{3+} ion as a sensibilizer for rare-earth ions in a terbium trifluoride single crystal, M. A. Dubinskii, P. Misra, *Howard Univ.;* B. N. Kazakov, A. L. Stolov, Zh. S. Yakovleva, *Kazan State Univ., Russia.* The results of Tb^{3+}–Re^{3+} donor–acceptor interaction analysis for rare-earth (Re^{3+}) doped TbF_3 single crystal are represented. Possible applications of Sm^{3+}—as well as Eu^{3+}—coactivated stoichiometric Tb-hosts for conversion of Argon-laser radiation into "yellow-orange-red" are discussed. **(p. 224)**

ThD9 • Stimulated emission without cavity in powders and single crystals of Nd-doped materials, M. A. Noginov, N. E. Noginova, H. J. Caulfield, P. Venkateswarlu, T. Thompson, M. Mahdi, *Alabama A&M Univ.;* V. Ostroumov, *Hamburg Univ., Germany.* Short-pulsed (≥300 ps) emission is found from powders of $NdAl_3(BO_3)_4$. $Nd_xLa_{1-x}Sc_3(BO_3)_4$ and $Nd:Sr_5(PO_4)_3F$, compared with that from single crystals, and described in terms of $^4F_{3/2}$ concentration and emission density. **(p. 227)**

ThD10 • Linear and nonlinear dispersion in solid-state solitary-wave lasers, Marco Santagiustina, Ewan M. Wright, *Univ. Arizona.* The theory of third-order dispersion in solitary-wave lasers is developed, and we show that its detrimental effects can be countered by nonlinear dispersion. **(p. 230)**

ThD11 • Growth and optical characterization of Nd:YVO_4 crystal fibers, F. S. Ermeneux, C. Gouteaudier, R. Moncorgé, R. Burlot, M. T. Cohen–Adad, *Univ. Lyon I, France.* The optical properties of good optical quality $Nd:YVO_4$ crystal fibers grown by the LHPG technique are studied and compared with those obtained with other crystals of different origins. **(p. 233)**

ThD12 • Ultrafast dynamics of excited-state absorption in V^{3+}:YAG saturable absorber, V. P. Mikhailov, K. V. Yumashev, N. V. Kuleshov, P. V. Prokoshin, N. N. Posnov, *International Laser Center, Belarus.* The results of excited-state absorption spectra measurements in V^{3+}:YAG solid-state saturable absorber with picosecond temporal resolution are reported. ESA from the $^1E(^1D)$ level and relaxation time from the $^1E(^1D)$ to the $^3T_2(^3F)$ state are estimated. **(p. 236)**

ThD13 • Small signal gain in chromium forsterite amplifiers, Iain T. McKinnie, *Univ. Otago, New Zealand;* Terrence A. King, *Univ. Manchester, UK.* We present the first gain measurements in a Cr:forsterite amplifier. Gain, polarization, and temporal response are studied for different crystal characteristics with a 1300 nm cw signal. **(p. 239)**

ThD14 • Compositionally tuned Nd lasers, Norman P. Barnes, Elka B. Ertur, *NASA Langley Research Center;* Brian M. Walsh, *Boston College;* Ralph L. Hutcheson, *Scientific Materials Corp.* Nd laser wavelengths can be continuously compositionally tuned in selected garnets. Data are presented on the compositional tuning of Nd:YGAG for several Ga to Al ratios. **(p. 242)**

GOLD ROOM

10:45am–12:30pm

ThE • Mid Infrared Lasers

Norman Barnes, *NASA Langley Research Center, Presider*

10:45am (Invited)

ThE1 • Recent developments in Cr^{2+}-doped II-VI compound lasers, Ralph H. Page, Laura D. DeLoach, Kathleen I. Schaffers, Falgun D. Patel, Stephen A. Payne, William F. Krupke, *Lawrence Livermore National Laboratory;* Arnold Burger, *Fisk Univ.* Medium-average-power, widely tunable mid-IR $ZnS:Cr^{2+}$ and $ZnSe:Cr^{2+}$ lasers are being developed. Crystal-growth techniques, slope efficiencies, tuning range, and diode-pumped laser designs are discussed. **(p. 246)**

11:00am

ThE2 • High power 2 μm wing-pumped Tm:YAG laser, R. J. Beach, S. B. Sutton, J. A. Skidmore, M. A. Emanuel, *Lawrence Livermore National Laboratory.* Using a scalable diode end-pumping technology, we demonstrate a compact Tm:YAG laser capable of generating greater than 25 W of cw 2 μm laser output power. **(p. 249)**

11:15am

ThE3 • 2 W single-frequency cw Tm,Ho:YLF ring laser, Andrew Finch, John H. Flint, *Schwartz Electro-Optics Inc.* We report on a diode-pumped, Thulium,Holmium:YLF ring laser that has produced over 2.0 W of single-frequency power with a pump power of 14 W. **(p. 253)**

11:30am

ThE4 • 1.55 μm-wavelength cw microchip lasers, Philippe Thony, Engin Molva, *LETI–CEA, France.* Erbium-doped microchip lasers are operated at 1.55 μm. Incident pump threshold of 18 mW and slope efficiency of 33% are measured under diode pumping. **(p. 256)**

11:45am

ThE5 • Continuous wave fiber laser operation at a wavelength of 3.9 micrometers, J. Schneider, C. Carbonnier, U. B. Unrau, *Technische Univ. Braunschweig, Germany.* Continuous wave fiber laser operation at 3.9 μm in a holmium-doped fluoride fiber is realized. Output powers of more than 10 mW are obtained. **(p. 259)**

12:00m

ThE6 • Slope efficiency of a pulsed 2.8-μm Er^{3+}:$LiYF_4$ laser, R. Spring, M. Pollnau, S. Wittwer, W. Lüthy, H. P. Weber, *Univ. Bern, Switzerland.* 40% slope efficiency from pulsed $Er^{3+}:LiYF_4$ is demonstrated under cw Ti:sapphire pumping. Decrease of efficiency with pump-pulse duration depends on upper-laser-level storage time. **(p. 262)**

12:15pm

ThE7 • Quasi-cw diode-pumped 2.8 μm laser operation of Er^{3+}-doped garnets, T. Jensen, G. Huber, K. Petermann, *Univ. Hamburg, Germany.* We investigate the laser performance of Er:YSGG and Er:GGG at 2.8 μm in quasi-cw operation up to 19 mJ output energy. A scalable diode-end-pumping technology transferred 230 mJ quasi-cw diode laser power into the crystals. **(p. 265)**

12:30pm–6:30pm

Free Time (For information on the City Highlights Tour, please see page 8.)

VENETIAN ROOM

6:30pm–7:30pm

Banquet Dinner Served

7:30pm–7:45pm

Dessert Served

VENETIAN ROOM

8:00pm–8:45pm

Nonlinear Optics: A Historical Overview

Nicolaas Bloembergen, *Harvard University*

GARDEN ROOM

7:30am–6:00pm
Registration

GOLD ROOM

8:00am–8:30am
FA • Plenary IV
Hagop Injeyan, *TRW, Presider*

8:00am (Invited)
FA1 • The challenge of solid-state lasers for ICF, Howard T. Powell, *Lawrence Livermore National Laboratory.* Development of megajoule-class, solid-state lasers for the National Ignition Facility and future ICF facilities requiring challenging levels of laser beam control and flexibility will be discussed. **(p. 270)**

8:30am–9:45am
FB • Spectroscopy and Characterization
Richard Moncorgé, *University of Lyon, France, Presider*

8:30am
FB1 • Excited-state absorption and stimulated emission measurements of Cr^{4+}-doped $Y_3Al_5O_{12}$, $Y_3Sc_{0.9}Al_{4.1}O_{12}$, and $CaY_2Mg_2Ge_3O_{12}$, S. Kück, K. L. Schepler, *USAF Wright Laboratory;* K. Petermann, G. Huber, *Univ. Hamburg, Germany.* Excited-state absorption measurements of different garnet crystals are presented and analyzed. Stimulated emission is observed between 1300 nm and 1750 nm for Cr^{4+}:$Y_3Al_5O_{12}$ and between 1300 nm and 1950 nm for Cr^{4+}:$Y_3Sc_{0.9}Al_{4.1}O_{12}$. **(p. 274)**

8:45am
FB2 • Spectroscopic studies of potential mid-IR laser materials, S. R. Bowman, L. B. Shaw, J. A. Moon, B. B. Harbison, *US Naval Research Laboratory;* Joseph Ganem, *Loyola College, Maryland.* Recent spectroscopic studies of erbium and terbium doped into low phonon energy host materials are reported. The prospects for new mid-infrared lasers with these materials are discussed. **(p. 277)**

9:00am
FB3 • Gain measurements in Dy^{3+}-doped $LaCl_3$: A potential 1.3 μm optical amplifier for telecommunications, K. I. Schaffers, R. H. Page, R. J. Beach, S. A. Payne, W. F. Krupke, *Lawrence Livermore National Laboratory.* $LaCl_3$:Dy^{3+} shows promise for providing the properties necessary for a 1.3 μm amplifier owing to the combination of large emission lifetime and strong pump absorption bands. **(p. 280)**

9:15am
FB4 • Investigation of luminescent properties of Sc:CaF_2 and Sc,Ce:CaF_2 crystals as promising new media for UV tunable solid-state lasers, S. B. Mirov, A. Yu. Dergachev, W. A. Sibley, *Univ. Alabama–Birmingham;* L. Esterowitz, *US Naval Research Laboratory;* V. B. Sigachev, A. G. Papashvili, *General Physics Institute, Moscow.* Wideband UV-visible luminescence under laser or cw lamp excitation is observed in γ-irradiated Sc and Sc-Ce doped CaF_2 crystals: 1) at 380 nm in Sc:CaF_2 and Sc:Ce:CaF_2 crystals, attributed to Sc^{2+} ions and 2) at 300 nm in Sc,Ce:CaF_2 crystals, due to Sc–Ce aggregate centers. **(p. 283)**

9:30am
FB5 • CrO_4^{3-} and MnO_4^{2-}: Broadband emitters in the NIR and potential laser systems, Thomas C. Brunold, Menno F. Hazenkamp, Hans U. Güdel, *Univ. Bern, Switzerland.* CrO_4^{3-} and MnO_4^{2-} doped crystals exhibit broadband emission between 11000 and 7000 cm^{-1} on VIS/NIR excitation. Thermal quenching is within acceptable limits. **(p. 286)**

TERRACE ROOM

9:45am–10:45am
FC • Spectroscopy Poster Session/Coffee Break and Exhibits

FC1 • Spectroscopy and optical amplification in Cr-doped $LiNbO_3$, J. M. Almeida, A. P. Leite, *Univ. Porto, Portugal;* R. M. De La Rue, C. N. Ironside, *Univ. Glasgow, UK;* J. Amin, M. Hempstead, J. S. Wilkinson, *Univ. Southampton, UK.* We present measured polarized absorption and emission cross-sections for Cr:$LiNbO_3$ and investigate the feasibility of active waveguide devices in this material system. **(p. 290)**

FC2 • High excited ion density effects on the effective fluorescence lifetime in Q-switched solid state lasers, Brian W. Baird, *Electro Scientific Industries;* Richard K. DeFreez, *Linfield Research Institute;* Eric M. Freden, *Utah State Univ.* A new expression for the pulse energy dependence at high excited ion densities is presented along with experimental measurements of fluorescence lifetimes in diode-pumped Nd:YLF. **(p. 293)**

FC3 • Self-quenching of the Nd $^4F_{3/2}$ manifold, Norman P. Barnes, *NASA Langley Research Center;* Elizabeth D. Filer, *Norfolk State Univ.;* Clyde A. Morrison, *Army Research Laboratories.* An alternate approach to describe self quenching of the Nd $^4F_{3/2}$ manifold is developed using computed self quenching and diffusion parameters. Disparate results for Nd:YLF, Nd:YAG, and Nd:$LaSc_3(BO_3)_4$ are explained. **(p. 296)**

FC4 • Multiphonon relaxation (MR) in the rare-earth ions doped laser crystals, T. T. Basiev, Yu. V. Orlovskii, K. K. Pukhov, V. B. Sigachev, M. E. Doroshenko, I. N. Vorob'ev, *General Physics Institute, Moscow.* The fluorescence kinetics decay from various multiplets of Tm^{3+} and Ho^{3+} ions in $Y_3Al_5O_{12}$, $Lu_3Al_5O_{12}$, and $LiYF_4$ laser crystals is directly measured. On the basis of these measurements the multiphonon relaxation rates of the transitions are determined and analyzed using the nonlinear theory of MR. **(p. 299)**

FC5 • Lack of correlation between Tm,Ho upconversion measurements, Kenneth M. Dinndorf, *Wright Laboratory;* Hans P. Jenssen, *CREOL.* We measure the average transfer parameter for $^5I_7$->$^5I_5$ upconversion in Tm,Ho:YLF using different techniques. The measurements cannot be correlated with existing theoretical models. **(p. 302)**

FC6 • Crystal growth and luminescence properties of Er^{3+}-doped YVO_4 single crystals, F. S. Ermeneux, R. Moncorge, *Univ. Lyon I, France;* P. Kabro, J. A. Capobianco, *Concordia Univ., Canada;* M. Bettinelli, *Univ. Studi Di Verona, Italy;* E. Cavalli, *Univ. Parma, Italy.* Optical properties of erbium ions doped yttrium vanadate single crystals are demonstrated. The radiative transition probabilities within the 4f manifolds are calculated using the Judd–Ofelt theory. **(p. 305)**

FC7 • ESA measurements of Cr^{4+}-doped crystals with wurtzite-like structure, S. Hartung, S. Kück, K. Petermann, G. Huber, *Univ. Hamburg, Germany.* Cw and time-resolved ESA measurements of Cr^{4+}-doped $LiAlO_2$ and $LiGaO_2$ at room temperature and at 10 K from 300 nm to 2500 nm are presented. **(p. 308)**

FC8 • Effects of radiation trapping on measured excited-state lifetimes, Markus P. Hehlen, *Los Alamos National Laboratory.* Efficient elimination of radiation-trapping artifacts in the $^2F_{5/2}$ lifetime of YAG:1%Yb^{3+} is achieved using a generally applicable refractive-index matched sphere. **(p. 311)**

FC9 • Far-infrared spectra of ultrahigh purity III-V and II-VI nonlinear crystals, Gregory S. Herman, *Univ. Arizona* and *Science Applications International Corp.;* Gianluigi Bertelli, *Old Dominion Univ.* and *SAIC;* Derrick Whitehurst, *Norfolk State Univ.;* Sudhir Trivedi, *Brimrose Corp. of America.* Far-infrared (FIR) transmission spectra are measured for many nonlinear crystals. Ultrahigh purity III-V and II-VI crystals are suitable for difference-frequency generation to the FIR. **(p. 314)**

FC10 • Time-resolved excited-state absorption measurements in Cr^{4+}-doped Mg_2SiO_4 and Y_2SiO_5 laser materials, N. V. Kuleshov, V. G. Shcherbitsky, V. P. Mikhailov, *International Laser Center, Belarus;* S. Kück, K. Petermann, G. Huber, *Univ. Hamburg, Germany.* Polarized ESA spectra have been measured in Cr^{4+}-doped Mg_2SiO_4 and Y_2SiO_5 crystals in the 200–900 nm region. Solid-state passive *Q*-switches based on these materials are proposed for lasers in the 550–800 nm spectral range. **(p. 317)**

FC11 • Spectroscopic evaluation of visible laser potential of several Pr^{3+}- and Tm^{3+}-doped crystals, Larry D. Merkle, Bahram Zandi, *Army Research Laboratory;* Bruce H. T. Chai, *CREOL.* Several oxide crystals are evaluated spectroscopically for potential visibly pumped, visible lasers. Tm:$Sr_5(PO_4)_3F$, Tm:$Ca_5(PO_4)_3F$, and Pr:$La_3Lu_2Ga_3O_{12}$ look promising, especially for their long fluorescence lifetimes. **(p. 320)**

FC12 • Photoconductivity and electro-motive force study of rare-earth-doped YSGG laser crystals, M. A. Noginov, N. Kukhtarev, N. E. Noginova, H. J. Caulfield, P. Venkateswarlu, M. Mahdi, *Alabama A&M Univ.* Linear correlation between the photocurrent and the population of 4f excited states is found in rare-earth-doped crystals. The model of the photoconductivity is discussed. **(p. 323)**

FC13 • Excited-state dynamics in the low-phonon materials Er^{3+}:BaY_2F_8 and $Cs_3Er_2Br_9$, M. Pollnau, W. Lüthy, H. P. Weber, K. Kramer, H. U. Güdel, *Univ. Bern, Switzerland;* R. A. McFarlane, *Hughes Research Laboratories.* By measurement of excited-state absorption and fluorescence, the population dynamics in Er^{3+}:BaY_2F_8 and $Cs_3Er_2Br_9$ are investigated. Differences in wavelength ranges, multiphonon relaxations, and interionic processes are discussed. **(p. 326)**

FC14 • Time-resolved Fourier spectroscopy of energy transfer in multisite (Yb,Ho)KYF_4, C. J. Schwindt, H. Weidner, R. E. Peale, *Univ. Central Florida.* Time-resolved FTS on the IR-pumped green-lasing crystal (Yb,Ho):KYF_4 reveals new information concerning upconversion and back-transfer processes. **(p. 329)**

FC15 • Radiative and nonradiative transition rates of Pr^{3+} in $LaCl_3$, L. B. Shaw, S. R. Bowman, B. J. Feldman, *US Naval Research Laboratory;* Joseph Ganem, *Loyola College, Maryland.* Radiative rates and fluorescence lifetimes are calculated for the lower lying states of Pr:$LaCl_3$ using the Judd–Ofelt theory and multiphonon emission probabilities. **(p. 332)**

FC16 • A multi-dimensional spectroscopic facility for the characterization of laser materials, Lee H. Spangler, *Montana State Univ.;* Ralph L. Hutcheson, *Scientific Materials Corp.* A new spectroscopic method with sub-wavenumber spectral and simultaneous 5 nanosecond temporal resolution covering the UV to IR in both excitation and emission is developed. **(p. 335)**

FC17 • Optical properties of Tm^{3+} in lanthanum beryllate, V. Sudesh, J. A. Piper, *Macquarie Univ., Australia;* D. S. Knowles, *Naval Command, Control and Ocean Surveillance Center;* R. S. Seymour, *Defence Science and Technology Organisation, Australia.* Optical properties of crystalline Tm:BeL grown by the Czechralski method indicate its promise as a mid-infrared laser medium with a higher emission cross-section than Tm:YAG. **(p. 337)**

FC18 • A powerful new technique for laser crystals: Time-resolved Fourier spectroscopy, H. Weidner, R. E. Peale, *Univ. Central Florida.* Time-resolved Fourier transform spectroscopy is demonstrated to be a powerful tool for studying dynamic effects in laser crystals. **(p. 340)**

GOLD ROOM

10:45am–12:30pm

FD • Novel Architecture

Douglas Anthon, *ATx-Telecom Systems, Presider*

10:45am

FD1 • Deformable membrane frequency tuning of microchip lasers, J. A. Keszenheimer, A. Mooradian, J. Prince, *Micracor Inc.;* S. Humphrey, *Rome Laboratory/OCPC.* An Nd:YAG microchip laser operating at 1.3 μm is frequency-tuned by use of a silicon nitride deformable-membrane output coupler. **(p. 344)**

11:00 am

FD2 • Single axial-mode oscillation of a coupled cavity Yb:YAG laser, Takunori Taira, Takao Kobayashi, *Fukui Univ., Japan;* William M. Tulloch, Robert L. Byer, *Stanford Univ.* Single axial mode operation of a Yb:YAG laser is achieved with a 33.9 mW threshold and 32% slope efficiency. An uncoated Yb:YAG crystal assisted with mode selection for the 913 nm Ti:Al_2O_3-pumped microchip laser. **(p. 347)**

11:15am

FD3 • 1 W cw 2.12 μm lamp-pumped room temperature YAG:Yb-Ho laser, A. A. Nikitichev, V. A. Pis'mennyi, *Vavilov State Optical Institute, Russia.* CW 2.12 μm YAG:Yb-Ho lamp pumped room temperature laser with the output power of 1 W is reported for the first time. The processes of energy transfer, creating the operating scheme of the laser, are studied. **(p. 350)**

11:30am
FD4 • Diode-pumped gas-cooled-slab laser performance, C. D. Marshall, L. K. Smith, S. Sutton, M. A. Emanuel, K. I. Schaffers, S. Mills, S. A. Payne, W. F. Krupke, *Lawrence Livermore National Laboratory;* B. H. T. Chai, *CREOL.* The first gas-cooled-slab laser with output powers up to 50 W are discussed. An InGaAs diode array pumped a 2 × 2 × 0.5 cm $Yb:Sr_5(PO_4)_3F$ slab. **(p. 353)**

11:45am
FD5 • Near-diffraction-limited output from a high-power diode-pumped laser via phase correction with aspheric diamond-turned optics, Jeffrey J. Kasinski, Ralph L. Burnham, *Fibertek Inc.* Diode-pumped Nd:YAG (1.06 μm) output of 1.3X-diffraction-limited, 0.76 J, 60 Hz (46 W) is achieved using a diamond-turned-aspheric lens to compensate thermal distortion; frequency doubling produced 30 W, 2.4X-diffraction-limited at 532 nm. **(p. 356)**

12:00m
FD6 • A novel design for high brightness fiber lasers pumped by high power diodes, P. Glas, M. Naumann, I. Reng, A. Schirrmacher, *Max-Born-Institut, Germany;* J. Townsend, *Univ. Southampton, UK.* We report lasing action in a newly developed ring (M-profile) fiber. With 600 mW pump power, and output power of 100 mW is obtained with a slope efficiency of 20%. **(p. 359)**

12:15pm
FD7 • Distributed-feedback ring all-fiber laser, D. Yu. Stepanov, J. Canning, I. M. Bassett, G. J. Cowle, *Univ. Sydney, Australia.* Low-threshold and narrow-linewidth single-frequency operation is achieved in a novel distributed-feedback ring all-fiber laser configuration; 6.5 kHz linewidth is demonstrated. **(p. 362)**

12:30pm–1:30pm
Lunch Break

GOLD ROOM

1:30pm–3:15pm
FE • Short Pulse Lasers II
Richard Wallenstein, *Kaiserslautern University, Germany, Presider*

1:30pm
FE1 • Broadband tuning of a femtosecond neodymium fiber laser, M. H. Ober, M. Hofer, R. Hofer, G. A. Reider, *Technische Univ. Wien, Austria;* G. D. Sucha, M. E. Fermann, D. Harter, *IMRA America Inc.;* C. A. C. Mendonca, T. H. Chiu, *AT&T Bell Laboratories.* Continuous tuning of a mode-locked Nd^{3+} fiber laser over 75 nm is reported. The pulse duration achieved is 300–400 fs over the entire tuning range. **(p. 366)**

1:45pm
FE2 • Femtosecond mode-locked Yb:YAG lasers, C. Hönninger, F. X. Kärtner, G. Zhang, U. Keller, *Swiss Federal Institute of Technology;* A. Giesen, *Univ. Stuttgart, Germany.* We passively mode-locked an Yb:YAG laser using high-finesse and low-finesse antiresonant Fabry–Perot saturable absorbers and achieved pulses as short as 540 fs at either 1.03 μm or 1.05 μm. **(p. 369)**

2:00pm
FE3 • Femtosecond visible Kerr lens mode-locked Pr:YLF laser, J. M. Sutherland, P. M. W. French, J. R. Taylor, *Imperial College, UK;* B. H. T. Chai, *CREOL.* We report femtosecond pulse generation using Kerr lens mode-locking of a new visible transition in a cw-pumped Pr:YLF. Thirteen other new laser lines are observed. **(p. 372)**

2:15pm
FE4 • Diode-pumped passively mode-locked 1.3 μm $Nd:YVO_4$ and Nd:YLF lasers using semiconductor saturable absorbers, R. Fluck, K. J. Weingarten, G. Zhang, U. Keller, *Swiss Federal Institute of Technology;* M. Moser, *Paul Scherrer Institute, Switzerland.* We demonstrate self-starting passively mode-locked diode-pumped 1.3 μm lasers using semiconductor saturable absorbers, achieving pulses as short as 4.6 ps in $Nd:YVO_4$ and 5.7 ps in Nd:YLF. **(p. 375)**

2:30pm
FE5 • Self-mode-locked solid-state intracavity Raman lasers, J. T. Murray, P. T. Guerreiro, L. K. Calmes, R. C. Powell, N. Peyghambarian, *Univ. Arizona;* W. Austin, *Lite Cycles Inc.* Passive mode-locking induced by an intracavity solid-state Raman medium is employed to mode-lock a 3.5 W cw arclamp-pumped 1.338 μm Nd:YAG laser and a 500 mW, 1.556 μm *Q*-switched Raman laser. **(p. 378)**

2:45pm
FE6 • Diode-pumped high-average power femtosecond fiber laser systems, M. E. Fermann, A. Galvanauskas, D. Harter, *IMRA America Inc.;* J. D. Minelly, J. E. Caplen, Z. J. Chen, D. N. Payne, *Univ. Southampton, UK.* The design constraints of fully diode-pumped high average power femtosecond erbium fiber laser systems are described. Average system output powers up to 260 mW are generated and pulse widths shorter than 400 fs are obtained. **(p. 381)**

3:00pm
FE7 • Passively Q-switched 180 ps Nd:LSB microchip laser, B. Braun, F. X. Kärtner, U. Keller, *Swiss Federal Institute of Technology;* J.-P. Meyn, G. Huber, *Univ. Hamburg, Germany.* We demonstrate single-frequency 180 ps passively *Q*-switched pulses from a Nd:LSB microchip laser with an antiresonant Fabry–Perot saturable absorber as a passive *Q*-switcher. **(p. 384)**

TERRACE ROOM

3:15pm–4:15pm
FF • IR Lasers II Poster Session/Refreshment Break and Exhibits

FF1 • Picosecond diode-pumped Cr:LiSAF laser seeded Ti:sapphire laser amplifiers, Franck Falcoz, Patrick Georges, Alain Brun, *Univ. Paris–Sud, France;* Frederic Estable, Luc Vigroux, *B. M. Industries, France.* We have developed a high-energy picosecond laser based on a diode-pumped Cr:LiSAF laser that is amplified in Ti:sapphire amplifiers. This system produces narrow-band 100 ps pulses at 846 nm with an energy of 100 mJ. **(p. 388)**

FF2 • High-repetition-rate mode-locked Ti:sapphire laser using a saturable Bragg reflector, Taro Itatani, Takeyoshi Sugaya, Tadashi Nakagawa, Yoshinobu Sugiyama, *Electrotechnical Laboratory, Japan;* Zhenlin Liu, Chengyou Liu, Shinji Izumida, Nobuhiko Sarukura, Tomoyuki Hikita, Yusaburo Segawa, *The Institute of Physical and Chemical Research, Japan.* We construct a high-repetition-rate (540 MHz) mode-locked Ti:sapphire laser with self-starting capability by use of a saturable Bragg reflector. **(p. 391)**

FF3 • Measurements of operation parameters and nonlinearity of a Nd^{3+}-doped fiber laser by relaxation oscillations, R. Böhm, V. M. Baev, P. E. Toschek, *Univ. Hamburg, Germany.* The efficiency of frequency doubling, cavity losses, and lifetimes of laser levels are measured in a Nd^{3+}-doped fiber laser by monitoring relaxation oscillations and using a novel four-level model. **(p. 394)**

FF4 • Tuning and stability properties of single-frequency diode-pumped coupled cavity Nd:YVO_4 laser, Peter Lichtenberg Hansen, Christian Pedersen, Torben Skettrup, Preben Buchhave, *Technical Univ. Denmark.* Frequency tuning and stability of a single-frequency coupled cavity Nd:YVO_4 laser have been investigated. Temperature tuning of 60 GHz has been measured for $\Delta T \approx 30°C$. **(p. 397)**

FF5 • Investigation of frequency stability and design criterion of ring lasers, Christian Pedersen, Peter Lichtenberg Hansen, Preben Buchhave, Torben Skettrup, *Technical Univ. Denmark.* A theoretical analysis and design criteria of ring lasers are presented. The frequency stability of two single-frequency diode-pumped solid-state ring lasers are measured. **(p. 400)**

FF6 • Single-frequency, coupled-cavity, gain-switched chromium forsterite laser, Iain T. McKinnie, Andrew Tiffany, Donald M. Warrington, *Univ. Otago, New Zealand.* Narrow bandwidth operation of a chromium (IV) laser is reported for the first time. Near-transform-limited pulses are obtained from a novel coupled-cavity laser. **(p. 403)**

FF7 • High-brightness cw-500-W Nd:YAG rod laser, Koji Yasui, *Mitsubishi Electric Corp., Japan.* Enhanced performance of a high-brightness, cw-pumped rod-geometry 500-W Nd:YAG laser is proved by the compensation of the thermally induced bifocusing lens. **(p. 406)**

FF8 • Q-switch and excited state absorption experiments with Cr^{4+}:LuAG single crystals, R. Moncorgé, H. Manaa, F. Deghoul, Y. Guyot, *Univ. Lyon I, France;* Y. Kalisky, *Nuclear Research Centre–Negev, Israel;* S. A. Pollack, *Optitron Inc.;* E. V. Zharikov, *General Physics Institute, Moscow;* M. Kokta, *Union Carbide Corp.* Nd:YAG laser *Q*-switching with 35% conversion efficiency using Cr^{4+}:$Lu_3Al_5O_{12}$(LuAG) as passive shutter is demonstrated. Transmission saturation curves and ESA spectra are recorded and analyzed. **(p. 409)**

FF9 • High average power diode-array-pumped frequency-doubled YAG laser, B. J. Le Garrec, G. J. Razé, *Centre d'études de Saclay, France.* We report the demonstration of a transversally diode array pumped Nd:YAG laser using 30 20-W cw linear diode arrays. At a 9 kHz repetition rate the laser produces 46 W average power at 532 nm when intracavity doubled with a KTP crystal, leading to a 2.3% optical/electrical efficiency. **(p. 412)**

FF10 • Precision distance measurements using frequency-stabilized Nd:YAG lasers, V. Mahal, E. Inbar, A. Arie, *Tel Aviv Univ., Israel.* Accurate distance measurements with large non-ambiguity range are achieved by two-wavelength interferometry using Nd:YAG lasers locked to sub-Doppler molecular transitions of iodine and cesium. **(p. 415)**

FF11 • Laser beam propagation in a thermally loaded absorber, Alphan Sennaroglu, Attila Askar, Fatihcan M. Atay, *Koç Univ., Turkey.* Beam propagation in a thermally loaded absorber is analyzed by a novel method. The formulation identifies dimensionless coefficients controlling thermally induced lensing and power-dependent transmission. **(p. 418)**

FF12 • Analysis of thermal effects in crystalline media using a dual-interferometer, J. M. Laurenzano, J. O. Grannis, *USAF Phillips Laboratory;* B. W. Liby, *Manhattan College.* Transient effects as a result of thermal loading in diode-pumped solid-state laser media using a novel dual-interferometer configuration are discussed. **(p. 421)**

FF13 • Compensation of polarization distortion of a laser beam in a four-pass Nd:glass amplifier by using a Faraday rotator, H. J. Kong, J. Y. Lee, H. S. Kim, K. Y. Um, J. R. Park, *Korea Advanced Institute of Science and Technology.* We present an experimental and numerical investigation of a four-pass Nd:glass laser amplifier, compensating the polarization distortion induced by thermal birefringence with use of a Faraday rotator. **(p. 424)**

GOLD ROOM

4:15pm–6:00pm

FG • Visible/Ultraviolet Lasers

Martin Fejer, *Stanford University, Presider*

4:15pm

FG1 • Highly efficient second harmonic generation of green light from picosecond pulses in bulk quasi-phase-matched lithium niobate, V. Pruneri, S. D. Butterworth, P. G. Kazansky, W. A. Clarkson, N. Moore, D. C. Hanna, *Univ. Southampton, UK.* 1.3 W average power of green light is generated by quasi-phase-matched frequency doubling of a quasi-cw mode-locked Nd:YLF laser with 60% average conversion efficiency. **(p. 428)**

4:30pm

FG2 • Ultraviolet application of $Li_2B_4O_7$ crystals: Generation of the fifth and fourth harmonic of Nd:YAG lasers, Ryuichi Komatsu, Tamotsu Sugawara, Koichi Sassa, *Mitsubishi Materials Corp., Japan;* Nobuhiko Sarukura, Zhenlin Liu, Shinji Izumida, Yusaburo Segawa, *The Institute of Physical and Chemical Research, Japan;* Satoshi Uda, Tsuguo Fukuda, Kazuhiko Yamanouchi, *Tohoku Univ., Japan.* We investigate nonlinear properties of $Li_2B_4O_7$ in the ultraviolet region and demonstrate the fifth and fourth harmonic generation of a *Q*-sw Nd:YAG laser. **(p. 431)**

4:45pm

FG3 • 560 mW, fifth harmonic (213 nm), flashlamp-pumped Nd:YAG laser system, Ruikun Wu, Michael J. Myers, John D. Myers, Scott J. Hamlin, *Kigre Inc.* A flashlamp-pumped, 200 Hz, *Q*-switched, TEM_{00}, Nd:YAG laser system with 10 W of fundamental average power is developed. By use of a nonlinear crystal frequency conversion system, 560 mW of fifth harmonic (213 nm) output is obtained. **(p. 434)**

5:00pm
FG4 • Efficient intracavity frequency doubling of a room temperature cw 930 nm Nd:$YAlO_3$ laser, T. Kellner, F. Heine, B. Struve, V. Ostroumov, K. Petermann, G. Huber, *Univ. Hamburg, Germany.* Efficient intracavity frequency doubling of a Ti:sapphire-pumped 930 nm Nd:$YAlO_3$ laser by use of nonlinear crystals LBO, BBO, and $LiJO_3$ is reported. Total blue cw output power of up to 150 mW using 2 W of incident pump power is achieved. **(p. 437)**

5:15pm
FG5 • A quadrupled Nd:FAP laser at 1.126 μm for a Hg^+ optical frequency standard, F. C. Cruz, J. C. Bergquist, *NIST, Boulder.* A single-frequency, narrowband quadrupled Nd:FAP laser at 1.126 μm is developed as the local oscillator for an optical frequency standard based on the $^{199}Hg^+$ S-D quadrupole transition at 281.5 nm. **(p. 440)**

5:30pm
FG6 • Ultraviolet picosecond pulses from an all-solid-state Ce:LiSAF master oscillator and Ce:LiCAF power amplifier system, Nobuhiko Sarukura, Zhenlin Liu, Shinji Izumida, Yusaburo Segawa, *The Institute of Physical and Chemical Research, Japan;* Mark A. Dubinskii, *Howard Univ.;* Vadim V. Semashko, Alexander K. Naumov, Stella L. Korableva, Ravil Yu. Abdulsabirov, *Kazan State Univ., Russia.* 290-nm, 590-psec, and 300-μJ pulses are obtained from a Ce:LiSAF/Ce:LiCAF MOPA system pumped by the fourth harmonic of an Nd:YAG laser. **(p. 443)**

5:45pm
FG7 • Ultrabroadband continuum generation by a self-trapped ultrashort Ti:Al_2O_3 laser pulse, Hajime Nishioka, Wataru Odajima, Yoshimasa Sasaki, Ken-ichi Ueda, *Univ. Electro-communications, Japan.* White-light ranging from IR to 150 nm was generated by a self-trapped femtosecond Ti:Al_2O_3 laser pulse in atmospheric pressure rare gases. Spectral intensity of 100 MW/nm is observed in the UV region. **(p. 446)**

6:00pm–6:15pm
Closing Remarks
Clifford Pollock, *Cornell University, Program Chair*

Wednesday, January 31, 1996

Plenary I

WA 8:15 am-8:45 am
Gold Room

Stephen Payne, *Presider*
Lawrence Livermore National Laboratory

Novel Uses of Lasers in Medicine

Kenton Gregory
Oregon Medical Laser Center
9205 Southwest Barnes Road
Portland, OR 97225-6622

Summary not available.

Wednesday, January 31, 1996

Ultraviolet/Blue Lasers

WB 8:45 am-9:45 am
Gold Room

Michio Oka, *Presider*
Sony Corporation, Japan

Highly-efficient first-order quasi-phase-matched frequency doubling to blue of a cw diode-pumped 946 nm Nd:YAG laser

V.Pruneri, R.Koch, P.G.Kazansky, W.A.Clarkson, P.St.J.Russell and D.C.Hanna
Optoelectronics Research Centre, University of Southampton
Southampton SO17 1BJ, U.K.
fax. + +44/1703/593142, tel. + +44/1703/593136, email. vp3@orc.soton.ac.uk

The generation of blue-light via frequency doubling has attracted growing interest over recent years, owing to its potential use in high density optical storage and in medicine. Traditionally, frequency doubling of infra-red lasers has been accomplished with nonlinear crystals which rely on birefringent phase-matching. This dependence on birefringent phase-matching has greatly restricted the range of suitable nonlinear materials as well as the range of wavelengths that can be efficiently doubled. The net result has been that cw frequency doubling efficiencies in single-pass configurations have tended to be rather low.

More recently, there has been increasing interest in the use of quasi-phase-matched nonlinear crystals. Quasi-phase-matching (QPM) has several advantages over birefringent phase-matching, including access to higher nonlinear coefficients and non-critical interaction geometries for any wavelength in the transparency range of the crystal. QPM can be achieved by an appropriate periodic modulation of the nonlinear coefficient [1]. Nonlinear gratings fabricated in crystals such as $KTiOPO_4$ (KTP) [2], $LiTaO_3$ [3] and $LiNbO_3$ [4,5] have been used for blue light generation via frequency doubling both in bulk and waveguide geometries. So far, however, cw blue power from QPM materials has been limited to only few mW in bulk [3] and ~20 mW [4] in waveguide geometries.

In this paper we report single-pass highly efficient cw blue light generation by first-order QPM-SHG in lithium niobate of a high power diode-pumped Nd:YAG laser which oscillates at 946 nm. The results indicate a d_{eff} of ~19 pm/V.

The lithium niobate sample, used in our experiment, had a thickness of 200 μm and a length of 6 mm, and was periodically poled by applying a high voltage pulse, of ~4.5 kV and ~300 ms duration, via liquid electrodes as described in refs. [5]-[8]. The period of domain reversal required was rather short (4.6 μm), so careful attention was paid to the significant spreading of the inverted domains during the poling process in order to obtain a domain reversal period with mark-to-space ratio close to the optimum at 50:50.

The fundamental source used in our frequency doubling experiment was a diode-pumped Nd:YAG laser oscillating on the quasi-three-level transition $^4F_{3/2}$ - $^4I_{9/2}$ at 946 nm. This laser was end-pumped by a beam-shaped 20 W cw diode bar [9] and produced a polarised output of 1.5 W at 946 nm with beam quality factor $M^2 \leq 1.5$. The output from this laser was collimated and then focused into the uncoated PPLN sample with a $1/e^2$ waist spot diameter of 58 μm.

Fig.1 shows the SH power as a function of crystal temperature. The curve follows the expected $sinc^2$

shape and the bandwidth FWHM of ~3 °C is seen to be in good agreement with the theoretical prediction shown in fig.1.

Fig.2 shows that the dependence of the generated blue power on the fundamental power is close to the expected quadratic behaviour and shows no sign of roll-off at higher power.

Following the Boyd and Kleinmann treatment [10] we have estimated that the nonlinear coefficient d_{eff} is ~19 pm/V and thus is close to the theoretical limit of 21 pm/V expected for an ideal first order QPM grating in PPLN. In arriving at this estimate we have taken account of the multimode nature of the fundamental source (i.e. several longitudinal modes were oscillating and the beam was not perfectly diffraction-limited).

The highest conversion efficiency we have achieved was for a fundamental beam with a slightly smaller spot size in the PPLN sample, of $1/e^2$ diameter 38 μm. In this case an internal SH power of 49 mW was generated for an internal fundamental power of 1.07 W, corresponding to a fundamental intensity at beam centre of ~190 kW/cm^2. This result corresponds to a conversion efficiency of ~4.6% and a corresponding normalised conversion efficiency of ~7.1 %/(W*cm). To the best of our knowledge this is the highest value reported for blue light generation in bulk periodically poled materials.

At the maximum conversion efficiency we measured the M^2 beam quality factor of the SH beam to be ~3. The origin of this degradation in beam quality relative to the fundamental has not yet been conclusively identified. Some contributions may be due to imperfect polishing of the end faces of the sample, as well as the onset of photorefractive damage. This is the subject of continuing further investigation.

We believe that there are good prospects for further increasing the cw blue output power by fabricating longer gratings and by scaling the power of the 946 nm Nd:YAG laser.

References

1. M.M.Fejer, G.A.Magel, D.H.Jundt and R.L.Byer, IEEE J.Quantum Electron. **QE-28**, 2631 (1992).
2. Q.Chen and W.P.Risk, Electron. Lett. **30**, 1516 (1994).
3. K.Mizuuchi and K.Yamamoto, Appl. Phys. Lett. **66**, 2943 (1995).
4. M.Yamada, N.Nada, M.Saitoh and K.Watanabe, Appl. Phys. Lett. **62**, 435 (1993).
5. J.Webjörn, V.Pruneri, J.R.M.Barr, P.St.J.Russell and D.C.Hanna, Electron. Lett. **30**, 894 (1994).
6. J.Webjörn, V.Pruneri, P.St.J.Russell and D.C.Hanna, Electron. Lett. **31**, 669 (1995).
7. V.Pruneri, J.Webjörn, P.St.J.Russell and D.C.Hanna, to be published in Appl. Phys. Lett.
8. V.Pruneri, J.Webjörn, J.R.M.Barr, P.St.J.Russell and D.C.Hanna, Optics Comm. **116**, 159 (1995).
9. W.A.Clarkson, R.Koch, K.I.Martin and D.C.Hanna, paper CMD4, Conference on Lasers and Electro-Optics 95, Baltimore, Maryland (USA).
10. G.D.Boyd and D.A.Kleinmann, J. Appl. Phys., **39**, 3597 (1968).

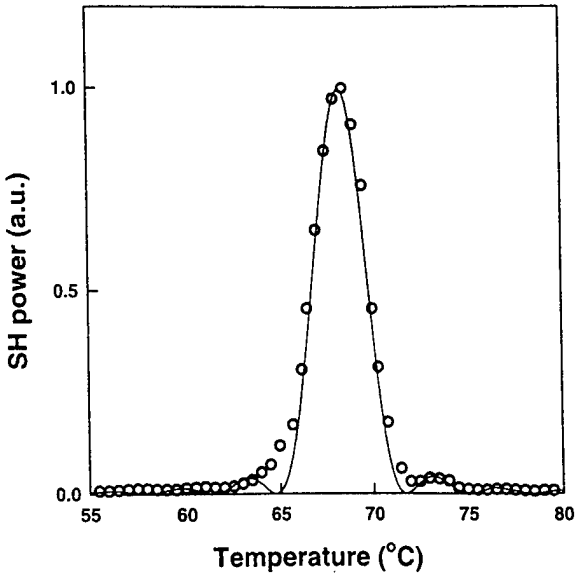

Figure 1 Temperature dependence of generated second harmonic power on the temperature of the crystal. The continuous line is the result of a computation for a perfect grating of the same length.

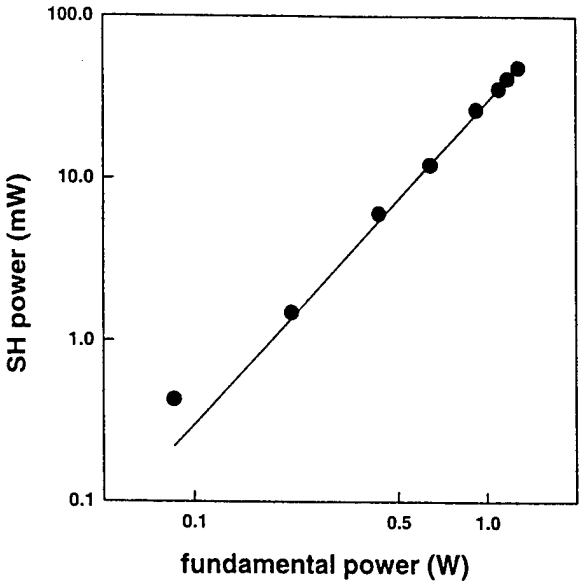

Figure 2 SH power as a function of the fundamental power. The powers relate to internal values for the uncoated sample. The continuous line is the best quadratic fit.

Efficient Ultraviolet Ce:LiSAF Laser Using Anti-Solarant Pump Beam

A. J. Bayramian, C. D. Marshall, and S. A. Payne
Lawrence Livermore National Laboratory
University of California
Livermore, California 94550
(510) 423-0570 FAX (510) 422-1930

G. J. Quarles and V. Castillo
Lightning Optical Corporation
Tarpon Springs, Florida 34689

Since the discovery that cerium-doped colquiriite ($LiCaAlF_6$ or LiCAF) offers a robust means of generating tunable ultraviolet radiation, interest in direct solid state laser sources for this purpose has been re-kindled.[1] Several research groups have been examining the potential performance available from Ce-doped $LiSrAlF_6$ (Ce:LiSAF), which can be pumped at 266nm and offers gain in the range of 280-320nm.[2,3] Since the LiSAF crystal is already commercially available with chromium dopants (i.e. Cr:LiSAF), the development of Ce:LiSAF may be expected to be somewhat more straightforward. In our previous report on this topic we characterized the ground and excited state cross sections, storage time of the upper laser level, and other relevant laser parameters.[3] We also noted that some level of UV-induced solarization is present in Ce:LiSAF, although the level of coloring is moderate and can recover after a short time.

In the present paper we have explored the solarization of Ce:LiSAF in considerable detail, and have found an interesting new effect. In particular, we observed that the color centers created by the 266nm fourth harmonic pump beam from the Nd:YAG laser can be bleached (destroyed) with the addition of the 532nm second harmonic from the laser. This effect permits the laser efficiency of the crystal to be significantly increased. On the basis of this promising result, it becomes feasible to imagine laser systems that allow for the introduction of both the normal 266nm pump beam as well as this anti-solarant 532nm pump beam.

Further exploration of the solarization and bleaching phenomena reveal that it is sensitive to the material preparation and the possible presence of co-dopants. For example, Fig. 1 below depicts the ultraviolet-induced spectra of two Ce:LiSAF samples containing 2% cerium in the melt, but with additional Na^+ or Mg^{2+} ions included in the starting materials. As can be readily seen, the magnesium codopants give rise to a far greater level of solarization, and also to a different shape for the spectrum itself. If we now measure the slope efficiency of a variety of crystals, and then plot this quantity against the actual loss at the 290nm operating wavelength of the laser, a clear correlation can be inferred

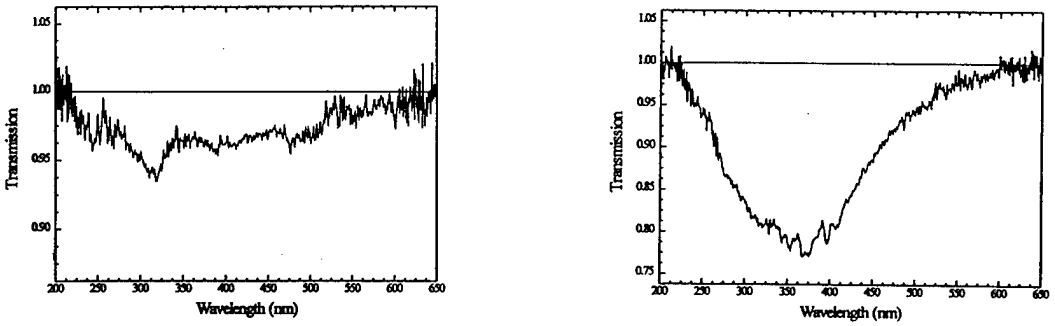

Fig.1:UV-induced solarization spectra in Ce:LiSAF crystals codoped with Na^{+} and Mg^{2+} ions (left- and right-hand sides, respectively).

from the data, (see Fig.2 below). On the basis of this analysis we can conclude that higher efficiencies would be possible from laser materials that are characterized by lower levels of UV-induced solarization loss. This objective can be approached from two directions: by including the preferred codopants, and by introducing the additional anti-solarant pump beam.

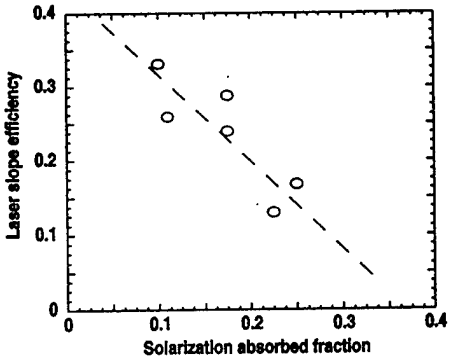

Fig.2: Plot revealing the correlation between the UV-induced solarization loss and the measured slope efficiency of the particular laser crystal.

The favorable influence of introducing the 532nm beam is evidenced from the data in Fig.3, where the rising fluence of the 532nm pump is found to increase the 290nm output of the laser from about 0.17mJ to 0.24mJ. Use of a simple model to fit the data in the figure suggests that the losses can be separated into bleachable and non-bleachable components, amounting to 19% and 27% (round-trip) in this case, respectively. The shape of the data in the plot suggests that the efficiency benefit from the 532nm beam saturates at about $10J/cm^2$. Using this technique, the two samples yielding the solarization spectra shown in Fig.1 experience slope efficiency enhancements of 33 to 47%, and from 1 to 8%. Finally, we mention that the non-bleachable portion of the loss may arise from a single-shot effect, whereas the anti-solarant co-pump pulse can only be expected to destroy the defects producing losses for the next laser shot.

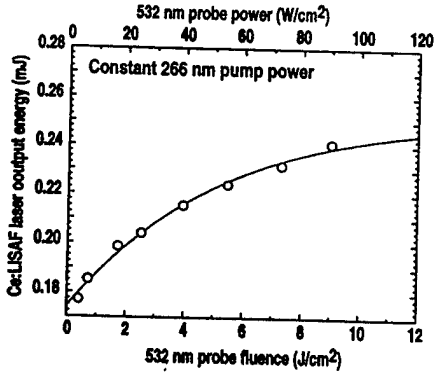

Fig.3: Output energy of Ce:LiSAF laser as a function of 532nm fluence, for a fixed energy input at 266nm.

A last piece of corroborating evidence advancing the concept of the anti-solarant effect is depicted in Fig. 4, where a 266nm beam is used to create the defects while a continuous-wave 457nm beam is used to monitor their decay. This experiment reveals that the decay time is strongly dependent on the intensity of the probe beam, varying from 0.4sec to less than 0.01sec in this experiment. An analysis shows that the findings of Figs. 3 and 4 are roughly consistent with one another.

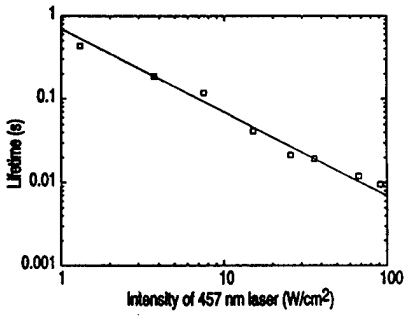

Fig.4: Plot of the defect decay time as a function of the intensity of the probe beam.

In summary, we are able to conclude that the performance of the Ce:LiSAF laser can be substantially improved by introducing the additional 532nm anti-solarant pump beam at a fluence of about 10J/cm^2. The spectrum characterizing the solarization effect extends from 220-600nm, thereby impacting the pump and gain regions. Separate experiments corroborate the observation that visible light is able to accelerate the decay of the defects.

References

1. M. A. Dubinskii, V. V. Semashko, A. K. Naumov, R. Y. Abdulsabirov, and S. L. Korableva, J. Mod. Opt 40, 1 (1993).

2. J. F. Pinto, et al., Electron. Lett. 30, 240 (1994).

3. C. D. Marshall, J. A. Speth, S. A. Payne, W. F. Krupke, G. J. Quarles, V. Castillo, and B. H. T. Chai, J. Opt. Soc. Am. B11,2054 (1994).

High efficiency UV light generation by CLBO

Y. Mori, M. Inagaki, S. Nakajima, A. Taguchi, A. Miyamoto,
W. L. Zhou and T. Sasaki
Department of Electrical Engineering, Osaka University
2-1 Yamadaoka, Suita, Osaka 565, Japan
TEL +81-6-879-7707
FAX +81-6-879-7708
Email: mori@pwr.eng.osaka-u.ac.jp

S. Nakai
Institute of Laser Engineering, Osaka University
2-6 Yamadaoka, Suita, Osaka 565, Japan

Borate crystals are of the great interest for nonlinear optics (NLO) to realize an all solid-state ultraviolet (UV) laser. Recently new borate crystal, $CsLiB_6O_{10}$ (CLBO) has been developed by the present authors [1-6], which exhibits excellent UV NLO properties and can be grown easily. CLBO possesses smaller walk-off angle, higher laser damage threshold, lager angular, spectral and temperature bandwidths compared to β-BaB_2O_4 (BBO) as shown in Table 1. For these reason it is considered to be the most suitable material for fourth (FOHG) and fifth harmonic generations (FIHG) of Nd:YAG laser. In this paper, we report on the high efficiency FOHG and FIHG of the 1.064 μm Nd:YAG laser radiation with type-I phase matching (PM) realized in CLBO crystal.

One unfavorable nature of CLBO is that it tends to be cracked during cutting and polishing of the crystal due to its relatively high fragility. The improvement of processing of CLBO made it possible to prepare a few cm^3 CLBO samples with surface roughness of 2~3 nm rms obtained by conventional optical polishing. More recently we developed a new subsequent dry etching process which can reduce the surface roughness of CLBO to less than 0.6 nm rms.

The Quanta-Ray GCR-190 Nd:YAG laser which can operate 10 Hz with pulse width of ~7ns was used to obtain FOHG and FIHG of Nd:YAG laser radiation in CLBO. The beam diameter was ~8 mm. The transverse dimensions of CLBO crystal used were 10 x10 mm^2 for FOHG and 11 x 11 mm^2 for FIHG. The fundamental was doubled in a KD_2PO_4 (KD*P) crystal with type-II PM to obtain 532 nm radiation. The 532 nm radiation was physically separated from the fundamental by using a mirror and then doubled in an uncoated 10 mm long CLBO crystal with type-I PM for FOHG. Fourth harmonic performance as a function of 532 nm input energy is shown in Figure 1. The 266 nm output energy was proportional to the square of the second harmonic energy. We obtained output energy of 204 mJ at 266 nm with 49% FOHG efficiency from the second harmonic of 420 mJ.

FIHG was obtained in an uncoated 5 mm long CLBO crystal by type-I sum frequency generation (SFG) of the fourth harmonic and the fundamental. The fundamental and all harmonics beams propagated co-axially and they were physically separated from each other by a fused silica prism. Figure 2 shows various harmonic energies as a function of fundamental energy. The output pulse energies of 80 mJ at 213 nm was obtained from fundamental energy of 790 mJ. The 213 nm output energy showed high stability for time interval as long as 5 hours. This 213 nm output energy is almost double than that obtained for BBO at the same fundamental input energy [7]. We could obtain a conversion efficiency of more than 10% from fundamental. However we must consider a loss of fundamental input energy for type-I SFG, because the mixing waves do not have the same polarization (fundamental wave is randomly elliptical polarized) in this experiment. Therefore, the use of the same polarization waves can lead to a higher FIHG efficiency.

In conclusion, we have studied FOHG and FIHG of Nd:YAG laser radiation at λ=266 nm and at λ=213 nm realized in CLBO crystals. More than 10% FIHG efficiency for 790 mJ of fundamental and 49% FOHG efficiency for 420mJ 532 nm radiation were demonstrated.

References

[1] T.Sasaki, I.Kuroda, S.Nakajima, K.Yamaguchi, S.Watanabe, Y.Mori and S.Nakai: Proc. of Advanced Solid-State Lasers Conference, Memphis, Tennessee, Jan. 30 - Feb. 2, 1995 (Paper WD3).

[2] Y.Mori, I.Kuroda, S.Nakajima, T.Sasaki and S.Nakai, Jpn. J. Appl. Phys. 34, L296 (1995).

[3] Y.Mori, I.Kuroda, S.Nakajima, T.Sasaki and S.Nakai, Appl. Phys. Lett. 67, 25 September (1995).

[4] Y.Mori, I.Kuroda, S.Nakajima, T.Sasaki and S.Nakai, CLEO'95 Technical Digest, paper CFC3.

[5] T.Sasaki, Y.Mori, I.Kuroda, S.Nakajima, K.Yamaguchi and S.Nakai, Acta Crystallographica C. in press.

[6] Laser Focus World, May 1995, p.46.

[7] W.Wiechmann, L.Y.Liu, M.Oka, Y.Taguchi, H.Wada, Y.Minoya, T.Okamoto and S.Kubota, CLEO'95 Post deadline papers, paper CPD19.

Table 1. Nonlinear optical properties of CLBO and BBO

Fundamental wavelength (nm)	Crystal	PM angle (deg.)	deff (pm/V)	Angular bandwidth (mrad•cm)	Spectral bandwidth (nm•cm)	Temperature bandwidth (°C•cm)	Walk-off angle (deg)
532+532 =266	CLBO	62	0.85	0.49	0.13	9.4	1.83
	BBO	48	1.32	0.17	0.07	4.5	4.80
1064+266 =213	CLBO	67	0.88	0.42	0.16	-	1.69
	BBO	51	1.26	0.11	0.08	3.1	5.34

Laser damage threshold at 1064 μm with 1.1 ns: CLBO 26 GW/cm^2, BBO 13.5 GW/cm^2

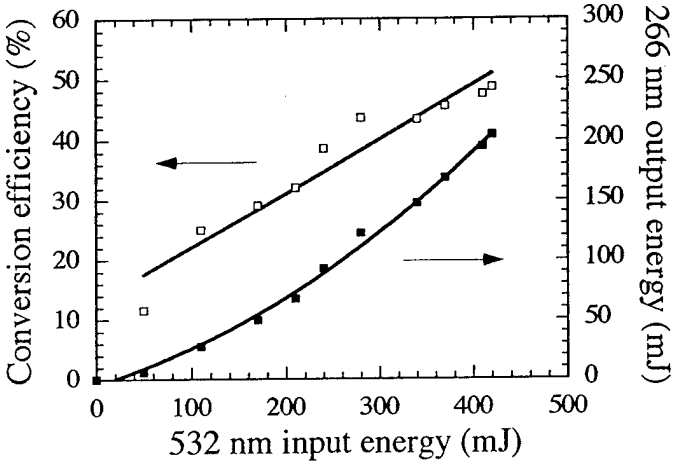

Figure 1. Fourth harmonic energy and conversion efficiency as a function of 532 nm input energy.

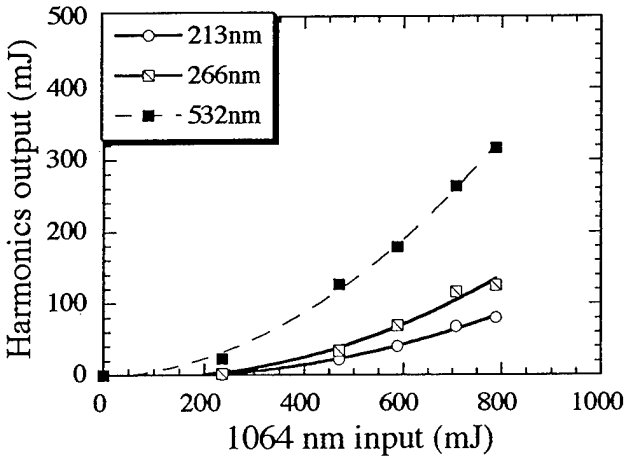

Figure 2. Harmonics output energies as a function of 1064 nm input energy.

CW 355 nm Generation by Doubly-Resonant Sum-Frequency Mixing in an External Resonator

Yushi Kaneda and Shigeo Kubota

Sony Research Center, Kubota Opto-Electronics Laboratory

6-7-35 Kitashinagawa, Shinagawa-ku, Tokyo 141, JAPAN

phone +81-3-5448-5621

fax +81-3-5448-5634

internet: kaneda@devo.crl.sony.co.jp

Continuous wave ultraviolet solid state lasers can be used in applications such as optical disk mastering systems, or as the replacement of UV argon lasers. We report generation of continuous wave 355 nm ultraviolet light, which corresponds to the third harmonic wavelength of 1064 nm Nd lasers.

Since the normalized nonlinear conversion efficiency is typically on the order of 10^{-5} W^{-1} to 10^{-3} W^{-1}, the enhancement of the input is necessary for a good conversion efficiency in the cw mode. In the sum-frequency mixing, two inputs at different wavelengths need to be enhanced as opposed to the SHG case, where only one wavelength needs to be enhanced. In order to simultaneously enhance both inputs, we utilize two independent single-frequency lasers as well as two independent servo loops. The first servo loop locks the mixing cavity to the first laser, while the second loop locks the frequency of the second laser to the external cavity. Double-resonance is achieved when both of the servo loops are closed. Enhanced fields are built up in the cavity at both input wavelengths under the double-resonance, hence increasing the nonlinear conversion efficiency.

Schematic of the experimental setup is shown in Figure 1. To generate the 355 nm output, 532 nm laser output and 1064 nm output are to be mixed. A diode-pumped intracavity doubled Nd:YVO_4 532 nm green laser is used as the first laser, and a commercial diode pumped Nd:YAG 1064 nm laser is used as the second laser. The mixing resonator is a bow-tie cavity consisting of 3 dual-high-reflection (dual-HR) mirrors and a dual-input coupler. The dual-HR mirrors are highly reflective at both 532 nm and 1064 nm, while the reflectivity of the dual input coupler is approximately 99 % at 532 nm and 99.3 % at 1064 nm. The dual input coupler and one of the dual HR mirrors are flat, while two of the dual-HR mirrors are ROC = 50 mm concave mirrors and have

high transmission at 355 nm. One of the resonator mirrors is mounted on a VCM,[1] providing cavity length control. The eigenmode of the resonator has two waists, one of which is between the two curved mirrors and tightly focused. The waist radii at the tighter waist are 22 μm at 532 nm and 31 μm at 1064 nm.

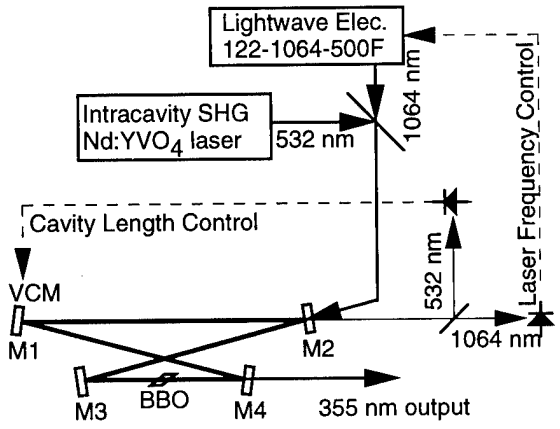

Figure 1: Schematic of the experimental setup. M1, 3, 4: dual HR mirrors, M2: dual input coupler.

A BBO crystal that is fabricated as shown in Figure 2 is placed at the tight-waist of the cavity. The angle of incidence is 59°, which is the center of two Brewster angles at 532 nm and 1064 nm, which are 58.85° and 59.15°, respectively. Incidence at an angle of 59° yields less than 0.1 % reflectivity for p-polarization, maintaining low loss of the cavity at both wavelengths, and 22 % reflectivity for s-polarization in which 355 nm is generated. Both green and infrared inputs are phase modulated, and then combined with the same focusing parameter using a dichroic mirror before incident on the mixing resonator.

The single-frequency 532 nm output is obtained by a laser head similar to what has been reported.[2] The laser head is pumped with a 4 W single-emitter laser diode (SDL-2382-P1), producing more than 500 mW of stable single frequency output at 532 nm.

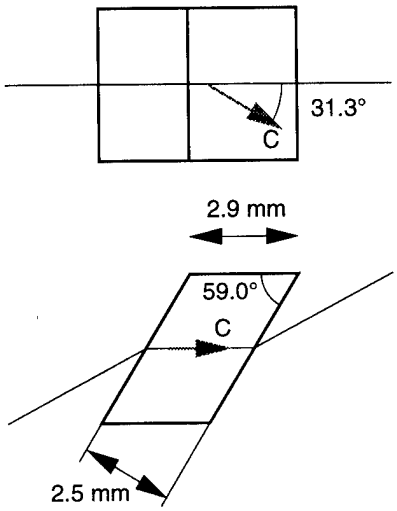

Figure 2: Schematic of BBO crystal configuration. The angle of incidence is ~59°, within 0.2° from the Brewster angle at both wavelengths.

The NPRO (Lightwave Electronics, Model 122-1064-500F) is employed as the laser source at 1064 nm. The NPRO operates in a single-longitudinal mode and has fast frequency tuning capability. The unit that is used in this experiment has an output power of approximately 560 mW. The frequency tuning coefficient of this unit is 4.3 MHz/V at low frequencies, giving 170 MHz tuning range when ±20 V is applied to the fast frequency tuning port.

The resonator frequency is adjusted by the VCM, using FM-sideband technique.[3] Since the green laser is free running and does not have the frequency tuning capability, the cavity has to be locked to the green laser frequency. With the mixing cavity locked to the green light, the 1064 nm laser is locked to the mixing cavity by controlling the oscillation frequency, providing the double resonance.

The incident powers onto the mixing resonator are 480 mW at 532 nm and 520 mW at 1064 nm. When both inputs are at the resonance, reflection from the input coupler reduces to 139 mW at 532 nm and 105 mW at 1064 nm, giving 71 % and 80 % of coupling efficiencies. These coupling efficiencies indicate good mode and impedance matching.

With both of the 532 nm and 1064 nm resonantly enhanced, 220 mW of 355 nm output is obtained outside the cavity. This output corresponds to the generation of more than 280 mW, taking the 22% reflectivity of the Brewster-face for s-polarization of the BBO crystal into account. The conversion efficiency from the total input power that is incident on resonator to the detected 355 nm power is 22 %. The internal conversion efficiency, which is defined as the efficiency from the total coupled power to the generated 355 nm power, is 37 %.

In conclusion, we have obtained 220 mW of 355 nm output by doubly-resonant sum-frequency mixing (DRSFM) between a frequency doubled Nd:YVO_4 green laser and a Nd:YAG laser.

References :

[1] M. Oka, N. Eguchi, L. Y. Liu, W. Wiechmann and S. Kubota, in *Conference on Lasers and Electro-Optics*, Vol. 8 of OSA Technical Digest Series (Optical Society of America, Washington D.C., 1994), paper CThM1.

[2] W. Wiechmann, L. Y. Liu and S. Kubota, in *Digest of Conference on Advanced Solid-State Lasers* (Optical Society of America, Washington D.C., 1995), paper WD4.

[3] R. W. P. Drever, J. L. Hall, F. V. Kowalski, J. Hough, G. M. Ford, A. J. Munley and H. Ward, Appl. Phys. B **31**, 97 (1983).

Wednesday, January 31, 1996

IR Lasers I
Poster Session

WC 9:45 am-10:45 am
Terrace Room

Miniature Nd:YAG Ring Lasers with High Single-Frequency Output Power at 946nm

I. Freitag, R. Henking, F. von Alvensleben, and A. Tünnermann
Laser Zentrum Hannover e.V., Hollerithallee 8, D-30419 Hannover, Germany
Tel.: (49)511 2788110, Fax: (49)511 2788100

Efficient sources of stable coherent radiation in the visible and UV spectral region are required for many scientific and commercial applications. Blue light sources in particular would be useful tools in fundamental quantum optics and communication technology. Hence, there has been considerable interest in the past few years in the development of direct blue lasers, for example II-VI semiconductor compounds such as ZnSe and ZnS, respectively. However, these lasers are in a very early stage of development and not suited for practical applications so far. Frequency conversion of solid-state lasers operating in the near infrared spectral region is a commonly applied technique for the realization of visible light sources. Efficient green light sources were realized by frequency conversion of Nd:YAG lasers operating at a wavelength of 1064nm with a conversion efficiency as high as 82% [1].

Applying Nd:YAG as active medium, the generation of coherent blue light is possible by second harmonic generation of the 946nm transition [2]. However, continuous-wave operation of the $^4F_{3/2}$-$^4I_{9/2}$ quasi-three-level transition in Nd:YAG is difficult to achieve because of the high ground state reabsorption [3, 4]. Furthermore, the 946nm transition has to compete with the much stronger $^4F_{3/2}$-$^4I_{11/2}$ transition at 1064nm which requires sophisticated optical coatings. The losses due to reabsorption are directly correlated with the lower laser level population. Hence, cooling of the active medium reduces the reabsorption losses. At room temperature the losses of the 946 nm laser radiation are still in the range of 7-8%·cm^{-1} and require optimization of the active medium length. In end-pumped configurations, short crystals show insufficient pump power absorption, whereas long crystals show high reabsorption losses. For excitation with diode arrays, the optimum length is in the range of a few mm. A maximum single-frequency output power of 250mW cw has been reported using a 3mm long Nd:YAG crystal in a linear twisted-mode cavity [2]. But, the efficiency at the low gain transition is sensitive to cavity losses and hence, the output power is decreased by the additional intracavity components. Therefore, it is desirable to use the non-planar ring laser concept to enforce single-frequency operation with high stability [5]. However, the conventional monolithic ring laser design is not practical for the quasi-three-level transition at 946nm because of the required small cavity dimensions.

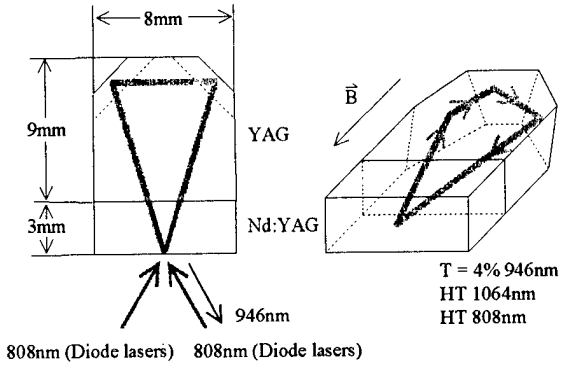

Fig. 1: Quasi-monolithic Nd:YAG ring laser

This contribution reports on the first 946nm operation of a diode-pumped Nd:YAG non-planar ring oscillator using a quasi-monolithic cavity (see Figure 1). The design of the laser with dimensions of 3·8·12mm^3 is identical to the previously reported monolithic ring lasers optimized for operation at 1064nm [6, 7], except that a composite design is applied which consists of one 0.9at.% Nd-doped and one undoped YAG crystal. Therefore, the length of the

active medium can be optimized, while the cavity dimensions remain large. The undoped YAG material closes the beam path without introducing additional reabsorption losses. In addition, it provides Faraday rotation required for the intrinsic optical diode which enforces unidirectional and single-frequency operation of the ring oscillator. Transverse mode stability of the cavity is provided by thermal lensing inside the Nd:YAG crystal due to absorption of the pump radiation. The properties of the dielectric mirror on the front facet of the quasi-monolithic Nd:YAG ring laser are extremely important for operation at the 946nm transition. They have to be highly transmitting at 808nm for efficient pump light coupling, and highly transmitting at 1064 nm to suppress the stronger $^4F_{3/2}$-$^4I_{11/2}$ transition. Finally, a defined output coupling at the 946nm laser wavelength is required. The ion-beam-sputtering technique was used for deposition of the dielectric coatings, to allow precise control of their parameters. A coating design was optimized for a transmission of the output coupler at the laser wavelength of 4%. At the 808nm and 1064nm wavelength, transmissions of 95% and 90%, respectively, are measured. The laser beam passes four surfaces during one cavity round trip. To reduce reflection losses, these surfaces are antireflection coated for the laser wavelength of 946nm.

High pump power densities are achieved by four 1W cw Siemens SFH 474801 diode lasers (see Figure 2). The temperature of the diode lasers is controlled by a thermoelectric cooler to tune the emission wavelength to the strongest absorption line in Nd:YAG at 808nm. Each diode laser has an emitting aperture of 1·200μm^2 and is equipped with a miniature cylindrical lens to compensate the astigmatism of the emitted radiation. A mode-selective excitation of the quasi-monolithic Nd:YAG ring laser is achieved by focussing the polarization coupled radiation of two diode lasers into each pump channel. Due to reabsorption losses, the laser threshold of higher order transverse modes is strongly increased and hence, the requirements for mode-selective pumping are strongly relaxed compared to the 1064nm transition [7].

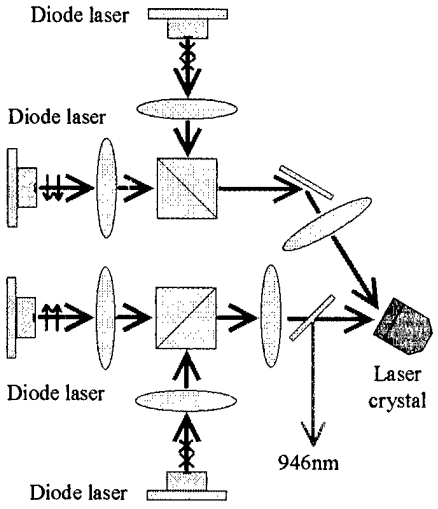

Fig. 2: Pump scheme

The laser crystals temperature is controlled by a thermoelectric cooler. At room-temperature, a maximum output power of more than 800mW cw is generated with a pump power of 5W cw (see Figure 3). The measured laser threshold of 2W cw is high, due to high reabsorption losses. However, the calculated optical slope efficiency of 26% allows efficient room-temperature operation at the quasi-three-level transition. Single-frequency operation was confirmed by a scanning Fabry-Perot interferometer, the 946nm wavelength with a monochromator. No emission at the stronger 1064nm transition was observed.

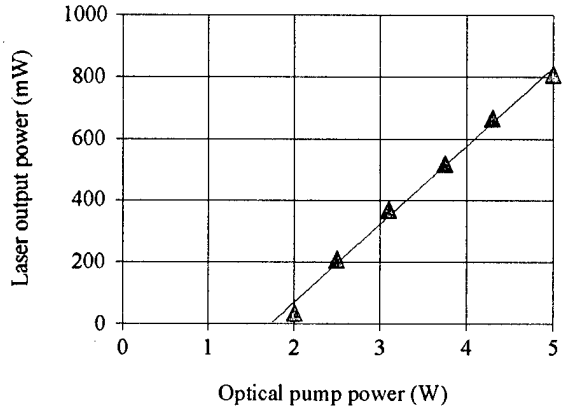

Fig. 3: Output power versus pump power

Because of the quasi-monolithic structure of the cavity, high intrinsic stability of the emitted radiation is guaranteed. The amplitude noise is low, and only dominated by the relaxation oscillation at a few 100kHz. For the maximum output power of 800mW the noise spectrum was detected with a low noise photo detector and an electrical spectrum analyzer with 2mW optical power at the detector (see Figure 4). The relaxation oscillation at 400kHz can be effectively reduced using an active feedback loop [8]. This noise spectrum is similar to those of monolithic Nd:YAG ring lasers operating at the 1064nm transition [9].

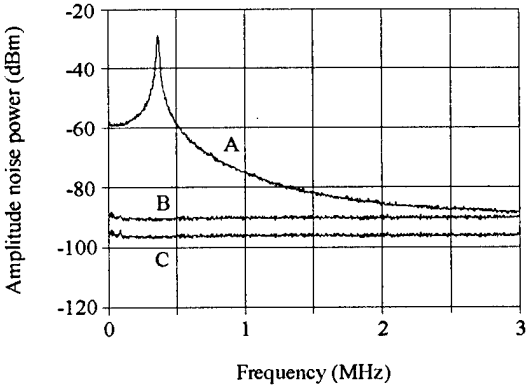

Fig. 4: Amplitude noise power spectra: A) Nd:YAG ring laser, B) White light source, C) Detector noise

In conclusion, the first realization of a diode-pumped Nd:YAG ring laser oscillating at the 946nm quasi-three-level transition has been demonstrated. Efficient room-temperature operation is achieved by a new quasi-monolithic non-planar ring laser design. A single-frequency output power of more than 800mW cw is generated at high amplitude and frequency stability. In future systems, the laser performance will be improved by diffusion bonding of the two laser crystals. This will eliminate the need for additional antireflection coatings on the Nd:YAG-YAG surface. The resulting reduction of laser threshold and increase of slope efficiency in combination with an optimized output coupling will allow output powers beyond 1W cw. With extra-cavity frequency conversion, the generation of powerful radiation in the blue spectral region is possible by conserving the high stability of the quasi-monolithic Nd:YAG ring oscillator.

References:

[1] R. Paschotta, K. Fiedler, P. Kürz, R. Henking, S. Schiller, and J. Mlynek, Opt. Lett. 19, 1325 (1994).
[2] G. Hollemann, E. Peik, and H. Walther, Opt. Lett. 19, 192 (1994).
[3] T. J. Fan, and R. L. Byer, IEEE J. of Quantum Electron. QE-23, 605 (1987).
[4] W. P. Risk, J. Opt. Soc. Am. B 5, 1412 (1988).
[5] T. J. Kane, and R. L. Byer, Opt. Lett. 10, 65 (1985).
[6] I. Freitag, I. Kröpke, A. Tünnermann, and H. Welling, Opt. Commun. 101, 371 (1993).
[7] I. Freitag, A. Tünnermann, and H. Welling, Opt. Commun. 115, 511 (1995).
[8] C. C. Harb, M. B. Gray, H.-A. Bachor, R. Schilling, P. Rottengatter, I. Freitag, and H. Welling, IEEE J. of Quantum Electron. QE-30, 2907 (1994).
[9] I. Freitag, A. Tünnermann, and H. Welling, Photonics West 1995, San Jose, CA, Technical Digest (SPIE Proceedings 2379), 335 (1995).

Experimental and Theoretical Investigations on the Intensity Noise Properties of Injection-Locked Lasers

I. Freitag, A. Tünnermann, and H. Welling
Laser Zentrum Hannover e.V., Hollerithallee 8, D-30419 Hannover, Germany
Tel.: (49)511 2788110, Fax: (49)511 2788100

C.C. Harb, D.E. McClelland, and H.-A. Bachor
The Australian National University, Canberra ACT0200, Australia
Tel.: (61)62 492747, Fax: (61)62 490741

T.C. Ralph
University of Auckland, Private Bag 92019, Auckland, New Zealand
Tel.: (64) 9 3737599 , Fax: (64) 9 3737445

Low noise lasers are useful tools for applications in both applied and fundamental research fields. One application in fundamental physics demanding an ultra-stable light source is the detection of gravitational wave with Michelson type interferometers. To measure the extremely small length changes of the interferometer arms caused by the gravitational waves, a high signal-to-noise-ratio is required. To increase this ratio, the power of the laser light source can be increased while the intensity noise should be reduced as close as possible to the fundamental limit set by the quantum properties of light.

The requirement for low noise laser systems operating at high output powers has motivated investigations of the phenomena known as injection locking. The mode structure and noise behaviour of a high power laser (the slave laser) can be improved by injecting the light of a laser oscillator (the master laser) that has high amplitude and frequency stability (see Figure 1). The injection locking technique is an estabilished field of research dating back to the 1960s. Single-frequency output powers up to 20W cw have been demonstrated by injection locking of Nd:YAG lasers [1-3]. These reports verified that high power lasers can be controlled by low power lasers with high stability. But until recently, it has been extremely difficult to investigate the basic injection locking properties, like quantum noise effects. This is due to several reasons including the lack of suitable theories that take into account the full dynamics of the coupled cavity and laser systems.

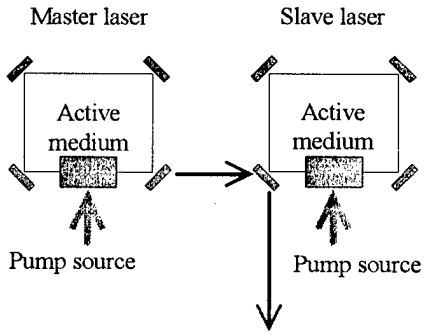

Fig. 1: Schematic setup of an injection-locked laser system

The aim of the collaboration between the Laser Zentrum Hannover e.V. and the Australian National University is to examine techniques for producing stable light source with high output power [4, 5]. We have developed a fully quantum mechanical model that can accurately describe injection-locked laser systems, and performed a set of experiments to test the validity of the model. Our model allows us to predict the behaviour of the injection-locked system by treating it as an example of cascaded optical systems [5]. The theoretical model describes the

intensity noise spectra of the two pump sources and calculates how this pump noise is coupled into both, the master and the slave laser, and finally how this generates the output noise spectrum. The advantage of our full quantum theoretical model over earlier classical models [6] is that both modulations signals as well as the noise close to the quantum noise level can be predicted.

The theoretical predictions of the model have been tested experimentally by using diode pumped non-planar Nd:YAG ring laser as both, the master and the slave laser (see Figure 2). Due to the high intrinsic frequency stability of these lasers [7-9], injection locking can be accomplished for hours without electronic stabilization, allowing investigation on the basic injection locking properties with no interference of an electronic feedback loop [10].

Two different types of experiments have been performed. The intensity noise spectra were recorded using a photo detector and a spectrum analyzer. The transfer functions for modulations of either the injected power or the slave lasers pump power through the entire system are determined via large modulations imposed using appropiate intensity modulators. The experimental observations can be summarized as follows:

i) Modulation of the slave laser pump power. The free-running slave laser has intensity noise due to an interaction between the atoms in the lasing medium, the cavity storage rate and the noise introduced from the pump source. This results in an transfer function which is dominated by the well known relaxation oscillations typically at a few 100kHz (see Figure 3a). The behaviour of the injection-locked slave laser is completely changed. It acts like a lowpass filter to pump noise (see Figure 3b). The transfer of modulation from the slaves pump intensity through to the injection-locked slave laser output is characterized by no attenuation at zero modulation frequency, followed by increasing attenuation with the modulation frequency until the signal falls below the slave lasers quantum noise level.

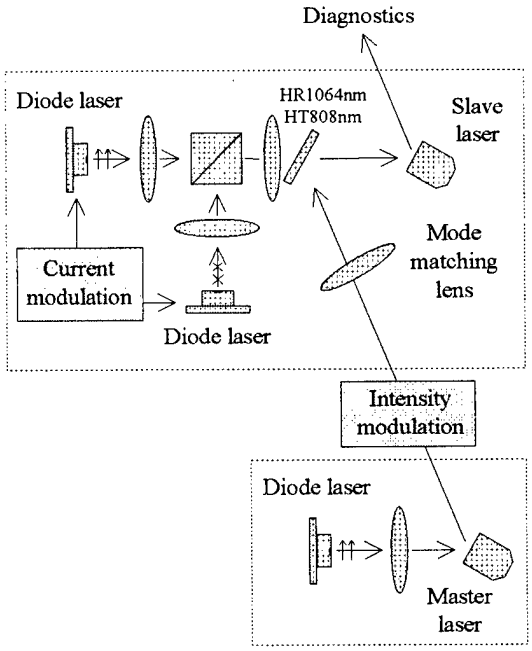

Fig. 2: Experimental setup for investigation of the intensity noise transfer in injection-locked solid state lasers

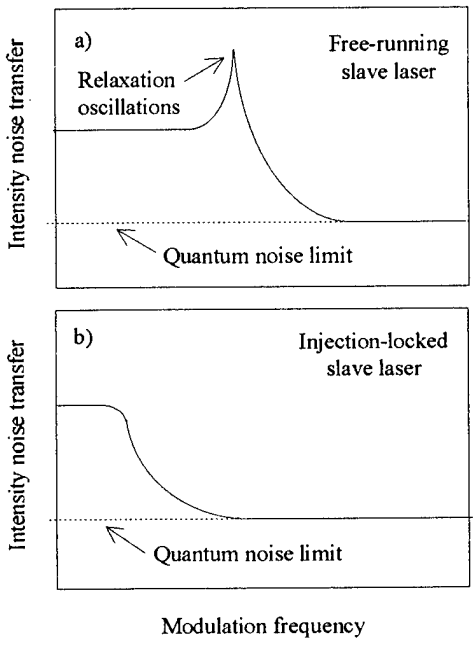

Fig. 3: Schematic diagram of the transfer functions for modulations of the slave lasers pump power

ii) Modulation of the injected power. For the free-running slave laser the injected signal is almost completely reflected at the slave lasers input mirror. The transfer of modulation of the injected signal through the injection-locked slave laser is more complicated, it can be best described by discussing three distinct frequency regions. At low frequencies, the dynamics of the slave laser responds too slowly, and hence any forced oscillation can not be followed. Therefore, the master laser has small influence at low frequencies. This influence increases in a frequency region located around the relaxation oscillation frequency of the slave laser. In this frequency region, the modulations of the injected signals are amplified by the square of the ratio $H = P_{slave} / P_{master}$ of slave to master laser power. The width of this amplification region is inversely proportional to H. In the final frequency region, there is neither attenuation nor amplification of the signal from the master laser. Modulations from the master are reflected off the cavity of the slave laser without entering. The reflected master signal coherently beats with the strong injection-locked slave carrier mode. In this frequency region, the noise floor is set by the quantum noise of the master laser beating with the slave mode. It is at the quantum noise limit of the slave laser if the master laser is quantum noise limited, but can be higher or lower if the master laser radiation is super or sub-Poissonian.

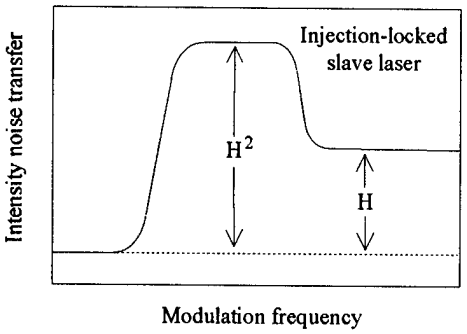

Fig. 4: Schematic diagram of the transfer function for modulations of the injected power

All experimental observations described above are predicted by the theoretical model which can now be used to tailor the performance of injection-locked high power laser systems and to optimize the position of the amplification region depending on the application of the laser. While not fully equivalent to a quantum noise limited high power laser, the injection-locked system will be extremely useful for generating high output powers with low noise.

References:

[1] D. Golla, I. Freitag, H. Zellmer, W. Schöne, I. Kröpke and H. Welling, Opt. Commun. 98, 86 (1993).

[2] I. Freitag, D. Golla, S. Knoke, W. Schöne, H. Zellmer, A. Tünnermann, and H. Welling, Opt. Lett. 20, 462 (1995).

[3] A. D. Farinas, E. K. Gustafson and R. L. Byer, Opt. Lett. 19, 114 (1994).

[4] C. C. Harb, M. B. Gray, H.-A. Bachor, R. Schilling, P. Rottengatter, I. Freitag, and H. Welling, IEEE J. of Quantum Electron. QE-30, 2907 (1994).

[5] C. C. Harb, T.C. Ralph, I. Freitag, D.E. McClelland, H.-A. Bachor, "*Intensity Noise Properties of Injection-Locked Lasers*", to be published.

[6] A. D. Farinas, E. K. Gustafson and R. L. Byer, J. Opt. Soc. Am. B12, 328 (1995).

[7] T. J. Kane, and R. L. Byer, Opt. Lett. 10, 65 (1985).

[8] I. Freitag, I. Kröpke, A. Tünnermann, and H. Welling, Opt. Commun. 101, 371 (1993).

[9] I. Freitag, A. Tünnermann, and H. Welling, Opt. Commun. 115, 511 (1995).

[10] I. Freitag and H. Welling, Appl. Phys. B 58, 537 (1994).

Spectroscopic Properties and Laser Oscillation of Yb/Er:$Ca_2Al_2SiO_7$ in the 1.6 μm eye-safe range

B. Simondi-Teisseire, B. Viana, A.M. Lejus and D. Vivien
Laboratoire de Chimie Appliquée de L'Etat Solide (ENSCP)
11Rue P&M Curie 75231 Paris cedex 05 - France
phone# (33)-1-44276707 fax# (33)-1-46347489
C. Borel, R. Templier and C. Wyon
C.E.A. L.E.T.I.(Technologies Avancées) C.E.N.G..
17 Avenue des Martyrs, 38054 Grenoble Cedex, France

Introduction

Radiation around 1.5μm ($^4I_{13/2}$->$^4I_{15/2}$ transition) has extensively been investigated over the last few years for eye safe measurement and communication applications. This paper describes the optical properties of Yb codoped Er:$Ca_2Al_2SiO_7$ (CAS) crystals. Ytterbium ions, well adapted to laser diodes pumping systems, have been considered in this work to sensitize the erbium infrared luminescence.

The Gehlenite $Ca_2Al_2SiO_7$ belongs to the melilite family. The Gehlenite structure presents some particular features: a structural disorder around the rare earth cations substituting Ca^{2+}, due to a statistical distribution of several cations with differents sizes and charges over a given set of site, high phonons energy ($\hbar\omega_{max}$ = 1020 cm^{-1}) and a low symetry ensuring strong electric dipolar transitions. These properties are favourable to a broad and intensive 1.55 μm emission ($^4I_{13/2}$ —> $^4I_{15/2}$ transition) well centered in the eye safe window [1].

Crystals of Er and Er/Yb Gehlenite have been grown at first by the melting zone process in order to analyse the optical properties and secondly by the Czochralski process for the laser experiments. Good optical quality has been obtained even with high doping level (10^{21} ions/cm^3).

Results

Emission cross sections have been determined by the Fuchtbauer Ladenburg and reciprocity methods. Similar results have been obtained in boyh cases (see Figure 1). Even at low erbium content the emission is broad and well centered in the eye safe window. At 1535 nm, the emission cross section value, 8 10^{-21} cm^2, is in the same range than for erbium doped orthosilicate YSO or phosphate glass. As the Er^{3+} ion presents a quasi four levels laser configuration, with reabsorption processes limiting the laser performance, we report on figure 2, for several population inversion ratios β, the efficient gain cross section $\sigma^{eff}(\lambda)$ taking into account the reabsorption and calculated by the following expression:

$\sigma^{eff}(\lambda) = \beta\sigma_e(\lambda) - (1-\beta)\,\sigma_a(\lambda)$. Laser action could be achieved for positive gain cross section i.e. at the longer wavelengths, where the reabsorption losses are minimized. Gain cross section begins to be positive for an inversion ratio β of 30% at 1570 nm.

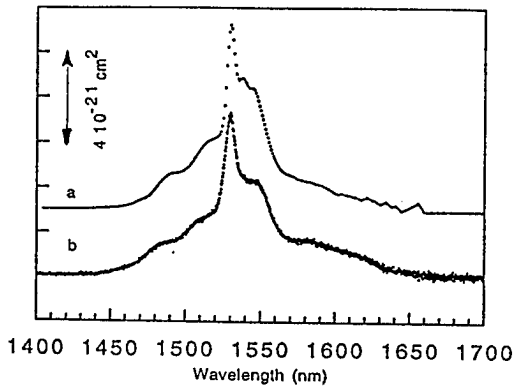

Figure 1: Stimulated emission cross section of $Ca_{1.98}Er_{0.02}Al_{2.02}Si_{0.98}O_7$ calculated by (a) the reciprocity method and (b) the Fuchtbauer Ladenburg method.

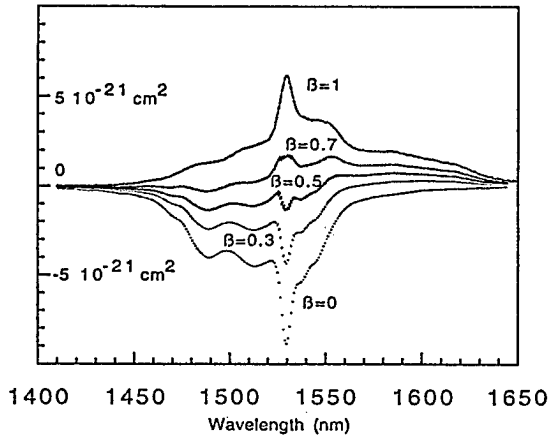

Figure 2:Gain cross section spectra for different values of the population inversion ratio. One can notice on these spectra that β=0 represents the absorption

The lifetime of the Er^{3+} $^4I_{13/2}$ level is 7.6 ms, a value favourable to the energy storage on this level, while the strong non radiative processes lead to small lifetimes values of all the other emitting levels [$\tau(^4I_{11/2})$=41 µs, $\tau(^4S_{3/2})$=7.6 µs and $\tau(^4F_{9/2})$=7.5 µs]. These small lifetimes values fasten the population mechanisms of the $^4I_{13/2}$ emitting level and limit the upconversion process [$^4I_{13/2}$;$^4I_{13/2}$->$^4I_{9/2}$;$^4I_{15/2}$]. The absorption of Er^{3+} in the diode emission range is low (3×10^{-21} cm^{-1}) but nevertheless, the Er^{3+} concentration should remain weak to limit the reabsorption process. Ytterbium ions is well adapted to the InGaAs laser diodes pumping systems (σ^{abs} for Yb^{3+} around 5×10^{-20} cm^2) and a relatively high concentration has been considered in this work to sensitize the erbium infrared luminescence as a good overlap is observe between the emission of the Yb^{3+} sensitizor and the absorption of the Er^{3+} activator ions.

The mechanisms of the Yb/Er energy transfer are analyzed in the codoped Yb;Er:CAS samples. The energy levels and the processes included in the model are shown in figure 3. Because of the low erbium concentration, Er^{3+} cross relaxation from the $^4S_{3/2}$ level is not included in the model and only the back transfer Er->Yb from the $^4I_{11/2}$ level is considered as there is a rapid decay of the $^4F_{7/2}$ and $^2H_{11/2}$ to the $^4S_{3/2}$ level and because the lifetime of this level is not affected by the presence of the Yb^{3+} ions. In order to measure the energy transfer rates, the samples were excited at 800 nm using a C.W. titanium sapphire. By this mean, the Yb ions are only excited through the Er->Yb energy transfer. Measurements of the fluorescence intensities of the 1 µm and 1.5 µm emission lead to the determination of the Yb-Er energy transfer rates $C_{Yb->Er} = 2\text{-}4\times10^{-16}$ cm^3s^{-1} and $C_{Er->Yb} = 4\times10^{-17}$ cm^3s^{-1}.

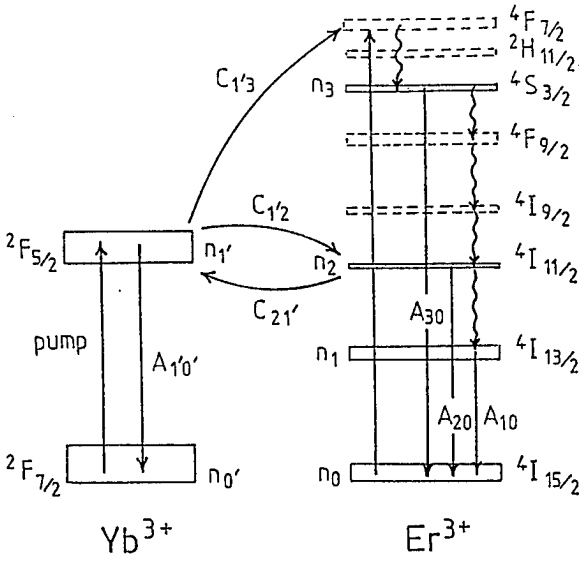

Figure 3: Energy levels and the processes included in the energy transfer modeling in the Yb;Er:CAS .

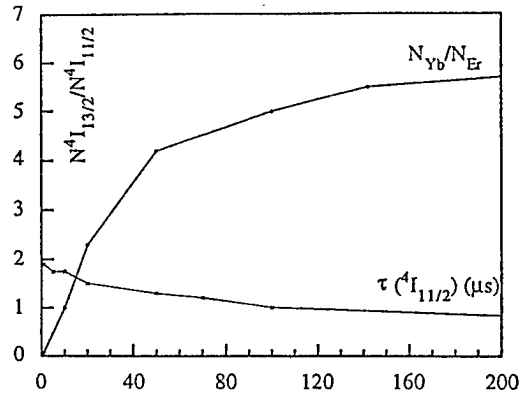

Figure 4: Population ratio of the $^4I_{13/2}$ and $^4I_{15/2}$ states (a) for various Yb/Er ratio and (b) various $^4I_{11/2}$ lifetimes

In the Yb;Er:CAS, rate equations are used for modeling the population on several Yb^{3+} and Er^{3+} states. The set of differential equations was solved numerically using a Range-Kutta procedure and all the input parameters are experimentally determined leading to the determination of the population inversion conditions. Pump energy flux, rare earth ions concentrations as well as codoping system to decrease significantly the $^4I_{11/2}$ Er^{3+} lifetimes are considered in the paper. Lifetimes of the $^4I_{11/2}$ level of the Er^{3+} can be decreased by introducing Ce^{3+} ions in the Er^{3+} vicinity according to the phonon assisted cross relaxation scheme [$^4I_{11/2}$(Er);$^2F_{5/2}$(Ce)->$^4I_{13/2}$(Er);$^2F_{7/2}$(Ce)] and experimental results indicate that for $6.6x10^{20}$ Ce^{3+} ions the $^4I_{11/2}$ lifetime is divided by 3.

A laser oscillation have been obtained using a plano-concave cavity (3 cm long) on a 2.2 mm long rod of $Ca_{1.923}Er_{0.007}Yb_{0.07}Al_{2.077}Si_{0.923}O_7$ crystal, pumped by a titanium sapphire laser at 976 nm. The threshold with a 1% transmission output mirror is 125 mW in the same order than those obtain recently for other silicate materials [3]. Further laser experiments are in progress on several gehlenite samples.

This research was supported by the DRET (France)

References

[1] B. Viana, D. Saber, A.M. Lejus, D. Vivien, C. Borel, R. Romero and C. Wyon OSA Proceeding on Advanced Solid-State Lasers 15, (1993) 242
B. Teisseire, A.M. Lejus, B. Viana, D. Vivien, Technical digest CLEO (1994) 192
[2] C. Borel, J.C. Souriau, Ch. Wyon, C. Li, R. Moncorgé , Mat. Res.Soc.Proc , 329, (1994) 253.
[3] T. Schweizer, T Jensen, E. Heumann and G. Huber Optics comm. 118 (1995) 557

HIGH ENERGY DIODE SIDE-PUMPED Cr:LiSAF LASER

Christyl C. Johnson
Donald J. Reichle
Norman P. Barnes
NASA Langley Research Center
Hampton, VA 23681

Gregory J. Quarles
Lightning Optical Corporation
Tarpon Springs, FL 34689

NASA Langley Research Center has recently demonstrated a diode-pumped Cr:LiSAF laser with a 30 mJ normal mode output energy at an optical to optical efficiency (laser diode output to Cr:LiSAF laser output) of 17%. In order to reach this level of output energy with a side diode-pumped system, scattering losses had to be minimized, coupling losses had to be minimized, and absorption in the mode volume had to be optimized. Therefore, a theoretical model which would provide for the optimization of the dopant concentration for a fixed rod radius was established.

An optimum Cr concentration can be determined by considering the absorption characteristics of the laser material. Since the Cr absorption features are relatively strong and Cr can be incorporated into $LiSrAlF_6$ in any desired concentration, an optimum Cr concentration can be determined by considering the distribution of absorbed energy. A simple example can be used to approximate the optimization process. In a side pumped laser rod geometry, it is difficult to extract the stored energy near the periphery of the laser rod. If the absorption coefficient is too large, too much of the stored energy is near the periphery where it is difficult to extract detracting from the efficiency. On the other hand, if the absorption coefficient is too small, too much of the pump radiation passes through the laser rod without being absorbed. Unabsorbed pump radiation does not contribute to the stored energy, detracting from the efficiency. Optimum concentration is a compromise of these two effects.

An approximate but closed form expression can be obtained to estimate the optimum concentration. Continuing with the example, consider a laser rod with radius a_r supporting a circular profile laser beam with radius w_c. For a pump beam which travels along the diameter of the laser rod, the pump energy absorbed within radius w_c is given by

$$E_{paw} = E_{p0}[\exp(-\beta_a(a_r-w_c))-\exp(-\beta_a(a_r-w_c))].$$

where E_{p0} is the incident pump energy and β_a is the absorption coefficient. Maximizing this quantity produces

$$\beta_a = \sigma_a N_S C_A = (1/2w_c)\ln((a_r+w_c)/(a_r-w_c))$$

where σ_a is the absorption cross section, N_S is the number density of active atom sites, and C_A is the concentration of the active atoms. More detailed calculations average over the various directions for the pump radiation as well as the pump wavelengths and hence the absorption

coefficient [1]. However, for diode pumping of a transition metal such as Cr, the variation in the absorption coefficient over the range of diode wavelengths is relatively small.

As a result of NASA Langley Research Center's efforts to produce a side diode-pumped 30 mJ Cr:LiSAF laser system, Langley has contributed to the development of two significant technologies for diode-pumped Cr:LiSAF laser systems. Through an SBIR contract, Langley has funded SDL to develop high power GaInP/AlGaInP diodes at 670 nm to be used as pumping sources. The laser diodes that have already been delivered under this contract were six-bar stacks, each emitting 360 W of output power. These laser diode arrays have been operated for nearly 10^6 shots and have not suffered any degradation in output power. Langley SBIR funding has also enabled Lightning Optical to develop the technology for the growth of LiSAF doped with various levels of Cr^{3+} suitable for optimized pumping with laser diodes. A systematic study and optimization of the parameters utilized in the Czochralski growth of high Cr doped LiSAF was conducted on the growth of thirteen boules with different chromium concentrations. Pieces from each boule were tested for final Cr concentration in the crystal and scatter loss per unit length. Concentration and spectroscopic analyses were compiled for each crystal, and subsequently, laser rods from the highest quality materials were fabricated and coated for testing in Langley's diode-pumped resonator. Finally, two representative spectroscopic samples were analyzed for defects, impurities, and scatter site identification.

Scatter sites in the original, higher-loss boules were investigated with various microprobe and x-ray analysis techniques. Scatter losses were determined to have come from impurities in the starting chemicals and oxygen contamination. A new materials processing technique was investigated, and this technique yielded high-doped Cr:LiSAF boules with less than 0.2%/cm scatter losses. This technique and the results from the analysis will be discussed further in this paper. These lower scatter losses were demonstrated in the final eight boules grown for this program, with the Cr-concentrations ranging from 0.8 at% Cr to 24.2 at% Cr in the crystal. For these higher doped materials, this represents an order of magnitude reduction in the scatter losses in the boule.

Experiments have been performed to verify the theoretical analysis using different Cr concentrations in $LiSrAlF_6$ and a side pumped laser diode arrangement, placing three 680 nm laser diode arrays of 360 W (60 mJ) each around the circumference of the Cr:LiSAF laser rod (see figures 1 and 2). Using the analysis, the optimum Cr concentration is approximately 0.015. Laser rods have been obtained having Cr concentrations ranging from 0.012 to 0.059. Normal mode laser performance has been obtained and compared with the expected results. The optimized laser system was acousto-optically Q-switched and tuned, via the use of a birefringent plate and dispersive prism in concert, over the region of 780-900 nm.

This paper will present a more detailed look at the theoretical model, laser performance characterization, Q-switched laser performance (output energy of 2.5 mJ), and wavelength tunability.

1. N. P. Barnes, M. E. Storm, P. L. Cross, and M. W. Skolaut, Jr. "Efficiency Of Nd Laser Materials With Laser Diode Pumping," IEEE J. Quant. Elect. QE-26, 558-569 (1990)

Figure 1. Resonator Congifuration

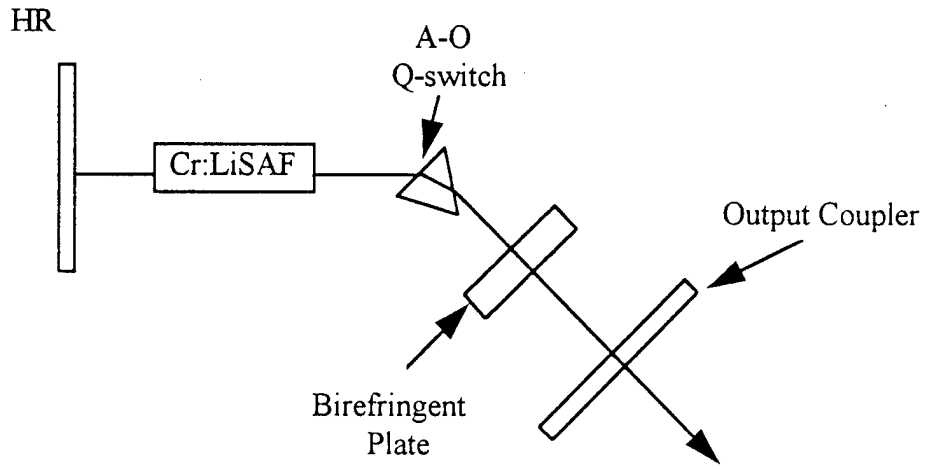

Figure 2. Laser Head Configuration

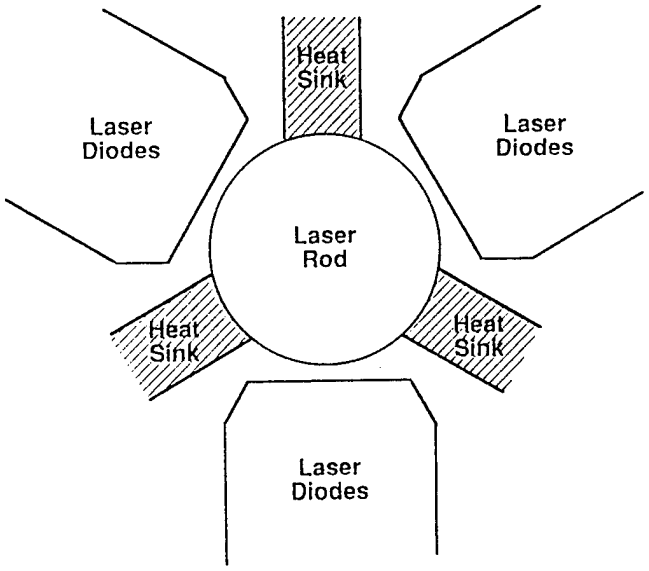

Lasing in diode-pumped thulium and thulium, holmium doped YAP

I. F. Elder and M. J. P. Payne
Defence Research Agency
St. Andrews Road
Malvern
Worcs WR14 3PS
United Kingdom

Tele +44 (0)684 896139
Fax +44(0)684 896270
E-Mail elder@dra.hmg.gb

Yttrium orthoaluminate (YAP) offers itself as a potentially useful laser host crystal, combining the mechanical strength of YAG with a natural birefringence (possessing orthorhombic structure)[1] which dominates any thermally induced birefringence. In addition, the emission cross-section of thulium in YAP is twice that of thulium in YAG[2].

We have assessed laser action in both Tm:YAP and Tm,Ho:YAP. The pump source for these experiments was a 500 μm wide aperture 3 W SDL Inc laser diode, temperature tuned to the 794 nm absorption peak of thulium in YAP. Dopant concentrations of 4.2% thulium and 0.28% holmium were chosen, yielding the same doping densities as the more common 6% thulium and 0.4% holmium in YAG. The YAP samples were grown inhouse by the Czochralski method.

Figure 1 depicts the design of the laser used in these experiments. The highly divergent output of the laser diode was initially collected by a 6.5 mm focal length spherical lens, which produced an astigmatic magnified image of the diode output facet. The 40 mm focal length cylindrical lens acted to reduce the divergence of the beam in the plane perpendicular to the diode p-n junction (corresponding to the wide dimension of the output facet, which was the many times diffraction limited orientation). The 10 mm focal length cylindrical lens was then positioned so as to overlap its focus with the diffraction limited focus produced by the spherical lens acting in the plane perpendicular to the diode p-n junction. The inclusion of the 40 mm focal length cylindrical lens allowed a greater depth of focus to be achieved with the 10 mm lens. Using these components, FWHM spot sizes of 50 to 100 μm could readily be achieved, with greater than 90% transmission through the optics train.

The gain element was either 2 or 3 mm long, and was polished plane/plane with the input face coated to be a high reflector at two microns, with high transmission of the pump beam; the other

end was antireflection coated at two microns. The resonator was completed with a flat output coupler. Using this simple design, resonators of length less than one centimetre could be built. A stable cavity mode was achieved by thermal lensing in the gain medium caused by heat deposition due to absorption of the pump beam. The laser crystal was mounted on a brass heatsink, the temperature of which was held at a constant 15°C by a thermoelectric cooler.

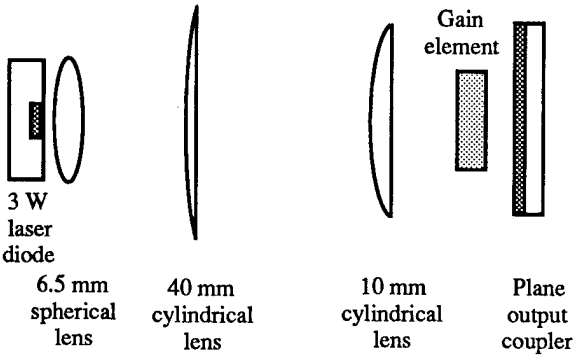

Figure 1 : Schematic of layout of laser experiments

Figure 2 shows a comparison of the output power behaviour of the two lasers. Note that different lengths of crystals were used. A range of output couplers was used with each crystal , and the plot shows the curve for the optimum output coupling in each case. For the thulium laser the optimum mirror transmission was 1.5%, while for the holmium laser the optimum mirror transmission was 2%. Threshold pump powers were approximately 1 W in both cases, but the slope efficiencies were markedly different, 19% for the holmium and 40% for the thulium laser. In terms of optical-to-optical conversion efficiency from the diode pump light to two micron laser light, 9% conversion was achieved with the holmium and 24% with the thulium laser.

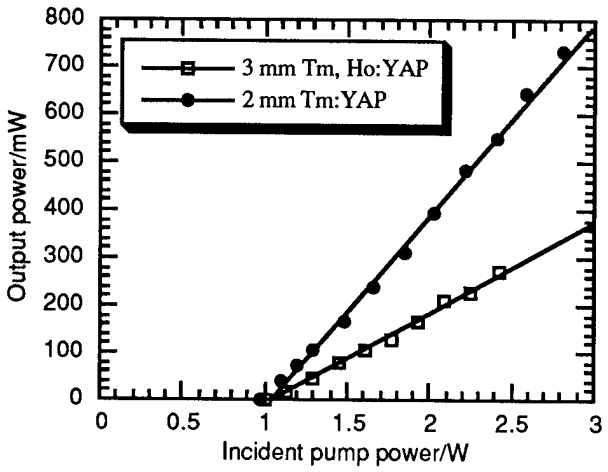

Figure 2 : Comparison of output power behaviour

The poorer performance of the holmium laser can be attributed to the increased losses introduced by upconversion in the double doped crystal compared to singly doped thulium. In the case of the former, bright green/yellow fluorescence is evident which is caused by emission in two bands, one centred on 545 nm, the other on 660 nm, while for the latter faint green/white fluorescence can be seen by eye, but could not be detected with the apparatus used to analyse the holmium upconversion fluorescence. Only a small fraction of the excitation generated via upconversion decays as fluorescence, the remainder decaying nonradiatively and thus depositing additional heat in the crystal. Therefore, under conditions of fixed absorbed pump power and fixed heatsink temperature, the temperature rise in the pumped volume of Tm,Ho:YAP will be higher than in Tm:YAP, increasing lasing threshold and reducing the maximum output power achievable.

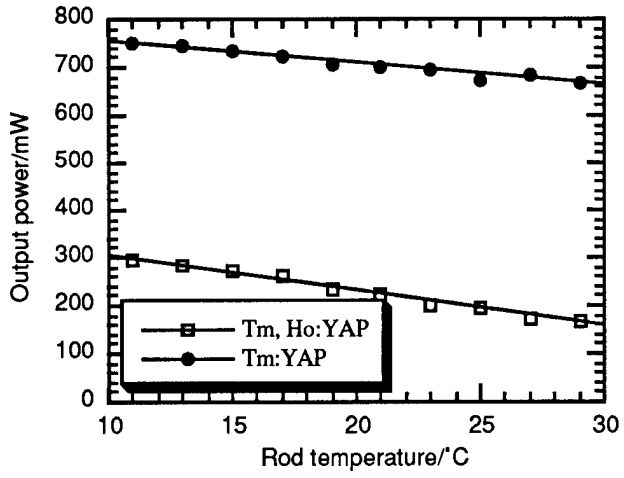

Figure 3 : Comparison of temperature tuning behaviour

Figure 3 illustrates the greater temperature sensitivity of the output power of the holmium laser compared to the thulium laser. A simple experiment was performed whereby the only parameter varied was the laser crystal heatsink temperature. The maximum output power of Tm:YAP was measured to change at -4.5 mW/°C, the corresponding value for Tm,Ho:YAP being -7.5 mW/°C. Examination of the energy level splittings in the ground state manifolds of thulium and holmium[3,4] reveals that at room temperature, the lower laser level in thulium contains slightly less than 1% of the total ground state population, while for holmium the lower laser level contains slightly greater than 1% of the total ground state population. The variation of maximum output power with heatsink temperature is a direct measure of the change in lasing threshold with temperature. The disparity in measured output power variations is significantly larger than the disparity in lower laser level populations, and is accounted for by considering the increased heat deposition in Tm,Ho:YAP. Further evidence of the deleterious effects of upconversion in Tm,Ho:YAP can be obtained by observing the fluorescence decay in the two micron waveband from the first excited state of holmium, and comparing this to the two micron fluorescence decay in singly doped thulium crystals. The holmium fluorescence was found not to possess a single exponential decay profile, with an effective lifetime of 2.5 ms determined by dividing the peak fluorescence signal by the area under the decay curve. In the case of Tm:YAP under identical excitation conditions the fluorescence decay was found to be a single exponential with lifetime 5 ms.

References

[1] 'CRC Handbook of Laser Science and Technology', Volume IV Part 2 (1986) & Volume V Part 3 (1987), M J Weber, Florida: CRC Press, Inc.

[2] 'Infrared Cross-Section Measurements for Crystals Doped with Er^{3+}, Tm^{3+}, and Ho^{3+}', S A Payne et al, IEEE Journal of Quantum Electronics, vol. 28, no. 11 (1992), pp 2619-2630

[3] 'Crystal field determination for trivalent thulium in yttrium orthoaluminate', J M O'Hare & V L Donlan, Phys. Rev. B, vol. 14, no. 9 (1976), pp 3732-3743

[4] 'Laser Crystals', A A Kaminskii, 2nd Edition, Berlin Heidelberg: Springer-Verlag (1990)

EFFICIENT PYRROMETHENE DOPED XEROGELS FOR TUNABLE SOLID-STATE LASERS

Mohammed Faloss, Michael Canva, Patrick Georges, Alain Brun, Frédéric Chaput* and Jean-Pierre Boilot*

Institut d'Optique Théorique et Appliquée
Unité de Recherche associée au CNRS N° 14
91403 ORSAY-FRANCE
Phone: 33 1 69 41 68 56
Fax: 33 1 69 41 31 92
Email: michael.canva@iota.u-psud.fr

* Groupe de Chimie du Solide
Laboratoire de Physique de la Matière Condensée,
École Polytechnique,
Unité de Recherche associée au CNRS N° 1254D
91128 PALAISEAU Cedex, FRANCE
Phone: 33 1 69 33 46 51
Fax: 33 1 69 33 30 04
E-mail: jpb@pmcsun1.polytechnique.fr

For decades, numerous efforts have been made in order to synthesize solid state dye doped materials for tunable lasers. About ten years ago, fluorescent dyes were incorporated in sol-gel matrices [1]. This stimulated a new start in this field [2-6]. A few years ago, the performances were very poor, especially concerning the lifetime and it was impossible to obtain more than a few thousands shots from the same area of the samples. During the last years, impressive progresses have been made, the materials being mainly made with polymers and xerogels matrices [7-10]. Progressively, significant improvements were obtained concerning the host matrix in terms of transparency. Meanwhile, new organic dye molecules have been synthesized leading to better performances. These molecules belong to the pyrromethene family. We especially tested the pyrromethene 597 dye, recently introduced by Exciton, which exhibits higher efficiency [11] than the classical rhodamine molecules. Furthermore, it also has a better behavior in terms of photodegradation and thermodegradation. These two properties are essential for our application, since we always test the samples by using the same area, so in the most hard conditions compared with real applications where the samples could be mounted on moving plates. In that case, and at each pump pulse, the sample's area used for the laser would be renewed, leading to a decrease of the local average temperature.

In this conference, we will report significant progresses obtained by trapping pyrromethene 597 molecules in a new xerogel matrix. We have been able to obtain more than 80 % slope efficiency and to gain more than an order of magnitude in terms of number of pulses emitted by the same sample area.

Gels are obtained by inorganic polymerization of a solution called sol, involving hydrolysis and polycondensation reactions. These chemical reactions are performed at room temperature and it is

possible to dope the sol with any organic molecules that are soluble in it. After gelification and drying, the molecules are trapped into the solid xerogel matrix.

Xerogel samples were prepared from alkoxysilane : vinyltriethoxysilane (VTEOS) or methyltriethoxysilane (MTEOS) according to similar published procedure [8]. The hydrolysis of silicon alkoxide was performed under acidic conditions with acetone as common solvent. The initial molar ratios alkoxysilane : water (pH=2.5) : acetone were respectively 1 : 3 : 3. After several hours hydrolysis at room temperature, a small amount of amine modified silane was added in order to neutralize the acidity of the medium and therefore to increase the condensation reaction rate. Acetonic solution of pyrromethene 597 was then added to yield a concentration between 10^{-5} and 10^{-3} mol.l^{-1}. Afterwards, the resulting sols were cast into polypropylene cylindrical-shaped moulds and sealed. Gelation occurred within one week at 40°C. The samples were left to dry for 3 weeks more at the same temperature. After drying, optically clear and dense inorganic-organic hybrid xerogels were obtained. Samples are hard enough to be machined and polished.

We tested the efficiency of our samples in a linear plano-concave laser cavity which consisted of a concave input mirror (10 m radius of curvature) and a flat output coupler (T=80% in the 550-650 nm range). The concave mirror supported a dichroic coating (high reflection in the 550-650 nm range and high transmission at 532 nm). The beam waist was about 400 µm. The xerogel samples were placed 2 cm from the output coupler and were pumped by a frequency doubled Q:switched Nd:YAG laser producing 8 ns pulses at a repetition rate up to 20 Hz. The figure 1 presents the output pulse energy, at 588 nm, versus the pump energy, corresponding to a 80% slope efficiency. We also tested the tunability by inserting a prism in the cavity. Our result show that the molecules keep their properties in the xerogel matrices and lead to roughly the same tunability (570-625 nm) than in solution.

The most important improvement presented here is the relatively high operating lifetime obtained with these new samples. In solid state dye lasers, the output energy tends to decrease, due to photodegradation and thermodegradation processes. To measure this, we recorded the evolution of the output energy emitted from the same point and at a fixed pump energy as a function of the number of previous pumping pulses. The lifetime corresponds to the number of pulses emitted before the output energy reach half the initial value. We tested our samples behavior at a 1 mJ pump energy, at 20 Hz repetition rate. In this case, we routinely obtain lifetimes in excess of 100,000 pulses and even up to 350,000 pulses [Fig. 2] which is one order of magnitude more than our previous results [8].

Finally we recently prepared oxygen free samples. Previous experiments have demonstrated that oxygen reacts with the molecules in the triplet excited state leading to the destruction of the molecules. With these xerogels, preliminary results indicate an interesting behavior, especially concerning the lifetime. In the same conditions than the other tests, about 2,000,000 pulses may be emitted. These results are consistent with previous experiments [9].

EFFICIENT PYRROMETHENE DOPED XEROGELS FOR TUNABLE SOLID-STATE LASERS

Mohammed Faloss, Michael Canva, Patrick Georges, Alain Brun, Frédéric Chaput* and Jean-Pierre Boilot*

Institut d'Optique Théorique et Appliquée
Unité de Recherche associée au CNRS N° 14
91403 ORSAY-FRANCE
Phone: 33 1 69 41 68 56
Fax: 33 1 69 41 31 92
Email: michael.canva@iota.u-psud.fr

* Groupe de Chimie du Solide
Laboratoire de Physique de la Matière Condensée,
École Polytechnique,
Unité de Recherche associée au CNRS N° 1254D
91128 PALAISEAU Cedex, FRANCE
Phone: 33 1 69 33 46 51
Fax: 33 1 69 33 30 04
E-mail: jpb@pmcsun1.polytechnique.fr

For decades, numerous efforts have been made in order to synthesize solid state dye doped materials for tunable lasers. About ten years ago, fluorescent dyes were incorporated in sol-gel matrices [1]. This stimulated a new start in this field [2-6]. A few years ago, the performances were very poor, especially concerning the lifetime and it was impossible to obtain more than a few thousands shots from the same area of the samples. During the last years, impressive progresses have been made, the materials being mainly made with polymers and xerogels matrices [7-10]. Progressively, significant improvements were obtained concerning the host matrix in terms of transparency. Meanwhile, new organic dye molecules have been synthesized leading to better performances. These molecules belong to the pyrromethene family. We especially tested the pyrromethene 597 dye, recently introduced by Exciton, which exhibits higher efficiency [11] than the classical rhodamine molecules. Furthermore, it also has a better behavior in terms of photodegradation and thermodegradation. These two properties are essential for our application, since we always test the samples by using the same area, so in the most hard conditions compared with real applications where the samples could be mounted on moving plates. In that case, and at each pump pulse, the sample's area used for the laser would be renewed, leading to a decrease of the local average temperature.

In this conference, we will report significant progresses obtained by trapping pyrromethene 597 molecules in a new xerogel matrix. We have been able to obtain more than 80 % slope efficiency and to gain more than an order of magnitude in terms of number of pulses emitted by the same sample area.

Gels are obtained by inorganic polymerization of a solution called sol, involving hydrolysis and polycondensation reactions. These chemical reactions are performed at room temperature and it is

possible to dope the sol with any organic molecules that are soluble in it. After gelification and drying, the molecules are trapped into the solid xerogel matrix.

Xerogel samples were prepared from alkoxysilane : vinyltriethoxysilane (VTEOS) or methyltriethoxysilane (MTEOS) according to similar published procedure [8]. The hydrolysis of silicon alkoxide was performed under acidic conditions with acetone as common solvent. The initial molar ratios alkoxysilane : water (pH=2.5) : acetone were respectively 1 : 3 : 3. After several hours hydrolysis at room temperature, a small amount of amine modified silane was added in order to neutralize the acidity of the medium and therefore to increase the condensation reaction rate. Acetonic solution of pyrromethene 597 was then added to yield a concentration between 10^{-5} and 10^{-3} mol.l^{-1}. Afterwards, the resulting sols were cast into polypropylene cylindrical-shaped moulds and sealed. Gelation occurred within one week at 40°C. The samples were left to dry for 3 weeks more at the same temperature. After drying, optically clear and dense inorganic-organic hybrid xerogels were obtained. Samples are hard enough to be machined and polished.

We tested the efficiency of our samples in a linear plano-concave laser cavity which consisted of a concave input mirror (10 m radius of curvature) and a flat output coupler (T=80% in the 550-650 nm range). The concave mirror supported a dichroic coating (high reflection in the 550-650 nm range and high transmission at 532 nm). The beam waist was about 400 µm. The xerogel samples were placed 2 cm from the output coupler and were pumped by a frequency doubled Q:switched Nd:YAG laser producing 8 ns pulses at a repetition rate up to 20 Hz. The figure 1 presents the output pulse energy, at 588 nm, versus the pump energy, corresponding to a 80% slope efficiency. We also tested the tunability by inserting a prism in the cavity. Our result show that the molecules keep their properties in the xerogel matrices and lead to roughly the same tunability (570-625 nm) than in solution.

The most important improvement presented here is the relatively high operating lifetime obtained with these new samples. In solid state dye lasers, the output energy tends to decrease, due to photodegradation and thermodegradation processes. To measure this, we recorded the evolution of the output energy emitted from the same point and at a fixed pump energy as a function of the number of previous pumping pulses. The lifetime corresponds to the number of pulses emitted before the output energy reach half the initial value. We tested our samples behavior at a 1 mJ pump energy, at 20 Hz repetition rate. In this case, we routinely obtain lifetimes in excess of 100,000 pulses and even up to 350,000 pulses [Fig. 2] which is one order of magnitude more than our previous results [8].

Finally we recently prepared oxygen free samples. Previous experiments have demonstrated that oxygen reacts with the molecules in the triplet excited state leading to the destruction of the molecules. With these xerogels, preliminary results indicate an interesting behavior, especially concerning the lifetime. In the same conditions than the other tests, about 2,000,000 pulses may be emitted. These results are consistent with previous experiments [9].

In conclusion we have shown significant improvements of performances of dye doped xerogels for solid state tunable lasers: more than 80% slope efficiency and a lifetime in the order of a few hundreds of thousands shots have been demonstrated.

References :

[1] Avnir D., Levy D. and Reisfeld R.
"The nature of the silica cage as reflected by spectral changes and enhanced photostability of trapped Rhodamine 6G"
J. Phys. Chem., **88**, 5956-5959, (1984).

[2] Gromov D.A., Dyumaev K.M., Manenkov A.A., Maslyukov A.P., Matyushin G.A., Nechitailo V.S. and Prokhorov A.M.
"Efficient plastic-host dye lasers"
J. Opt. Soc. Am. B, **2**, 1028-1031, (1985).

[3] Salin F., Le Saux G., Georges P., Brun A., Bagnall C. and Zarzycki J.
"Efficient tunable solid-state laser near 630 nm using sulforhodamine 640-doped silica gel"
Optics Letters, **14**, 785-787, (1989).

[4] Whitehurst C., Shaw D.J. and King T.A.
"Sol-gel glass solid state lasers doped with organic molecules"
SPIE, **1328**, Sol-Gel Optics, 183-193, (1990).

[5] Reisfeld R., Brusilovky D., Eyal M., Miron E., Burstein Z. and Ivri J.
"A new solid state tunable laser in the visible"
Chemical Physics Letters, **160**, 43-44, (1989).

[6] Knobbe E.T., Dunn B., Fuqua P.D. and Nishida F.
"Laser behavior and photostability characteristics of organic dye doped silicate gel materials"
Applied Optics, **29**, 2728-2733, (1990).

[7] R.E. Hermes, T. Allick, S. Chandra and J.A. Hutchinson
"High-efficiency pyrromethene doped solid-state dye lasers"
App. Phys. Lett., 63, 877-879, (1993).

[8] M. Canva, A. Dubois, P. Georges, A. Brun, F. Chaput, A. Ranger and J.P. Boilot,
"Perylene, Pyrromethene and Grafted Rhodamine Doped Xerogels for Tunable Solid State Laser," SPIE **2288** Sol-Gel Optics III, 298-309, (1994).

[9] M.D. Rahn and T.A. King,
"Lasers based on doped sol-gel composite glasses,"
SPIE **2288** Sol-Gel Optics III, 382-391, (1994).

[10] B. Dunn, F. Nishida, R. Toda, J.J. Zink, T.H. Allik, S Chandra and J.A. Hutchinson,
"Advances in dye-doped sol-gel lasers,"
Mat. Res. Soc. Symp. Proc. **329**, 267-277, (1994).

[11] Pavlopoulos T.G., Boyer J.H., Thangaraj K., Sathyamoorthi G., Shah M.P. and Soong M.L.
"Laser dye spectroscopy of some pyrromethene-BF2 complexes"
Applied Optics, **31** (33), 7089-7094, (1992).

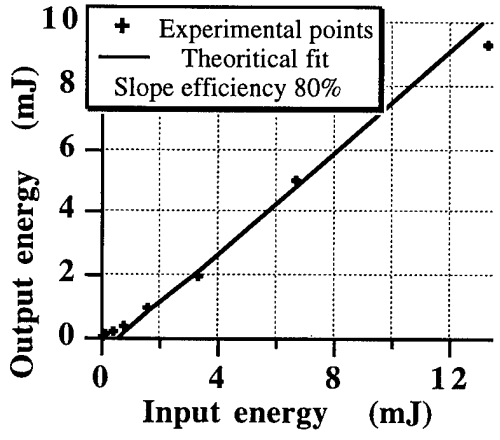

Figure 1 : Efficiency of a solid state pyrromethene 597 laser.

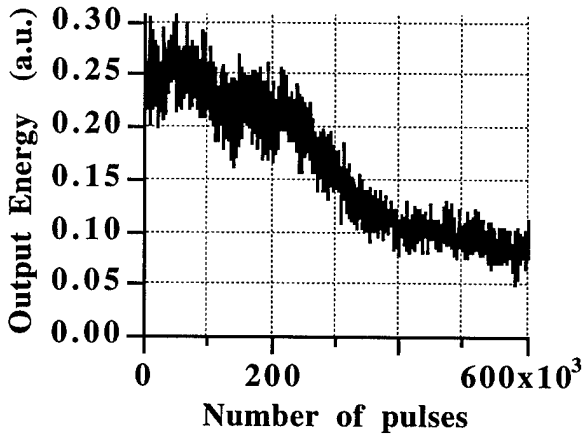

Figure 2: Output energy evolution of a solid state pyrromethene 597 laser.

High Average Power Scaling of a Compact, Q-Switched, Diode Pumped, Nd:YAG Laser

J. L. Dallas and R. S. Afzal

NASA/Goddard Space Flight Center
Greenbelt, MD 20771
Phone: (301) 286-4047, Fax: (301) 286-1750
E-mail: joe_dallas@gsfc.nasa.gov

NASA-Goddard is developing a breadboard laser for spaceborne altimetry which requires the conflicting specifications of high efficiency, small size, TEM_{00} mode, high energy, short pulsewidths (< 6 ns), 40 Hz repetition rate, and billion shot lifetime. As an extension to this research, we have investigated scaling this laser to higher repetition rates to support lidar programs desiring greater sampling resolution. Pushing a laser to higher average powers is usually limited by enhanced pumped induced thermal aberrations. The magnitude of these aberrations and their effect on the laser performance are a function of the laser design. We have investigated these parameters using the highest power laser diode bars commercially available to pump a Nd:YAG slab following an innovative pump scheme previously reported.[1] In a particularly simple laser design, we obtained 4 ns Q-switched pulses in a range from 40 to 975 Hz, with over 2.4 mJ in a gaussian-like mode. Under CW operation, over 6 watts output with a 41 % slope efficiency was measured. The small size, high efficiency, and high repetition rate of this laser makes it an attractive source for many applications; including broad coverage air and spaceborne lidar, chemical remote sensing, and micro-machining.

A number of approaches have been taken to efficiently capture and direct the highly diverging light from the extended source of high power laser diodes.[2,3,4] Most of these techniques excel for CW diodes. High power Quasi-CW (QCW) bars typically have many more individual emitters and poorer beam quality than CW bars. Our laser utilized a 100 W, QCW, water cooled, laser diode (SDL-3255-C1) in a very simple configuration. The output was initially focused in the vertical axis by an uncoated, 1 mm diameter, cylindrical glass rod. A stripe of light was formed 5 mm from the diode with over 80 % of the power transmitted through a 300 μm slit placed at the focal point. The diode/rod module was positioned to side pump a Nd:YAG slab (Figure 1). The 1.2 x 5 x 13 mm crystal was fabricated to provide a seven bounce zig-zag path through the medium. Its ends were uncoated with anti-parallel Brewster faces. The 5 x 13 pump face was anti-reflection (AR) coated and the opposite face was high-reflection (HR) coated for the diode wavelength of 808 nm. The HR side was mounted to a water cooled heat sink using a silicon elastomer. A 10 cm long optical cavity was established by a 2.5 m radius of curvature HR mirror and a flat 75 % reflecting output coupler. The cavity modes were apertured in the horizontal axis by the thickness of the Nd:YAG slab and receive gain in the vertical axis only within the narrow pump stripe region.

The pump diode was driven with 110 amp, 200 μs pulses at a 500 Hz repetition rate. Though the diode was specified to lase at 808 nm while at 500 Hz, this 10 % duty factor is 2.5 times the vendor recommended value. The Nd:YAG laser yielded 2.75 watts of average, long pulse, power with 8.7 watts of incident pump power. A slope efficiency of 44.8% was measured. The spatial profile maintained a single, gaussian-like mode from 10 to 500 Hz.

A KD*P electro-optic Q-switch, thin film polarizer, and quarter-wave plate were added to this cavity. The output coupler was changed to a 60 % reflector. Upon Q-switching at 500 Hz, pulsewidths of 4 ns

(FWHM) were produced with an energy of 2.4 mJ. The output beam's spatial profile, at 500 Hz, remained single lobed with an M^2 of 2.1. To study the source of performance degradations, this laser was placed within a station for autonomously monitoring its vital signs: power, pulsewidth, beam profile, coolant temperature, diode drive current, and Q-switch drive voltage.[5] At 500 Hz, it ran continuously for 5.5 months accumulating 7 billion shots. The energy per pulse degraded by only 38 % to 1.5 mJ and the pulsewidth increased by 37 % to 6.5 ns. These performance degradations were directly attributable to the decay of the pump diode output power and an upward shift of its emission wavelength.

The diode pump was replaced and coupled directly to the Nd:YAG slab without the glass focusing rod. This alternate pumping method preserved the laser performance. The laser was Q-switched at a range of repetition rates from 500 to 975 Hz. At 975 Hz (19.5 % duty factor), over 2.5 mJ per 4 ns pulse was obtained (Figure 2). The spatial profile became more elliptical at higher repetition rates yet remained single lobed. The M^2 measured 3.0, 2.7, and 1.9 for 950, 750, and 500 Hz respectively. Second and fourth harmonic generating nonlinear crystals (KTP/KDP) were placed in series outside the cavity. Without any optimization, the incident 80 MW/cm^2 peak intensity beam created 1.3 W at 532 nm and 280 mW at 266 nm, at a frequency of 950 Hz..

At the extremum of higher repetition rates, the QCW laser diode was replaced with a 20 W CW diode (SDL-3470-S). The cavity was shortened to 6 cm with a 3.0 m radius of curvature HR mirror and 94 % reflecting output coupler. Directly coupling the diode to the slab yielded 6 watts output for 17 watts pump with a slope efficiency of 41% and an $M^2 = 3.1$. Using a low power CW Nd:YAG probe laser, a small signal gain coefficient of 0.31 was measured.

Removing the cylindrical focusing rod from the diode pumping scheme simplifies the design, reduces the number of parts, eases the alignment procedure, and slightly decreases the ellipticity of the beam profile, without effecting performance. A model was derived which calculates the expected inversion distribution within the slab given the diode divergence angles, its distance from slab, and the lasing medium's material properties. The full divergence angle of the CW diode was measured to be 32° at the FWHM point and 57° at $1/e^2$. The QCW diodes diverge similarly. With the diode emitters located 250 μm from the Nd:YAG slab, a $1/e^2$ pump stripe radius of 400 μm is predicted. The induced fluorescence was imaged by removing the cavity end mirrors and looking down the optical axis with a filtered CCD camera. The $1/e^2$ stripe radius was measured to be 368 μm, in agreement with the model. This stripe is larger than what was produced when using the diode focusing rod yet it remains smaller than the 426 μm bare cavity eigenmode, for efficient energy extraction.

Thermal lensing scales with the pump distribution as well as average power.[6] The induced optical path difference (OPD) was measured at various average pump powers using a Wyko interferometer (Figure 3). A reference fille was recorded for the un-pumped, mounted slab which takes into account fabrication errors, end effects, alignment tilts, and stressed generated distortions. This reference was subtracted from the OPD distribution recorded at each pump power. According to Tidwell *et al.*, the actual thermal distortion is decreased while lasing by a factor of 10-15%.[7] The distributions reveal the source and strength of the thermal aberrations. Defocus and spherical are the largest induced Seidel aberrations. The mixing provided by the zig-zag path effectively minimizes the OPD along one axis. The thermal effects in the uncompensated axis change the cavity eigenmode and deform the intracavity beam yet still allows only lowest order transverse mode operation. The quality of the beam suffers as indicated by the M^2 values in Figure 2.

In conclusion, we have demonstrated a simple scheme for producing a high repetition rate, high average and peak power, Q-switched laser. The use of coupling optics has been eliminated, creating a simple and easily assembled design. Lowest order transverse mode operation is assured with beam quality scaling with repetition rate. The high gain and short cavity length allow for the creation of short Q-switched pulsewidths. Efficient harmonic generation into the green and UV is made possible by the high peak powers. We have mapped-out the performance characteristics of the laser over various repetition rates and billions of shots lifetime. Future work includes parametric studies through modeling of the cavity dynamics.

References

1. R. S. Afzal and M.D. Selker, Opt. Lett. **20**, 465-467 (1995).
2. W.L. Nighan, D. Dudley, M.S. Keirstead, in *Conference on Lasers and Electro-Optics,* 1995 Technical Digest Series, Vol. 15 (Optical Society of America, Washington, D.C., 1995), CMD5
3. W.A. Clarkson, A.B. Neilson, and D.C. Hanna, in *Conference on Lasers and Electro-Optics,* 1994 Technical Digest Series, Vol. 8 (Optical Society of America, Washington, D.C., 1994), p. 360.
4. Th. Graf and J.E. Balmer, *Advanced Solid State Lasers*, 1995 Technical Digest, (Optical Society of America, Washington, D.C., 1994), WC6
5. J.L. Dallas, R.S. Afzal, and M.A. Stephen, Submitted for Publication in Applied Optics.
6. M.E. Innocenzi, H.T. Yura, C.L. Fincher, and R.A. Fields, Appl. Phys. Lett., **56**, #19, 1831-1833 (1990).
7. S.C. Tidwell, J.F. Seamans, M.S. Bowers, and A. K. Cousins, IEEE JQE, **28**, #4, 997-1009 (1992).

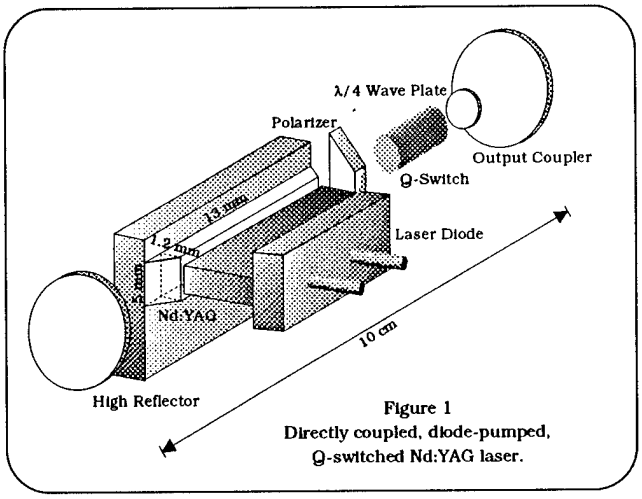

Figure 1
Directly coupled, diode-pumped, Q-switched Nd:YAG laser.

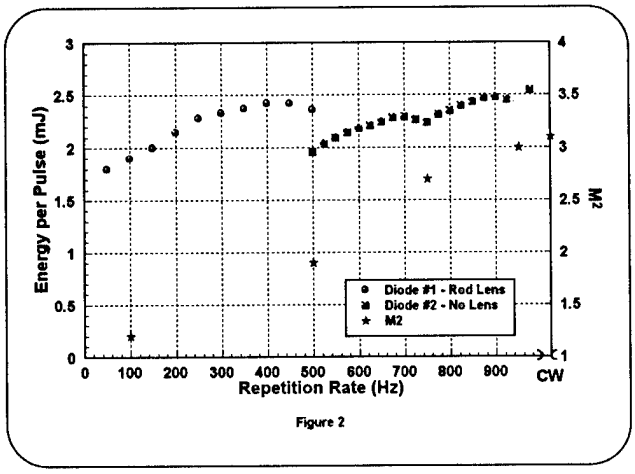

Figure 2

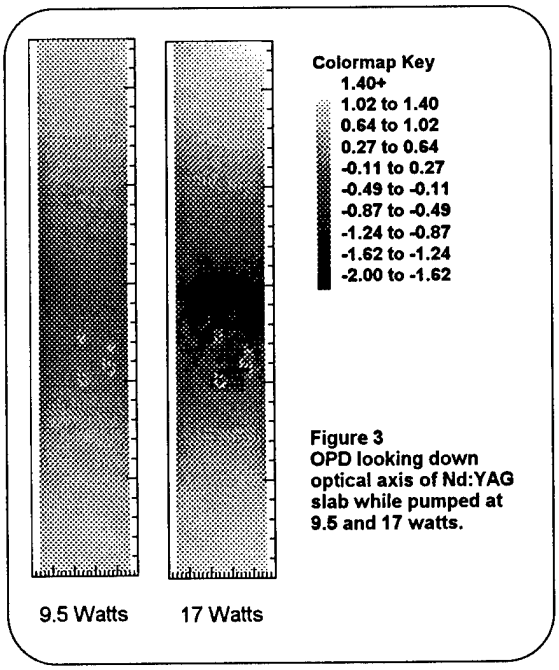

Figure 3
OPD looking down optical axis of Nd:YAG slab while pumped at 9.5 and 17 watts.

Enhanced Performance Flashlamp-Pumped Ti:Sapphire Laser with Phase Conjugate Resonator.

N. W. Hopps, M. R. Dickinson and T. A. King.
Laser Photonics Group,
Department of Physics and Astronomy, University of Manchester,
Manchester M13 9PL, United Kingdom.
Tel: +161 275 4292 Fax: +161 275 4293

INTRODUCTION

Phase conjugation by stimulated Brillouin scattering (SBS) has been shown to compensate for beam distortions in lasers caused primarily by the thermal loading of the laser material upon pumping. This technique utilises the phase-conjugate nature of the scattered radiation [1] to accomplish aberration corrections. Such systems are used for both laser amplifiers and oscillators [2].

This paper describes the development and performance of, to the authors' knowledge, the first reported flashlamp-pumped titanium:sapphire laser incorporating a Brillouin mirror.

LASER DESIGN

The laser was based on a titanium:sapphire laser rod with dimensions of 8 mm by 200 mm, pumped using two xenon filled flashlamps. This system, with a conventional back mirror with a radius of curvature of 5 m and a flat output coupler with 50% reflectivity, could deliver about 1.5 J for 300 J input in ~5 μs, with a shot-to-shot stability of 2%.

The SBS oscillator is shown in figure 1. Initially, laser oscillations build up between the output coupler and the diffraction grating. This radiation induces a hypersonic wave in the SBS medium [3]. Further incident radiation enhances the sound wave and scatters from it. A large component of the scattered radiation is phase-conjugate with the incident light. Hence, a phase conjugate resonator (PCR) is established between the output coupler and the SBS cell.

The output coupler was flat with 50% reflectivity. The Littrow grating had 1200 lines per millimetre and provided coarse tuning and narrowed the spectral width of the laser to ~200 GHz. A solid etalon, with broad-band coatings, could be used to reduce the linewidth further to ~10 GHz. An intra-cavity telescope focused the laser oscillations into a cell containing the SBS medium and also expanded the cavity modes onto the grating. The lens focal lengths were 50 mm and 85 mm. Both liquid (acetone) and gaseous (SF_6 at 20 atm) SBS media were investigated.

It has been demonstrated that the SBS reflectivity is enhanced by ensuring the Brillouin downshifted radiation can oscillate as a longitudinal mode of both the conventional Littrow cavity and the PCR [3]. Therefore, when using SF_6, the optical length of the conventional resonator and PCR was set to 180 cm and 120 cm, respectively. Acetone required a shorter cavity with optical lengths of 114 cm and 85 cm.

RESULTS

1) Energy measurements

Losses introduced by the Littrow grating caused a much diminished output. By monitoring how much energy is lost as the zeroth order of diffraction and comparing it with the energy transmitted through the output coupler, the amount of stimulated Brillouin scatter was estimated without interfering with the laser cavity itself. The ratio of output from both

ends of the laser was seen to increase by a factor of ~3 for each medium, indicating significant SBS reflectivity. Large shot-to-shot energy variations can be explained as SBS reflectivity variations in each pulse.

Bubbles were formed in the acetone at the focus of the telescope when the laser was fired. The resulting disturbance caused a reduction in efficiency of the scattering process. When the repetition rate of the laser was greater than 0.5 pulses per second, laser action became intermittent. Results for SF_6, however, are more encouraging. In this case, the energy transmitted through the output coupler increased to ~240 mJ as a consequence of the stimulated scattering in the cell. This would be expected when the cell itself does not introduce significant loss, since the greatest losses, seen at the grating, become less influential as the SBS reflectivity becomes large. The fact that the output stability exceeds that of the acetone based system, suggests that the SBS reflectivity varies less when using the gaseous medium. This would be expected because it has a faster recovery time. The energy stability is still poorer than with no SBS cell present, however. The energy readings for SF_6 were taken with the cavity lengths appropriate for the acetone Brillouin downshift. This is because the cavity length was such that diffraction losses overcame the benefit of having properly matched longitudinal modes.

These measurements were taken without the etalon since SBS was readily achievable and the improvement in SBS reflectivity, which may be expected by using a narrower linewidth, was more than compensated for by the lower intensities caused by the additional loss of the etalon.

2) Temporal profile measurements

The temporal profile of the laser emission with no SBS cell present shows the familiar relaxation oscillations on a time scale of the cavity decay time. However, when an SBS medium is inserted into the cavity, the output forms distinct spikes approximately 60 ns long (see Fig 2). This is the case for both acetone and SF_6 as the scattering medium. This is the passive Q-switching phenomenon which has previously been reported in neodymium lasers with SBS mirrors [3-6]. When the loss in the part of the cavity between the SBS cell and the grating was increased by inserting an etalon or an aperture, the number of peaks in one pulse was reduced and higher peak powers obtained ,as expected.

Each peak in figure 2 exhibits modulation with a period which very closely matches the round trip time of the phase-conjugate cavity (8 ns). When the cavity was shortened to match the acetone downshift and SF_6 used, the resultant trace shows modulation with a period equal to the conventional cavity round trip time. This suggests that the SBS process is less effective under these conditions. Acetone always produced modulation with the period of the conventional round trip time.

3) Spectral profile measurements

Spectral profiles were taken using a pulsed laser spectrum analyser (Burleigh PLSA-3500). Figures 3 and 4 shows the effect on the linewidth of introducing a Brillouin medium (acetone) into the laser cavity. SF_6 yielded similar results. With no SBS cell, the spectral width is ~250 GHz. However, when the Brillouin medium is introduced, the linewidth shows a pronounced decrease to ~7 GHz. It appears that the Brillouin process is enhancing one frequency at the expense of the others, which is expected since the SBS reflectivity is greatest for the frequency with the highest intensity.

4) Divergence measurements

The divergence of the beam was measured with and without each Brillouin medium. A significant reduction in divergence was observed in each case, with a minimum of roughly twice the diffraction limit for SF_6, an improvement of a factor of ~8.

It was observed that ~10% of the shots using an SBS medium produced a highly extended spot with obvious structure, corresponding to very few high order transverse modes. This would occur if these modes were excited before lower order modes could be established.

The research was funded by the UK Ministry of Defence.

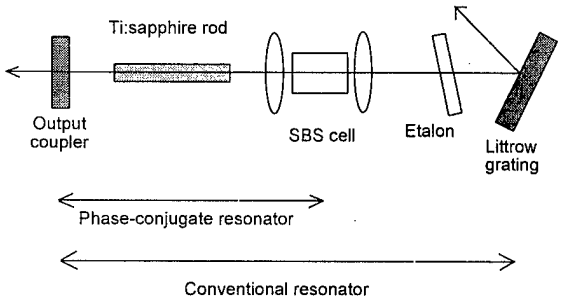

Figure 1: Schematic of the SBS laser resonator.

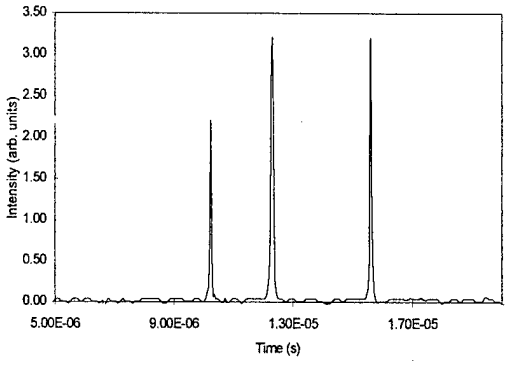

Figure 2: Temporal profile of laser pulse with 20atm SF_6 SBS cell.

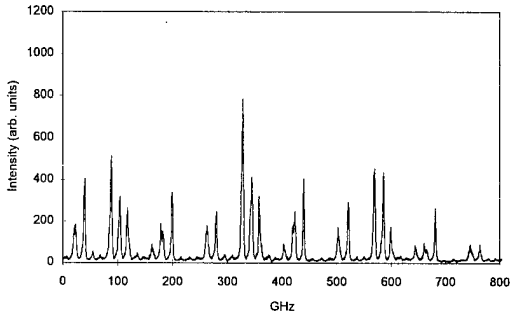

Figure 3: Etalon fringes produced by spectral output of laser with no SBS cell.

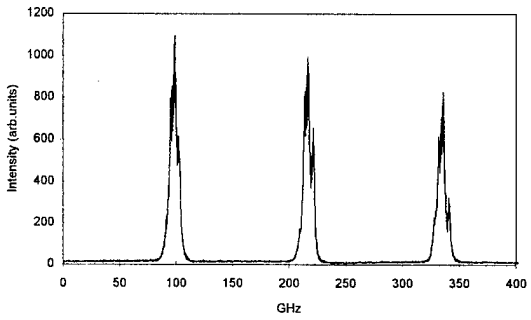

Figure 4: Etalon fringes produced with acetone SBS cell.

REFERENCES

1. P. Suni and J. Falk, "Theory of phase conjugation by stimulated Brillouin scattering." J. Opt. Soc. Am. B **3**, 12, 1681-1691 (1986)
2. For example: J. Soan, M. J. Damzen, V. Aboites, M. H. R. Hutchinson, "Long-pulse self-starting stimulated-Brillouin-scattering resonator." Opt. Lett. **19**, 11, 783-785 (1994)
3. H. Meng and H. J. Eichler, "Nd:YAG laser with phase-conjugating mirror based on stimulated Brillouin scattering in SF_6 gas." Opt. Lett. **16**, 569-571 (1991)
4. N. Il'ichev, A. A. Malyutin, P. P. Pashinin, "Laser with diffraction limited divergence and Q-switching by stimulated Brillouin scattering." Sov. J. Quantum Electron. **12**, 9, 1161-1164 (1982)
5. J. Eichler, R. Menzel, D. Schumann, "10-W single-rod Nd:YAG laser with stimulated Brillouin scattering Q-switching mirror." Appl. Opt. **31**, 24, 5038-5043 (1992)
6. S. Seidel and G. Phillipps, "Pulse lengthening by intracavity stimulated Brillouin scattering in a Q-switched, phase-conjugated Nd:YAG laser oscillator." **32**, 36, 7408-7417 (1993)

Slope efficiency and gain measurement of highly Cr^{4+}-doped forsterite

Takashi Fujii, Masahiro Nagano and Koshichi Nemoto

Electrophysics Department, Komae Research Laboratory,
Central Research Institute of Electric Power Industry
11-1 Iwado Kita 2-chome, Komae-shi, Tokyo 201, Japan
Telephone: +81-3-3480-2111, Facsimile: +81-3-3488-6697
e-mail address: fujii@komae.denken.or.jp

A chromium-doped forsterite (Cr: Mg_2SiO_4) laser is a tunable laser, for which wavelength tunability from 1167 nm to 1345 nm[1] and from 1130 nm to 1367 nm[2] has been reported. It is attractive for applications in optical communication, LIDAR and spectroscopy. Moreover, its second-harmonic generation is expected to cover the wavelength region from 585 nm to 670 nm which is useful for various isotope separations[3].

Up to now the chromium concentration in forsterite has been rather low (~0.04 at.%)[4,5]. Therefore, the absorption coefficient of the crystal at the pump beam wavelength of 1064 nm has been small. Recently, improvement of the growth technique has enabled doping of higher Cr^{4+} concentration[6]. By using the highly Cr^{4+}-doped forsterite, the pump radiation can be used more efficiently, which leads to a decrease of crystal length. Moreover, diode pumping can be realized.

In this paper, we report the laser oscillation characteristics and the gain measurement of a forsterite sample which has a high chromium concentration of 0.13-0.14 mol% ($1.8\text{-}1.9\times 10^{19}$ cm^{-3})[7,8]. The chromium-doped forsterite is treated in the space group Pmnb, and the lattice parameters of a unit cell are a = 5.99 Å, b = 10.20 Å and c = 4.76 Å.

The chromium-doped forsterites used in the experiment were $5\times5\times5$ mm^3 cubic samples grown by Mitsui Mining and Smelting Co., Ltd. Laser oscillation experiments of the highly chromium-doped forsterite was performed. Two samples which was AR-coated centered at 1200 nm on different crystal faces were tested. One was AR-coated on the crystal faces perpendicular to the a-axis, and the pump beam was propagated along the a-axis. The other was AR-coated on the crystal faces perpendicular to the c-axis, and the pump beam was propagated along the c-axis. The experimental setup for laser oscillation is almost equal to that shown in previous paper[7]. A hemispherical resonator was formed by a 115-mm-radius back mirror and a flat output mirror. Three output mirrors of which transmissions T in the 1150-1250 nm spectral range are 29.0 %, 9.2 % and 1.3 % were employed. The angles of resonator mirrors were adjusted to obtain the highest output energy. The crystal was longitudinally pumped with 1064 nm pulses from a Q-switched Nd: YAG laser (Quanta-Ray DCR-2) operating with a 10 Hz repetition rate. The pump beam was polarized along the b-axis.

Figure 1 shows the output laser energy versus absorbed pump energy with the three output mirrors of different transmission for the forsterite sample which is AR-coated on the crystal faces perpendicular to the a-axis. In the case of using the 29.0 % transmission mirror, the maximum output energy of over 1.2 mJ was obtained with the absorbed pump energy of 8.6 mJ. Moreover, the slope efficiency of 25 %, which is the maximum value yet achieved in the case of pulse operation to our knowledge, was obtained. 70 % of the input pump energy was effectively absorbed even though the crystal was only 5 mm thick. Although the length of

the gain region of this experiment is only 5 mm, we can achieve high slope efficiency due to high population inversion density. The threshold absorbed pump energy was slightly larger because the pump beam spot size was larger than the cavity mode spot size. Figure 2 shows the output laser energy versus absorbed pump energy for the forsterite samples when the pump beam was propagated along the a-axis and the c-axis. In this experiment, the two samples which were AR-coated on the crystal faces perpendicular to the a-axis and the c-axis were used for each respective pump beam propagating direction. The laser output characteristics are almost equal in both cases. The fluorescence characteristics, especially the polarization, differ between the fluorescence emitted along the a-axis and the c-axis[8]. However, in the laser output characteristics, no significant differences were observed between the two cases of lasing direction in the crystal.

One pass gain of the highly chromium-doped forsterite was measured by pump-and-probe technique. The forsterite sample was pumped by 1064 nm pulses from a Q-switched Nd: YAG laser (Quanta-Ray GCR-250) operating with 10 Hz repetition rate. The pump beam was focused to the radius of 1.4 mm at the crystal surface by a 1500 mm focal length lens. The 1224 nm output beam of 6 μJ from a optical parametric oscillator (OPO, Quanta-Ray MOPO-730) was used as the probe beam and was focused to the radius of 600 μm at the crystal surface by a 700 mm focal length lens. The OPO was pumped by 355 nm pulses from the same Nd: YAG laser used for pumping of the forsterite sample. The delay time between pump and probe beam was 10 nsec at the crystal. The pump beam and probe beam were polarized along the b-axis of the crystal. In order to compensate the fluctuation among each pulse, a part of the probe beam separated by a beam splitter before incident to the sample was used as a reference beam. The waveforms of the probe beam passing through the sample and the reference beam were monitored by a fast detector with the delay time between both beams of 20 nsec. Figure 3 shows the probe beams and the reference beams with and without pumping. The forward tail of the amplified probe beam is the residual pump beam. The average one pass gain of 1.7 was obtained when pumping energy density was 0.84 J/cm^2. Moreover, we calculated the effective gain cross section using this data and the order of the effective gain cross section, which was roughly estimated, was in agreement with previously published values[9].

In conclusion, laser oscillation was achieved using the forsterite sample which has a high chromium concentration of 0.13-0.14 mol% and was only $5\times5\times5$ mm^3. The maximum output energy of over 1.2 mJ, and high slope efficiency of 25 %, which is the highest value achieved in the case of pulse operation to our knowledge, were obtained. The one pass gain measured by pump-and-probe technique was 1.7 for 5 mm gain length when pumping energy density was 0.74.

References

1. V. Petricevic, S. K. Gayen, and R. R. Alfano, Appl. Opt. **28** (1989) pp.1609-1611.
2. V. G. Baryshevskii, M. V. Korzhik, A. E. Kimaev, M. G. Livshits, V. B. Pavlenko, M. L. Meil'man, and B. I. Minkov, Zh. Prikl. Spektrosk. **53** (1990) pp. 7-9.
3. I. L. Bass, R. E. Bonanno, R. P. Hackel, and P. R. Hammond, Appl. Opt. **31** (1992) pp. 6993-7006.
4. V. Petricevic, S. K. Gayen, and R. R. Alfano, Appl. Phys. Lett. **52** (1988) pp.1040-1042.
5. V. Petricevic, A. Seas, and R. R. Alfano, Optics Lett. **16** (1991) pp. 811-813.
6. Y. Yamaguchi, K. Yamagishi, and Y. Nobe, J. Crystal Growth **128** (1993) pp. 996-1000.
7. T. Fujii, M. Nagano, and K. Nemoto, in Advanced Solid-State Lasers, Memphis, Tennessee (1995).
8. T. Fujii, M. Nagano, and K. Nemoto, in Solid State Lasers and Nonlinear Crystals, Proc. SPIE 2379, pp. 68-72 (1995).

9. V. Petricevic, S. K. Gayen, and R. R. Alfano, in Advanced Solid-State Lasers (1990) pp. 73-78.

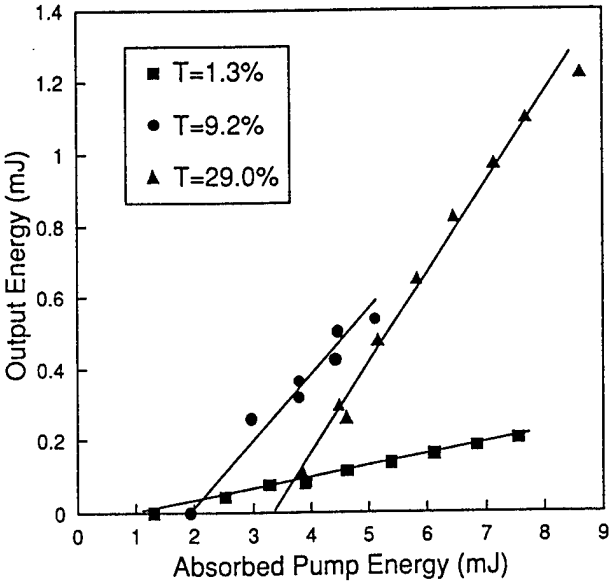

Fig. 1. Output laser energy versus absorbed pump energy of 0.13-0.14 mol% chromium concentration forsterite with three output mirrors of different transmission when pumped by 1064 nm from Nd: YAG laser.

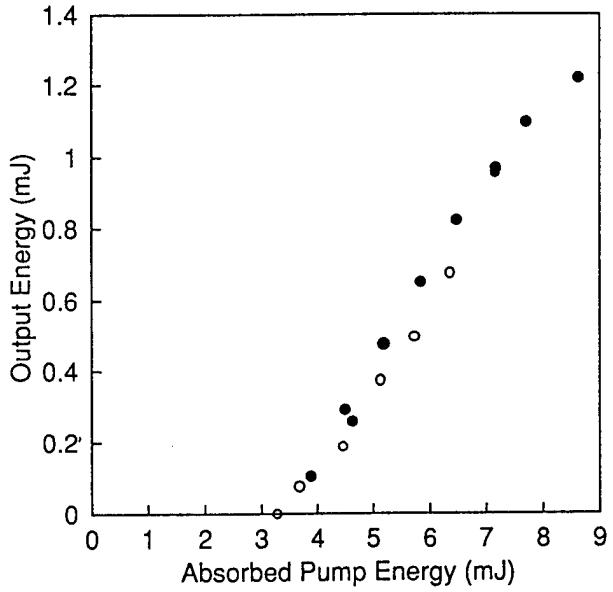

Fig. 2. Output laser energy versus absorbed pump energy of 0.13-0.14 mol% chromium concentration forsterite when pumped by 1064 nm from Nd: YAG laser: ● pump beam was propagated along a-axis and ○ along c-axis.

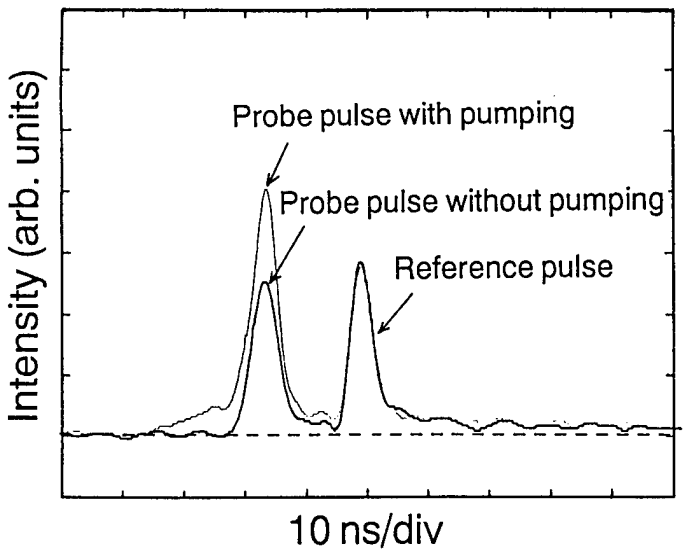

Fig. 3. Pulse waveforms of probe and reference beams with and without pumping in gain measurement by pump-and-probe technique.

Passive Q-switching of the Erbium:Glass Laser Using Er^{3+}:CaF_2

Marly B. Camargo,[a] Robert D. Stultz,[b] and Milton Birnbaum
Center for Laser Studies
University of Southern California
DRB 17, University Park
Los Angeles, CA 90089-1112
Tel.: (213) 740-4235, Fax: (213) 740-8158

Eyesafe Er:glass lasers (1.54 μm) are interesting and useful for a large number of applications such as communications, optical atmospheric studies, traffic enforcement, obstacle avoidance, and air defense.[1-4] Many applications require short 1.5 μm pulses with high peak power which can be obtained by Q-switching the Er:glass laser. A saturable absorber Q-switch is the simplest and least expensive Q-switch option, also permitting a very compact resonator size.

Er:glass is a three-level laser where the 1.54 μm transition, $^4I_{13/2} \rightarrow {}^4I_{15/2}$, terminates in the ground-state. Consequently, many Er-doped materials may be used as saturable absorber Q-switches because of the significant overlap of the Er^{3+}:host absorption spectra with the Er:glass emission spectrum.

Er:CaF_2 possesses a broad, continuous absorption spectra nearly coincident with the emission spectrum of the Er:glass (Fig. 1). The shorter effective relaxation lifetime of Er:CaF_2 avoids the free-running problems encountered with other Er-doped crystal Q-switches, such as Er^{3+}:$Ca_5(PO_4)_3F$ (or Er:FAP).[5] The Er:CaF_2 crystals used in these experiments, with 2.0 and 3.5% of Er, were obtained from Optovac, Inc.

Undoped CaF_2 crystals have the cubic structure of fluorite with space group Fm3m.[6] The divalent cations (Ca^{2+}) are at (0,0,0) with the fluorine ions at ±(1/4,1/4,1/4) in an FCC lattice. The presence of Er^{3+}, which replaces the Ca^{2+} ion, distorts the otherwise cubic symmetry due to several possible charge compensation mechanisms, i.e. multiple sites with various crystalline field symmetries are possible. As a result, the optical spectra of Er^{3+} in CaF_2 are complex and characterized by the presence of a large number of overlapping inhomogeneously broadened electronic and/or vibronic lines. The broad (full width at half maximum ≈ 66 nm) absorption band of our (3.5%)Er:CaF_2 crystal with the maximum around 1.54 μm is shown in Fig. 1, along with Er:glass (Kigre QE-7) fluorescence. The absorption spectrum for the (2%)Er:CaF_2 was the same, except the peak absorption coefficient was 2.7 cm^{-1}, instead of 4.4 cm^{-1}.

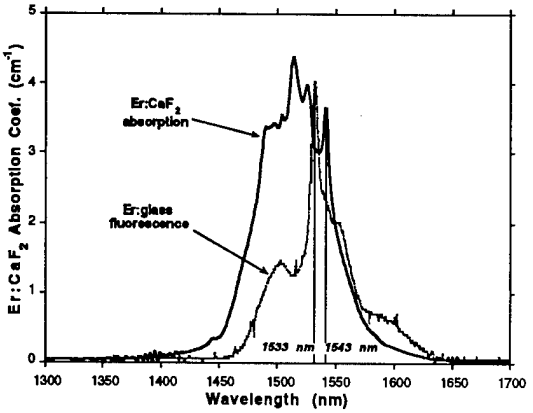

Figure 1. (3.5%)Er:CaF_2 absorption and Er:glass fluorescence.

An Er:glass laser, passively Q-switched with a U^{2+}:SrF_2 saturable absorber Q-switch,[7] was used as the excitation source for the lifetime experiments. The laser output energy was 5 mJ and the pulsewidth was 138 ns, full width at half maximum (FWHM). This Q-switched laser had a wavelength of 1533 nm. The Er-crystals were placed near the focus of a +15 cm focal length lens, used to concentrate the laser beam into a 400 μm spot and produce an incident fluence of about 4 J/cm^2.

The crystal fluorescence (Fig. 2) was collected using a fast (f/1.2) glass lens. The light signal was detected by a Ge photodiode (Judson, J16-series). A thin silicon crystal was placed in front of the Ge

diode to block possible emissions associated with Er^{3+} energy levels higher than $^4I_{13/2}$.

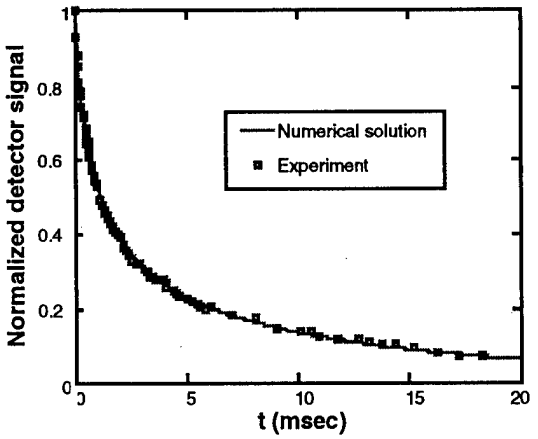

Figure 2. (3.5%)Er:CaF_2 fluorescence.

Multi-ion processes are strong in Er:CaF_2, typically resulting in highly nonexponential $^4I_{13/2}$ fluorescence decays, even with relatively low Er concentrations. An attempt to model the observed decay rates in terms of pair theory[8] proved unsuccessful. Instead, we used the following rate equation for the Er^{3+} $^4I_{13/2}$ population density (m), which includes both quadratic and cubic terms:

$$\frac{dm}{dt} = - \alpha_1 m - \alpha_2 m^2 - \alpha_3 m^3 \qquad (1)$$

Using the method of partial fractions, equation (1) can be put in the following closed transcendental form:

$$\mu\left(\frac{1+a\mu}{1+a}\right)^{\frac{a}{b-a}}\left(\frac{1+b\mu}{1+b}\right)^{\frac{b}{a-b}} = e^{-\alpha_1 t} \qquad (2)$$

where $\mu \equiv m/m_0$, m_0 is the initial ($t = 0$) value of m, and a, b are defined by:

$$a \equiv \frac{F_1 + [F_1^2 - 4F_2\alpha_1]^{0.5}}{2\alpha_1} \quad b \equiv \frac{F_1 - [F_1^2 - 4F_2\alpha_1]^{0.5}}{2\alpha_1} \qquad (3)$$

where $F_1 \equiv \alpha_2 m_0$, $F_2 \equiv \alpha_3 m_0^2$. We numerically solved equation (2), and adjusted the parameters a, b, and α_1 to yield the best fit to the measured Er:CaF_2 fluorescence (solid curve in Fig. 2). When Q-switching, the faster decay near the excitation time ($t = 0$) is important. With the (2%)Er:CaF_2 crystal, the initial (effective) lifetime was about 45 μs, whereas the slower (exponential) component was over 12 ms.

The absorption cross-section for Er:CaF_2 was obtained by bleaching the 2% crystal with a short pulse (14 ns, FWHM) of 1543 nm light from a Raman-shifted Nd:YAG laser, with a spectral linewidth of less than 1 nm. The measured Frantz-Nodvik saturation fluence ($h\nu/\sigma_{eff}$) yielded an effective absorption cross section (σ_{eff}) of 1.43 x 10^{-20} cm^2.

Two Er:CaF_2 samples were used to perform the Q-switch experiments: a) 1.0 mm thick piece with 2.0% Er concentration, and b) a 1.1 mm thick piece with 3.5% Er concentration. Both switches were cut and polished with flat and parallel surfaces, and were used uncoated. Since the Er:CaF_2 absorption cross-section value is comparable to that of glass, intracavity focusing was necessary to obtain Q-switching.[5]

The Q-switched resonator cavities, both of which possessed stable Gaussian modes, are shown in Fig. 3. The cavity shown in Fig. 3a was flat-flat and with mirror reflectivities of 100% and 88% (outcoupler), at 1533 nm. The length was 21 cm, and a +7.6 cm lens was used to focus the laser beam into the Q-switch. The output mirror in Fig. 3b had a 94% (1533 nm) reflectivity, with a 2.5 cm radius of curvature. The cavity length in this case was 17.5 cm, and a +5 cm intracavity lens was used. All the resonator internal components (except the Q-switches) were AR-coated at 1.54 μm. The Q-switches were always positioned between the output mirror and the intracavity lens, close to the Gaussian beam waist.

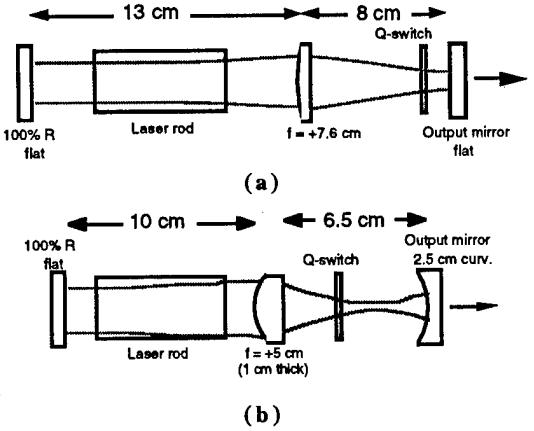

Figure 3. Er:glass resonator cavities.

The $Er:CaF_2$ Q-switch results were obtained using a QE-7S, 3 x 50 mm Er:glass rod, pumped by a Xenon flashlamp with a FWHM pulsewidth of approximately 600 μs. The free-running laser had a threshold of about 14 J with an output slope efficiency of 0.51% for the cavity in Fig. 3b.

The results for both 2% and 3.5% $Er:CaF_2$ Q-switches are summarized in Table I. The best results were obtained with the (2%)$Er:CaF_2$ switch, using the cavity in Fig. 3b. A typical output pulse obtained is shown in Fig. 4, for this configuration. The Q-switched pulse was recorded using a fast InGaAs photodiode, and the Q-switched output energy was measured using a Scientech calorimeter.

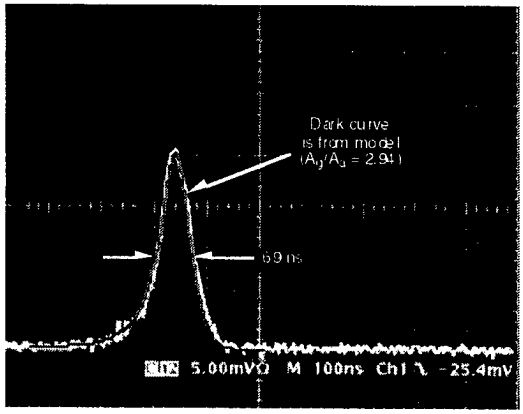

Figure 4. Q-switched pulse.

A saturable absorber Q-switch rate equation model was applied to the (2%)$Er:CaF_2$ Q-switch. Using the parameters from Table I (losses due to Fresnel reflections from the uncoated surfaces were also included), and the measured value for the absorption cross-section (σ_{eff}), the theoretical model predicted a pulsewidth of 18 ns and an output energy of 36.6 mJ. When the focusing parameter,[5] A_g/A_s, was adjusted to 2.94 in the model, the simulated output pulse shape was identical to experiment (see Fig. 4). The corresponding theoretical output energy was 19.3 mJ.

In conclusion, we have demonstrated a new saturable absorber Q-switch material, $Er^{3+}:CaF_2$, for the 1.54 μm Er:glass laser. We achieved reliable operation with output pulses of 11 mJ, 69 ns in a 17.5 cm laser cavity. The $Er:CaF_2$ did not exhibit any of the free-running problems previously encountered with Er:FAP, because of the rapid initial decay of its $^4I_{13/2}$ level. The theoretical modeling for the Q-switched pulse shapes was in good agreement with experimental data.

a) Permanent address: Instituto de Pesquisas Energeticas e Nucleares, CP 11049, CEP 05422-970, S. Paulo, SP, Brazil, Financial support: CNPq/RHAE.

b) Permanent address: Hughes Electro-Optical Systems at El Segundo, CA 90245-0902.

References

1. D. W. Anthon and T. J. Pier, SPIE Proceed. **1627**, 8 (1992).
2. S. E. Sverkov, B. I. Denker, V. V. Osiko, and Yu. E. Sverkov, SPIE Proceed. **1627**, 42 (1992).
3. H. S. Keeter, D. S. Dewald, and M. A. Woodwall, SPIE Proceed. **1627**, 21 (1992).
4. S. J. Hamlin, J. D. Myers, and M. J. Myers, SPIE **1419**, 100 (1991).
5. K. Spariosu, R. D. Stultz, M. Birnbaum, T. H. Allik, and J. A. Hutchinson, Appl. Phys. Lett. **62**, 2763 (1993).
6. R. W. G. Wyckoff, Crystal Structures, Vol. 1, 2nd ed., (Wiley, New York, 1963), Chap. IV, pp. 239-243.
7. R. D. Stultz, M. B. Camargo, S. T. Montgomery, M. Birnbaum, and K. Spariosu, Appl. Phys. Lett. **64**, 948 (1994). See also Erratum: Appl. Phys. Lett. **65**, 3153 (1994).
8. R. A. McFarlane, M. Robinson, S. A. Pollack, D. B. Chang, and H. Jenssen, OSA Proceed. on Tunable Solid-State Lasers **5**, 179 (1989).

Table I. Summary of $Er:CaF_2$ Q-switched laser experiments.

Q-switch; Thickness (mm)	Resonator cavity; Er:glass rod; Intracavity lens f.l.	Internal transmit. at 1533 nm	A_g/A_s (calc.)	Output mirror reflect. (%)	Output Energy (mJ)	Thresh. (J)	Free-run. output energy (mJ)	Q-sw. pulsewidth (ns)
(2.0%)Er: CaF_2; 1.0	Fig. 3b; 3 x 50 mm QE-7S; +5cm	0.80	12.9	94	11	46	162	69
(3.5%)Er: CaF_2; 1.1	Fig. 3a; 3 x 50 mm QE-7S; +7.6cm	0.72	6.2	88	3.3	205	not measured	129

Efficient single-transverse-mode laser-diode side-pumped thulium and holmium lasers - Modelling and experiment

Gunnar Rustad, Harald Hovland, and Knut Stenersen
Norwegian Defence Research Establishment
P.O.Box 25, N-2007 Kjeller, Norway
Tel: +47 63 80 73 80 Fax: + 47 63 80 72 12
Email: gunnar.rustad@ffi.no

Thulium- and holmium-doped lasers are important sources in the eyesafe 2 μm spectral region, and have extensive applications in remote sensing, medical, and military technology. During the last decade, the development of efficient high-power laser-diode-arrays as pump sources has stimulated the interest in thulium- and holmium-doped lasers. This is particularly due to the favorable properties of thulium with respect to diode pumping, such as a strong absorption band at a diode emission wavelength around 785 nm and an efficient cross-relaxation process yielding 2 ions in the upper laser level per absorbed pump photon.

The objective of this work has been to develop lasers with a compact design and output energies in the 10 mJ range, which is typical for e.g. military laser range finding. Due to the low stimulated emission cross-section and the quasi-3-level nature of thulium and holmium lasers, relatively high pump powers are required to achieve such energies. This is difficult to obtain with end-pumped geometries, whereas side-pumped geometries may produce considerably higher pulse energies [1, 2]. However, side-pumping is often regarded as less attractive due to its lower efficiency caused by the poorer overlap between the gain profile and the resonator mode. We have improved this overlap by applying a dielectric coating which is highly reflective at the laser wavelength to the cylinder surface of the laser rod, except in two AR-coated slits directly in front of the laser-diodes. The pump light is coupled into the rod through these slits, as indicated in Figure 1. The multi-pass pumping geometry allows the pump light to be absorbed within a narrow rod cross-section, which is important for the efficiency of quasi 3-level lasers. The threshold for laser operation is significantly reduced, and this allows efficient operation to be obtained with as few as two quasi-CW 60 W laser-diode-arrays.

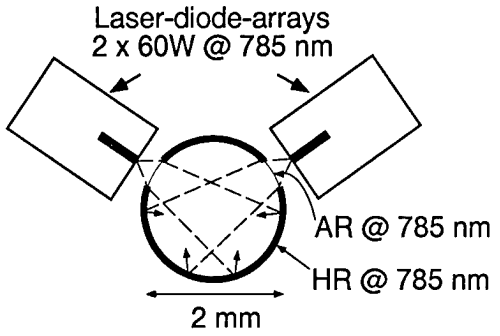

Figure 1 End view of the rod with barrel coating. The rod and the laser-diode-arrays are 1 cm long.

A detailed theoretical description of the laser is required in order to design efficient lasers with these materials. The population inversion in thulium- and holmium-doped lasers is limited by strong upconversion loss processes, particularly in the Tm:Ho-doped materials, and reduced pump rates due to depletion of the ground state. In Tm:Ho-lasers, the energy-transfer and back-transfer between the $^3F_4$ and $^5I_7$ energy manifolds result in an equilibrium between the populations in the two manifolds which will be displaced towards thulium as the holmium ground state is depleted. We have developed numerical models for the thulium- and holmium-doped lasers, accounting for these processes in addition to the spatial distributions of the gain and the resonator mode [3], and our lasers have been designed on the basis of results from such simulations.

To reduce the threshold of the laser, it is important to reduce the number of laser ions needed to be excited to obtain optical transparency in the laser material. This is done by reducing the dopant concentration, the rod length, and the gain medium and resonator mode cross-sections. In the thulium laser, the reduction of dopant concentration is limited by the reduced cross-relaxation efficiency at dopant concentrations below ~3% [4]. We used a 3.3% Tm:YAG rod for most of our experiments, but we also obtained laser operation with a 2.0% Tm:YAG rod. In the holmium laser, one of the limiting factors for the dopant concentration is that the equilibrium of the upper level populations is displaced towards thulium when the holmium dopant concentration is reduced. In our work, we used a 6% Tm, 0.5% Ho:YAG rod. The lengths of the rods were limited by the dimensions of the laser-diode-arrays, and were chosen to be 1.0 cm long. Our special pump geometry allows us to use quite narrow rod diameters and still have efficient absorption of the pump. The chosen 2 mm diameter was limited by manufacturing difficulties.

The pump intensity profile was calculated by a ray-tracing algorithm taking into account the spatial and spectral distributions of the pump light from the diodes. We calculated pump absorption efficiencies in the range of 60-80% in a 2 mm diameter 3%-6% Tm:YAG rod, assuming a R=90% coating along the cylinder surface. This is a conservative estimate of the reflectivity, but was used to account for small areas in the coating which were damaged. The pump intensity profile was then used to calculate the population inversion in the rod, accounting for upconversion losses and reduced pump rate due to ground-state depletion. Free-running laser operation was simulated by assuming that the laser operated in CW mode after threshold was reached and during the rest of the pump pulse, i.e. $E_{out} \approx P_{out,CW}(T_P - T_{th})$, where T_P is the pump pulse length, T_{th} is the time from the start of the pump pulse until threshold is reached, and $P_{out,CW}$ is the output power in CW operation. Q-switched operation was simulated by first calculating the population inversion profile at the end of the pump pulse and then applying split-step calculations accounting for the diffraction of the laser field and saturation of the gain [5]. The numerical simulations were fit to the experimental results by varying the round-trip losses.

Single-shot experimental results from free-running and Q-switched operation are compared with the results of such simulations in Figure 2. The significantly poorer performance of the Tm:Ho:YAG laser in Q-switched mode compared to free-running mode was reproduced in the simulations. The reduced output stems partly from the fact that the fraction of the population inversion that is stored

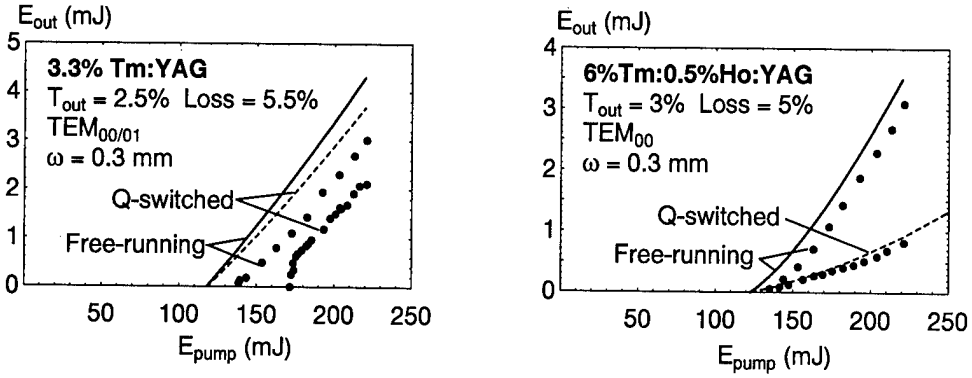

Figure 2 Comparison of single-shot experimental results and numerical simulations based on the developed models for Tm:YAG and Tm:Ho:YAG rods. Total roundtrip loss equals T_{out} +Loss. In Q-switched operation with Tm:YAG, optical damage occurred and the laser operated in a TEM_{01} mode.

in thulium (about 50%) cannot be extracted in a single Q-switched pulse, and partly from the significant upconversion losses which increase with increasing population inversion. The effect of upconversion in Q-switched Tm:Ho:YAG is shown in Figure 3, where the calculated round-trip gain in the laser material at the end of 1 and 2 ms pump pulses is shown as function of the upconversion parameter covering the range of published values (2.4-14·10^{-17} cm^3/s [6]). In the experiments, the laser oscillated in the fundamental mode. During the Q-switched experiments, optical damage occurred on the AR-coated surface on the Tm:YAG laser rod, which led to a higher threshold value and that the laser oscillated in the TEM_{01}-mode.

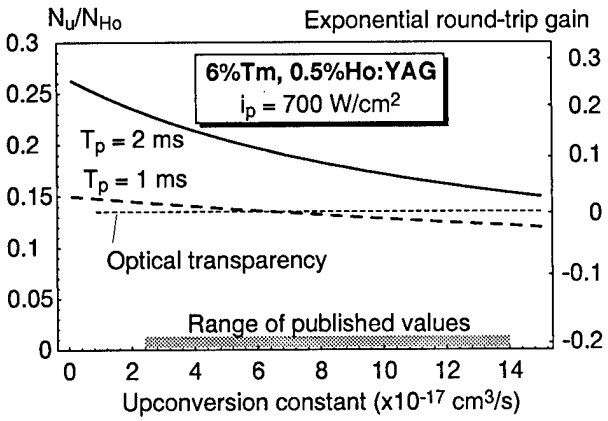

Figure 3 Calculated relative inversion of the holmium laser ions at the end of 1 and 2 ms pump pulses as function of the upconversion constant. The pump intensity is a typical value in our geometry. The exponential round-trip gain was calculated assuming room temperature and a 1cm long material.

In this work, the Q-switched output was limited to ~2 mJ, and the optical efficiencies were in the 1-2% range. A limiting factor has been the relatively high round-trip loss (~5%) and the small output coupling. The efficiency should be improved significantly by increasing the pump energy and the output coupling. The narrow dimensions of the rod make single-transverse-mode operation easily achievable. Future work will include efforts to reach 10 mJ/pulse at 10 Hz pulse rate. To obtain this and to reduce the danger for optical damage, the pump energy, the output coupling and the mode size must be increased. A geometry including 4 single-stripe-arrays is currently under investigation.

[1] S. R. Bowman, J. G. Lynn, S. K. Searles, B. J. Feldman, J. NcMahon, W. Whitney, D. Epp, G. J. Quarles and K. J. Riley, Opt. Lett. **18** (1993), 1724-1726.

[2] M. G. Jani, N. P. Barnes, K. E. Murray and G. E. Lockard, Opt. Lett. **18** (1993), 1636-1638.

[3] G. Rustad, Dr Scient-thesis, University of Oslo, Norway, 1994.

[4] G. Armagan, A. M. Buoncristiani, W. C. Edwards, A. T. Inge and B. DiBartolo, OSA Proceedings on Advanced Solid State Lasers, vol 6, H. P. Jenssen and G. Dubé, eds, (Optical Society of America, Washington, DC, 1990), 144-149.

[5] H. Ajer, S. Landrø and K. Stenersen, OSA Proceedings on Advanced Solid State Lasers, vol 20, T. Y. Fan and B. H. T. Chai, eds, (Optical Society of America, Washington, D.C., 1994), 20-24.

[6] R. R. Petrin, M. G. Jani, R. C. Powell and M. Kokta, Opt. Mater. **1** (1992), 111-124.

Simultaneous lasing of Nd^{3+}:$Sr_5(PO_4)_3F$ at 1.059 and 1.328 μm

X.X. Zhang
Melles Griot, New Laser Products, Auburn, MA 01501
Tel.: (508) 832-3282, Fax: (508) 832-0390

M. Bass and B.H.T. Chai
CREOL - Center for Research and Education in Optics and Lasers
University of Central Florida, Orlando, FL 32826

P.J. Johnson and J.C. Oles
Lightning Optical Corporation, Tarpon Springs, FL 34689

L.K. Cheng
E.I. duPont de Nemours & Co., Wilmington, DE 19880

Nd^{3+} doped strontium fluorapatite, $Sr_5(PO_4)_3F$ or S-FAP, has recently gained a great deal of interest for some novel laser applications because of its unique spectroscopic properties. Excellent lasing performances have been demonstrated in laser-pumped, [1] diode-laser-pumped, [2] and lamp-pumped [3] operation. Nd^{3+}:S-FAP is of particular interest because of its high efficiency, low threshold laser performance at the 1.3 μm line. [1, 3-4] In this paper we report the simultaneous generation of 1.059 and 1.328 μm lasers in Nd^{3+}:S-FAP. Through the sum-frequency generation of these two wavelengths, laser emission at 589 nm was demonstrated.

The emission cross section at 1.328 μm is 2.4×10^{-19} cm^2, [4] only a factor of 2.2 smaller than that at 1.059 μm, in Nd^{3+}:S-FAP. In addition, the loss at 1.328 μm was found [4] to be about 3 times smaller than that at 1.059 μm. Both of these are very favorable factors for the realization of simultaneous lasing at both wavelengths.

An S-FAP rod (102 mm in length by 6.3 mm in diameter) containing 1.0 mole % Nd^{3+} in the melt (~ 5.5×10^{19} Nd^{3+} ions/cm^3 in the crystal) was fabricated for laser testing. The c-axis of the crystal was perpendicular to the longitudinal axis of the rod. Both ends of the rod were cut flat and parallel and were anti-reflection coated at both 1.328 and 1.059 μm with the coating optimized at the former wavelength. The rod was placed inside a 4-inch, close-coupled laser head and tested in a Schwartz Electro-Optics Laser 1-2-3 system. A xenon flashlamp was used as the pump source. The distance between the electrodes of the flashlamp was 85 mm and the flashlamp discharge duration was ~ 300 μs.

The optical cavity consisted of a curved high reflector (for both wavelengths) and a flat output coupler about 30 cm apart. The radius of curvature of the high reflector was 50 cm. In order to design the output coupler, the condition for simultaneous lasing was assumed to occur when the laser threshold is the same for both wavelengths. The laser threshold was studied as a function of the output coupling reflectivity while the laser operated at each individual wavelength. Based on this information, a relation was obtained between the reflectivities for both wavelengths. It was found that a wide range of choices of output coupler reflectivities could satisfy the condition.

Two output coupling mirrors were prepared with the intention to produce a reflectivity of 54 % at 1.328 μm and 26 % at 1.059 μm. As it turned out, one of them has a reflectivity of 54.5% at 1.328 μm and 31.6 % at 1.059 μm, and the other has a reflectivity of 55 % at 1.328 μm and 35.5 % at 1.059 μm. Simultaneous lasing was indeed achieved for the first mirror. Lasing occurred, however, only at 1.059 μm when the second mirror was used. The output energies at each wavelength as a function of pump energy are given in Fig. 1 when simultaneous lasing occurred using the first mirror. It can be seen that more than 1 joule has been achieved for each wavelength. Fig. 2 gives the temporal waveforms for each lasing wavelength as well as the waveform of the flashlamp pulse. The simultaneity of both lasing wavelengths is clearly indicated in Fig. 2 and has been confirmed by the fact that yellow light at 589 nm was observed when a $RbTiOAsO_4$ (RTA) crystal was placed in the output beam path.

Simultaneous lasing in cw mode is currently being investigated.

References:

1. X.X. Zhang, P. Hong, G.B. Loutts, J. Lefaucheur, M. Bass, and B.H.T. Chai, "Efficient laser performance of Nd^{3+}:$Sr_5(PO_4)_3F$ at 1.059 and 1.328 μm," Appl. Phys. Lett., Vol. 64, pp. 3205-3207, 1994.
2. W. Wiechmann, M. Oka, S. Kubota, and B.H.T. Chai, "Efficient intracavity-doubled laser diode pumped Nd:SFAP green laser," in *Advanced Solid-State Lasers*, OSA Technical Digest (Optical Society of America, Washington, D.C., 1995), pp.200-202.

3. X.X. Zhang, M. Bass, and B.H.T. Chai, "Flashlamp pumped neodymium doped strontium fluorapatite lasers," OSA Proc. Advanced Solid-State Lasers, B.H.T. Chai and S.A. Payne, eds. (Optical Society of America, Washington, DC, 1995), in press
4. P. Hong, X.X. Zhang, M. Bass, and B.H.T. Chai, "Nd^{3+}-doped apatite crystals for diode-pumped 1.06- and 1.33-μm lasers," in *Conference on Lasers and Electro-Optics*, Vol. 8, 1994 OSA Technical Digest Series (Optical Society of America, Washington, D.C., 1994), p. 159.

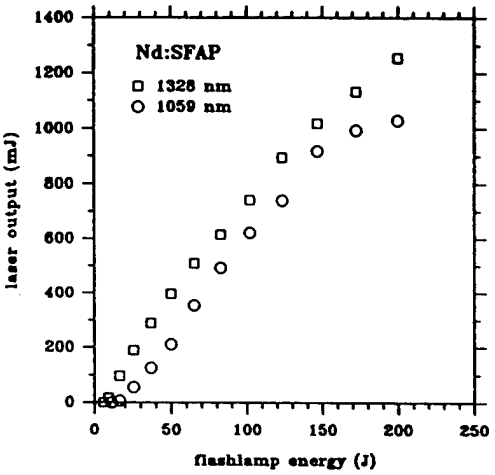

FIG. 1. Laser output energies at each wavelength as a function of input energy for Nd^{3+}:S-FAP when operating simultaneously at 1.059 and 1.328 μm.

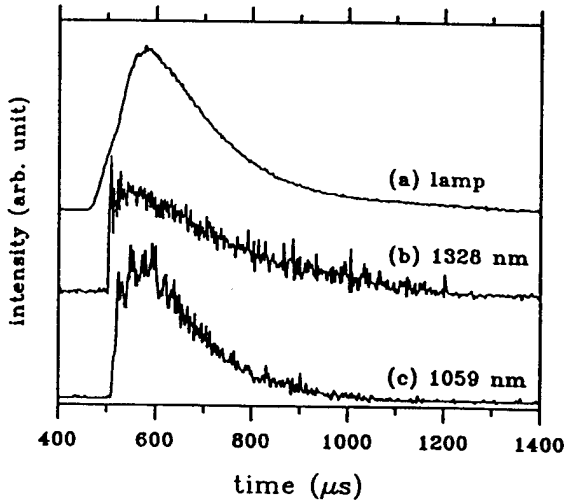

FIG. 2. Lasing temporal waveforms of Nd^{3+}:S-FAP in long pulse dual-wavelength operation.

Comparison of spectroscopic and laser properties of Cr^{4+}:$Y_xLu_{3-x}Al_5O_{12}$ crystals.

A.I. Zagumennyi, Yu.D. Zavartsev, P.A. Studenikin,
V.I.Vlasov, V.A. Kozlov, I.A. Shcherbakov, and A.F. Umyskov.

General Physics Institute,38 Vavilov Str., Moscow 117942, RUSSIA.
Tel./ Fax: +7-095-135-02-11.e-mail: zagumen@physlab.msk.ru

Recently, the large attention is given to crystals with garnet structure $Y_3Al_5O_{12}$ (YAG), $Y_3Sc_2Ga_3O_{12}$ (YSGG), $Gd_3Sc_2Ga_3O_{12}$ (GSGG), $Lu_3Al_5O_{12}$ (LAG) with so named fototroped Cr^{4+} centers [1-3]. With these crystals a passive modes synchronization [4] and passive Q-switch in a resonator of Nd lasers at λ = 1,06 μm [5] are carried out. Cr^{4+}:$Y_3Al_5O_{12}$ crystals lasing in region of 1,35÷1,55 μm [6,7]. CW laser action of a Cr^{4+}:$Lu_3Al_5O_{12}$ crystals demonstrated in the range 1370÷1470 nm [8]. The Cr^{4+} ions were used as sensitiser of the Ho and Er luminescence [9]. In this letter we report on the spectroscopic and laser properties of this Cr^{4+}:$Y_xLu_{3-x}Al_5O_{12}$ crystals.

Crystals of mixed yttrium/lutecium aluminum garnet $Y_xLu_{3-x}Al_5O_{12}$ ($0 \le x \le 3.0$), were grown by Czochralski technique in a radio frequency heated iridium crucible. The orientation of growth was <100>. The growth pooling rate was 3,2mm/h; rotation rate - 15÷20 r/min; growth atmosphere - 98% of N_2 + 2% of O_2.

Lattice constants of crystals at room tempera-ture were determined by a powder defraction method. The lattice constants were changed between 11.89÷12.01A for Cr^{4+}:$Y_xLu_{3-x}Al_5O_{12}$ when $0 \le x \le 3.0$. The low temperature unit-cell dimensions were calculated with approximate factors of thermal expansion of the $Y_3Al_5O_{12}$ and $Lu_3Al_5O_{12}$ crystals.

Measured at room temperature and 77K the transmission spectra of the Cr^{4+}:$Y_xLu_{3-x}Al_5O_{12}$ crystals are submitted in Fig.1. The chemical formulas, measured and calculated physical parameters of investigated crystals are listed in Table 1.

It is shown that the integral describing the crystal-field strength ρ_4 is directly propotional to $1/a_o^5$, where a_o is a lattice constant.

The shift of the emission spectra of Cr^{4+} ions in the Cr^{4+}:$Lu_3Al_5O_{12}$, Cr^{4+}:$Y_{1,5}Lu_{1,5}Al_5O_{12}$, Cr^{4+}:$Y_{0,6}Lu_{2,4}Al_5O_{12}$ and Cr^{4+}:$Y_3Al_5O_{12}$, crystals was determined for 925 nm excitation.

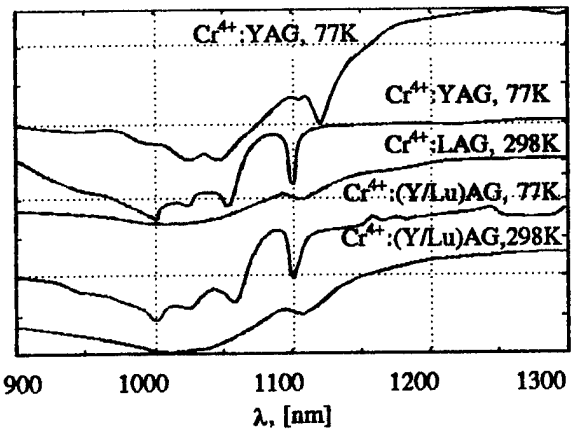

Fig.1. Transmission spectra of the Cr^{4+}-doped crystals at various temperature.

The absorption and luminescence spectra is shifted to the higher energies when the lattice constants of the crystals are reduced, Table 1. The luminescence lifetime of the Cr^{4+} $^3B_2$ ($^3T_2$) level has been measured at room temperature and liquid nitrogen temperature for Q-switched 1064-nm excitation Table 1.

The luminescence decay rate $W=1/\tau$ (inverse luminescence lifetime) of the Cr^{4+} $^3B_2(^3T_2)$ level is described by the linear dependence on the crystal-field strength ρ_4 (Fig.2.).

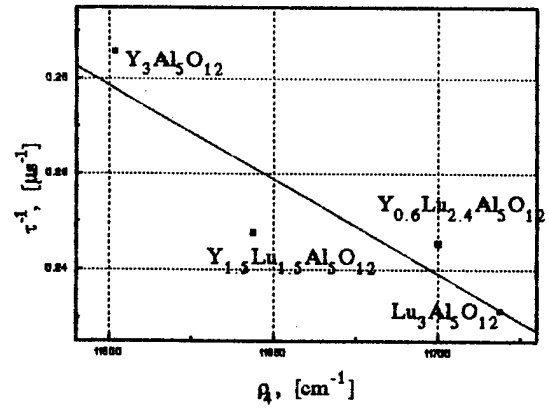

Fig.2. Influence of crystal-field strength on the decay rate of the Cr^{4+} $^3B_2(^3T_2)$ level.

The energy of the $^3E(^3T_2)$ and $^3B_2(^3T_2)$ levels is directly proportional to a_o^{-5} (Fig.3). With increasing of the crystal field strength the split of the $^3T_2$ sublevels is increased.

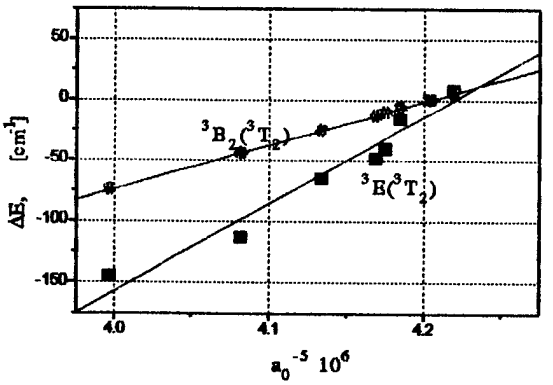

Fig.3. Displacement of energy $^3E(^3T_2)$ and $^3B_2(^3T_2)$ levels as function of crystal-field strength.

Saturable absorption measurements were performed by using the two Ge diodes, a digital oscilloscope and the Q-switch Nd:YAG laser with the pulse duration 10 ns at half-width as the source. The transmittance measurements as a function of 1.06 μm input energy are plotted in Fig. 4. The dependence of the transmission T on the excitation pulse energy can be written as

$$T=\ln[1+T_0(\exp(\alpha E)-1)]/\alpha E,$$

where E is an excitation pulse energy, T_0 is an internal initial transmission and α is a coefficient. The theoretical transmittances are plotted along with the experimental data (dashed curve).

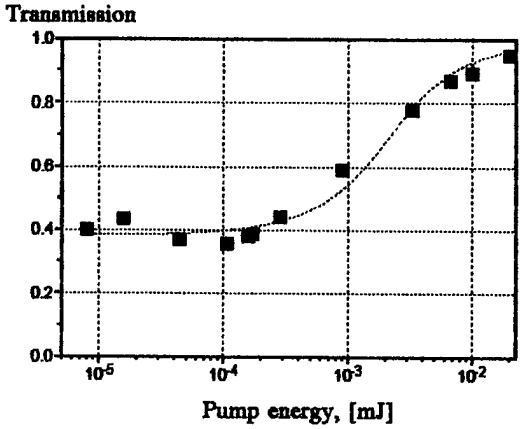

Fig.4. Experimental and theoretical Cr^{4+}:$Y_xLu_{3-x}Al_5O_{12}$ internal transmission as a function of the 1.06 μm pump pulse energy.

Cr^{4+}:$Y_xLu_{3-x}Al_5O_{12}$ crystals have been used for passive Q-switching of CW diode-pumped Nd:$GdVO_4$ laser. The surfaces of the vanadate crystal were coated with a antireflection coating for 1.06 μm on the one side and a dual band (1.06 μm and 0.808 μm) 99.6% reflection and 96% transmission coating, respectively, on the other side. The Cr^{4+} crystal had the 95% initial transmission.

The lasing experiments were performed in the cavity formed by HR surface of laser crystal and the curved mirror having a 10-cm radius of curvature and 3.9 % transmission at 1.06μm.

In passive Q-switching regime the pulse duration and pulse repetition rate depend on both the initial transmission of used the Cr^{4+}-crystals and the angle between the $GdVO_4$ C-axis of and the $Y_xLu_{3-x}Al_5O_{12}$ <001>-axis. During the rotation of the Cr^{4+} crystal the laser pulse repetition rate was changed from 28 μsec up to 50 μsec, the pulse duration was changed from 80 ns up to 200 ns, Fig.5.

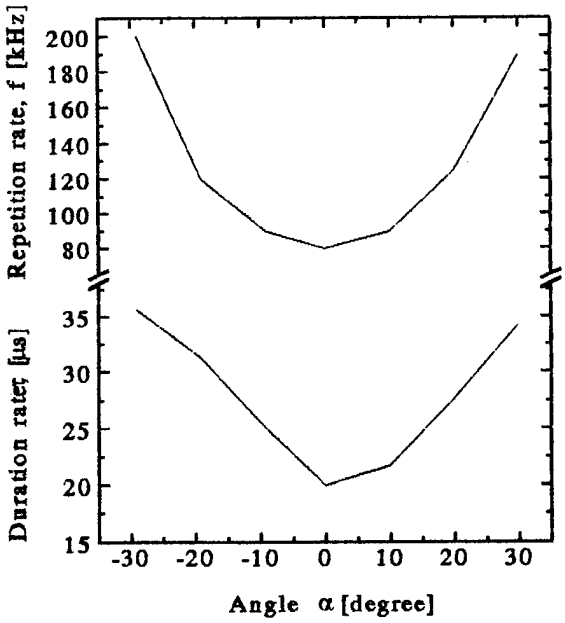

Fig.5. Pulse duration and pulse repetition rate in passive Q-switching regime for Cr^{4+}:$Y_{1.5}Lu_{1.5}Al_5O_{12}$ crystals at 1,06 μm.

The obtained peak power in giant pulse was up to 10 W for CW pump power of 175 mW.

This work was supported by the Volksvagen Fondation.

References.

1. Eilers H., Hoffman K.P., Dennis W.M., Jacobsen S.M., Yen W.M. Appl.Phys.Lett., v.61 (1992) p.2958
2. Chen W., Spariosu K., Stultz R., Kuo Y.K., Birnbaum M. and Shestakov A.V. Optics Communications v.104 (1993), p.71-74.
3. Eilers H., Hommerich U., Jacobsen S.M. and Yen W.M., Hoffman K.P., Jia W. Phys.Rev B v.49, (1994) p.15505-15513].
4. M.I.Demchuk, A.M.Zabasnov, I.A.Shcherbakov, Sov. J. Quantum Electron., v.14, (1987) p.423]
5. D.M.Andrauskas and C.Kennedy, in *Proceedings on Advanced Solid State Lasers,* ed.by G.Dube and L.Chase (OSA), USA, Washington v.10 (1991) p.393
6. N.I.Borodin, V.A.Zhitnyuk, A.G.Ohrimchuk, A.V.Shectakov, Izvestia Akademii nauk SSSR v.54 (1990) p.1500-1506
7. K.Spariosu, W.Chen, R.Stultz, M.Birnbaum, and A.V.Shestakov, Optics Letters, v.18 (1993) p.814-816.
8. J.Zhang, Y.Kalisky, G.H.Atkinson, M.Kokta in *Technical digest on Advanced Solid State Lasers*, (OSA), USA, (1995) p.182-186
9. V.B.Sigachev, M.E.Doroshenko , N.N.Basiev, G.B.Louts, B.Chai. Sov. J. Quantum electron., v.22 (1995), p.33-36

Table 1.

Chemical formula	Charge compen -sator	Lattice constants, nm	T, °K	Absorption maximum shift, nm	Lumine-scence shift, nm	Tetrahed-ron angle θ, degree.	Radial integral ρ_4, cm^{-1}	Lifetime τ, μs
$Lu_3Al_5O_{12}$	Ca^{2+}	11.9086	298	5	-	-	-	-
$Lu_3Al_5O_{12}$	Mg^{2+}	11.9122	298	6	0	52.8	11720	4.3
$Lu_3Al_5O_{12}$	Mg^{2+}	-	77	0	-	-	-	29.0
$Y_{0.6}Lu_{2.4}Al_5O_{12}$	Mg^{2+}	11.9324	298	8	2	52.8	11700	4.0
$Y_{0.6}Lu_{2.4}Al_5O_{12}$	Mg^{2+}	-	77	2	-	-	-	29.5
$Y_{1.5}Lu_{1.5}Al_5O_{12}$	Mg^{2+}	11.9627	298	14	5	52.8	11640	4.04
$Y_3Al_5O_{12}$	Ca^{2+}	12.0133	298	18	10	52.8	11600	3.5

Novel Geometries for Copper Vapour Laser Pumped Ti:Sapphire Lasers

W.J.Wadsworth, D.W.Coutts and C.E.Webb
University of Oxford, Atomic and Laser Physics, Clarendon Laboratory, Oxford OX1 3PU, UK.

Telephone: +44 1865 272259 Fax: +44 1865 272400 E.Mail:w.wadsworth1@physics.oxford.ac.uk

Introduction

Copper vapour laser (CVL) pumped Titanium Sapphire lasers have proved to be excellent sources of high repetition rate tuneable near infrared radiation. The CVL wavelengths at 511 and 578 nm are well matched to the absorption band of Ti:Sapphire and CVLs are unique as pump lasers in that they operate at high repetition rate (2-24 KHz) and high average power (up to 500 W in a single unit). Research carried out in our laboratory and elsewhere on pumping of Ti:Sapphire lasers by CVLs has shown that high efficiencies for conversion into the infrared can be obtained. The infrared beam has excellent beam quality, allowing efficient non-linear conversion into the blue and ultraviolet [1,2,3,4]. Hitherto only longitudinal pumping geometries have been considered. This is because the emission cross-sections of Ti:Sapphire are so low that to obtain a reasonable gain with the modest pump energies available from CVLs, a pumped volume which presents a small area across the direction of the Ti:Sapphire laser axis must be used. This is most simply attained with spherical focusing optics in a longitudinal pumping geometry. With low power CVLs (up to 10 W per crystal face) this has proved to be a robust and efficient method, offering excellent beam quality, low threshold (<0.6 W), and slope efficiencies up to 30% [1,3] giving the highest output power to date of 5 W at 780 nm. The problem which arises with higher pump powers is surface and bulk damage to the Ti:Sapphire crystal by the tightly focused pump beam. The small and well defined focal spot with a large depth of focus required for longitudinal pumping also requires a CVL resonator producing a low divergence output. Most studies have used CVLs with unstable resonators which provide excellent beam quality, particularly on small lasers. However for higher power pump lasers, it is more difficult to obtain high beam quality from a single oscillator unit, and a two unit (master oscillator / power amplifier) combination must be used [5]. Recently more highly doped Ti:Sapphire crystals have become available with absorption depths of around 2 mm at 511 nm. This prompted us to investigate the possibilities for transverse pumping by a high power CVL. The transverse geometry eliminates the need for high beam quality in the pump laser because it allows the use of very short focal length cylindrical lenses, as the depth of focus required is only 1 mm compared with lengths of about 10 mm in longitudinal pumping geometries. A plane-plane resonator may therefore be used on the CVL which offers the maximum power extraction and great simplicity. Furthermore the line focus of the pump beam on the crystal has a low power density and so crystal damage is eliminated. The resulting laser unit is relatively insensitive to the alignment of the pump laser beam and may be implemented as a compact add-on to a high power CVL.

Experimental layout

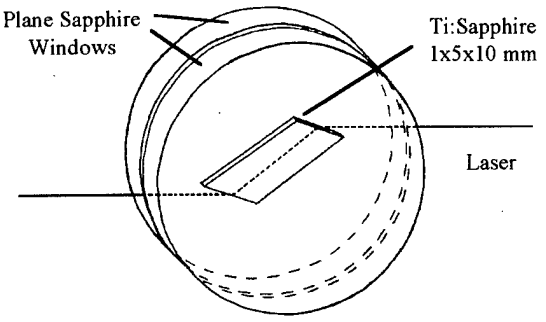

Figure 1 Ti:Sapphire crystal mount

Our initial investigations have been carried out using a modified Oxford Lasers CU40 as the pump laser. This has a 42 mm x 1.5 m active volume and delivers up to 65 W at 6.5 KHz. The CVL is run with a plane-plane resonator with an intracavity polarising beamsplitter to polarise the output parallel to the c-axis of the Ti:Sapphire crystal. This is the simplest form of CVL resonator and offers the maximum power extraction, though with rather poor beam quality (~500 times diffraction limit). The Ti:Sapphire crystal is doped at 0.25% (the highest doping level obtainable from Union Carbide) which corresponds to absorption depths of 2 mm at 511 nm and 4 mm at 578 nm, with a figure of merit of >150. The crystal is held between two undoped sapphire windows which conductively cool the laser crystal through its front and back surfaces (Figure 1). The windows are water cooled from their edges using a recirculating chiller, and the temperature may be set between -5 and +60 °C.

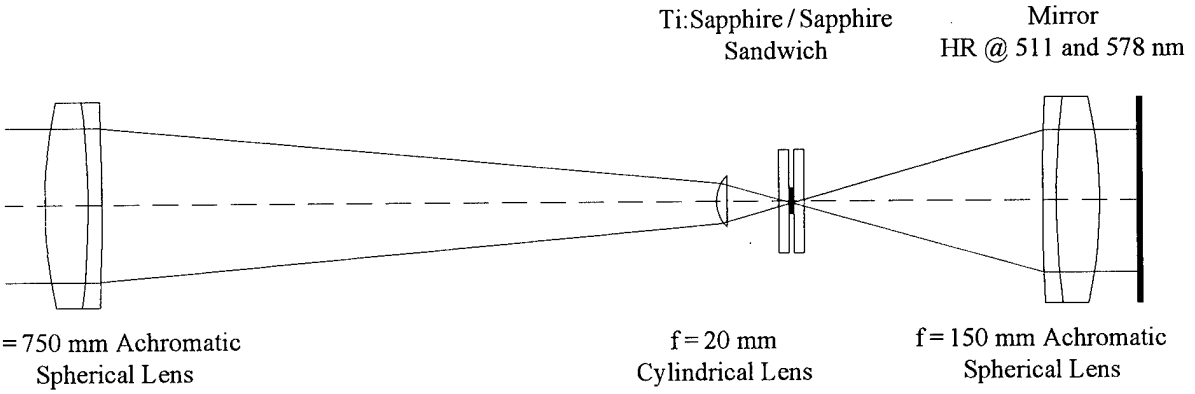

Figure 2 The CVL pump beam focusing geometry

The pump beam focusing geometry is shown in Figure 2. A f=750 mm lens is placed 610 mm from the crystal which serves to reduce the diameter of the CVL beam from 42 mm to the 10 mm length of the crystal. The line focus is 10 mm long and 0.5 mm high, obtained by using a f=20 mm cylindrical lens. For effective pump use, given the 2 mm absorption depth at 511 nm, a double pass of the pump beam is required in the 1 mm thick laser crystal and this is achieved by imaging the focus back onto itself with a lens and mirror. The Ti:Sapphire laser cavity is formed perpendicular to the plane of Figure 2. Two-mirror cavities are used, with a plane R=80% output coupler and HR back mirror of 250 mm radius of curvature. The cavity length was kept as short as possible to increase the cavity mode size and so to get the best power extraction from the large pumped volume. In practise the crystal mount allows a minimum cavity length of 60 mm. The crystal is cut so that the c-axis lies perpendicular to the lasing direction, and the pump and Ti:Sapphire lasers are both polarised parallel to this. The crystal end faces are Brewster cut in the direction of the Ti:Sapphire laser.

Results

The Ti:Sapphire laser performance is shown in Figures 3 and 4. The fraction of the output power of the CVL absorbed in the crystal is only 33%, partly because a double pass of the crystal represents only one absorption depth, but mainly because none of the faces of the sapphire windows, the laser crystal or the cylindrical lens are anti-reflection coated. The lasing threshold is high, and this, together with the limited absorbed power, restricts the output power to 4 W. Higher reflectivity output couplers should reduce the threshold without significantly reducing the slope efficiency, improving the overall efficiency which is already comparable with longitudinally pumped systems at 28% [1,3]. The build up time (50 ns) and pulse length (10 ns FWHM) of this laser are much shorter than that of the longitudinally pumped lasers previously reported, despite the lower round trip gain, since the cavity round trip time is very short. The high peak power associated with the short pulse should allow high efficiency non-linear frequency conversion of this laser.

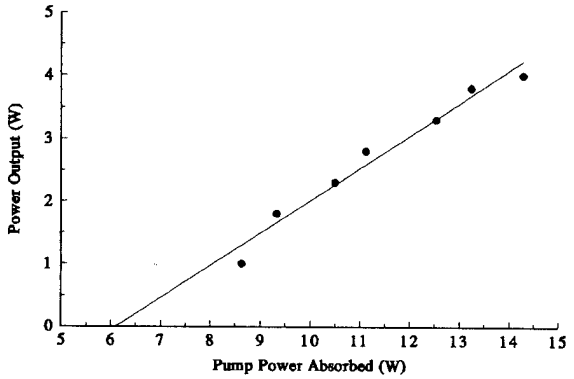

Figure 3 Efficiency of the Ti:Sapphire laser

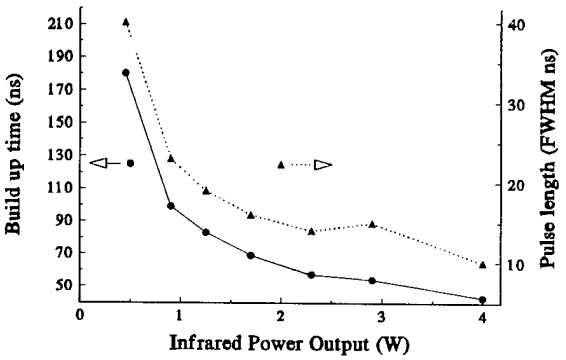

Figure 4 Build up time and pulse lenth of the Ti:Sapphire laser

The transverse mode structure is poor, being double-lobed in the horizontal direction. This is a consequence of the large pumped volume and the small cavity mode size. The pumped region of the Ti:Sapphire crystal acts as a strong positive astigmatic GRIN lens, which tends to reduce the cavity mode size in practical cavities containing the crystal. We are undertaking further detailed investigations in order to be able to design a cavity with a fundamental mode which matches the pumped volume. The mode matching is monitored by imaging the end of the crystal onto a CCD camera. This can then be used to observe the crystal fluorescence when it is pumped, and to observe the depletion of the fluorescence by the laser mode when a cavity is formed around the crystal. Reducing the crystal temperature may help as the thermal properties of sapphire improve with decreasing temperature (thermal conductivity increases and *dn/dT* decreases). Preliminary results indicate that this does indeed reduce the lensing effects.

References

[1] M.R.H.Knowles and C.E.Webb, (1993) Optics Letters **18** pp607-609
[2] K.Takehisa and A.Miki, (1992) Applied Optics **31** pp2734-2737
[3] I.J.Evans, W.J.Wadsworth and C.E.Webb, (1994) CLEO/Europe paper CWL3, Technical Digest p273
[4] D.S.Knowles and D.J.W.Brown, (1995) Optics Letters **20** pp569-571
[5] D.W.Coutts, (1995) IEEE J. Quantum Electronics **31** pp330-342

Laser operation and spectroscopy of Cr^{3+}:Yb^{3+}:Ln^{3+}:YSGG.

Yu.D.Zavartsev, A.A.Zagumennyi, V.V.Osiko, P.A.Studenikin, I.A.Shcherbakov, A.F.Umyskov

General Physics Institute, 38 Vavilov Str., Moscow 117942, RUSSIA.
Tel./ Fax: +7-095-135-02-11; E-mail: zavart@physlab.msk.ru

The crystals with a garnet structure, in particular the gallium garnet crystals co-doped by rare-earth (Ln^{3+}) and chromium ions are widely used as active media for solid-state lasers. The Ln^{3+} concentration in gallium garnets doped by Cr^{3+} ions has to be considerably high for the efficiency energy transfer $Cr^{3+} \rightarrow Ln^{3+}$. However some levels of Ln^{3+} ions have a concentrational quenching so a low Ln^{3+} concentration is interest because it will allow to realise a new lasing possibilities of Ln^{3+} ions. In addition the lasing threshold of three-level lasers is decreased at low concentration.

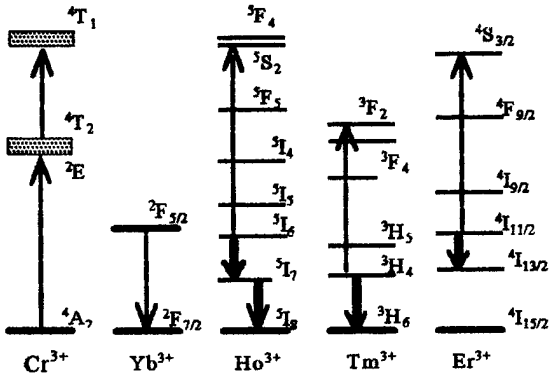

Fig.1. Electronic energy levels and transition mechanisms of the co-doped Cr^{3+}:Yb^{3+}:Ho^{3+}: YSGG, Cr^{3+}:Yb^{3+}:Tm^{3+}:YSGG and Cr^{3+}:Yb^{3+} Er^{3+}:YSGG active laser media.

We present the results of the investigations of Cr^{3+}:Yb^{3+}:Ln^{3+}:YSGG crystals, where Ln^{3+} are Ho^{3+}, Tm^{3+}, Er^{3+} ions. In these crystals Cr^{3+} ions efficiently absorb the emission of the pumping lamp and transfer the energy to Yb^{3+} ions. Ytterbium has strong absorption bands over the range 910-1030 nm and near resonant energy transfer to the Tm $^3H_5$, Ho $^5I_6$ and Er $^4I_{11/2}$ levels and so can be used as a sensitiser Fig.1. Thus Cr^{3+}:Yb^{3+}:Ln^{3+}:YSGG crystals are suitable objects both for pumping with flashlamps and for diode pumping at 920-970 nm.

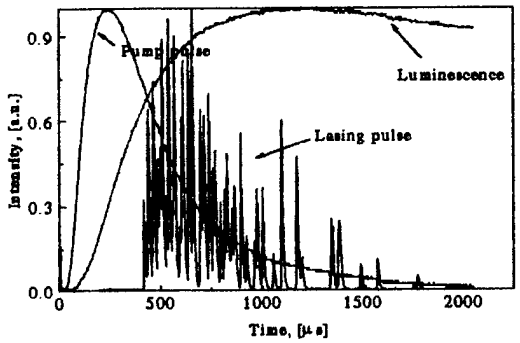

Fig. 2 Pump pulse (1), lasing pulse (2) and fluorescence of the Tm $^3H_4$ level (3) of the Cr^{3+}:Yb^{3+}:Tm^{3+}:YSGG crystal. Pumping energy is 45 J.

The Yb^{3+} concentration is equal to such value that the energy transfer to the lasing Ln^{3+} ions are migratory-promoted, but not only static. Such mechanism of energy transfer $Cr^{3+} \rightarrow Yb^{3+} \rightarrow Ln^{3+}$ allows to decrease considerably the concentration of the lasing Ln^{3+} ions and to realise the laser channels possible only at low concentration.

The experiments were carry out with the Czochralski grown crystals: 1) *Cr^{3+}:Yb^{3+} :Ho^{3+}:YSGG* (Cr^{3+} is $5 \cdot 10^{19}$ cm^{-3}, Yb^{3+}- $6 \cdot 10^{21}$ cm^{-3}, Ho^{3+} is $5 \cdot 10^{19}$ cm^{-3}), 2) *Cr^{3+}: Yb^{3+}:Tm^{3+}:YSGG* (Cr^{3+} is $5 \cdot 10^{19}$ cm^{-3}, Yb^{3+} is $2 \cdot 10^{21}$ cm^{-3}, Tm^{3+} is $2 \cdot 10^{20}$ cm^{-3}), 3) *Cr^{3+}:Yb^{3+}:Er^{3+}:YSGG* (Cr^{3+} is $5 \cdot 10^{19}$ cm^{-3}, Yb^{3+} is $1 \cdot 10^{21}$ cm^{-3}, Er^{3+} is $2 \cdot 10^{20}$ cm^{-3}). The laser rods 4 mm diameter and 65 mm long without coating were used for the lasing experiments.

The Cr^{3+}:Yb^{3+}:Tm^{3+}: YSGG crystal. In that crystal the energy is transferred to the

Tm $^3H_4$ level according to scheme $Cr^{3+} \rightarrow Yb^{3+} \rightarrow Tm^{3+}$ Fig.1. The lifetime of the $^3H_4$ level of Tm^{3+} ions is equal 13 msec. The lasing is achieved on the $^3H_4 \rightarrow {}^3H_6$ transition in the high reflectivity mirrors cavity, Fig.2. The threshold of lasing is equal 35 J, Fig.3. When the output mirror had the 87 % reflectivity the laser action was not achieved up to 200 J of the pumping energy.

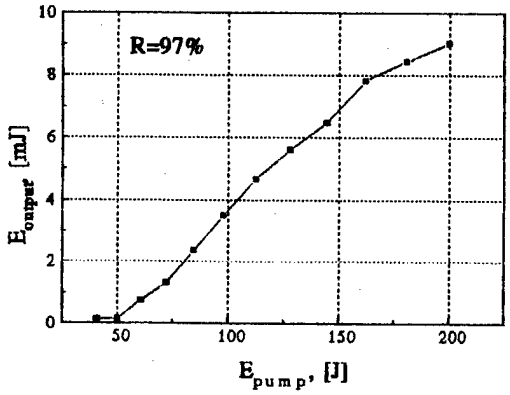

Fig.3 Input-Output curve for 2 μm lasing of Cr^{3+}:Yb^{3+}:Tm^{3+}:YSGG.

It is known that the lasing efficiency on the Cr^{3+}:Tm^{3+}:YSGG crystals achieves 6 %. In the Cr^{3+}:Yb^{3+}:Tm^{3+}:YSGG crystal the Tm concentration was taken out such that the concentration quenching of the Tm $^3F_4$ level was insignificant. Taking into account that the lifetime of the $^2F_{5/2}$ level of Yb^{3+} ions shortens from 700 μsec in Cr^{3+}:Yb^{3+}:YSGG crystal to several μsec in Cr^{3+}:Yb^{3+}:Tm^{3+}: YSGG crystal, the calculated efficiency of energy transfer $Cr^{3+} \rightarrow Yb^{3+} \rightarrow Tm^{3+}$ is more than 90%. The addition of Yb^{3+} ions into the Cr^{3+}:Tm^{3+}:YSGG system makes possible the process of the interaction of the excited Yb $^2F_{5/2}$ and Tm $^3H_4$ levels:

$$^2F_{5/2}\,(Yb^{3+}),\ ^3H_4\,(Tm^{3+}) \rightarrow {}^2F_{7/2}\,(Yb^{3+}),\ ^3F_2\,(Tm^{3+}). \qquad (1)$$

As a result the Tm $^3H_4$ level is depleted and the efficiency of 2μm lasing has a saturation. The excitation from the Tm $^3F_2$ level relaxes to the metastable $^3F_4$ level. However the lasing on the Tm $^3F_4 \rightarrow {}^3H_5$ transition (λ=2.3 μm) in the high reflectivity mirrors cavity was not achieved.

The Cr^{3+}:Yb^{3+}:Ho^{3+}:YSGG crystal. In that crystal the energy is transferred to the Ho upper laser levels according to scheme $Cr^{3+} \rightarrow Yb^{3+} \rightarrow Ho^{3+}$ (Fig.1). The calculated efficiency of energy transfer is more than 90%. The lifetimes of the $^5I_6$ and $^5I_7$ levels of Ho^{3+} ions are equal 0.47 msec and 9.8 msec respectively. As a result the 3 μm channel of lasing $^5I_6 \rightarrow {}^5I_7$ is self terminated. The oscillation in 3 μm laser channel without self termination was obtained in the high reflectivity mirrors cavity because then the 2 μm laser channel depleted the lower laser level of 3 μm channel. The cascade lasing was demonstrated, to our knowledge for the first time, on the Ho $^5I_6 \rightarrow {}^5I_7 \rightarrow {}^5I_8$ transitions at 3 μm and 2 μm at room temperature with the flashlamp pumping [2]. The achieved cascade lasing efficiency is 0.17% at 1150 μsec pulse duration.

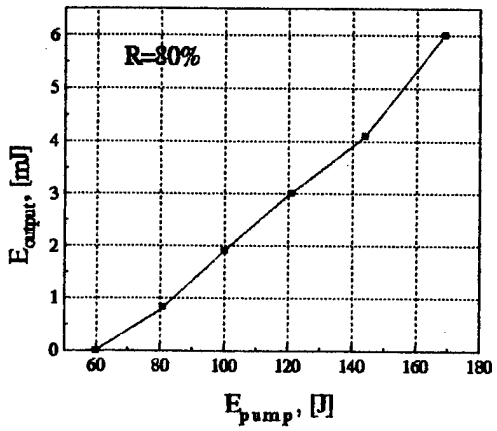

Fig.4 Input-Output curve for 3μm lasing of Cr^{3+}:Yb^{3+}:Er^{3+}:YSGG.

Upconversion occurs in this system whereby the excited Yb $^2F_{5/2}$ and Ho $^5I_6$

levels interact to produce a ground state Yb^{3+} and an excited Ho^{3+} ion:

$$^2F_{5/2}(Yb^{3+}), {}^5I_6(Ho^{3+}) \rightarrow {}^2F_{7/2}(Yb^{3+}), {}^5S_2(Ho^{3+}). \quad (2)$$

This undesirable process depletes the population of the Ho $^5I_6$ upper laser level and results in saturation of the lasing efficiency of both laser channels. Its effect can be minimised using high Yb and Ho concentrations, as these make the $Yb^{3+} \rightarrow Ho^{3+}$ energy transfer rate so fast that it dominates the upconversion rate (2) [3].

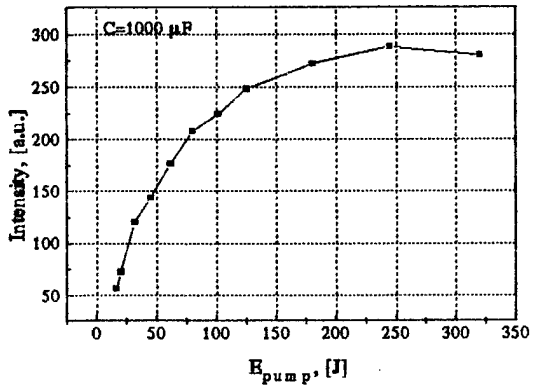

Fig.5 1.5 μm fluorescence emission strength of erbium as a function of pump energy.

The Cr^{3+}:Yb^{3+}:Er^{3+}:YSGG crystal. In this crystal the energy is transferred to the Er $^4I_{11/2}$ level according to scheme $Cr^{3+} \rightarrow Yb^{3+} \rightarrow Er^{3+}$ Fig.1. The energy gap between the Er $^4I_{11/2}$ and Yb $^2F_{5/2}$ levels is small, and as a result both levels are populated. The lifetimes of the Er $^4I_{11/2}$ and $^4I_{15/2}$ levels are equal 1.6 msec and 8.1 msec respectively, the lifetime of the Yb $^2F_{5/2}$ level is equal 1.6 msec. The lasing was achieved on the Er $^4I_{11/2} \rightarrow {}^4I_{13/2}$ transition at 3 μm in the 80% reflectivity mirrors cavity. The threshold of the lasing is equal 60 J Fig.4. However the laser action on the Er $^4I_{13/2} \rightarrow {}^4I_{15/2}$ transition at 1.5 μm was not achieved up to 320 J of the pumping energy. The 1.5 mm fluorescence emission strength was measured as a function of pump energy Fig.5. With the increasing of the pump energy value the population of the Er $^4I_{13/2}$ level is saturated. The interaction of the excited Yb $^2F_{5/2}$ and Er $^4I_{11/2}$ levels

$$^2F_{5/2}(Yb^{3+}), {}^4I_{11/2}(Er^{3+}) \rightarrow {}^4F_{7/2}(Yb^{3+}), {}^4S_{3/2}(Er^{3+}) \quad (3)$$

results in the saturation of lasing efficiency.

Conclusion. Cascade laser action on the 3 μm Ho $^5I_6 \rightarrow {}^5I_7$ and 2 μm Ho $^5I_7 \rightarrow {}^5I_8$ transitions was achieved. An undesirable upconversion process were discovered in all the investigated systems, though its effect can be minimised for the Cr^{3+}:Yb^{3+}:Ho^{3+}:YSGG system using the high Yb and Ho concentrations, as these make the energy transfer rate so fast that it dominates the upconversion rate.

REFERENCES.

1. Denisov A.L., Zagumenniy A.I., Luttz G.B., Semenkov S.G., Umyskov A.F. - Kvantovaya Elektronika, 1992, v.19, No 9, pp.842-844.
2. Zavartsev Yu. D., Osiko V.V., Semenkov S.G., Studenikin, P.A., Umyskov A.F. - Kvantovaya Elektronika, 1993, v.20, No 4, pp.366-370.
3. Morris P.J., W.Luthy, H.P.Weber, A.I.Zagumennyi, I.A.Shcherbakov, A.F.Umyskov - J.Quant.Spectrosc.Radiat. Transfer, 1994, v.52, No 5, pp.545-554.

Narrow band volume holographic 532 nm optical filter

Michael A. Krainak
Mail Code 717
Phone: (301) 286-2646 Fax: (301) 286-1750
email: mike_krainak@ccmail.gsfc.nasa.gov

Robert S. Afzal
Mail Code 924
Phone: (301) 286-5669 Fax: (301) 286-1761
email: rob@eib1.gsfc.nasa.gov

NASA Goddard Space Flight Center, Greenbelt, MD 20771

Anthony W. Yu
Hughes STX Corporation
7701 Greenbelt Road, Suite 400, Greenbelt, MD 20770
Phone: (301) 286-5611 Fax: (301) 286-1750
email: anthony_w_yu.1@gsfc.nasa.gov

Koichi Sayano
Accuwave Inc.
1651 19th Street
Santa Monica, CA 90404
Phone: (310) 449-5540 Fax: (310) 449-5539

Many laser ranging, altimetry, and cloud and aerosol lidar[1] direct detection systems incorporate frequency doubled Nd:YAG lasers. These systems typically require a high throughput, narrow band, 532 nm optical filter to improve the optical receiver signal to noise ratio in the presence of background illumination (e.g., Sun light). Many filter technologies have been suggested. For example, a high throughput, narrow band, 532 nm active filter has recently been reported[2]. However, a passive filter is much more attractive for airborne and space borne systems where size, weight, power, and reliability are important. In this paper, we report on the experimental performance of a volume holographic filter formed in photorefractive lithium niobate with a 532 nm center wavelength. This type of filter has been manufactured previously at the 657[3] nm and 1548[4] nm wavelengths. The details of the filter fabrication are presented in References 3 and 4.

The spectral response of the 532 nm volume holographic filter was measured by tuning a Pyrromethene-BF_2 dye laser. This is shown in Figure 1. The full width at half maximum (FWHM) bandwidth is 16 pm. The maximum filter throughput is 14%. A new version of the filter should have a four-fold increase in throughput (> 50%), but requires linearly

polarized light. The filter was also tested with a CW frequency doubled Nd:YAG laser. The Nd:YAG laser crystal was on a thermoelectric cooler (TEC) controlled mount so that the laser could be temperature tuned (10 pm/°C). The filter was also mounted on a TEC controlled mount and could be tuned 2.5 pm/°C. The frequency doubled Nd:YAG laser light passed through the filter.

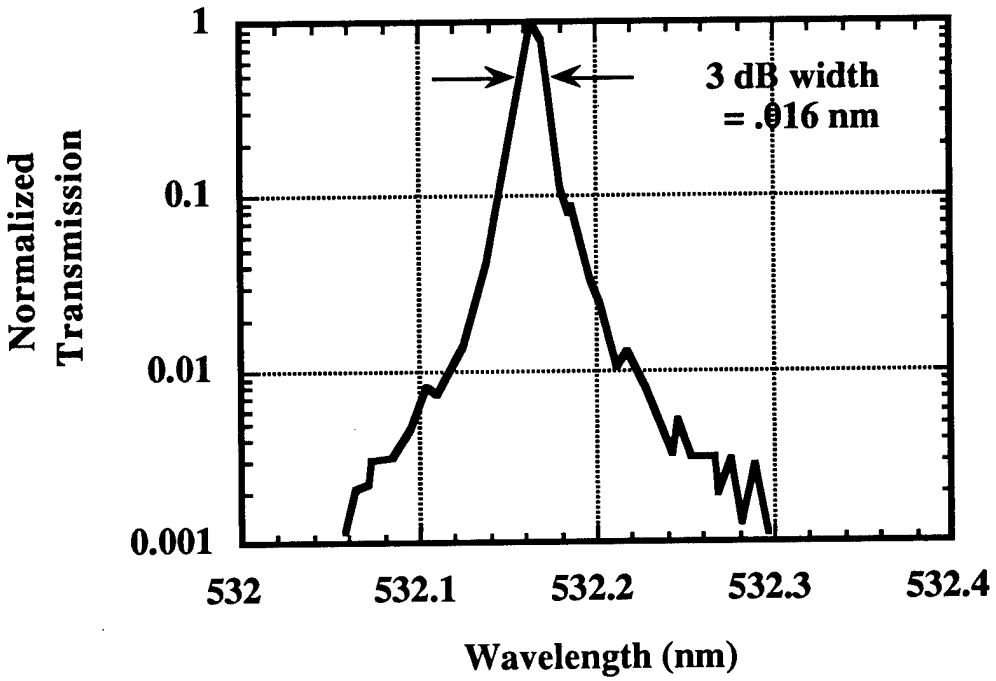

Figure 1. Normalized transmission spectrum of the volume holographic filter. The maximum filter throughput is 14%.

NASA is working on an Earth observing instrument called the Geoscience Laser Altimeter System (GLAS). The GLAS instrument will use a Q-switched Nd:YAG laser transmitter[5] for ice sheet elevation measurement and for atmospheric cloud/aerosol profiling. The fundamental wavelength is used for altimetry measurement and the frequency doubled output is intended for atmospheric lidar measurements. The cloud lidar link budget requirements disallow use of the 1064 nm wavelength, at present, due to the lack of availability of high quantum efficiency photon counting detectors at the 1064 nm wavelength. However, both high pulse energy laser radiation and a high quantum efficiency photon counting detector are available at the 532 nm wavelength. Therefore, a 532 nm center wavelength optical filter is required for the GLAS cloud/aerosol lidar. The

desire for daytime cloud lidar operation leads to a filter bandwidth requirement of less than 20 pm. Since the laser wavelength must remain within this filter pass band, the absolute laser wavelength stability required is +/- 5 pm. The GLAS laser transmitter must be wavelength stabilized to the center wavelength of the optical filter. We will injection lock the Nd:YAG laser to maintain this stability. Our present plan is to use the 532 nm GLAS receiver volume holographic filter as the reference standard for injection locking the GLAS transmitter Nd:YAG oscillator. In this way the transmitter and receiver will be locked together. Since the filter center wavelength can be temperature tuned to the laser operating wavelength, locking to the filter is preferable to locking the laser to an atomic absorption line[6]. We will present these volume holographic filter reference standard injection locking results. We will also present results of the improved throughput 532 nm volume holographic filter.

References

1. "Micro pulse lidar", James D. Spinhirne, IEEE Transactions on Geoscience and Remote Sensing, Vol. 31, No. 1 pp. 48-55 (1993).

2. "Induced-dichroism-excited atomic line filter at 532 nm", S. K. Gayen et al. Optics Letters Vol. 20 No. 12 1995 pp. 1427-1430 (1995).

3. "Volume holographic narrow-band optical filter", George A. Rakuljic and Victor Leyva, Optics Letters Vol. 18 No. 6 1993 pp. 459-461 (1993).

4. "Narrow bandwidth volume holographic optical filter operating at the Kr transition at 1547.82 nm", Victor Leyva, George A. Rakuljic and Bruce O'Connor, Applied Physics Letters Vol. 65 No. 9 pp. 1079-1081 (1994).

5. "A simple, high efficiency, TEM00 diode laser pumped, Q-switched laser", R.S. Afzal and M.D. Selker, Technical Digest Advanced Solid State Laser Conference, Memphis,TN paper MD6-1 (1995).

6. "Frequency stabilization of the 1064-nm Nd:YAG lasers to Doppler-broadened lines of iodine", Ady Arie and Robert L. Byer, Applied Optics Vol. 32 No. 36 pp. 7382-7386 (1993)

Wednesday, January 31, 1996

Parametric Oscillators

WD 10:45 am-12:30 pm
Gold Room

David Nabors, *Presider*
Coherent Laser Group

High-power, high-repetition-rate optical parametric oscillator based on periodically-poled $LiNbO_3$

W. R. Bosenberg, A. Drobshoff
Lightwave Electronics Corporation, Mountain View, CA 94043
(415) 962-0755, Fax (415) 962-1661

L. E. Myers,
USAF Wright Laboratory, WL/AARI, Wright-Patterson AFB, OH 45433

Introduction

Frequency conversion via quasi-phasematching is an old idea that has received a lot of attention recently because of new developments in poling techniques applied to ferroelectric crystals [1]. Periodically-poled lithium niobate (PPLN) is one example that offers high nonlinear coefficients, low optical loss, and "engineerable" phasematching properties that allow noncritical phasematching anywhere in its transmission range (0.35 - 4.2 μm). PPLN is quickly becoming the crystal of choice for low peak power mid-infrared frequency conversion. This paper describes the first multi-watt operation of a PPLN optical parametric oscillator (OPO).

PPLN Crystal Fabrication

The PPLN material is fabricated using the electric-field poling method [1]. 0.5 mm thick $LiNbO_3$ wafers are poled using liquid electrodes. Standard lithography produces a patterned electrode with period lengths suitable for nonlinear frequency conversion (15 - 32 μm). Applying an electric field of ~21 kV/mm to the electrodes permanently reverses the sign of the nonlinear coefficient in a pattern dictated by the electrode. Several PPLN crystals were fabricated for this work, and all exhibited identical performance in the OPO, indicating good reproducibility in the fabrication process. The crystals had a 29.5 μm quasi-phasematching period which generated signal and idler wavelengths of 1.54 μm and 3.45 μm, when pumped at 1.064 μm (for a crystal temperature of 70 °C). The crystals were 15 mm long and had antireflection coatings on their 15 mm x 0.5 mm apertures. A different crystal was used to collect the data in Fig. 3. This crystal had seven separate quasi-phasematching gratings of period 26 - 32 μm (in integral micron steps) as described in [2]. The multi-grating crystal was 19 mm long, and had no antireflection coatings on its end-faces.

1.064 μm Pump Source

The pump source was a standard Lightwave Electronics model 210-s laser, which is a cw-diode-pumped, q-switched Nd:YAG laser. The laser operates at repetition rates of 0 - 50 kHz. The average power for repetition rates above 10 kHz was 5.8 W, and the maximum pulse energy (at rep. rates below 1 kHz) was 1.5 mJ. The pulse durations at 1 kHz, 10 kHz, and 20 kHz were 22 ns, 40 ns, and 63 ns , respectively.

PPLN OPO and Results

The OPO resonator was a half-symmetric linear cavity. The input coupler had a 50 mm radius of curvature, and reflectivities of 3 %, 99 %, and ~10 % at the pump, signal, and idler wavelengths. The output coupler was flat, and had reflectivities of 2 %, 60 %, and 20 % at the pump, signal, and idler. The physical OPO cavity length was 30 mm. The PPLN crystal was mounted in an oven operated at a temperature of ~70 °C to avoid photorefractive damage caused by the unphasematched second harmonic generation of the pump [1]. For operation at lower repetition rates (1 - 25 kHz), the pump was focused to a spot diameter of 180 μm ($1/e^2$). For operation at higher repetition rates (15 - 30 kHz), the pump was focused to a diameter of 120 μm.

Fig. 1 shows the output of the OPO vs. input at 10 kHz. The threshold was measured to be 1.1 W, which corresponds to ~20 MW/cm^2. At 5.8 W pump, we generated 2 W of 1.54 μm radiation and 0.6 W of 3.45 μm radiation. No thermal effects in the PPLNwere observed as indicated by the linearity of the output vs. input. With the 180 μm pump spot diameter, the OPO could be run at repetition rates of 5 - 25 kHz (a maximum pulse energy). We reduced the size of the pump focus to 120 μm to operate at higher repetition rates (lower peak powers). As Fig. 2 indicates the OPO operated over 15 - 32 kHz with the smaller pump spot. The zero walkoff in PPLN allows tighter focusing and use of longer crystals, hence operation at even higher repetition rates (30 - 50 kHz) should be possible with a properly configured device.

Using the multiple-grating PPLN crystal described in the crystal fabrication section, we tuned the OPO over 2.8 - 4.8 μm by translating the uncoated crystal. The output power for the tunable OPO could be improved by a factor of ~2 by using AR coatings. Reduced absorption of the extraordinary polarized light relative to the ordinary polarized light in $LiNbO_3$ is responsible for the robust operation at wavelengths longer than 4.3 μm.

Conclusions

We have demonstrated a high-power, high-repetition-rate OPO on PPLN. This device generated 2 W at 1.54 μm and 0.6 W at 3.45 μm from 5.8 W of pump. The device was operated over repetition rates of 0 - 32 kHz, and could be tuned over the important 3 - 5 μm spectral range.

This work was supported by an Army Phase I SBIR contract administered by Night Vision and Electronic Sensor Directorate, Ft. Belvoir, VA.

References

[1] L. E. Myers, R. C. Eckardt, M. M. Fejer, R. L. Byer, W. R. Bosenberg, and J. W. Pierce, "Quasi-phasematched optical parametric oscillators in bulk PPLN", accepted for publication J. Opt. Soc. Am. B, November 1995. and references therein.

[2] L. E. Myers, R. C. Eckardt, M. M. Fejer, R. L. Byer, and W. R. Bosenberg "Grating tuned, quasi-phasematched optical parametric oscillator in periodically poled $LiNbO_3$", submitted for publication Opt. Lett Sept. 1995).

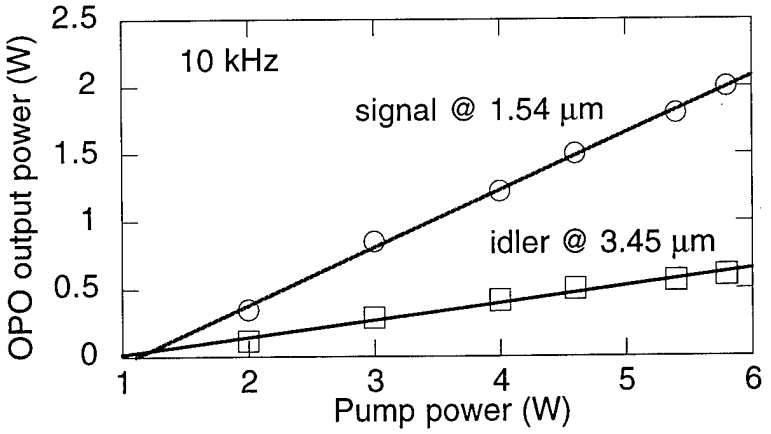

Fig. 1 Output vs. input of the PPLN OPO running at 10 kHz repetition rate.

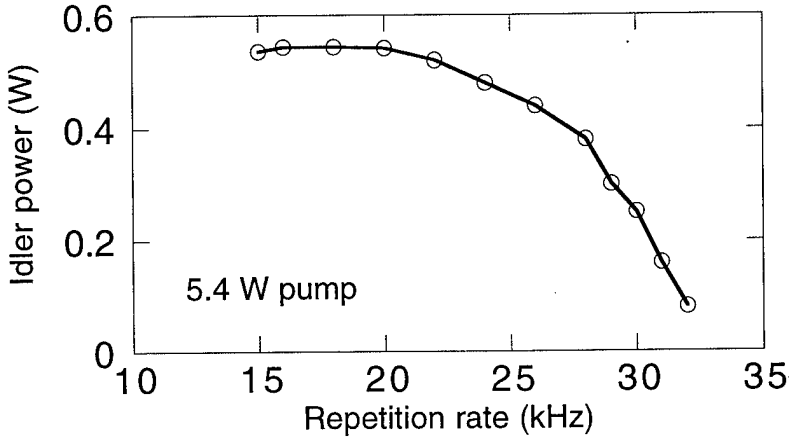

Fig. 2 Idler power (at 3.45 μm) vs. repetition rate with a pump diameter of 120 μm.

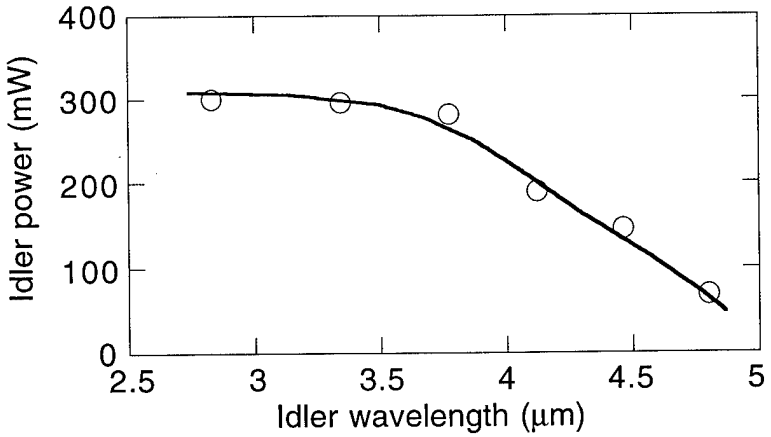

Fig. 3 Power out vs. wavelength for the OPO using the uncoated, multi-grating PPLN crystal at 10 kHz rep. rate. The OPO is tuned in discrete steps by translating the crystal through the pump beam. Use of an AR coated crystal would increase the output by a factor of ~2.

Synchronous Pumping of a Periodically Poled Lithium Niobate Optical Parametric Oscillator

T.P. Grayson, L.E. Myers
USAF Wright Laboratories
WL/AARI-2, Bldg. 622
Wright-Patterson AFB, OH 45433-7700
513-255-9614
513-155-6489 (fax)
graysotp@aa.wpafb.af.mil

M.D. Nelson, Vince Dominic
University of Dayton
Center for Electro-Optics
Dayton, OH 45469

In the past year much work in the nonlinear optics community has focused on the process of quasi-phase-matching (QPM) in frequency conversion devices.[1,2,3,4] QPM offers significant improvements over traditional birefringent phase-matching since the technique allows customization of the phase-matching function. This permits wavelength selection over the entire transmission window of the material. It also allows for utilization of nonlinear coefficients that are larger by more than an order of magnitude and eliminates problems associated with walk-off, resulting in much greater gain and efficiency.

One technique for which QPM is particularly appealing is the synchronous pumping of optical parametric oscillators (OPO). When a mode-locked laser is used as an OPO pump source, the pulses are very short, anywhere from 100 ps down to around 10 fs, but they arrive at a very high repetition rate, as high as 100 MHz. If such a laser were used to directly pump an ordinary OPO, the short pump pulse would traverse the cavity before the signal had time to build-up through multiple passes of amplification. This results in very poor efficiencies and may even make attainment of the oscillating threshold impossible. An alternate technique is synchronous pumping, taking advantage of the high pulse repetition rate of these lasers. By adjusting the OPO cavity length such that the cavity round trip time is equal to the time between pump pulses, one insures that there is always a pump pulse available to amplify the signal on each pass through the nonlinear medium.

The technique of synchronous pumping is divided into two sub-classes based upon the nature of the pump source, which may be either a cw or a Q-switched mode-locked laser. With a cw mode-locked laser, the pulses arrive in a continuous stream, while with a Q-switched mode-locked laser, the short mode-locked pulses arrive in bursts determined by the Q-switch firing. The amplitude of these pulses is shaped by the Q-switch envelope. Use of Q-switched mode-locking in a Nd:YAG laser results in mode-locked pulses with very high peak energies compared to a cw mode-locked laser, but with the sacrifice of longer pulses. A Q-switched mode-locked OPO has potential applications in the area of laser radar where short pulses are advantageous for fine range resolution, but where high peak energy is very important for long range applications.

The authors have recently demonstrated a Q-switched mode-locked synchronously pumped OPO using potassium titanyl arsenate (KTA).[5] The pump laser was a Q-switched mode-locked Nd:YAG laser operating at a wavelength of 1.064 μm and a Q-switch repetition rate of 1 kHz. The Q-switch envelope was approximately 350 ns. The 100 ps long mode-locked pulses were spaced by approximately 13 ns, resulting in approximately 26 pulses per burst. The typical average pump power into the OPO cavity was around 3 W. While this laser exhibits reasonably high peak pulse

energy, the long pulse durations result in modest peak powers and correspondingly modest nonlinear gain. The small gain was countered by using a tight beam waist, but the usefulness of focusing is limited by damage considerations and walk-off. Furthermore there are a limited number of pump pulses per Q-switch burst, limiting the useful lifetime of the OPO cavity.

Our attention has now turned to QPM, implemented with periodically poled lithium niobate (PPLN). As described above, the large nonlinearity and lack of walk-off associated with PPLN make it ideally suited for this type of OPO device. Furthermore, while damage is typically the limiting factor when using a PPLN device, the modest peak powers available from the pump laser make damage a minor concern for this device.

The OPO built for this experiment is identical to the KTA OPO. The same pump source that was described above is used with PPLN. The cavity layout is shown below in Fig. 1. HWP1 and LP are a half-wave plate and linear polarizer used in tandem as a variable attenuator. HWP2 is used to select the pump polarization for OPO operation or for alignment using the second-harmonic generated in an LBO crystal. The pump light is mode-matched into the cavity using lenses ML1 and ML2. The cavity itself begins with two spherical dielectric mirrors surrounding the PPLN crystal. Both mirrors have radii of curvature of 26.2 mm to provide a cavity waist of approximately 80 μm. HR is coated for high transmission at 1.064 μm and high reflectivity at 1.5 μm, while OC is coated for 70% reflection of 1.5 μm and high transmission of 3.44 μm to avoid idler feedback. HR and OC are both tilted so that the optical path travels out at angles, avoiding the corners of the crystal. The rapidly diverging light is collimated by lenses CL1 and CL2, and protected aluminum mirrors CM1 and CM2 form the ends of the folded linear cavity. CM2 is mounted on a translation stage which permits fine tuning of the length of the cavity to match the round-trip time to the pump pulse separation time. Signal light exits the cavity through OC.

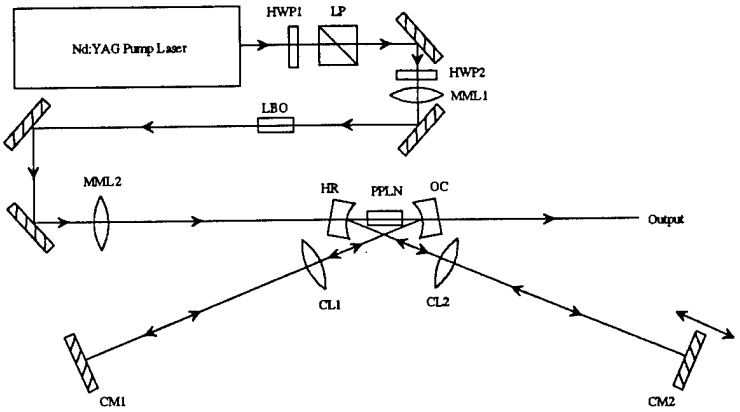

Fig. 1: Schematic illustration of the experimental layout of the synchronously pumped PPLN OPO.

The PPLN crystal is 15 mm long and has a 20 mm X 0.5 mm aperture. The QPM grating has a period of approximately 29.75 μm, produced using a standard field poling technique. This grating is predicted to produce 1.54 μm at a temperature of about 118°C. Since no heaters were used for this experiment, the actual operating wavelength at room temperature, measured using a monochrometer, was 1.528 μm.

With 2.77 W of average pump power entering the OPO, only 158 mW of signal radiation was detected, for a conversion efficiency of 5.7%. This poor result is largely due to the large intracavity losses caused by the lenses and aluminum mirrors. A better indication of OPO performance is the pump depletion. Depletion data are shown below. Fig. 2 shows the measured percentage of pump

depletion as a function of the average pump power. These data may be used to calculate the total signal power produced. Depletion percentage is converted to an energy efficiency using the ratio of pump to signal photon energies. This efficiency is multiplied by the pump power to give a total signal power. Results are shown in Fig. 3. The resulting slope efficiency measured from the plot is 61% with an extrapolated threshold value of 0.21 W. This threshold agrees well with the measured oscillation threshold of 0.16 W.

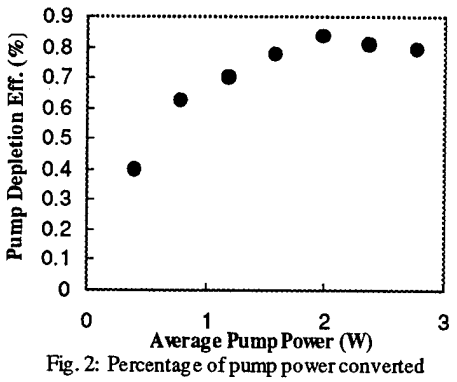

Fig. 2: Percentage of pump power converted into OPO radiation as a function of average pump power.

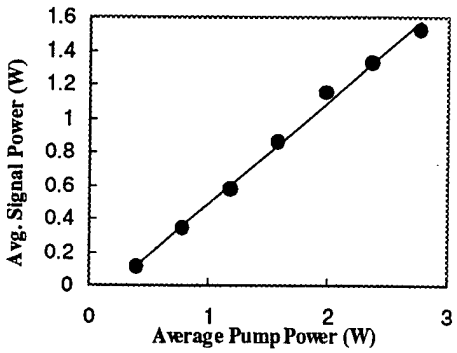

Fig. 3: Average signal power calculated from pump depletion as a function of average pump power. Solid line is a linear regression.

This performance greatly exceeds that of the KTA OPO, for which the calculated slope efficiency and threshold were 15% and 0.92 W, respectively. All system parameters, including mode-matching, are the same for both KTA and PPLN except for the slight wavelength difference. This should not have a significant effect on performance, as the optical coatings and detector response are flat over this wavelength range. Nevertheless, if performance is skewed by the wavelength, it will be worse for PPLN, since the system design and coatings were optimized for 1.540 μm.

To summarize, we have demonstrated for the first time synchronous pumping of PPLN. QPM is shown to be particularly advantageous for use with a Q-switched mode-locked pump because of the significantly higher single-pass gain it provides. For identical OPO parameters the PPLN performance was far superior to KTA. Q-switched mode-locked pumping of PPLN or other QPM materials is an efficient means of producing bursts of very short, eye-safe pulses for use with applications such as laser radar.

1. L.E. Myers, G.D. Miller, R.C. Eckardt, M.M. Fejer, R.L. Byer, W.R. Bosenberg, Opt. Lett. **20**, 52 (1995).

2. W.R. Bosenberg, A. Drobshoff, D.C. Gerstenberger, L.E. Myers, R.C. Eckardt, M.M. Fejer, R.L. Byer, paper PD8, Advanced Solid State Lasers Conference, Memphis, TN, (Optical Society of America, Washington, D.C., 1995).

3. L. Goldberg, W. K. Burns, R. W. McElhanon, Opt. Lett. **20**, 1280 (1995).

4. C. J. van der Poel, J. D. Bierlein, J. B. Brown, S. Colak, App. Phys. Lett. **57**, 2074 (1990).

5. T. P. Grayson, M. D. Nelson, Vince Dominic, submitted to J. Opt. Soc. Amer. B, Aug. 1995.

Effect of Cavity Design on Optical Parametric Oscillator Performance

William A. Neuman and Stephan P. Velsko

Lawrence Livermore National Laboratory
P.O. Box 808, L-493, Livermore, California 94550
(510) 423-8187, Fax (510) 422-1930
Email neuman1@llnl.gov

Optical parametric oscillators (OPOs) offer an efficient means of generating coherent, tunable radiation in frequency regimes not directly accessible with current laser technology. The utility of OPOs depends on their ability to efficiently convert the pump light into the longer wavelength signal and idler beams and the quality of the output beams produced. These characteristics are dependent both on the input pump laser and the resonator cavity design. Recent experimental results[1,2] have indicated that unstable resonators have advantages over more traditional flat-flat or stable resonators in achieving high conversion efficiency with good output beam quality. In this paper we investigate the OPO performance theoretically as a function of the resonator cavity design. The reported experimental findings of references 1 and 2 are supported by our calculations.

The model developed is time-dependent and includes diffraction, three-wave mixing, crystal absorption, and variable reflectivities and curvatures of the mirrors. The model solves the coupled field equations for the three waves using a spit-step operator approach in the crystal. The three-wave mixing and crystal absorption are treated with a second-order, predictor-corrector algorithm and the diffraction is treated using Fourier transform techniques. The propagation is limited to uniaxial crystals or biaxial crystal propagation in a principal crystal plane. The time dependency is treated by discretizing the pulse envelope in increments of the cavity round trip time. Each of these time slices is propagated through the cavity applying the appropriate boundary conditions at the mirrors. Fields can be injected (or extracted) at both mirrors to accommodate experimental conditions. Non-ideal input fields are treated by permitting Gaussian, super-Gaussian, and Hermite-Gaussian transverse beam shapes as well as phase aberrations described by Zernike polynomials. The input temporal pulse shape can be either Gaussian or super-Gaussian and can be specified individually for each input field.

The pump laser assumed for the study is a pulsed YAG laser at 1.064 μm with a 20 ns FWHM Gaussian temporal pulse profile. The parametric oscillator studied is singly-resonant and has a 30 mm $LiNbO_3$ crystal. The crystal is cut at the phase-matching angle for generation of 1.5 μm signal and 3.6 μm idler waves (~47° to the crystal z-axis). The signal wave is resonated in the cavity and the mirrors are assumed 100% transmissive for the pump and idler waves. The output coupler is assumed to reflect 60% at the signal wavelength and the only loss considered is a 10% transmission of the signal wave at the input coupler. A linear cavity geometry is assumed with a physical length of 125 mm.

Three cavity types are considered, a long-radius, hemispherical stable cavity, a flat-flat cavity, and a positive branch, confocal unstable cavity. The stable resonator has a 10 m radius back mirror and a flat output coupler. Multiple unstable resonator magnifications are used ranging from M=1.02 to M=1.2. The unstable resonators use a uniform partially-transmitting curved output coupler in contrast to a spot mirror. This is considerably simpler experimentally and affords more uniform near-field output profiles of the resonated wave. The effective unstable resonator feedback is a combination of the beam expansion and the output coupler reflectivity. The reflectivity of the output coupler is varied to maintain approximately constant effective feedback between the different unstable resonator magnifications and the stable and flat-flat cavities.

The energy output generated with the different cavity types is shown in Figure 1 for an unaberrated, Gaussian spatial input pump profile with a waist of ω_o=3 mm. The conversion efficiency is the poorest for the stable resonator, particularly at high input pump energies. The stable resonator mode for this cavity configuration is ~0.7 mm, which is significantly smaller than the pump size. This poor mode

matching results in reduced energy conversion. As the magnification of the unstable resonator increases, the output idler energy increases. The magnification cannot be continually increases, however, since the effective output coupling is dependent on both the magnification and output coupler transmission. At M=1.2 the beam expansion results in a signal intensity reduction of 31% on each round trip. For an effective output coupler reflectivity of 60% the transmission of the signal wave for this magnification is only 13.5% (effective reflectivity is R_{oc}/M^2). At this magnification the useable output signal energy has decreased significantly compared to the lower magnification cavities as seen in Figure 2 for a 100 mJ input pump. The flat-flat resonator is shown as M=1 and the stable resonator is included at M=0.96 for comparison.

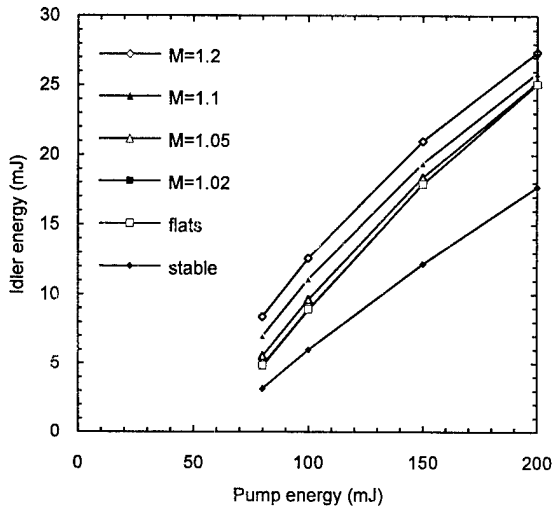

Figure 1. Comparison of the energy conversion for unstable, flat-flat, and stable OPO resonator cavities.

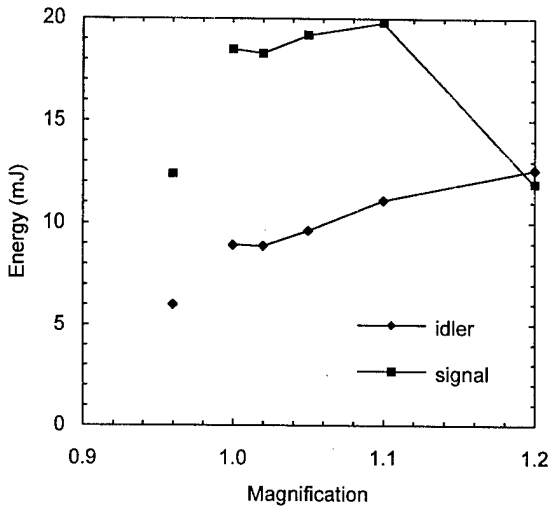

Figure 2. Comparison of the OPO output energy as a function of unstable resonator magnification for a 100 mJ input pump pulse. The flat-flat cavity result is plotted at M=1.0 and the stable cavity is plotted at M=0.96 for comparison.

Similar trends in the output energy conversion are seen for pump beams with super-Gaussian spatial profiles. For a super-Gaussian beam with a radius of 3 mm the output energy is ~20% lower for the flat-flat and unstable cavities at 100 mJ input pump energy. The peak intensity of the Gaussian beam is higher than that of the super-Gaussian beam for equivalent radii and energy (~60% higher). This larger peak intensity enables the Gaussian pump to reach threshold earlier in the pulse than the pump with the super-Gaussian spatial profile, resulting in increased energy conversion. The stable cavity again converts the least amount of energy and the conversion is significantly lower than with the Gaussian input pump (2 verses 6 mJ for the Gaussian and Super-Gaussian pumps, respectively). The transverse beam shape effect is more pronounced with the stable resonator because of the poor mode matching with the pump beam size. Since the stable cavity mode is smaller than the pump beam only the central portion of the pump beam is efficiently converted and in this region the super-Gaussian intensity is significantly lower than with the Gaussian profile.

The output beam divergence is also a function of the cavity type as seen in Figure 3 for a 100 mJ Gaussian input pump pulse. Multiplication of the beam divergence by the wavelength yields the half angle which contains ~82% of the beam energy. The unstable resonator produces the output with the minimum divergence. At M=1.2 the output beams are approximately 1.2 times diffraction limited based on the divergence of a Gaussian beam with ω_o=3 mm. Note the beam quality is very good for magnifications as small as M=1.1. This is potentially useful for OPOs operated at lower energies where increased feedback is required for efficient energy conversion.

The unstable resonator also performs better than the more traditional resonators when pumped by aberrated input beams. The energy conversion for an astigmatic input pump beam is shown in Figure 4. The input pump has 1 λ of astigmatism across the 3 mm radius and has a super-Gaussian transverse intensity profile. The 1 λ of astigmatism results in an input beam quality of ~3 TDL as compared to a 3 mm radius flat-phase, flat-top beam. The conversion efficiency is highest for the unstable resonator and lowest for the stable cavity. The output beam divergence also was best for the unstable resonator which produced an output beam quality approximately the same as the input pump beam over the range of input energies investigated. The output beam quality from the flat-flat and stable cavities degraded monotonically as the input pump energy increased, the flat-flat cavity producing the lower output divergence. Although the flat-flat cavity performed better at the 1 λ aberration level the stable cavity was found to perform comparably or better than the flat-flat cavity with larger (2-3 λ) astigmatic aberrations, particularly at higher input pump energies. With these higher aberrated conditions the unstable resonator still performed better than the other resonator types.

In summary, the effect of resonator cavity type on OPO performance has been investigated theoretically with a time-dependent model including diffraction, three-wave mixing, and pump beam aberration effects. Under the conditions analyzed, an unstable resonator is found to out perform flat-flat and stable resonators in both energy conversion and output beam divergence. This result is found with unaberrated and astigmatically aberrated input pump beams.

This work was performed under the auspices of the U. S. Department of Energy by Lawrence Livermore National Laboratory under contract W-7405-Eng-48.

1. A. Kaz and L. R. Marshall, OSA Proceedings on Advanced Solid-State Lasers, **20**, 466, (1994).
2. B. C. Johnson, V. J. Newell, J. B. Clark, and E. S. McPhee, submitted to JOSA B, (1995).

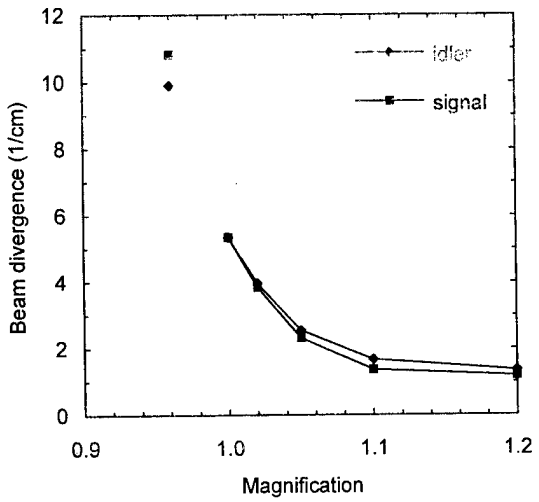

Figure 3. Comparison of the OPO output beam divergence as a function of unstable resonator magnification for a 100 mJ input pump pulse. The flat-flat cavity result is plotted at M=1.0 and the stable cavity is plotted at M=0.96 for comparison.

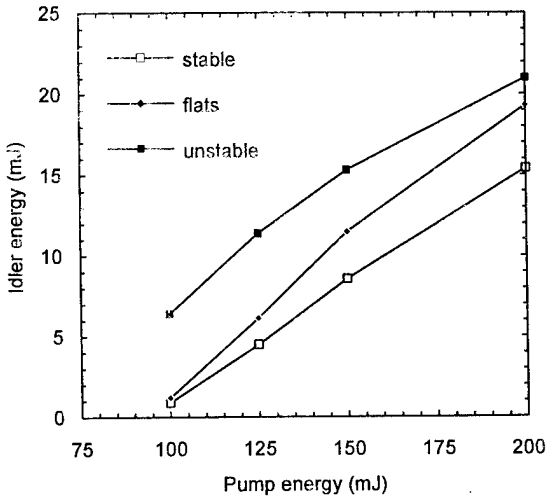

Figure 4. OPO performance with an astigmatic input pump pulse (1 λ of astigmatism). The input pump beam quality is ~3 TDL. The unstable resonator has a magnification of 1.1.

Continuous-wave mode-locked operation of a picosecond $AgGaSe_2$ optical parametric oscillator in the mid infrared

Chr. Grässer, S. Marzenell, R. Beigang and R. Wallenstein.
Fachbereich Physik
Universität Kaiserslautern
Erwin-Schrödinger-Str.46,
D-67663 Kaiserslautern, Germany

Optical parametric oscillators (OPO's) are well suited for the generation of powerful ps and fs light pulses in the near infrared region up to 4 μm [1,2]. The spectral region of the mid infrared can in principle be covered, using the nonlinear crystals like $AgGaS_2$, $AgGaSe_2$ and $ZnGeP_2$. Their broad transmission range and birefringent properties allow the generation of radiation between 1.3 and 12 μm [3,4]. Due to the high absorption coefficient in the visible and near infrared a pump source with a wavelength longer than approximately 1.3 μm has to be used. This contribution reports on what we believe is the first demonstration of continuous-wave mode-locked operation of a $AgGaSe_2$-OPO in the mid infrared spectral region. The $AgGaSe_2$-OPO was pumped by the 40 ps long pulses of the 1.55 μm signal radiation of a Nd:YLF laser pumped cw mode-locked KTP-OPO.

The experimental-setup consists of three components: the cw mode-locked Nd:YLF pump laser, the KTP-OPO and the $AgGaSe_2$-OPO. A commercial actively mode-locked Nd:YLF laser (Coherent Antares 76) with up to 18 W average power and 50 ps pulse width synchronously pumped the KTP-OPO. We used a 15.8 mm long KTP crystal with an antireflection coating for 1.053 μm and 1.55 μm cut for type II phase matching with $\Theta=90°$ and $\phi=0°$. A signal output power of 4.1 W at 1.55 μm was obtained with a 10% output coupler. The signal conversion efficiency was about 20%. An uncoated 0.3 mm etalon provided improved spectral stability and pulse quality. The pulses were bandwidth limited with a 40 ps pulse length and a bandwidth of 10 GHz. The signal radiation was focused by a f=80 mm lens into the $AgGaSe_2$ crystal through one of the curved resonator mirrors. The $AgGaSe_2$ crystal (4x4x6 mm^3) was cut for type I phase-matching ($e \rightarrow o+o$) at $\Theta=70°$. It was antireflection coated for the signal wave at 2.2 μm. Because of the small walk-off angle of 0.4° the pumping was collinear. The signal resonant cavity consisted of two spherical mirrors with a radius of curvature of 100 mm and two plane mirrors which defined a beam waist $w_0=33$ μm at the crystal's position. The coatings of the resonator mirrors were high reflective in the region of 1.85 μm to 2.58 μm.

Tuning of the $AgGaSe_2$-OPO was accomplished by rotating the crystal. A typical tuning curve is shown in Fig.1 together with the signal and idler wave calculated from Sellmeier coefficients. The calculation predicts that a variation of the phase-matching angle from 50° to 90° should result in a tuning range of the signal and idler wave which extends from 1.78 μm to 12 μm. The OPO signal and idler wave were tuned from 2.0 μm to 2.56 μm and from 3.95 μm to 6.93 μm, respectively, using two mirror sets for the resonant signal wave. The large external angle of the crystal limited the operating range to wavelength from 2.0 μm to 2.56 μm which corresponds to phase matching angles from $\Theta=60.5°$ to $\Theta=79.5°$.

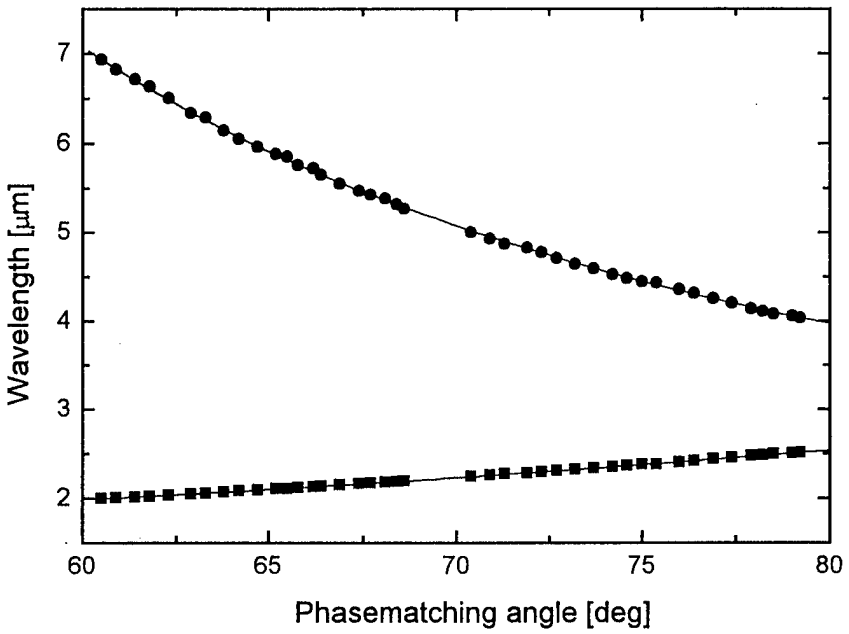

Fig. 1. Tuning curve of the $AgGaSe_2$-OPO pumped at 1.55 µm. Symbols represent experimental data, the theoretical curve was calculated with Sellmeier equations.

Fig. 2. shows the average output power of the signal and idler wave at a wavelength of 2.41 µm and 4.34 µm as a function of the 1.55 µm-pump power. The threshold pump power of 800 mW measured in front of the focusing lens corresponds to about 600 mW inside the crystal. This power loss is due to a 25 % reduction at the focusing lens, the input mirror and the crystal's surface. This threshold power is in agreement with the calculated value of 480 mW assuming a round trip loss for the signal wave of 11 %. At input powers of 2.4 W the total power of signal and idler output exceeded 520 mW. For pump powers higher than 2.2 W the output starts to saturate. The reason for this saturation is not investigated in detail but may be caused by reconversion of signal and idler radiation into pump radiation at a pump power value 3 times above threshold. Also an

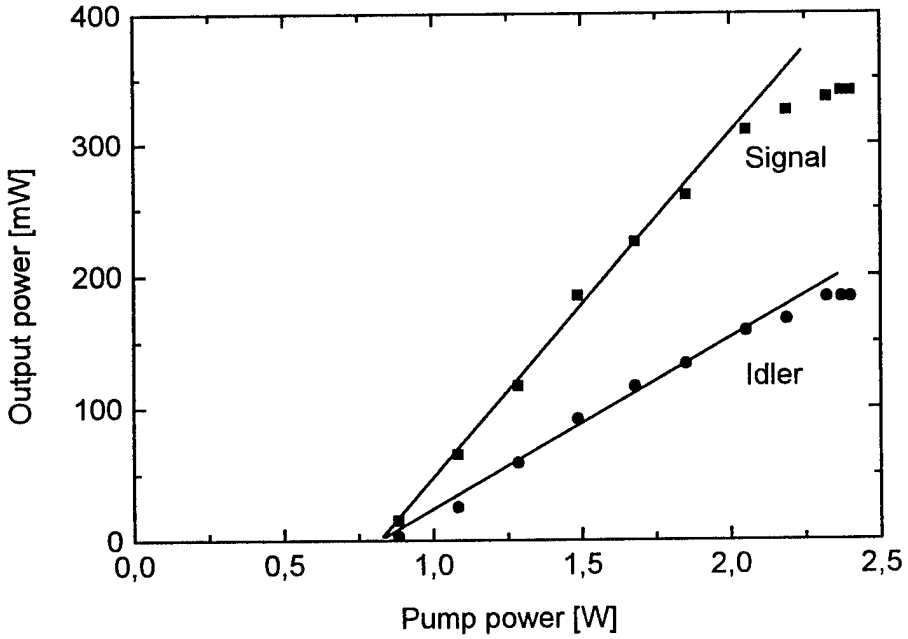

Fig. 2. Signal and idler output power as function of the pump power.

increased thermal lensing effect in the crystal resulting in a reduction of the Q-value of the resonator may cause a reduction of the output power. The external efficiency was 21 % with a slope efficiency of 39 %. The measured pump depletion of 50 % indicates that 0.9 W of the pump power was converted into signal and idler power. According to the Manley-Rowe relation this corresponds to 0.58 W signal and 0.32 W idler power. These values are in good agreement with the measured power taking into account the losses for both waves.

Thermal problems caused by absorption of pump or signal wave radiation are a major concern in cw mode-locked operation of a $AgGaSe_2$-OPO. Our investigation showed, that absorption of the intracavity signal wave power was the main reason for crystal damage. Keeping the signal intensity inside the crystal below $I_{av} \sim 110$ kW/cm^2 did not cause any damage. This can be easily done by adjusting the output coupling to the available pump power.

These first results clearly indicate that the synchronously pumped $AgGaSe_2$-OPO is an efficient source for widely tunable mid infrared ps pulses. Shorter pulses will be obtained by using as pump light, e. g. , the 1.5 μm signal radiation of a mode-locked Ti:sapphire-laser-pumped CTA-OPO. In first experiments this OPO generated 0.9 ps pulses at 1.5 μm with an average power of up to 700 mW. The results of these investigations which are present in progress as well as the prospect for the generation of mid infrared fs pulses will be discussed in detail.

1. Special issue on optical parametric oscillators: J. Opt. Soc. Am. B **10**, 2162 (1993).
2. Special issue on optical parametric oscillators: Appl. Phys. B **60**, 411 (1995).
3. Cheung, K. Koch, G.T. Moore, Opt. Lett. **19,** 631 (1994).
4. Komine, J.M. Fukumoto, W.H. Long, Jr and E.A. Stappaerts, IEEE STQE **1**, 44 (1995).

Improved OPO brightness with a GRM non-confocal unstable resonator

Suresh Chandra and Toomas H. Allik
Science Applications International Corporation
1710 Goodridge Drive, McLean, VA 22102
(703)704-3268, Fax (703)704-1752

J. Andrew Hutchinson
U.S. Army CECOM
Night Vision & Electronic Sensors Directorate
Fort Belvoir, VA 22060

Mark S. Bowers
Aculight Corporation
40 Lake Bellevue, Suite 100
Bellevue, WA 98005

Plano-parallel resonators are the most commonly used cavities with optical parametric oscillators (OPOs) pumped by a Q-switched Nd:YAG laser or its harmonics. Simple in construction, plano-parallel resonators normally produce excellent efficiencies, but, for all but very low pulse energies (< 1 mJ), they produce large beam divergence and consequently low brightness. Good beam quality from high energy OPOs is of interest particularly when the OPO output is used in further nonlinear frequency conversion processes. Recently, it has been demonstrated that an unstable confocal resonator, with a convex outcoupler mirror, can improve OPO beam divergence resulting in improved doubling efficiency to the OPO second harmonic.[1] In this paper, a non-confocal unstable resonator with a gradient reflectivity mirror (GRM) is investigated for improving the beam brightness of a fixed-frequency, high energy β-barium borate (BBO) OPO. This resonator design has a well defined transverse mode distribution that provides improved mode matching with super-Gaussian pump sources. It has been

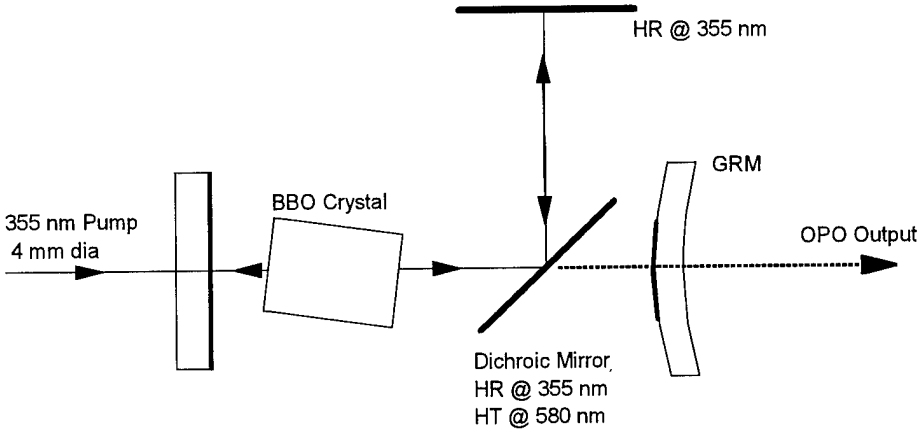

Fig. 1: Double pass pump, non-confocal GRM unstable resonator.

previously demonstrated to greatly improve the beam brightness of a solid-state dye laser over that obtained using a plano-parallel resonator [2].

A comparison between plano-parallel and unstable resonators was performed with 355 nm pumping of BBO. The double-pass pump, singly resonant oscillator is shown in Fig. 1. The pump laser was a Continuum Surelite **II** Nd:YAG laser that had a 4 ns pulse width and operated at a 5 Hz repetition rate. The BBO crystal was cut at $\theta = 32.1°$ and was 7 mm x 7 mm in cross section and 10 mm long. The cavity length was approximately 7 cm. The dichroic input rear mirror was 90% transmitting at 355 nm with maximum reflectivity near the signal wavelength of 580 nm. The GRM was obtained from the National Optics Institute of Canada. The GRM was formed on a 2 m convex radius of curvature surface while the back AR coated surface was 2 m concave. It was a supergaussian mirror of reflectivity profile $R(r) = R(0) \exp[-(r/r_o)^4]$, where r is the distance from the center, $R(0) = 30\%$ and $r_o = 2.4$ mm. The GRM and rear mirror form a non-confocal unstable cavity with a geometric magnification of 1.4. The slightly diverging output was collimated with an external lens. The stable resonator used a plano mirror that had approximately 30% reflectivity at 580 nm.

Fig. 2 shows the input/output efficiencies for the two resonators for a 4 mm pump diameter. The slope efficiency for the GRM unstable resonator is slightly lower than that of the stable resonator. It should be noted that the reflectivities of both outcouplers were not optimized. The far-field beam divergences were determined by focusing the OPO beam with a 2 m *f.l.* mirror and measuring the energy transmitted through apertures ranging between 1-5 mm

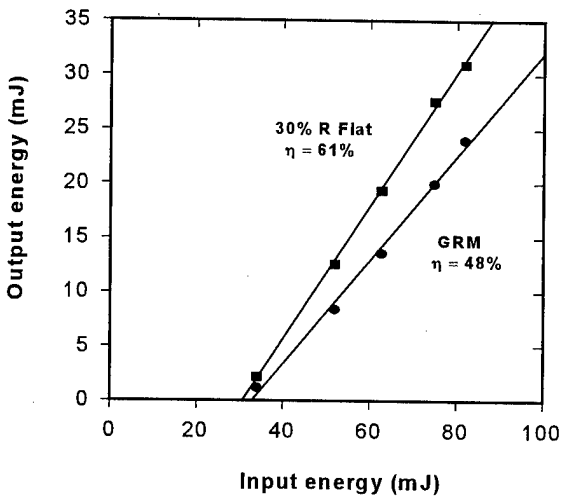

Fig. 2: OPO slope efficiency comparison between the stable and GRM unstable resonator for energies incident on BBO crystal.

in diameter. The radial intensities plotted in Fig. 3 are derived from the energy transmitted through aperture measurements. The figure shows the improvement in brightness obtained through the use of a GRM and an unstable resonator as compared to the standard plano-parallel resonator.

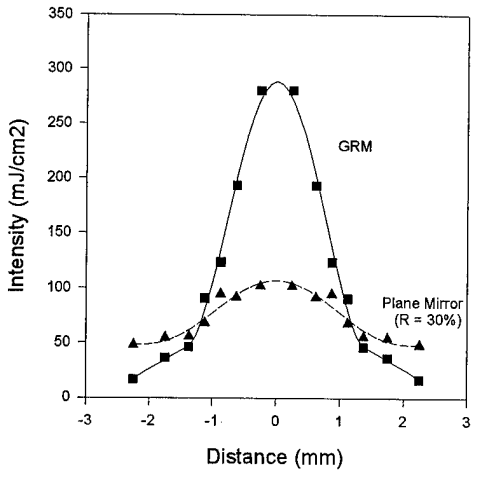

Fig. 3: Far field radial intensity distribution for the stable and the GRM unstable resonator.

The authors thank Walt Bosenberg of Lightwave Electronic Corporation for helpful discussions.

References

[1] J. Clark, B. Johnson and V. Newell, "Frequency doubling of narrowband high energy optical parametric oscillators," in Solid State Lasers and Nonlinear Crystals, Gregory J. Quarles, Leon Esterowitz, L. K. Cheng, Editors, Proc. SPIE Vol. **2379**, 256, 1995.

[2] "Non-confocal unstable resonator for solid state dye lasers using a gradient reflectivity mirror", S. Chandra, T.H. Allik and J.A. Hutchinson, Optics Letters *(accepted for publication).*

A KTA OPO Pumped by a Q-switched, Injection-seeded Nd:YAG Laser

T. Chuang, Jeffrey Kasinski and Horacio R. Verdún
Fibertek, Inc. 510 Herndon Parkway, Herndon VA 22070
Tel: (703) 471-7671; FAX: (703) 471-5806

The applications of potassium titanyl arsenate ($KTiOAsO_4$), or KTA, in optical parametric oscillators have increased dramatically, particularly when the fundamental pump sources are lasers with wavelengths near 1 μm and the signal wavelengths are near 1.5 μm. The primary reason for this is due to the fact that KTA possesses a much lower absorption beyond the 3 μm wavelength than does KTP. Usually, the wavelength beyond 3 μm is the idler wavelength when a KTA or a KTP OPO is pumped by a Nd:YAG or a Nd:YLF laser. The absorption at the 3 μm wavelength generates some thermal related effects to the OPO, such as thermal lensing, which are difficult to overcome or correct. This reason alone, and the fact that KTA is similar to KTP in many ways, including the damage threshold and nonlinear coefficients, make it likely that KTA will replace KTP in certain OPO applications where the thermal effects must be avoided.

In a recent project, in which a single longitudinal mode (SLM) laser wavelength at 1.53159 μm must be generated for the purpose of the eye-safe wind shear lidar detection in the lower atmosphere, a KTA crystal was chosen to form an OPO pumped by an injection-seeded, Q-switched and diode-pumped Nd:YAG laser. The choice was based upon two considerations. First, the lower absorption at 3 μm in a KTA crystal allowed simpler design approaches. Second, when pumped by a Nd:YAG laser, a KTA OPO operated at near noncritical phase matching (NCPM) can produce the desired wavelength. Because of these, a KTA OPO was constructed with a diode-pumped, Q-switched and injection-seeded Nd:YAG laser.

The structure of the Nd:YAG laser was based on that already reported by Kasinski, et al. [1] The pumping sources were 80 diode bars, arranged in a circular manner to provide a circularly uniform gain profile. A KD*P Q-switch was employed to produce short pulses. The SLM operation of the Nd:YAG laser was achieved by injecting an SLM seed laser into the laser cavity. Operated at 30 pulses per second (PPS), the laser produced 19 mJ of energy with a pulsewidth of ~ 20 ns. Its transverse mode profile was nearly diffraction limited. The SLM operation of the laser was verified by the pulse buildup time advance and the elimination of the mode beating in the laser pulse.

The KTA crystal used in this work was grown by Crystal Associates, Inc. Its dimensions were 5 mm x 5 mm x 15 mm. It was cut at $\theta = 90°$ and $\phi = 15°$, with a cutting accuracy of 0.25°. Both the entrance and exit faces were anti-reflection coated for 1.064 and 1.532 μm. The pump beam propagated on the xy plane along the 15 mm dimension with its polarization on the xy plane. The polarization for the signal wave was parallel to that of the pump beam, while that for the idler wave was along the z-axis. These cut angles gave rise to a Type II phase matching near NCPM, as compared to a conventional x-cut NCPM where ϕ is equal to 0°. The calculated signal wavelength at $\phi = 15°$ was 1.5316 μm, while that at $\phi = 0°$ was 1.534 μm. The walk-off angle at the $\theta = 90°$ and $\phi = 15°$ cut was found to be ~ 2 mrad, while the effective nonlinear coefficient, d_{eff}, was calculated to be 4.37 pm/V,[2] which was ~ 3% smaller than that at $\theta = 90°$ and $\phi = 0°$. Therefore, a KTA OPO operating at $\theta = 90°$ and $\phi = 15°$ should be almost as efficient as that operated at $\theta = 90°$ and $\phi = 0°$.

The OPO resonator consisted of a flat/flat type cavity design and was a singly resonant cavity at the signal wave. The input mirror had a high reflection (HR) coating at 1.5 μm and a high transmission (HT) coating at 1.064 μm. The output mirror had an HR coating at 1.064 μm and $\sim$ 60% reflection at 1.5 μm. Since the gain of an OPO greatly depends on the cavity round trip time, the OPO cavity length was kept as short as possible. The cavity length was $\sim$ 2.5 cm for this work.

The input-output relation for the OPO was measured. The result is presented in Fig. 1. The beam diameter for the pump laser was measured to be 1.2 mm. Three curves are presented in the figure. One is for the unseeded pump laser, another one is for the seeded one. The maximal output energy obtained was $\sim$ 6.7 mJ with the unseeded pump laser, while that for the seeded pump laser was $\sim$ 7.5 mJ. The OPO conversion efficiency (defined as the ratio of the OPO output energy to the incident pump energy on the crystal) is plotted against the incident pump intensity, as illustrated in Fig. 2. Similar to Fig. 1, there are three curves in Fig. 2. One is for the unseeded pump, another one is for the seeded pump. The threshold for OPO with the unseeded pump was $\sim$ 14 MW/cm^2, while that for the seeded pump was $\sim$ 9 MW/cm^2. The conversion efficiency for the seeded pump at 50 MW/cm^2 incident intensity was as high as 49%. For the unseeded pump, however, the highest conversion efficiency was $\sim$ 42%, occurring at 66 MW/cm^2 incident intensity. One important point conveyed by Fig. 2 is that, beyond 50 MW/cm^2 incident pump energy, the conversion efficiency for the OPO with the seeded pump seemed to enter a region of oscillation, indicating perhaps that the conversion oscillated back and forth between the pump and the signal (idler) waves as the pump intensity was increased. The OPO wavelength was measured indirectly to be 1.5322 μm. This value is 0.6 nm apart from the targeted wavelength of 1.5316 μm. The discrepancy is believed to be due to the accuracies of the measurement instrument (0.5 nm resolution) and the crystal angle cutting.

To better understand the performance of the OPO, we conducted a model calculation based on the well known three-wave coupled equations.[3] The model took into account the pump depletion and made assumptions that 1) the temporal pulse shape of the pump was Gaussian, 2) the spatial profile of the pump was a plane wave and 3) there was a single frequency in the OPO cavity. Some of the experimental parameters were used in the calculation, such as the pump pulsewidth, pump beam diameter, OPO cavity length and mirrors' reflectivities of the OPO cavity. The results of the calculation are given in Figs. 1 and 2 respectively. It is clear in both figures that the calculated results are in closer agreement with those obtained with the seeded pump. This is understandable since the conditions in the case of the seeded pump are closer to those in the model calculation. Note that the calculated conversion efficiency shown in Fig.2 also exhibits a tendency of oscillation beyond 42 MW/cm^2. The model calculation provided us confidence that the OPO performed appropriately.

Fig. 3 shows two oscilloscope traces. The first is that of the seeded pump pulse and the second, the OPO pulse. A huge pump depletion is evident in the figure. The pulsewidth of the OPO pulse is about 20 ns, simply following that of the pump pulse.

In conclusion, we have demonstrated a KTA OPO at near NCPM, pumped by a diode-pumped, Q-switched and injection-seeded Nd:YAG laser. The angle variation along the crystalline angle of ϕ provides a method for blue wavelength tuning while maintaining phase matching close to NCPM, hence preserving the merits of NCPM as much as possible.

1. Jeffrey Kasinski, et.al. IEEE J. Quant. Elect. 28, 977 (1992)
2. K. Kato, IEEE J. Quant. Elect. 30, 881 (1994)
3. Orazio Svelto, "Principles of Lasers", 2nd edition, Plenum Press

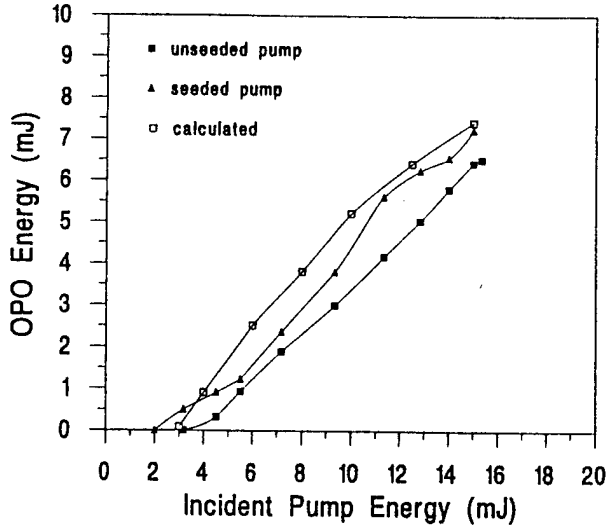

Fig. 1 The performance of the OPO, with a calculated result.

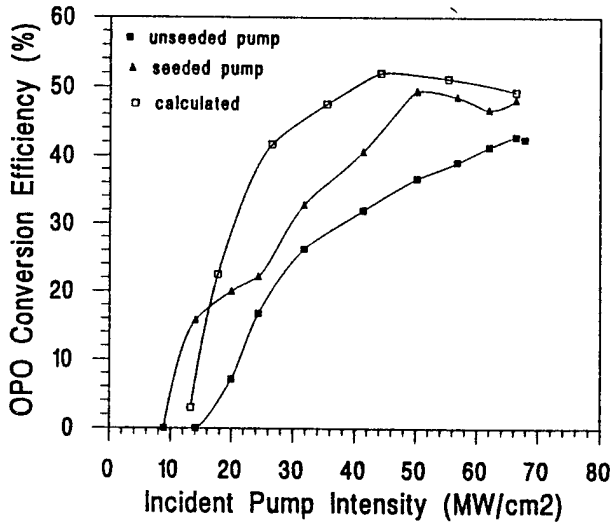

Fig. 2 The conversion efficiency of the OPO, with a calculated result.

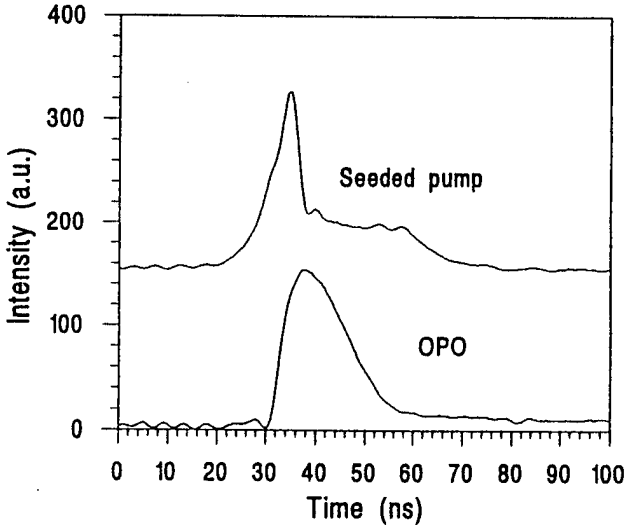

Fig. 3 The oscilloscope traces of the seeded pump and OPO pulses.

Synchronous pumping of an optical parametric oscillator using an amplified quasi-cw pump envelope.

S. D. Butterworth, W. A. Clarkson, N. Moore, G. J. Friel and D. C. Hanna

Optoelectronics Research Centre, University of Southampton

Southampton, U.K., SO17 1BJ

Tel +44 1703 593144 Fax +44 1703 593142 E-mail sdb@orc.soton.ac.uk

There are many experimental situations where laser power requirements are well in excess of those available from cw lasers, but where the alternative of Q-switched lasers is not suitable, due to the excessive intensity or the pulse duration being too short for the intended application. As an example, a laser producing pulses in the μsec regime can provide quasi-cw pumping conditions for short lifetime laser transitions, eg. Ti:sapphire. Thelong quasi-cw pump pulse can provide sufficient time for frequency selection to be effective in Ti:sapphire or in optical parametric oscillators (OPO's), with Mhz linewidths achievable in principle. Thus with long pulses many of the benefits of cw operation can be retained, but at higher powers

By pulse-slicing the laser at pulse repetition rates equal to the inverse fluorescence lifetime, and then subsequent amplification, high power extraction and maximum pulse energy in the amplified pulse are achieved. Thus for example by using Nd:YLF (τ_f≈450μsec), operation at 2kHz with say 10μsec pulses allows pulse power with up to 50 times that which could be extracted cw but without the associated thermal penalties that such high power cw generation would incur.

In our present system we use a simple end-pumped double-pass amplifier to achieve small signal gains of ~34 for a modest pump power of 4Watts. We have used this arrangement to amplify 10μsec pulse envelopes from a cw additive-pulse mode-locked (APM) Nd:YLF laser. These amplified pulses then have sufficient peak power to allow efficient single-pass harmonic generation in lithium triborate (LBO), whereas previously when operating cw efficient SHG required the extra complexity of a resonant enhancement cavity.

This amplification scheme offers considerable flexibility in the choice of operating parameters such as repetition rate, pulse duration and the shape of the pulse envelope.

The experimental arrangement used for this demonstration is shown in figure 1. The output of the APM laser consisted of 2psec pulses at 105MHz with average cw power of 540mW. The cw beam was pulse-sliced by an acousto-optic modulator (AOM), with the diffracted beam being then amplified. A maximum diffraction efficiency of 70% was measured with this device. The pulse shape, length and repetition rate were all freely adjustable by modulation of the RF drive to the AOM. An area of increased flexibility was provided by the use of an arbitrary waveform generator, AWG (Tektronix AWG 2005). This allowed control of the pulse envelope to the amplifier, so that gain saturation during the pulse could be offset by a corresponding increase in the input signal thus enabling flat-topped output pulse envelopes to be produced (see figure 2 for a comparison).

The amplifier consisted of a 6mm long by 4mm dia. Nd:YLF rod with 1.1% doping. The crystal was AR coated at 1.047μm on one face, with the other face coated to be HR@1.047μm and HT @~0.8μm through which end-pumping took place. The signal beam entered the crystal with a small angle to the face normal allowing a double pass and separation of the input and amplified beams. The pump diode was a 4W device (SDL 2382-P1), operating at 796nm.

The two output lobes of the diode are superimposed in the rod by first separating them and then after polarisation rotation of one half, re-combining via a polarising beam splitter cube (PBC). This arrangement shown in figure 1 and described elsewhere[1] allows enhancement of the pump beam brightness, an important step in maximising the gain.

The basic approach for achieving largest gain is to minimise the pumped volume within the absorption length of the crystal. Circularity of the pump beam is not required and as such the signal beam was shaped to match the elliptical pump beam. Through a combination of crossed cylindrical lenses (f3 and f4 in figure 1) of focal length 100mm and 60mm respectively we achieved a pump beam at the laser rod with $1/e^2$ intensity radii of 175μm by 44μm. To ensure maximum gain the input signal beam was focussed with a pair of cylindrical lenses, f5 and f6 of respective focal lengths 150mm and 250mm to produce an elliptical spot of size 176μm by 57μm, such that the signal beam overlapped the most intensely pumped region of the gain medium.

Using this arrangement, a double-pass cw gain of 4.4 was obtained for an input power of 270mW. This value was considerably reduced by saturation from the small signal gain (SSG) value of 34. By using the AOM to provide pulse envelopes from the cw mode-locked pulse train with short envelope lengths and low enough repetition rates, it would be possible to access essentially the full of the small signal gain. In practice, we opted for an envelope length of 10μs at 2KHz repetition frequency, which gave an envelope energy gain of 20, reduced from the SSG by saturation. Using square input pulses we achieved a maximum amplified power of 5W (averaged over the sliced-pulse envelope), a factor of 5 greater than was available from this system under cw conditions [1]

The M^2 beam quality factor of the output beam was measured to be ~1.05, confirming that amplification did not introduce significant beam distortion. Further confirmation of the beam quality was provided by harmonic generation. A 15mm long LBO crystal was used for single-pass doubling. A generated single-pass SH power of 2.5W was measured (envelope average), this is significantly greater than that achieved under cw conditions, where an enhancement cavity was used to achieve 0.65W.

The SH beam was subsequently used to drive a synchronously-pumped OPO again based on LBO. The singly resonant OPO was basically the same as that described elsewhere [1], which had a threshold of 170mW under cw pumping conditions, for a signal wave of 950nm and an output coupling of 2.5%. The corresponding pulsed threshold was 475mW (envelope average). Figure 2 shows the typical temporal behaviour of the OPO for a pump power of 1.7W in a flat-topped pulse. As an inset the behaviour is shown without the pulse-shaping via the AWG. Here, the pump pulse shows a drop in power as saturation of the amplifier occurs during the pulse. It should be noted that a penalty is paid when using the shaped envelope in that significantly higher power was available with the unshaped pulse (2.5 W cf. 1.7W flat-topped). After a build-up time of ~2μsec, oscillation occurs with a large depletion of the pump (50%) as shown in figure 2. The output powers obtained for 1.7W of pump were 250mW for the signal at 950nm and 150mW for the idler at 1164nm. These results indicate performance close to that observed for the cw pumped oscillator, so the expectation is that, with further optimisation of the setup, the performance of the cw oscillator will be fully reproduced in this pulsed fashion, with tuning from 0.65μm to 2.65μm [1].

The experiment described here was chosen as a demonstration of the concept for using high gain amplification of long pulses to create a quasi-cw pump source with power substantially greater than would be available in cw operation. There is much scope for extending the capabilities of such a source, particularly by moving to higher power diode pumps, particularly in the form of a diode bar with output beam shaped for longitudinal pumping [2]. An advantage demonstrated here even in our non-optimised arrangement, and with modest pump power, has been the ability to achieve

efficient single-pass doubling for a long, quasi-cw pulse, without the complexity of a resonant enhancement cavity as needed for cw operation.

Acknowledgements

This work has been funded by the Engineering and Physical Science Research Council, UK. We also thank Tektronix, UK for the generous loan of the arbitrary waveform generator used in these experiments.

References.

1. S. D. Butterworth, S. Girard and D. C. Hanna, J. Opt. Soc. Am. B, **12**, vol 11 (1995) to be published.

2. W. A. Clarkson, A. B. Neilson and D. C. Hanna, CLEO Europe technical digest, Paper CFH6, p.410-41 (1994)

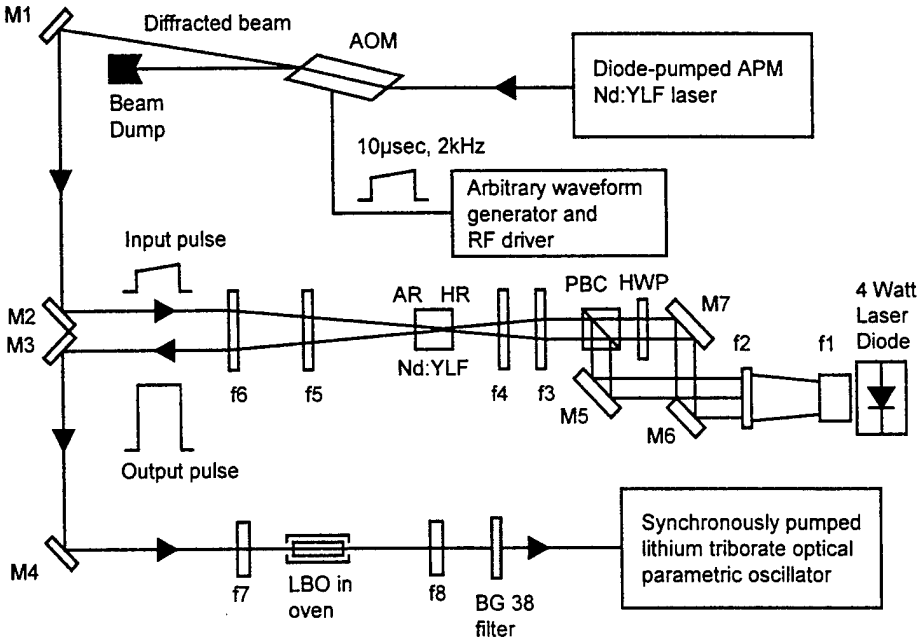

Figure 1. Schematic layout of the experiment. AOM-acousto-optic modulator, HWP-half-wave plate, PBC-polarizing beam-splitter cube, M1-M4, HR@1.047µm, f1-f8, lenses, M5-M7, HR@0.8µm.

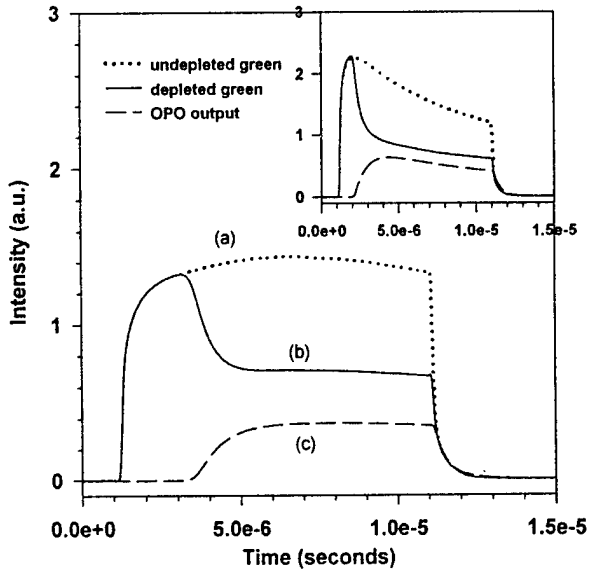

Figure 2. Temporal behaviour of the synchronously pumped quasi-cw OPO. The traces shown are a) the undepleted pump pulse, b)the depleted pump pulse and c) the OPO output. Shown inset is the same behaviour but using a square input pulse to the amplifier to show the saturation as it occurs over the pulse.

Short Pulse Lasers I

WE 1:30 pm-3:15 pm
Gold Room

Paul French, *Presider*
Imperial College of Science and Technology, U.K.

Saturable Bragg Reflector Modelocking of Cr^{4+}:YAG Laser Pumped By a Diode-Pumped Nd:YVO_4 Laser

B.C. Collings
Princeton University, Engineering Quad, Olden Street, Princeton, New Jersey, 08544
(609) 258-2856 FAX (609) 258-1954

S. Tsuda, W.H. Knox, J.B. Stark,
J.E. Cunningham, W.Y. Jan, R. Pathak
AT&T Bell Laboratories, Holmdel, NJ 07733
(908) 949-8365 FAX (908) 949-2473

K. Bergman
Princeton University, Engineering Quad, Olden Street, Princeton, New Jersey, 08544
(609) 258-1174 FAX (609) 258-1954

The utilization of the nonlinear optical Kerr effect has rapidly advanced the progress in the generation of ultrashort optical pulses at many wavelengths [1]. In 1991, Shestakov et al. reported the first room temperature CW lasing of Cr^{4+}:YAG [2] in the 1550 nm telecommuncations window of optical fiber, and Kerr-Lens-Modelocking (KLM) has produced 46 fs pulses [3,4]. The absorption band is centered around 1000 nm [5]. In this paper, we use a diode pumped Nd:YVO_4 laser to pump a Cr^{4+}:YAG laser and we demontrate femtosecond self-starting passive modelocking using a new Saturable Bragg Reflector (SBR) epitaxial semiconductor structure. In addition, we compare SBR modelocking in this laser with KLM and discuss the relative merits of the two modelocking schemes.

Tsuda *et al.* recently demonstrated that a low-loss intracavity saturable bragg reflector structure consisting of a single GaAs quantum well embedded in an AlAs/AlGaAs Bragg reflector (shown in Figure 1) can be used to passively modelock argon-pumped Ti:Sapphire lasers and diode-pumped Cr:LiSAF lasers, resulting in self-starting 90-100 fs pulses around 860 nm [6]. In the present case, we are interested in extending this technique to 1550 nm using Cr:YAG as the gain medium. We show two cavity configurations: SBR and KLM cavities (Figures 2a and 2b). The SBR modelocking cavity consists of an astigmatically-compensated Z configuration with focusing mirrors of 10 cm radii of curvature and two brewster cut SF10 prisms to provide the dispersion compensation, with a 20mm brewster-brewster cut Cr^{4+}:YAG crystal (IRE-POLUS). The Cr^{4+}:YAG crystal was pumped through one of the focusing mirrors by a diode pumped Nd:YVO_4 laser (Spectra-Physics OEM) capable of delivering up to approximately 10 W of CW power at 1060 nm.

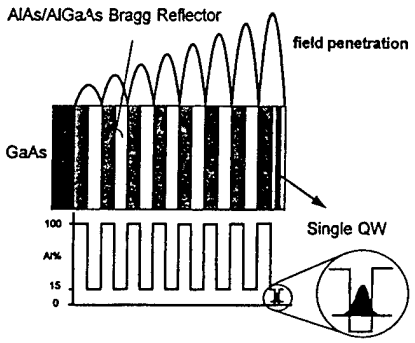

Figure 1)

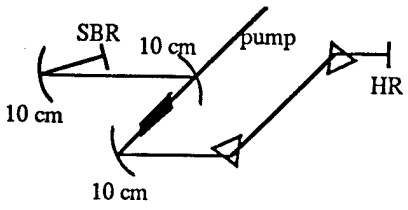

Figure 2a)

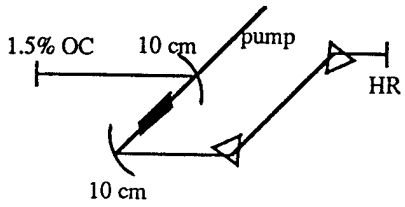

Figure 2b)

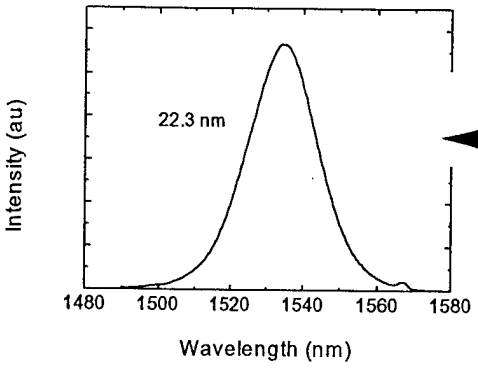

Figure 3a)

SBR

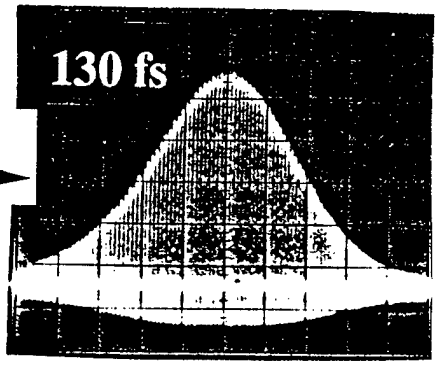

Figure 3b)

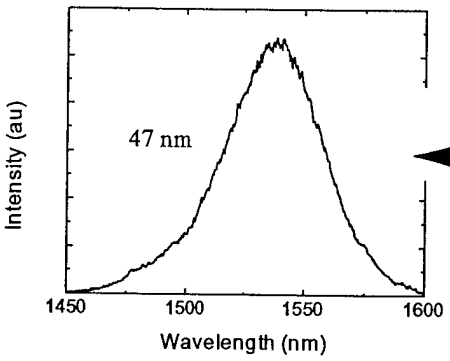

Figure 4a)

KLM

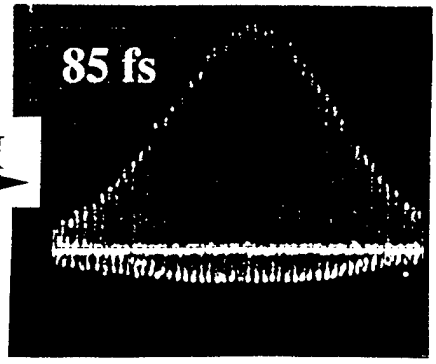

Figure 4b)

Modelocking with the SBR was obtained at wavelengths between 1530 and 1550 nm Figures 3a and 3b show a typical spectrum and autocorrelation. In SBR mode, we obtained 30-50 mW output powers with pulsewidths in the range 110-130 fs, in a self-starting TEM_{00} mode. The repetition rate is 140 MHz. To operate in KLM mode wherein the modelocking dynamics are controlled by self-focusing modelocking, we remove the SBR and focusing mirror from the cavity (Fig. 2b) and carefully adjust the cavity alignment and pump focusing to obtain modelocking. Since KLM is not self-starting, we used the SBR in a weakly-coupled external cavity to start the KLM. We were also able to start the KLM by vibrating an intracavity mirror. Figures 4a and 4b show the typical spectrum and autocorrelation in KLM mode. We obtained 150 mw average power and pulsewidths of ~85 fs.

In the case of intracavity SBR modelocking, several mechanisms are possible : purely passive modelocking caused by the ultrafast transient reflectivity of the SBR [6], or KLM that is continuously self-started by the ultrafast transient reflectivity. A mixture of these effects is also possible, however it appears that SBR dominates over KLM for the majority of cavity alignments. We will discuss this further.

References

1. D.E. Spence, P.N. Kean, and W. Sibbett, *Opt. Lett.*, **16**, pp. 42
2. A. V. Shestakov, N. I. Borodin, V. A. Zhitnyuk, A. G. Ohrimtchyuk and V. P. Gapontsev, CLEO Conf., Post-deadline Paper CPDP11, 1991.
3. P. M. W. French, N. H. Rizvi and J. R. Talyor, *Opt. Lett.*, **18**, 1993, pp. 39-41.
4. Y. Ishida and K. Naganuma, *Opt. Lett.*, **19**, 1994, pp. 2003-5.
5. A. Sennaroglu, C.R. Pollock and H. Nathel, *J. Opt. Soc. Am. B.*, **12**, 1995, pp. 930-7.
6. S. Tsuda, W. H. Knox, E. A. de Souza, W. Y. Jan and J. E. Cunningham, *Opt. Lett.*, **20**, 1995, pp. 1406-8.

An efficient diode-based Ti:sapphire ultrafast laser

Murray K. Reed, Michael K. Steiner-Shepard and Daniel K. Negus
Coherent Laser Group, Coherent Inc., 5100 Patrick Henry Drive, Santa Clara, CA 95054 U.S.A.
(408) 764-4305 fax (408) 764-4818

Kerr-lens modelocked Ti:sapphire lasers pumped by cw argon-ion lasers are widely used as sources of 100-fs optical pulses [1, 2]. Producing a reliable source of sub 100-fs pulses that uses a solid-state-diode pump would greatly simplify the use of ultrafast measurement techniques. Recently much research has centered on the development of such a source using AlGaInP 670-nm diodes to pump Cr:LiSAF and related materials [3,4,5]. and powers greater than 100 mW at 860-nm using two 400-mW diodes have been reported. An alternative approach to a diode-pumped ultrafast laser is pumping Ti:sapphire with a solid-state green source: doubled Nd:YAG or Nd:YLF pumped with diodes [6,7]. While this is necessarily more complicated it has the advantage of using longer-life GaAlAs 808-nm diodes and allowing pumping of the modelocked laser with a TEM-oo mode. We have used our commercially available YAG SHG source, the Coherent DPSS-532, which uses a single 4-W laser diode pump, to pump such a laser. An output power of 175-mW at 790-nm with 53-fs pulses is produced. Second harmonic generation with a 2-mm BBO crystal produces 30-mW at 395-nm.

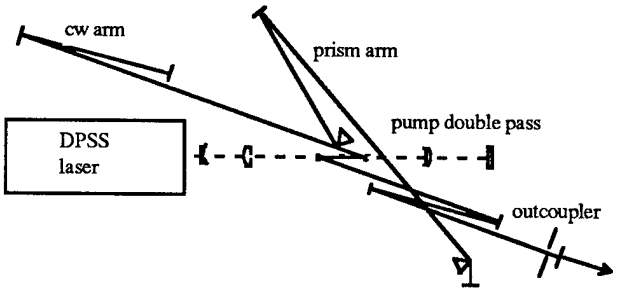

Figure 1. DPSS pumped ultrafast Ti:sapphire laser layout

As outlined by Harrison and coworkers [6] the design philosophy for a low power pumped laser is simple: "use a short heavily doped Ti:Al_2O_3 crystal in a resonator with a small waist in crystal." We find optimum performance using an uncoated 5.0-mm long Brewster rod of 0.20% doped crystal (Crystal Systems) placed in a symmetric z-fold cavity using 7.5 cm radius of curvature mirrors. The laser can be operated in either an empty cavity or, by insertion of two fused silica prisms separated by 70 cm, in a dispersion compensated cavity.

The diode-pumped solid state (DPSS) laser is a two mirror Nd:YAG ring laser with an intracavity KTP crystal for SHG. When pumped with the rated 4.0-W from a 500-μm aperture laser diode (SDL-2382-P1) the laser produces 780 mW of cw power at 532-nm. The output is pure TEM-oo with a measured M^2 of <1.05 in both axes. Single-pass absorption is less than 80% so we relay the pump back through the crystal for a double pass to improve efficiency. The total laser cavity loss is less than 2%, dominated by the absorption loss in the crystal. With a 4% outcoupler we observe a laser threshold around 200-mW of pump and a slope efficiency near 40%. At rated output the laser cw power is more than 210-mW.

Kerr-lens modelocking in the dispersion compensated cavity is stabilized by optimizing the distances between the laser cavity fold mirrors and the laser crystal and slightly closing a vertical slit near the outcoupler. To start the modelocking we use a vibrating voice coil drive on the outcoupler. When optimized the modelocking starts routinely with only a slight vibration drive which is then turned off. The modelocked output power is then reduced to 175-mW at rated power. The spectrum, in this easy starting configuration, is shown below. Centered at 790-nm the 21-nm main pulse is flanked by two spikes associated with strong self-phase-modulation. These can be removed by aperturing with slits in the prism leg if required.

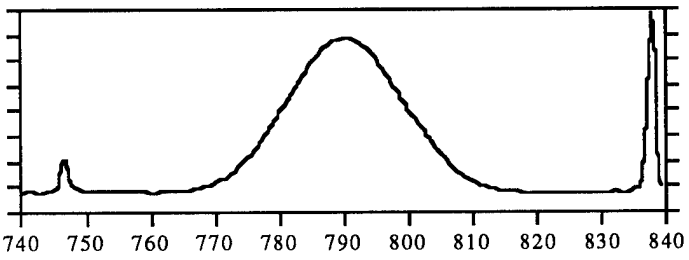

Figure 2. **Ti:sapphire laser spectrum**

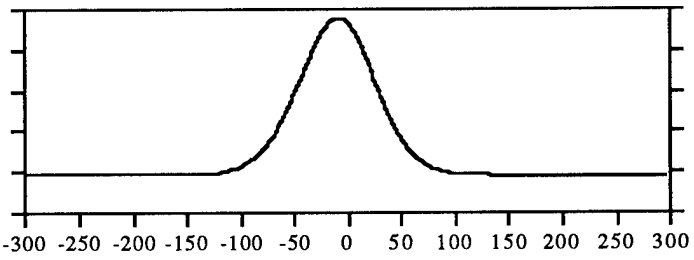

Figure 3. **Ti:sapphire laser autocorrelation**

The pulse autocorrelation is shown above. The FWHM of 82-fs corresponses to a 53-fs pulsewdith if a $sech^2$ pulse shape is assumed. The cavity is optimized for power output and not for transform limited pulses so pulses are strongly chirped, around 1.7 times transform limited, and can be externally prism compressed to shorter than 40-fs.

Second harmonic generation of this output is performed with a 2-mm thick Type-I BBO crystal. The output is focused with a 40-mm lens to a waist diameter of 30-μm in the crystal . With 170 mW input over 30-mW of output at 395-nm is produced. Since the BBO group velocity mismatch between fundamental and harmonic pulses is 200-fs/mm the SHG pulselength generated by the 2-mm crystal is expected to be broadened to longer than 100-fs.

We believe this architecture may offer a more reliable path to diode based ultrafast lasers than the systems pumped with 670-nm diodes. This device is now being optimized for operation at 500-mW of pump power to guarantee lifetimes of more than 10,000 hours . We presently have 100-mW of modelocked output in this configuration. We are also investigating self-starting operation, optimized time-bandwidth product performance and multipass SHG for improved efficiency in UV conversion and will present these results at the meeting.

REFERENCES

1 D. K. Negus and L. A. Spinelli, U.S. Patents Number 5,079,772 (Jan. 7, 1992) and 5,097,471 (Mar. 17, 1992), "Mode-locked Laser Using Non-linear Self-Focusing Element" .

2. For example see the Special Issue on Ultrafast Optics and Electronics, IEEE J. Quantum Electron. **QE-28**, 2084 (1992).

3. M. Dymott and A. Ferguson,Opt. Lett. **20**, 1157 (1995).

4. V. P. Yanofsky, F. W. Wise, A. Cassanho and H. P. Jenssen,Opt. Lett. **20**, 1304 (1995).

5. D. Kopf, K. J. Weingarten, L. R. Brovelli, M. Kamp and U. Keller, Opt. Lett. ,**19**, 2143 (1995).

6. J. Harrison, A. Finch, D. M. Rines, G. A. Rines and P. F. Moulton,Opt. Lett. **16**, 581 (1991).

All-Solid-State Diode-Pumped Tunable Femtosecond Cr:LiSAF Regenerative Oscillator/Amplifier

R. Mellish, R. Jones, N. P. Barry, S. C. W. Hyde, P. M. W. French and J. R. Taylor

Femtosecond Optics Group, Physics Department,
Imperial College, London SW7 2BZ, U.K.
Tel. : 44-171-594 7706 Fax. : 44-171-589 9463 email: paul.french@ic.ac.uk

C. J. van der Poel and A. Valster

Philips Optoelectronics Centre
Prof. Holstlaan 4, 5656 AA Eindhoven, The Netherlands

All-solid-state Cr:LiSAF lasers can replace Titanium-doped sapphire (Ti:Al_2O_3) lasers for many applications, delivering reasonably high c.w. average power levels, ultrashort picosecond and femtosecond pulse operation and narrow line-width operation. We report here the first all-solid-state tunable Cr:LiSAF femtosecond laser oscillator/amplifier system which is pumped by AlGaInP semiconductor diodes. The oscillator generates pulses of less than 55 fs, tunable from 835 - 910 nm, with up to 70 mW average output power in a single beam. The shortest pulsewidths measured to date are 25 fs. This diode-pumped oscillator is used to seed a diode-pumped regenerative amplifier which delivers pulses energies as high as 2.7 μJ (measured before the grating compressor) at a repetition rates up to 25 kHz. The compressed pulses were of ~ 1 μJ energy and ~ 200 fs duration.

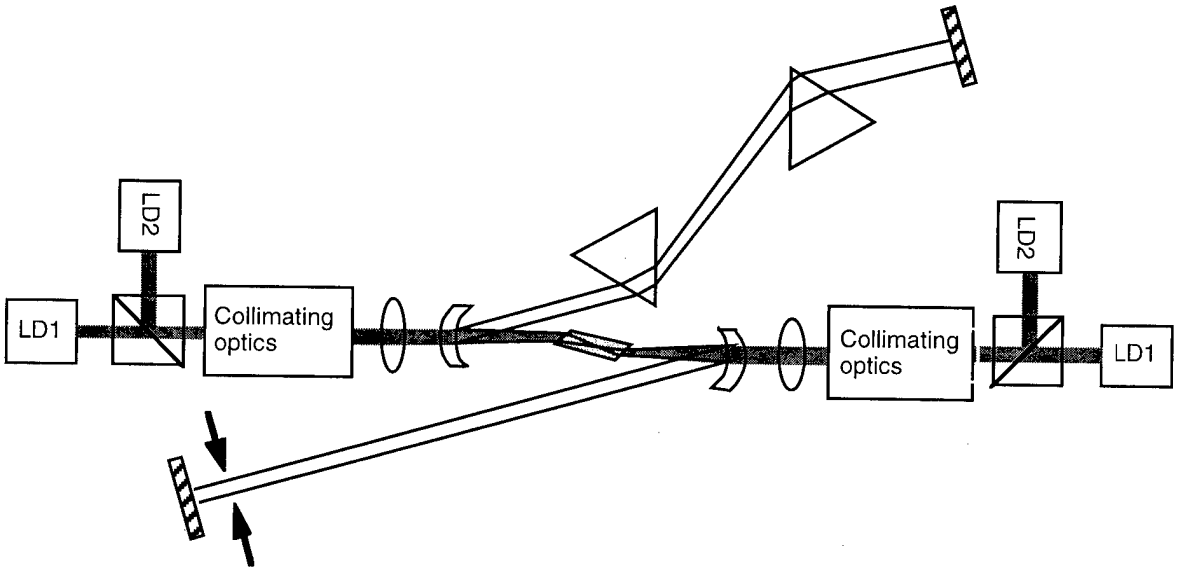

Figure 1. Schematic of diode-pumped KLM Cr:LiSAF femtosecond laser oscillator

Previously we had employed AlGaInP diodes of 160 μm stripe-width to pump the first tunable picosecond all-solid-state Cr:LiSAF laser [1] and the first femtosecond all-solid-state Cr:LiSAF laser oscillator [2]. The latter device employed an intracavity MQW semiconductor saturable to achieve femtosecond pulse generation with the relatively low intracavity power levels available with these pump diodes. We now report an improved oscillator which is pumped by much brighter diodes of 50 μm stripe-width. The resulting intracavity power levels were sufficient to achieve Kerr Lens Mode-locking (KLM) in the cavity shown in Figure 1. Each pump diode provided 300 mW which after polarisation-combined and beam shaping, resulted in a total of 900 mW of pump radiation being absorbed in the 1.7 % doped laser rod. The cavity mirrors were all of 99.9 % reflectivity except the output coupler. With an output coupler of 0.12 % transmission, the laser delivered pulses of less than 40 fs duration with up to 70 mW average output power. This mirror operated near the edge of its reflectivity curve and this limited the available bandwidth. Using a 0.05 % transmission mirror with a flat reflectivity profile centred on 840 nm, this laser tuned from 835 - 910 nm generating pulses shorter than 55 fs. KLM was initiated by either tapping a mirror or using an acousto-optic modulator on one of the quartz prisms. The amplitude stability was better than 1 %. Replacing the output coupler with a high reflector produced pulses as short as 24 fs with a time-bandwidth product of 0.39. Figure 3 shows the autocorrelation trace of these pulses. This measured duration was limited by the autocorrelator used. We note that slightly shorter pulses have been reported from a similar laser, although with less output power [3]. We are now working to simplify our femtosecond laser oscillator and have observed KLM in an end-pumped laser.

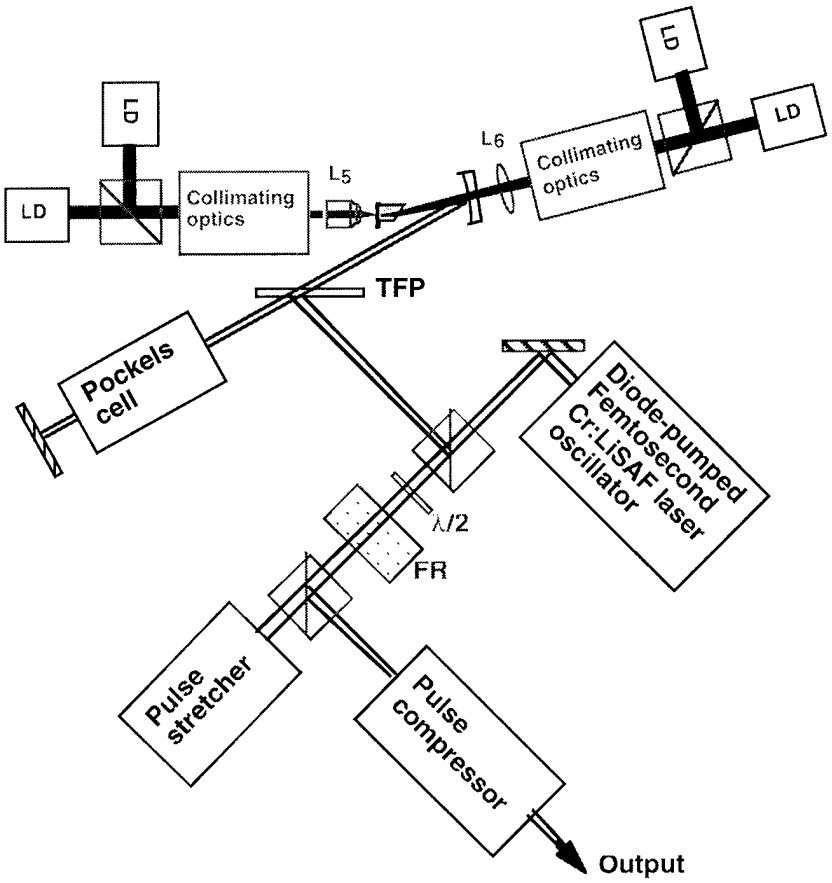

Figure 2. Schematic of diode-pumped Cr:LiSAF femtosecond laser oscillator/amplifier system

Figure 2 shows the configuration of the diode-pumped regenerative amplifier. This was considerably improved compared to our earlier system [4] which was previously demonstrated to amplify the pulses from an argon ion-pumped Spectra Physics Tsunami laser oscillator and tuned from 805 - 875 nm. Improving the mirror reflectivity's to 99.9 % and pumping with four full power (300 mW) diodes with improved beam-shaping permitted us to amplify 100 fs pulses of 200 pJ from the diode-pumped Cr:LiSAF oscillator to energies as high as 2.65 μJ (measured before the compressor). The output energy of this regenerative amplifier remained constant as a function of pulse repetition rate up to 25 kHz, the maximum possible with our pockels cell driver. Figure 4 shows the recompressed pulses from the all-solid-state diode-pumped oscillator/amplifier. These pulses were of ~ 200 fs duration due to uncompensated third order group velocity dispersion (GVD) in the stretcher, compressor and regenerative amplifier cavity. This amplifier can be considerably simplified by either eliminating the grating stretcher or using an optical fibre to dispersively broaden the pulses.

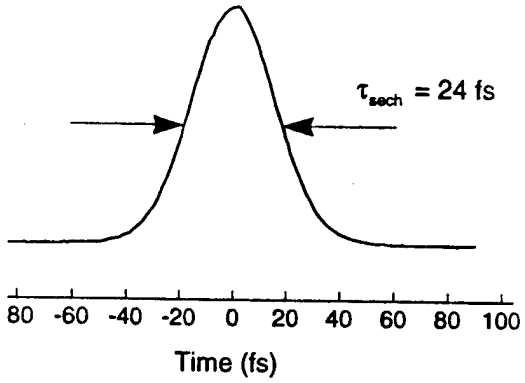

Figure 3 Autocorrelation trace of shortest pulses from the tunable all-solid-state KLM Cr:LiSAF laser oscillator

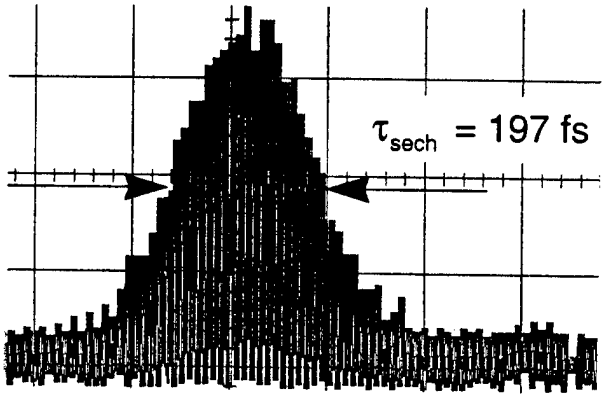

Figure 4 Autocorrelation trace of μJ pulses from the tunable all-solid-state Cr:LiSAF laser oscillator/amplifier system

This all-solid-state diode-pumped laser technology has the potential to provide low-cost compact devices for ultrafast instrumentation. We have already used the femtosecond oscillator described above in a two photon microscope developed by Carl Zeiss, Oberkochen. This will be discussed. Other applications include medical imaging, the measurement of surface micro-roughness using second harmonic generation and electro-optic sampling. The amplified pulses are sufficiently intense for continuum generation and parametric generation e.g. [5]. In the near future, the demonstration of low threshold and/or self-starting [6] KLM diode-pumped lasers will greatly simplify the oscillator design. Furthermore, the use of higher power pump diode arrays will permit significantly higher powers to be obtained from both oscillators [7] and amplifiers. We anticipate many new applications for versatile, low-cost, ultrafast all-solid-state lasers.

References

[1] P. M. W. French, R. Mellish, J. R. Taylor, P. J. Delfyett and L. T. Florez, Electron. Lett., **29**, (1993) 1263
[2] R. Mellish, P. M. W. French, J. R. Taylor, P. J. Delfyett and L. T. Florez, Electron. Lett., **30**, (1994) 223
[3] M. J. P. Dymott and A. I. Ferguson :"18 fs pulse generation from a diode-pumped self-mode-locked Cr:LiSAF ", in *Conference on Lasers and Electro-optics*, Paper CWM1, Volume 15, 1995 OSA Technical Digest Series(Optical Society of America, Washington, DC, 1994) pp 251-252
[4] S. C. W. Hyde, N. P. Barry, R. Mellish, P. M. W. French, J. R. Taylor, C. J. van der Poel and A. Valster, Opt. Lett., **20**, (1995) 160
[5] M. K. Reed, M. K. Steiner-Shepard and D. K. Negus, Opt. Lett., **19**, (1994) 1855
[6] F. Falcoz, F. Balembois, P. Georges and A. Brun, To be published in Optics Letters
[7] D. Kopf, J. Aus der Au, U. Keller, G. L. Bona and P. Roentgen, Opt. Lett., **20**, (1995) 1782

Self-Starting Diode-Pumped Femtosecond Cr:LiSAF Laser

Franck Falcoz, François Balembois, Patrick Georges,
Gérard Roger and Alain Brun

Institut d'Optique Théorique et Appliquée
Unité de Recherche associée au CNRS N° 14
B.P. 147
91403 ORSAY-FRANCE

Since its first demonstration in 1991 by Spence et al in Ti:sapphire [1], Kerr Lens Mode-locking has revolutionized the world of ultrafast solid-state lasers. Pulses shorter than 10 fs have been obtained in self-mode-locked Ti:sapphire [2]. However these lasers require the use of green pump light, coming from an argon ion laser or from a diode-pumped frequency doubled Nd:Yag laser. In order to develop a compact and efficient ultrafast laser, Cr:LiSAF is well suited due to its large absorption band in the red, where high power laser diodes are now available. Femtosecond pulses have already been obtained in diode-pumped Cr:LiSAF lasers by using different methods such as: multiple quantum well or anti-resonnant Fabry Perot saturable absorber [3-5] and regenerative mode locking [6]. We now report on a self starting Kerr lens mode-locked diode-pumped Cr:LiSAF laser that produces sub-100 fs pulses.

To pump the laser, we used two single stripe GaAlInP diodes from Applied Optronics with a 1x100 μm^2 emitting area and producing 400 mW at 670 nm. The relatively good beam quality allowed us to pump the amplifying crystal through the cavity mirrors and to use a classical X fold cavity configuration as shown in the figure 1. The LiSAF crystal was placed at the focus point of two concave mirrors M_1 and M_2. These mirrors had a radius of curvature of 100 mm, a highly reflective coating between 800-900 nm and an antireflection coating at 670 nm. The cavity was ended by two plane mirrors M_3 (highly reflection coating) and the output coupler M_4. We used a 5 mm long Brewster cut LiSAF crystal, from Lightning Optical Corporation, with 1.5 % doping level in order to reduce the thermal effects wich occur in higher doped crystals. The absorption was around 95 % at 670 nm. The following pumping scheme was used to reshape the beam coming from the diode and to compensate the astigmatism. A first objective (f=15 mm) collimated the diode beam. Then a cylindrical afocal system with a magnification of 10 modified the beam in the direction parallel to the junction of the diode. Finally in order to focus the diode through the cavity mirror we used an objective with a long focal length (f=100 mm, doublet). Taking into account the transmission of the reshaping optics, the total absorbed pump power was 300 mW for each pump way. With a CCD camera, we measured a pumping spot size of around 60×30 μm^2 in diameter. Two SF 10 prisms with a tip to tip distance of 250 mm were used to compensate the group velocity dispersion in the cavity. A slit near the output coupler initiated and enhanced the pulsed regime and another slit after the prisms allowed us to tune the cavity wavelength.

To optimize the femtosecond operation, we carefully adjusted the cavity parameters (concave mirrors separation and crystal position) in agreement with the approach presented by Cerullo et al [7].

In order to increase the intracavity power and to improve the non linear effects we used a low transmission output coupler (0.1%). In this configuration we achieved self-starting KLM without the need of any starting mechanism. To study this self-starting mechanism, we first blocked the cavity over a period of several seconds and then we unblocked the laser. Typical behaviour of the laser is shown on Fig. 2. After one second of cw emission, the laser became unstable and turned to the femtosecond regime. When the cavity was blocked over a shorter period (typically less than one second) the build-up time was reduced to around 200μs. Self-sustaining fs regime over several hours of operation have been obtained.

To compensate the positive group velocity dispersion introduced by the output coupler (8 mm thick) and the autocorrelator elements (focusing lens and beamsplitter), we added an external sequence of four fused silcate prisms (prisms separation: 30 cm) between the laser and the autocorrelator. Pulses as short as 55 fs (assuming a $sech^2$ pulse shape) at 850 nm with an average output power of 10 mW were produced with a corresponding spectrum width of 16.7 nm. The time bandwidth product was 0.38 indicating that the pulses were not completely transform limited. This can be explained by the asymmetry of the pulse spectra which could be due to third order dispersion in the SF10 prisms.

In order to obtain higher ouptut power we tried to use the 1 % output coupler. In this case, we did not achieve a self-starting regime. To start the femtosecond regime, we used a simple moving mirror and we were abble to obtain femtosecond pulses. Then we could stop the shaker and the laser still operated in this regime for a long period. With the SF10 prisms, 70 fs pulses at 850 nm were produced with a spectrum width of 11.7 nm corresponding to a time-bandwidth product $\Delta t \Delta \nu$ of 0.34. This value indicates that the pulses were close to transform limited. However, we removed the SF10 prisms and added two LaK31 prisms in the cavity in order to reduce the third order dispersion in the cavity. In that case we have obtained transform limited pulses of 45 fs with an average output power of 30 mW and a spectrum of 18.5 nm (Fig.3).

In conclusion, we report on a simple and compact **self starting** diode-pumped femtosecond Kerr lens mode-locked Cr:LiSAF laser. In this regime, 55 fs pulses with 10 mW average power have been obtained. We also demonstrated that a simple moving mirror can be used to initiate the femtosecond regime (like in fs Ti:Sapphire laser) and pulses as short as 45 fs have been produced.

References:

[1] D.E. Spence, P. N. Kean, and W. Sibbett, Opt. Lett. 16, 42 (1991).
[2] J. Zhou, G. Taft, C. Huang, M. Murname, and H. C. Kapteyn, Opt. Lett. 19, 1149 (1994).
[3] P. M. W. French, R. Mellish, J. R. Taylor, P. J. Delfeytt and L.T. Florez, Electron. Lett. 29, 1262 (1993).
[4] D. Kopf, K. J. Weingarten, L. R. Brovelli, M. Kamp, and U. Keller, Opt. Lett. 19, 2143 (1994).
[5] S. Tsuda, W.H. Knox, E.A. de Souza, W.Y. Jan and J.E Cunningham, Opt. Lett. 20, 1406 (1995).
[6] M. J. P. Dymott, and A. I. Ferguson, Opt. Lett. 19, 1988 (1994).
[7] G. Cerullo, S. De Silvestri, and V. Magni, Opt. Lett. 19, 1040 (1994).

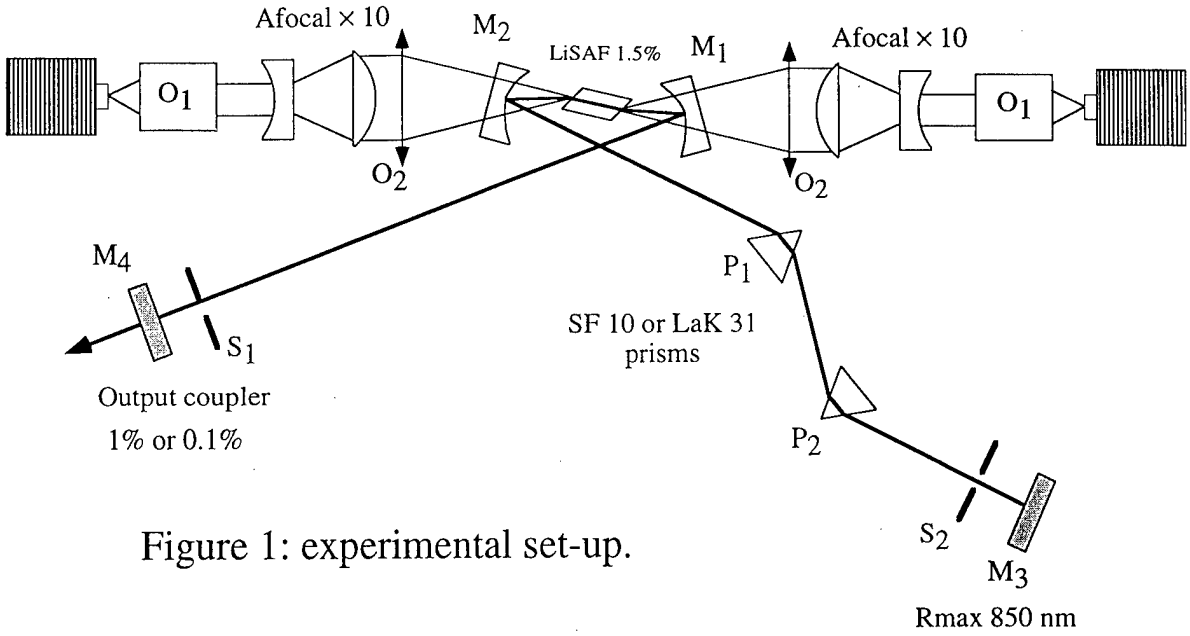

Figure 1: experimental set-up.

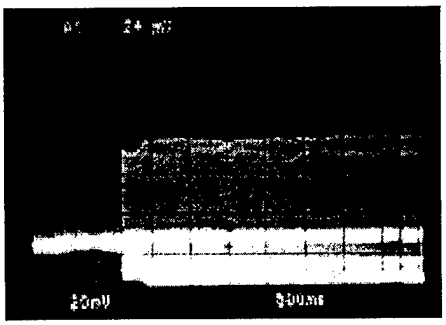

Figure 2: self starting behavior of the laser.

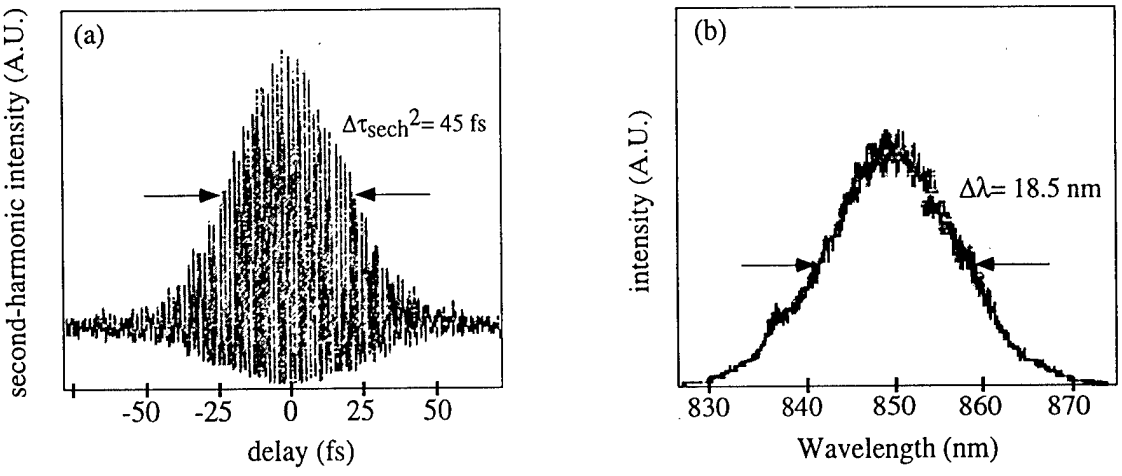

Figure 3 : interferometric autocorrelation and spectrum of the shortest femtosecond pulses produced.

Self-starting femtosecond diode pumped Cr:LiSGAF laser

V. P. Yanovsky and F. W. Wise
Department of Applied Physics, Cornell University , Ithaca NY 14853 ph. (607) 255 9956, fax (607) 255 7658

Until recently most attention in the development of compact, all-solid-state (i.e., diode-pumped) femtosecond laser oscillators has been devoted to Cr:LiSAF (Cr^{3+}:$LiSrAlF_6$). A relatively new crystal of the Colquiriite family, chromium-doped LiSrGaF (Cr:LiSGAF) possesses spectroscopic properties very similar to those of Cr:LiSAF, but has lower thermal expansion coefficient and anisotropy of thermal expansion. We recently reported the generation of 50-fs pulses from a Kerr-lens modelocked (KLM) diode-pumped Cr:LiSGAF laser.[1] Although KLM is a wavelength-tunable and inexpensive technique, it is generally not self-starting. In addition it demands more critical alignment than saturable absorber modelocking methods. These include modelocking using saturable mirrors (SM) with a multiple quantum well used either as a mirror directly[2] or embedded into anti-Fabry-Perot-saturable absorber (AFPSA)[3], or a single quantum well in a multilayer mirror. In the last case the SM is also called a saturable Bragg reflector (SBR).[4]

Here we report the first self-starting modelocking of a Cr:LiSGAF laser. We use a SM with a single quantum well in the top layer of the mirror[4] as a mode locker. The laser generates transform-limited 96-fs pulses at 40 mW average power. Because SM rely on wavelength-dependent absorption of the quantum well structure, the laser operation wavelength must be carefully chosen in order to obtain the best performance. We present the pulsewidth dependence on the wavelength and on the intracavity dispersion for the SM containing a single quantum well.

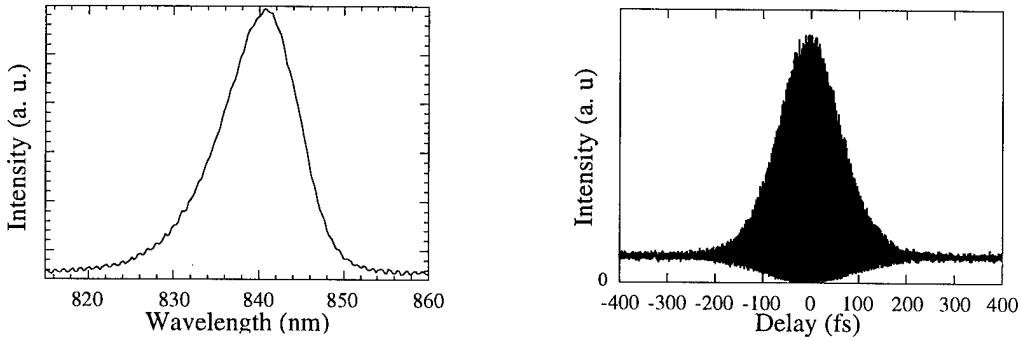

Fig. 1. Spectrum and interferometric autocorrelation of Cr:LiSGAF laser.

The laser resonator is similar to that used in our KLM-mode locked Cr:LISGAF laser[1], except that the end plane high reflector has been replaced with a 20 cm curved high reflector with the SM in its focus.The SM contains a 10-nm-thick single quantum well in the top layer of the quarter-wave dielectric mirror[4]. The high reflectance spectral range of the mirror is shifted by 30

nm to shorter wavelengths compared to the SBR described in Ref. 4 in order to be centered on the maximum of the Cr:LiSGAF gain curve.

To locate the quantum well spectral position *in situ* we recorded the cw tuning curve of the laser. A narrow adjustable slit was installed inside the cavity near the output coupler. The slit width was adjusted to ensure that the laser power did not exceed 10 mW. At this power level the laser operates cw with no tendency for Q-switching or mode locking. The dashed curve in Fig. 2 shows the tuning curve with the SM. The solid curve shows the tuning curve obtained similarly except that the SM was replaced by a high reflector. Both curves behave similarly from the short wavelength edge of the spectrum to about 815 nm, where the quantum well absorption losses become comparabe to the passive losses of the cavity. In between 842 nm and 854 nm the losses, introduced by the absorption of the quantum well added to other passive cavity loses (including losses introduced by the slit) exceed gain and the laser is below threshold. The long-wavelength edge of the tuning curve at 857 nm is caused by the drop of the semiconductor mirror reflectivity at longer wavelengths.

Stable mode locking is achieved for output powers between 15 and 40 mW and pump powers between 430 and 600 mW, respectively. The laser is aligned for a TEM_{00} mode. To modelock the laser, the wavelength is tuned between 841 and 849 nm. Tuning in this wavelength region is performed by placing a knife edge near the output coupler. As the knife edge blocks the short wavelength part of the spectrum where the maximum of the gain curve is, the laser tends to oscillate near the knife edge and moving the knife tunes the lasing wavelength. The shortest pulses are achieved at the center wavelength of 841 nm (Fig. 1). We infer 96-fs pulsewidth from the autocorrelation assuming a Gaussian pulse shape. The corresponding spectral width is 10.6 nm and the time-bandwidth product is 0.44.

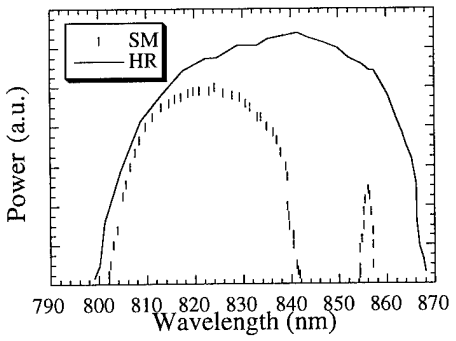

Fig.2 CW tuning curve with saturable mirror (dashed curve) and with saturable mirror replaced by a high reflector (solid curve).

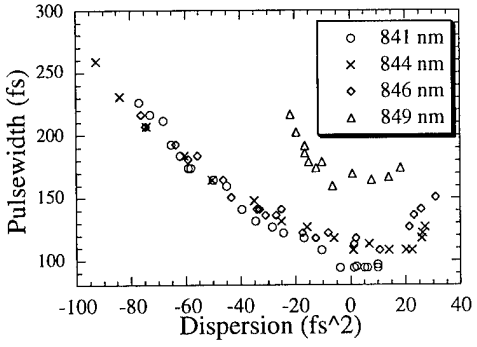

Fig.3 Pulsewidth dependence on intracavity dispersion

To optimize the laser performance we plot the dependence of the pulsewidth on the intracavity dispersion for a set of four lasing wavelengths (Fig. 3). The intracavity dispersion is changed by varying the prism insertion into the laser beam. The upper and lower dispersion value on the curves are limited by the onset of instabilities. There is a minimum in pulsewidth at about

zero dispersion for all four wavelengths. All curves, which have points corresponding to positive and negative dispersion values are roughly symmetrical relative to the zero dispersion points. This is expected with fast saturable absorber modelocking and is in contrast to the asymmetric dependence found with KLM[5,6]. To check additionally that modelocking is due to the saturable absorber rather than KLM we replaced the SM with a high reflector. No mode locking was found without the SM.

For fixed dispersion, the pulses are shorter at shorter wavelengths. Further reduction in the pulse duration by going to shorter wavelengths is limited by the onset of Q-switching instabilities. Thus for the shortest wavelength (841 nm) we were able to modelock the laser only at negative and zero dispersion. At wavelengths longer than 850 nm the laser operates only cw. This can be explained by higher losses compared to the losses at shorter wavelengths. Indeed, taking into account the quantum well absorption spectrum [7], one can conclude from Figure 2 that the heavy-hole exciton absorption should be in the vicinity of 850 nm. In addition, the reflectivity of the semiconductor mirror drops at wavelengths longer than 857 nm. This also can contribute to losses for a pulse with a spectrum 10 nm wide and centered at 850 nm. Note that in Reference 4 where an SBR was used with a diode pumped Cr:LiSAF laser, the best performance was also found displaced from the exciton absorption maximum by 10 nm but to longer wavelengths rather than to shorter. To check if higher losses at longer wavelengths are responsible for the apparent asymmetry of the modelocking behavior relative to the absorption band of the quantum well, we conducted experiments with a Ti:sapphire laser, with the expectation that the higher-gain Ti:sapphire laser should not be susceptible to losses to the same extent as the low-gain diode-pumped laser. Unlike in the case of Cr:LISGAF laser, we observed the best modelocking performance of the Ti:sapphire laser and a shortest pulse at 850 nm, the absorption maximum of the heavy-hole exciton. We believe that increasing the pump power or decreasing losses introduced by the quantum well by burying the absorber deeper into the mirror[4] will lead to the best modelocking performance, which should be observed on the exciton resonance for the Cr:LiSGAF laser as well.

In conclusion, we demonstrated a self-starting Cr:LiSGAF laser by using a saturable mirror. Pulsewidth dependence on the wavelength in the vicinity of the quantum well absorption band is shown. A lower-loss saturable mirror or higher gain is needed to realize the best mode-locking performance.

References:

1.V. P. Yanovsky, F. W. Wise, A. Cassanho and H. P. Jenssen, Opt. Lett. 20, 1304 (1995).
2. P. M. W. French, R. Mellish, J. R. Taylor, P. J. Delfyett, and L. T. Florez, Opt. Lett. 18, 1934 (1993).
3. D. Kopf, K. J. Weingarten, L. R. Brovelli, M. Kamp, and U. Keller, Opt. Lett. 19, 2143 (1994).
4. S.Tsuda, W. H. Knox, E. A. de Souza, W. Y. Jan, and J. E. Cunningham, Opt. Lett. 20, 1406 (1995).
5. H. A. Haus, J. G. Fujimoto, and E. P. Ippen, IEEE Journal of Quantum Electron. 28, 2086 (1992).
6. B. Proctor, E. Westwig and F. Wise, Opt. Lett. 18, 1654 (1993).
7.. W. H. Knox, R. L. Fork, M. C. Downer, D. A. B. Miller, D. S. Chemla, C. V. Shank, A. C. Gossard, and W. Wiegmann, Phys. Rev. Lett., 54, 1306 (1985).

47 fs pulse generation from a prismless self-mode-locked Cr:LiSGaF laser.

I. T. Sorokina, E. Sorokin, and E. Wintner

Technical University of Vienna
Gusshausstr. 27/359, A-1040 Wien, Austria
tel. 043-1-58801-3703, fax 043-1-5042477, e-mail: sorokina@ps1.iaee.tuwien.ac.at

A. Cassanho

Lightning Optical Corp., 431 E. Spruce str., Tarpon Springs, FL 34689 USA

H. P. Jenssen

University of Central Florida, CREOL 12424 Research Parkway, Suite 400, Orlando, FL 32826 USA

R. Szipöcs

Research Institute for Solid State Physics
Budapest, P.O. Box 49, H-1525, Hungary

Within the last few years remarkable progress has been made in the field of Kerr-lens mode-locked (KLM) Cr:LiSAF lasers, producing pulses as short as 18 fs [1]. Recently the KLM lasers based on a Cr:LiSGaF crystal [2] have been reported [3-5], operating in the comparable resonator design at substantially higher average mode-locked output powers.

Obviously, the major trend in the femtosecond technology nowadays goes towards the compact and reliable all-solid-state femtosecond laser sources. However, the standard KLM lasers still contain a pair of Brewster-angled prisms for providing a net negative group delay dispersion (GDD) for dispersion compensation. A constraint set by the minimum prism separation on the resonator length can be removed by the replacement of prisms by dispersive dielectric mirrors. Basically, there are two types of dispersive mirrors: Gires-Tournois interferometers (GTI) [6,7], which are essentially etalons, and chirped dielectric mirrors [8]. The chirped mirrors exhibit nearly constant GDD over a much larger bandwidth than can be obtained by using GTI for dispersion control, which resulted in the development of a femtosecond Ti:Sapphire oscillator generating pulses as short as 7.5 fs [9]. On the other hand the GTI mirrors have an advantage of negligibly low intrinsic loss, and relatively high, and adjustable (through changing of the angle of incidence) GDD, thus, being well suited for intracavity applications in femtosecond lasers. We performed the lasing experiments with both chirped and GTI mirrors. The results indicate that at the present state of research it is unlikely that the chirped mirrors for dispersion compensation will work in Cr:LiSGaF or Cr:LiSAF, like they do in Ti:Sapphire. This is mainly due to a significantly lower gain in these laser materials in comparison to that in Ti:Sapphire laser. However, the results demonstrate feasibility of successful implementation of GTI mirrors. Besides, due to the poor thermal conductivity and the presence of upconversion in these crystals, one should work with low doped and therefore relatively long crystals (typically of a few mm in comparison to 1.5 mm in Ti:Sapphire), thus, leading to the necessity to compensate a higher material dispersion. This means that in order to provide the necessary dispersion compensation a considerably larger number of reflections from dispersive mirrors is required (about 20 per round trip in comparison to 7 in Ti:Sapphire). This automatically increases the intracavity losses, which can not be tolerated in these lasers due to a five times lower output coupling than in Ti:Sapphire.

Here we report what is to our knowledge the first demonstration of femtosecond operation of a Cr:LiSGAF laser, using the dielectric multilayer mirrors, designed as GTI. In this way a Kr-pumped KLM laser was constructed, employing no intacavity prisms or mode-locking elements for starting and producing highly stable bandwidth-limited sub-50 fs pulses at λ=835 nm.

The cavity is a standard X-cavity, consisting of two curved (R = 100 mm) folding mirrors, one of which is dispersive, three flat dispersive mirrors, the Cr:LiSGAF crystal (8 mm long, 0.75 % Cr) and a 2.3 % output coupler (Fig.1). The best performance was achieved in a nearly symmetrical configuration, which contradicts our experience with a prism-controlled resonator, where a slight assymmetry was always favourable in order to achieve an optimum trade-off between stability and maximum self-amplitude modulation. The implemented dispersive mirrors exhibited low scattering losses (less than 0.1 %) with the maximum GDD of $\approx -100fs^2$, which is twice as high as that of the corresponding chirped mirrors ($\approx -50fs^2$).

An interferometric chirp-free autocorrelation trace of the laser pulses is shown in Fig.2. A corresponding pulse spectrum is given in Fig.3. Assuming a $sech^2$ pulse shape we obtained a pulse length of 47 fs. The interesting characteristic feature of the pulse spectrum is the presence of a narrow side-band around λ=880 nm. Our view of the origin of this effect as well as its quantitative analysis will be given in the presentation. We will also compare the performance of a GTI controlled Cr:LiSGaF laser with that of its prism-controlled forerunner.

In conclusion, we demonstrated what is to our knowledge the first prismless femtosecond KLM Cr:LiSGaF laser, producing stable nearly bandwidth-limited 47 fs pulses. The reported preliminary results are far from representing the ultimate performance achievable with a GTI controlled LiSGaF laser. Ways of improving the pulse duration will be discussed. At this stage the new prismless KLM laser represents a significant step towards the development of a robust compact all-solid-state femtosecond laser source.

References

1. M. J. P. Dymott and A. I. Ferguson, CLEO'95 Technical Digest, paper CWM1, 251 (1995)
2. L. K. Smith, S. A. Payne, W. L. Kway, L. L. Chase, B. H. T. Chai, IEEE J. Quantum Electron, **QE-28**, 2612 (1992).
3. I. T. Sorokina, E. Sorokin, E. Wintner, A. Cassanho, H. P. Jenssen, CLEO/EUROPE'94 Technical Digest, paper CThN3
4. I. T. Sorokina, E. Sorokin, E. Wintner, A. Cassanho, H. P. Jenssen, M. A. Noginov, OSA Proceedings on ASSL'95, Memphis (1995)
5. V. P. Yanovski, F. W. Wise, A. Cassanho, H. P. Jenssen, Opt. Lett., **20**, 1304 (1995).
6. J. Heppner, J. Kuhl, Appl. Phys. Lett.,**47**, 453 (1985)
7. P. M. W. French, G. F. Chen, and W. Sibbett, Optics Commun.,**57**, 263 (1986)
8. R. Szipöcs, K. Ferencz, Ch. Spielmann, F. Krausz,Opt. Lett., **17**, 1605 (1992).
9. Ch. Spielmann, M. Lenzner, R. Szipöcs, A. Stingl, F. Krausz, OSA Annual Meeting, paper MMM 1, Portland, OR (1995).

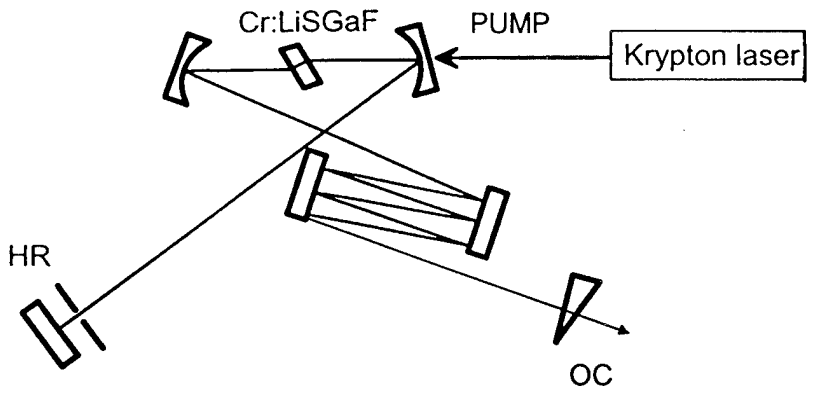

Figure 1. Schematic diagram of a compact prismless KLM Cr:LiSGaF laser.

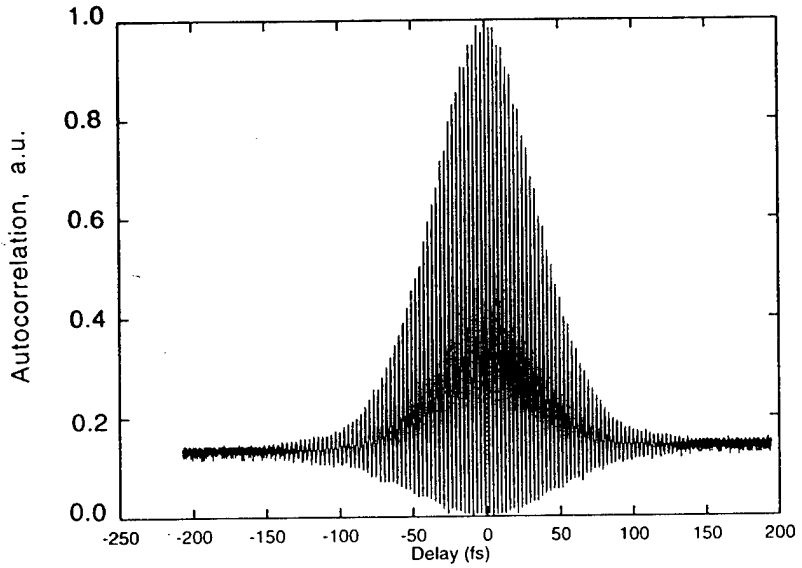

Figure 2. Interferometric autocorrelation trace of the passively mode-locked 47 fs pulses.

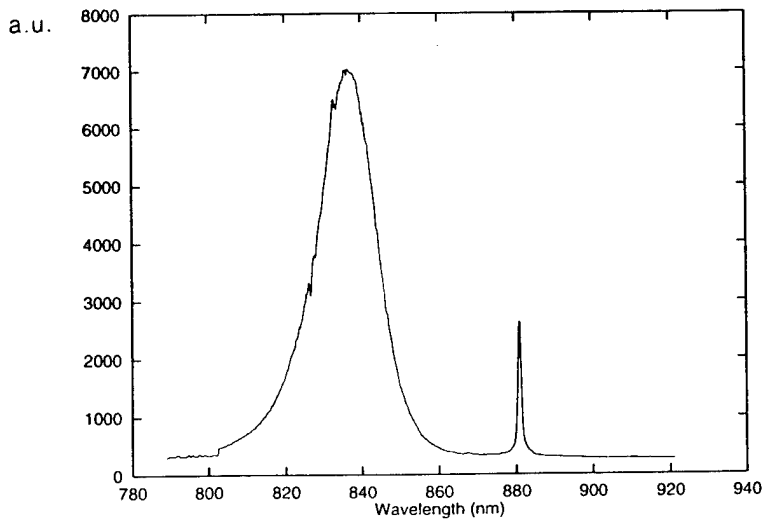

Figure 3. Spectrum of the output pulse.

Infrared femtosecond pulse generation with a 250 kHz Ti:sapphire pumped β-BaB_2O_4 optical parametric amplifier

Murray K. Reed and Michael K. Steiner-Shepard (408) 764-4305 fax (408) 764-4818
Coherent Laser Group, Coherent Inc., 5100 Patrick Henry Drive, Santa Clara, CA 95054 U.S.A.

Extending the tuning range of Kerr-lens modelocked Ti:sapphire lasers by using ultrafast optical parametric amplifiers (OPA) is now common [1, 2]. We first demonstrated that it is possible to operate an OPA system with pulse energies of only a few microjoules with a 400-nm pumped, β-barium-borate (BBO) Type-I OPA [3,4]. In this paper we describe a low energy threshold 800-nm pumped, BBO Type-II OPA designed to be converted through difference frequency mixing in $AgGaS_2$ to the midinfrared from 3-μm to 10-μm, as demonstrated by Seifert et al [5] with a higher energy system.

The pump for this system was a compact Ti:sapphire mode-locked oscillator and regenerative amplifier system, the Coherent RegA, which uses a single argon-ion laser to pump both the oscillator and the amplifier components. This produces 800-nm wavelength, 100-fs pulses with μJ level pulse energies at repetition rates up to 300 kHz.

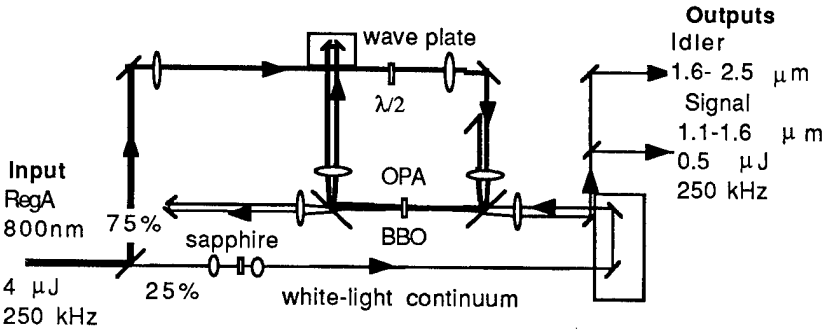

Figure 1: Optical parametric amplifier layout.

The OPA architecture involves splitting the 800-nm wavelength RegA output into two portions: one part (25%) generates a broadband whitelight continuum to seed the OPA while the other part (75%) is rotated in polarization by 90° to provide the pump for the OPA. A typical continuum spectrum, recorded with Si and InGaAs detectors, shows an exponential decay of intensity with wavelength in the infrared, however there may be a plateau, like that seen in the visible, beyond the noise level of our spectrometer. The possibility of seeding of an OPA out to beyond 1.6-μm is therefore not obvious.

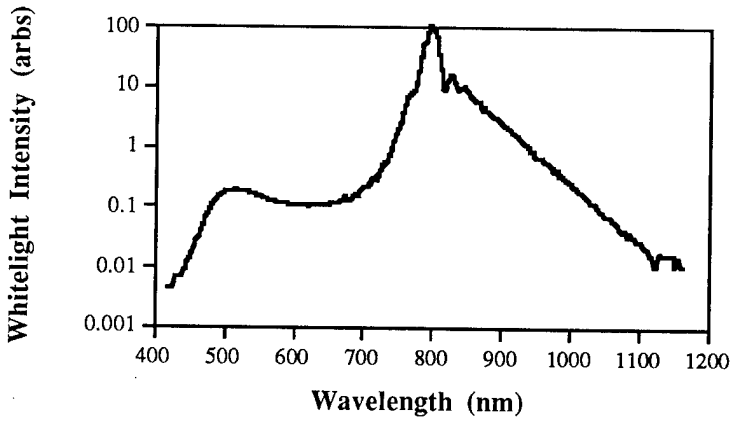

Figure 2: White-light continuum spectrum

The whitelight beam in the OPA is reflected with protected silver mirrors throughout the system, to allow maximum tuning. The two pulses, the 800-nm OPA pump and the whitelight OPA seed, are refocused,

recombined on a dichroic mirror, and mode-matched in a 3-mm long Type-II BBO OPA crystal cut at $\theta = 32^{o}$. The signal output from the OPA is tunable across the infrared by just rotating the OPA crystal for phase-matching and then slightly varying the whitelight to pump relative optical delay to allow the appropriate seed wavelength to temporally overlap with the pump pulse. The OPA is typically operated in a double-pass configuration, as shown in Figure 1, to allow compensation for GVM walkoff between the pump and signal pulses in the OPA crystal and optics. The first-pass weakly saturates the amplifier while the second-pass extracts 10 to 20% of the pump energy. Both passes are kept in the same horizontal plane so the first-pass gain peak is matched on the second-pass.

For femtosecond OPAs pump self-focusing in the OPA crystal creates a limit to the drive intensity possible and the group velocity mismatch (GVM) walkoff between the pump, signal and idler pulses creates a limit to the useful crystal length. While Type-I BBO has lower GVM and can support longer crystals and hence higher gain, the Type-II geometry has the advantage of allowing operation through degeneracy with polarizations ideal for the difference frequency mixing to the mid infrared. We therefore choose to use a Type-II crystal and picked a 3-mm crystal length as close to optimum for 100-fs pulselengths in the presence of 50 fs/mm GVM.Figure 3 shows the OPA phasematching curve, wavelength versus phasematching angle θ, calculated from the Sellmeier coefficients given by Kato [6] and experimentally measured. We see efficient OPA signal seeding well beyond 1.6-μm.

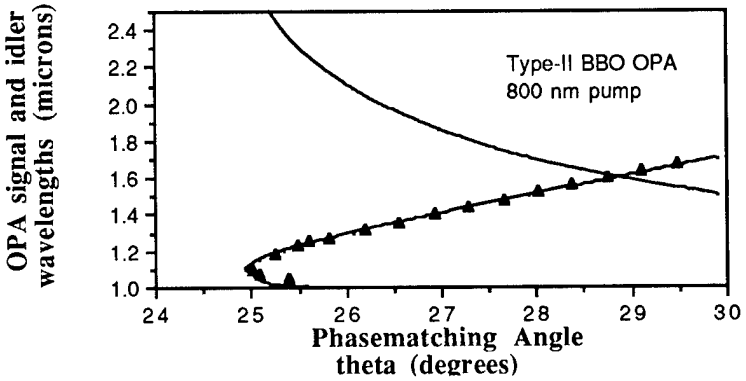

Figure 3: Optical parametric amplifier phasematching curve

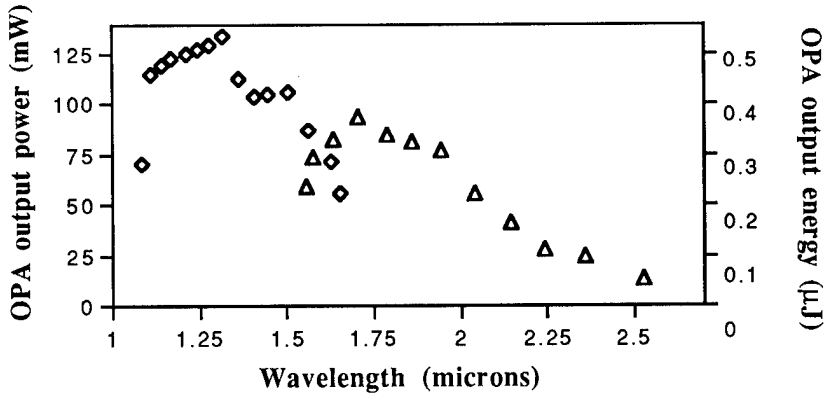

Figure 4: Optical parametric amplifier tuning curve

Figure 4 shows the OPA signal and idler energy versus wavelength measured at 250-kHz repetition rate with 4-μJ pump energy from the RegA. The double-pass OPA gain is more than 10000, so the amplified spectrum rises well above the whitelight background level. We separated the signal and idler components by using dielectric mirrors and used a thermal power meter. The total power generated was around 190-mW over most of the tuning range. Below 1.1-μm we pass the phasematching inflection point and the increase in GVM strongly reduces the gain while above 1.6-μm we are probably limited by the declining energy in the continuum seed. The first pass power ranged from around 30-mW at the peak down to 5-mW at the spectrum limits.

The signal bandwidths were measured with a InGaAs spectrometer and the signal pulses lengths were measured with a noncollinear SHG autocorrelator using a BBO crystal. The spectra and pulses both showed

some side lobe structure at most wavelengths when the OPA was optimized for maximum power output. The bandwidth and autocorrelation FWHM were measured over the tuning range with this condition. The results show that the bandwidths are near that expected for 100-fs pulses and the time bandwidth product is less than 1 over most the range except around the phasematching curve inflection point near 1.15-μm

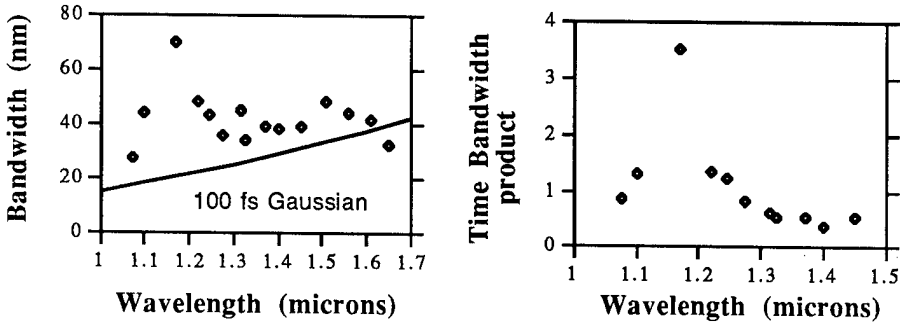

Figure 5: Optical parametric amplifier spectral quality

The spectral quality can be improved by small adjustments of the OPA delays or by reducing the drive levels. Focusing the OPA output into a 1-mm Type-I BBO crystal converts the signal to the second harmonic. The signal SHG generated could excede 10-mW with this crystal. Examples of spectraly optimized signal SHG spectra, normalised and recorded for a range of wavelengths across the signal tuning range, are displayed in Figure 6. The spectra are all Gaussian-like in shape.

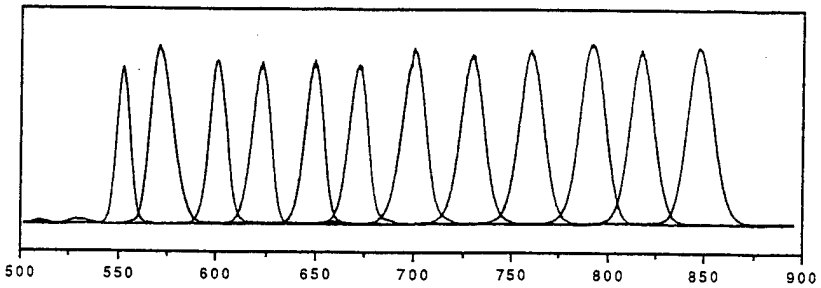

Figure 6:

We measured the pump Gaussian $1/e^2$ radii at the OPA crystal as ω_o= 120-μm x 140-μm which gives an intensity of 100-GW/cm^2 with the measured pump inputs to the crystal of 2.75-μJ of energy in 100-fs. The focused pump intensity is limited to this level by backing off the OPA crystal from the input beam focal waist to avoid beam distortion from pump self-focusing. For higher intensities we see a rapid change in the spotsize and shape of the 800-nm output beam and continuum generation in the OPA crystal.

The OPA gain should be reduced by the spatial walk-off of the extraordinary polarized pump beam. The BBO walkoff of 4° means that 140-μm radius beams separate by 75% in 3-mm and it appears that the pump and signal are aligned, for maximum output, in a slightly non-collinear geometry that compensates for this walk-off.

In conclusion we have demonstrated the use of microjoule energy, 100-fs pulses from a 250-kHz Ti:sapphire regenerative amplifier system to drive the efficient operation of a Type -II BBO optical parametric amplifier and produce high power tunable output from 1.0-μm to 1.6-μm and 1.6-μm to 2.5-μm. Taking these signal and idler outputs and difference frequency mixing in $AgGaS_2$ to the midinfrared from 3-μm to 10-μm is the next goal for this work.

REFERENCES

1. F. Seifert, V. Petrov, and F. Noack, Opt. Lett. **19**, 837 (1994).
2. See the JOSA B special issue on optical parametric devices November 1995
3. Murray K. Reed, Michael K. Steiner-Shepard and Daniel K. Negus, Opt. Lett. **19** , 1855 (1994).
4. Murray K. Reed, Michael S. Armas, Michael K. Steiner-Shepard and Daniel K. Negus, Opt. Lett. **20**, 605 (1995).
5. F. Seifert, V. Petrov, and M. Woerner, Opt. Lett. **19**, 2009 (1994).
6. K. Kato, IEEE JQE, **QE-22**, 1013 (1986).

Wednesday, January 31, 1996

Nonlinear Frequency Conversion
Poster Session

WF 3:15 pm-4:15 pm
Terrace Room

Raman spectroscopic and nonlinear optical properties of barium nitrate crystal

P. G. Zverev, T. T. Basiev
General Physics Institute, Vavilov str, 38
Moscow, 117333, Russia

and

W. Jia, H. Liu
Department of Physics, University of Puerto Rico
Mayaguez, PR 00681-5000

Barium nitrate crystal was found to be a promising nonlinear medium for stimulated Raman scattering (SRS). Previously it was shown that $Ba(NO_3)_2$ crystal can be used for developing solid state Raman shifters in the eye safe spectral region, and with an external cavity or an intracavity configuration the quantum conversion efficiency can reach up to 70% [1].

The characteristic feature of SRS is the Stokes losses that are absorbed in the nonlinear medium, resulting in the heating of the working channel. With Nd:YAG pumping (1.064 μm) these losses equals to the scattering of at least 11% of the incident energy for the first Stokes oscillation, 22% for the second Stokes. This energy causes changes of the spectral and optical properties of the Raman crystal. These effects will be discussed in the report. Firstly, we will consider the linewidth broadening of the Raman mode with increase of crystal temperature that results in the reduction of SRS gain coefficient. Secondly, the self-focusing effect due to the third-order nonlinear susceptibility will be taken into account.

The gain of the SRS process is determined by the peak cross section of the SRS active mode and is inversely proportional to the spectral linewidth. Thus, the knowledge of linewidth broadening is important to evaluate the parameters of the material as a Raman medium. In case of homogeneous broadening the linewidth (FWHM) is determined by the vibrational relaxation time τ_2 of the mode as $\Delta\Omega = (\pi c \tau_2)^{-1}$ and so these parameters can be obtain from either spectral, or temporal domain.

The coherent anti-Stokes probe scattering technique was used to measure the decay time of the Raman active mode in our experiments. This involves the excitation of SRS in a nonlinear medium by a picosecond pump pulse. A delayed probe beam travelling at a small angle provides the coherent anti Stokes scattering signal, whose intensity is measured with respect to the delay time. By analyzing the shape of the relaxation curve it is possible to measure a vibrational relaxation time which can be even an order of magnitude shorter than the laser pulse duration. This experiment allows us to obtain linewidth broadening of A_g Raman mode in $Ba(NO_3)_2$ crystal at temperature below 300 K. The relaxation time of the mode was measured to be 230 ± 10, 145 ± 10 and 50 ± 3 ps at 11, 100 and 200 K, respectively.

Direct measurements of the A_g Raman mode linewidth at room temperatures or higher were made by spontaneous Raman scattering with Ar laser excitation. The full width of the line (FWHM) was found to be 0.56 ± 0.1 cm^{-1} at room temperature, increasing to 1.1 ± 0.15 cm^{-1} at 413 ± 3 K and finally to 3.5 ± 0.2 cm^{-1} at 600 ± 5 K. The room temperature values obtained by these two different techniques are in a good agreement with each other, although the uncertainty in these values is relatively large as it was limited by the temporal and spectral resolutions of the experimental setups.

The obtained results are discussed in terms of multiphonon relaxation processes.

Another effect caused by the Stokes losses in the Raman crystal is the self-focusing. A simple Z-scan technique is known to provide precise measurements of the magnitude and sign of the third order nonlinear refractive index [3]. A mode locked Nd:YAG laser (1.064 μm) with a pulse duration of 35 ± 5 ps and a repetition rate of 10 Hz was used as a light source for our Z-scan experiments. The spatial profile of the laser output in the far field was measured to be almost Gaussian. The beam was focused into the sample by a lens with 800 mm focal length. The $Ba(NO_3)_2$ crystal, 20 mm long, was placed on a positioning stage with a stepper motor driver controlled by a microprocessor system to an accuracy of about 20 μm. The energy of the transmitted beam was measured by a photodiode placed after the aperture in the far field. A dichroic mirror placed in front of the photo diode reflects all the Stokes components and transmits only the pump radiation. Fig.1 (a) shows the Z-scan data without and with 50% aperture. The absorption of the pump beam in the focal position is due to SRS. The result of division of the two data sets is presented at Fig.1 (b). The observed Z-scan dependence exhibit a behavior typical to the nonlinear medium with the positive third order nonlinearty resulting in a self-focusing of the pump and scattered beams inside the crystal.

1. P. G. Zverev and T. T. Basiev, in *Advanced Solid-State Lasers,* OSA Technical Digest (Optical Society of America, Washington, D.C., 1995), pp. 380-382.

2. P. G. Zverev, W. Jia, H. Liu, and T. T. Basiev, Optics Lett. (1995), (to be published).

3. M. Sheik-Bahae, A. A. Said, T. H. Wei, D. J. Hagan, and E. V. Van Stryland, IEEE J. Quantum. Electron., **QE-26,** 760 (1990).

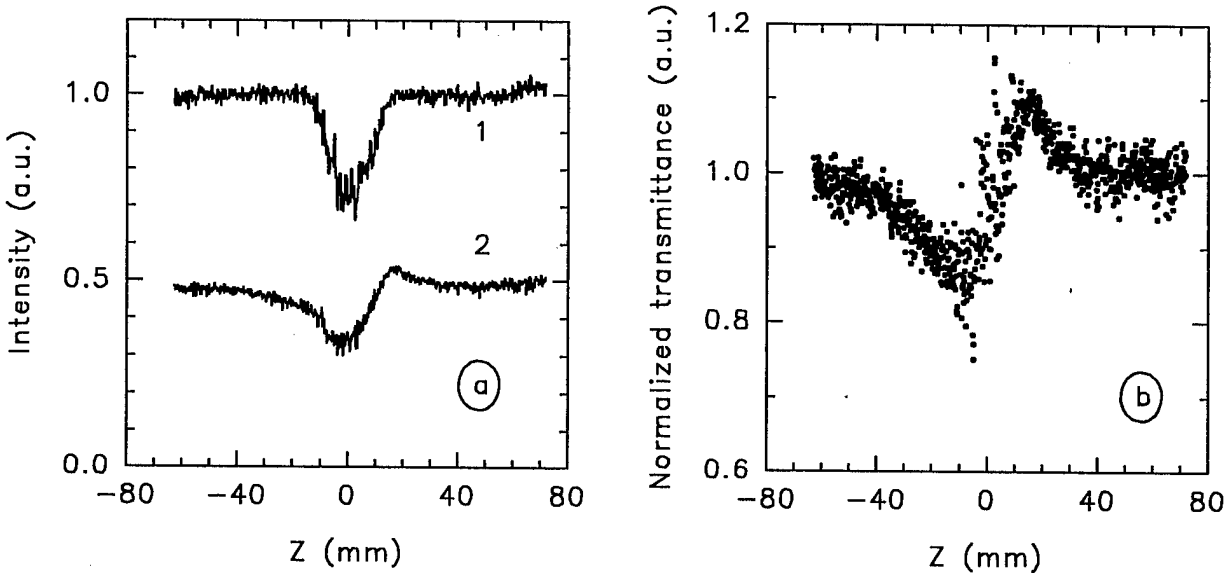

Fig.1. Open (1) and closed (2) aperture Z-scan in $Ba(NO_3)_2$ Raman crystal (a) and the result of division of the two data sets (b), exhibiting positive third order nonlinearity.

High Power Nonlinear Generation of UV

W.D. Marsh, D. Richter and J.C. Barnes
NASA Langley Research Center
Hampton VA 23681-0001
804-864-8062

Introduction

There is an increasing need to develop high power UV sources for performing remote sensing of Ozone in the atmosphere. Current systems operate by doubling the frequency of tunable dye lasers. [1] While energies approaching 100 mj/pulse are available with dye systems, they need daily dye replacement. A solid state system based on nonlinear frequency conversion of Nd:YAG light will provide a robust source of UV. Such systems have the potential for remote sensing from space.

Initial work done by Larry Marshall [2] demonstrated a solid state nonlinear frequency conversion technique to convert 25% of Nd:YAG fundamental at 1064 nm to 289 nm. While the output energy was low, the high conversion efficiency provided the motivation to investigate energy scaling to obtain output energies of 100 mj/pulse. The 289 nm light was generated by mixing tripled YAG with the 1570 nm output of a KTP-OPO in a LBO-Sum Frequency Generation crystal. This required four nonlinear crystals; CD*A doubler, KDP tripler, KTP-OPO and a LBO-SFG crystal. By energy scaling we have demonstrated 40 mj/pulse at 289 nm with 1 J/pulse of pump.

Summary

Our pump source for our experiment was a Continuum YG-682 Nd:YAG laser. The pump laser had an output of 1 joule/pulse at 10 Hz in an 8 ns pulse. The spacial profile of the output was donut shaped with a measured beam quality of 2.5 times diffraction limited. The spectral bandwidth of the pump was 160 pm FWHM at 1064 nm. (See Fig. 1)

A 20% beamsplitter was used to send 200 mj of pump to a 20 mm long KTP optical parametric oscillator. The pump beam was double passed through the KTP crystal. The KTP OPO yielded 80 mj of 1570 nm with a divergence of 9 mrad full width. The large divergence of 9 mrad is attributed to the 20 mm cavity length and the large pump radius of 4.5 millimeters.

The other 800 mj of pump was sent to a CD*A doubler and KDP tripler to yield 220 mj of 355 nm. The 220 mj of tripled yag was sent through an optical delay leg of 30 cm to synchronize the 355 nm pulse with the 1570 nm pulse of the KTP-OPO. The 355 nm was combined with the 1570 nm on a dichroic beam combiner and sent to

a 2.5 X reducing telescope. After the reducing telescope the 355 and 1570 were sent through a 15 mm long type II LBO sum frequency generation crystal. Since the LBO was non-critically phased matched for these wavelengths the 289 nm output generated was a substantial 40 mj/pulse. The 289 nm beam had a divergence of 3 milliradians. The measured spectral bandwidth of the 289 nm beam was 120 pm FWHM which was well within our system requirements of < 500 pm.

Theory

Conversion efficiencies of nonlinear processes such as described above are strongly dependent on phase matching conditions. Perfect phase matching would mean that the conservation of momentum and energy would apply for the entire content of the input beams; in our case 1570 nm and 355 nm. Perfect phase matching would allow ~100% conversion efficiency with a suitably long crystal (~10 cm).

However, perfect phase matching is impossible since the input beams have non-zero values for divergence and spectral bandwidth. In quantifying the parameters which affect conversion efficiency, terms like angular bandwidth, spectral bandwidth and temperature bandwidth products are used to describe the tolerances for various nonlinear interactions. For example, in our experiment, the bandwidth products for sum frequency generation in LBO are 0.74 mrad*cm , 6.8 C*cm and 0.42 nm*cm for angular, temperature and spectral products respectively.

The angular bandwidth product of 0.74 mrad*cm means that for a 1 cm crystal an input beam with a divergence of 0.74 mrad could only be converted 50% of the maximum conversion expected for a 1 cm long crystal. If the maximum conversion efficiency was 42% then an input beam with 0.74 mrad divergence could only be converted with an efficiency of 21%. Therefore, in trying to develop an efficient nonlinear frequency conversion process, the bandwidth products should be as large as possible or the divergence, spectral bandwidth and crystal temperature gradients should be minimized.

The angular bandwidth product can be greatly enhanced by using noncollinear phase matching in which the input beams cross at a slight angle inside the nonlinear crystal. For example, computer models have shown that the angular bandwidth product for BBO can be increased from 1 mrad*cm to 36 mrad*cm as the angle between the input beams is changed from 0 degrees to 5.5 degrees. Recent experimental data has confirmed this result.[3]

Spectral bandwidth products cannot be significantly increased by noncollinear phase matching, so to improve conversion efficiency, the input beams must be line narrowed by a suitable technique such as injection seeding. Since the output of our KTP-OPO was 0.6 nm and the bandwidth product of the LBO-SFG is 0.42 nm*cm, this implies a conversion efficiency reduction of >50% due to spectral content alone. Injection seeding of the OPO will greatly enhance the overall conversion efficiency.

Temperature bandwidth products cannot be enhanced, but are usually large enough that problems only arise when significant thermal loading is present in the nonlinear crystal. If linear and nonlinear absorption is small in the nonlinear crystal, this parameter is usually neglected. If absorption is not negligible, thermal management by use of suitable crystal holders mitigates some of the thermal loading losses.

Experimental Setup

[Figure 1]

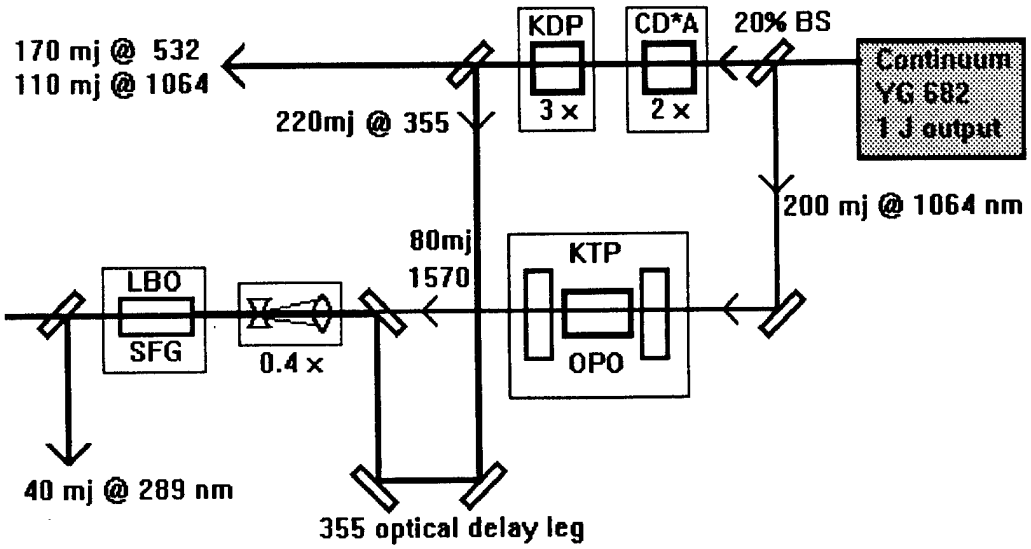

Conclusions

A nonlinear frequency conversion process has been developed to generate 40 mj/pulse of 289 nm with 1 joule/pulse of Nd:YAG pump. Significant improvement in conversion efficiency is expected when injection seeding of the OPO and noncollinear sum frequency generation are implemented. A solid state UV source capable of ~100 mj/pulse at 289 nm should be possible.

References:

[1] UV DIAL System, NASA LaRC Hampton VA 23681-0001, Dale Richter and Ed Browell 804-864-5370. System deployed on DC-8 aircraft Sept 1995.

[2] Larry Marshall and Alex Kaz, "**High Efficiency All Solid State UV Laser Source**", 1994 post deadline CLEO paper # CP-D19.

[3] W. Marsh, Noncollinear Phase Matching performed at Coherent Laser Group Inc., Santa Clara CA, Sept 5-8 1995. Future publication of Data pending. 804-864-8062

Phase-matched second-harmonic generation in ion-implanted $KNbO_3$ channel waveguides

D. Fluck and P. Günter

Nonlinear Optics Laboratory, Institute of Quantum Electronics,

Swiss Federal Institute of Technology, ETH-Hönggerberg,

8093 Zürich, Switzerland.

St. Bauer and Ch. Buchal

Institut für Schicht und Ionenforschung,

Forschungszentrum (KFA) Jülich,

52425 Jülich, Germany.

Compact all-solid-state blue lasers are of considerable technological interest in applications such as optical data storage, xerography and spectroscopy. Frequency doubling of near infrared diode lasers (DLs) offers the potential of robust, compact and reliable blue laser sources. $KNbO_3$ is one of the candidate materials for high efficiency frequency doubling of near-infrared DLs into the blue-green spectral range thanks to its high nonlinear optical coefficients, the favourable noncritical phase-matching possibilities for wavelengths around 860 nm and 980 nm at room temperature and its high threshold to optical damage [1-3]. With a fundamental power of typically 100 to 200 mW available from single-mode DLs, either resonant or waveguide structures are required to achieve high conversion efficiencies. Resonant schemes have been proven to be highly efficient, but are relatively complex and rather bulky [4]. Phase-matched second-harmonic generation (PM SHG) using waveguides is potentially efficient and ultra-compact. Recently, the formation of low-loss channel waveguides in $KNbO_3$ by multiple-energy ion implantation [5] and blue-light generation by Cerenkov-type frequency doubling of a diode laser has been demonstrated [6].

Here, we report for the first time on PM SHG in ion-implanted $KNbO_3$ channel waveguides. Up to 1.3 mW blue light at 441 nm is generated in a 5.8 mm long $KNbO_3$ channel waveguide for an incident fundamental power of 200 mW from a Ti-sapphire laser (Fig. 1). The channel

waveguides were produced by single-energy irradiation with 2 MeV He^+ ions and doses from $7.5 \cdot 10^{14}$ to $3 \cdot 10^{15}$ cm^{-2} using structured photoresist on the $KNbO_3$ samples as a direct implantation mask. The photoresist was about 6 μm thick and had four sets of channels with widths between 7 μm and 19 μm and a spacing of 100 μm between adjacent channels. The loss coefficients of these channel waveguides were between 3 and 9 $dBcm^{-1}$ at a wavelength of 860 nm and between 14 and 20 $dBcm^{-1}$ at 457 nm, respectively. The effect of the waveguide loss on the SH output power is shown in Fig. 2. The relatively high waveguide losses limit the useful waveguide length and the maximum attainable conversion efficiency. This clearly demonstrates that waveguide loss is one of the key parameter of guided wave frequency doubling devices.

Further optimisation of the photoresist shielding mask to produce narrower channel guides, post-implantation low-temperature annealing to reduce the waveguide losses [7], repoling in order to restore the nonlinear optical coefficient [8], and the selection of homogeneous $KNbO_3$ substrate crystals [9] is anticipated to increase the conversion efficiency by more than a factor of fifteen. Therefore, we envision the generation of more than 10 mW SH blue light by frequency doubling 200 mW single-mode DLs in $KNbO_3$ channel waveguides.

REFERENCES

[1] P. Günter, Appl. Phys. Lett. 34 (1979) 650.

[2] J.-C. Baumert, P. Günter, H. Melchior, Opt. Commun. 48 (1983) 215.

[3] I. Biaggio, P. Kerkoc, L.-S. Wu, P. Günter, B. Zysset, J. Opt. Soc. Am. B 9 (1992) 507.

[4] W. J. Kozlovsky, W. P. Risk, W. Lenth, B. G. Kim, G.-L. Bona, H. Jaeckel, D. J. Webb, Appl. Phys. Lett. 65 (1994) 525.

[5] D. Fluck, P. Günter, M. Fleuster, Ch. Buchal, J. Appl. Phys. 72 (1992) 1671.

[6] D. Fluck, T. Pliska, P. Günter, M. Fleuster, Ch. Buchal, D. Rytz, Electron. Lett. 30 (1994) 1937.

[7] T. Pliska, D. H. Jundt, D. Fluck, P. Günter, J. Appl. Phys. 77 (1995) 6114.

[8] D. Fluck, T. Pliska, M. Küpfer, P. Günter, Appl. Phys. Lett. 67 (1995) 748.

[9] T. Pliska, F. Mayer, D. Fluck, P. Günter, D. Rytz, M. Fleuster, Ch. Buchal, J. Opt. Soc. Am. B12 (1995) October.

The surface roughness of the films is measured using atomic force microscopy. For both $LiNbO_3$ and $LiTaO_3$ thin films, the rms roughness is less than 1% of the film thickness. The films with smaller rocking curve widths have the lowest rms roughness, between 0.4 and 0.6%. Low propagation loss is achieved with films which are thicker than 400 nm [2]. Typically, the loss is lower than 5dB/cm at 632.8 nm for the fundamental modes TE_0 and TM_0.

For bulk $LiNbO_3$ and $LiTaO_3$, the -Z and -Y faces etch faster in HF than the +Z and +Y faces. We have etched the films to determine the sign of their polarization as grown. The $LiNbO_3$ films do not get etched after several hours and remain shiny. Also, $LiNbO_3$ films grown on $LiTaO_3$ show clearly that the Y faces etch with different etching rates. We can conclude that the films are +Z oriented as grown. The conclusion is not as clear with the $LiTaO_3$ thin films because, like with bulk, the etch rates of the two polarizations are closer. But, as the films etch uniformally, we can conclude that the polarization is uniform.

Phase matching and quasi phase matching conditions

Phase matching using modal dispersion can be achieved in the thin films. We have observed phase matching in our thin films, using as the IR source, a tunable 0.5 W cw laser diode SDL-8630 emitting between 1035nm and 1065nm. For a $LiTaO_3/Al_2O_3$ film, 400 nm thick, the TM_0 mode can phase match with the TM_1 mode at the harmonic wavelength. The interaction is not very efficient as the overlap between the two modes is small. To obtain an efficient interaction between the two fundamental modes, QPM is necessary.

In bulk, proton exchange deadens the nonlinearity of the material [3],[4]. We have used proton exchange to modulate the d_{33} nonlinear coefficient and thus obtain a 0/+/0/+ type modulation. Like in bulk [5], the thin films showed an etch rate difference in HF between the exchanged and the non exchanged regions (see Fig.1). The index change due to the proton exchange process has to be taken into account for the calculation of the QPM period. Moreover, it depends on the duty cycle. Uniform exchange in $LiNbO_3$ thin films, using benzoic acid, leads to an increase for the extraordinary index around 0.14 and an index decrease around 0.05 for the ordinary index. This is slightly larger than what is observed in bulk. For $LiTaO_3$ thin films, the extraordinary index variation is, like in bulk, smaller. It is around 0.002. The index decrease is around 0.04 for the ordinary index.

In a first effort, we have focused on $LiTaO_3/Al_2O_3$ structures as the index variation due to proton exchange is smaller, thus reducing the loss due to the scattering of the grating and also making the dependence of the period less sensitive to the exchange conditions (temperature, duty cycle). Figure 2 represents the variation of the 1st order QPM period versus the film thickness, for a $LiTaO_3$ thin film periodically exchanged. First order QPM involves grating periods lower than 3 μm. We have chosen to work with 2nd and 3rd order QPM. Four gratings, 5x5 mm^2 large with period increments of 0.2 μm, are patterned in a SiO_2 mask. The proton exchange is done at 220°C. The endfaces of the planar waveguide are then polished for end-fire coupling.

A $LiTaO_3$ film, 580 nm thick, exchanged during 3 h 45 min, with a period of 5.9 μm and a duty cycle close to 70% (75% is optimum for second order QPM) has demonstrated 2nd order QPM between the two fundamental TM modes for a pump

wavelength of 1046 nm. The film exhibits loss of 10 dB/cm at 632.8 nm for the fundamental modes after proton exchange (loss were lower than 5 dB/cm before the exchange). The loss reduces the conversion efficiency and if it is assumed to be around 6 dB/cm in the IR and 15 dB/cm in the green, the conversion efficiency is reduced by a factor of 80% over the value obtained with no loss for a 5 mm propagation length [6]. About 25 mW of pump were measured at the output of the planar waveguide and approximately 500 nW of green were generated. This is consistent with the calculated efficiency for this device of 0.3% /Wcm^2 assuming a 1 mm wide waveguide.

QPM has been demonstrated in thin films. There are still technological problems to overcome. Loss for the film as grown and after the process is the main concern. Alternatives to obtain more efficient QPM in the films have to be studied. For example, Ti-indiffusion would create a +/- type modulation of the d_{33} nonlinear coefficient in $LiNbO_3$. We will report on any progress.

This work is supported in part by the Department of Commerce Advanced Technology Program 70NANB2H1241.

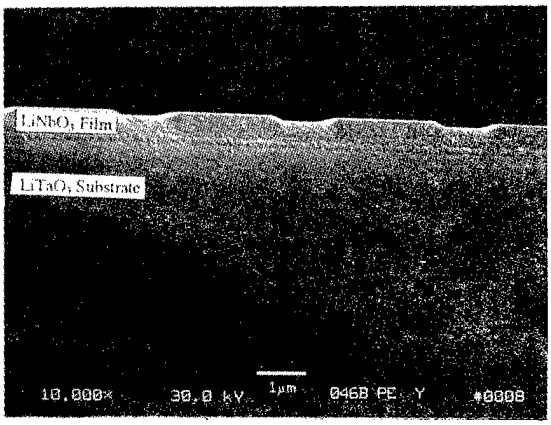

Figure 1: Y face of a periodically proton exchanged and slightly etched in HF, $LiNbO_3$ thin film grown on $LiTaO_3$. Longer etch removes entirely the exchanged regions.

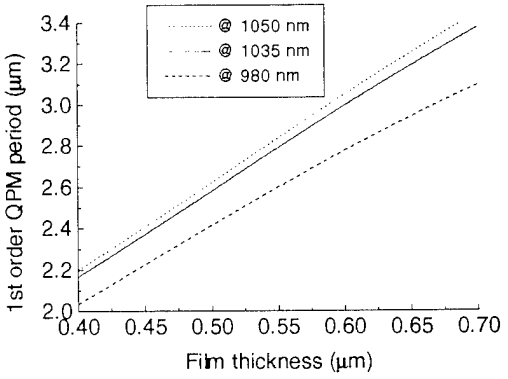

Figure 2: 1st order QPM period versus the film thickness for a $LiTaO_3$ thin film grown on sapphire and periodically exchanged at different wavelengths.

[1] F. Armani-Leplingard et al., Integrated Ferroelec., vol. 6, no. 1, (1995), pp: 337-344
[2] D.K. Fork et al., MRS Symp. spring 1995, paper U5.6
[3] H. Åhlfeldt et al., Electron. Lett., vol. 29. no. 9, (1993), pp: 819-821
[4] F. Laurell et al., Appl. Phys. Lett., vol. 60, no.3, (1992), pp: 301-303
[5] F. Laurell et al., J. Ligthwave Technol., vol.10, no.11, (1992), pp: 1606-1609
[6] F. Armani-Leplingard et al., ASSL'95 technical digest, pp: 155-157

Efficient tunable intra-cavity OPO in the mid-IR

A. Englander, R. Lavi, and R. Lallouz

Non-Linear Optics Group
Soreq NRC
Yavne 81800, Israel
Phone: 972 8 434777 Fax: 972 8 434401

Recently highly efficient Optical Parametric Oscillators (OPO) with a wide tuning range in the mid-IR have been demonstrated. [1] One of their drawbacks however is the requirement for powerful pump sources due to the high threshold for the onset of the parametric process. The effectiveness of increasing power density by focusing the pump beam is limited by the walk-off angle of the non-linear crystal which prevents the use of small pump beam diameters. A way to circumvent this problem is to place the OPO inside the cavity of the pump laser and to take advantage of the intense fluence inside this cavity (a factor of (1+R)/(1-R) greater than the fluence outside the cavity, where R is the reflectivity of the output mirror).

The intracavity OPO systems demonstrated in the past operated either near the degenerate point around 2.12μm with temperature tuned $LiNbO_3$ [2-3] pumped by flash-lamp pumped Nd:YAG source, or in a non-critical phase matching configuration with KTP,[4] so that just a limited range of tunability was achieved. Recently, Prasad and Geiger [5] presented an approach using Nd:MgO:$LiNbO_3$ crystal, which is an non-linear material that exhibits lasing action.

A highly efficient, all solid-state, continuously tunable, critically phased matched intra-cavity optical parametric oscillator based on a $LiNbO_3$ crystal and a diode pumped Nd:YAG pumping source is presented here. The experimental setup is shown schematically in Fig. 1.

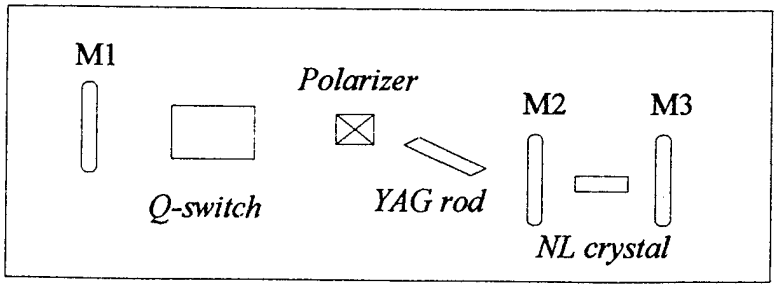

Fig 1. : Schema of laser and OPO cavities.

The pump cavity was a conventional hemispherical resonator with a 4 m concave back mirror (M1) and a flat outlet mirror. The laser head contained a 2.5 mm diameter Nd:YAG rod. A side pumping configuration was employed with a 4-bar diode array (SDL 3254-A4) mounted side by side to the laser rod in a close coupled configuration.

The laser rod which was cut at Brwester angle at both ends for better coupling between the pumped area and the TEM_{00} mode of the cavity, had an AR coating stripe at 810nm on the side facing the diode and an HR coating stripe at the same wavelength on the opposite side, in order to assure double passing of the diode light. The Nd:YAG barrel was rough grinded except for the two polished stripes. The diode laser produced a total of 360 W peak power at current of 120 A. A KD*P Q-switch and a polarizer were mounted between the laser head and the back mirror. The laser cavity was 30 cm long. Fig. 2 shows the output energy obtained with the laser operating under diode pulsewidth of 100 μsec and 68% reflectivity of the output mirror. The overall light to light efficiency was 15.6% with 0.24 slope efficiency. The beam diameter was 1.5 mm with quality of 1.5 x diffraction limit.

The intra-cavity OPO consisted of the same resonator components as used by us for a demonstration of a high efficiency, extra-cavity OPO (see ref. 1). It consisted of two flat mirrors and a nonlinear crystal, and was placed instead of the laser's outlet mirror. The 6x6x20 mm^3 $LiNbO_3$ crystal was cut at $\theta = 48°$ and was AR coated at the pump and signal wavelengths (R<1%). Reflection at the idler wavelength was less than 5% per face. The "input" coupler, M2, was coated for HT at 1064 nm and HR at 1400-1600 nm. The output coupler, M3, was an undoped YAG blank coated for HR at 1064 nm and at 1400-1600 nm and for HT at the idler wavelengths. The OPO, 3 cm in length, acted as a singly resonating cavity for the signal wave. The pump wave was locked between the laser back mirror (M1) and the output coupler of the OPO (M3) whereas the idler was free to exit the laser through M3. The output energy of the idler as a function of the diode pump energy is shown in Fig. 2.

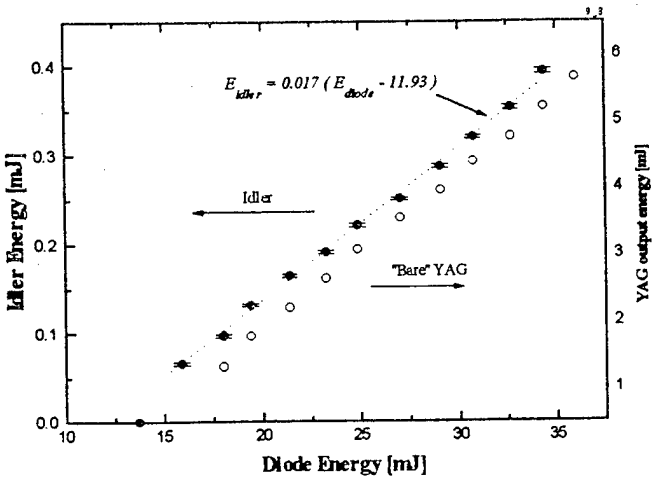

Fig 2: Idler vs. diode pump energy. Output of the "bare" laser shown at right.

Fig. 3 shows the conversion efficiency obtained from diode light to idler light as a function of diode laser energy.

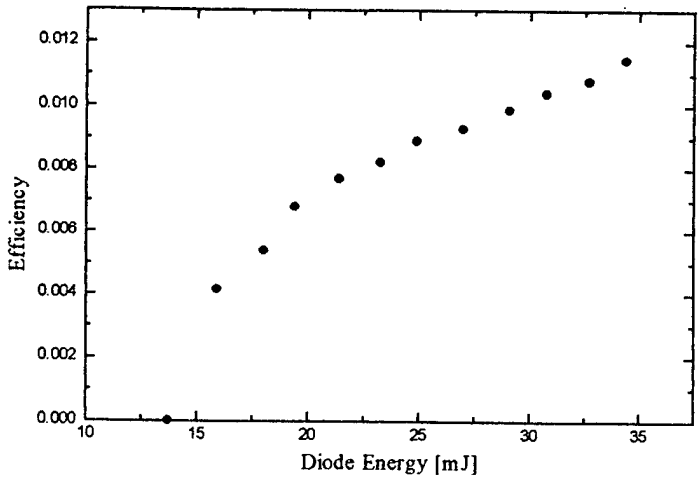

Fig 3: Idler Conversion efficiency

The angle tuning range covered by the idler extended from 3.45 to 4.10 μm without significant loss of energy. It should be noted that when the OPO was placed externally to the laser no conversion process was observed.

When the $LiNbO_3$ crystal was replaced by a 10 mm $KNbO_3$ crystal cut at $\theta = 42°$, a maximum idler energy of 250 μJ was measured at 35 mJ diode pump level. The idler tuning range with this crystal was somewhat broader: from 3.2 μm to 4.6 μm (with 50% energy losses at the edges).

In summary, we have demonstrated a compact low threshold source for the mid IR in a configuration of an intra-cavity all solid state OPO based on a diode pumped Nd:YAG laser and a $LiNbO_3$ or $KNbO_3$ crystal. The total internal conversion efficiency of this device from diode light to signal and idler waves was above 4%.

References

1. A. Englander and R. Lavi, in Advanced Solid-State Lasers, PD2 (1995).
2. E.O. Ammann, J.M. Yarborough, M.K. Oshman and P.C. Montgomery, App.Phys. Lett. **16**, 309 (1970).
3. J. Falk, J.M. Yarborough and E.O. Ammann, IEEE J. Quantum Electron.7, 359 (1971).
4. L.R. Marshall, A. Kaz and R. Burnham, in Conference on Lasers and Electro-Optics, Vol. 11 of 1993 OSA Technical Digest Series (Optical Society of America, Washington, D.C., 1993), CThK7.
5. N.S. Prasad and A.R. Geiger, in Conference on Lasers and Electro-Optics, Vol. 15 of 1995 OSA Technical Digest Series (Optical Society of America, Washington, D.C., 1995), CTuI28.

Ultraviolet Tunable Cr:LiSAF Laser System for Detection of Chemical and Biological Agents

Eric Park, James Gorda, Martin Richardson
Center for Research and Education in Optics and Lasers
University of Central Florida
12424 Research Parkway, Orlando, Florida 32816
PH: (407) 658-3925
FAX: (407) 658-6880
e-mail: dino@newton.creol.ucf.edu

Jay Fox
US Army CECOM
Night Vision & Electronics Directorate
Ft. Belvoir, Virginia 22060

Cynthia Swim
US Army CBDCOM
Edgewood Research, Development, & Engineering Center
Aberdeen Proving Ground, Maryland 21010

Abstract

We describe the design and construction of a MOPA configuration Cr:LiSAF based laser system utilizing frequency tripling to generate tunable radiation in the ultraviolet region. Application to the detection of biological and chemical agents, most specifically tryptophan, is discussed. Configuration of the Cr:LiSAF oscillator including the use of a 3 plate birefringent filter to allow tunability of the output in the infrared is detailed along with the design of a two pass Cr:LiSAF amplifier to increase the energy output of the narrowed spectrum. Finally, a pair of β Barium Borate (BBO) crystals is used to generate the second and third harmonics (2ω & 3ω) of the fundamental output thereby producing the desired radiation in the ultraviolet region.

Summary

Laser Induced Fluorescence (LIF) has been shown to be a promising technique for the detection of biological and chemical agents. Issues of strong frequency dependence for atmospheric propagation of lightwaves in the ultraviolet region coupled with the specific frequencies of absorption and secondary fluorescence of the agents of particular interest have initiated a search for the most efficient laser source for a stand-off detection system[1].

Cr:LiSAF, a member of the Colquiriite family of crystals, has been developed as a laser material and possesses a number of properties suitable for the aforementioned application. In particular, Cr:LiSAF displays a broad emission spectrum covering a region from nearly 780nm to 1000nm in wavelength[2]. It is desirable to be able to produce tunable UV radiation from approximately 250nm to 310nm. Third harmonic generation from a Cr:LiSAF system could cover this range and analysis of possible alternative sources shows that Cr:LiSAF would be the most efficient in generating the desired light.

Various methods of tuning Cr:LiSAF have been demonstrated including the use of an intracavity birefringent filter[3] and the intracavity use of a reflection grating[4] in the Littman configuration[5]. We detail the design of a Cr:LiSAF oscillator which is tunable with a birefringent filter, a two stage Cr:LiSAF amplifier, and a pair of BBO crystals for the generation of the 3ω output.

The oscillator utilizes a 4mm diameter, 65mm long Cr:LiSAF crystal in a dual flashlamp pumped head[6,7]. Energy to the flashlamps is 65 J while the flashlamp pulse length is 150μs. The cavity is formed between a 5 meter radius high reflecting mirror and a 65% reflective planar output coupler separated by 90 cm. The oscillator is Q-switched utilizing a KD*P Pockels Cell. A broadband thin film polarizer is also introduced into the cavity to establish preferential polarization along the c-axis of the Cr:LiSAF. Spectral tuning of the cavity is accomplished with a 3-plate birefringent filter (BRF). The BRF is inserted intracavity and rotated to select the desired wavelength of infrared output from the oscillator. Tuning has been accomplished over a range from 820nm to 890nm and is expected to be extended with the use of an improved break-free BRF. An intracavity etalon narrows the linewidth further to a value $\Delta\lambda$=.8nm. The pulse ouput of the oscillator has been measured to be 40ns with an energy of 30mJ.

The oscillator output beam width of 1.4mm is expanded in a 4x telescope and introduced into a 10mm diameter, 105mm long Cr:LiSAF amplifier. The amplifier is also flashlamp pumped with energy of 300J and pulse duration of 190μs. Single pass gain of the amplifier has been measured to be 4.2. The amplifier is used in the system in a two pass configuration leading to a total gain of 17.6. Energy in the amplified pulse is near .5J.

Finally, the amplified pulse is telescoped back down in diameter by a factor of 5 and taken into the first of a pair of β Barium Borate non-linear crystals. The first crystal is Type I phase matched for second harmonic (2ω) generation. The second crystal is used in Type II phase matching to mix the ω & 2ω for 3ω generation. Efficiency of BBO for 2ω is near 50% while that for 3ω is near 25% leading to an overall frequency conversion efficiency of approximately 10%. Thus, tunable output in the ultraviolet is on the order of 50mJ in the spectral range of 273nm to 297nm.

Continuing development of this system to increase output energy in the ultraviolet includes optimization of the non-linear harmonic generation and modification to the oscillator cavity design to reduce intracavity losses and increase the energy available per pulse from the cavity. The desire for increased energy output stems directly from the relationship between output energy and the rated stand-off distance of the chemical/biological detection system. Increased stand-off detection translates to increased time to take protective measures against the presence of a hazardous agent.

1) Richardson, et.al., "Cr-Doped LiSAF- A new Solid-State Laser for CBD", Proceedings of the Third Workshop on Standoff Detection for Chemical and Biological Defense, October, 1994, Williamsburg, VA. pg. 119
2) S.Payne, L.Chase, G. Wilke, "Optical Spectroscopy of the new Laser Materials, $LiSrAlF_6:Cr^{3+}$ and $LiCaAlF_6:Cr^{3+}$", Journal of Luminescence, 44, (1989) 167-176
3) H.Zenzie, Y.Isyanova, "High Energy, High Efficiency Harmonic Generation from a $Cr:LiSrAlF_6$ Laser System", Optics Letters, Vol. 20, No. 2, Jan. 15, 1995, pg. 169-171
4) J.Early, C.Lester, C.Quick, J.Tiee, T.Shimada, N.Cockroft, "Continuously Tunable Narrow Linewidth Q-Switched Cr:LiSAF Laser for Lidar Applications", Technical Digest on Advanced Solid State Lasers, Optical Society of America, Washington, D.C. 1995, Paper MB-1.
5) M.Littman, H.Metcalf, "Spectrally Narrow Pulsed Dye Laser without Beam Expander", Applied Optics, Vol. 17, No. 14, 15 July 1978, pg. 2224-2227
6) P.Beaud, M.Richardson, Y.Chen, B.Chai, "Optical Amplification Characteristics of Cr:LiSAF and Cr:LiCAF under Flashlamp-Pumping", IEEE Journal of Quantum Electronics, Vol. 30, No. 5, May 1994, pg 1259-1266
7) P.Beaud, E.Miesak, Y.Chen, B.Chai, M.Richardson, "Flashlamp Pumped Cr:LiSAF Regenerative Amplifier", Proceedings on Advanced Solid State Lasers, Optical Society of America, 1992, Vol. 13, pg 109-112

Application of Laser and Related Materials to Demonstrate Large Nonlinear Optical Effects and Diffraction Efficiency

Ian McMichael and Tallis Y. Chang
Rockwell International Science Center
1049 Camino Dos Rios
Thousand Oaks, CA 91360
(805) 353-4508, -4423 Fax

Mikhail Noginov
Center for Nonlinear Optics and Materials
Department of Physics
Alabama A&M University
P.O. Box 1208
Normal, AL 35762

Harry Tuller
Materials Science & Engineering Department
Massachusetts Institute of Technology
77 Massachusetts Avenue
Cambridge, MA 02139

Laser and related materials can be used to demonstrate large nonlinear optical effects using cw lasers. For example, we have demonstrated a gain of 22 times for a weak probe beam by using a moving grating technique with a strong pump beam in Cr:$YAlO_3$.[1] Since these materials are solid state, they are much easier to use than metal-vapors that also have large optical nonlinearities. Photorefractives are solid state materials that can be used to demonstrate large nonlinear optical effects using cw lasers, but their nonlinear optical response is typically non-local and not proportional to intensity. Thus, laser and related materials may play an important role in nonlinear optics by providing convenient solid state materials, with a local nonlinear optical response proportional to intensity, that will allow researchers to demonstrate large nonlinear optical effects using cw lasers.

In this summary we first present results of a simple model of the optical nonlinearity in laser materials. We believe these results can be used to find rules of thumb for developing materials in which one can obtain large refractive index changes. As an example of such a material, the second section of the summary describes our experiments with chromium-doped yttrium aluminate (Cr:$YAlO_3$). Our hope is that this work will stimulate others to help us in the search for better materials and understanding.

Results of a Simple Model of the Optical Nonlinearity of Laser Materials

The optical nonlinearity in laser materials results from the light induced population of a metastable state and the accompanying change of the refractive index. The long lifetime of the metastable state makes it possible to achieve a large population of the metastable state, and thus a large change in refractive index, using relatively low power cw lasers. At least as long ago as 1977, it was suggested[2] that the dominant contribution to the light induced change of the refractive index in ruby could be explained by considering just the strong charge-transfer (CT) transitions.[3-5] In ruby, the CT transitions are allowed transitions in which an electron is transferred from a nonbonding orbital, localized predominantly on the O^- ligands, to an antibonding orbital on the metal ion, and it results in a very strong absorption in the UV at approximately 180 nm. This suggestion continues to be used in the literature to explain the

nonlinear refractive index of laser materials. If we follow this suggestion, then we can show that the maximum index change Δn_{max} is given by,

$$\Delta n_{max} = n_2 I_S = \frac{(n_0^2+2)^2}{18 n_0} N \frac{e^2}{\varepsilon_0 m} \left(\frac{f_1}{\omega_1^2 - \omega^2} - \frac{f_0}{\omega_0^2 - \omega^2} \right)$$

where n_2 is the nonlinear refractive index, $I_S = h\nu/\sigma\tau$ is the saturation intensity, h is Planck's constant, ν is the frequency of the light interacting with the material, σ is the absorption cross-section, τ is the metastable state lifetime, n_0 is the linear refractive index, N is the number density of the active species (i.e. Cr for the case of ruby), e is the elementary charge, ε_0 is the permittivity of vacuum, m is the electron mass, f_1 and ω_1 are the oscillator strength and angular (i.e. $\omega = 2\pi\nu$) frequency for the transition from the metastable state to the CT state, respectively, f_0 and ω_0 are the oscillator strength and angular frequency for the transition from the ground state to the CT state, respectively, and ω is angular the frequency of the light interacting with the material. This expression is closely related to that for the polarizability used by Powell and Payne.[6]

Assuming we can detune the light frequency to reduce absorption, and that τ is long enough that we can reach I_S with a cw laser, then this equation gives the figure-of-merit for obtaining a large refractive index change. It indicates that one desires a large linear refractive index, a large doping, large oscillator strength for the transition from the metastable state to the CT state, small oscillator strength for the transition from the ground state to the CT state, a CT state that is closer to the metastable state, and a metastable state that is close to the laser frequency. However, when one considers a CT state closer to the metastable state, at some point one must include the resulting absorption. Also note that under these conditions the two frequency dependent terms in this equation can have the same negative sign and combine to yield an even larger effect.

Experiments Demonstrating a Large Optical Nonlinearity in Cr:$YAlO_3$

Figure 1 is a simplified schematic of the setup used to measure gain for a weak probe in a moving grating experiment. This is a powerful technique that can be used to determine both the real and imaginary parts of the nonlinear refractive index and the decay time for the metastable state.[7] Light from an argon laser is split into a weak probe beam $I_2(0)$ and a strong pump $I_1(0)$, with a fixed ratio $I_2(0)/I_1(0)$ = 1/1000. The frequency of the pump is shifted by approximately 5 Hz with respect to the probe by reflecting it from a mirror mounted to a piezoelectric transducer and driven by a triangle-wave voltage source. The grating formed by the interaction of the pump and probe in the crystal of Cr:$YAlO_3$ results in amplification for the probe when the mirror is moving in one direction, and attenuation when the mirror moves in the opposite direction.

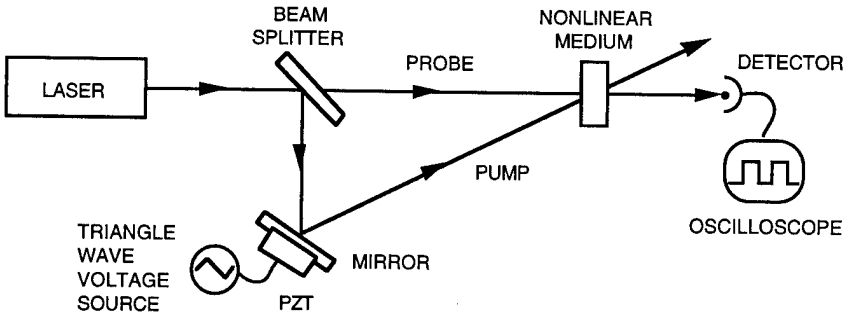

Fig. 1 Schematic of the setup to measure gain for a weak probe in a moving grating experiment.

Figure 2 (a) shows the gain for the probe beam as a function of the pump beam intensity for the range from 0 to 80 W/cm^2. The circles are the measurements, and the line is a theoretical fit,[1] using n_2 as the only adjustable parameter, that yields $n_2 = 3.2 \times 10^{-7}$ cm^2/W.

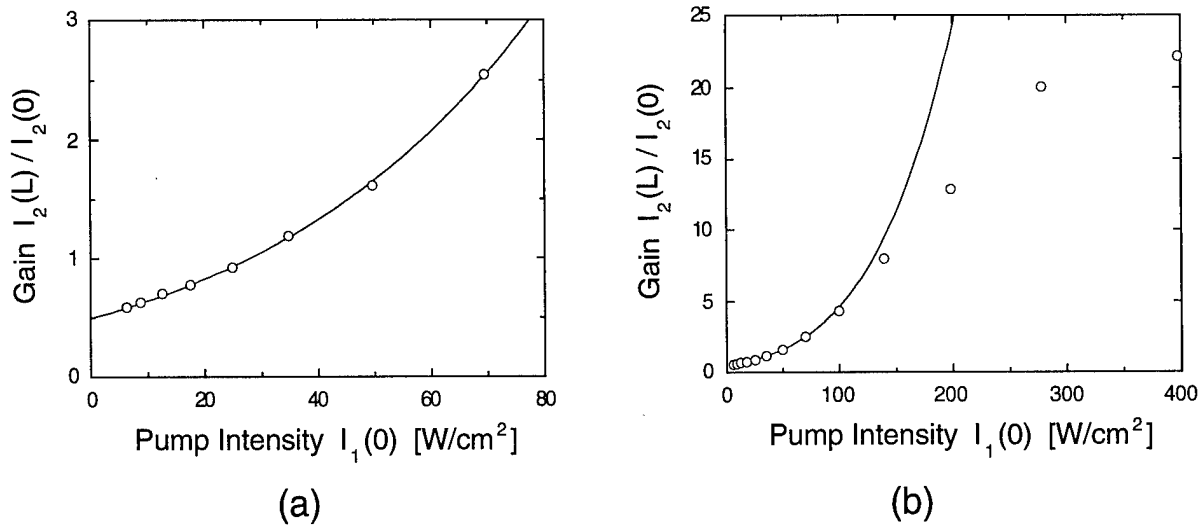

Fig. 2 Gain vs. pump intensity: (a) from 0 to 70 W/cm^2, and (b) from 0 to 400 W/cm^2.

Figure 2 (b) shows the gain for the range from 0 to 400 W/cm^2. Using n_2 as determined from the fit for the lower intensity range of Fig. 2(a), the line in Fig. 2(b) represents projections based on the previously mentioned theoretical expression.[1] A gain of 22 times was obtained at approximately 400 W/cm^2, but the measured gain does not increase with intensity as much as the simple theory predicts (a gain of 200 at 400 W/cm^2). This may be due to a "beam break-up" that results from spatial nonuniformities of the nonlinear refractive index change in the interaction region, or it may be due to other decay processes for the metastable state such as upconversion.[8] We are currently exploring the second possibility.

Conclusion

We discuss results of a model[6] that can be used to identify existing materials with large nonlinearities or to guide the development of new materials. We also presented experiments using Cr:$YALO_3$ demonstrating that large nonlinear optical effects can be achieved using laser materials. Again, laser and related materials may play an important role in nonlinear optics by providing convenient solid state materials with a local response proportional to intensity, that will allow researchers to demonstrate large local nonlinear optical effects using cw lasers. We hope is this will stimulate others to help us in the search for better materials and understanding.

References

1. I. McMichael, et. al., Opt. Lett. **19**, 1511 (1994).
2. T. Venkatesan and S. McCall, Appl. Phys. Lett. **30**, 282 (1977).
3. D. McClure, J. Chem. Phys. **36**, 2757 (1962).
4. T. Kushida, IEEE J. Quantum. Electron. **QE-2**, 524 (1966).
5. H. Tippins, Phys. Rev. **B 1**, 126 (1970).
6. R. Powell and S. Payne, Opt. Lett. **15**, 1233 (1990).
7. I. McMichael, P. Yeh, and P. Beckwith, Opt. Lett. **13**, 500 (1988).
8. M. Noginov, et. al., "Interaction of Excited Cr^{3+} Ions in Laser Crystals," *OSA Proceedings on Advanced Solid-State Lasers*, G. Dubé and L. Chase, eds. (1991), Vol. 10, pp. 21-24.

Synthesis and Study of Nonlinear Single Crystals $CeSc_3(BO_3)_4$

V.A. Lebedev, V.F. Pisarenko, Yu. M. Chuev
Kuban State University
Krasnodar, Russia

Conditions of the crystalization of $LnSc_3(BO_3)_4$ (Ln= La, Ce, Gd, Nd, Yb, Er) systems in trigonal (R32) or monoclinic (C2/c) modification and spectral-luminescent characteristics Cr^{3+}, Nd^{3+}, Yb^{3+}, Er^{3+} in these crystals were studied.

Modification of the optical transmission of flux grown $KTiOPO_4$ crystal by growth in nitrogen ambient

Akio Miyamoto, Yusuke Mori, Takatomo Sasaki, and Sadao Nakai

Department of Electrical Engineering and Institute of Laser Engineering,

Osaka University,

2-1 Yamadaoka, Suita, Osaka 565, Japan.

Tel +81-6-879-8727, Fax +81-6-879-7708

E-mail:amiyamoto@ile.osaka-u.ac.jp

KTP ($KTiOPO_4$) crystals exhibit excellent nonlinear optical properties in the visible range, namely large nonlinear coefficients and wide temperature and angular acceptance. However, as reported by several authors, KTP tends to suffer from reduced optical transmission in the visible and near-UV spectral regions at wavelengths significantly different from its 370nm UV cutoff [1,2]. Since absorption in the visible and near-UV is undesirable from the standpoint of the material's most important applications, there have been some reports concerning the improvement of this absorption [3,4]. The reason and detailed mechanism for this absorption, however, have not been revealed yet. In the present work, we could increase the transmission in the range below 550 nm by growing crystals in nitrogen ambient, and revealed that the absorption related to the reduced transmission is caused by Pt impurity.

KTP crystals were grown from $K_6P_4O_{13}$ (K6) flux in the temperature range between 975°C and 950°C using a platinum crucible in a vertically cylindrical electric furnace. Three kinds of oxygen concentration in the growth ambient, 5%, 21% (air) and 80%, were used. New solutions were prepared for each growth run because crystals grown from the solution which has been used for many times tend to become yellowish. Single KTP crystals 40mm long in c axis were obtained in each ambient by a three week growth. A yellowish KTP crystal was grown in the case of 80% oxygen, while a colorless KTP crystal was obtained in the 5% oxygen case. Figure 1 shows the absorption coefficient spectrum of each grown crystal. The dependence of the absorption coefficient on the oxygen concentration is clearly seen in Fig. 1, particularly in the range below 550 nm. In order to clarify the origin of this absorption, impurities in the grown crystals have been analyzed by inductively coupled plasma emission spectrometry (ICP). Although Cr, Fe and V, which have been reported as an absorbance of KTP [5], were below the detection level (less than 1 ppm), a

significant change in Pt concentration was observed between two crystals. Pt concentration in the crystals grown in 80% oxygen ambient was 18 ppm, which was roughly four times greater than that grown in 5% oxygen ambient, 4.3 ppm. From the data shown in Fig. 1, the absorption coefficients of KTP grown in 80% oxygen ambient are approximately four times greater than that grown in 5% oxygen ambient in the range from 400 to 550nm. This agreement suggests that Pt impurity causes the absorption of KTP crystals.

Spatial distributions of absorption coefficient and concentration of Pt impurity on growth distance were also measured. The large KTP crystal grown in an air ambient described in Ref. [6] was investigated. Figure 2 shows the absorption coefficient at 400 nm and Pt impurity concentration as a function of growth distance in the same (011) growth sector. Both the absorption coefficient and Pt concentration increased in the same way along the growth direction. This strong correlation between absorption coefficient and Pt concentration suggests that Pt atoms from crucible is the origin for this absorption.

Similar phenomenon has been reported in a phosphate glass [7,8]. These reports showed the increase of Pt concentration with the oxygen content. This phenomenon was explained as follows: The oxide platinum, PtO_2, is made in the melt by the oxidation of the Pt on the crucible wall. This PtO_2 is incorporated in the crystal as an ion Pt^{2+}. The absorption observed in KTP may be explained by this mechanism observed for the phosphate glass.

In conclusion, we found that growth in nitrogen ambient is useful for avoiding the incorporation of Pt leading to a lower absorption in the visible and near-UV spectral regions.

References

[1] R.F.Belt, G.Gashurov and Y.S.Lir, Laser Focus, 21, No. 10, 110(1985)

[2] D.J.Gettemy, W.C.Harker, G.Lindholm and N.P.Barnes, IEEE, J.Quantum Electron. 24(1988)2231

[3] P.F.Boudui, R.Blachman and R.G.Norwood, Appl.Phys.Lett. 61,1369(1992)

[4] A.Miyamoto, T.Nakai, Y.Mori, Y.Okada, T.Sasaki and S.Nakai, CLEO Pacific Rim '95 Technical Digest, 86(1995)

[5] T.F.McGee, G.M.Blom and G.Kostecky, J.Crystal Growth 109(1991)361

[6] T.Sasaki, A.Miyamoto, A.Yokotani and S.Nakai, J. Crystal Growth 128 (1993) 950.

[7] J.H.Campbell, E.P.Wallerstein, J.S.Hayden, D.L.Sapak, D.E.Warrington, A.J.Marker III, H.Toratani, H.Meissner, S.Nakajima and T.Izumitani, Lawrence Livermore National Laboratory. Report UCRL-53932. 1989

[8] J.H.Campbell, E.P.Wallerstein, H.Toratani, H.E.Meissner, S.Nakajima and T.S.Izumitani, Glastech. Ber. Glass Sci. Technol. 68(1995)59.

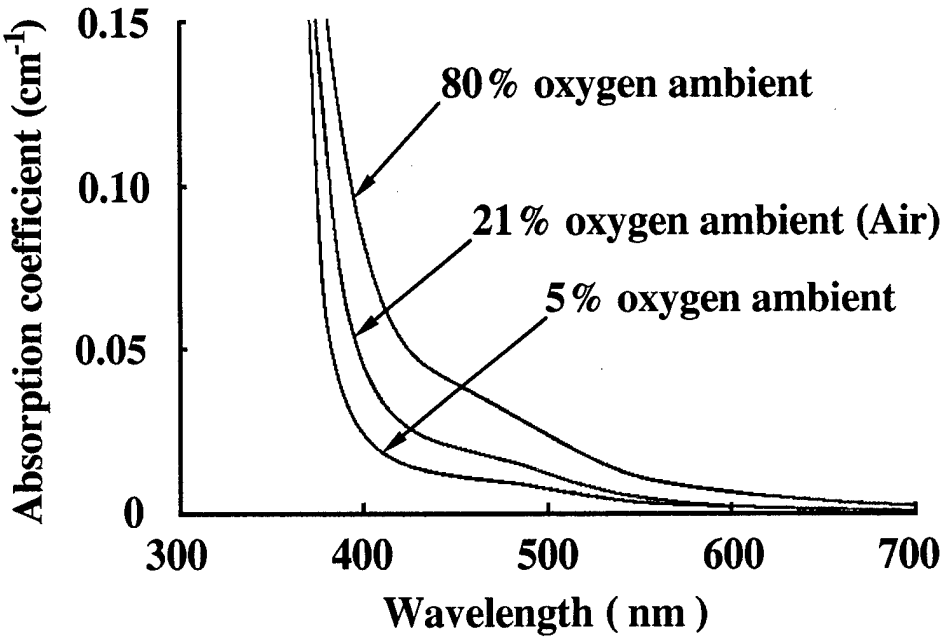

Fig. 1. Optical absorption spectra of KTP crystals grown in various ambient

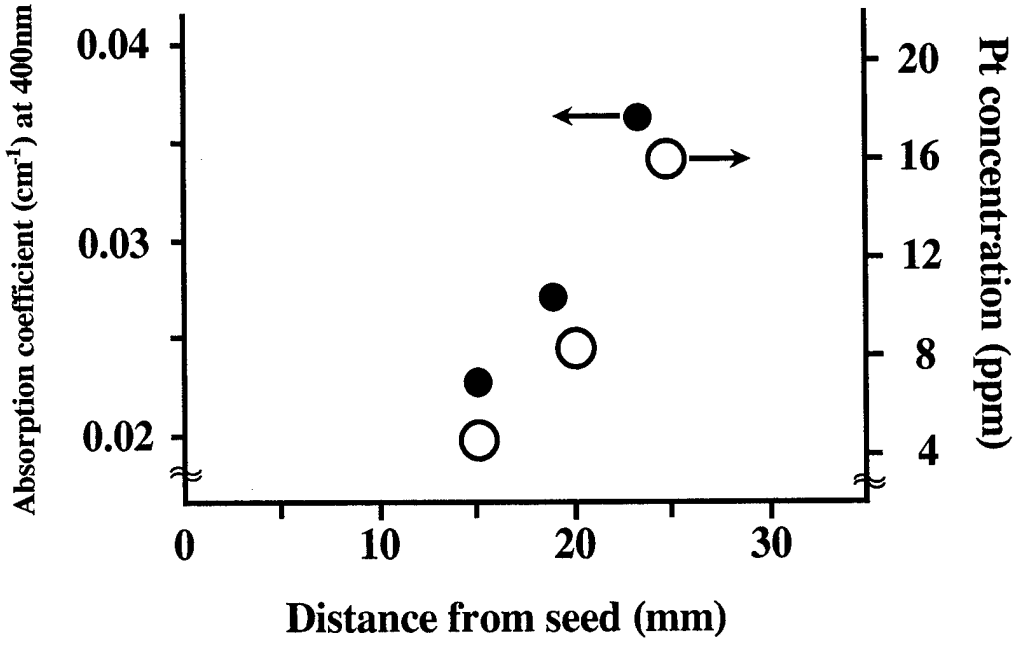

Fig. 2. Spatial distribution of absorption coefficient and Pt concentration in grown crystal to growth direction (the perpendicular to (011) surface)

A 10 mW frequency doubled diode laser at 491 nm

D. Fluck, T. Pliska, and P. Günter

Nonlinear Optics Laboratory, Institute of Quantum Electronics,

Swiss Federal Institute of Technology, ETH-Hönggerberg,

8093 Zürich, Switzerland.

Compact all-solid-state blue lasers are attractive for applications such as optical recording, xerography, spectroscopy and display systems. Frequency doubling of near infrared diode lasers (DLs) offers the potential of a robust and reliable blue laser source. $KNbO_3$ crystals are very attractive for frequency doubling of near infrared DLs into the blue-green spectral range due to its high nonlinear optical coefficients and the favourable noncritical phase-matching possibilities for wavelengths around 860 nm and 980 nm at room temperature [1, 2]. Second-harmonic generation (SHG) with DLs in $KNbO_3$ has been demonstrated in single-pass [3], resonant [4, 5] and waveguide [6] configurations. Resonant schemes have been proven to be highly efficient, but are relatively complex. The second-harmonic (SH) output power from single-pass and waveguide frequency doubling schemes has been limited in the past by the relatively low power available from single-mode narrow linewidth DLs. Recently, monolithically-integrated master-oscillator power-amplifier (M-MOPA) DLs with more than 1 Watt continuous-wave (CW) output power has been demonstrated which allowed efficient generation of blue-green light by single-pass SHG in $KNbO_3$ crystals [7, 8].

We report the generation of 10 mW coherent diffraction limited CW 491 nm light by direct single-pass frequency doubling a 750 mW M-MOPA DL in a $KNbO_3$ crystal with a conversion efficiency of 1.7 %/W which is more than a factor of four higher than reported so far for frequency doubling a 980 nm M-MOPA DL [7].

The M-MOPA DL (SDL 5760-A6) consists of a distributed Bragg reflector master oscillator, a flared amplifier, and collimating optics. The output beam with a diameter of about 3 mm was focused with an 80 mm, anti-reflection (AR) coated, plan-convex lens into a 17 mm long b-cut $KNbO_3$ crystal. The crystal was AR coated at both the fundamental and SH wavelengths. The SH radiation was collimated with a 30 mm, AR coated lens to provide an output beam with a diameter of about 1 mm. The crystal was placed in a small oven with AR coated windows to ensure a homogeneous crystal temperature.

Operation of the MOPA laser diode at an oscillator and amplifier current of 264 mA and 2.5 A, respectively, provided a maximum power of 760 mW incident on the $KNbO_3$ crystal. At a crystal temperature of 18.7 °C a maximum output power of 10 mW of second-harmonic radiation at 491 nm was generated with a conversion efficiency of 1.0 %/Wcm. Fig. 1 shows the measured temperature tuning curve. The full width at half maximum (FWHM) was 0.56 °C. From the dispersion of the refractive indices of $KNbO_3$ a theoretical acceptance width of 0.35 °C is calculated [2], and hence, the birefringence of this 17 mm long crystal is slightly inhomogeneous. For optimum Gaussian beam focusing we expect a normalised conversion efficiency of 1.7 %/Wcm for a homogeneous $KNbO_3$ crystal with a nonlinear optical coefficient of $d_{31} = 11.3$ pm/V [9]. The discrepancy between the measured and the theoretical normalised conversion efficiency of about 40 percent can be fully explained by the crystal inhomogeneity.

The beam quality of the SH radiation was measured with a laser beam analyser. The beam parameter M^2 was 1.0 and 1.1 in the direction perpendicular and parallel to the junction of the diode laser. Fig. 2 shows a typical plot of the second-harmonic power as a function of time. Measured over a period of more than six hours the drift of the SH power was smaller than 3 %. The inset in Fig. 2 shows the intensity fluctuations in the time domain measured over a period of 10 µs. The root-mean-square value of the power fluctuations in the frequency band between 10 Hz and 100 MHz was less than 0.1 %.

The excellent beam quality, the low noise, and the small long-term drift make this type of blue-green all-solid-state laser source very suitable for applications. We envision the generation of up to 50 mW SH power at 491 nm by using homogeneous $KNbO_3$ crystals and a 1 Watt M-MOPA DL.

REFERENCES

[1] P. Günter, Appl. Phys. Lett. 34 (1979) 650.

[2] I. Biaggio, P. Kerkoc, L.-S. Wu, P. Günter, B. Zysset, J. Opt. Soc. Am. B 9 (1992) 507.

[3] P. Günter, P. M. Asbeck, S. K. Kurtz, Appl. Phys. Lett. 35 (1979) 461.

[4] W. J. Kozlovsky, W. P. Risk, W. Lenth, B. G. Kim, G.-L. Bona, H. Jaeckel, D. J. Webb, Appl. Phys. Lett. 65 (1994) 525.

[5] C. Zimmermann, V. Vuletic, A. Hemmerich, T. W. Hänsch, Appl. Phys. Lett. 66 (1995) 2318.

[6] D. Fluck, T. Pliska, P. Günter, M. Fleuster, Ch. Buchal, D. Rytz, Electron. Lett. 30 (1994) 1937.

[7] R. Waarts, S. Sanders, R. Parke, D. Mehuys, R. Lang, S. O'Brien, K. Dzurko, D. Welch, D. Scifres, IEEE Photon. Technol. Lett. 5 (1993) 1122.

[8] L. Goldberg, D. Mehuys, Appl. Phys. Lett. 65 (1994) 522.

[9] D. A. Roberts, IEEE J. Quatum Electron. QE-28 (1992) 2057.

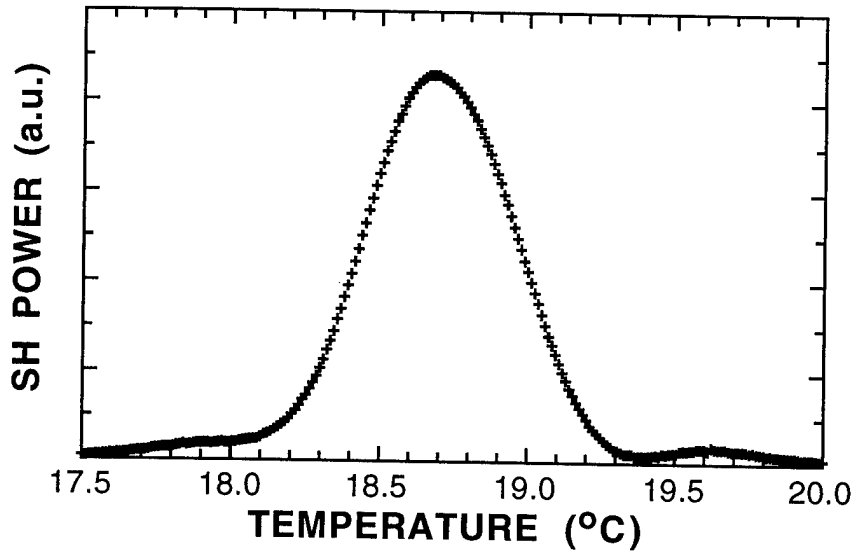

Fig. 1: Temperature tuning curve for noncritical phase-matched frequency doubling a 982 nm M-MOPA laser diode in a 17 mm long b-cut $KNbO_3$ crystal.

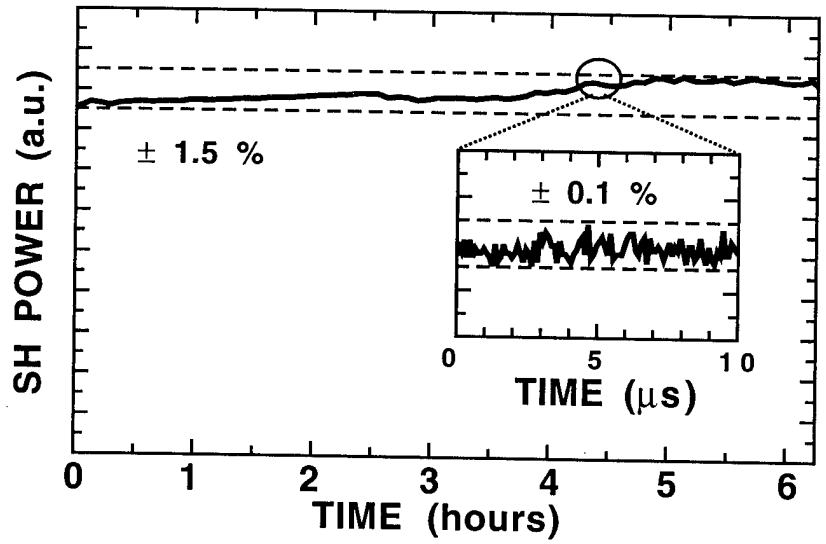

Fig. 2: Long-term stability and short-term fluctuations (inset) of the SH power at 491 nm for single-pass frequency doubling a 750 mW M-MOPA DL in a $KNbO_3$ crystal at a temperature of 18.7 °C.

SEMI-ANALYTICAL MODEL OF THE PULSED OPTICAL PARAMETRIC OSCILLATOR ; COMPARISON WITH EXPERIMENT

T. Debuisschert, J. Raffy, J.P. Pocholle

Laboratoire Central de Recherches, THOMSON-CSF
Domaine de Corbeville, 91404 Orsay Cedex, France
tel : (33) (1) 69-33-91-85
fax : (33) (1) 69-33-08-66
e-mail : Debuisschert @ lcr.thomson.fr

Optical Parametric Oscillators (OPO) have been the scope of a lot of studies in those recent years. Although many experiments have been performed with pulsed OPO's, few models have been proposed to describe them. The study of the threshold in pulsed regime have been proposed [1], but few work has been done concerning the OPO pumped high above threshold. The pulsed OPO's work in transient regime, thus a dynamical model is necessary. The conversion can be very high, and can exceed 50% [2]. That shows that the small gain approximation which is often used to describe the non-linear coupling in cw OPO's is no more valid in the case of pulsed OPO's. Moreover, in the case of Singly Resonnant OPO's, the mirrors have a high transmission for one of the fields. Thus, the low loss cavity approximation does not hold as well. Consequently, the non-linear coupling and the loss induced by the cavity must be studied without making any assumption on the fields intensities.

Our purpose is to perform a model which is as simple as possible and which describes adequatly the pulsed OPO. We solve the problem partly analytically, what leads to a better understanding of the problem than a complete numerical resolution. The physical effects which play a role in the problem can be set in three categories. First, the nonlinear coupling and the cavity losses. They describe the gain and the losses in the OPO and are the fundamental effects. Second, diffraction which is responsible of a spread of the wavefronts which are propagating in the cavity. It induces a loss of coherence of the fields and perturbs the non-linear coupling. Diffraction becomes important when the beams are focused. Third, walk-off and absorption. They appear more as secondary effects than the previous ones. Walk-off does not appear in the case of non-critical birefringence phase-matching, and the absorption can be very low in the case of very good quality crystals such as $LiNbO_3$. For the sake of simplicity, our model takes only the non-linear coupling and the cavity losses into account. We consider weakly focused pump beams so that their diffraction can be neglected (Rayleigh length >> cavity length). This assumption allows a ray approach [3] of the non-linear coupling which can be studied analytically [4].

The non-linear coupling equations rely on the amplitudes of the fields. Depending on their initial values, the conversion can occur from the pump beam to the signal and idler beams or from the signal and idler beams to the pump beam. We consider that the signal and idler fields are resonant with the cavity and thus no detuning is introduced in one round-trip. Moreover the initial phases of the signal and idler fields are not imposed by the interaction, so they can adjust themselves to zero to optimise the energy transfer. We can thus consider that all three fields are real. Nevertheless their sign can change during the interaction inducing conversion back and forth from the pump beam to the signal and idler beams. With the assumption of real fields, the three non-linear equations can be solved analytically thanks to energy conservation arguments and a geometrical approach. We obtain the dependence of the fields α_j along the propagation direction. The indices 0, 1 and 2 hold for the pump, signal and idler fields respectively. The pump field dependence is given by :

$$\alpha_0(Z) = \frac{-R_1.sn(R_1.Z,k).\alpha_2(0).\alpha_1(0)+R_1^2.\alpha_0(0).dn(R_1.Z,k).cn(R_1.Z,k)}{R_1^2-\alpha_0^2(0).sn^2(R_1.Z,k)} \quad (1)$$

In that case, the input signal field is supposed greater than the idler field. In the other case the indices 1 and 2 have to be permuted. Analog expressions give the axial dependence of the signal and idler fields. Z is a normalised length with respect to the non-linear coefficient. R_1, R_2 and k are defined by $R_1^2 = \alpha_1^2(0)+\alpha_0^2(0)$, $R_2^2 = \alpha_2^2(0)+\alpha_0^2(0)$ and $k = R_2 / R_1$. The functions $sn(R_1.Z,k)$, $dn(R_1.Z,k)$ and $cn(R_1.Z,k)$ are Jacobian elliptic functions. They are periodic functions depending on the parameter k. Their period is inversely proportionnal to R_1, thus to the input fields amplitudes. That dependence of the period with initial conditions is directly related to the non-linearity of the problem and has important consequences on the overall conversion. The analytic solutions allow to relate directly the fields going out of the crystal to the incoming fields. In particular, it is not necessary to assume that one of the field is zero at the entrance of the crystal. We consider a linear cavity OPO with a round-trip time which is much smaller than the pump pulse duration. We consider that the pump, signal and idler fields are single frequency modes. The signal and idler fields evolutions are calculated by propagating them in one complete round-trip, taking into account the non-linear interaction in both directions and the mirrors losses. When the OPO is pumped over oscillation threshold, the signal and idler fields experience a net gain on the total round-trip. Anyhow, there is a need of a perturbation to make them getting out of the unstable equilibrium state where no photons at all are present in the two fields. This role is played by quantum fluctuations which lead to the presence of one half energy quantum in the signal and idler modes even in the absence of any pumping.

In a first step, one can consider a simple model where the three fields are quasi-plane waves with a gaussian transverse dependence. In that case, overlap integrales can be calculated between the fields what leads to a set of equations which are analog to that obtained with a plane waves approach. Only the normalised non-linear coefficient differ. A simulation based on such an approach leads to some discrepancy with experience. Analysing the temporal pump depletion profiles, one sees that just after the beginning of the efficient pump conversion, a complete conversion of the incoming pump field occurs, leading to a very steep temporal variation. The temporal profile can exhibit other temporal oscillations for high pumping levels. We have never observed such temporal profiles experimentally. This suggest that the quasi-plane wave model is unsufficient to describe adequately the dynamics of the OPO.

To improve the agreement of the model with experiment, we have studied the transverse profiles of the fields. This is directly suggested by the form of expression (1). The period of the oscillations is a fonction of the input fields amplitudes. Even if the initial beams are gaussian, their transverse distribution is not uniform. Thus the period of the solutions has a transverse variation. Assuming a radial symetry of the problem, the period increases with r. At the output of the crystal, it is now no more possible to have the same value of a field for each value of r. When computing the total power of the beams, there is a blurring of the oscillations due to their radial dependence. In particular, it is no more possible to obtain a uniform zero value for the pump field so that the complete depletion of the incoming pump field is no more possible. This leads to a better agreement of the calculated depletion profile with the experimental one.

We have compared our model with our experimental results [2]. The OPO consists of a 5 cm long $LiNbO_3$ crystal with a d_{eff} of 4.6 pm/V which is inserted in 5.5 cm long cavity. The input mirror has a reflexion of 10 % for the idler and is R_{max} for the signal at 1.54 μm. The output mirror has a reflexion of 30 % for the signal and the idler. The laser is a Q-switch Nd:YAG providing pulses of 20 ns at 1.064 μm. The calculated input pump, depleted pump

and signal profiles are given for input energies of 30 mJ (fig. 1) and 40 mJ (fig. 2). Experimental input pump and depleted pump profiles corresponding to an input energy of 40 mJ are shown on figure 3. The calculated temporal profiles show a good agreement with the experimental ones. In particular it does not display any complete conversion of the incident pump power at any time of the interaction. For high pumping energies, there is a slight oscillation which appears on the temporal pump profile. This is attributed to back conversion from the signal and idler fields to the pump field. We have compared the conversion efficiency between the pump energy and the signal energy in both experimental and theoretical case for the same OPO configuration (fig. 4). Although the threshold and the high level efficiency are slightly underestimated, the general agreement is quite good taking into account that there is no adjustable parameter in the model.

Our model shows clearly the importance of the transverse structures of the fields wave-fronts in the OPO. They are mainly driven by the non-linear coupling rather than the cavity. The model can be improved introducing the effects of diffraction. This should lead to a decrease of the contrast of the transverse structures and a decrease of the conversion from the signal and idler fields back to the pump field.

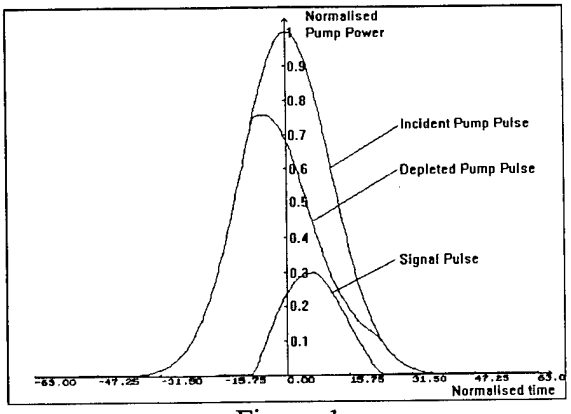

Figure 1

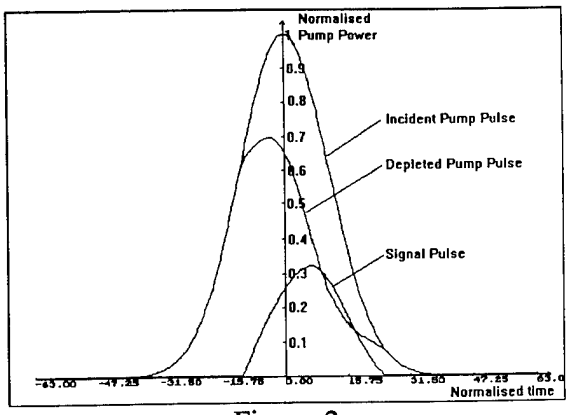

Figure 2

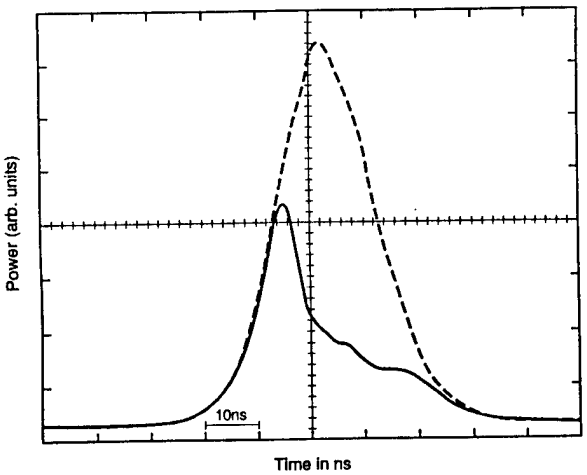

Figure 3

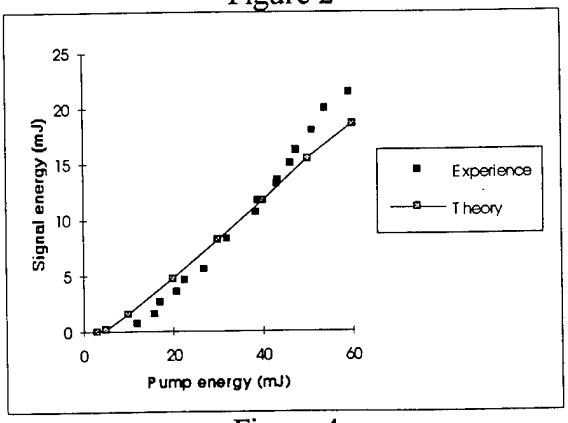

Figure 4

[1] S. J. Brosnan and R. L. Byer, IEEE J. Quantum Electron. **QE-15**, 415-431 (1979)

[2] J. Raffy, T. Debuisschert, J.-P. Pocholle and M. Papuchon, "$AgGaSe_2$ OPO pumped by a $LiNbO_3$ OPO", OSA Proceedings on Advanced Solid-State Lasers, Vol. 15, pp 127-130 (1993)

[3] G. D. Boyd and A. Kleinman, J. Appl. Phys. **39**, 3597 (1968)

[4] J. A. Armstrong, N. Bloembergen, J. Ducuing and P. S. Pershan, Phys. Rev. **127**, 1918 (1962)

Analysis of incoherence effect of single-mode pump on second-harmonic generation

W. -L. Zhou, Y. Mori, T. Sasaki, and S. Nakai
Department of Electrical Engineering and Institute of Laser Engineering,
Osaka University, 2-1 Yamadaoka, Suita, Osaka 565, Japan
Fax. 0081-6-879-7708, Email: wlzhou@ile.osaka-u.ac.jp

After three decades development of second-harmonic generation (SHG), large disparities in absolute nonlinear optical coefficient values measured by various techniques (SHG, Maker-fringe and fluorescence scattering) are remained unsolved.[1,2] A more precise treatment on this problem is seem to be vital. We have developed an analysis on the incoherence effect of a single-mode pump on its SH intensity. We define that a single-frequency wave is strictly monochromatic, namely perfect coherent, while a single-mode wave is of finite spectral bandwidth and thus partially not coherent. The former is usually utlized in the theoritical treatment of SHG, while the latter is met in pratical SHG experiments. Assumptions of lossless and dispersionless of the SHG crystal are adopted in the following analysis.

Consider a pump wave $E(z) = E_0 \exp j(kz + \phi(z))$ propagats through the SHG crystal of length L along the z direction, where the time related terms are omitted. E_0 and k are amplitude and wave vector, and the phase $\phi(z)$ is z-dependent for single-mode wave but constant for single-frequency wave. The induced second-order nonlinear polarization is expressed as $P(z) = \chi E^2(z)$, where χ is the nonlinear optical coefficient. The polarization field serves as the source of the SH wave in every element Δz (refered to SH subwave) along the z direction. The field of SH subwave $\Delta E_{SH}(z)$ is of course proportinal to the local polarization as $\Delta E_{SH}(z) = KP(z)\Delta z$, where K is a constant. The total strength of the SH field, $E_{SH}(L)$, at the crystal output surface results from the superposition of all the subwaves propagating along the z direction, i.e., $E_{SH}(L) = \sum \Delta E_{SH}(z) \exp jk_{SH}(L - z)$, where k_{SH} is the wave vector of the SH subwaves and $k_{SH} = 2k$ when phase matched. In the case of single-frequency pump, the total SH field at $z=L$ obtained under phase-matching condition is

$$E_{SH}(L) = K\int_0^L P(z) \exp j2k(L - z)dz = KL\chi E_0^2 \exp j(2kL + \phi) \quad , \qquad (1)$$

and thus the SH intensity $I_{SH}(L) = (KL\chi E_0^2)^2$.

However, in the case of single-mode pump, Eq. (1) can not be integreted due to the z-dependent phase $\phi(z)$. In fact, SH subwaves radiated from different positions will superpose partially in intensity rather solely in field strength since they are patially phase related. It is necessary to resolve the single-mode pump into such waves that have no z-dependent phases. The concept of damping wave may be useful for this purpose. It is known that phase disturbances of a single-mode laser beam give rise to the broadening of spectral bandwidth. On the other hand, e. g., a Lorentzian distributed spectrum can be expressed as an exponential damping wave by Fourier transformation. This is to say that on the average these phase disturbances are responsible for a damping amplitude. For simplicity,

we use square-root damping wave to express the present single-mode pump (then the spectrum is the square of a *sinc* function). The intensity of the square-root damping wave is triangularly distributed with a peak of E_0^2. Define the coherence length (L_c) as the half-maximum fullwidth, and thus the duration of the damping wave is $2\,L_c$. The damping wave is assumed to be radiated from a point source, which must periodically emit the similar damping waves to maintain a constant intensity of the pump wave. Taking the position at z=0 (incident facet of the crystal) as the starting point, we can then demonstrate the single-mode pump as an array of damping waves as shown in Fig. 1. These damping waves (denoted by i, ii, iii and so on) are identical but randomly phased since they are radiated at different times, and therefore mutually superposed with the intensity. One can find that the model shown in Fig. 1 is consistent with an exact single-mode wave in the intensity and phase relation.

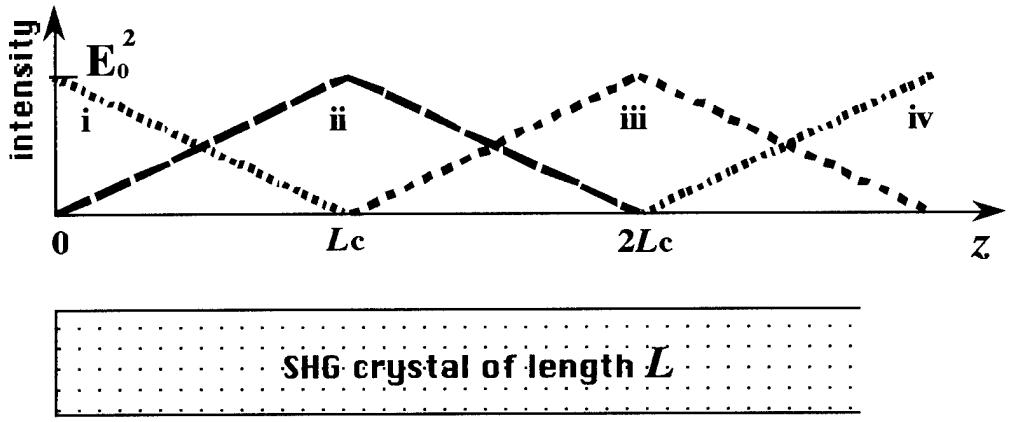

Fig. 1. Single-mode pump resolved to square-root damping waves inside SHG crystal. The intensity is remained constant.

From Fig. 1 the single-mode pump can be expressed as the summation of two square-root damping waves in any positions as respected to the starting point. For $L \le L_c$, these two damping waves are written as

$$E_i(z) = E_0\sqrt{(1 - z/L_c)}\exp j(kz + \phi_i)$$
$$E_{ii}(z) = E_0\sqrt{(z/L_c)}\exp j(kz + \phi_{ii}) \qquad (2)$$

where the phases ϕ_i and ϕ_{ii} are random and z-independent. In the same way as Eq. (1), we can finaly obtain the SH intensity at $z = L$ as $I_{SH}(L) = (KL\chi E_0^2)^2 M$ with

$$M = (\frac{L_c}{L})^2\{(\frac{L}{L_c})^2(1 - \frac{L}{2L_c})^2 + \frac{1}{4}(\frac{L}{L_c})^4$$
$$+[(\frac{L}{L_c} - \frac{1}{2})\sqrt{\frac{L}{L_c}(1 - \frac{L}{L_c})} + \frac{1}{4}\arcsin(\frac{2L}{L_c} - 1) + \frac{\pi}{8}]^2\} \qquad (L \le L_c) \qquad (3)$$

The factor M (refered as incoherence factor) demonstrates the influence of incoherence of the single-mode pump on SHG. It can also be expressed as the similar as Eq. (3) for $L \ge L_c$.

Figure 2 shows the dependence of the incoherence factor M on the ratio of L/L_c. As mentioned above the SH subwaves superpose partially with the intensity and thus the final SH intensity would be smaller than that of single-frequency pump. On the other hand, we know that a multimode pump with N randomly phased modes (accurately N single-line frequencies) will enhance its SH intensity with a factor of 2-1/N compared to single-frequency pump.[3,4] A single-mode pump with a finite bandwidth can be considered as a quasi-multi-frequency one and therefore an enhancement factor might be involved. This is the reason why the value of M is above unity when $L/L_c \leq 1.1$. The mximum of M value is 1.253 at L/L_c=0.62, corresponding to a single-mode pump at 1064 nm with a bandwidth of 0.07 nm if L=1 cm.

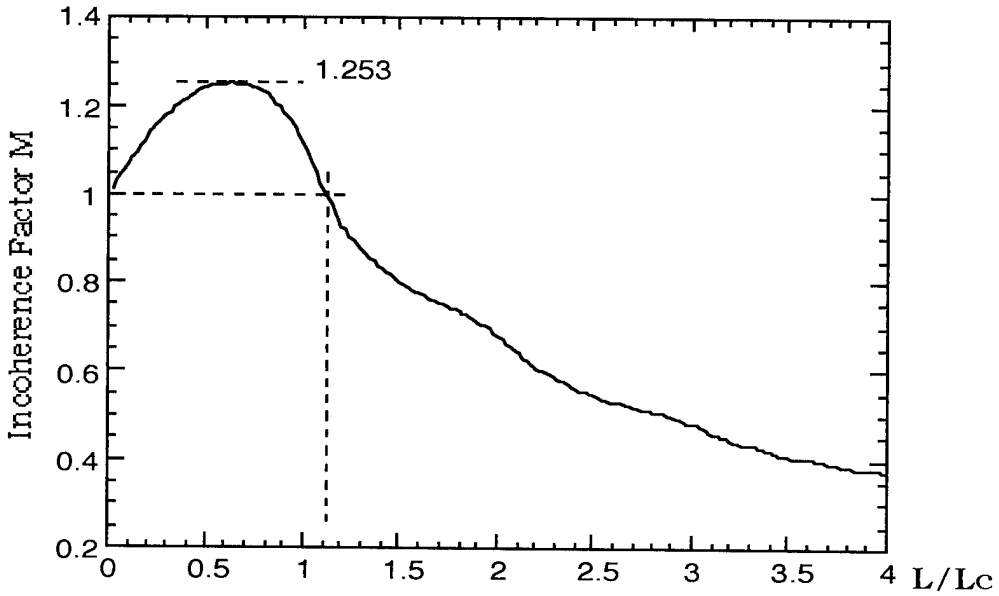

Fig. 2. Dependence of incoherence factor on the ratio of crystal length (L) and laser coherence length (L_c).

It is worth to notice that when $L/L_c \rightarrow 0$, $M \rightarrow 1$. This is corresponding to two special cases: the single-frequency pumped SHG where $L_c \rightarrow \infty$ and the non-phase-matched SHG or Maker-fringe technique where the effective crystal length is very small. The former is pratically impossible, while the latter is one of the standard methods to determine the nonlinear optical coefficient. It is interesting to indicate the fact that the nonlinear optical coefficient value (e. g. d_{22} of BBO) measured by the Maker-fringe technique is usually smaller than that by the SHG method.[5]

1) D. A. Roberts, IEEE J. Quantum Electron. 28, 2057 (1992).

2) R. Eckardt, H. Masuda, Y. X. Fan, and R. L. Byer, IEEE J. Quantum Electron. 26, 922 (1990).

3) N. Bloembergen, *Nonlinear Optics* (Benjamin, New York, 1965) p. 131.

4) F. Zernike and J. Midwinter, *Applied Nonlinear Optics* (Wiley-Interscience, New York, 1973) p. 108.

5) C. T. Chen, *Development of New Nonlinear Optical Crystals in the Borate Series* (Harwood Academic, Switzerland, 1993) p. 59.

A Diode Array Pumped Continuous Wave Blue Microchip Laser

David G. Matthews[1], Neil MacKinnon[2], Richard S. Conroy[1] and Bruce D. Sinclair[1]

[1] J. F. Allen Physics Research Laboratories, School of Physics and Astronomy, University of St. Andrews,St. Andrews, Fife, KY169SS, Scotland, U.K.
Tel: +44 1334 463118 Fax: +44 1334 463104 Email: dgm1@st-and.ac.uk

[2]I E Optomech Ltd, Crabtree Farm, Newnham, Northants., NN113ET, England, U.K.
Tel: +44 1327 704916 Tel: +44 1327 300052 Email: 75522.1670@compuserve.com

Compact all-solid state blue and green lasers are desired as replacements for low power cw Argon ion lasers. Arguably the solid-state laser technology offering the ultimate in minaturisation and potential for low cost mass-production is the microchip format. Our group recently reported 130mW of green generated in a composite-material microchip device [1 ,2]. We report here on the successful operation of a Nd:YAG/$KNbO_3$ composite material blue microchip laser generating 1mW of 473nm cw radiation diode-pumped, and 9mW when Ti:sapphire pumped.

The composite material microchip laser consisted of a 1mm thick 1.1% Nd:YAG crystal polished plane-parallel and bonded to a nominally 1.5mm thick plane-parallel $KNbO_3$ crystal angle cut for type I critical phase matching of 946nm radiation at T_{pm} =45°C. The crystal set was coated for high reflectance at 946nm and high transmittance at 1064nm, 1320nm and 473nm, whilst measurements indicated a 28% reflectance at 810nm. A stable cavity is formed by the pumped surface deformation and thermal lensing induced by the absorption of the pump radiationβ].

The threshold for the quasi-three level $^4F_{3/2}$ - $^4I_{9/2}$ Nd transition is reduced by the higher lying Z_5 stark level (848cm^{-1}) in the $^4I_{9/2}$ manifold in YAG compared to that for Nd:YVO_4 (439cm^{-1}). However the low absorption coefficient of 1.1% Nd:YAG (0.85mm^{-1}) at 810nm compared to 3% Nd:YVO_4 (12mm^{-1}) makes YAG less desirable as a microchip medium. More significantly as Nd:YAG is isotropic it was expected that in order to generate efficiently the 946nm fundamental in the correct polarisation for second harmonic generation would require insertion of a polariser. Potassium Niobate ($KNbO_3$) was selected as the doubling material due to its high nonlinearity (d_{eff} =13pm/V) and an ability to be birefringently phase-matched for second harmonic generation of the 946nm fundamental.

In initial experiments an 850mW cw Ti:sapphire laser tuned to λ_p=808.5nm was focused to a spot size of 17±5μm within the crystal set. The 28% reflectance of the input coating and the 49.2% absorption within the Nd:YAG crystal led to a maximum absorbed power P_{abs} of 279mW.

The blue and 946nm output powers as a function of the absorbed pump power were measured, as shown in figure 1. As the pump power was reduced additional heat was required to ensure that the $KNbO_3$ crystal remained phase-matched to maximise the blue output power.

The maximum blue power P_{blue} of 4.3mW was generated at P_{abs}=279mW. As the crystal coating specifications on both sides were identical we can expect similar outputs emitted from both the input and output surfaces. The 1.02° walkoff between the fundamental and second harmonic introduced by the 1.5mm long $KNbO_3$ was calculated to have reduced the conversion efficiency by only 23%. A second crystal set with the $KNbO_3$ angle cut to phase-match at the lower T_{pm}= 40°C produced a single-direction blue output power of 9.2mW Ti:sapphire pumped. The

crystal heat sink temperature T_x which maximised the blue output power, at full pump power, was 36.6°C. The short non-linear crystal length resulted in an acceptably broad temperature bandwidth of 2°C FWHM, figure 2.

The spatial quality of both the 946nm and blue output beams suggest TEM_{00} transverse mode operation with < 1:1.1 ellipticity. At full pump power and at optimum temperature (T_x=36.6°C) three blue frequencies and three axial modes centred at 946.2nm with a mode spacing of 0.25nm were present. The calculated longitudinal 946nm mode spacing for this cavity was 0.1nm, suggesting that adjacent modes are prevented from oscillating due to spatial hole burning. No parasitic laser oscillation was detected at either 1064nm or 1320nm.

Intensity fluctuations due to mode coupling in green microchip lasers, 'green noise', have been reported[1,2]. In our blue microchip laser 'blue noise' was present producing intensity fluctuations the depth and spectral content of which varied with crystal temperature. A RF spectrum analysis indicated both distinct frequency and random noise are present dependent on the operating conditions. One such noise spectrum was characterised by 9% peak to peak fluctuation at around 2MHz. It is expected that this noise is caused by mode coupling due to sum frequency mixing as suggested by Baer[4].

An examination of the polarisation of the output beams showed that the 946nm radiation was strongly linearly polarised and orthogonal to the linearly polarised blue output. That the blue radiation was strongly polarised is a condition of the phase-matching geometry of the $KNbO_3$ crystal [5]. However as Nd:YAG is isotropic there is no intrinsic mechanism to ensure that the 946nm output is optimally linearly polarised parallel to the $KNbO_3$ ab-plane and is thus phase-matched for optimum blue generation. Under all experimental conditions (varying T_x and P_{abs}) the laser chose to oscillate polarised parallel to the ab-plane. This may have been due to stress effects in the Nd:YAG or the positioning of the fundamental modes across the gain profile.

A 2Watt (200x1μm emitter) diode laser and an aspheric lens pair were used to focus the λ_p=808.5nm pump beam into the crystal producing a maximum absorbed power of P_{abs} = 647mW. A maximum blue output power of P_{blue}=0.954mW was observed, figure 3. In each case the crystal heat sink temperature was maintained at T_x=26.9°C. An attempt at adjusting T_x at each pump power for optimum blue output proved difficult producing bistability in the output power.

The polarisation of the fundamental and blue outputs were linear and orthogonal to each other and displayed the same insensitivity to pump power and crystal heat sink temperature observed with Ti:sapphire pumping. Intensity noise of approximately 10% was again present.

At maximum pump power two axial modes were present centred at 946.2nm with a mode separation of 0.25nm. Single axial mode operation was only observed just above threshold. The blue output showed a single spot of high ellipticity (1:1.7) whilst the fundamental beam had three spots consistent with TEM_{00} and TEM_{10} transverse modes.

Investigations are in progress to determine the optimum angle cut temperature and crystal lengths along with a clarification of the mechanisms leading to the polarisation eigenmodes observed and means by which the blue noise may be eliminated.

We acknowledge the support of the UK EPSRC (grant GR/K14766). The subject matter and results reported here are subject to pending UK and international patent applications.

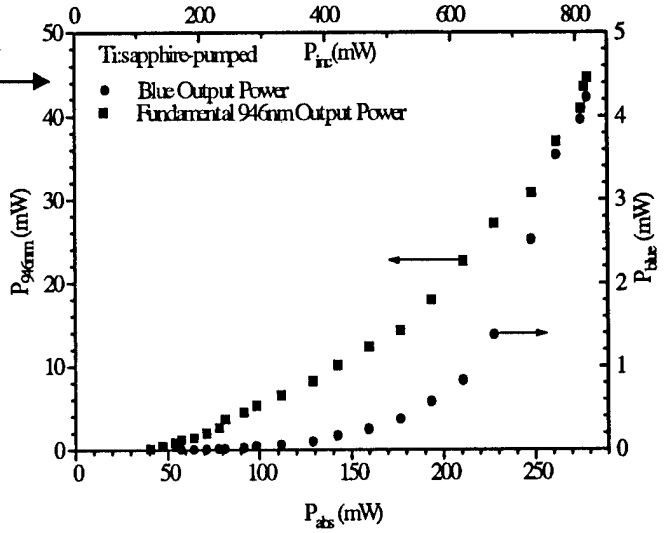

Figure 1. Ti:sapphire pumped: Blue and 946nm laser output power as a function of pump power (P_{inc} -incident, P_{abs} -absorbed) at the T_x which optimised the blue output at each pump power.

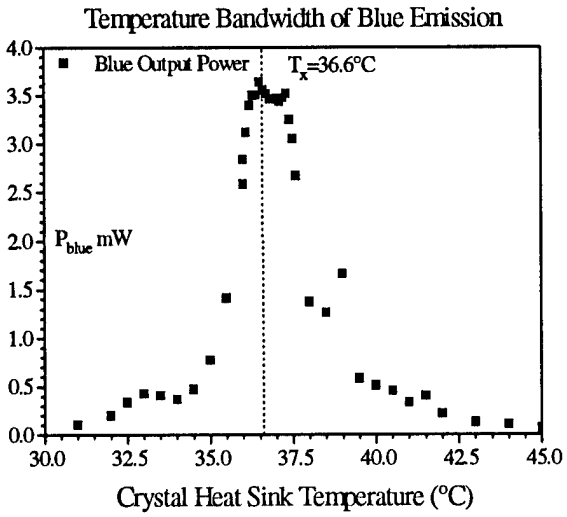

Figure 2. Blue laser output power as a function of crystal heat sink temperature at maximum Ti:sapphire pump power P_{abs}=279mW.

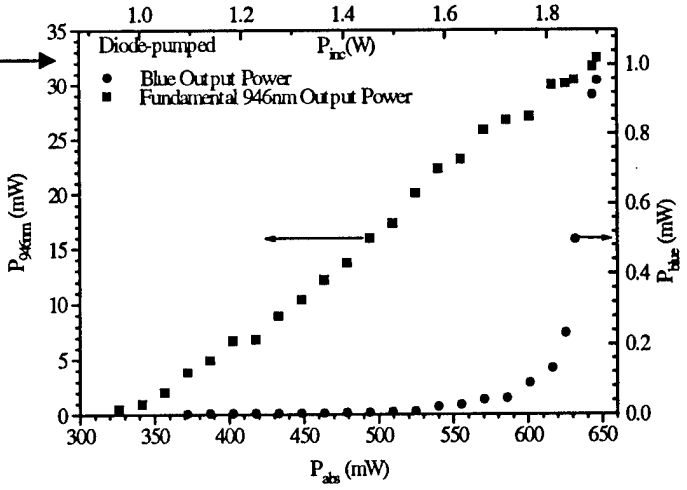

Figure 3. Diode pumped: Blue and 946nm laser output power as a function of pump power (P_{inc} -incident, P_{abs} -absorbed) at T_x=26.9°C which optimised blue output at maximum pump power P_{abs}= 647mW.

1. N. MacKinnon and B. D. Sinclair, Opt. Comm. **105**, 183 (1994).
2. N. MacKinnon et al., in *Conference on Lasers and Electro-Optics*, Vol. 8 of 1994 OSA Technical Digest Series (Optical Society of America, Washington D.C., 1994), paper CTuP2.
3. J. J. Zayhowski, Lincoln Laboratory Journal, **3** 428 (1990).
4. T. Baer, J. Opt. Soc. Am. B **3**, 1175 (1986).
5. I. Biaggio et al., J. Opt. Soc. Am. B **9**, 507 (1992).

Intracavity, frequency-doubled, miniaturized Nd:$YAlO_3$ blue laser at 465 nm

Joseph H. Zarrabi, Paul Gavrilovic and Shobha Singh

Research Division, Polaroid Corporation, Cambridge, Massachusetts 02139

The vast majority of Nd^{3+} solid-state lasers demonstrated so far have been operated on either $^4F_{3/2}$ => $^4I_{11/2}$ (1.06 μm) or $^4F_{3/2}$ => $^4I_{13/2}$ (1.3 μm) transitions. In addition to these four-level transitions in Nd doped crystals, the three-level $^4F_{3/2}$ => $^4I_{9/2}$ transition yields ~ 0.93 - 0.95 μm emission. Frequency doubled lasers operating on this transition generate coherent blue emission. There are disadvantages to these quasi three-level lasers, the major one being the lower stimulated emission cross section of the $^4F_{3/2}$ => $^4I_{9/2}$ transition in comparison to $^4F_{3/2}$ => $^4I_{11/2}$. Another disadvantage is significant reabsorption loss due to population of the terminal laser level. Solid-state lasers exhibiting reabsorption loss have been modeled previously and it was shown that there is an optimum crystal length for minimum threshold pump power[1].

Previously, intracavity frequency doubling of 946 nm emission in Nd:YAG has been used in different experiments to generate blue light[2]. In all these experiments, the laser cavity consisted of a separate input mirror, Nd:YAG crystal, a $KNbO_3$ crystal, and an output mirror, along with other optical components such as a quarter wave plate for mode stabilization.

In this paper we report on a plano-plano, microcavity blue laser consisting of a 1.2 mm-thick piece of neodymium-doped yttrium orthoaluminate (Nd:$YAlO_3$) and a 1.3 mm- thick $KNbO_3$ crystal. This composite microcavity laser generated 15 mW of blue emission at 465 nm when pumped with a Ti:Sapphire laser.

Yttrium orthoaluminate ($YAlO_3$) is an orthorhombic crystal derived from the Y_2O_3-Al_2O_3 material system, as is YAG. The crystal field splitting of of the $^4I_{9/2}$ manifold in Nd:$YAlO_3$ is smaller than the crystal field splitting Nd:YAG: ΔE_{YAlO3} = 670 cm^{-1} vs. ΔE_{YAG} = 857 cm^{-1}. Since resonant loss in a quasi-three level laser is proportional to exp($-\Delta E/kT$), the threshold pump power for 930 nm transition in Nd:$YAlO_3$ is higher than for the 946 nm transition in Nd:YAG. On the other hand, since the 930 nm output of Nd:$YAlO_3$ is polarized, a higher SHG conversion efficiency is expected. The polarized nature of emission at 930 nm in Nd:$YAlO_3$ was the motivation for this work.

The Nd:$YAlO_3$ crystal was cut and polished into 3x3x1.2 mm plates. Before fabrication, the polarized absorption and emission cross sections of Nd^{3+} were measured. The Nd concentration was determined to be 0.9 +/- 0.05 atomic percent by electron probe analysis. The absorption coefficient of

uncoated, polished plate of Nd:$YAlO_3$ at 813 nm in the direction parallel to the a-axis was measured to be $\alpha = 11.6\ cm^{-1}$.

The input face of the Nd:$YAlO_3$ crystal was coated with a dielectric stack having high reflectivity (> 99.7 %) at 930 nm and high transmission (> 80 %) at 800-820 nm. The other side of the Nd:$YAlO_3$ crystal was coated for high reflectivity at the pump band of 800-820 nm and high transmission (T >96%) at 930 nm. The $KNbO_3$ crystal was 1.3 mm thick, angle cut for type-I frequency doubling and phase-matched at 930 nm at T=52.7 °C. Its input was AR coated for 900-950 nm while the opposite output face was coated for high reflectivity at 930 nm (99.7 %).

The pump beam from a Ti:Sapphire laser was focused to a spot diameter of ~ 25 μm by a f=25 mm spherical lens. The Nd:$YAlO_3$ crystal was mounted such that the a-axis of the crystal was parallel to the polarization of the pump beam. The pump beam was tuned to 813.2 nm, the wavelength of the strongest absorption band in 800-820 nm region in Nd:$YAlO_3$. The absorption efficiency at 813.2 nm was determined to be 0.9 by measuring the amount of unabosrbed pump power in a small angle reflective geometry. The $KNbO_3$ crystal was mounted on a fixture attached to a thermoelectric cooler in order to temperature tune for exact phase-matching at 930.3 nm. The Nd:$YAlO_3$ crystal was mounted on a separate fixture, passively cooled at room temperature and was not attached to the $KNbO_3$ Crystal. The spacing between the Nd:$YAlO_3$ and the $KNbO_3$ crystals was adjustable.

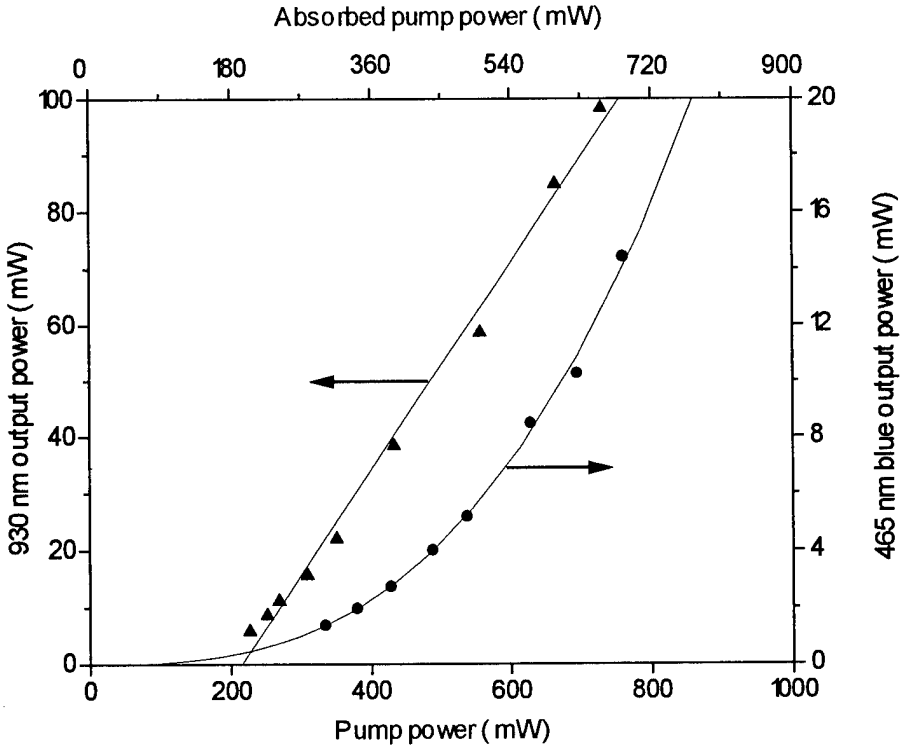

Fig. 1

Figure1 shows a plot of the fundamental output power at 930 nm and the corresponding SHG output at 465 nm. The output was in a TEM_{00} mode with a measured fundamental beam waist radius of ~ 60 μm.

The blue power obtained by SHG of the 930 nm fundamental has beed estimated to be be around 45 mW. The estimated SHG blue output power is three times higher than measured value of 15 mW. The reason behind this discrepancy is not clear. It is possible that output mirror reflectivity is lower than 0.997 as it was intended. The blue output of the current design can be improved significantly if we replace the unoptimized L=1.3 mm $KNbO_3$ with a longer crystal. A better high reflector (r = 0.999) on the output face of the $KNbO_3$ will also increase the intracavity power leading to higher blue output. Finally, the Nd:$YAlO_3$ and $KNbO_3$ crystals can be attached to each other permanently if the sides facing each other are uncoated to form a monolithic microcavity blue laser.

In order to compare the SHG blue output power of Nd:$YAlO_3$ against the Nd:YAG, a 1-mm thick, 1% doped Nd:YAG crystal which was coated simultaneously with Nd:$YAlO_3$ crystals, was pumped at 807 nm. Using the same 1.3 mm $KNbO_3$ crystal as frequency doubler and output mirror, the Nd:YAG laser generated 4.83 mW of blue output power at 473 nm and 101 mW of IR output. The absorbed pump power was ~ 504 mW. For this experiment, the $KNbO_3$ phase-matching temperature was 67.7 °C. Thus for the same intracavity fundamental power, the SHG output power is higher in the Nd:$YAlO_3$ than in the Nd:YAG laser. This difference is due to the fact that the fundamental beam in Nd:$YAlO_3$ is linearly polarized while in the case of Nd:YAG it is partially polarized. Theoretically, a 4:1 SHG power ratio is expected between linearly polarized and unpolarized fundamental beams. The observed SHG power ratio is in close agreement with this expectation, with the small discrepancy being attributed to slight birefringence in the Nd:YAG crystal.

In conclusion, a Ti:Sapphire pumped microcavity blue laser consisting of Nd:$YAlO_3$ and $KNbO_3$ crystal with 15 mW of output power at 465 nm has been demonstrated. The $KNbO_3$ crystal was oriented for type-I intracavity frequency doubling at 930.3 nm. The blue output power of this unoptimized laser can be significantly improved by using a longer $KNbO_3$ crystal with higher reflectivity coating at the fundamental wavelength.

1 - T. Y. Fan, R. L. Byer, IEEE J. Quantum Electron.. **QE-23**, 605 (1987).

2 - W. P. Risk, R. Pon and W. Lenth, Appl. Phys. Lett., **54**, 1625 (1989).

Infra-red to visible nonlinear up-and-down conversion processes using $AgGaS_2$ crystals

J.-J. Zondy, D. Touahri and O. Acef

Laboratoire Primaire du Temps et des Fréquences (BNM-LPTF),
Bureau National de Métrologie/ Observatoire de Paris,
61, Avenue de l'Observatoire, 75014, Paris (France).

Phone: 33-1-40512222; Fax: 33-1-43255542; e-mail: zondy@opdaf1.obspm.fr

We report various frequency up-and-down CW parametric conversion processes of an optical frequency synthesis and measurement chain [1] connecting a CO_2 laser reference standard (λ_R=10.2 μm, ν_R=29 THz) to an AlGaAs diode laser frequency-stabilized to a hyperfine component of the $5S_{1/2}$-$5D_{5/2}$ two-photon transition of rubidium vapor at λ_0 = 0.778 μm (ν_0= 385 THz ≈ 13 ν_R) [2].

The synthesis of the 13th harmonic of the CO_2 laser (fig.1) uses as transfer oscillators a tunable KCl:Li color center laser delivering 15 mW single mode power ($\Delta\nu$<1 kHz) at λ_1 = 2.52 μm ($\nu_1 \approx 4\nu_R$); and two extended-cavity diode lasers (ECDL): a near-IR AlGaAs diode at λ_3= 0.842 μm ($\nu_3 \approx 12\ \nu_R$), and a mid-IR InGaAsP diode at λ_2= 1.26 μm ($\nu_2 \approx 8\ \nu_R$).

The InGaAsP diode laser frequency is compared to the reference frequency via the second-harmonic generation (SHG) of the color center laser in a type-I (ooe)-cut 10 mm long $AgGaS_2$ crystal (θ= 43°). Owing to the high nonlinearity of silver thiogallate ($d_{36} \approx 12$ pm/V), the SHG conversion efficiency is 20 times higher than that of type-II phase-matched KTP in a former version of that frequency chain [3,4]. About 6 nW of harmonic power is obtained with a fundamental power of 15 mW and a beam waist of 120 μm. The 13th harmonic (at 0.778 μm) of the CO_2 laser is generated by type-I (ooe) frequency up-conversion (SFG) of the AlGaAs transfer ECDL ($\nu_3 \approx 12\ \nu_R$) using a 15 mm long $AgGaS_2$ crystal (θ= 43°). A conversion efficiency of about 500 $\mu W/W^2$ has been measured for that sum-frequency process with equal near-IR and IR beam parameters of $2z_R$= 160 mm [5]. To fulfill the frequency measurement, the frequency of the near-IR diode laser should be compared to the reference frequency, either by SFG of the color-center laser with the mid-IR diode laser ($4\nu_R+8\nu_R= 12\nu_R$) or by DFG of the near-IR diode with the color center laser ($12\nu_R-4\nu_R= 8\nu_R$). That (ω, 2ω, 3ω) mixing process is type-I (ooe) non-critically phase-matched (θ= 90°) in silver thiogallate and can be temperature-tuned to cover the whole tuning range of the KCl:Li laser (2.5-2.8 μm). The crystal (15 mm long) is mounted on a thermo-electric cooler and the room-temperature (T= 25°) phase-matching corresponds to a KCl:Li wavelength of 2.538 μm. Because of power convenience, optical parametric amplification (OPA) at 1.26 μm by difference-mixing the AlGaAs diode and the color center lasers has been implemented, yielding more than 250 nW generated radiation from pump and idler powers of about 15 and 10 mW and corresponding waists of 50 μm and 90 μm.

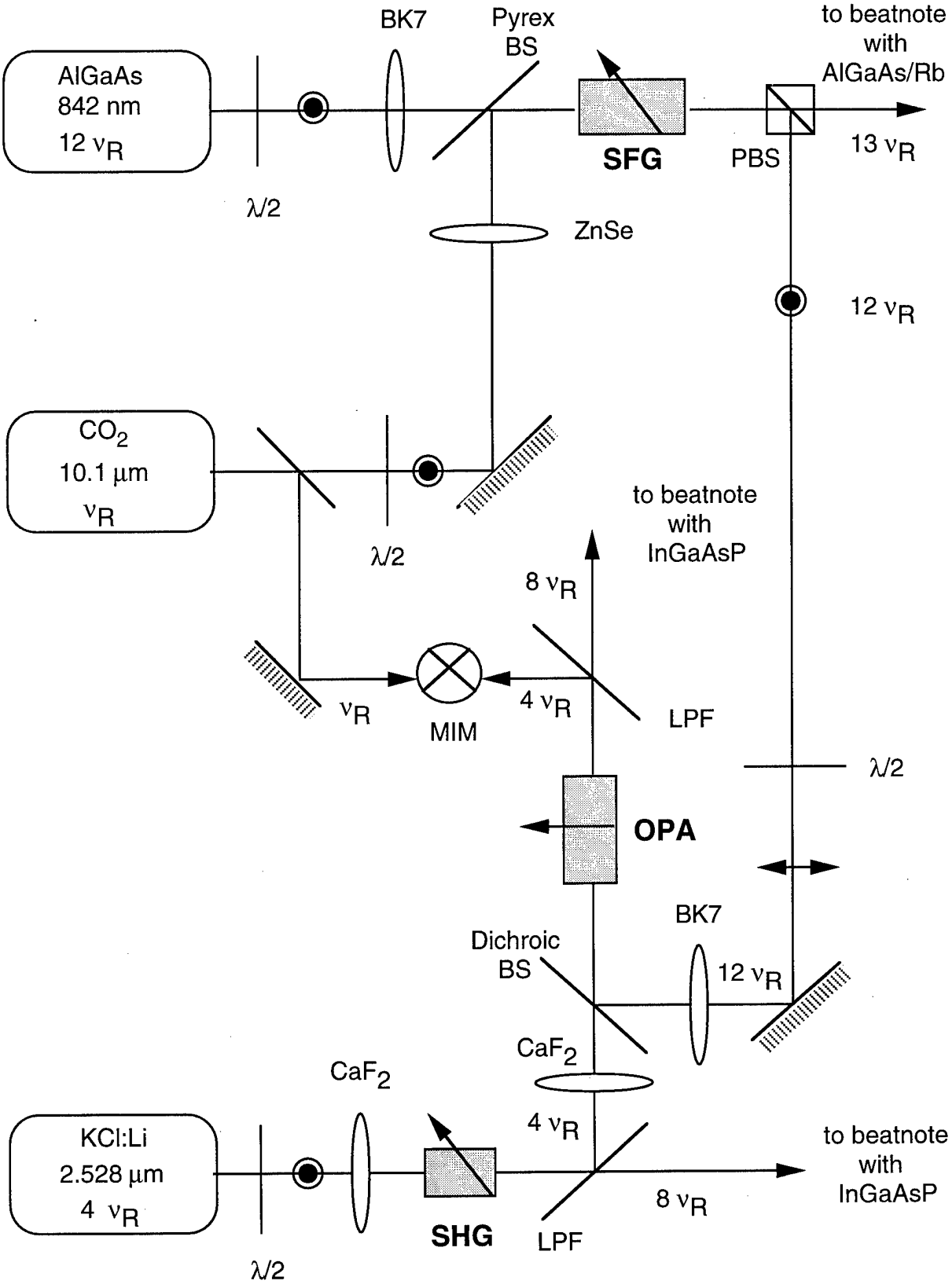

Fig 1: Experimental set-up for SHG, SFG and OPA with $AgGaS_2$ crystals. MIM: metal-insulator-metal point contact diode for the beatnote detection of the KCl:Li laser. LPF: low-pass (λ_c= 2 μm) interference filter .PBS: near-IR polarizing beamsplitter.

Owing to the wide wavelength range involved in that frequency synthesis chain (10.2 to 0.778 μm) employing $AgGaS_2$ as a nonlinear mixer, the dispersion of the nonlinear coefficient of this material can be measured as well as an accurate determination of its thermo-optic index coefficients. The measured aborption coefficients (less than $1\%.cm^{-1}$ in the near-and-mid IR for samples of american origin) and the estimated small signal OPA gain ($\Gamma = 1.2\ 10^{-2}\ P_3$ where P_3 is the near-IR pump power in Watt) of our $AgGaS_2$ sample for the (indirect) third harmonic synthesis of the color center laser frequency opens up the possibility to develop a doubly resonant OPO-based 3:1 optical frequency divider using $AgGaS_2$ pumped by a low-power (tens of mW) AlGaAs near-IR diode lasers. Such a DROPO would conveniently replace the use of both the KCl:Li and InGaAsP lasers in our frequency chain.

References

1 - J.-J. Zondy, D. Touahri, O. Acef, L. Hilico, M. Abed and A. Clairon, Proc. of the OE'Lase/SPIE conf. on "*Laser frequency stabilization and noise reduction*", Photonic West'95, San Jose(CA), Feb. 95,Vol. **2378**, pp. 147-155 (1995).

2 - R. Felder, D. Touahri, O. Acef, L. Hilico, J.-J. Zondy, A. Clairon, B. de Beauvoir, F. Biraben, L. Julien, F. Nez and Y. Millerioux, same volume as above except pp. 52-57.

3 - O. Acef, J.-J. Zondy, M. Abed, D.G. Rovera, A.H. Gérard, A. Clairon, Ph. Laurent, Y. Millerioux and P. Juncar, Opt. Comm. **97**, pp. 29-34 (1993).

4 - J.-J. Zondy, M. Abed and A. Clairon, J. Opt. Soc. Am **B11**, pp. 2004-2015 (1994).

5 - D. Touahri, O. Acef and J.-J. Zondy, "*30 THz up-conversion of an AlGaAs diode laser using $AgGaS_2$: Bridging several THz frequency gap in the near-IR* ", to appear in Optics Letters (1995).

Visible picosecond pulse generation in a frequency doubled optical parametric oscillator based on LiB_3O_5

S. French, M. Ebrahimzadeh and A. Miller

The J. F. Allen Research Laboratories, School of Physics and Astronomy, University of St. Andrews, Fife KY16 9SS, Scotland, United Kingdom

The current increase in interest in the field of time-resolved ultrashort spectroscopy has lead to the need for widely tunable pulses in the visible wavelength region. Over the past decade, synchronously pumped or passively mode-locked dye lasers have been the main source for high-repetition rate picosecond and femtosecond applications in the visible[1]. These systems are however complicated and suffer from limited tunability because of the need for different dye/pump laser configurations. However, the green-to-red spectral range is of increasing importance, for example, for research on wide band gap semiconductors such as AlGaInP. There has recently been an increasing interest in optical parametric oscillators (OPOs) for the generation of ultrashort pulses. In particular, the emergence of the self-mode-locked Ti:sapphire laser as the pump source has enabled reliable operation of OPOs in the femtosecond time domain. However, there have previously been only two reports on Ti:sapphire-pumped OPO in the picosecond regime. By using KTP as the nonlinear crystal, Nebel [2] et al reported a device with a tunable range of 1.52-1.214 μm (signal) and 2.286-2.871 μm (idler), while we recently demonstrated an OPO based on temperature-tuned LiB_3O_5 (LBO). This system was pumped by a picosecond Ti:sapphire laser and produced tunable 1.1 ps pulses over the wavelength range 1.18 μm to 1.828 μm [3]. Here, we report a new source of picosecond visible pulses based on an OPO that uses LiB_3O_5 as the nonlinear crystal which is externally frequency doubled by a further LiB_3O_5 crystal and is synchronously pumped by picosecond pulses from a self-mode-locked Ti:sapphire laser. The unique feature of the described OPO is its accessible tuning range of 584-771 nm that is not fully obtainable from either the Ti:sapphire or frequency doubled Ti:sapphire laser. The combination of the LiB_3O_5 OPO, frequency doubled LiB_3O_5 OPO and the Ti:sapphire pump laser represents a highly versatile source of picosecond pulses with extended tunability from 584 nm to 2.27 μm. The configuration of the Ti:sapphire-pumped picosecond LiB_3O_5 OPO is similar to that described in detail previously[4]. The OPO cavity a standing-wave, folded arrangement formed by two concave reflectors and a plane mirror. The OPO is singly-resonant and the pump is single-pass. The mirrors are highly reflecting (R>99.7%) for wavelengths centred at 1.4 μm and have high transmission (T>95%) over 0.75-1.1 μm. The LiB_3O_5 crystal is 30 mm in length and 3 mm x 3 mm in aperture. It is cut for type I noncritical phase-matching (NCPM) along the x-axis ($\theta=90°$, $\phi=0°$) and the end faces are AR-coated at 1.4 μm. While LiB_3O_5 possesses smaller nonlinear coefficients than KTP, its NCPM allows the use of long interaction lengths, thus preserving high conversion efficiencies. Moreover, temperature-tuning in LiB_3O_5 enables broadband parametric generation under type I NCPM, a feature not available to KTP. The magnitude of the group velocity mismatch in LiB_3O_5 is also as low as 14 to 18 fs/mm, almost an order of magnitude smaller than in KTP.[2] Therefore, much longer crystal lengths can be used in LiB_3O_5 OPOs to maintain high efficiencies with minimal increase in spatial and temporal walk-off effects. The second harmonic generation (SHG) was carried out by using two NCPM LiB_3O_5 crystals which were temperature tunable, one is 16 mm in length and 3 mm x 3 mm in aperture and is cut for type I NCPM along the x-axis ($\theta=90°$, $\phi=0°$) with the end faces being AR-coated at 1.4 μm. The other is also 16 mm in length and 3 mm x 3 mm in aperture but is cut for type II NCPM along the z-axis ($\theta=0°$, $\phi=0°$) with the end faces again AR-coated at 1.4 μm. Two crystal were necessary so that the full signal range could be frequency doubled while keeping the phase-matching temperature in the 20-50°C range[5]. This prevented the need for any peltier cooling or nitrogen purge systems which would lead to system complexity. These characteristics make LiB_3O_5 highly desirable for use in ultrashort-pulse OPOs and as a frequency doubling crystal. The pump laser is a commercial self-mode-locked Ti:sapphire laser (Spectra-Physics, Tsunami) which is configured for picosecond operation. It delivers a maximum average output of 2.0 W for 12 W of argon ion pump. The duration of the output pulses is typically 1.1-2 ps and the repetition rate is 81 MHz. The pump beam is focused to a spot radius of ~25 μm inside the crystal, using a 10-cm focal length lens. An optical isolator is located between the two cavities and a half-wave plate is used to yield a pump polarisation along the y-axis of the crystal. With the available mirrors set, we have demonstrated a total signal (idler) tuning range from 1.290 to 1.534 μm (1.610 to 1.973 μm) for a range of pump wavelengths from 770 to 800 nm, by varying the crystal temperature between 117.1° and 230°C for more detailed discussion of the OPO see[6]. Using a 5% output coupler (OC) on the OPO we obtained signal powers as high as 300 mW with the power over the entire tuning range staying for the most part above 50 mW.

In Fig. 1. the power in the second harmonic is shown as a function of wavelength it can be seen that the power rises to as high as 68 mW at 645 nm, with greater than 10 mW being achieved for almost the entire tuning range of 584-771 nm.

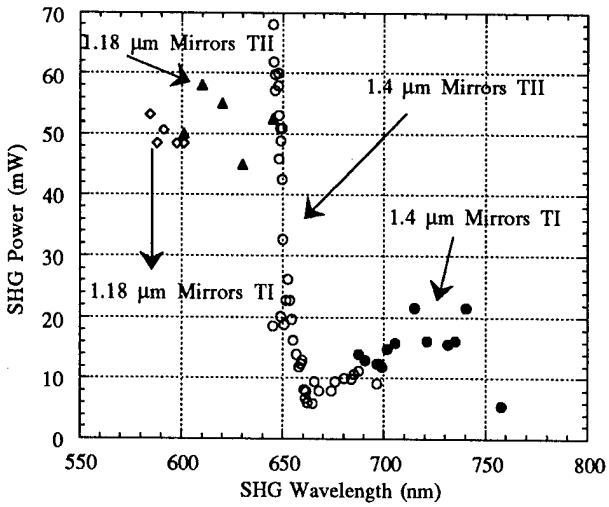

Fig. 1. Second harmonic power as a function of wavelength, for a Ti:sapphire laser pump power of 2.0 W.

In Fig. 2 (a) and (b), typical interferometric autocorrelation and spectrum of the signal pulses at a wavelength of 625 nm are shown. The pulse duration deduced from the autocorrelation is 880 fs ($sech^2$ pulse profile assumed). The spectrum has a smooth profile with a spectral width of 0.5 nm, giving a time-bandwidth product of 0.338. Therefore, these pulses are essentially transform-limited. We observe variations in the pulse duration between 860 and 880 fs across the SHG tuning range which is found to follow the pulse durations of the signal wave. However, we observe that the SHG pulses remain essentially chirp-free and transform-limited across the tuning range, with dispersion compensation in the cavity required only for signal wavelengths below 1.2 μm which are in the positive LBO GVD regime.

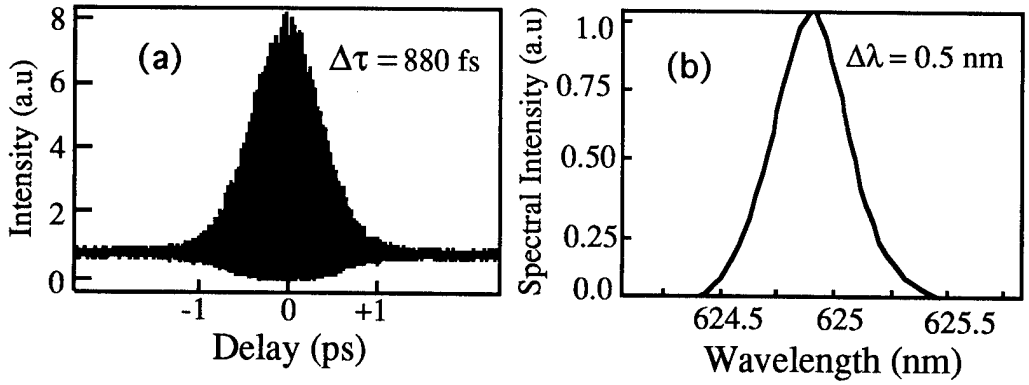

Fig. 2. Typical (a) interferometric autocorrelation and (b) spectrum of the output SHG pulses at 625 nm, indicating a time-bandwidth product $\Delta\tau\Delta\nu$=0.338. The signal pulse duration is 1.01 ps and pump pulse duration is 1.1 ps.

References

1. R. L. Fork, B. I. Greene, and C. V. Shank, Appl. Phys. Lett. 38, 671 (1981).
2. A. Nebel, C. Fallnich, R. Beigang, and R. Wallenstein, J. Opt. Soc. Am. B 10, 2195 (1993).
3. M. Ebrahimzadeh, S. French, W. Sibbett, and A. Miller, Opt.Lett. 20, 55 (1995).
4. J. M. Dudley, D. T. Reid, M. Ebrahimzadeh, and W. Sibbett, Opt. Commun. 104, 419 (1994).
5. S. Lin, B. Wu, F. Xie, and C. Chen, J. Appl. Phys. 73 (3), 1029. (1993).
6. M. Ebrahimzadeh, S. French, and A. Miller, (accepted) J. Opt. Soc. Am. B (1995).

Temperature (-32°C to +90°C) Performance of a 20 Hz Potassium Titanyl Phosphate Optical Parametric Oscillator

Robert D. Stultz and Michael E. Ehritz
Hughes Electro-Optical Systems
2000 E. El Segundo Blvd., E1/D109
El Segundo, CA 90245-0902
Tel.: (310) 616-4963, Fax: (310) 616-4468

Optical parametric oscillators (OPOs) using Potassium Titanyl Phosphate (KTP) in a non-critically phase-matched (NCPM) configuration are known to provide efficient eyesafe wavelength conversion from 1 to 1.5 μm [1]. Laser systems which incorporate OPOs are often required to operate over large temperature ranges, and components which necessitate temperature control typically add significant complexity and cost to the overall design. We have measured key performance parameters of a NCPM KTP OPO over a temperature range of greater than 120°C. OPO slope efficiency and threshold are found to be extremely insensitive to temperature. Also, the signal wavelength shift is close to that predicted by theory.

The 1.06 μm (multi-mode) pump laser was flashlamp pumped with a 0.25 x 4.25 inch Nd:YAG rod, and was electro-optically Q-switched with a full-width at half-maximum (FWHM) output pulsewidth of 18 ns. A spherical thermal compensation lens was inserted in the 1.06 μm pump resonator for 20 Hz operation. No lens was used at 1 Hz. A 1.5x beam reducing telescope was used to increase the incident pump intensity in the OPO.

The room and high-temperature OPO cavity consisted of two flat fused-silica mirrors of 100% (HR) and 70% (outcoupler) reflectivity at 1.57 μm. The pump beam was input through the 1.57 μm HR mirror which was also highly transmitting (HT) at 1.06 μm. The OPO outcoupler was HR at 1.06 μm. The cavity length was 5 cm. The optical axis of the OPO cavity was tipped by a few milliradians, relative to the pump beam, in order to prevent the back-reflected pump from re-entering the 1.06 μm resonator.

For elevated temperature operation, the KTP crystal was mounted on a resistive-type heater. The heater temperature was controlled by varying the current through the heater using a DC power supply. The crystal was otherwise open to the ambient atmosphere.

The OPO configuration for the low-temperature measurements is shown in Fig. 1. The hot end of a thermo-electric (TE) cooler was mounted to a heat exchanger block which was lowered to -29°C using an RT-4 Neslab refrigerated cooler (with methanol as the coolant). The crystal temperature was further reduced and controlled using the TE cooler. The cavity length had to be increased to 6.5 cm, due to the use of a small Plexiglass chamber. Ultrapure (dry) N_2 was constantly flowed through this chamber to prevent condensation on the KTP crystal. N_2 was also blown across the external window surfaces. The same OPO mirrors were used as at room and high temperatures.

Type II, non-critical phase-matching, with $\phi = 0°$, $\theta = 90°$, was used in all cases. A slight optical wedge as a result of a transverse thermal gradient produced at the extreme temperatures was compensated for by adjusting the tilt on one of the OPO cavity mirrors.

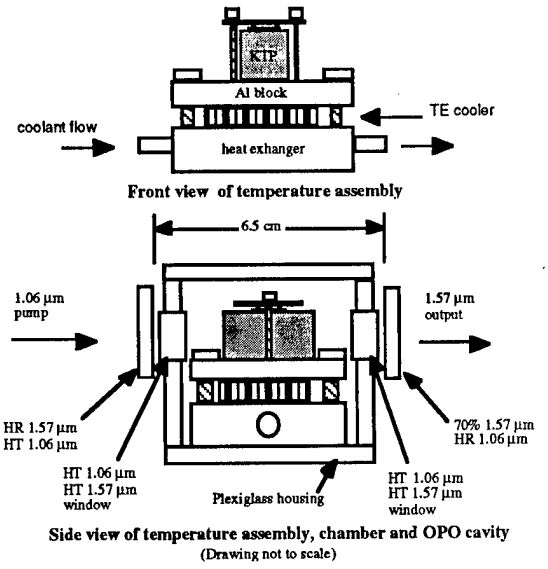

Figure 1. Low temperature set-up.

The OPO shot-to-shot variation was reasonably small over all temperatures. A typical example of pump, signal energy versus time is shown in Fig. 2 (KTP is at +90°C). The 1.06

μm (pump) input energy is shown in the upper part of the figure as negative-going traces. The OPO output (1.57 μm) is displayed in the lower part of the figure (positive-going traces).

The 86% pump divergence (at the input of the OPO cavity) was about 2.5 mrad at both PRFs, with a pump beam diameter of about 4 mm. The room temperature OPO signal divergence (see Fig. 3) was nearly identical at the two pulse repetition frequencies (PRFs). The near-field beams for both the pump and the signal were relatively smooth, but slightly elliptical in shape. The signal beam was roughly 25% smaller than that of the pump. Beam divergence was not measured at the various temperatures, but near and far-field beam profiles did not significantly change in appearance.

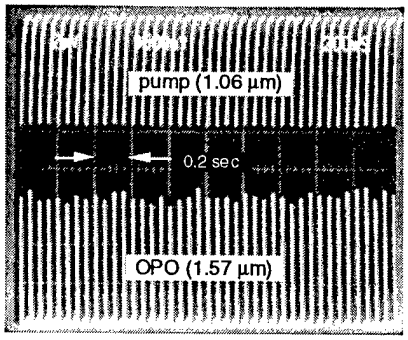

Figure 2. 20 Hz pump, signal with KTP at +90°C.

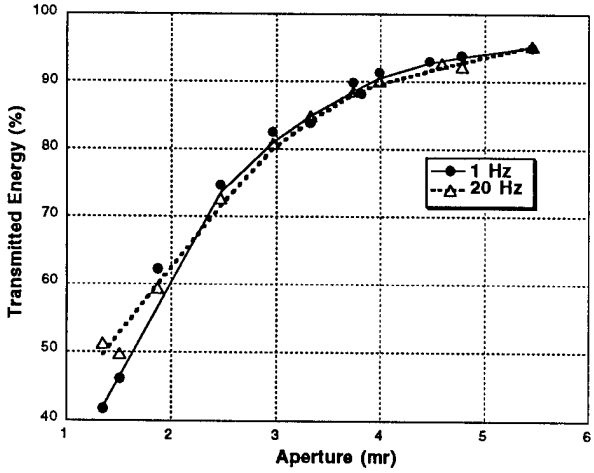

Figure 3. Room temperature signal (1.57 μm) beam divergence at 1 and 20 Hz PRF.

Slope efficiency versus PRF at room temperature is shown in Fig. 4. The relative difference between 1, 20 Hz was almost exactly the same over the entire temperature range tested.

Both pump and signal wavelengths were measured using a 1/2 meter Jarrell-Ash monochromator with a Judson Ge (J16 series) photodiode. The pump wavelength was 1064.4 nm (independent of KTP crystal temperature). The measured signal wavelength dependence on temperature is shown in Fig. 5. The theoretical curve was calculated using Sellmeier equations and *dn/dT*'s from references [2] and [3], respectively.

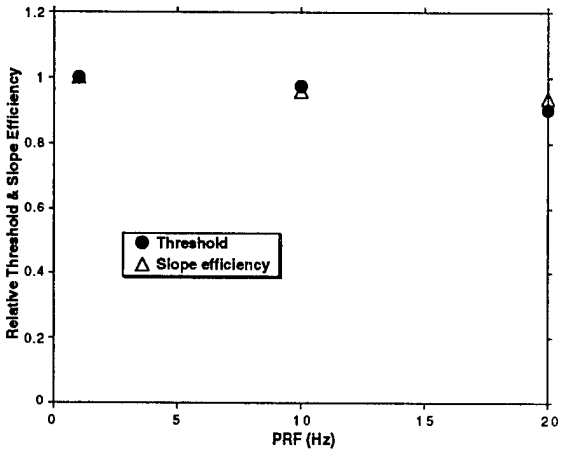

Figure 4. Relative threshold and slope efficiency versus PRF.

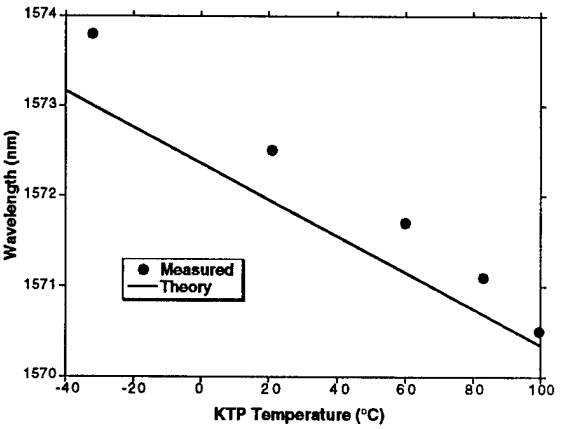

Figure 5. Signal wavelength versus KTP temperature.

Threshold and slope efficiencies for room and elevated temperatures are shown in Fig. 6. Both parameters were extremely insensitive to temperature variations. Theoretical OPO threshold for the 5 cm cavity, calculated using ref. [4] and a nonlinear coef. (d_{eff}) of 2.7 pm/V, determined using ref. [5], is 18 MW/cm^2. This

compares well to the 16 MW/cm^2 measured experimentally.

The increase of threshold with the 6.5 cm cavity (Fig. 7) may be accounted for by the increase in OPO cavity length and the insertion of the window losses. The expected increase in threshold for the 6.5 cm cavity is about 14%, theoretically. We observed a 12% increase (at room temperature), experimentally. A further slight increase (8%) was observed at low temperature (Fig. 7).

In conclusion, we have demonstrated the stable performance of a 1.5 μm KTP OPO over a large (120°C) temperature and PRF range, without the need for temperature control.

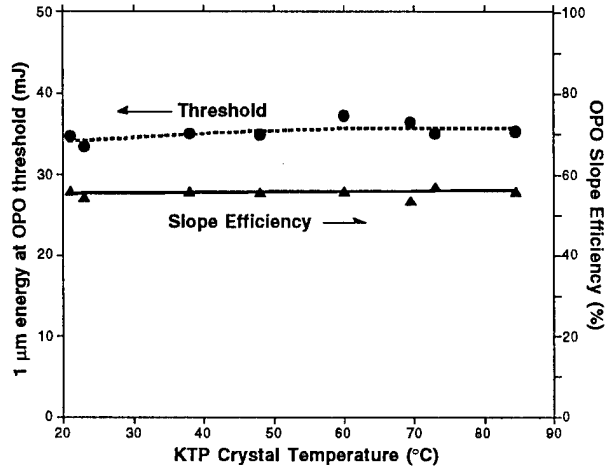

Figure 6. OPO threshold and slope efficiency as a function of KTP crystal temperature at 1 Hz PRF (5 cm long OPO cavity).

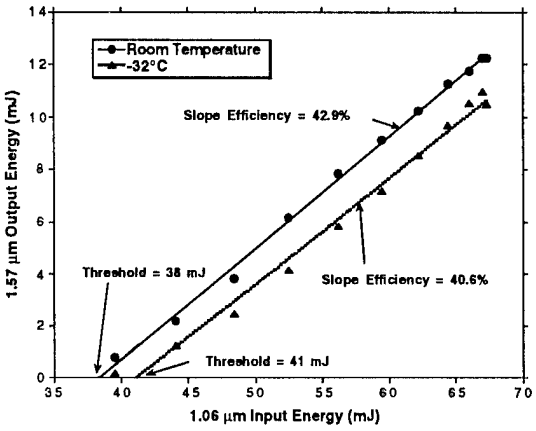

Figure 7. 1 Hz room and low temperature slope efficiencies (6.5 cm long OPO cavity).

References

1. L. R. Marshall, J. Kasinski, and R. L. Burnham, "Diode-pumped eye-safe laser source exceeding 1% efficiency," Opt. Lett. **16**, 1680 (1991).
2. L. T. Cheng, L. K. Cheng, and J. D. Bierlein, "Linear and Nonlinear Optical Properties of the Arsenate Isomorphs of KTP," SPIE Proceedings **1863**, 43 (1993).
3. J. D. Bierlein, "Potassium Titanyl Phosphate (KTP): Properties, Recent Advances and New Applications," SPIE Proceedings **1104**, 2 (1989).
4. S. J. Brosnan and R. L. Byer, "Optical Parametric Oscillator Threshold and Linewidth Studies," IEEE J. Quantum Electron. **QE-15**, 415 (1979).
5. R. C. Eckardt, H. Masuda, Y. X. Fan, and R. L. Byer, "Absolute and Relative Nonlinear Optical Coefficients of KDP, KD*P, BaB_2O_4, $LiIO_3$, MgO:$LiNbO_3$, and KTP Measured by Phase-Matched Second-Harmonic Generation," IEEE J. Quantum Electron. **26**, 922 (1990).

A Single Mode Grazing Incidence BBO OPO with a Large Scanning Range.

J. M. Boon-Engering[1], W. E. van der Veer[1,2], E. A. J. M. Bente[1] and W. Hogervorst[1].

[1]Laser Centre Vrije Universiteit, Department of Physics and Astronomy, De Boelelaan 1081, 1081 HV Amsterdam, The Netherlands. tel:+31-20-4447951, fax:+31-20-4447899.
[2]Nederlands Centrum voor Laser Research B.V. Postbus 2662, 7500 CR Enschede, The Netherlands. tel:+31-53-893965, fax:+31-53-338065.

Introduction

Optical parametric oscillators (OPO's) are attractive solid state sources of coherent radiation with an extensive tuning range and high efficiency. In practice, however, realising devices for spectroscopic applications has been difficult. While the output from a free running OPO exhibits a broad spectral bandwidth, many applications require narrow linewidth, or even single longitudinal mode (SLM) operation. As with other tunable laser sources, considerable reduction in the OPO bandwidth may be achieved by injection seeding with a narrow-band laser[1] or through the use of intracavity elements such as etalons. Another technique to reduce the spectral bandwidth is to use a cavity in a grazing incidence configuration[2]. This configuration has previously been used successfully to minimise the bandwidth of dye lasers and titanium sapphire lasers. In those devices SLM oscillation is obtained using a high efficiency, high resolution grating, a short cavity length (to maximise longitudinal mode separation) and careful control of the beam diameter. For scanning devices the pivot point of the tuning mirror is extremely critical, and in practice active stabilization of the end mirror is required. In this paper we present a SLM grazing incidence BBO OPO with a demonstrated scanning range of up to 5 cm^{-1}, using an actively-controlled, piezo-mounted end mirror. The signal for this position control is derived from the observed frequency output spectrum of the OPO. The scanning capabilities of this system are a.o. demonstrated in an iodine absorption experiment.

OPO setup and stabilization scheme

The OPO is shown schematically in Fig. 1. It consists of two BBO crystals in a grazing incidence cavity. The BBO crystals, in a walk-off compensated configuration, are used in the cavity to obtain a sufficiently high gain[3]. The crystals are cut for type I phase matching (e -> o + o). The size of both crystals is 7 x 5 x 12 mm^3.The total optical cavity length is 6.8 cm, corresponding to a free spectral range (FSR) of 2.2 GHz. The cavity consists of a piezo-mounted end mirror, a holographic diffraction grating and a tuning mirror. Inside the cavity a 355 nm absorption filter is placed behind the two crystals to prevent the residual pump light from damaging the grating. The end mirror acts as a high reflector for the signal wave (570-710 nm) and has a high transmission for the pump wavelength (355 nm). The tuning mirror is mounted on a piezo-controlled rotation stage. The grating has a periodicity of 1800 grooves/mm and is placed at grazing incidence relative to the cavity axis. The OPO is pumped at 355 nm by a 10 Hz repetition rate injection seeded Nd:YAG-laser (Spectra Physics GCR-4). The pump laser

diameter is reduced by a factor of 2 using a telescope. The resulting beam diameter is 2.5 mm ($1/e^2$ values). The OPO is scanned by controlling the angle of the tuning mirror with a piezo. The voltage over the piezo is scanned under software control. The output of the OPO is monitored using a spectrum analyser, consisting of an etalon (FSR of ~10 GHz, resolution of ~200 MHz) and a diode array. Each laser shot the OPO spectrum is read into a PC and the mode structure analysed. When additional modes start to appear in the spectrum, the software will via a DAC-controlled high voltage supply, correct the position of the end mirror. Also when the OPO is not scanning this stabilization is active to correct for thermal drift.

Experimental results

In Fig. 2 the single shot spectrum of the OPO as measured with the etalon is given. As can be seen this is a single mode output, and several modes of the etalon can be observed. It also shows that the linewidth of the OPO is less than 300 MHz. The system was operated in the wavelength range of 580-630 nm. At λ=610 nm about 100 μJ output pulses were obtained at a pump energy of 60 mJ. The pump energy is limited by optical damage on the end mirror. The scanning capability of the system is nicely demonstrated in an iodine absorption experiment. A fraction of the OPO output is send through a 50 cm long iodine cell. The OPO output intensity and transmission through this cell are monitored by photodiodes. A typical scan result is given in Fig. 3. It shows the OPO scanning SLM over 5 cm^{-1} at λ=610 nm. The scan length is limited by the translation range of the piezo controlling the tuning mirror. The spectrum in Fig. 3 is normalized on the output intensity of the OPO, which shows considerable intensity variations. During the scan the angle of the two BBO crystals is not changed.

Conclusions

An actively-stabilized, SLM grazing-incidence BBO OPO has been demonstrated with a scan range of about 5 cm^{-1}. In the stabilization scheme the spectral output of the OPO is analysed in order to derive a feedback to the OPO cavity. By using suitable mirrors and gratings this setup can be used to produce scannable, SLM output over the complete 355 nm pumped BBO OPO range. The maximum obtainable scan range will depend on wavelength. At this moment several experiments are in preparation. Firstly the OPO will be used in spectroscopic applications in different wavelength regions, which is of importance to determine accurate values for the linewidth. Secondly the OPO system will be pumped by a near diffraction limited pump source, to study the effects on efficiency, stability and linewidth.

We gratefully acknowledge the support of Urenco (Capenhurst) Ltd.

References

[1] J. M. Boon-Engering, W. E. van der Veer, J. W. Gerritsen and W. Hogervorst, Opt. Lett. **20**, 380 (1995).
A. Fix, T. Schröder, R. Wallenstein, J. G. Haub, M. J. Johnson and B. J. Orr, J. Opt. Soc. Am. B **10**, 1744 (1993).

[2] W. R. Bosenberg and D. R. Guyer, J. Opt. Soc. Am. B **10**, 1716 (1993).

[3] W. R. Bosenberg, W. S. Pelouch, and C. L. Tang, Appl. Phys. Lett. **55**, 1952 (1989)

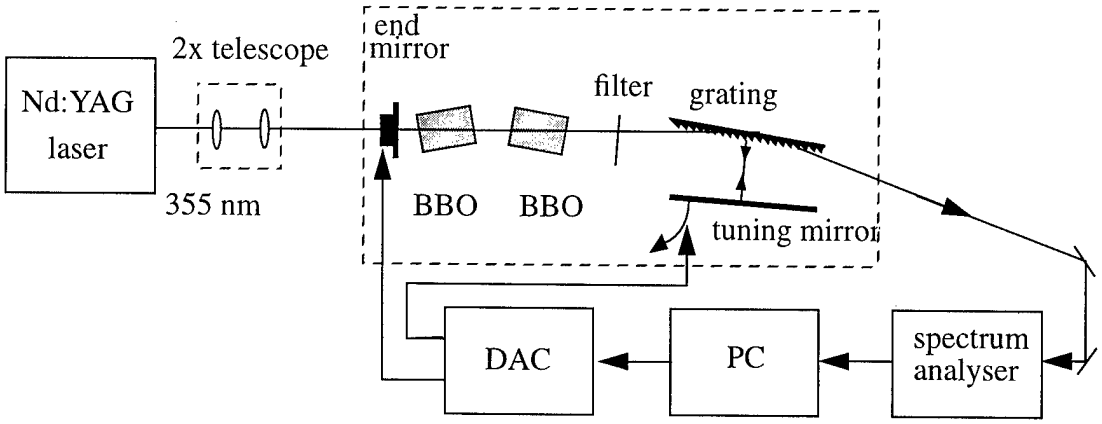

Fig. 1: Experimental setup and stabilization scheme.

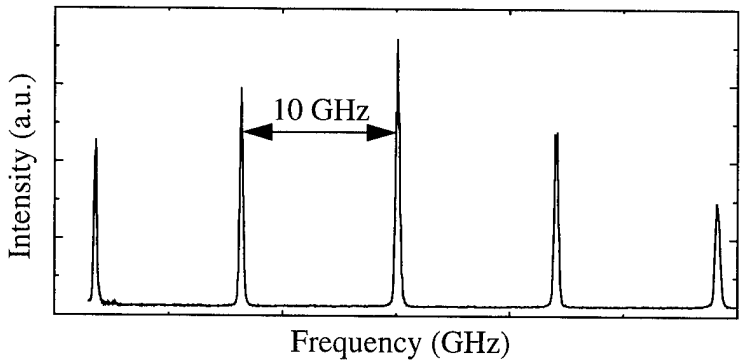

Fig. 2: Etalon spectrum of the output of the OPO.

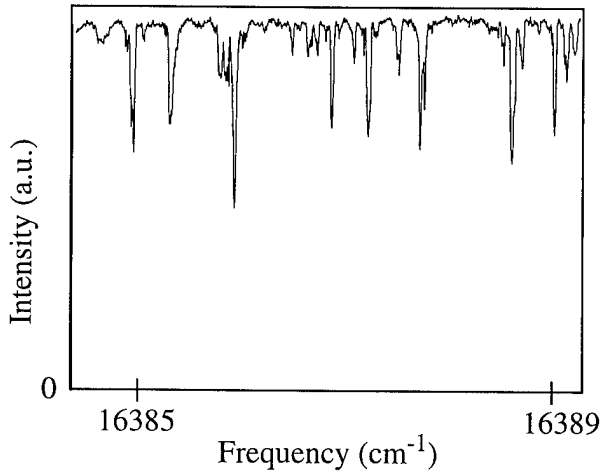

Fig.3: Iodine absorption spectrum as measured with the scanning OPO. The spectrum is normalized on the output intensity of the OPO.

LD-Pumped Nd:YAG Green Laser System

Yoichiro MARUYAMA, Masaki OHBA, Masaaki KATO,
and Takashi ARISAWA

Department of Chemistry and Fuel Research
Japan Atomic Energy Research Institute
Shirakata, Tokai-mura, Naka-gun Ibaraki-ken 319-11, JAPAN
FAX:(29)282-5572

Compact Nd:YAG laser with high beam quality and high average power are very attractive light source for the application of the pumping of tunable lasers such as Ti:Al_2O_3 laser and dye laser, material processing such as drilling and machining, and so on. A zigzag slab Nd:YAG laser is the adequate candidate for generating high quality, high average power laser beam[1,2,3,4], and this will become more reliable and compact with laser diode pumping. The efficient and stable frequency conversion are also important for the application. We constructed a zigzag slab Nd:YAG green laser system and its characteristic was studied.

In Fig. 1, the schematic of the Nd:YAG laser MOPA system is shown, which consists of an oscillator and an amplifier. The oscillator is a LD pumped pulsed zigzag slab Nd:YAG laser with E/O Q-switch. The dimension of the YAG crystal is 3 mm x 3 mm x 75 mm and the concentration of the Nd^{3+} is 1 %. The total reflector of the laser cavity is a 1-m-radius concave mirror and the reflectance of the output coupler is 50 %. The maximum average power of the laser diode is about 150 W at the peak current of 35 A and the pulse duration of 150 μs. The maximum pulse repetition frequency (PRF) of the LD is1 kHz. The pulse duration of the YAG laser is around 30 ns. The maximum average power of the Nd:YAG laser oscillator is 14 W at the maximum rating of the LD. The intensity profile of the oscillator laser beam is near Gaussian. The laser head of the YAG laser amplifier is the same as that used in the oscillator. For the generation of second harmonic, type II KTP crystals of which dimension is 5mm x 5mm x 5mm, are used. For the generation of third and fourth harmonics, BBO crystals are used.

The characteristics of single- and double-pass amplification are

shown in Fig. 2. ● is the average output power for the single-pass configuration at the LD pulse duration of 150 μs and ▲ at the LD pulse duration of 185 μs. ■ shows the average output power for double-pass configuration and the average power of 43 W was obtained. Fig.3 shows the wave front (a), the wave front from which defocus component is removed (b) and the far field pattern (c) of the amplified laser beam. The wave front distortion measured is about 3.5 λ. Most of the distortion is composed of defocus which is mainly due to the effect of concave rear reflector. The wave front distortion from which defocus component is removed is around 0.4 λ. In Fig.4, the average power of second harmonic and the conversion efficiency are shown. The input beam diameter is adjusted by a lens with the focal length of 400 mm to obtain almost the same incident power at the input surfaces of each crystal. The incident power was around 20 MW/cm^2. The output power of second harmonic increased linearly with the length of KTP crystal and the output power of 15.5 W was obtained. The energy conversion efficiency is about 57 %. Using double-pass configuration, the average green power of 19 W was obtained.

Using LD pumped zigzag slab Nd:YAG laser MOPA system operated at the pulse repetition frequency of 1 kHz, the maximum average power of 43 W was obtained at the wavelength of 1064 nm. And average power of the second harmonic were 15.5 W for single-pass and 19 W for double-pass configuration, respectively. The fourth harmonic obtained is 2.3 W for the input power of 13 W of 532 nm.

References

1) J.M.Egglestone,T.J.Kane,J.Unternahrer,R.L.Byer,IEEE,J.Q.E, QE-20,289(1984)

2) M.Hermann, J.Honig, L.Hackel, CTuC5, Conference on Lasers and Electro-Optics 1995, Batimore, Maryland, May21-26 (1995)

3) M.Hermann, L.Hackel, CTuM4 Conference on Lasers and Electro-Optics 1995, Batimore, Maryland, May 21-26 (1995)

4) H.Injeyan, R.J.St.Pierre, J.G.Berg, R.C.Hilyard, M.E.Weber, M.G.Wickham, R.Senn, G.Harpol, C.Florentino, F.Groark, M.Farey, CThC1, Conference on Lasers and Electro-Optics 1994, Anaheim, California, May5-13 (1994)

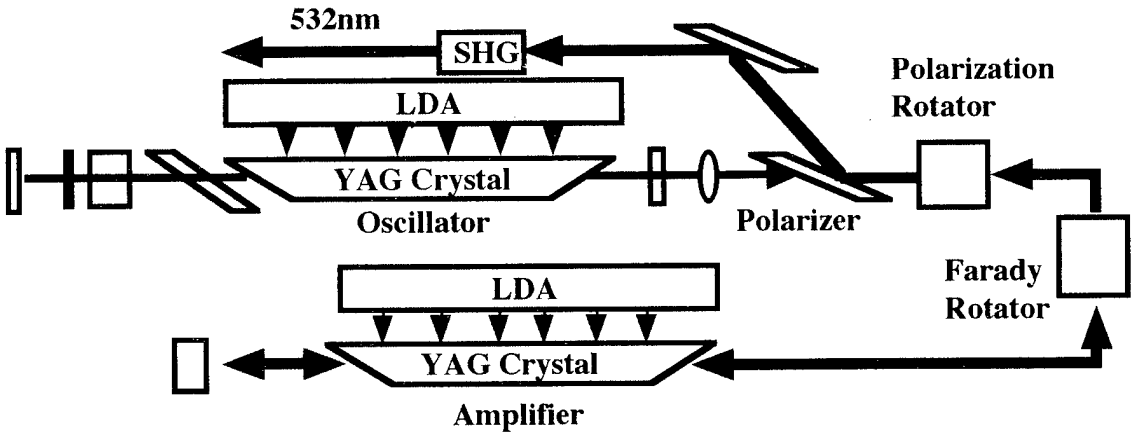

Fig.1 Schematic of LD-pumped Nd:YAG laser MOPA system

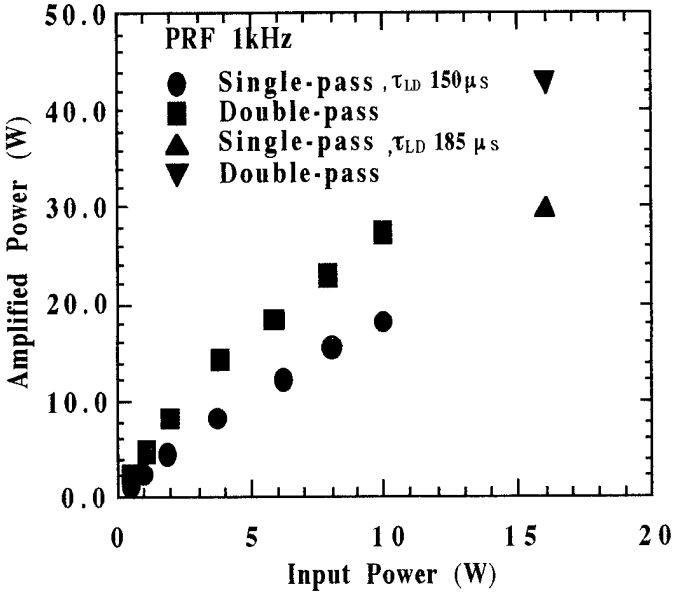

Fig.2 Characteristics of single and double-pass amplification

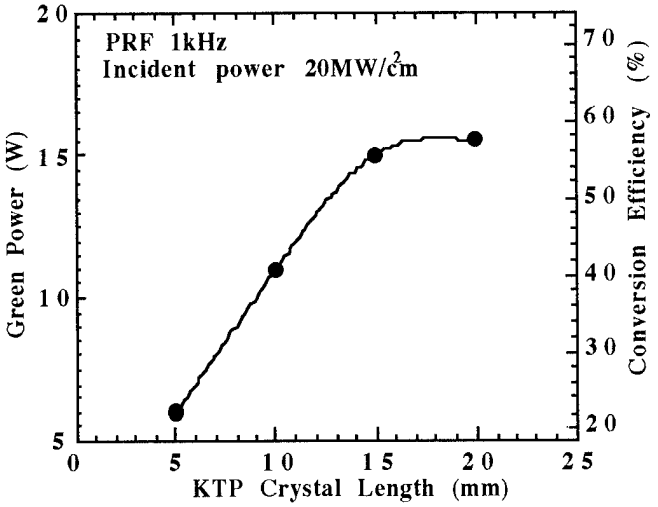

Fig.4 Green power and conversion efficiency as a function of crystal length

(a) Wave front

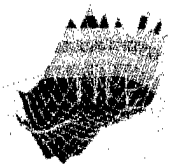

(b) Wave front from which defocus is removed

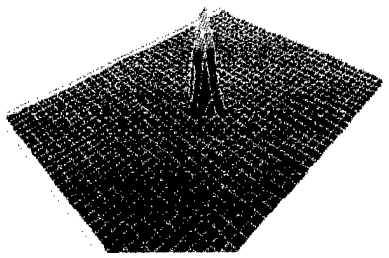

(c) Far field pattern

Fig.3 Wave front and far field pattern

Wednesday, January 31, 1996

Near Infrared Lasers

WG 4:15 pm-6:00 pm
Gold Room

Joseph F. Pinto, *Presider*
U.S. Naval Research Laboratory

1-W continous-wave diode-pumped Cr:LiSAF laser

D. Kopf and U. Keller
Ultrafast Laser Physics Laboratory, Institute of Quantum Electronics, Swiss Federal Institute of Technology, ETH Hönggerberg, HPT, CH-8093 Zürich, Switzerland
Tel: [011] 41 1 633 21 52, Fax: [011] 41 1 633 10 59, e-mail: kopf@iqe.phys.ethz.ch
WWW: http://iqe.ethz.ch/~kopf/ULP.html

R. J. Beach and M. A. Emanuel
Lawrence Livermore National Laboratory, P.O. Box 808, L-250, Livermore, California 94550

We demonstrate a diode-pumped Cr:LiSAF laser with a pure (not quasi) cw output power of 1 W. This is to our knowledge the highest reported average output power from a Cr:LiSAF laser. We show that optimized mode-matching of the pump and lasing mode and efficient cooling can lead to output powers in the 1 W range. Previously, Cr:LiSAF has been thought to be restricted to milliwatt output powers because of the material's thermal limitations due to upper-state lifetime quenching [1], thermal lensing, and non-diffraction-limited focussing conditions of broad area emitting diode-laser arrays.

Cr:LiSAF is an interesting gain medium for a variety of laser applications. Its broad emission bandwidth supports both wavelength tunability and femtosecond pulse generation. Diode-pumping makes it a potentially inexpensive replacement for Ar-ion pumped Ti:Sapphire lasers. In terms of femtosecond pulse generation, we have demonstrated self-starting mode-locking of a diode-pumped Cr:LiSAF laser with pulse widths below 50 fs using an antiresonant Fabry-Perot saturable absorber [2]. More recently, we have also improved the saturable absorber design for wavelength tunability of mode-locking over a range of 30 nm. Moreover, a loss-optimized saturable absorber has been used to achieve mode-locked output powers in excess of 100 mW, showing that saturable absorbers are well suited to generate mode-locking at little expense in output power compared to CW operation.

Motivated by the need for higher output power from the Cr:LiSAF laser, we have recently applied optimized mode-matching of the lasing mode to the asymmetric pump beam and obtained 400 mW [3], limited by the available pump power. Higher power pump diodes are diode-laser bars which have been demonstrated to produce up to 40 W [4, 5] at 690 nm from a 1 cm wide bar. However, to pump Cr:LiSAF with such a bar, we have to combine optimized mode-matching with an efficient cooling mechanism.

The laser setup is shown in Fig.1. We used a high-power diode-laser array emitting at 690 nm from a 1 cm wide facette. This diode bar is mounted on a silicon micro channel cooling plate for efficient heat removal [4, 5]. The diode was operated up to an output power of 12 W. The pump diode beam is imaged into the crystal to a spot with a diameter of 3 mm x 70 μm. The

full-angle divergence is 30° in the tangential direction, corresponding to 1800 times the diffraction limit. In the sagittal plane, the diode beam is nearly diffraction limited (5x after the microlens). The absorption length of the 0.8% Cr-doped LiSAF crystal is about 4 mm such that the absorbed heat is deposited in a volume of approximately 3 mm x 4 mm x 100 µm. The generated heat is then cooled with a mainly one-dimensional heat flow (Fig.2). The crystal is only 1 mm high, allowing for efficient cooling to a copper heat sink.

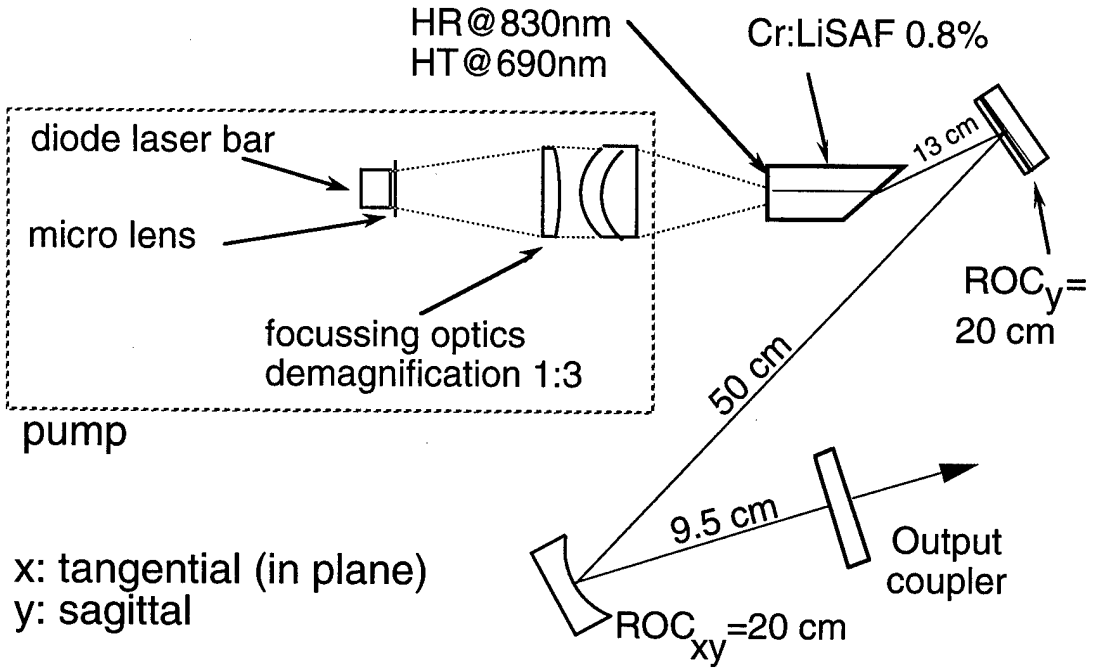

Fig.1: Laser setup

The crystal heat sink temperature is 16°C. Numerical heat flow simulations [6] based on the material parameters given in Ref.[7] showed that a thermal load of 10 W results in a temperature rise of only a few tens of degrees C, for which upperstate lifetime quenching is negligible. In addition, the temperature profile across the Cr:LiSAF cross section was found to be sufficiently small to prevent severe thermal lensing and therefore an unstable cavity mode.

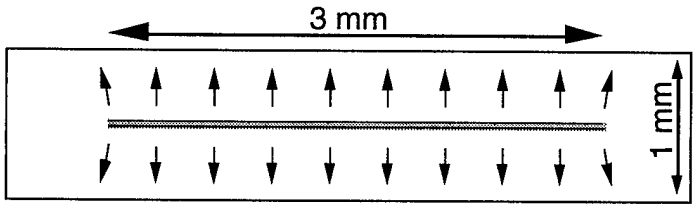

Fig.2: Cross section view of Cr:LiSAF crystal (not to scale) as pumped by the strongly asymmetric diode beam (shaded area). Heat is mostly one-dimensional (arrows).

The laser cavity consists of a flat 1% output coupler, a curved folding mirror and a cylindrical mirror which focusses the lasing mode to a ~2 mm x 130 µm waist in diameter in the Cr:LiSAF

gain medium (Fig.1). Therefore, the lasing mode is matched to the pump beam within a factor of 1.5 in both the tangential and the sagittal plane. The output power as a function of absorbed pump power is shown in Fig. 3 and has a slope efficiency of 17.5%. At a maximum absorbed power of 8.4 W we obtained a CW output power of 1 W without significant saturation as expected from temperature profile calculations.

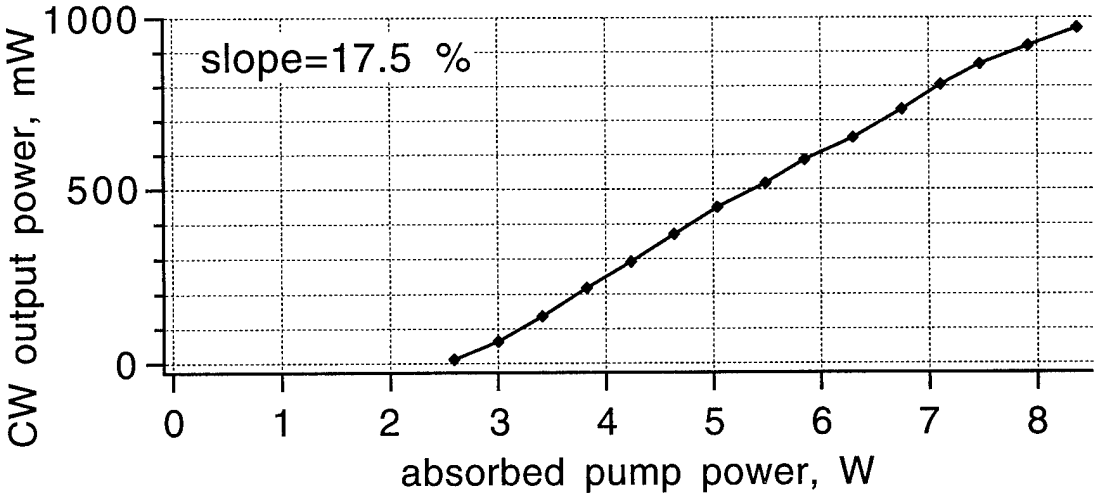

We measured the output beam quality with a moving-slit beam scan at two positions, and determined the beam to be near-diffraction-limited with an M_x^2=2.3 in the tangential plane. In the sagittal plane the beam was diffraction limited. We attribute this less-than-perfect beam quality to the pump beam which tends to have higher intensity at the edges of the diode-laser array and therefore supports higher order modes. We think that further engineering will lead to diffraction limited output.

The authors would like to thank H. Hediger and P. Brühwiler from the ETH workshop for help with the mechanical setup.

References:

1. M. Stalder, M. Bass, B. H. T. Chai, *J. Opt. Soc. Am. B* **9**, 2271 (1992)
2. D. Kopf, K. J. Weingarten, L. R. Brovelli, M. Kamp, U. Keller, Conference on Lasers and Electro-Optics, CLEO 1995, paper CWM2
3. D. Kopf, J. Aus der Au, U. Keller, G. L. Bona, P. Roentgen, *Optics Letters* **20**, 1782 (1995)
4. M. A. Emanuel, R. J. Beach, J. A. Skidmore, D. Hudson, W. J. Benett, B. L. Freitas, N. W. Carlson, Conference of Lasers and Electro-Optics, CLEO 1994, paper CMH2
5. J. A. Skidmore, M. A. Emanuel, R. J. Beach, W. J. Benett, B. L. Freitas, N. W. Carlson, R. W. Solarz, *Applied Physics Letters* **66**, 1163 (1995)
6. J. G. Korvink, J. Funk, H. Baltes, *Sensors and Materials* **6**, 235 (1994)
7. S. A. Payne, L. K. Smith, R. J. Beach, B. H. T. Chai, J. H. Tassano, L. D. DeLoach, W. L. Kway, R. W. Solarz, W. F. Krupke, *Applied Optics* **33**, 5526 (1994)

Efficient, Single-mode, 1.5-mJ, Passively *Q*-Switched Diode Pumped Nd:YAG Laser

Robert S. Afzal
Code 924, NASA-GSFC
Greenbelt, MD 20771
(301) 286-5669 (V) - 1761 (F)
Internet - rob@eib1.gsfc.nasa.gov

and
John J. Zayhowski and T. Y. Fan
MIT Lincoln Laboratory
Lexington, MA 02173
(617) 276-6701 (V) - 6721 (F)

Most field-deployed military and space solid state lasers are *Q*-switched Nd:YAG lasers either flashlamp or diode laser pumped. These lasers are often electro-optically *Q*-switched using nonlinear crystals such as $LiNbO_3$ or KD*P that require kilovolt electrical pulses with rise times of tens of nanoseconds. Now that diode laser pump sources are maturing the next high risk item in these lasers is the *Q* switch. Both the high-voltage switching electronics and the nonlinear crystals themselves have been a common source of failure. In space systems that need to operate in vacuum, the high-voltage switch presents added constraints to avoid failures due to discharge at critical pressures sometimes encountered during system test and operation.

The most common *Q*-switch crystal is lithium niobate. This crystal has the advantages of low insertion loss and low switch voltage($\approx$ 1-3 kV). The device has had problems caused by pyroelectricity, piezoelectricity and low damage threshold. The effect of these properties is manifested during test and operation by compromising the laser performance either by loss of hold-off or catastrophic optical damage to the crystal coatings. Failures of this type lead directly to significant cost increases and schedule risk. Through the years much effort has been placed in studying $LiNbO_3$ to mitigate these problems with various degrees of success. Usually the system test and operation is limited in order to not exceed the limited bounds of operation of the electro-optic crystal. This usually translates into increased system testing cost and limited range of operation.

Our efforts have concentrated on solving these problems by eliminating electro-optic *Q*-switching and high-voltage electronics all together. We have demonstrated a single-mode, passively *Q*-switched, diode pumped Nd:YAG laser using Cr^{4+}:YAG as a saturable absorber[1] in a standing-wave linear cavity. This laser is based on the same design used for breadboard development of the Geoscience Laser Altimeter System (GLAS)[2] transmitter. The passively *Q*-switched laser generated 1.5-mJ, 3.9-ns pulses in a single lowest-order transverse and longitudinal mode at $\approx$ 3% electrical to optical efficiency. The pulse energy and width were stable up to 100-Hz repetition rate which was only limited by the duty cycle of the diode. Previous work on passively *Q*-switching Nd:YAG lasers with Cr^{4+}:YAG[3] or F_2^-:LiF[4] did not demonstrate the pulsewidth or efficiency needed for GLAS.

A schematic of the laser is shown in Figure 1. The laser consists of a Nd:YAG zig-zag slab, a single close-coupled 100-W quasi-cw diode pump array and a 5-cm long resonator formed by a R=60% flat output coupler and a 2.5-m radius-of-curvature high reflector. The Cr^{4+}:YAG samples were polished flat, antireflection coated, mounted and placed in the resonator on either side of the active medium. The samples had typical absorption coefficients of 1.5 cm^{-1} at 1064 nm; the unsaturated loss was varied by choosing different lengths of material. In long-pulse operation (without saturable absorbers in the cavity) many higher order transverse modes oscillated. While *Q*-

switching, however, the presence of the saturable absorber ensured lowest-order single transverse-mode operation by acting as a spatial filter with a soft aperture. The laser threshold was measured using combinations of the three saturable absorbers of differing loss to determine the single-pass gain (Figure 2). Figure 3 shows the laser pulse energy and pump duration as a function of unsaturated loss in the resonator.

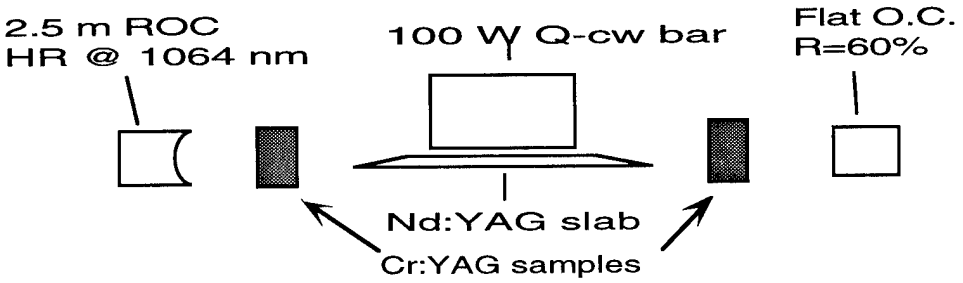

Figure 1 - Schematic of the laser

Cr^{4+}:YAG was chosen as the passive material because of several factors. For long life (billion shot life times) in a field environment Cr^{4+}:YAG has the promise of minimal photobleaching and is fairly insensitive to thermal variation, implying that the laser could be temperature cycled without affecting performance. Figure 4 shows the absorption of Cr^{4+}:YAG for several different temperatures. Cr^{4+}:YAG can also be coated with high quality high optical damage threshold anti-reflection coatings.

This laser's performance compares favorably to the same laser electro-optically switched that generated 2.3-mJ, 4.3-ns pulses in single transverse but multi-longitudinal modes[5]. For a lidar and altimetry transmitter the significantly improved pulse-width stability (improved from 20% to <5% variation) and single-frequency operation holds many advantages over the EO-switched device. The 1.5-mJ pulse energy is sufficient to efficiently seed traditional single and multipass amplifier chains to achieve greater pulse energies. Single mode operation provides very stable (<5% variation in width and peak, instrument limited) pulse waveforms for accurate timing as well as wavelength control to match narrow band filters[6] in lidar receivers.

This work was funded by the NASA Code X Laser Sensing RTOP.

References:

1) D. Andrauskas, and C. Kennedy, *OSA Proceeding on Advanced Solid State Lasers*, Hilton Head, SC, Mar 18-20, 1991, Vol. 10, p.393

2) J.B. Abshire, J.C. Smith and B.E. Schutz, *Proceedings 17th International Laser Radar Conference*, July 25 - 29, 1994, Sendai, Japan, paper 26D5, p. 215

3) I. J. Miller, A. J. Alcock, and J.E. Bernard, *OSA Proceeding on Advanced Solid State Lasers,* L. Chase and A. Pinto, eds. (Optical Society of America, Washington DC, 1992), Vol. 13, p. 322

4) Y. Isyanova, and D. Welford, *OSA Proceeding on Advanced Solid State Lasers,* A. Pinto and T.Y. Fan, eds. (Optical Society of America, Washington DC, 1992), Vol. 13, p. 322

5) R. S. Afzal, M. D. Selker, *Opt. Lett.,* Vol. 20, No. 5, p.46, March 1, 1995

6) M. Krainak, K. Sayano, "Narrow-band Volume Holographic 532 nm Optical Filter," paper submitted to this meeting.

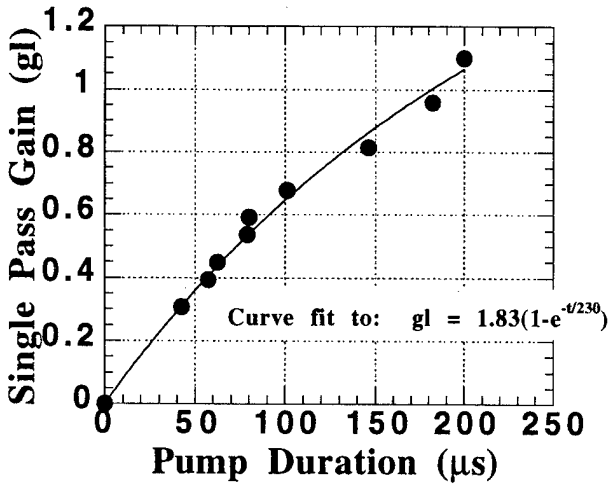

Figure 2 - Single pass gain of the laser as a function of pump duration. This data was obtained by determining the laser threshold for different amounts of unsaturated single pass loss.

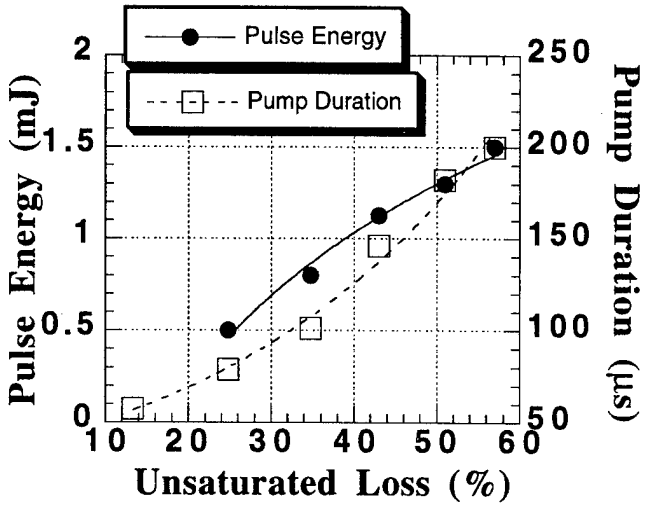

Figure 3 - Laser output pulse energy as a function of intracavity single pass unsaturated loss. Also plotted is the pump duration for when the laser reached threshold. The diode pump was at 100 W and R=60% for the output coupler.

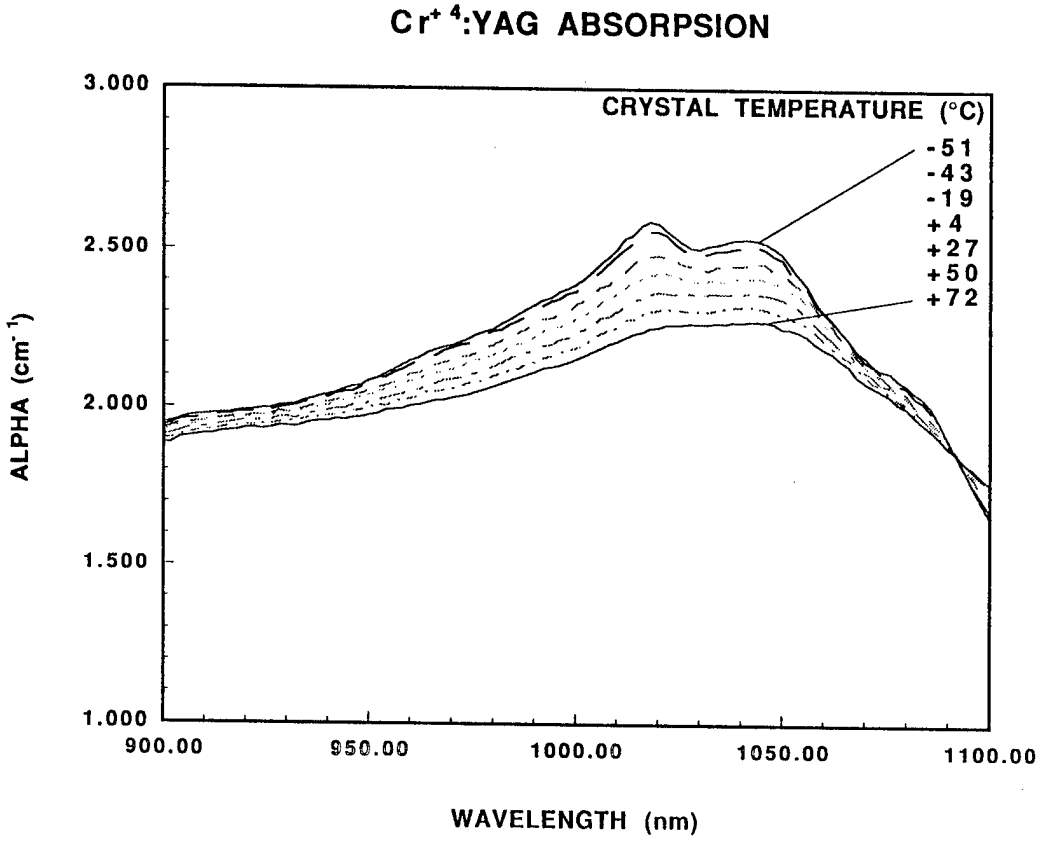

Figure 4 - Single pass unsaturated absorption spectra of Cr^{4+}:YAG taken at seven different crystal temperatures.

Cw-diode-pumped Nd:$GdVO_4$-laser passively Q-switched with Cr^{4+}:YAG as saturable absorber.

I.V. Klimov, V.B. Tsvetkov, I.A. Shcherbakov
General Physics Institute, Russian Academy of Sciences
Tel.: 7-095-132-83-90, FAX: 7-095-135-02-70
Vavilov str., 38, 117333 Moscow, Russia

J. Bartschke, K.-J. Boller, and R. Wallenstein
Fachbereich Physik, Universität Kaiserslautern
Tel.: 49-63-205-2327, FAX: 49-631-205-3906
67653 Kaiserslautern, Germany

Because of their unique absorption and emission properties, several Cr^{4+}-doped crystals have been used as passive Q-switch or as laser active material for the generation of tunable radiation in the 1.5 μm-range [1].
In most of the Q-switched systems the laser crystal was an optically isotropic Nd-doped garnet. In these systems the output pulse parameters are determined primarily by the initial transmittance of the Cr^{4+}-crystal. In lasers based on anisotropic crystals the polarisation dependence of the saturation intensity in the Cr^{4+}-doped Q-switch material becomes important. The angle dependence of the absorber transmittance (without taking ESA or any other unsaturable processes into account) can be estimated from the following equation [2, 3]:

$$T = (\cos\theta)^2 \, e^{\frac{-\alpha l}{1 + \frac{Q(\cos\theta)^2}{Q_s}}} + (\sin\theta)^2 \, e^{\frac{-\alpha l}{1 + \frac{Q(\sin\theta)^2}{Q_s}}}$$

where α is the unsaturated absorption coefficient, l is the absorber length, θ is the angle between one of the crystal axes and the polarization of the laser beam, Q is the energy density of the laser beam (J/cm^2) and Q_s the saturation energy density (J/cm^2).
The dependence of T on θ is thought to be caused by a preferred orientation of the absorbing dipoles along the crystal axes. As a result, the saturation intensities for the polarization parallel or nonparallel to one of the axes are different, with a maximum difference equal to a factor of 2 for a rotation by 45°. Rotation of the resonator internal Cr^{4+} crystal, should thus change the output parameters of linearly polarized lasers like Nd:$GdVO_4$, or Nd:YAG (operated with an intracavity polarizer).
In this paper, we demonstrate the influence of the polarization dependent saturation intensity of a Cr^{4+}:YAG passive Q-switch on the output parameters of a Nd:$GdVO_4$-laser pumped by a cw laser diode. In the experiments a 0.4mm long AR-coated Cr^{4+}:YAG-crystal ([100]-cut, initial transmittance T_0=0.91) was inserted into the 24mm long linear resonator of a Nd:$GdVO_4$-laser. The laser was pumped by a 1W laser diode (SDL-2462). One facet of the 2mm long Nd:$GdVO_4$ crystal was high reflective for 1.06 μm and served as rear mirror of the cavity.. The other facet was AR-coated. The output

coupler (R=0.93) was a spherical mirror with a radius of curvature of r=200mm. The Cr^{4+}:YAG could be rotated by 360°. The dependence of the pulse duration, the pulse energy and the output repetition rate on the rotation angle of the Q-switch are shown in the figures 1 and 2. As seen from these figures there is a strong dependence of the output parameters on the Q-switch angle. For instance, the pulse duration changes from ~170ns to ~30ns for a Q-switch rotation by 45°. Simoultanously the pulse repetition rate varies from 40kHz to 300kHz.

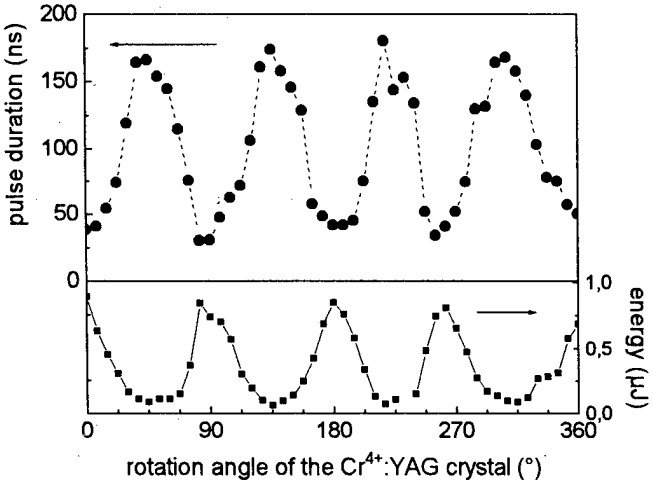

Fig. 1: Pulse duration and energy versus angle position of the Q-switch.

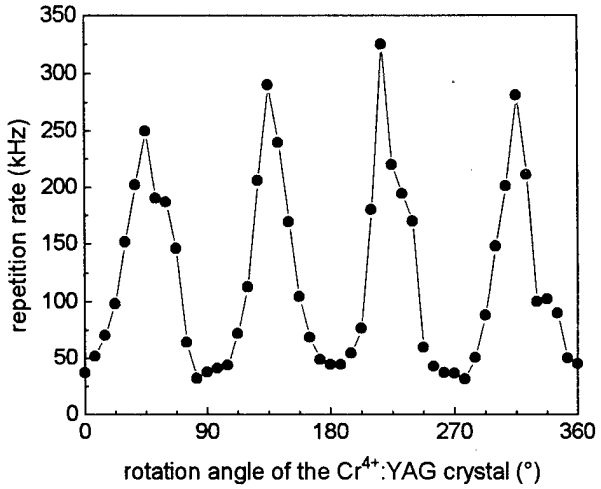

Fig. 2: Repetition rate versus angle position of the Q-switch.

In the experiments we noted that the angle position for shortest pulse duration, maximum pulse energy and highest average power is also the position for a most stable pulse amplitude and repetition rate. In comparision to the average output power, the pulse power, defined as $P=E_{pulse}/t_{pulse}$, depends even stronger on the crystal orientation. The maximum and minimum values of the pulse power are different by almost two orders of magnitude.

The experimental results, shown in the figures 1 and 2 were the base for the determination of the optimum angle position of a Cr^{4+}:YAG crystal in a short cavity Nd:$GdVO_4$-laser (cavity length 2.6mm, OC 7%). The output of this laser was a continuous train of pulses, with a duration of ~2.6ns (FWHM). The average power was 75 mW, the repetition rate 32.5 kHz when pumped with ~800mW (absorbed power).

It should be noted that a Nd:$GdVO_4$ laser with a Cr^{4+}:GSGG-Q-switch (length 2mm, AR-coated, [100]-cut, initial transmittance ~0.6) generated output pulses with similar duration (~2.2ns) and energy (~2µJ), but the output power (~22 mW) was three times lower and the repetition rate ~10kHz. Due to the small initial transmittance of Cr^{4+}:GSGG, laser oscillation was restricted to an angle position of the Q-switch crystal where one crystallographic axis was parallel to the polarization of the laser light.

These results clearly indicate that the angle position of the Cr^{4+}-crystal is a crucial parameter for passively Q-switched lasers based on anisotropic crystals like Nd:$GdVO_4$. The results obtained can be understood from the "two threshold" nature of passive Q-switching [4]. The time interval between the beginning of the pumping process and

the start of the laser pulse (which is the time to accumulate the population inversion), consists of two parts: first, the time until the gain exceeds the unsaturated losses; second, the time necessary for the intracavity intensity to reach a level which starts to saturate the absorption. In isotropic (non polarization dependent) saturable absorbers the second time is fixed. The laser paramenters thus depend on the initial transmittance and, consequently, on the first time interval. For polarization dependent absorbers (like Cr^{4+}-crystals) rotation of the crystal changes it's saturation intensity and, thus, varies the second time interval. Because of the low slope of the initial intracavity intensity, even a small change of the absorber saturation intensity can dramatically change the pre-lasing time interval.
Rotation of the Cr^{4+}-Q-switch thus allows the operation of a passively Q-switched laser system with output parameters which can be varied over a wide range. It is very likely that similar results can be obtained for other lasers of anisotropic crystals, like LiCAF, LiSAF etc., which can be passively Q-switched with Cr^{4+}-doped saturable absorbers.

References:

1. A. Sennaroglu, C.R. Pollock, and H. Nathel, "Efficient continuous-wave chromium-doped YAG laser", J. Opt. Soc. Am. B, Vol. 12, No. 5, p.930, 1995
2. H.Eilers, K.R.Hoffman, W.M.Dennis, S.M. Jacobson, and W.M.Yen "Saturation of 1.064 μm absorption in Cr, Ca:$Y_3Al_5O_{12}$ crystals", Appl. Phys. Lett. 61, p. 2958, 1992
3. Bufetova G.A., Klimov I.V., Nikolaev D.A., Tsvetkov V.B., and I.A. Shcherbakov , to be published.
4. A.E. Siegman "Lasers", University Science Books, California, 1986, p. 1026

Laser performance of a new ytterbium doped phosphate laser glass

U. Griebner, R. Koch, H. Schönnagel
Max-Born-Institut für Nichtlineare Optik und Kurzzeitspektroskopie
Rudower Chaussee 6, D-12489 Berlin, Germany
Phone: (+30) 6392 1452, Fax: (+30) 6392 1459, e-mail: griebner@mbi.fta-berlin.de

S. Jiang, M.J. Myers, D. Rhonehouse, S.J. Hamlin
Kigre Inc.
100 Marshland Road, Hilton Head Island, SC 29926
Phone: 803-681-5800, Fax: 803-681-4559

W.A. Clarkson, D.C. Hanna
Optoelectronics Research Centre
University of Southampton, Southampton, SO17 1BJ, U.K.

Ytterbium based lasers have attracted much attention due to their low heat generation, simple electronic structure (absence of unwanted processes such as excited state absorption and concentration quenching) and broad absorption and emission bandwidths.
The inherently small quantum defect in Yb^{3+} lasers is a motivating interest for operation at higher power levels. Efficient laser action has been demonstrated in Yb:YAG [1] and several other Yb-doped crystals [2]. There is also much interest in Yb^{3+} in glass host materials. Yb-doped silica fiber lasers have been investigated in detail [3]. Laser properties of ytterbium in fluoride phosphate glasses are described in [4].
In this paper, we present laser performance of a new ytterbium doped phosphate glass composition designated QX/Yb. QX laser glasses have demonstrated significant enhancement in thermal loading capabilities over conventional phosphate based laser glasses. Average output powers of greater than 110 watts have been produced from QX/Nd at 1054 nm, and 7 watts from QX/Er at 1540 nm in lamp pumped configurations. More recent data has proven that over 15 watts may be extracted from lamp pumped QX/Er at 1540 nm [5,6].
The QX/Yb:phosphate glass was doped with 5 wt% Yb_2O_3 and exhibits a fluorescence lifetime of approximately 2 ms. The absorption and emission spectra are shown in Fig.1. The Yb:phosphate glass spectra are much smoother compared to Yb:YAG.

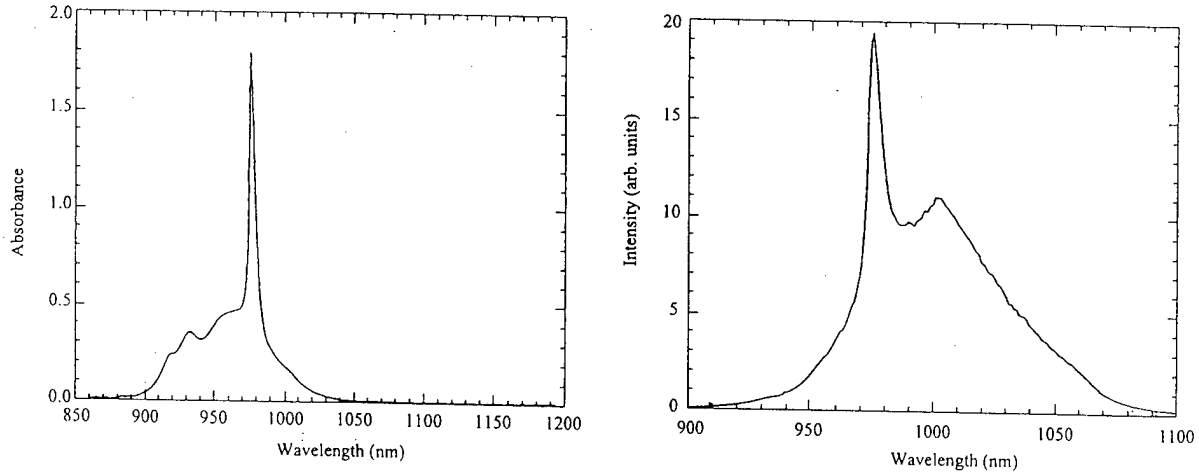

Fig.1: Absorption (left) and emission spectra of QX/Yb:phosphate glass

The laser experiments were performed by using a diode pumped Nd:YAG laser operating at 946 nm. This laser was end-pumped by a 20 W diode bar using the beam-shaping technique described in [7]. With a non-optimized cavity design this laser produced a stable output of 2.6 W with good beam quality ($M^2 \sim 2$). The output of this laser was focused into a 4 mm thick Yb-doped glass sample by a lens with a focal length of 40 mm resulting in a $1/e^2$ spot radius of about 40 μm. Due to the losses of the non-optimized components in the pumping scheme only about 1.5 W of pump power were obtained at the sample.
To investigate the lasing characteristics of the Yb:phosphate glass, we choose a nearly hemispherical laser cavity with a radius of the outcoupling mirror of 50 mm. The mirrors were HR-coated (R_1 = 99.9% and R_2 = 97%) for the lasing wavelengths. 49% of the available pump power were absorbed in a double-pass by the active material.
The cw-lasing characteristics of the Yb:phosphate glass laser are shown in Fig.2. A slope efficiency of 43% with respect to the absorbed pump power and a maximum output power of 250 mW have been obtained. It is important to note that these results have been achieved at room temperature without any cooling of the active material.

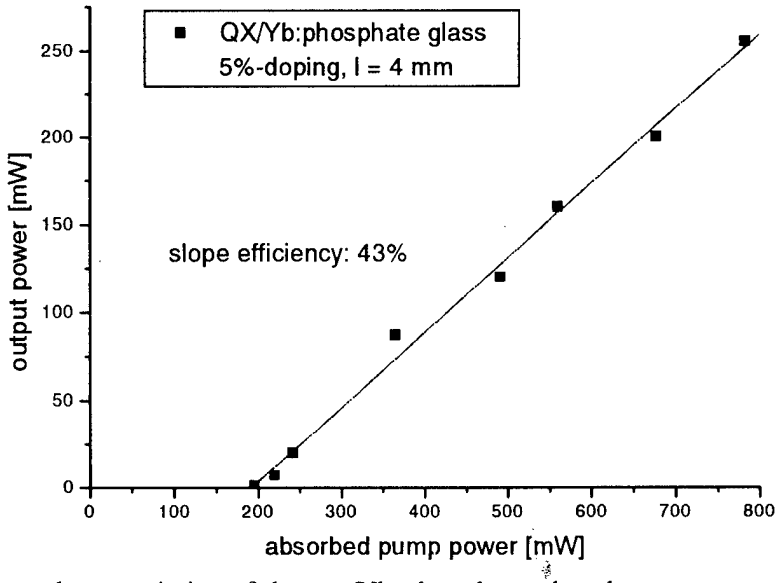

Fig.2: Input-output characteristics of the cw-Yb:phosphate glass laser

Laser operation has been demonstrated in the range from 1025 nm - 1060 nm with spectral widths of 1.0 to 3.0 nm (FWHM). This behaviour can not be explained by temperature and etalon effects only. The observed dependence on the resonator length delivered a clue for an effect influencing the spectral characteristics. In a slightly different experimental situation we have measured the pump light distribution perpendicular to the resonator axis at the location of the waist in a configuration with a $1/e^2$ spot radius of about 80 μm and calculated the corresponding gain distribution for two specific wavelengths - 1030 nm and 1050 nm -, depicted in Fig.3. The required pump power density to reach the laser threshold is about 4.5 kW/cm^2 due to the thermal population of the lower laser level. In areas of lower pump power density reabsorption takes place in dependence on the wavelength. In this way, the reabsorption acts as a spectral selective aperture. This behaviour is demonstrated by the wavelength dependent waist diameter $2w_0$ of the laser mode. The small-signal gain coefficient exceeds 0 if $2w_0$ = 160 μm for λ = 1030 nm and $2w_0$ = 180 μm for λ = 1050 nm, respectively (Fig.3). As a result, the lasing wavelength can be tuned by changing the mode volume of the laser. Fig.4 illustrates this effect. Emission in the range between 1036 nm and 1055 nm has been achieved only by varying the resonator length. The preliminary explanation is consistent with these observations.

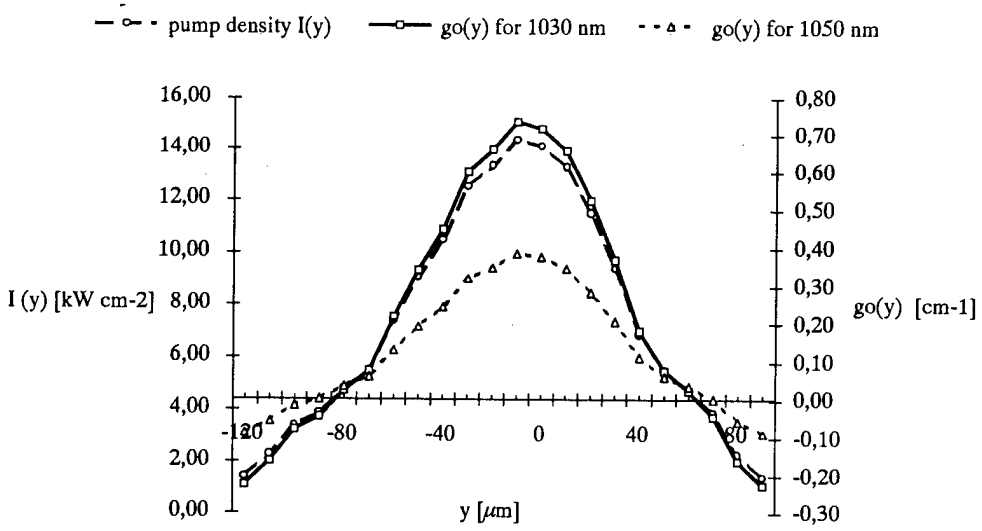

Fig.3: Measured pump power density I(y) and calculated gain distribution $g_0(y)$ for two wavelengths across the beam waist y

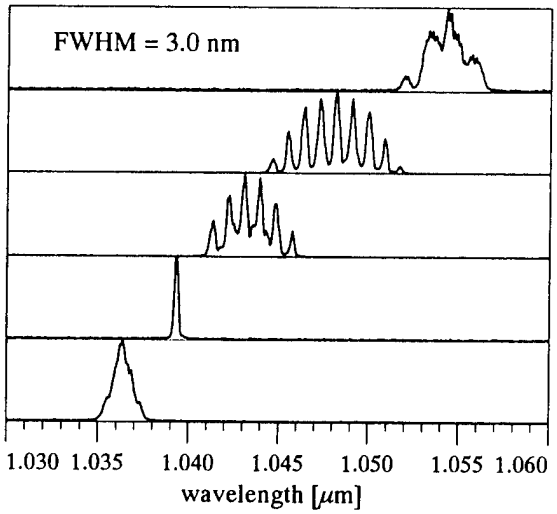

Fig.4: Emission spectra of the Yb:phosphate glass laser in dependence on the mode volume (increasing resonator length from the bottom to the top)

First results of diode-pumping the Yb-doped phosphate glass and investigations with higher Yb-dopand concentrations will be reported. This glass is a prospective candidate for lasers in the range of several watts with the potential of broad tunability.

References:

[1] T.Y. Fan, S. Klunk, F. Henein, Opt. Lett. **18**, 423 (1993)
[2] L.D. Deloach, S.A. Payne, L.L. Chase, L.K. Smith, W.F. Krupke, IEEE J. Quantum Electron. **29**, 1179 (1994)
[3] H.M. Pask, R.J. Carman, D.C. Hanna, A.C. Tropper, C.J. Mackechnie, P.R. Barber, J.M. Dawes, IEEE J. Selected Topics in Quantum Electron. **1**, 2 (1995)
[4] E. Mix, E. Heumann, G. Huber, D. Ehrt, W. Seeber, Adv. Solid-State Lasers, Memphis TN, Tech. Dig., paper WB5-1, p.230 (1995)
[5] S. Jiang, J.D. Myers, R. Wu, G.M. Bishop, M.J. Myers, S.J. Hamlin, SPIE **2379**, 17 (1995)
[6] S. Jiang, J.D. Myers, D.L. Rhonehouse, G.M. Bishop, M.J. Myers, S.J. Hamlin, Conference on Lasers and Electro-Optics, Tech. Dig. Series 1995, **15**, p.232 (1995)
[7] W.A. Clarkson, R. Koch, K.I. Martin, D.C. Hanna, Conference on Lasers and Electro-Optics, Tech. Dig. Series 1995, **15**, p.17 (1995)

Diode Pumped Continuous-Wave Yb Laser in Fluoride Phosphate Glasses

T. Danger, E. Mix, E. Heumann, and G. Huber
Institut für Laser-Physik, Universität Hamburg, Jungiusstr. 9a, D-20355 Hamburg, Germany,
Tel.: ++49-40-4123-5243, Fax: ++49-40-4123-6281

D. Ehrt and W. Seeber
Otto-Schott-Institut, Universität Jena, Fraunhoferstr. 6, D-07743 Jena, Germany,
Tel.: ++49-3641-636168, Fax: ++49-3641-636172

Yb^{3+}-doped materials exhibit a very small quantum defect, so in laser experiments losses by nonradiative relaxation processes are quite low [1]. The high potential of Yb^{3+} systems was recently demonstrated by diode pumped high power tunable laser action of Yb:YAG [2]. First experiments with Ti:sapphire laser pumping have shown that Yb-doped fluoride phosphate glasses, whose structure and compounds were described in Ref. 3, are also promising laser materials [4]. In this work the laser characteristics of these glasses and the influence of slight changes of the compounds were investigated under diode pumping. The glasses were produced in Jena, while the laser experiments were performed in Hamburg.

For the cw laser experiments, which were carried out at room temperature, a hemispheric resonator with an output mirror of r = -5 cm radius of curvature was used. The collimated beams of two laser diodes operating around 968 nm were alligned with a polarizing beam splitter and focused into the investigated glass with a lens of 3 cm focal length. The glass was mounted on a water cooled copper block. Using small transmission values ($T \leq 2$ %) of the output mirror, laser action was observed for several glasses between 1.055 μm and 1.06 μm.

In Fig. 1 the laser characteristics of two Yb-doped fluoride phosphate glasses with an Yb concentration of $5 \cdot 10^{20} cm^{-3}$ and a length of d = 4 mm are compared. The maximum output power was about 150 mW for the S2 (with a content of 2 mole-% strontium phosphate) and 140 mW for the S4 (4 mole-% strontium phosphate) glass. The corresponding absorbed pump power, which was calculated from the incident pump power using the absorption coefficient and thickness of the investigated glass, was 530 mW (47 % of the incident pump power) in both cases. Slope efficiencies up to 64 % were achieved, taking into account only the upper parts of the curves. The absorbed pump powers at threshold were 118 mW (S2) and 186 mW (S4) for T = 1 %.

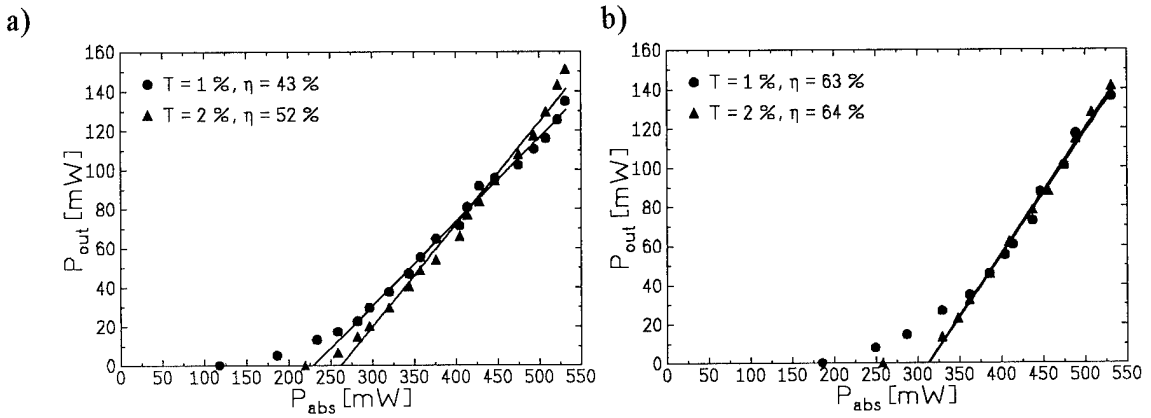

Figure 1: Input output curves of diode pumped fluoride phosphate glasses, a) S2 and b) S4

Performance of a Q-switched Yb:$Sr_5(PO_4)_3F$ laser*

Camille Bibeau, Raymond J. Beach, and Stephen A. Payne
University of California
Lawrence Livermore National Laboratory
P.O. Box 808 L-493
Livermore, CA 94550
(510) 422-7798

Yb-doped apatites have spectroscopic and laser properties that make them useful as laser materials. In particular, recent experimental work with Yb:S-FAP has shown this material to be a promising candidate for high energy laser systems due to its long storage lifetimes[1]. Furthermore, the strong pump and emission lines at 900 and 1047 nm make this material highly suitable for diode pumping thereby increasing the overall efficiency of the system.

In this work, we will describe the Q-switched operation of a Yb:S-FAP laser with diode pumping and "lens duct" irradiance conditioning in an end-pumped cavity geometry (Fig.1). The 900 nm pump source consisted of a 22 bar array of microchannel cooled 1.5 cm long InGaAs diodes. The radiation from each diode bar was optically conditioned to reduce the output divergence angle (fast axis) with a cylindrical microlens from 60 degrees to 0.6 deg. The pump light was focused or concentrated down to a 2.9 x 2.9 mm area with a fused silica lens duct to allow for end-pumping of the laser rod. The rectangular laser rod (3x3x25mm) was coated with a multilayer $\lambda/4$ stack of silicon dioxide and hafnium dioxide for high reflectance at 1047 nm and high transmission at 900 nm coating at the pump end of the rod, thus allowing one end of the rod to perform as a high reflector for the laser cavity. A conjugate coating was placed at the output end of the rod. A pump beam with a pulse length of 500 μs and an energy of 400 mJ produced an output energy of 34 mJ with an approximate pulse length of 40 ns at the FWHM. (Fig. 2) The measured pulse length is similar to the predicted pulse length of 13 ns from a straightforward calculation of the cavity dynamics of a single mode laser system. We might expect that the highly multimode nature of the laser beam will contribute to the lengthening of the Q-switched pulse. A polarizer and electro-optic Q-switch provided the modulated cavity loss. A mirror with a 50% reflective coating and a 4 m radius of curvature was used as the output coupler. An intensity profile of the beam showed a peak to valley modulation of 1.6:1 (Fig. 3) which we predict could be improved upon with an unstable resonator configuration.

A plot of the free running laser energy as a function of the diode current is shown in Fig. 4. The overlaid Q-switched data is also shown for different surface conditions of the laser rod. The highest output energy of 34 mJ was achieved when two whole sides of the rod orthogonal to c-axis were ground and two sides of the rod parallel to c-axis were partially ground. The grinding is necessary due to the anisotropic gain of Yb:S-FAP. This aspect coupled with the rectangular geometry of the laser rod allows for the undesirable amplification of parasitic modes to develop in the plane orthogonal to the lasing axis (c-axis). An obvious solution to this problem usually involves only grinding the sides of the rod which are orthogonal to the c-axis. However, we have found that partial grinding of the surfaces parallel to the c-axis is helpful. Although a small fraction of the pump light was lost through scattering we found that the parasitic threshold could be increased from 8 mJ to 34 mJ (~4x). After the surfaces were ground, we found that the limiting factor for higher output energies was no longer due to parasitic population clamping but could be attributed to laser induced damage of the dichroic coatings.

In addition to the measurements of the Q-switched laser energetics, we have developed a computer model of the laser in order to estimate the performance and improve the efficiency of our design. Included in the model is a computer code that tracks the intensity of the diode light as it propagates through the lens duct. The code is capable of calculating the optical efficiency and the pump irradiance profile at the output and at several planes beyond the lens duct. A computer simulation of the

fast axis intensity profile of the pump beam at the output of the lens duct is shown in Fig 5. The experimental profile is shown in Fig. 6. The dip in the middle of the profile is accurately modeled by our code. We also measured the beam profile at several planes beyond the exit surface. The camera profiles showed a divergence of the beam along the slow axis but virtually none along the fast or microlens conditioned axis. Employing the etendue invariance principle we can estimate the divergence of the diode array light from the beam profile data and compare the results with the code predictions. We find that experimentally, the beam divergence is 180 mrad at the exit of the lens duct along the slow axis. This compares well with the numerical result of 190 mrad assuming that the slow axis divergence of the diode array is 35 mrad (full angle). We can also estimate the optical efficiency of the lens duct based on the geometry of the diode stack array and the lens duct. The code predicts an optical efficiency of the 92% whereas experimentally we find the efficiency to be 70%. We believe wide angle scattering in the fast axis can account for the difference. We will present the details of our computer code along with the experimental data and comparisons.

Acknowledgments

We would like to thank C. Marshall for his valuable help and advice and the use of his experimental facility and laser system for making these measurements. We would also like to thank G. Graham and L. Smith for their help with the experiments and C. Petty for his assistance with the diode cooling system. In addition, we would like to acknowledge M. Emanuel and the diode group for their support and advice.

References

(1) C. D. Marshall, L. K. Smith, R. J. Beach, M. A. Emanuel, K. I. Schaffers, S. A. Payne, "Diode-pumped Ytterbium-doped $Sr_5(PO_4)_3F$ Laser Performance," submitted to IEEE J. Quant. Elect.

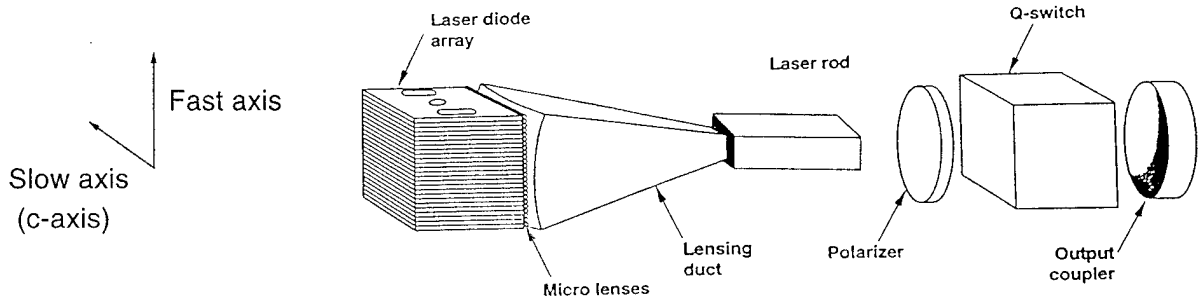

Fig.1 A schematic of the laser. With a 50%, 4m output coupler we produced 34 mJ in a 40 ns pulse.

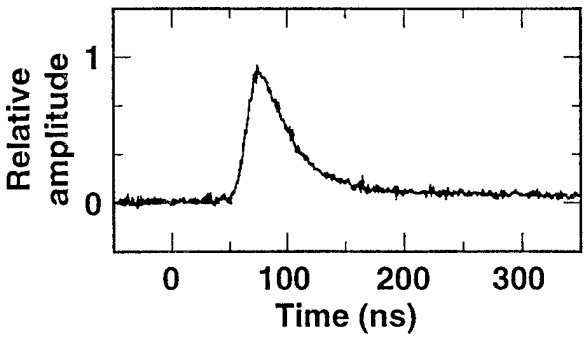

Fig. 2 . Q-switched temporal profile for Yb:S-FAP. Pulse width at FWHM is 40 ns.

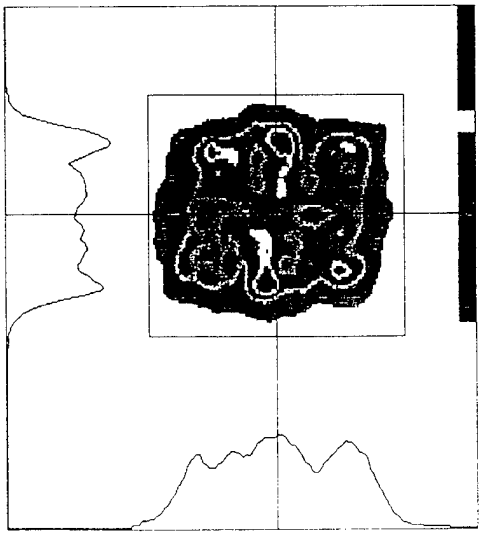

Fig. 3 Spatial beam profile. Peak to valley modulation is 1.6:1 for 34 mJ output.

Yb–absorption results in a strong green fluorescence indicating an effective population of the $^4S_{3/2}$–level of Er by the Yb–Er energy transfer. In addition, the broad and strong absorption of Yb makes diode pumping possible.

In the experimental set–up a 4 mm long Yb(5%),Er(1%):YLF crystal was placed in a nearly concentric cavity formed by two R = -50 mm mirrors. The input mirror was high reflecting at the laser wavelength (1.234 μm) and high transmitting around the pump wavelength between 920 and 980 nm. The transmission of the output coupler was 1% at 1.234 μm.

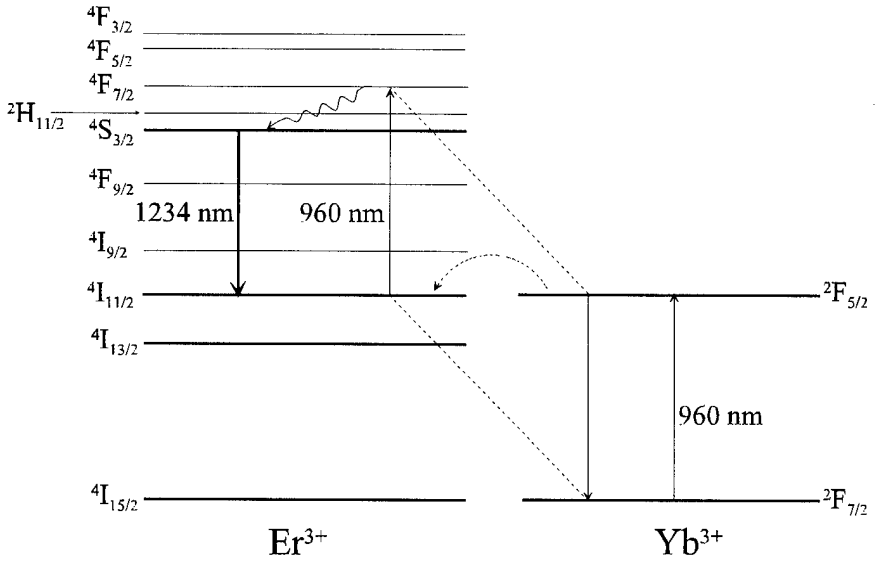

Fig. 1. *Schematic diagram of the pump mechanism used to populate the upper laser level.*

At first, a Ti:sapphire laser was used as a pump source tuned to the maximum of the Yb–absorption at 960 nm and focused with a 50 mm focal length lens into the crystal. The excitation scheme is shown in Fig. 1. In a first step Yb is efficient excited by absorption of the pump radiation. In the second step Yb–ions transfer their excitation energy to Er–ions: Yb($^2F_{5/2} \rightarrow {}^2F_{7/2}$), Er($^4I_{15/2} \rightarrow {}^4I_{11/2}$). As a third step the upconversion process Yb($^2F_{5/2} \rightarrow {}^2F_{7/2}$), Er($^4I_{11/2} \rightarrow {}^4F_{7/2}$) takes place and populates effectively the upper laser level $^4S_{3/2}$ of Er. The upconversion depletes simultaniously the lower laser level $^4I_{11/2}$ which is a prerequisite for cw lasing.

Fig. 2 shows the performance of the cw Yb,Er:YLF–laser at 1.234 μm using a Ti: sapphire laser as pump source. The maximum output was 160 mW at 1.1 W of absorbed power. The slope efficiency was about 14.3%.

For diode pumping experiments, two 1 W laser diodes at 968 nm coupled via a polarizing beam splitter were used for excitation. The pump radiation was focused into the 4 mm long Yb,Er:YLF sample by a 30 mm focal length lens. The crystal was placed in a hemisperical cavity close to the high reflecting plane mirror. The output coupler with R = -50 mm had a transmission of 1% at 1.234 μm. Cw lasing was obtained easily but the output of 16 mW at 1.4 W incident power was low compared with the excitation

of the Ti:sapphire laser. Because of the broad spatial area of the laser diode beam the average excitation density inside the crystal was about four times smaller than in the case of Ti:sapphire laser pumping. Furthermore, the wavelength of the laser diodes could not be tuned to the maximum of the Yb–absorption and one of the diode beams was polarized in σ–direction where the absorption coefficient is significantly smaller compared with the π–direction.

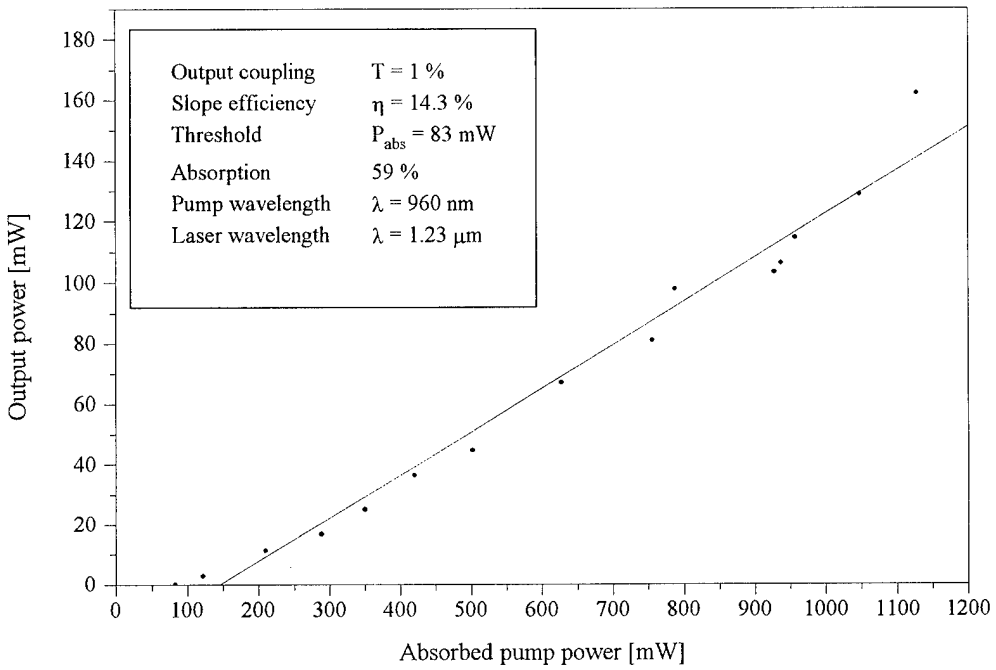

Fig. 2. *Input–output curve at* 1.234 μm *for an output coupling of* 1% *when pumped with a Ti:sapphire laser.*

Conclusions

In conclusion, room temperature upconversion pumped cw lasing of Yb,Er:YLF at 1.234 μm was demonstrated to our knowledge for the first time. Laser operation under Ti: sapphire laser excitation as well as under diode pumping was shown. Due to the strong dependence of the upper laser level population from the Yb–Er interaction the efficiency might be improved significantly by optimization of the Er and Yb dopant levels. Further experiments are in progress.

References

[1] F. Heine *et al.*, Appl. Phys. Lett. **65**(4), 383 (1994)
[2] Yu. K. Voronko *et al.*, Sov. Phys. JETP **21**, 1023 (1965)
[3] S. A. Pollack *et al.*, Appl. Phys. Lett. **54**(10), 869 (1989)
[4] A. A. Kaminskii, Sov. Phys. Dokl. **31**(10), 823 (1986)
[5] V. Petricevic *et al.*, Opt. Lett. **14**(12), 612 (1989)
[6] F. Heine *et al.*, ASSL Technical Digest, Memphis, Tennessee, paper WD2, 267 (1995)

Thursday, February 1, 1996

Plenary II

ThA 8:00 am-8:30 am
Gold Room

Clifford Pollock, *Presider*
Cornell University

Lasers for Material Processing in Advanced Manufacturing Applications

Andrew C. Tam

IBM Almaden Research Center,
650 Harry Rd., San Jose, CA 95120-6099
Tel: 408-927-1943; FAX: 408-927-3008

Traditional "workhorse" lasers for industrial laser processing are carbon dioxide lasers, lamp-pumped Nd:YAG lasers, and to a less extent, argon and krypton ion lasers. These have been widely used in various industries, including welding, drilling, cutting, surface hardening, printing, and entertainment. In the past several years, new laser sources have become mature, reliable, and readily available for new applications in industrial materials processing; particularly noticeable are excimer lasers and high-power diode lasers as well as diode-pumped solid-state lasers. This paper concentrates on some novel applications of these new laser sources in "hi-tech" manufacturing of semiconductor and data-storage devices.

The excimer lasers, in particular, the XeCl, KrF, and ArF lasers, are of much interest for the processing of materials ever since their discoveries in mid-1970's because of their ultraviolet wavelengths, short pulse duration in the tens of nsec, high pulse energy and the lack of spatial coherence or speckle effects. These features promote strong interactions of the excimer laser beam with many materials, particularly, polymers and dielectric materials, while the traditional laser sources do not produce desirable results. Early excimer lasers were only suitable for laboratory use; their frequent breakdown, short gas lifetime and high maintenance needed precludes any extensive applications in a production environment. Since the mid-1980's, "industrial quality" excimer lasers have become available using improved materials in the laser chamber and gas processor, better electronics, and modular design so that service maintenance can be done quickly. It is then possible to use such lasers for manufacturing applications. For example, such lasers are now extensively used in the selective localized removal of polymers as in wire-stripping /1/. With the high peak-power available over a relatively large area in the ultraviolet, micromaching applications are now possible using projection imaging systems as in photography; this can be done for ceramics /2/ as well as for other materials /3/. Besides the above applications based on the ablative removal of materials, the excimer lasers have also found applications in lithography, thin-film deposition /3/ and "laser cleaning" /4/. In particular, the technique of laser cleaning is of interest in the manufacturing of sub-quarter-micron linewidth devices, since traditional cleaning methods are often inadequate for cleaning off particles smaller than 0.1 micron.

More recently, diode-pumped solid-state lasers have become highly reliable and widely available commercially at reasonable cost for implementation in manufacturing. The advantages of such laser sources are their long lifetimes, near-zero maintenance, small size, low cost, high stability, good beam quality, high efficiency, and requiring little or no cooling, gas or other special facilities.

With Q-switching, such a laser source can produce a train of highly reproducible pulses at the tens of KHz repetition rate, with pulse width typically on the order of 10 nsec and pulse energy on the order of tens of μJ. While such a pulse energy seems small, the beam can be focussed to a near-diffraction-limited spot to produce a local laser fluence of many J/cm^2. Since the pulse train is at a high repetition rate, the focussed laser spot can be rapidly moved to cover a large area in a short time. This is the technique of laser processing using the moving dot approach, rather than the large-area imaging approach as is common for the excimer lasers which is limited in repetition rate typically to a few hundred Hz. Since the diode-pumped solid state lasers are superior to the excimer lasers in terms of cost, size, reliability and facility requirements, they are the preferred choice for laser sources in manufacturing whenever possible. Their applications will even be broader when high harmonic generation becomes broadly available to bring their wavelengths into the mid-ultraviolet and beyond. The Q-switched diode-pumped Nd:YLF laser is of particular interest to us, since this provides higher repetition rate with better pulse stability compared to the diode-pumped Nd:YAG laser. Such lasers have been implemented in various manufacturing processes, for example, in a "laser texturing" process /5/ whereby a special landing zone on a magnetic disk is produced by making tens of thousands of microscopic "bumps" of heights on the order of tens of nm in this zone. When the magnetic head lands on this zone, it is supported by hundreds of such bumps so that it does not stick onto the surface, which would happen if it lands onto the otherwise ultra-smooth disk surface used for high-density data recording.

References:

/1/ "Pulsed laser stripping of polyurethane-coated wires: A comparison of KrF and CO2 lasers", J. H. Brannon, A. C. Tam, and R. H. Kurth, J. Appl. Phys. **70**, P. 3881 (1991).

/2/ "Excimer laser ablation of ferrites", A. C. Tam, W. P. Leung, and D. Krajnovich, J. Appl. Phys. **69**, P. 2072 (1991).

/3/ See for example "Laser ablation in materials processing: Fundamentals and Applications", edited by B. Braren, J. J. Dubowski, and D. P. Norton, MRS Symposium Proceedings **285**, Materials Research Society, Pittsburgh, 1993.

/4/ "Laser-cleaning techniques for removal of surface particulates", A. C. Tam, W. P. Leung, W. Zapka, and W. Ziemlich, J. Appl. Phys. **71**, P. 3515 (1992).

/5/ "A new laser texturing technique for high performance magnetic disk drives", P. Baumgart, D. J. Krajnovich, T. A. Nguyen, and A. C. Tam, IEEE Trans. Mag., Sept, 1995 (in press).

Thursday, February 1, 1996

Plenary III

ThB 8:30 am-9:00 am
Gold Room

Clifford Pollock, *Presider*
Cornell University

Military and Dual Use Applications In The Next Decade

Rudolf G. Buser
CECOM RDEC
Night Vision and Electronic Sensors Directorate

Sensing Devices for military and related applications as well as forward working dual use concepts will be discussed. As baseline present/near term sensor requirements are analyzed; existing limitations due to physics and technology principals established; and possible pathways to solutions indicted.

Thursday, February 1, 1996

High Power Lasers

ThC 9:00 am-9:45 am
Gold Room

Christopher Clayton, *Presider*
Phillips Laboratory

69 W Average Power Yb:YAG Laser

Hans Bruesselbach and David S. Sumida
Hughes Research Laboratories
3011 Malibu Canyon Road, M/S RL65
Malibu, CA 90265-4799
(310) 317-5204 and (310) 317-5355; FAX (310) 317-5679

High power InGaAs laser diodes now enable the power scaling that Yb^{3+} lasers, by virtue of their small quantum defect and consequently low thermal load [1], merit [2]. The simple $[Xe]4f^{11}6s^2$ electronic structure has no excited state absorption, upconversion, or concentration quenching. Recent spectroscopy [2-6] has clarified the seven energy levels' positions, cross sections, and lifetimes, even as laser results [7-12] begin to tap the tremendous potential. Yb:YAG is favored for power scaling because of its broad pump bands and excellent thermo-mechanical properties. InGaAs diodes are used for pumping, so the dark-line-defect-related reliability problems [13] of AlGaAs are absent [14]. Fully exploiting these advantages requires different laser pump-head architectures than usual for four-level Nd^{3+} systems, because Yb^{3+} at 1.03 μm is quasi-three-level. Doped volumes not pumped to inversion are a loss. Ten watts of output power has been reported from chilled face-pumped active Yb:YAG mirror disks [11]. End pumped devices at 13 W have been reported [12], and proposed for scaling to kilowatt powers [15]. End-pumping efficiency, even multi-pass, is limited [16] to <80% because the medium becomes transparent when pumped to high inversion [17]. End-pumping is prone to parasitics when the active medium lightguides the pump, and, as with active mirrors, power scaling requires progressively higher brightness diodes and/or complex transport optics.

We have developed a multi-kilowatt-scalable side-pumped technology using an integrating pump cavity [18] with impingement cooling of the laser crystal [18]. To anchor our pump-cavity, thermal-management, and laser-kinetics modeling, we tested a small prototype head, shown in Figure 1, in an oscillator. We here report the first results of 69 W average power, 150 W quasi-cw power, and 173 mJ in a ~1 msec pulse, representing the highest pulse energy and highest power to date for a Yb:YAG laser.

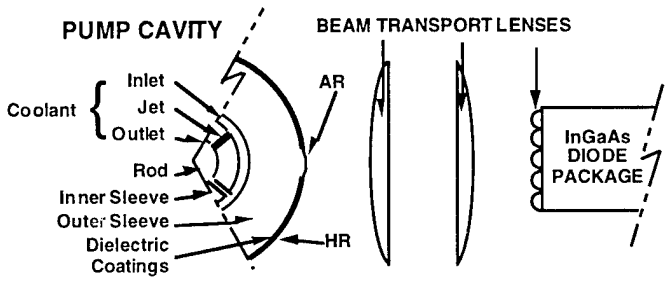

Figure 1. Schematic of one third of pump head, section perpendicular to rod axis; other two thirds identical.

Only the 2-mm diameter, 20-mm long, 1-at. % Yb^{3+} doped part of the rod volume is inside the integrating pump cavity. Both rod ends, outside the cavity, are undoped YAG, diffusion bonded to the center section (total rod length 31 mm). This facilitates mounting, coolant routing, and optical access. The rod is cooled with 15°C methanol impinging from laser-drilled holes in the inner sleeve. The outer sleeve is solid glass. Arranged symmetrically as three groups of three five-bar diode arrays each, 45 bars (SDL) transversely pump the rod. Diode bars are inherently bright enough to efficiently couple into our pump cavity, but presently available stacked-bar packaging, intended for slab face-pumping, for us required lossy adaptations. As purchased, each

five bar package is pre-collimated (we measured ~2° full angle for 90% power) with an ~80% transmitting microlens array in the bars' fast axis. The slow axis had ~12° divergence. We imaged the diodes onto the rod through AR-coated slots in the pump cavity barrel using 3 lens pairs. Except for these slots, all the pump cavity's outside walls are dielectrically coated to reflect the 941 nm pump band. Because the slots were fabricated before the divergence was measured, the beam shapes and slot sizes are mismatched. This and lens vignetting unfortunately left the diode-to-slot transport efficiency at only 52%, resulting in 1212 W quasi-cw pump power entering the pump cavity.

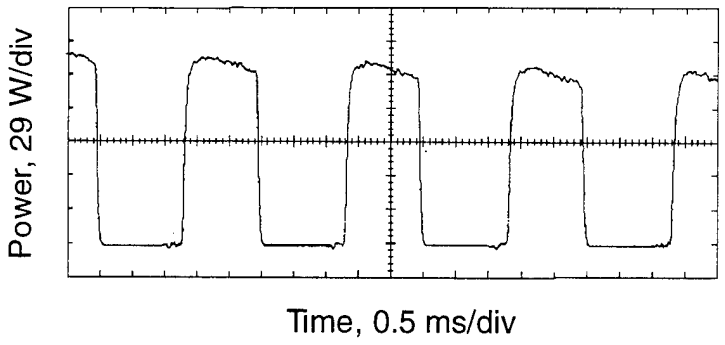

Figure 2. Quasi-cw lasing output, measured with silicon photodiode. Ordinate calibrated to 29 W/div, abscissa is 0.5 msec/div. ~90% output reflctor. 72 A pump diode current pulses started approximately 150 μsec before lasing, evidenced by electrical noise at baseline.

Pulse duration was typically 1.1–1.3 ms, the longest recommended for the diode bar thermal mounting. We varied the pulse rate to vary the duty factor. Operating at 52% duty factor for 4 seconds out of every 10 seconds kept us within the diodes' <20% duty cycle rating, and allowed corroboration of our rod thermal management modeling. The rod approaches thermal equilibrium with time constant $a^2/\alpha \approx 1$ sec given by the diffusion equation; a = 1 mm is the rod's radius, and $\alpha = 0.038$ cm^2/sec is the thermal diffusivity for Yb:YAG, extrapolating from our thermal conductivity measurements of doped and undoped Yb:YAG [19]. The rod's thermal-lensing back focal length after 4 seconds of absorbing ~300 W of pump was measured to be approximately 15 cm, consistent with earlier reported heat deposition numbers (12% [1] x 300 = 36 W of heat) for Yb:YAG.

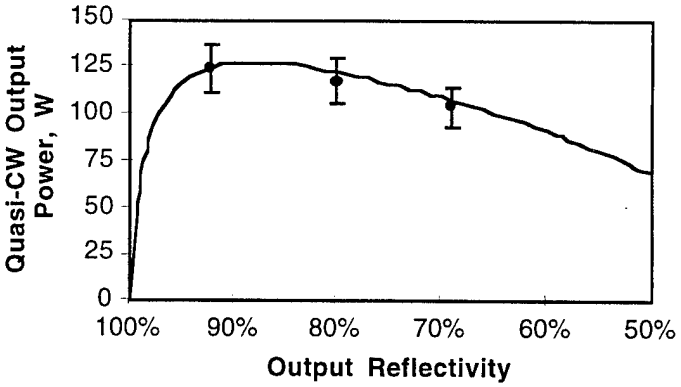

Figure 3. Rigrod analysis output power prediction as a function of output mirror reflectivity, assuming 26% pumping efficiency, compared with experiment.

Our oscillator had two flat mirrors spaced by ~10 cm, one with 99.6% reflectivity. Figure 2, an oscillograph of the output power measured with a silicon photodiode, shows typical quasi-cw performance operating at 52% duty-cycle. The average power was 69 W. Output is present 46% of the time, making the quasi-cw output power 150 W. Lasing begins 150 μsec after the start of each diode pump pulse.

We imposed Rigrod-type analysis on quasi-cw lasing data, as plotted in Figure 3, at a lower power level than Figure 2. Modeling the pump cavity efficiency at approximately 26% and round-trip resonator loss of 1.3% gave the best fit to the data. Detailed computer pump head

modeling [20] predicted 58% pump cavity efficiency. Out-of-specification polishing of the pump cavity's inner sleeve, causing unwanted scattering, explained much of the discrepancy. This was verified in the model, and confirmed experimentally by improving the sleeve polish, which made the pumping efficiency 29%, and allowed 150 W operation — the data seen in Figure 2. Replacing the coolant with index-match fluid to suppress the significant remaining scattering at the sleeve-coolant interfaces made the pump efficiency 40%, and the cw output during the 250 mJ pulses became 250 W at low (~1%) duty cycle. We think the remaining discrepancy is from the 95% spectral overlap, out-of-specification fabrication, diode misalignment, and the model not taking pump saturation into account. Modeled efficiencies approach 80% and 90% respectively for the 3-mm and 4-mm rods in the 3 kW design, because larger rods absorb more per pass and expose more area to the pumps, allowing a smaller-slotted, less lossy integrating cavity.

In summary, we have demonstrated the highest power and pulse energy to date for a side-diode-pumped Yb:YAG laser at room temperature. The measured thermal and optical performance was firmly linked to models, allowing interactive design and comfortable extrapolation to kilowatt-level average powers. High PRF Q-switched laser operation and true cw-pumped operation is currently in progress.

References:

1. T. Y. Fan, IEEE J. Quantum Electron. **29**, 1457 (1993).
2. D. S. Sumida, T. Y. Fan, and R. Hutcheson, OSA Tech. Dig. of the Advanced Solid State Laser Meeting, 224 (1995).
3. L. D. DeLoach, S. A. Payne, L. L. Chase, L. K. Smith, W. L. Kway, W. F. Krupke, IEEE J. Quantum Electron. **29**, 1179 (1993).
4. D. S. Sumida and T. Y. Fan, OSA Tech. Dig. of the Advanced Solid State Laser Meeting **20**, 100 (1994).
5. D. S. Sumida and T. Y. Fan, Opt. Lett. **19**, 1343 (1994).
6. D. C. Hanna, Opt. Comm. **99**, 211 (1993).
7. P. Lacovara, H. K. Choi, C. A. Wang, R. L. Aggarwal, and T. Y. Fan, Opt. Lett. **16**, 1089 (1991).
8. T. Y. Fan, S. Klunk, and G. Henein, Opt. Lett. **18**, 423 (1993).
9. I. Chartier, C. Wyon, D. Pelenc, B. Ferrand, D. P. Shepherd, and D. C. Hanna, Material Research Society Symposium Proc. Vol. **329**, 179 (1993).
10. D. S. Sumida and T. Y. Fan, LEOS Annual Meeting Conf. Proc., vol. 2, 419 (1994).
11. A. Geisen, H. Hugel, A. Voss, K. Wittig, OSA Tech. Dig. of the Adv. Solid-State Laser Meeting, 227 (1995).
12. C. Marshall, S. A. Payne, L. K. Smith, K. I. Schaffers, C. Orth, R. Beach, H. T. Powell, and W. F. Krupke, LEOS Annual Meeting Conference Proceedings, vol 2., 417 (1994).
13. R. G. Waters, D. P. Bour, S. L. Yellen, and N. F. Ruggieri, IEEE Photonics Tech. Lett. **2**, 531 (1990).
14. S. L. Yellen, R. G. Waters, Y. C. Chen, B. A. Soltz, S. E. Fischer, D. Fekete, and J. M. Ballantyne, Electronics Letters **26**, 2083 (1990).
15. S. A. Payne, C. D. Orth, and W. F. Krupke, LEOS Technical Digest, 704 (1993).
16. T. Y. Fan, in *Solid State Lasers: New Developments and Applications*, M. Inguscio and R. Wallenstein, ed. (Plenum, N.Y. 1993), p 189.
17. L. K. Smith, S. A. Payne, W. F. Krupke, L. D. DeLoach, W. L. Kway, and B. H. T. Chai, OSA Tech. Dig. of the Adv. Solid-State Laser Meeting, 188 (1993).
18. Patent Pending.
19. B. A. Wechsler and D. S. Sumida, in *CRC Handbook of Laser Science and Technology, Supplement 2: Optical Materials*, M. J. Weber, ed., (CRC Press, Boca Raton, 1995) p. 608.
20. D. Rock, SPIE Conference Proceedings Vol. 675, "Stray Radiation V", 18-20 August 1986, Robert Breault, ed., pgs. 9, 85-94, 105.

High-Power Near-Diffraction-Limited and Single-Frequency Operation of Yb:YAG Thin Disc Laser

A. Voss[1], C. Stewen[1], M. Karszewski[1], A. Giesen[1], U. Brauch[2]

[1]Universität Stuttgart, Institut für Strahlwerkzeuge,
Pfaffenwaldring 43, D-70569 Stuttgart, Germany
(phone: +49 (711) 685-6846, fax: +49 (711) 685-6842, e-mail: giesen@ifsw.uni-stuttgart.de)

[2]Deutsche Forschungsanstalt für Luft- und Raumfahrt, Institut für Technische Physik,
Pfaffenwaldring 38-40, D-70569 Stuttgart, Germany
(phone: +49 (711) 6862-512, fax: -49 (711) 6862-349, e-mail: u.brauch@dlr.de)

Recently, Ytterbium doped materials are of increasing interest for high power and high efficient laser operation [1-3]. To demonstrate the excellent qualification of the thin-disc laser concept for high-power applications with highest beam quality (TEM_{00} or even single frequency) we will present our results obtained with diode-pumped Yb:YAG discs.

The thin disc is pumped by a fibre bundle made of up to 120 fibres (125/140 µm core/cladding diameter, N.A. 0.37) with an output power of 1.2 W each (up to 148 W total) at 940 nm. As reported earlier [1], the pump light is imaged onto the center of the crystal disc by means of a spherical mirror. The front side of the 0.3 (0.4) mm thick crystal is AR coated for the pump and the emission wavelength (AR 940/1030 nm) whereas the back side is HR-coated for both wavelengths (HR 940/1030 nm). The pump light not absorbed is re-imaged at the crystal again with three other spherical mirrors and one flat mirrror [1]. This leads to four double-passes of the pump light, allowing to increase the local effective pump power density within the crystal by roughly a factor of three compared to the available power density at the end of the fibre bundle (approx. 6 kW/cm²). The 11 (8) at. % doped crystal is mounted onto a copper heat sink, using an indium-foil in between to ensure an optimal heat conduction. The temperature of the heat sink is controlled either by Peltier elements (+20 °C to -30 °C) or by methanol as cooling fluid (0 °C to -80 °C).

With 19 and 37 individually fibre coupled laser diodes output powers of up to

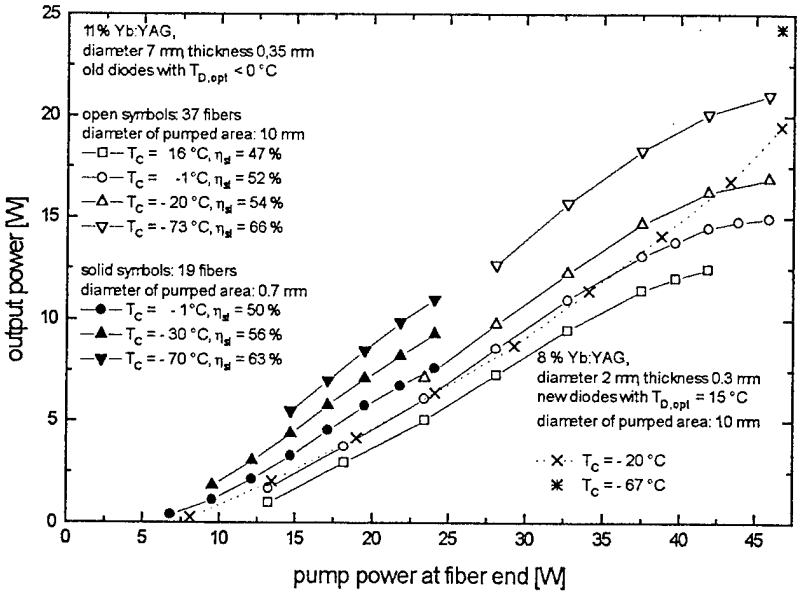

Fig. 1: Output power vs. pump power using 19 and 37 fibre bundles.

11 W and 24 W (fig. 1), respectively, have been achieved with near diffraction limited beam quality ($M^2 < 1.8$). Simultaneously, total optical efficiencies (relative to the fibre bundle output power) of up to 52 % have been obtained. As expected, the threshold (approx. 6 W and 12 W, respectively) scales proportional to the area of the pumped region (0.7 and 1.0 mm respectively).

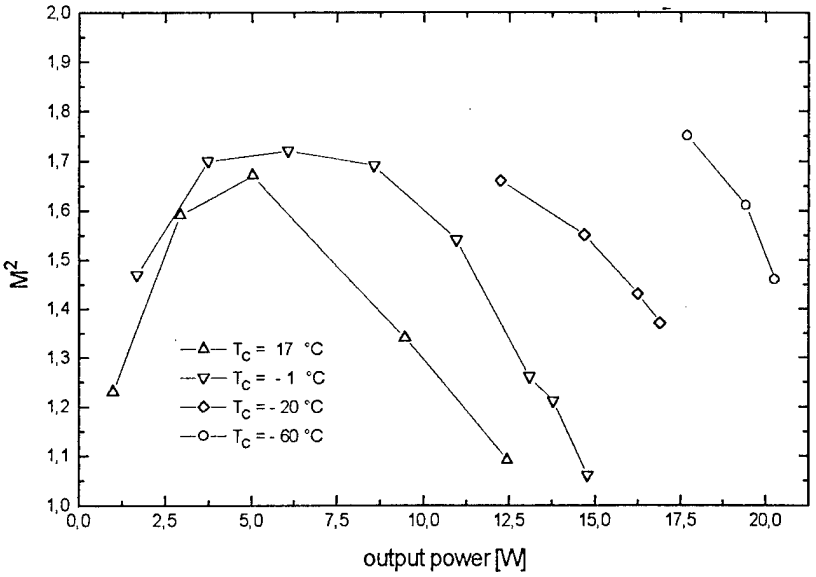

Fig. 2: Beam quality vs. output ower at various cooling fluid temperatures.

With a previous set of laser diodes a significant reduction of the slope efficieny has been observed at maximum output power (fig. 1, solid lines), which has been attributed to a current-dependent wavelength shift of the laser diodes, operating at a temperature above optimum at maximum current (5 °C instead of < 0 °C). This could be confirmed by using a new set of laser diodes with a shorter center wavelength (fig. 1, dashed line). In this case, the diodes reach the optimum wavelength at maximum current, which results in an increase in slope efficiency when approaching the maximum power.

Fig. 2 shows the beam quality measured with a Coherent Modemaster as a function of the output power for different cooling fluid temperatures T_C. Depending on T_C, the resonator reaches its stability limit due to thermal lensing at different pump powers. Close to the limit the beam quality is best ($M^2 < 1.1$). The good beam quality near threshold originates from the "aperture guiding" effect which induces higher losses for the higher transversal modes. This effect depends on the reabsorption in the unpumped regions of the quasi-three level system and is therefore strongest at high temperatures and low gains (near threshold). At low temperatures, the resonator remains stable even at maximum pump power. The range of beam qualities accessible by merely changing the pump power is reduced in this case. Nevertheless, the beam quality can be optimized further by varying the resonator length.

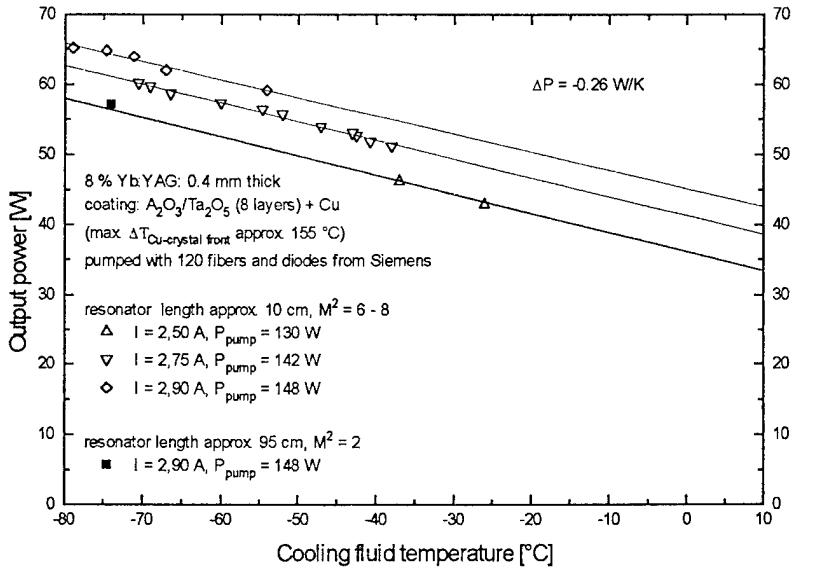

Fig. 3: Ouput power using a bundle of 120 fibres.

With 120 laser diodes output powers of up to 65 W have been achieved in multimode operation ($M^2 \approx 8$) using a 8 % doped, 0.4 mm thick crystal with a diameter of 7 mm (pumped diameter 1.9 mm, see fig. 3). The total efficiency exhibits a slope of - 0.20 %/K, which means 20 % efficiency reduction (> 40 % relative) for 100 K temperature rise, which demonstrates the importance of a low temperature difference between crystal and cooling fluid, which is, in the moment, dominated by the heat resistance of the HR-coating (estimated temperature drop: 60 - 100 K). By employing a longer resonator, the beam quality could be improved drastically (M^2 = 2.0) with only 10 % reduction of the output power (57 W). With new high power laser diodes we plan to realize near diffraction limited output powers in the range of 200 W in the near future.

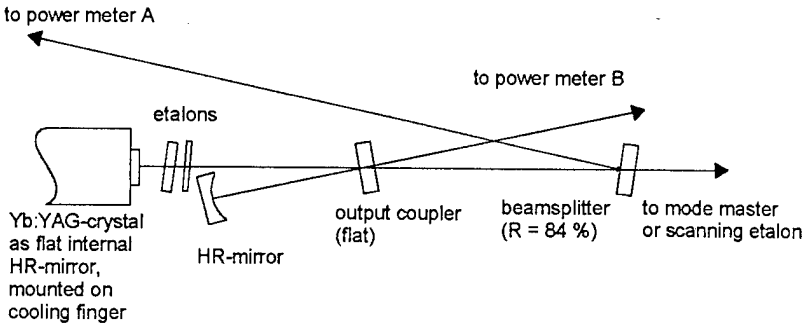

Fig. 4: Experimental setup for single frequency operation

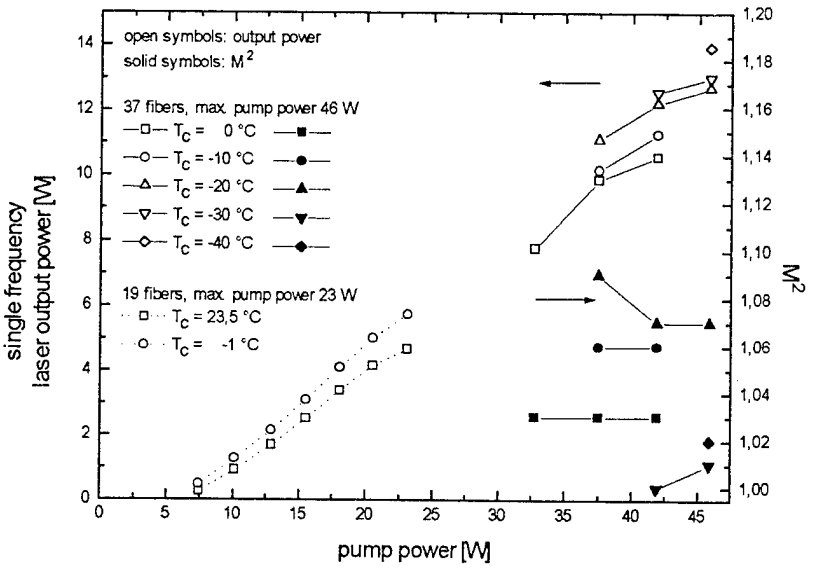

Fig. 5: Output power and beam quality in single frequency operation.

The ability to achieve excellent beam qualities with only minor losses in efficiency even at relatively high output powers, encouraged us to investigate also the possibility of single frequency operation of the Yb:YAG thin disc laser. As can be seen in fig. 4, a folded resonator with a flat folding mirror, which served as output coupler, was used. With only two addidional etalons (1 mm, 30 % reflection and 0.1 mm, uncoated) single frequency operation has been obtained, as confirmed by measurements with a scanning etalon. Fig. 5 shows the output powers and beam qualities achieved with this setup using 37 (17) diodes. At a cooling fluid temperature of -40 °C the maximum output power was 14 W (45.5 W pump power) with a beam quality of $M^2 = 1.02$.

[1] A. Giesen, L. Berger, U. Brauch, M. Karszewski, C. Stewen, A. Voss, „Recent Results of the Scalable Diode-Pumped Yb:YAG Thin Disk Laser", in *Advanced solid-State Lasers,* OSA Technical Digest (Optical Society of America, Washington D. C., 1995) pp. 227 - 229

[2] T. Y. Fan: IEEE J. Quant. Electron. **29**, 1457 (1993)

[3] C. D. Marshall, S. A. Payne, L. K. Smith, R. J. Beach, M. A. Emanuel, H. T. Powell, W. F. Krupke, „Diode-pumped Yb:$Sr_5(PO_4)_3F$ laser performance", in *Advanced solid-State Lasers,* OSA Technical Digest (Optical Society of America, Washington D. C., 1995) pp. 218 - 220

High Power Operation of Nd:YAG Rod Lasers Pumped by Fiber-coupled Diode Lasers

D. Golla, M. Bode, S. Knoke, W. Schöne, F. von Alvensleben, and A. Tünnermann
Laser Zentrum Hannover e. V., Hollerithallee 8, D-30419 Hannover, Germany
Tel.: (49)511 2788110, Fax: (49)511 2788100

Diode-pumped solid-state lasers operating at high cw power levels are attractive sources for various applications in materials processing and nonlinear frequency conversion. Commonly, bare diode laser arrays are used as pump sources which fulfill the requirements in terms of reliability and efficiency [1, 2]. However, the laser head design of these systems is very sophisticated. Compared to linear diode arrays, fiber-coupled diode lasers as pump sources have many advantages for a simple design and small laser head size. Any failure of individual diode lasers only requires plugging in the corresponding fiber connector to a new diode laser. There is only a bundle of optical fibers that is attached to the laser head, which allows nearly free adjustment of the pump light distribution inside the laser active medium.

In end-pumped rod lasers highly efficient TEM_{00} mode operation has been achieved because of mode-selective pumping [1]. However, end-pumped single laser head configurations are not scalable to output powers beyond 100 W [3]. Side-pumped slab lasers using fiber-coupled diode lasers have achieved a great reduction of thermally induced effects due to a nearly uniform pump light profile [4], but output powers are so far limited to about 70 W. Based on fiber-coupled diode lasers, side-pumped lasers for high power operation at excellent beam qualities have been developed.

A rod laser system has been designed, as shown in Fig. 1. The pump arrangement allows linear pump power densities up to 150 W/cm, considering the effectively pumped rod length of 32 mm. The Nd:YAG rod (length 56 mm, diameter 4 mm, Nd-doping level 0.9 at. %) has a polished barrel, which reduces the scattering losses for the pump light.

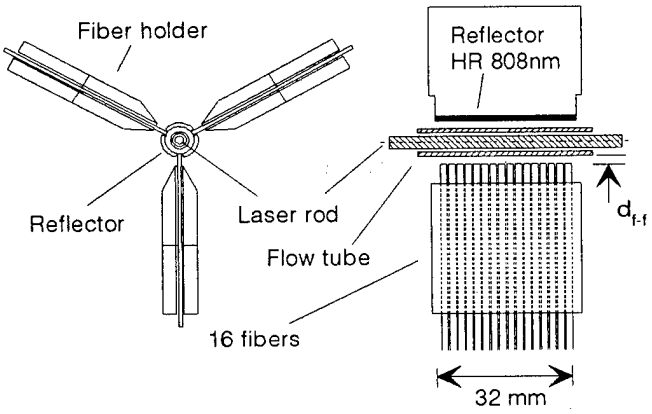

Fig. 1 Laser head, side-pumped by fiber-coupled diode lasers

The endfaces of the rod are antireflection coated at 1064 nm. For direct water cooling the laser rod is mounted inside a flow tube, which is antireflection coated at 808 nm. The optical pump source consists of fiber-coupled diode lasers (Jenoptik Laserdiode) with a nominal output power of 10 W each at 808 nm.

Each pump module consists of 16 fibers (core diameter of 800 µm, total diameter of 1.5 mm and 0.22 N.A.) (see Fig. 1). The fibers are mounted side by side with a spacing of 0.5 mm. The pump modules are arranged in a threefold symmetry around the laser rod with a total pump power of approximately 370W. The diode laser radiation directly irradiates the laser rod, and does not require any additional focusing optics. The spacing d_{ff} (see Fig. 1) between the fiber ends and the flow tube can be varied from 0.5 to 20 mm.

For sufficient absorption of the diode laser radiation, pump light reflectors are mounted around the rod [5]. Nearly 340 W of the total pump power are absorbed, due to the double-pass of the radiation in the laser rod. In order to reduce the thermally-induced effects for efficient laser performance in multimode and TEM_{00} mode operation, the pump light distribution in the laser rod has been investigated by imaging the fluorescence at 1064 nm onto a CCD camera for different distances between the fiber ends and the flow tube. For these measurements only a small cross-section in the laser rod was excited by 3 fiber-coupled diode lasers. Fig. 2 depicts the pump light distributions for two fiber-to-flow tube spacings.

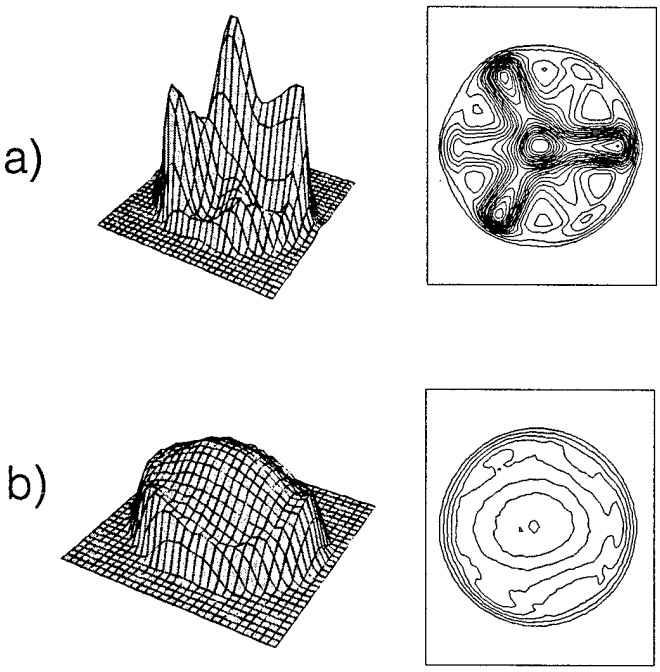

Fig. 2: Measured pump light distribution for fiber-to-flow tube spacings of 1 mm (a) and 13 mm (b).

Short fiber-to-flow tube spacings cause very inhomogeneous pump light distributions with a high gain on the center axis of the rod. In order to determine the influence of the pump light distribution on thermo-optical effects, the focal length of the thermally-induced lens was measured. Applying a pump power of 370 W a focal length of about 14 cm is measured for a fiber-to-flow tube spacing of 1mm while the focal length is increased to 21 cm for a spacing of 13 mm. The reduction of thermally-induced optical effects is due to a more uniform pump power deposition for greater distances between the fiber ends and the laser rod, and a nearly parabolic temperature distribution inside the laser rod.

Despite the large fiber-to-flow tube spacings the laser output power and optical slope efficiencies in multimode operation keep nearly constant. The laser performance in multimode operation at a laser wavelength of 1064 nm was investigated in linear flat-flat resonators with one highly reflecting mirror and one partly transmitting mirror. The cavity mirrors were separated by about 100 mm. At a fiber-to-flow tube spacing of 7 mm, a maximum multimode output power of more than 160 W cw was obtained for a pump power of 370 W cw. The laser output power relative to the pump power behind the fiber ends is plotted in Fig. 3. From these data, an optical slope efficiency of 46% was determined, and a corresponding pump power at laser threshold of 27 W. For larger fiber-to-flow tube spacings, the output powers only slightly decreased. The observed efficiencies are comparable with that obtained for end-pumped systems [1].

Because of the reduced thermally-induced effects, large fiber-to flow tube spacings are preferrable for high beam quality and TEM_{00} mode operation. Therefore, we chose a fiber-to-flow tube spacing of 13 mm. Moreover, for efficient and reliable TEM_{00} mode operation, we built linear flat-flat resonators which are stable against both focal length fluctuations and misalignment. The highly reflective mirror is positioned 78 cm from the principal plane of the laser rod; the output coupler is 22 cm from the other principal plane. This yields a TEM_{00} mode spot size of approximately 1.4 mm inside the laser rod. For these conditions, it is not necessary to use any aperture for suppressing higher order modes. At a pump power of 370 W, a TEM_{00} mode output power of more than 62 W cw is generated, which to our knowledge is the highest reported TEM_{00} mode output power for a single laser rod.

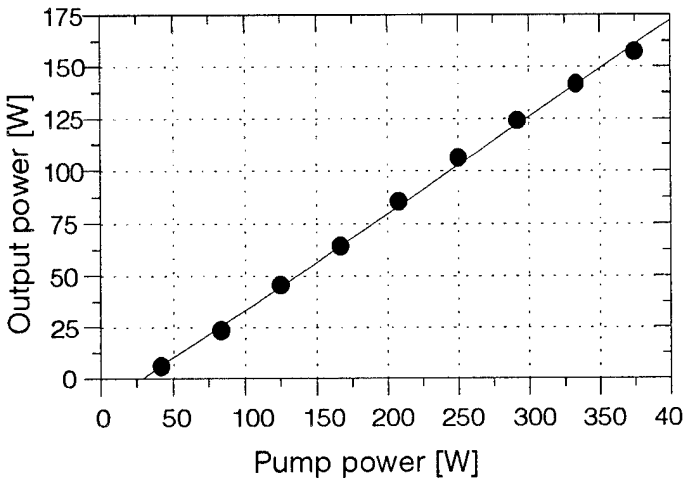

Fig. 3: Optical output versus pump power. Slope efficiency:46%, laser threshold: 27 W

Further theoretical investigations concerning high power TEM_{00} mode operation indicate that uniformity of the pump light distribution and the applied pump power density are key points for an enhanced efficiency. The excitation of a laser rod from many sides leads to a more homogeneous pump light distribution, so that optical aberrations are minimized. Moderate linear pump power densities also favor efficient TEM_{00} mode operation The average temperature inside the laser rod is reduced, yielding a negligible population of the lower laser level. This results in minimal aberration-related losses and allows a larger spatial overlap between the TEM_{00} mode and the pumped volume. As a consequence, in a five-fold pump scheme, optical-to-optical efficiencies of more than 25% in TEM_{00} mode operation are obtained. This corresponds to an output power of 61 W with 240 W of pump power and 120 W/cm of linear pump power density.

In summary, a diode-laser side-pumped, 160 W cw Nd:YAG laser with an optical slope efficiency of 46% and an overall electrical efficiency of more than 8% has been demonstrated. TEM_{00} mode output powers of more than 60 W have been described with optical-to-optical efficiencies of more than 25%. These devices will be well suited for efficient second harmonic generation with expected output powers of several ten watts in diffraction limited beam quality.

This research was supported by the German Ministry of Science, Education, Research and Technology under contract 13 N 6361.

References

[1] S. C. Tidwell, J. F. Seamans, and M. S. Bowers, Opt. Lett. **18**, 116 (1993).
[2] D. Golla, S. Knoke, W.Schöne, G. Ernst, M. Bode, A. Tünnermann, and H. Welling, Opt. Lett. **20**, 1148 (1995).
[3] S. C. Tidwell, J. F. Seamans, M. S. Bowers, and A. K. Cousins, IEEE J. Quantum Electron. **28**, 997 (1992).
[4] R. J. Shine, A. J. Alfrey, and R. L. Byer, Opt. Lett. **20**, 459 (1995)
[5] D. Golla, S. Knoke, W. Schöne, G. Ernst, A. Tünnermann, and H. Welling, Proc. Soc. Photo-Opt. Instrum. Eng. **2379**, 120 (1995).

Thursday, February 1, 1996

Novel Architectures Poster Session

ThD 9:45 am-10:45 am
Terrace Room

High Resolution Doppler Lidar Employing a Diode Pumped Injection-Seeded Tm:Lu,YAG Transmitter

Christian J. Grund
NOAA / Environmental Technology Laboratory
R/E/ET2
325 Broadway
Boulder, CO 80303
303-497-6870
cgrund@etl.noaa.gov

Introduction

Great strides in understanding atmospheric boundary layer processes have been achieved in recent years using Large Eddy Simulation models (LES). LES models give insight into the formation of structures, and the transport processes for heat, moisture, and momentum between the surface and the atmosphere. Progress in the development and verification of realistic models depends upon accurate measurements of the temporal evolution of spatially resolved turbulent and mean winds. Over the past several decades these measurements have been acquired by tower-, aircraft-, and balloon-borne *in situ* sensors. More recently, radar, sodar and lidar remote sensors have been developed to overcome some of the spatial and temporal sampling, and cost limitations inherent to *in situ* sensors. However, continued model improvements are still limited by the lack of temporal, spatial, and velocity resolution available from current wind measurement instrumentation. Measurements of the turbulent fluctuations of the wind with better than 50 m spatial resolution covering volumes of a few km^3/sec to distances >10 km are needed to provide the observations from which to improve boundary layer simulation models, or from which turbulent flux measurements can be obtained. Of particular interest are the improvement of vertical resolution in the boundary layer entrainment zone, higher resolution observations of the nocturnal and neutral (or shear-driven) boundary layers, and day/night boundary layer transition processes. Also of interest are the development of momentum flux and, in combination with other remote sensors, chemical species flux (e.g., O_3, H_2O_v), the measurement of ice crystal fall speeds in cirrus clouds and the impact of shear on cloud morphology, the measurement of synoptic scale divergence and vorticity, the observation of complex terrain flows, and improved range in high humidity environments facilitating ocean boundary layer studies.

The NOAA Environmental Technology Laboratory has addressed the limitations of current measurement technologies by designing, developing, and constructing a high spatial and temporal resolution solid-state coherent Doppler lidar with an operating wavelength near 2 μm. The High Resolution Doppler Lidar (HRDL) employs a high repetition rate, eye-safe wavelength, laser-diode-pumped, solid-state Tm:Lu,YAG pulse laser transmitter, and a high-speed alt-azimuth scanner. To facilitate operation from ships, the scanner is corrected in real time for platform attitude. A standard shipping container (seatainer) has been modified as a lidar van enabling low-cost shipment of the system world-wide.

The HRDL has recently been field tested from a ship at sea for 4 weeks during the Marine Boundary Layer Experiment (MBLEX), and has simultaneously demonstrated 30 m range resolution and 5 cm/s velocity resolution. The technology used to achieve this performance is discussed.

Design and Performance

The Doppler frequency shift, Δf_{Dop}, for a given wind velocity, V, is inversely proportional to the laser wavelength ($\Delta f_{Dop} = 2V / \lambda$), while the Fourier transform width of a fixed pulse length, τ_p, is constant with wavelength ($\Delta f_p = 1 / 2\pi\tau_p$). To simultaneously improve both velocity resolution and range resolution over previous CO_2 laser based technologies operating near 10.6 μm (typically 0.5 m/s and 300 m), requires operation at shorter wavelengths. Gas pulse lasers also generally exhibit serious chirp, which further degrades velocity resolution for distributed atmospheric targets. As wavelength is shortened, however, signal degradation due to turbulence and background light become limiting factors in system performance. Eye-safety[1] also becomes a serious issue at wavelengths <1.45 μm which limits applications for a scanning boundary layer lidar. A compromise between competing performance issues lead to a search for laser operating in the 1.5 - 2.5 μm region having the beam quality required for coherent lidar and the high repetition rate needed to support rapid scanning. Tm:YAG and Tm,Ho:YAG lasers can meet the requirements. Tm:YAG was originally chosen over Tm,Ho:YAG primarily because the latter system

requires significant cooling (-20° C) to achieve good efficiencies. Near room temperature operation is an important consideration for field operation in the presence of high humidity and other adverse environmental conditions. Fortunately, good room temperature InGaAs detectors are also available at this wavelength, and 20 dB of shot noise can be obtained. Lidar specifications are given in Table 1, and a simplified schematic of the lidar system in fig. 1. Last year, a switch was made to Tm:Lu,YAG (4% Tm, 50% Y, 50% Lu) because the peak of fluorescence in this material coincides with a good atmospheric transmission window [2], enabling best laser efficiency and maximum system range.

To provide the required spatial resolution during volume sector scans while allowing profiles to be averaged to reduce speckle noise requires an accurate high-speed scanner and a relatively high laser pulse repetition rate. For these reasons, CW diode-pumping and acousto-optic Q-switched operation were chosen for the laser transmitter. This approach also minimizes the cooling requirements on the laser crystal and the thermal lensing and birefringence effects on the laser cavity, as well as cooling-water flow-induced laser head vibration and the resultant frequency jitter.

The power oscillator is injection-seeded to provide the narrow bandwidth and frequency stability needed to implement coherent detection in the receiver. A single temperature-stabilized reference laser (CLR Photonics CLR-2) provides both the local oscillator for coherent detection and a frequency-shifted beam for injection seeding. The reference laser has operated flawlessly for over 2 years, and has maintained the same frequency within the resolution of a Burleigh WA-10 wavemeter, despite exposure to vibration, accelerations and temperature extremes associated with transport and field operations. A single 100 MHZ intra-cavity acousto-optic modulator is used to accomplish both the seed light frequency shift and Q-switched operation of the slave laser[3]. The slave laser cavity output coupler (5% T, 300 mm RC) is mounted on a piezo-electric translator (PZT) to facilitate locking to the seed laser frequency. The rear cavity end mirror is coated onto the laser rod. Initially, lock is achieved by observing and minimizing the Q-switch build-up time from pulse to pulse by varying the PZT voltage. Once seeding is obtained, the output pulse beat note (with the reference oscillator) is used to fine-tune the laser cavity length. In the event acoustic vibration in the cavity degrades lock loop performance, the loops are also set up to facilitate implementation of a hill-climbing or ramp-and-fire servo schemes. However, during ship operations, stable operation was obtained using frequency alone for feedback, despite large amplitude 5 Hz vibrations induced by the ship's prop, and 0.5 g, 4 s period accelerations in all directions due to rough sea conditions.

Each end of the power oscillator Tm:YAG crystal is pumped with ~9 W of 785 nm light delivered by a 0.22 NA 400-μm diameter optical fiber and coupled into the rod by a pair of lenses. The pump energy for each fiber is generated by five temperature-controlled 3-W laser diodes. The module was built for us by Lightwave Electronics. An interesting characteristic of the pump light delivered in this way is that the apparent source position for individual diodes appears at a different depth within the fiber, causing the focal position of each diode to vary along the pump volume in the laser rod.

Although designed to develop 10 mJ/pulse with a 200 ns pulse width, optical coating damage has limited injection seeded performance to < 5mJ/pulse. In practical field operation, only .8 - 1 mJ/pulse can be maintained. The problem is due to thermal lensing and subsequent narrowing of the laser mode by the pump beam, resulting in excessively high fluence at the rod face. Field experience suggests that under typical marine boundary layer aerosol conditions, ~3-5 km range can be expected with 0.8 mJ/pulse averaging 12 pulses to achieve 5 cm/s velocity resolution in 30 m range gates. At a 1 kHz pulse rate the laser develops 1.2 mJ/pulse in 300 ns wide pulses (injection seeded).

Continuing development will include pulse and pump laser improvements, correction of data system shortcomings, and adaptation to aircraft. Current analysis is centered on establishing the absolute accuracy of the measurements (casual target observations suggest no bias), and calculation of wind profiles and kinetic energy fluxes from MBLEX. The system will again be deployed on a ship next March and from an aircraft in the Fall.The feasibility of using 2 μm DIAL for water profiling is also under investigation[4].

Acknowledgments

This lidar system was partially funded under Army Research Office contract ARO 117-92. Shipboard measurements were made possible under Office of Naval Research grant N00014-93-F-0029. This work would not have been possible without the contributing efforts of : Raul Alvarez, Kathleen Healy,Jim Howell, David Larson, Ron Richter, Scott Sandberg, and Ann Weickmann.

References

1. American National Standard for the Safe Use of Lasers. The Laser Institute of America, ANSI Z136.1-1993.
2. Kmetec, J.D., T.S. Kubo. T.J. Kane, and C.J. Grund, "Laser Performance of Diode-Pumped Thulium-doped $Y_3Al_5O_{12}$, $(Y,Lu)_3Al_5O_{12}$, and $Lu_3Al_5O_{12}$ Crystals, **Optics Letters 19** , 186-188 (1994).
3. Coherent Technologies Inc. patent applied for (1993), used with permission.
4. Grund, C.J, and R.M.Hardesty, and B. J. Rye, 'Feasibility of tropospheric water vapor profiling using infrared heterodyne differential absorption lidar', Proceedings, ARM Science Team Meeting, San Diego, CA, March, 1995.

Table 1. Lidar Specifications	Goal	Demonstrated
Radial velocity measurement range:	≤ 1 cm/s to ≥ 50 m/s	5 cm/s - 22 m/s
Velocity measurement accuracy:	< ±1 cm/s	not established
Measurement range:	≥ 15 km	5 km (marine)
Range resolution:	≤ 50 m	30 m
Pulse repetition frequency:	100 - 300 Hz	200 Hz - 1 kHz
Operating wavelength:	2.0218 μm	2.0218 μm
Transmitted pulse energy:	10-20 mJ	5 mJ (see text)
Telescope	0.2 m dia., Mersenne	.2 m dia Mersene
Detectors	InGaAs, 10 dB shot noise	20 dB shot noise

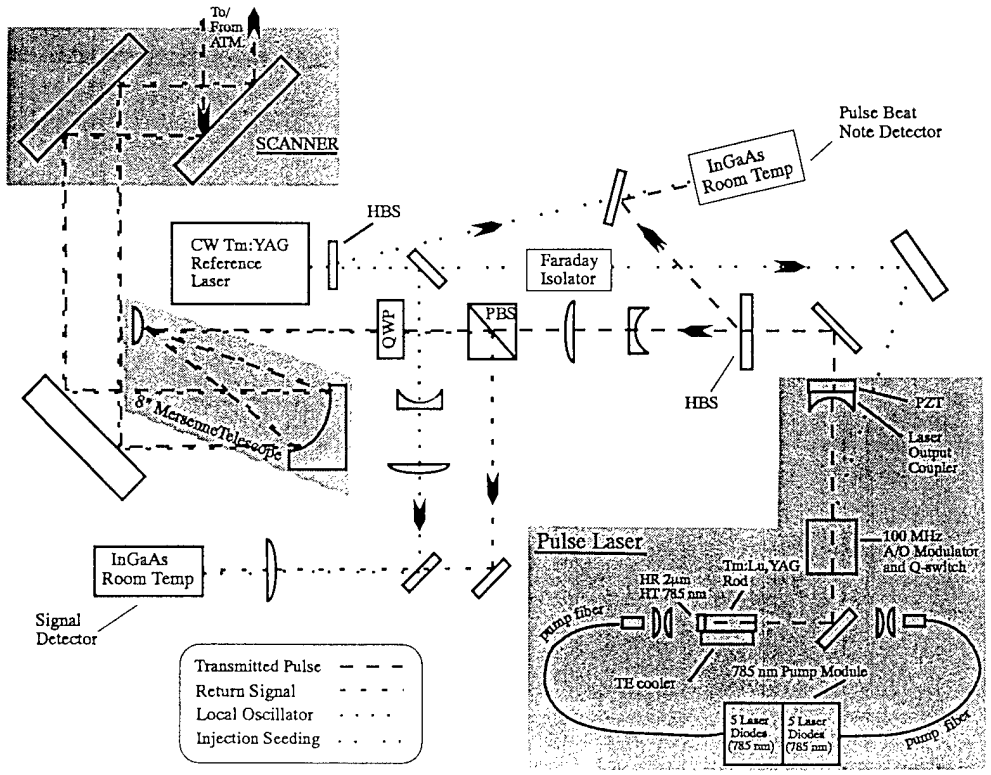

Fig. 1 Simplified schematic of the NOAA 2-μm Tm:Lu,YAG coherent Doppler lidar system (WP = wave plate, Q = 1/4, H = ½, BS = beam splitter, HBS = holographic beam splitter, PBS = polarization beam splitter, DBS = dichroic beam splitter.

Dual-rod Cr:LiSAF oscillator/amplifier for remote sensing applications

James W. Early, Charles Lester and Nigel J. Cockroft
Chemical Science and Technology Division
Los Alamos National Laboratory, MS E535
Los Alamos, NM 87545
505-667-3305, FAX 505-665-4637
cockroft@lanl.gov

Christyl Johnson and Donald Reichle
NASA Langley Research Center
Hampton, VA 23681
804-864-1553, FAX 804-864-8809

David W. Mordaunt
Stratonics, Inc.
4 Jenner Street, Suite 190
Irvine, CA 92718
714-727-1895, FAX 714-727-1742

Chromium-doped LiSAF has many attributes desirable for remote sensing LIDAR applications. The broad tunability (0.78-1 μm) [1-2], especially in combination with nonlinear harmonic generation, has broad potential for species specific measurement techniques. A long fluorescence lifetime (67 μsec) enables good energy storage and high Q-switched pulse energy output for long range LIDAR measurement. Broad absorption bands in the red, blue and UV enable very efficient coupling of both flashlamp excitation and 670 nm diode-laser pump energy. We have been developing the flashlamp-pumped, tunable Cr:LiSAF laser system for lidar applications. Recent demonstrations using dual-lamp excitation of a single laser rod have achieved average power output of 11 Watts with pulse energy exceeding 3 Joules for long pulse (20-30 μsec) and Q-switched pulse energies of 0.45 J (23 nsec) [3]. The system has been used to perform high quality water vapor DIAL measurements and metal ion fluorescence measurements. The configuration giving the highest quality results was a Littman grating cavity design that provided continuous tunability over 100 nm with a linewidth of 2 GHz [4].

One of the difficulties experienced in the LiSAF development experiments has been the occurrence of thermally-induced microstructure damage at an average electrical power to the lamps of 450 W (for a 0.6 x 10 cm rod). Results to date led us to conclude that the intrinsic thermo-mechanical limitations of LiSAF can best be overcome by the use of a dual-rod gain configuration. We report results of the evaluation of a dual rod design for both amplifier and oscillator applications.

Dual-Rod Amplifier

To demonstrate the feasibility of long range temperature measurement using Cr:LiSAF-based water vapor DIAL, we performed the integration of a diode-pumped Cr:LiSAF oscillator with a dual-rod, double-pass, flashlamp-pumped amplifier. The oscillator was successfully injection seeded by a tunable diode laser with linewidth of less than 2 MHz. A single birefringent plate filter was used in the cavity to center the gain curve on water vapor lines around 820 nm. The Q-switched output from this laser was double-passed through a 0.25 inch x 10 cm long rod and a 7 mm x 10 cm long rod. Each rod was pumped with dual Xenon flashlamps driven by a 60 μsec (FWHM) electrical pulse.

Figure 1 shows the gain achieved for the amplifier as a function of electrical pump energy delivered to each of the two pump heads. For example, a gain of approximately 120

corresponded to an input energy from the oscillator of 0.14 mJ and an amplifier output of 17 mJ. Saturation of the amplifier gain was not observed up to 0.5 mJ, the highest oscillator energy evaluated. The gain determined from these experiments was 0.27 cm^{-1} at the 75 J excitation level. This result significantly exceeds the previously reported level of 0.12 cm^{-1} for 100 J excitation. A possible explanation for the increased gain is improved material quality and improved optical coupling to the 7 mm LiSAF rod relative to the previously studied 0.25 inch diameter rods. The oscillator experiments described below support this conclusion.

Dual-Rod Cr:LiSAF Oscillator

The 1.5% Cr doped, 0.25 inch and 7 mm diameter rods were also configured in a linear oscillator cavity of length 61 cm, with a 1.5 m radius of curvature high reflector and a flat dielectric output coupler. Figures 2a and 2b compare the laser performance of each of the two heads operating separately in this configuration. The 0.25 inch diameter head performance is characteristic of the best previous results. The 7 mm head results clearly exceed this performance and demonstrate a record low threshold of 15 J pump energy and a record slope efficiency of 7.9%.

Figure 3 shows the output characteristics of this configuration as a function of electrical energy delivered to both heads simultaneously. As expected, for a given input energy level, the output energy exceeds the sum of the output for the two heads when operating separately. For example, an output greater than 3 J per pulse was obtained for pump energies of less than 50 J per head. The primary purpose for considering the dual-rod design was to enable an increase in the pulse repetition rate of the laser without thermally damaging the LiSAF rods. Details will be presented of successful demonstrations of 16 W output at 10 Hz while exciting each rod with 290 W of pump power, well below the 450 W damage limit. An average power of 7.8 W was achieved at 20 Hz. Significantly higher output powers are expected at high PRFs for configurations with lower output coupling.

References

1. M. Stalder, B. H. Chai and M. Bass, Appl. Phys. Lett. **58**, 216 (1991).
2. T. Ditmire and M. D. Perry, Opt. Lett. **18**, 426 (1993).
3. T. Shimada, J. W. Early, C. S. Lester and N. J. Cockroft, OSA Proceedings on Advanced Solid-State Lasers, T. Y. Fan and B. H. Chai, eds., Vol. 20, p. 188 (1994).
4. J. W. Early, C. S. Lester, c. R. Quick, J. J. Tiee, T. Shimada and N. J. Cockroft, Technical Digest on Advanced Solid-State Lasers (OSA), paper MB1-1, Memphis, TN, 1995.

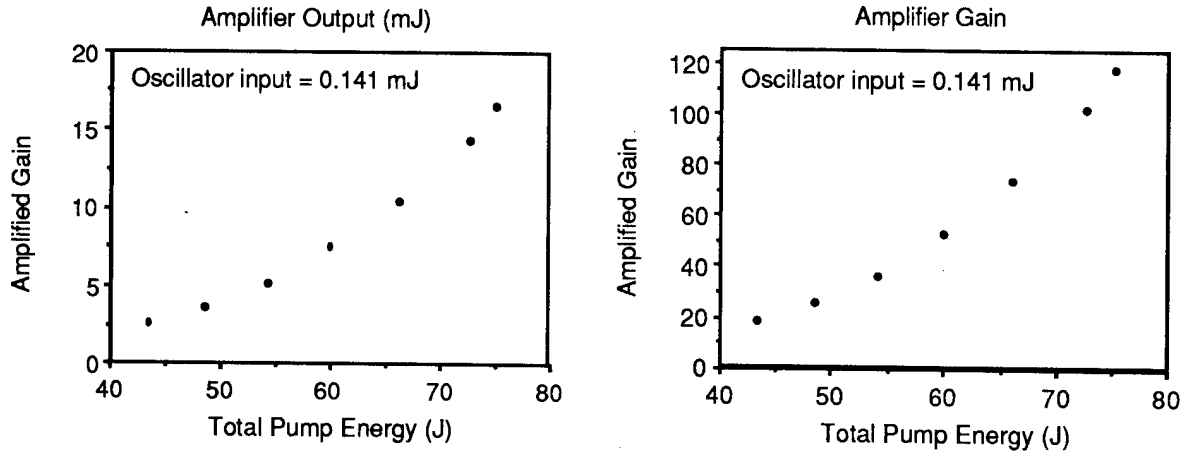

Figure 1. Double-pass amplifier output and gain as a function of electrical pump energy for a constant oscillator input of 0.141 mJ.

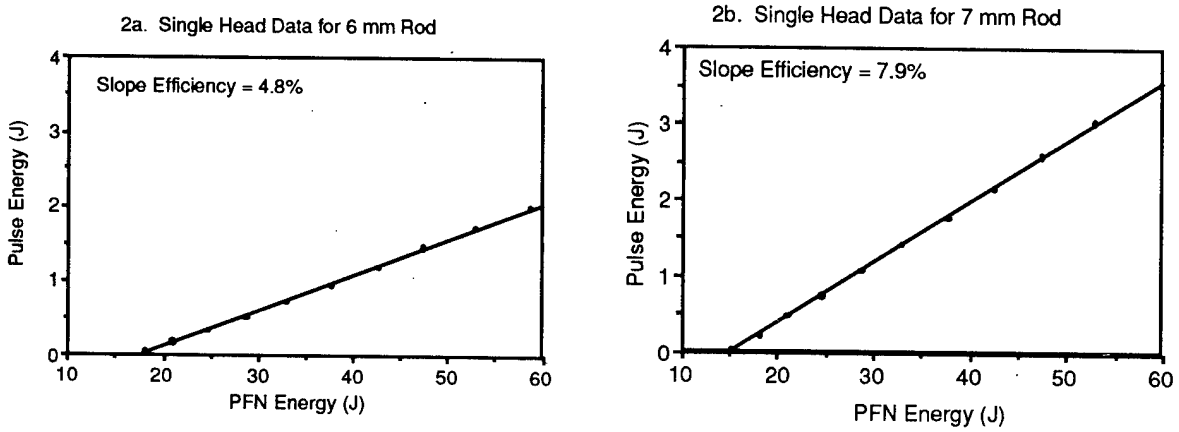

Figure 2. Oscillator performance for each of the two heads operating separately.

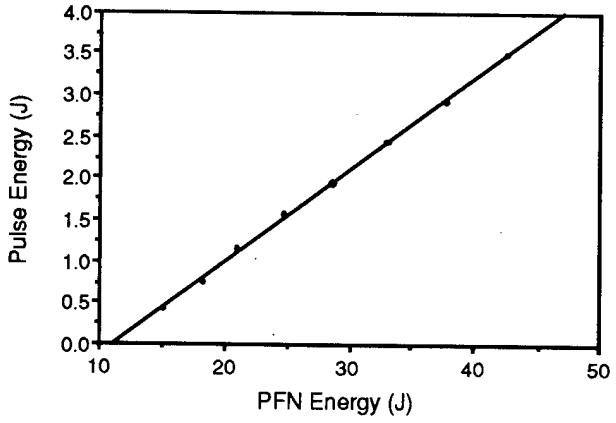

Figure 3. Output energy of the dual-rod oscillator as a function of pump energy per head.

Yb^{3+},Er^{3+} Codoped Materials for Planar Optical Waveguide Amplifiers

Markus P. Hehlen, Timothy R. Gosnell, Nigel J. Cockroft
Los Alamos National Laboratory, Mailstop E535, Los Alamos, NM 87545.

Allan J. Bruce, W.H. Grodkiewicz, Gerry Nykolak,
Joseph Shmulovich, Ruby Ghosh, M.R.X. Barros
AT&T Bell Laboratories, 600 Mountain Ave., Murray Hill, NJ 07974.

The superb performance of silica optical fibers and Er^{3+} doped fiber amplifiers (EDFA) led to a revolution of high-speed telecommunication in the last decade.[1] In long-distance networks amplification is required to compensate for signal attenuation and losses in the silica fiber, and with the use of Er^{3+} all-optical rather than electro-optical amplification can be achieved.[2] The Er^{3+} energy-level structure permits pumping of the $^4I_{9/2}$ excited state around 980 nm by high-power semiconductor lasers and subsequently the $^4I_{13/2}$ state is populated by multiphonon relaxation. In a predominantly radiative transition this state relaxes to the $^4I_{15/2}$ ground-state multiplet by emitting around 1.55 μm, a wavelength which matches the low-loss wavelength region of silica fibers. Significant inhomogenous broadening of the optical transitions in the disordered glass host allows wavelength multiplexing, and it is possible to operate several channels with different wavelength at multi gigabit per second rates in a single fiber link. EDFA's consist of various components including several meters of doped fiber, splitters, multiplexers, filters, and pump lasers, typically resulting in a bulky and costly device. Although not inhibitive for main trunk optical data networks these drawbacks hinder the realization of fiber-to-the-home. Today, individual consumers are still linked by conventional copper-wire technology which involves low-speed, service-intensive, electronic components creating bottlenecks in the overall data capacity. Planar optical waveguide amplifiers (POWA) on the other hand may solve these problems and provide complete optical transparency of the telecommunication networks. As shown in Figure 1, all of the components of an optical amplifier can be incorporated on a single chip using silicon optical bench technology. The resulting device is more cost effective and enables the miniaturization needed in future consumer applications.

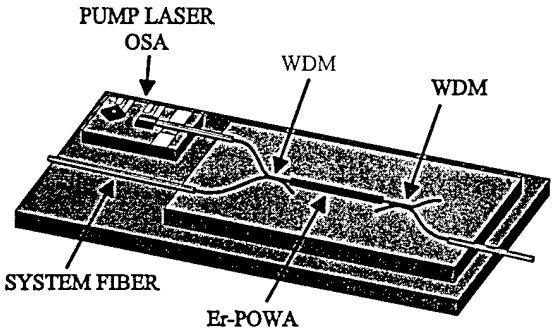

Figure 1: Conceptual design of a Er^{3+} POWA module which integrates all of the components on a small silicon chip.[3]

Integrating an Er^{3+} doped waveguide material on a small silicon chip requires a reduction of the amplifier length by about two orders of magnitude relative to a typical EDFA. As a consequence, ion densities have to be substantially increased in order to still maintain sufficient absorption of pump light over the short POWA. This can be achieved by increasing the Er^{3+} concentration, an approach which however is limited by the onset of ion-ion interactions at higher dopant concentrations. In contrast to a typical EDFA doped at ~200 ppm, the Er^{3+} ions in a highly doped POWA can no longer be regarded isolated. Processes such as upconversion and energy migration to defects with subsequent multiphonon relaxation lower the quantum yield of the 1.55 µm emission and thus degrade amplifier performance (Figure 2). Alternatively, the Er^{3+} ion can be sensitized by Yb^{3+} which also absorbs around 980 nm and the $^2F_{5/2}$ state of which can efficiently transfer its excitation to the $^4I_{9/2}$ (Er^{3+}) state. As shown in Figure 3, the absorption profile of Yb^{3+} is not only considerably broader than the one of Er^{3+}, offering much higher flexibility in the selection of the pump laser, but also the Yb^{3+} peak absorption coefficient is about an order of magnitude greater, allowing pump-light absorption over a short path length.

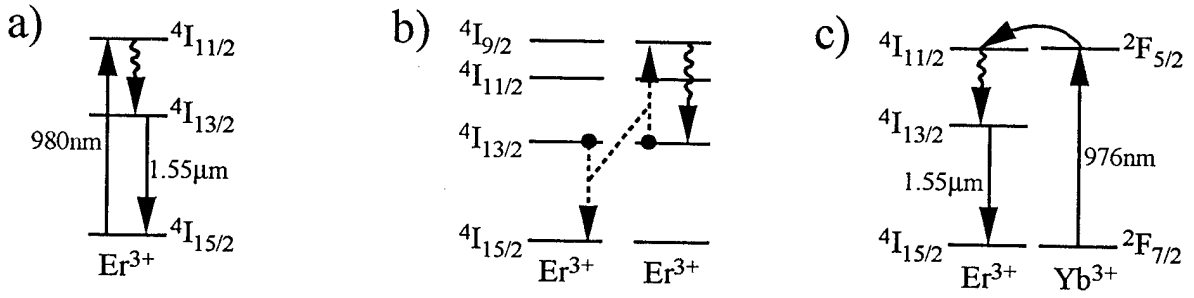

Figure 2: a) Direct excitation of $^4I_{9/2}$ (Er^{3+}) and subsequent multiphonon relaxation to $^4I_{13/2}$. b) Two-ion processes quenching $^4I_{13/2}$ population. c) Yb^{3+}-Er^{3+} codoped system using Yb^{3+} excitation followed by Yb→Er energy transfer.

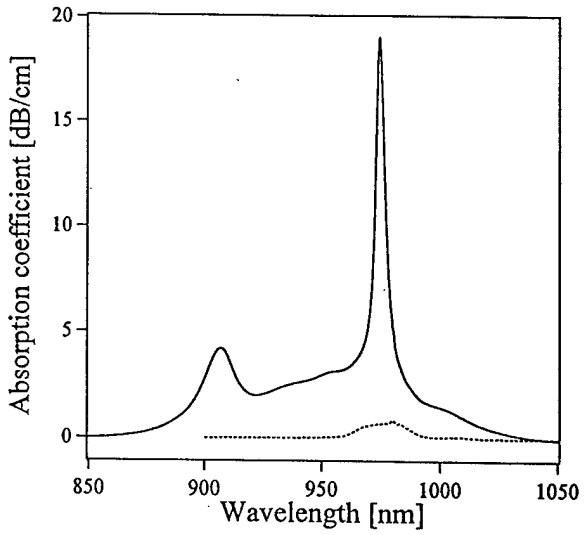

Figure 3: Room-temperature absorption spectra of a 0.4%Er^{3+} doped (dashed) and a 0.4%Er^{3+}, 0.8%Yb^{3+} codoped (solid) sodalime glass.

A codoped POWA relies on a sequence of nonradiative processes between pump-light absorption by Yb^{3+} and 1.55 μm emission by Er^{3+}. $^2F_{5/2}$ excitations created on Yb^{3+} ions have to migrate through the Yb^{3+} sub-lattice, to be transferred to the $^4I_{11/2}$ state of Er^{3+}, and finally to relax to the $^4I_{13/2}$ emitting state (Figure 2c). Relaxation to the $^4I_{15/2}$ state, providing 1.55 μm gain, is found to be predominately radiative (Figure 4). The correlation between the decay of $^2F_{5/2}$ (Yb^{3+}) population and the rise of $^4I_{13/2}$ (Er^{3+}) population is shown in Figure 5 indicating the existence of this sequence of energy-transfer processes. Various factors such as glass composition, ion densities, and phonon properties contribute to the overall efficiency of these energy transfer steps.

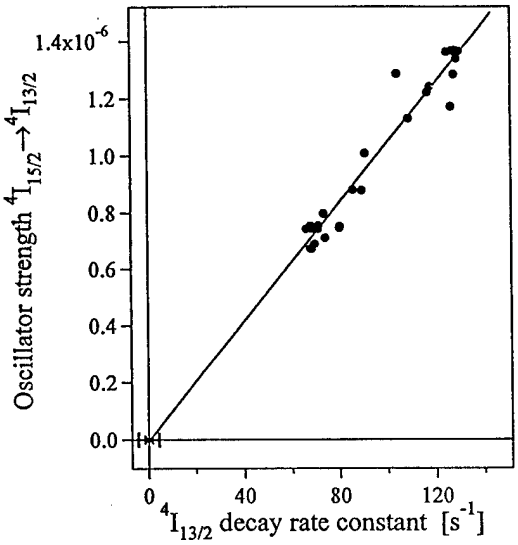

Figure 4: $^4I_{15/2}\leftrightarrow{}^4I_{13/2}$ oscillator strength versus $^4I_{13/2}$ room-temperature lifetime for a series of Er^{3+}-doped silica-based glasses. The zero x-axis intercept of the linear fit shows the unimportance of multiphonon relaxation processes from $^4I_{13/2}$.

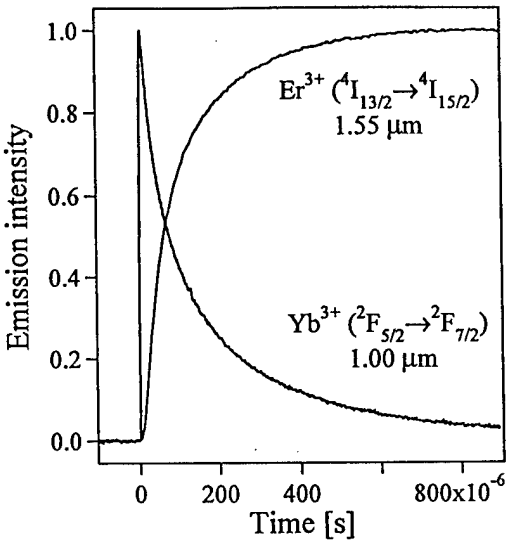

Figure 5: Comparison of the $^2F_{5/2}$ (Yb^{3+}, 1 μm) decay and $^4I_{13/2}$ (Er^{3+}, 1.55 μm) rise dynamics in a 0.4% Yb^{3+}, 0.4% Er^{3+} doped sodalime glass at room temperature.

In this paper we present the results of a spectroscopic characterization of an extensive series of glass samples. The study includes the concentration dependence of erbium quantum yields both in Er^{3+} and Yb^{3+}-Er^{3+}-codped silica-based glasses, the relevance of pump-induced heating effects and the power dependence of energy transfer and annihilation effects.

1 P. Cochrane, R. Heckingbottom, D. Heatley, Opt. Phot. News **8**, 15 (1994).

2 E. Desurvire, *Erbium-Doped Fiber Amplifiers*, John Wiley, New York 1994.

3 J.V. Gates, A.J. Bruce, J. Shmulovich, Y.H. Wong, G, Nykolak, M.R.X. Barros, R. Ghosh, Proc. MRS, 1995, *in press*.

Far infrared p-Ge laser: Temperature dependent laser dynamics

Kijun Park, [1, 2] Robert E. Peale, [3, 1] Henry Weidner, [3] Jin J. Kim [1, 3, 2]

Center for Research and Education in Optics and Lasers (CREOL) [1]
Department of Electrical & Computer Engineering, [2] Department of Physics [3]
University of Central Florida, Orlando, Florida 32816-2700
(407)823-3076 (V), (407)823-5112 (F), rep@physics.ucf.edu

Lasing in p-Ge is based on transitions between light and heavy hole bands at ~100 μm wavelengths. An electric field accelerates holes to regions where light and heavy hole energies are non-degenerate, and a perpendicular magnetic field prevents inelastic phonon scattering for the light holes only, giving rise to population inversion. Fig. 1 demonstrates the suitability of our instrumentation for measuring radiation in the 70 to 130 μm region. Fig. 2 presents a schematic of our new idea, a permanent magnet in Voigt geometry. Fig. 3 presents the emission intensity over more than 4 decades vs. E and B fields for a p-Ge laser using the traditional superconducting magnet in Faraday geometry. In Fig. 4, the intensity using our Voigt configured permanent magnet clearly shows the sharp threshold behavior for the lasing onset. Fig. 5 shows emission intensity and electric-pulse dynamics and reveals a 2 μs delay for the lasing onset and an ~80 ns rise time. Fig. 6 shows that the beam profile is Gaussian. Fig. 7 presents the temperature dependence of the peak intensity for temperatures below 4.2 K for the first time. A surprising observation is the steep decrease below 1.8 K, which is similar to features in the thermal conductivity and specific heat of liquid helium. Fig. 8 shows that the lasing-onset delay is temperature dependent but that the quench dynamics are temperature independent. The repetition rate data in Fig. 9 indicate a ~30 ms thermal time constant for the Ge rod, so that a simulation of Joule heating on μs time scales may neglect cooling. The results of this simulation are displayed in Fig. 10 and explain much of the temperature dependence in the pulse dynamics. A complete description of effects and modeling will be presented.

FIGURE CAPTIONS

Fig. 1. Cryostat window transmission spectra. The responses of two different detectors are shown. For the bolometer, the long pass filters (LPF) used are indicated.

Fig. 2. Schematic of the laser with a Voigt configured permanent magnet. For the top view, the directions of the magnetic- and electric-fields applied to the sample, and the propagation vector of the emission are shown.

Fig. 3. Output intensity as a function of electric and magnetic fields for a p-Ge laser in Faraday configuration using a superconducting magnet.

Fig. 4. Output intensity as a function of electric field for a p-Ge laser using a Voigt-configured permanent magnet.

Fig. 5. Typical temporal shapes of laser pulse, voltage, and current at 4 K.

Fig. 6. Beam profile measured 93 mm from the face of the p-Ge rod. The sample temperature is 4 K. The solid line is a Gaussian fit to the data.

Fig. 7. Temperature dependence of lasing. Open circles show the emission detected by a Si-composite bolometer. The dashed lines show the specific heat and the solid line shows thermal conductivity of liquid helium.

Fig. 8. Temperature dependence of the temporal behavior of the laser output. The Ge:Ga detector was used. Initial sample temperatures were 1.9, 2.1, 2.3, 2.5, 3.2, 3.5, 3.8, 4.0, 4.2, 4.4, 4.8, and 5.1 K, respectively. The large arrow emphasizes the common time when the lasing is quenched.

Fig. 9. Output intensity versus repetition rate for Faraday and Voigt geometry at 4 K.

Fig.10. Simulation of Ge lattice temperature rise under Joule heating with no cooling. Initial lattice temperatures are between 2 K and 9 K. The large arrow indicates the common time when the lasing is quenched. The E-field turns off at 3.7 μs.

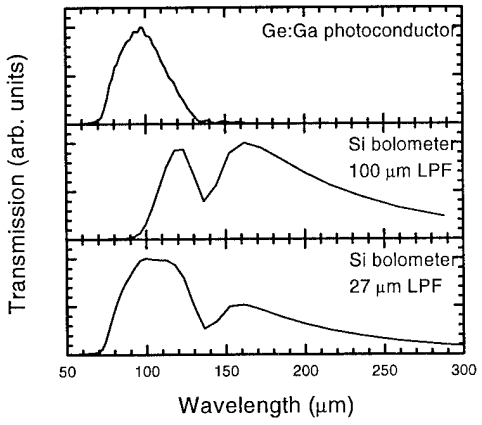

Fig. 1.

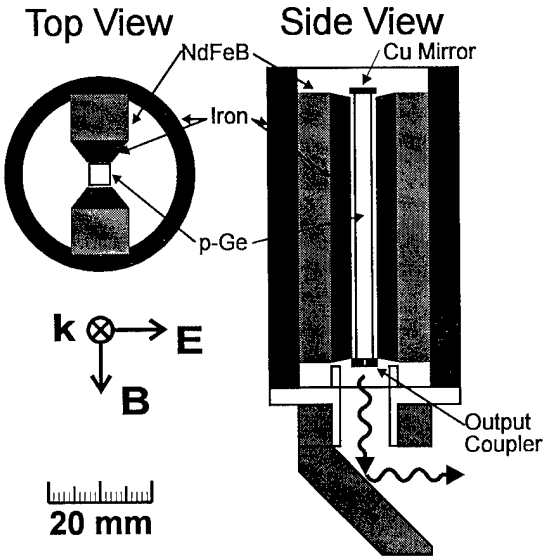

Fig. 2.

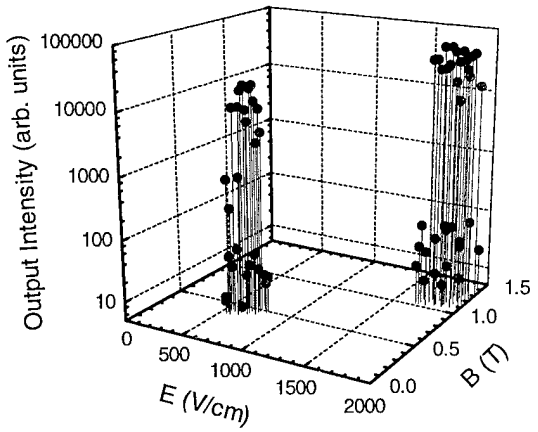

Fig. 3.

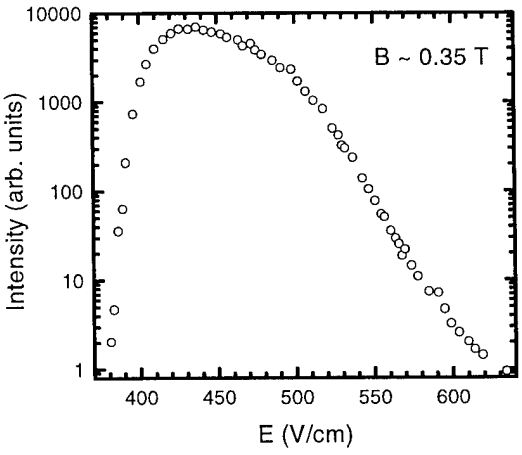

Fig. 4.

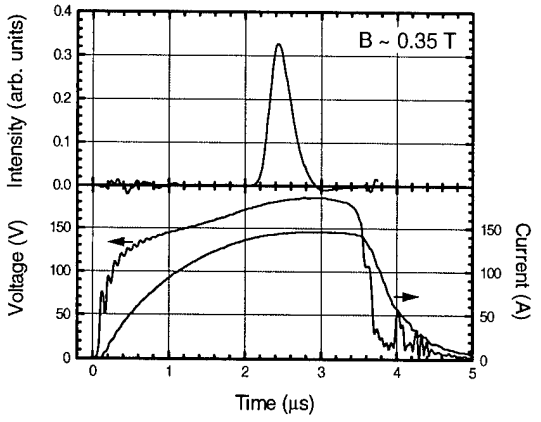

Fig. 5.

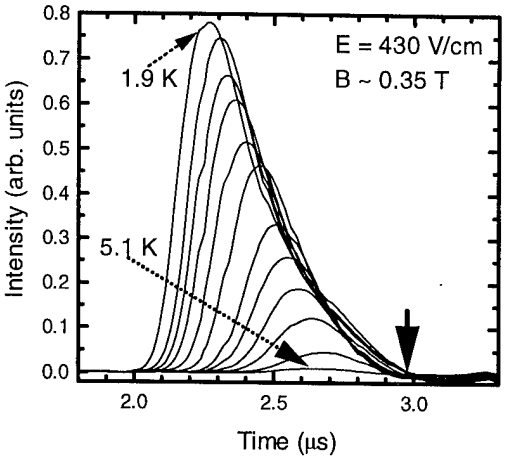

Fig. 8.

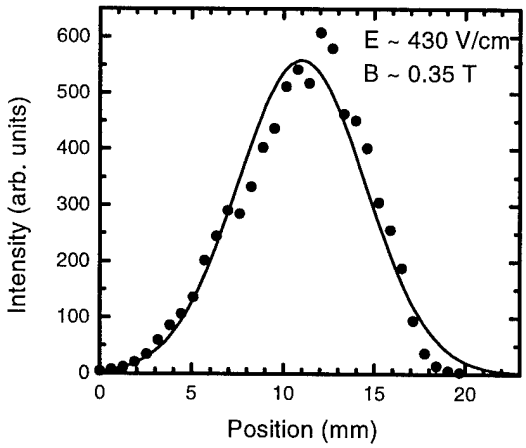

Fig. 6.

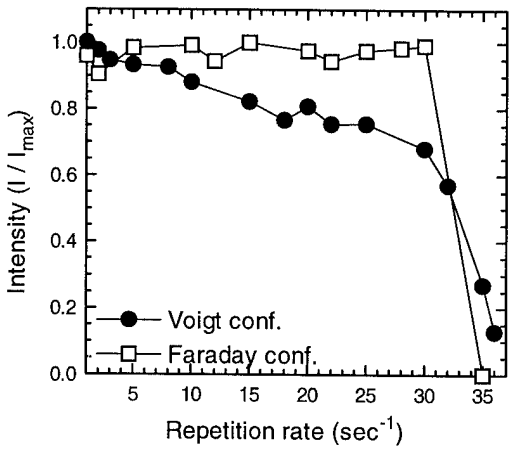

Fig. 9.

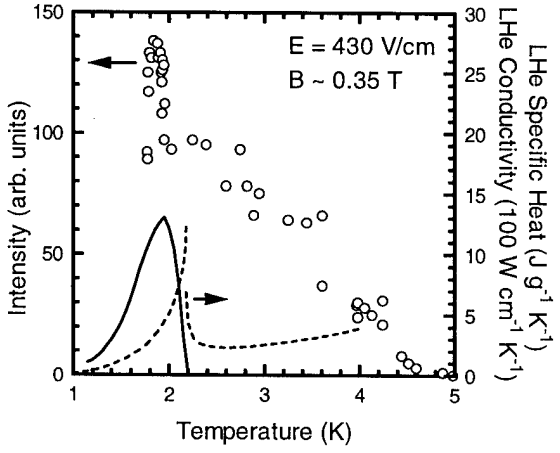

Fig. 7.

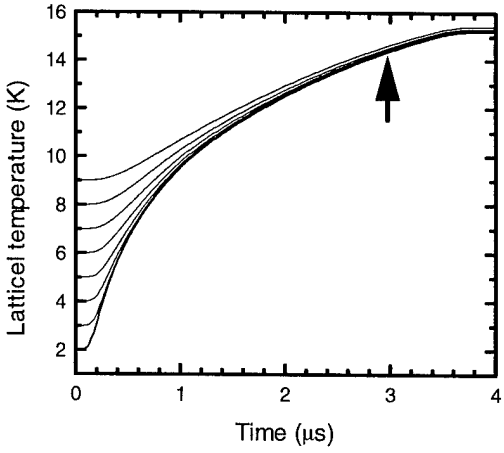

Fig. 10.

Phase conjugator of the light beams based on Nd:YAG-rod with the reciprocal feedback.

O.L. Antipov , S.I. Belyaev and A.S. Kuzhelev

Applied Physics Institute of the Russian Academy of Science

603600, 46 Uljanov Str., Nizhny Novgorod, Russia.

Tel.: 8312364068 ; Fax.: 8312363792

The effect of self-pumped phase conjugation (SPPC) of the light beam in the inverted laser crystal (LC) by the parametric generation in the scheme with the feedback loop (FL) has been investigated last years. Two possibilities of SPPC have been studied: the first process is the generation of PC-wave in the resonator with the "holographic" mirror induced in the interference field of mutually-coherent pumping waves (the incident pump and the one passing through FL) in LC [1]; the second process is the simultaneous scattering of the pumping waves in LC with FL [2]. Both schemes require the amplitude and phase nonreciprocity of FL, that makes the experimental setup more complicated.

In this report we present, in the first time, the investigations of SPPC in the inverted Nd:YAG-rod with reciprocal FL.

In our experiments the multi-longitudinal mode beam (having the frequency band about $0.02\,cm^{-1}$) of Nd:YAG-laser with the pulse duration about 0.65 ms after passing through the polarization isolator was directed into the flash-lamp pumped Nd:YAG-rod with the FL-scheme (Fig.1).

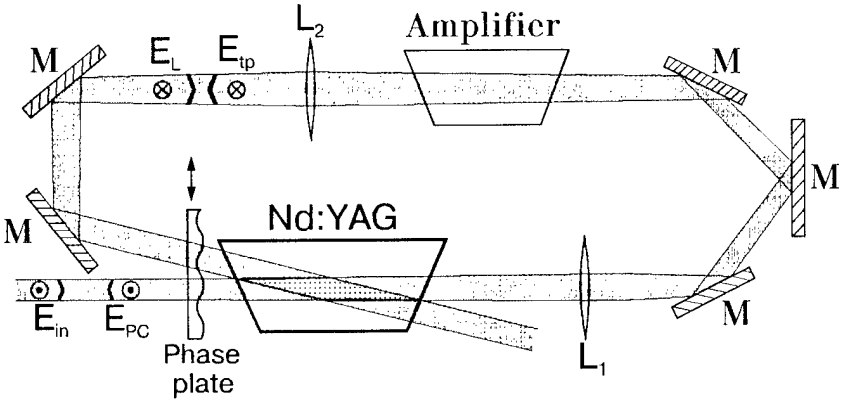

Fig 1. Experimental scheme. E_{in} - input pump, E_{tp} - transmitted pump, E_L - luminescence wave, E_{PC} - phase conjugated wave; Nd:YAG - inverted crystal rod; M- mirrors, L- lenses.

We observed generation of the PC-beam having the same polarization as the input pump polarization (the depolarized component was about 6%). The experiments showed the generation threshold both for the pumping wave intensity and the gain of the "nonlinear" rod. This threshold decreased with increasing of the amplification coefficients in the feedback loop .

The quality of the phase conjugation measured as the ratio of the power generated backward to the pump at the 1.2..1.5 PC-beam diffraction limit to all the backward propagating power (at the 25..30 diffraction limit) achieved the value 0.7..0.8 in the experiments with the input speckled beam.

The theoretical investigation shows that the nonreciprocities of FL for the realization of SPPC by the saturation of the resonant transition in inverted LC is not necessary when there is a real part of resonant susceptibility. In this case the refractive index grating of inverted LC is induced by the increasing of the population relaxation in the interference field of the optical waves. The simultaneous scattering of the intersecting pumps by the refractive index grating give the scattering waves which haves the complex amplitude conjugated to the backward propagating pumps. As a result, the wave phase conjugated to the input pump is generated.

The estimation of the generation threshold shows that in our experimental scheme the SPPC in the reciprocal scheme can be realized when the real part of the polarizability is by 10 times greater than its imaginary part.

The ratio was measured experimentally. For this goal the beam of the He:Ne laser was launched into the amplifier . The refractive index changing was registered by the movement of the interference field of rod-end reflections during the optical pumping of the Nd:YAG-rod. The measured ratio of the real and imaginary parts of the polarizability was about 10..15. This fact confirms our theoretical estimations.

Thus, we realized the SPPC of the laser beams in the inverted Nd:YAG-rod with reciprocal FL. The advantages of such a phase conjugator are the low generation threshold, the high reflection coefficient and the possibility to operate with high average power laser beams having a wide frequency band.

1. M.J.Damzen,R.P.M.Green,G.J.Crofts, *Opt. Lett.*,**19**, (1994), 134.

2. O.L.Antipov, S.I.Belyaev, A.S.Kuzhelev, *JETP Let.*, **60**, (1994), 165.

Fundamental studies of a pulsed high gain Nd:$YV0_4$ amplifier

P. Dekker , J.M. Dawes and J.A. Piper
Centre for Lasers and Applications, School of Mathematics, Physics, Computing and Electronics
Macquarie University, North Ryde, NSW 2109, Australia
Phone: 61-2-8508911, Fax: 61-2-8508983
email: dekker@macadam.mpce.mq.edu.au

Introduction

In recent years much attention has been directed towards the high gain laser crystal Nd:YVO_4, due to its strong polarised absorption and large emission cross section. This is most effective with end pumped microchip style lasers, where slope efficiencies as high as 50 % [1] are typical. Transversely pumped Nd:YVO_4 has also been demonstrated previously [2,3], with single pass gains as high as 1500 when the crystal was pumped by a 60 W quasi-cw laser diode. The high gain available effects the temporal characteristics of the output pulse, [4]. Here we present a system, portrayed in Fig 1, combining the best attributes of both geometries, using a high gain transversely pumped Nd:YVO_4 crystal to amplify a Q-switched end pumped Nd:YVO_4 oscillator. Our best performance to date at 10 Hz is 150 μJ pulse energy with a 6 ns pulsewidth.

End Pumped Nd:YVO_4

The oscillator cavity consists of a 2 % Nd doped Nd:YVO_4 crystal (1 x 3 x 3 mm), an acousto-optic q-switch and a separate output coupler (2.5 cm RoC, 15 % T). A maximum diode pump power of 415 mW (after delivery optics) is focussed to a spotsize of 100 μm at the face of the crystal. Without the q-switch the maximum cw TEM_{00} output power of 190 mW at 1.06 μm, with a slope efficiency of 45 %, is attained, typically with 2 axial modes. Single frequency output of 150 mW is achieved by slightly adjusting the cavity length [5], typically 2 cm. Q-switched operation using an acousto-optic modulator gave pulse energies and pulsewidths of 2.4 μJ and 6 ns respectively at pulse repetition frequencies up to 10 kHz.

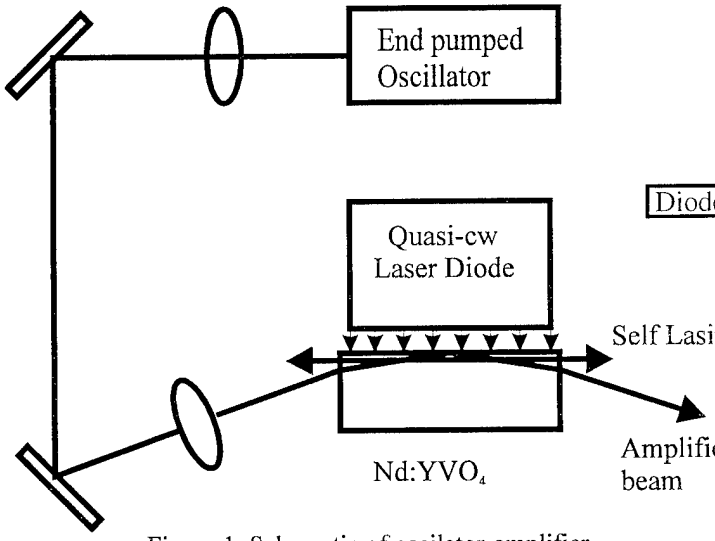

Figure 1 Schematic of oscilator-amplifier

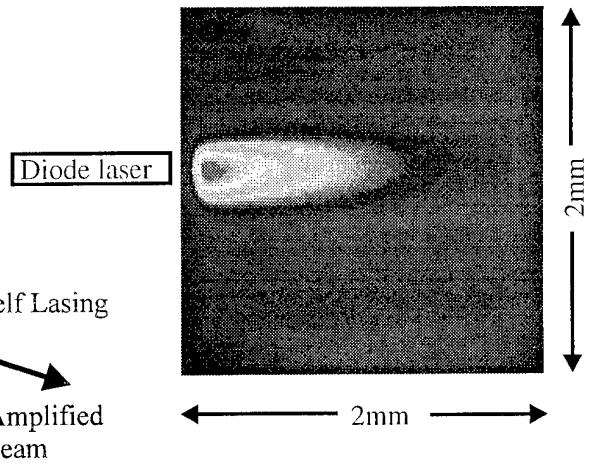

Figure2 Image of ASE in slab

Transversely Pumped Nd:YVO_4

The transversely pumped Nd:YVO_4 slab (2 x 2 x 10 mm) has been operated as an oscillator as well as an amplifier. The slab was pumped by a 80 W (16 mJ) quasi-cw laser diode array which was butted up to the laser crystal, with a minimum separation between the laser diode and the Nd:YVO_4 crystal of 184 μm. At 1 % Nd concentration, the absorption at the pump wavelength (808 nm) is 8 cm^{-1} for the a axis of the crystal. In an oscillator configuration with a short plane parallel cavity the output is very assymetrical largely determined by the strong gain at the pump face and the diffraction at the crystal ends. A maximum long pulse energy of 3.8 mJ at 1.06 μm has been obtained from this resonator. In fact the gain is sufficiently that the reflections from the ar coated crystal ends support laser oscillation. To overcome this unwanted oscillation the laser diode was rotated by an angle of 5° with respect to the crystal. To improve the beam quality Bernard et al designed their oscillator such that the oscillating beam makes a single reflection off the pump face of the Nd:YVO_4 laser crystal. This tends to circularise the beam as the diffraction at the crystal ends balances the tendency for the gain to stretch the mode [2,3]. We used the same approach with our oscillator-amplifier combination.

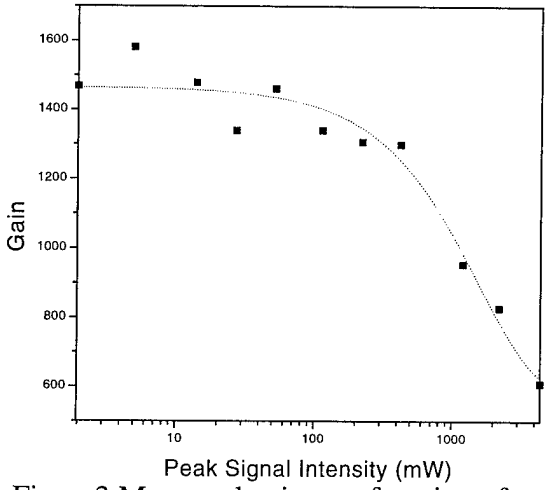

Figure3 Measured gain as a function of input peak power

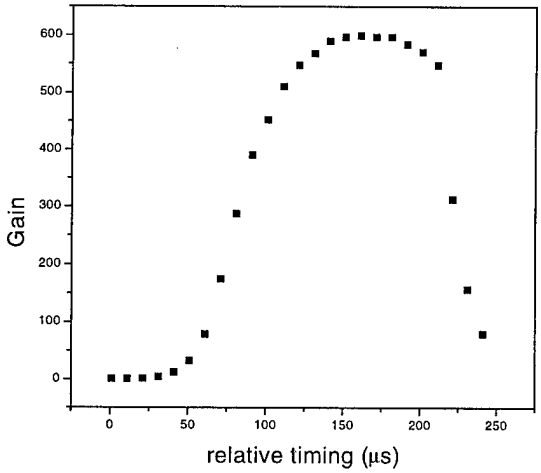

Figure4 Measured gain during amplifier pump pulse

Measurement of Gain and ASE

The spatial distribution of the gain and ASE were recorded by a CCD array. The gain distribution was measured by illuminating the entire amplifier crystal with a cw Nd:YVO_4 laser and recording the image with and without transverse diode pumping. The ASE was also recorded, shown in Fig 2, with maximum pump power absorbed by the Nd:YVO4 crystal and with the diode as close to the laser crystal as possible. The distribution of the gain can be adjusted by tuning the pump wavelength around the absorption peak to change the gain depth and by moving the pump diode away from the laser crystal to change the width. The smallest $1/e^2$ gain distribution was measured to be 300 x 700 μm. Fig 3 shows the measured gain in the slab as a function of the input signal peak power/pulse energy. Temporal studies of the gain, such as in Fig 4, show that the average gain is reduced near the end of the pump pulse where high ASE is present. The gain was measured by changing the timing between the q-switched pulse and the amplifier pump. Fig 5 shows the temporal behaviour of the ASE generated by the amplifier over the period of the pump for different diode-slab separations.

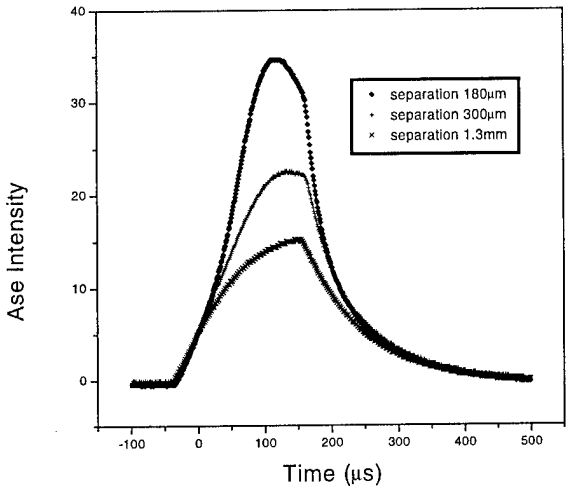

Figure5 ASE intensity during pump pulse for different diode-slab separations

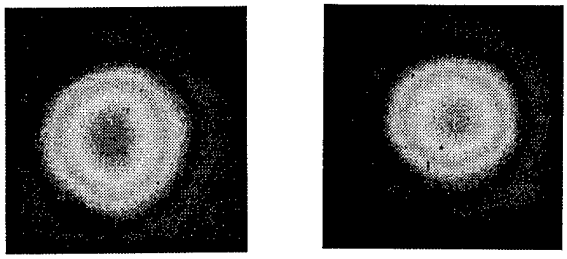

Figure 6 Beam profiles of the oscillator and amplifier (right).

Oscillator-Amplifier Characteristics

The arrangement is shown in Fig 1. Initial experiments were performed at a repetition frequency of 10 Hz, with the quasi-cw diode at max power of ~80 W, pulsewidth of 200 µs. A maximum small signal single pass gain of 1600 was measured in this system. At our maximum probe energy the gain has been reduced to 150, resulting in an amplified pulse energy of 150 µJ and pulsewidth of 6 ns. A much larger signal intensity is required to effectively remove all the stored energy. The spatial profile and indeed the gain are also a function of the angle, diameter and divergence of the probe in the amplifier. With a small diameter, well collimated signal beam the gain can be maximised by reducing the probe angle until diffraction becomes noticeable on the output. Examples of the beam profiles of the oscillator and amplifier are shown in Fig 6. These are not noticeably affected by thermal gradients in the crystal at 10Hz repetition rate.
The effect of the self lasing noted in the previous section is to reduce the amplified energy by approximately 25%. While this depends on the angle of the probe, it can be prevented by tilting the diode array with respect to the Nd:YVO_4 slab.

Conclusion

A q-switched end pumped single mode Nd:YVO_4 oscillator has been amplified using an transversely pumped Nd:YVO_4 slab. A maximum gain of 1600 and pulse energy of 150 µJ were obtained. Temporal and spatial studies of the gain and ASE suggest that higher gain is possible as the gain is significantly depleted by the self lasing in the amplifier and by ASE. Further work on increasing the amplified repetition frequency and on a combination oscillator - amplifier contained on the same crystal is underway.

References

1. R.A Fields, M. Binbaum and C.L. Fincher, Appl. Phys. Lett. **51**, 1885-1886 (1987).
2. J.E. Bernard and A.J. Alcock, Optics Letters, Vol **18**, 968-970 (1993).
3. J.E. Bernard, E. McCullough, and A.J. Alcock, Optics Comm **109**, 109-114 (1994).
4. J.E. Bernard and A.J. Alcock, Optics Letters, Vol **19**, 1861-1863 (1994).
5. G.J.Kintz and T.Baer, IEEE J. Quantum Electron **26**, 1457-1459 (1990).

Conductively Cooled Diode-Pumped Slab Laser

A.D.Hays, N. Martin and R. Burnham

Fibertek, Inc.

510 Herndon Parkway

Herndon, VA 22070

Cooling is a primary concern for space based laser system. The use of fluid cooling with its coolant lines, pumps and potential for leaking makes this approach unsuitable for most space applications. Conductive cooling of the laser diode array and zig-zag slab is relatively simple since both components have flat surfaces which the heat generated may flow across. The zig-zag slab design also provides birefringence correction and two pass absorption for small pump mode volumes.

The oscillator is comprised of a Porro prism and flat 20 % R output coupler. A waveplate and KD*P Pockels cell are used to holdoff and Q-switch the cavity. Besides the Brewster faces of the slab a thin film polarizer is also required to spoil the cavity Q. Cavity length is minimized to produce the shortest pulselength possible. The 18 bounce Nd:YAG zig-zag slab is 2.0 mm thick. Approximately 80% of the incident pump energy is absorbed in the 4 mm total path length. Fifteen 1-cm quasi-cw laser diode bars operating in series pump the Nd:YAG slab. To confine the highly divergent pump light a quasi-collimating cylinder lens is placed between the facets and slab. The laser diode energy is confined to a stripe approximately 1 mm wide. A cross section of the pump head is shown in Figure 1. Since the pump volume does not fill the entire width of the slab, significant cylinder lensing is observed due to the nonuniform pumping. Originally the resonator employed two dielectric mirrors to form the cavity. Unfortunately this produced an extremely elliptical mode volume which made efficient extraction of the TEM_{00} mode difficult. When the back dielectric mirror was replaced with a Porro prism the fundamental mode output dramatically improved. Using the porro prism reduced the ellipticity of the beam to 1: 1.1 and increased the effective thermal lens focal length to greater than 10 m. Mode profile and energy per pulse does not change as the repetition rate is varied between 1 and 100 Hz. The repetition rate is limited only by the laser diode duty cycle.

The Q-switched output energy is 20 mJ at a laser diode drive current of 65 A for a 200 μsec pump pulse with lasing threshold occuring at 32 A. The laser diode array

threshold is approximately 22 A drive current. Pulse-to-pulse energy stability is approximately 3% RMS for operation over a one hour period. Small signal gain is 1.79 neper. Given the small signal gain g_0l, round trip loss L, and the cavity round trip time t_r, the theoretical pulselength [1] is given by:

$$\tau_p = \frac{t_r}{L}\left\{\left[\frac{\ln\left(\frac{2g_0l}{L}\right)}{\frac{2g_0l}{L}}\right]\left[\frac{1}{1-\left[\frac{\frac{2g_0l}{L}-1}{\frac{2g_0l}{L}\ln\left(\frac{2g_0l}{L}\right)}\right]\left[1+\ln\left[\frac{\frac{2g_0l}{L}\ln\left(\frac{2g_0l}{L}\right)}{\frac{2g_0l}{L}-1}\right]\right]}\right]\right\} = 4.3 \text{ nsec}$$

The pulselength is shown in Figure 2 and has a FWHM of 5 nsec. Calculation of beam quality using a lens and Spiricon CCD camera show the beam is 1.41 mm-mrad full diameter-full angle which is 1.05 times the diffraction limit of 1.35 mm-mrad.

Currently the oscillator is being tested with a similarly designed amplifier. Results obtained for the space qualified MOPA system will be discussed.

Reference

[1] John J. Degnan, "Theory of the Optimally Coupled Q-Switched Laser," IEEE J. Quant. Electr., vol. 25, pp. 214-220, 1989.

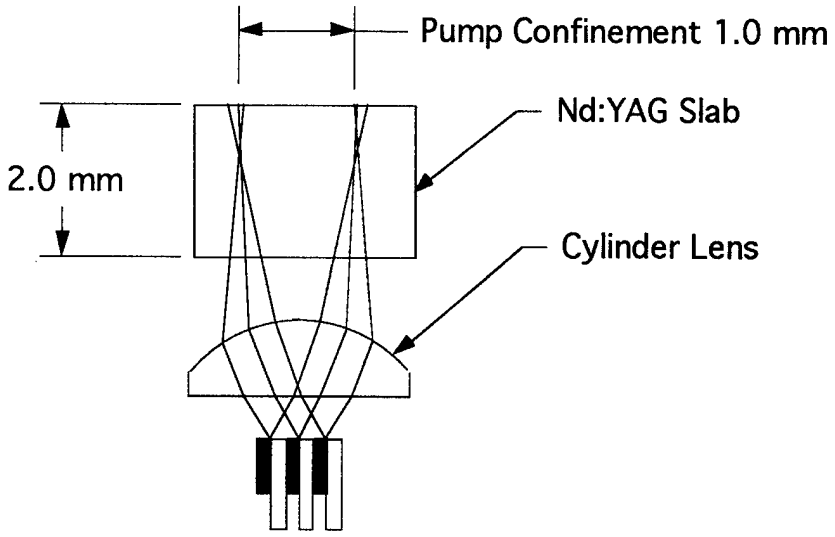

Figure 1. Cross section showing pump confinement using a cylinder quasi-collimating lens.

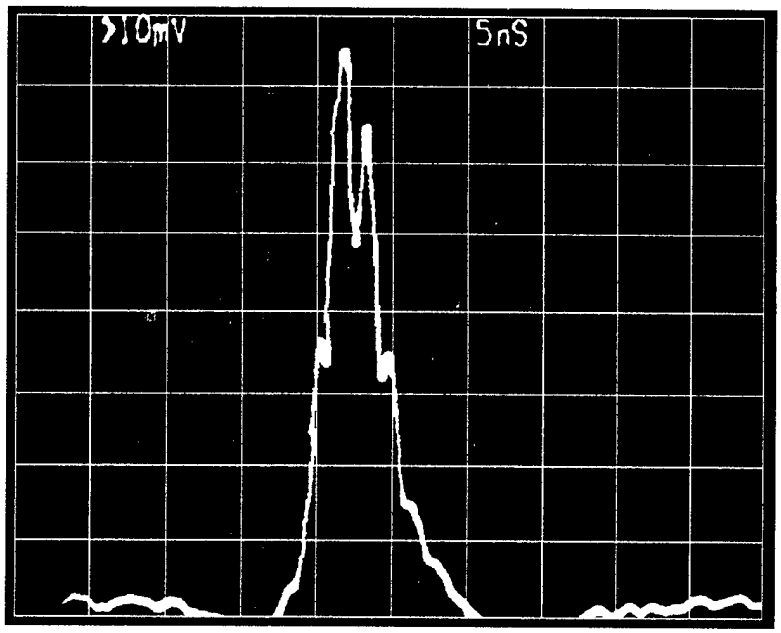

Figure 2. Q-Switched pulseshape with 20 mJ output energy at 50 Hz rep rate, 5 nsec/div

Tb^{3+} ion as a sensibilizer for rare-earth ions in a terbium trifluoride single crystal

M.A.Dubinskii and P.Misra
Laser Spectroscopy Laboratory, Department of Physics and Astronomy
Howard University, Washington, DC 20059, USA
Phone: (202)806-4913, FAX: (202)806-4429

B.N.Kazakov, A.L.Stolov and Zh.S.Yakovleva
Kazan State University
Kazan, Tatarstan 420008, Russia
Phone: (7-8432)318-716, FAX: (7-8432)-387067

The Tb^{3+} ion did not attract much attention of scientists involved in the search for new laser materials as a real laser-related ion, mostly due to the negative results of many efforts aimed at obtaining laser action from Tb^{3+}-containing single crystals in the past. In fact, only once have researchers succeeded in obtaining laser actin from Tb^{3+} itself [1]. There are two examples, though, of a successful application of Tb^{3+} as a donor-ion to sensibilize the fluorescence of other ions, some of them (e.g., Sm^{3+}) also being considered as the least prospective among the actinides in terms of obtaining laser radiation. In both cases concentration of Tb^{3+} ions in the laser crystals reached 100%. Thus, efficient sensibilization of Sm^{3+} ion by Tb^{3+} ion provided low-temperature (110-130 K°) orange $^4G_{5/2}$ - $^6H_{7/2}$ laser action at 593.2 nm from TbF_3: Sm^{3+} (0.3 at.%) single crystal with conventional flashlamp-pumping [2]. A high concentration of donor ions played a positive role in the above case, not only due to the fact that the high concentration itself helps to overcome the problem of low cross-sections (of the order of 10^{-21} cm^2) of absorption transitions characteristic of the Tb^{3+} ion, but also due to the significant concentration broadening of absorption lines, and besides, as supposed in [2], also due to a favorable changing of the donor-acceptor interaction parameters as the Tb^{3+} concentration increases. Efficient donor-acceptor interaction between the Tb^{3+} and Sm^{3+} ions also made possible the recent observation of room temperature orange CW $^4G_{5/2}$ - $^6H_{7/2}$ laser action at 605 nm from the $LiTbF_4$: Sm^{3+} (1 at.%) single crystal pumped by an Ar-ion 488 nm laser line [3]. The latter result, in fact, prompts one to reconsider the application potential of the Tb^{3+} ion by including the use of it as a sensibilizer for rare-earth ions (probably also other than only Sm^{3+}) for devising reliable CW Ar-ion laser linear frequency converters.

All of the above considerations stimulated our efforts to analyze the "sensibilization power" of Tb^{3+} ion - with respect to different rare-earth ions - in TbF_3: Re^{3+} (where Re^{3+} denominates any rare-earth ion) single crystal compounds. One can study donor-acceptor interactions either by changes in decay kinetics of the metastable donor state or by changes in the stationary fluorescence intensity in the presence of acceptor ions in the host. Our analysis was based on studying the metastable $^5D_4$ level fluorescence quenching by different Re^{3+} ions (from the Pr, Nd, Sm, Eu, Dy, Ho, Er, Tm, Yb sequence), as suggested by Van Vitert [4]. We have compared the quenching probabilities for the $^5D_4$ (Tb^{3+}) level for different doping ions in TbF_3. The probability of excitation transfer from donor the $^5D_4$ (Tb^{3+}) level to the acceptor ion under the assumption of single-exponential decay can be derived from the equation:

$$W_{Tb\text{-}Re} = 1/\tau - 1/\tau_o \ ,$$

where τ_o and τ are the lifetimes of the $^5D_4$ level *without* and *with* the presence of Re^{3+} impurity, respectively.

Table represents the $W_{Tb\text{-}Re}$ obtained for TbF_3: Re^{3+} crystals containing 1 at.% of impurity ions each. The fluorescence lifetime for the $^5D_4$ level in a pure TbF_3 single crystal was

found to be 780 μs at room temperature and 970 μs at 77 K°. The represented data show that the highest donor-acceptor energy transfer probability was observed with those doping ions for which direct resonance interaction with the $^5D_4$ level takes place with no lattice phonons involved. Energy transfer for these ions is also temperature insensitive. Such interaction for Er^{3+}, Ho^{3+}, Pr^{3+}, and Sm^{3+} ions is accomplished through the $^4F_{7/2}$, $^4F_3$, $^3P_0$ and $^4G_{7/2}$ states, respectively.

Table. Fluorescence lifetimes of $^5D_4$ (Tb^{3+}) level and probabilities of excitation transfer from $^5D_4$ (Tb^{3+}) to impurity ions in TbF_3: Re^{3+} crystal

Re	τ, μs		$W_{Tb\text{-}Re} \times 10^{-4}$, s^{-1}	
	300 K°	77K°	300 K°	77K°
Pr	8	---	12.4	---
Nd	6.5	---	16.5	---
Sm	3	3	33	33
Eu	42	156	2.2	0.5
Dy	160	430	0.5	0.13
Ho	9	---	11	---
Er	10	10	10	10
Tm	140	180	0.6	0.4
Yb	400	620	0.12	0.04

From the above data, it is obvious that Sm^{3+} is the best choice as an acceptor for the Tb^{3+} donor, and the excitation transfer from Tb^{3+} to Sm^{3+} occurs resonantly in accordance with the scheme:

$$Tb^{3+}\ (^5D_4 - {}^7F_6) : Sm^{3+}\ (^6H_{5/2} - {}^4G_{7/2})\ .$$

The resonance character of energy transfer was confirmed by comparison of the $^5D_4$ - $^7F_6$ fluorescence spectrum of the Tb^{3+} ion with the $^6H_{5/2}$ - $^4G_{7/2}$ absorption spectrum of Sm^{3+} ion in YF_3 single crystal, as represented in Figure. (YF_3 single crystal is isostructural analog of TbF_3 with quite close crystal field constants and often used for clarifying the spectroscopic situations with "self-activated" TbF_3). Note that resonant conditions are being satisfied for several energy-exchange channels simultaneously. The backward energy transfer through the same channels is not possible due to the fast nonradiative decay of the $^4G_{7/2}$ Sm^{3+} level:

$$^4G_{7/2} \rightarrow {}^4G_{5/2} + 2300\ cm^{-1}.$$

Considering the possibility of "laser situation" for the impurity ions listed in Table, one should also take into consideration possible "backwards quenching" of acceptor fluorescence levels by the lower-lying donor levels. Our studies show that, in fact, only two Re^{3+} ions incorporated in TbF_3, of the studied nine, are potentially suitable for obtaining lasing - Sm^{3+} and Eu^{3+}. The fluorescence of others is completely quenched due to the interaction with Tb^{3+} ions of the host. For the same reason, according to our data, the presence in the host crystal of minor amounts of other ions uncontrollably depletes the $^5D_4$ state, and may essentially depress the sensibilization effect.

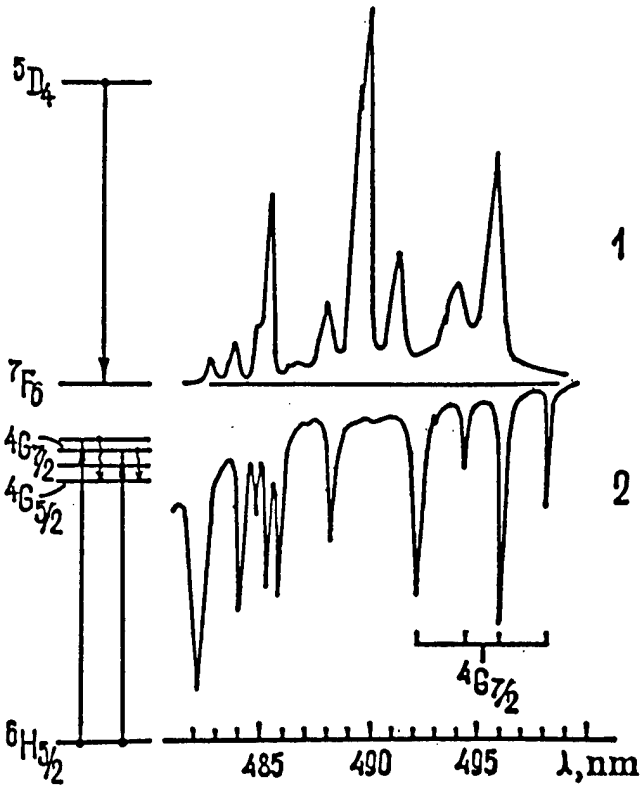

Figure. Fluorescence spectrum ($^5D_4$ - $^7F_6$) of Tb^{3+} ion (1) and absorption spectrum ($^6H_{5/2}$ - $^4G_{5/2}$, $^4G_{7/2}$) of Sm^{3+} ion (2) in YF_3 single crystal at 77 K°.

The above analysis enables one to explain the observed efficiency of Tb^{3+} - Sm^{3+} donor-acceptor pair for TbF_3 host crystal. Prediction that Tb^{3+} - Eu^{3+} pair might also be a good choice for an Ar-ion laser frequency converter seems to be practical.

Laser experiments implementing Ar-ion laser for pumping of TbF_3: Sm^{3+} as well as TbF_3: Eu^{3+} samples are now in progress.

Acknowledgment. Financial support from the NASA Lewis Research Center (Grant #NAG3-1677) is gratefully acknowledged.

References

1. H.P.Jenssen, D. Castleberry, et al. In: Digest of Techn. Papers, *CLEO* (IEEE/OSA, Washington, DC, 1973), p. 47.
2. B.N.Kazakov, M.S.Orlov, M.V.Petrov, et al. Opt. Spectrosc. (USSR) **47**, 1217 (1979).
3. H.P.Jenssen. In: *Advanced Solid-State Lasers* , OSA Techn. Digest (Opt.Soc. of Amer., Washigton, DC, 1995), p.73.
4. L.G.Van Vitert. - J. Electrochemical Society **114**, 1048 (1967).

Stimulated emission without cavity in powders and single crystals of Nd doped materials

M. A. Noginov*, N. E. Noginova, H. J. Caulfield**, P. Venkateswarlu*,
T. Thompson, M. Mahdi
*Center for Nonlinear Optics and Materials, **Center for Applied Optical Science, Department of Physics, Alabama A&M University, P. O. Box. 1268, Normal, AL 35762.
V. Ostroumov
Institute of Laser Physics, Hamburg University, Jungiusstrasse 9-11, D 20355, Hamburg, Germany

In late 70's, stimulated emission without mirrors was observed in small samples of high-gain Nd doped crystals designed for microlasers, see for example Ref. [1]. In 1986, stimulated emission characterized by short radiation pulses and narrowing of the spectral line was observed in powders of Nd doped materials [2]. Spectral and temporal behavior of emission from powders was studied in more details in Refs. [3-6]. In contrast to single crystals, where two parallel polished faces, in principle, can form a cavity, no such effects are likely in powders. However, theoretical models accounting for intra-particle modes supporting stimulated emission have been discussed in the literature, see for example Ref. [3]. A surprising result was recently reported in Ref. [7], where the threshold of stimulated emission in the gain scattering media (liquid laser dye with scatterers) not decreased but increased when the reflection off the cell walls was allowed.

In the present paper, we studied room temperature stimulated emission in the powders of $NdAl_3(BO_3)_4$, $Nd_xLa_{1-x}Sc_3(BO_3)_4$, and $Nd(2\%):Sr_5(PO_4)_3F$ (Nd:SFAP) laser materials, compared stimulated emission in powders to that in single crystals, and described the main features of the observed emission with the simple model accounting for $^4F_{3/2}$ excited state concentration and emission energy density. The study of the mechanism of stimulated emission in small, high-gain volumes of active media can be useful for design and optimization of microlasers. Moreover, the powders of laser crystals are the very interesting object to study, because they turn to be the simplest and least expensive solid-state source of short-pulsed narrow-line stimulated emission that can be useful in "photonic paints" [8] and other applications.

The main experimental results of this study are as follows:

1) After the pump energy (λ_{pump}=532 nm or 805-808 nm, τ_{pump}=10-20 ns) exceeded some threshold value, the Nd emission spectrum narrowed down to a single line (≥2 A), Fig. 1.
2) The spectrally narrow light was emitted in one or several short pulses. In the powder of $NdAl_3(BO_3)_4$, the duration of the pulses varied from 300 ps to 1300 ps, Fig 2.
3) In powders of the three laser materials studied, pumped at different wavelengths, the threshold gain varied from 2.5 to 16 cm^{-1}.

4) In $NdAl_3(BO_3)_4$ at the pump energy two times greater than the threshold energy, ≈ 0.2% of energy stored at the level $^4F_{3/2}$ went to the stimulated emission channel.
5) At higher thresholds, stimulated emission was also obtained in single crystals of the same three laser materials studied. According to Table 1, preparation of the material in the powder form (scattering), appreciable large volume, and polished plane-parallel surfaces in the bulk crystals (feedback) helped to reduce the threshold of stimulated emission in Nd:SFAP samples. However, the above dependence was not seen in a few plates of $Nd_xLa_{1-x}Sc_3(BO_3)_4$ and Nd:$GdVO_4$ we studied. Moreover, in the 8 mm thick polished sample of Nd:SFAP, stimulated emission was predominantly directed perpendicular to the plane-parallel polished faces, but no angular dependence of emission intensity was found (within ±30°) in thinner plates of $Nd_xLa_{1-x}Sc_3(BO_3)_4$ and Nd:$GdVO_4$. Probably, more samples need to be studied to increase the confidence in the experimental results on single crystals.

Sample (Nd:SFAP), λ_{pump}=805 nm	Powder (V≥1 mm)	8 mm polished plate	1.5 mm polished plate	0.8 mm unpolished plate
Threshold, mJ/cm^2	170	625	920	1080

Table 1. Thresholds of stimulated emission in the powder and single crystals of Nd:SFAP.

6) In the mixture of two powders (≈1/6 $NdAl_3(BO_3)_4$ and ≈5/6 $NdSc_3(BO_3)_4$), first several short emission pulses appeared at 1063.1 nm ($NdAl_3(BO_3)_4$), after that emission jumped to 1061.5 nm ($NdSc_3(BO_3)_4$). The first pulse in 1061.5 nm series coincided in time and was damped by the last pulse in 1063.1 nm series. This implies that individual components do not operate independently and that many particles behave collectively to produce stimulated emission pulses.

The threshold behavior of stimulated emission and short emission pulses we described with a simple model close to that for laser relaxation oscillations. From the literature we did know the whole set of spectroscopic parameters for the materials studied. The only unknown parameter in our system was the time τ_{phot}, that in the case of lasers has a meaning of a photon life-time in the cavity and a meaning of the photon life-time in the pumped volume in the case of stimulated emission without cavity. We used τ_{phot} as an adjustable parameter to fit the experimental threshold of stimulated emission and found in $NdAl_3(BO_3)_4$ powder τ_{phot}=10 ps. At the index of refraction n=1.5, this time corresponds to the average 2 mm photon path in the pumped volume, close to the linear size of the pumped medium in our experiment (≈1 mm).

The appearance of calculated emission pulses was very similar to that observed experimentally, Fig. 3. The calculated threshold of stimulated emission is inversely proportional to a small-signal amplification, that is typical for lasers (as well as experimental and calculated input/output curves and calculated dependence of $^4F_{3/2}$ excited state concentration on the pump energy).

The more detailed account of the experimental results and the theoretical model will be presented at the conference.

The work was done under the support of the MRCE-NSF grant #HRD-9353548, ARO Grant #DAA L 03-91-G-0316, and (for H. J. C.) the Air Force Office of Scientific Research. Authors acknowledge the assistance of Ms. C. Cochrane of AA&MU, Prof. G. Huber of Hamburg University, and Prof. M. Bass and Dr. X. X. Zhang of CREOL at the University of Central Florida.

1 - G. Huber , in Current Topics in Materials Science, Vol. **4**, E. Kaldis, editor, 1980, p. 1.
2 - V. M. Markushev, *et al.*, Sov. J Quantum Electronics, **16**, p. 281 (1986).
3 - V. M. Markushev, *et al.*, Sov. J Quantum Electron., **20**, p. 773 (1990).
4 - N. É. Ter-Gabriélyan, *et al.*, Sov. J Quantum Electron., **21**, p. 840 (1991).
5 - N. É. Ter-Gabriélyan, *et al.*, Sov. J Quantum Electron., **21**, p. 32 (1991).
6 - C. Gouedard, *et al.*, J Opt. Soc. Am. B, **10**, p. 2358 (1993).
7 - R. M. Balachandran, N. M. Lawandy, Opt. Lett., **20**, p. 1271 (1995).
8 - N. M. Lawandy, *et al.*, Nature, **368**, p. 436 (1994).

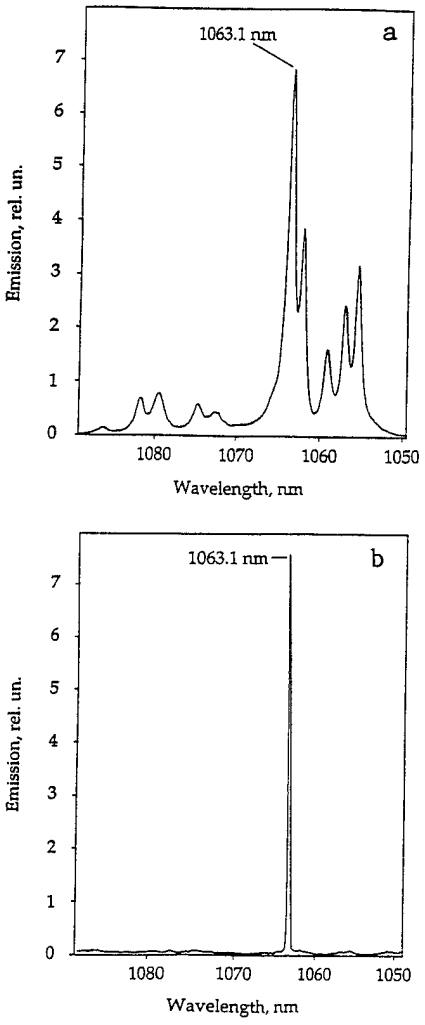

Figure 1. a) Emission spectrum of $NdAl_3(BO_3)_4$ powder below the threshold (≈30 mJ/cm^2), b) emission spectrum of $NdAl_3(BO_3)_4$ powder above the threshold (≈240 mJ/cm^2), λ=1063.1 nm.

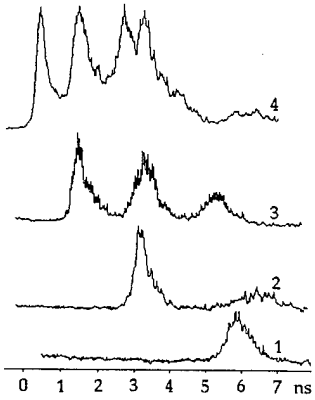

Figure 2. Pulses of stimulated emission from $NdAl_3(BO_3)_4$ powder 1) near the threshold (200 mJ/cm^2), 2) at x=1.6 times threshold energy, 3) x=1.9, 4) x=3.9.

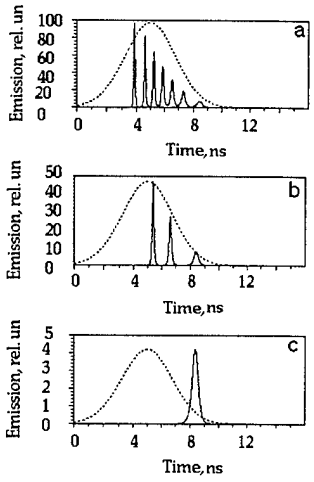

Figure 3. Calculated dynamics of stimulated emission in $NdAl_3(BO_3)_4$ at pumping density equal to 1000 mJ/cm^2 (a), 400 mJ/cm^2 (b), and 200 mJ/cm^2 (the threshold) (c).

Linear and nonlinear dispersion in solid-state solitary-wave lasers

Marco Santagiustina and Ewan M. Wright
Optical Sciences Center, University of Arizona,
Tucson, Arizona 85721, tel 520 621 2406, fax 520 621 6778

It is well known that the actual and fundamental constraint to pulsewidth compression in solid-state solitary lasers is linear dispersion and not the gain bandwidth [1, 2]. Theoretically the shortest pulses are attained close to the zero of the group velocity dispersion (GVD), but then third-order dispersion (TOD) must be considered. TOD infact induces an energy transfer from the solitary pulse to a linear dispersive wave, i.e. radiation, at a certain phase-matched frequency [3]. Thus as the pulse circulates in the cavity its amplitude decreases, its width broadens [4] and finally, if the TOD is too large, self-mode-locking is halted [5, 6], because of the overwhelming losses.
In this study we present a model to quantify the effects of TOD-induced radiation and we propose a new method to suppress them, exploiting the nonlinear dispersion (NLD), which can be strongly enhanced if the laser cavity incorporates a nonlinear element such that the center frequency is in the vicinity of a two-photon resonance [7].
The master equation, describing the circulation of the pulse envelope q reads in dimensionless units [4]

$$iq_z + \frac{\beta_2}{2}q_{tt} + |q|^2 q + i\beta_3 q_{ttt} = igq + i\beta q_{tt} + i\gamma_1|q|^2 q - i\gamma_2|q|^4 q, \tag{1}$$

where the following effects have been considered: negative GVD ($\beta_2 = 1$), Kerr nonlinearity, TOD (β_3), bandwidth limited amplification (g, β), self-amplitude modulation (γ_1, γ_2). Precise definitions of each coefficient and elaborations on their physical origins can be found in Refs. [8, 9] and are thus omitted here. The subscripts z and t indicate derivatives with respect to distance and time, once more expressed in soliton units ($z_0 = t_0^2/|k''|$, $t_0 = t_{fwhm}/1.763$). By means of a soliton perturbation theory (SPT) that takes into account the radiation [10] we find a system of coupled equations for the amplitude $\eta_0(z)$ and frequency $\mu_0(z)$ of a soliton, defined by:

$$q_s(z,t) = 2\eta_0 sech[2\eta_0(t-\xi)]e^{i2\mu_0(t-\xi)+i\delta}. \tag{2}$$

For the sake of brevity we present only the final results, i.e. the evolution equations for the soliton parameters (see also [9]):

$$(\eta_0)_z = \frac{2}{3}\eta_0[3g - 4\beta(\eta_0^2 + 3\mu_0^2) + 8\gamma_1\eta_0^2 - \frac{128}{5}\gamma_2\eta_0^4] - \\ -\frac{2\beta_3^2\pi^2\mu_r^2(\mu_r^2+\eta_0^2)^2}{|\mu_r - 6\beta_3\mu_r^2 - \mu_0|}sech^2\left[\frac{\pi}{2\eta_0}(\mu_0 - \mu_r)\right] \tag{3}$$

$$(\mu_0)_z = -\frac{16}{3}\beta\mu_0\eta_0^2 + \frac{(\mu_0-\mu_r)2\beta_3^2\pi^2\mu_r^2(\mu_r^2+\eta_0^2)^2}{\eta_0|\mu_r - 6\beta_3\mu_r^2 - \mu_0|}sech^2\left[\frac{\pi}{2\eta_0}(\mu_0-\mu_r)\right] \tag{4}$$

where μ_r is the phase-matched frequency, that can be calculated equating the radiation and soliton wavevectors [3]. Setting the left-hand sides of eqs. (3,4) to zero we find the stationary operating conditions for the dynamical system. The bifurcation diagram is presented in figure 1, for the amplitude, and compared with the numerical solutions of the master equation (1), with very good overall agreement. The value predicted for the bifurcation, beyond which mode-locking is halted, is 0.3975, in good agreement also with experiments [5]. For example, taking the data of a Ti:sapphire laser [1, 5], $t_0 \simeq 7fs, k'' = -50fs^2/m$ and $\beta_3 = 0.3975$, yields a TOD $k''' = -6\beta_3|k''|t_0 \simeq -800fs^3/m$,

which reflects experimental values for laser instability. We present also, in figure 2, the predicted pulse broadening, assuming (2) as a solution, and compare it with the steady-state pulsewidth of the numerical solutions.

Another interesting physical phenomenon captured by eqs. (3,4) is the decrease in the radiation emission, due both to a decrease of the amplitude and a soliton frequency shift. We note by inspection of the coupled equations that the $sech^2$ factor decreases with increasing amplitude η_0, and increases with the difference $\mu_0 - \mu_r$, which tends to grow according to eq. (4). In particular, μ_0 always change oppositely to μ_r ($|\mu_0| \ll |\mu_r|$ is always true), in such a manner that the soliton spectrum shifts to increase the effective total dispersion in order to preserve its stability.

It is particularly interesting to consider the possibility to compensate the TOD with the NLD, which is enhanced in the vicinity of a resonance. A two-photon resonance, for frequencies just below the half of the bandgap, is a good choice to enhance both the nonlinearity and the NLD without a concomitant increase of absorption [7]. The new term that must be added to the master equation is then able to suppress the emission of radiation from the soliton [7]. The new master equation is

$$iq_z + \frac{\beta_2}{2}q_{tt} + |q|^2 q + i\beta_3 q_{ttt} + i\alpha|q|^2 q_t = igq + i\beta q_{tt} + i\gamma_1|q|^2 q - i\gamma_2|q|^4 q, \qquad (5)$$

where α is the NLD coefficient [7]. Using a perturbative approach it is possible to show [7] that, as sources of radiation, NLD and TOD have the same form but are out of phase; Thus we can define an effective coefficient for radiation emission. When $\beta_3 \leq \alpha/6$ the TOD is overcompensated but no other radiation field appears due to the lack of a phase-matching condition for the NLD; Thus the effective coefficient is $\beta_{eff} = 0$. Otherwise if $\beta_3 > \alpha/6$ we may define $\beta_{eff} = \beta_3 - \alpha/6$ [7]. The modified bifurcation diagram, obtained by substituting β_{eff} to β_3 in the SPT equations, is in agreement with the numerical solutions of the new master eq. (5) (figure 3). A similar agreement is reached for the predicted pulsewidth (figure 4). Note that the bifurcation takes place for larger values of TOD and that the pulsewidth is always shorter.

In conclusion a model to study TOD-induced radiation in the solitary lasers has been developed and agrees both with the numerical solution of the master equation and the reported experiments. We have also shown, through numerical solutions and perturbative techniques, that nonlinear dispersion, enchanced in the vicinity of a two-photon resonance, can effectively suppress this radiation. Shorter pulses are then made possible by exploiting this new effect.

References

[1] F. Krausz, M.E. Fermann, T. Brabec, P.F. Curley, M. Hofer, M.H. Ober, C. Spielmann, E. Wintner, A.J. Schmidt, *IEEE J. Quant. El.*, **QE-28**, 2097 (1992).

[2] C. Spielmann, P.F. Curley, T. Brabec, F. Krausz, *IEEE J. Quant. El.*, **QE-30**, 1100 (1994).

[3] P.K.A. Wai, C.R. Menyuk, Y.C. Lee, H.H. Chen, *Opt. Lett.*, **11**, 464 (1986).

[4] H.A. Haus, J.D. Moores, L.E. Nelson, *Opt. Lett.*, **18**, 51 (1993).

[5] P.F. Curley, C. Spielmann, T. Brabec, F. Krausz, E. Wintner, A.J. Schmidt, *Opt. Lett.*, **18**, 54 (1993).

[6] T. Brabec, S.M.J. Kelly, *Opt. Lett.*, **18**, 2002 (1993).

[7] M. Santagiustina, E.M. Wright, *Opt. Lett.*, to be published (1995).

[8] H.A. Haus, J.G. Fujimoto, E.P. Ippen, *IEEE J. Quant. El.*, **QE-28**, 2068 (1992).

[9] Y. Kodama, M. Romagnoli, S. Wabnitz, *El. Lett.*, **28**, 1981 (1992).

[10] J.N. Elgin, *Phys. Rev. A*, **47**, 4331 (1993).

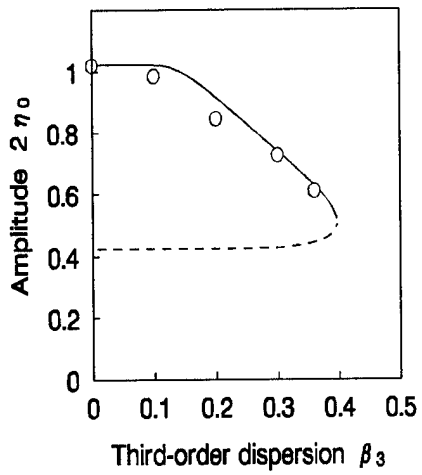

Figure 1: Bifurcation diagram for the amplitude; the solid (dashed) line is the stable (unstable) branch as a result of the SPT. Dots are the steady-state solutions of the master equation (1). Lasers parameters are $g = -0.0025, \beta = 0.051, \gamma_1 = 0.05, \gamma_2 = 0.025$.

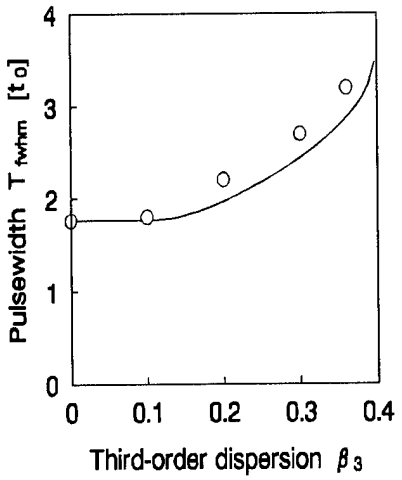

Figure 2: Comparison of output pulsewidth as a result of the SPT (solid line) and from the numerical solutions of eq. (1). Laser parameters are the same of figure 1.

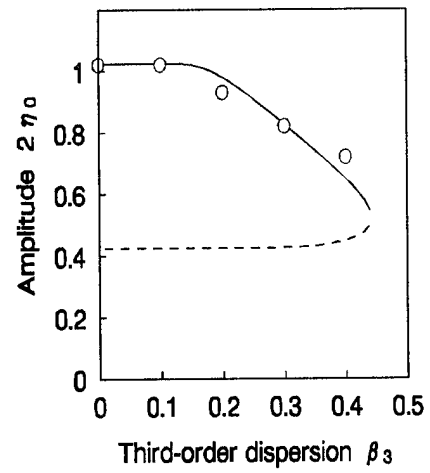

Figure 3: The same of figure 1, but including the NLD. The dots are now solutions from eq. (5) with $\alpha = 0.6$, which reflects a physical value for NLD [7]. Other laser coefficients are the same of previous figures.

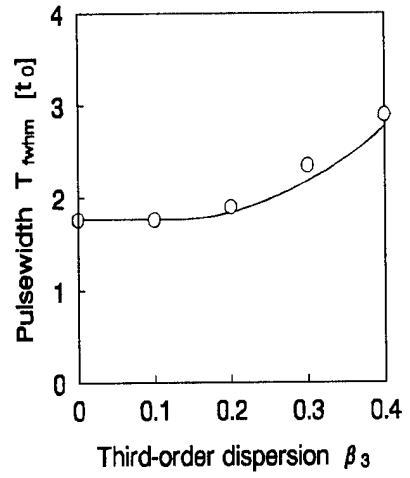

Figure 4: The same of figure 2, but including NLD ($\alpha = 0.6$) like in figure 3.

Growth and optical characterization of Nd:YVO_4 crystal fibers

F.S. Ermeneux, C. Gouteaudier, R. Moncorgé, R. Burlot, M.T. Cohen-Adad

Université de Lyon I, URA 442 CNRS, 69622 Villeurbanne, FRANCE
tél. (33) 72 43 12 08 Fax. (33) 72 43 11 30

Because of its particular optical properties, such as broad and strong absorption around 800 nm and large stimulated emission cross section around 1.06 μm, Nd^{3+} doped YVO_4 (and analogs like $GdVO_4$) is now one the most attractive crystalline material for diode-pumped solid-state minilaser applications [1]. However, though its laser performance, laser thresholds and slope efficiencies, are generally good, significant variations can be observed between crystals coming from different suppliers and/or grown by using different techniques. Though it is now admitted that the Czokralski method is the most viable technique for the growth of large and high quality YVO_4 crystals for commercial uses, other methods such as HTSG (flux method) have proved to be interesting too for rapid and low cost fabrication of good quality samples and for spectroscopic and laser evaluations [2].

We report here in this paper the results of a detailed study of the spectroscopic properties of good optical quality crystal fibers grown in our laboratory by the Laser Heated Pedestal Growth (LHPG) technique and, for comparison, of various other crystals coming from different sources and grown by different techniques, with the aim of trying to relate these properties with the structure and composition of the crystals.

It is of practical importance for a better understanding of the physico-chemistry and a better reproducibility of the crystals; it is also important from the fundamental point of view. Indeed, there two questions that need to be addressed more specifically: the one concerns the multisite character of the optical transitions, this having been only partially studied in the past [3,4], and the other, which results of the former, concerns the polarization sensitivity and the homogeneous/inhomogeneous nature of the absorption band around 800 nm, the one of interest for diode pumping.

Several crystal growth experiments using the LHPG method were performed to optimize growth conditions by varying the Nd_2O_3, Y_2O_3 and V_2O_5 proportions of the starting powders, the growth atmosphere, the laser power and the pulling rate. Better results than reported previously [5] for undoped crystals were apparently obtained. A special attention was addressed to the preparation of the ceramic feed rods, in particular to the pressing, the solid state reaction and the sintering conditions. Post growth thermal treatments were also necessary to reduce the strains in the crystals and change their coloration from yellow-green to blue, the typical color of Nd:YVO_4. Good optical quality single crystals in the form of about 1.5 mm in diameter up to about 2 cm long faceted fibers were thus obtained starting from 48.1% Y_2O_3, 51.4% V_2O_5 and 0.5% Nd_2O_3 component proportions.

Three other good quality crystals were also studied parallelly: two of them were grown by using flux techniques, the one labelled FB starting with from powders of Nd_2O_3, Y_2O_3 and $Pb_2V_2O_7$ and the other labelled FS starting from powders of Nd_2O_3, Y_2O_3, V_2O_5, Na_2CO_3 and B_2O_3; the third one labelled CZ was grown by using the Czokralski technique starting, as in the LHPG technique, from powders of Nd_2O_3, Y_2O_3, V_2O_5.

Polarized absorption/transmission spectra were recorded between 400 and 850 nm and at 12 and 300 K. The shape and the position of several lines, in particular that corresponding to the optical transition to the $^2P_{1/2}$ energy level around 434 nm, were registered as a function of temperature between 12 and 300 K. Polarized emission spectra were also recorded at low and high temperatures in the visible as well as in the infrared spectral domains from 400 to 2000 nm. Finally, time-resolved and site selective emission and excitation spectra were recorded at low temperature by exciting with a narrow-line Raman shifted dye laser in the excited and metastable levels $^4F_{5/2}$ and $^4F_{3/2}$ around 800 and 880 nm, respectively.

Three categories of Nd^{3+} sites corresponding to various multiplet Stark splittings are clearly evidenced. The ones labelled Site 1 and corresponding to the 15-18 cm^{-1} $^4F_{3/2}$ Stark splitting usually reported in the literature are the majoritory sites and are probably associated with regular Y^{3+} sites in the YVO_4 structure. However, as shown in Fig. 1, the structure of the excitation spectrum reveals that these category of sites give rise to many closely spaced lines which probably correspond to slight perturbations of the local environment of the Nd^{3+} ion. The excitation spectra corresponding to the Sites 2 and 3, with a $^4F_{3/2}$ Stark splitting of about 25 cm^{-1}, are more clearly defined and are probably associated to Nd^{3+} ions in more particular situations, such as ions with oxygen vacancies in their vicinity. The same complicated excitation structure associated with the Nd^{3+} sites 1 and the simple one associated with the Nd^{3+} sites 2 have been found in all the samples. The one associated with the Nd^{3+} sites 3 seem to be more specific of the LHPG crystal but this has to be checked again.

We show in Fig.2 the emission spectra resulting from selective laser excitation of the three categories of sites. It is worth noting that excitation of the site 1 Nd^{3+} ions give emission lines as sharp as the ones associated with the Nd^{3+} sites 2 and 3.

In summary, good optical quality crystal fibers have been grown and studied. We have identified, in these fibers as well as in other crystals of different origins, at least 2 kinds of Nd^{3+} sites, and it might be possible to use the low temperature excitation spectra corresponding to these sites, in conjunction with more classical techniques such as X-ray diffraction, for refined crystal quality evaluation.

Acknowledgments:
Thanks are expressed to Prof. M. Bettinelli and Dr. D. Rytz for providing us with the flux grown crystals labelled FB and FS in the text and Dr. Y. Kalisky for the Czokralski grown sample noted CZ. We also thank the Thomson society for its interest in this work and its financial support.

References:

1. L.Deshazer, Laser Focus febr. 1994, pp 88-93
2. G. Mizell, W. R. Fay, Th. Alekel, D. Rytz, SPIE vol. 2115 (1994) 52
3. Kh. Bagdasarov, G.A. Bogomolova, A.A. Kaminskii, V.I. Popov, Sov. Phys. Dokl. 13 (1968) 516
4. D. Sardar, R.C. Powell, J. Appl. Phys. 51 (1980) 2829
5. S. Erdei, F.W. Ainger, J. Cryst. Growth 128 (1993) 1025, Mat. Res.Soc. Symp. Proc. vol. 329 (1994) 245

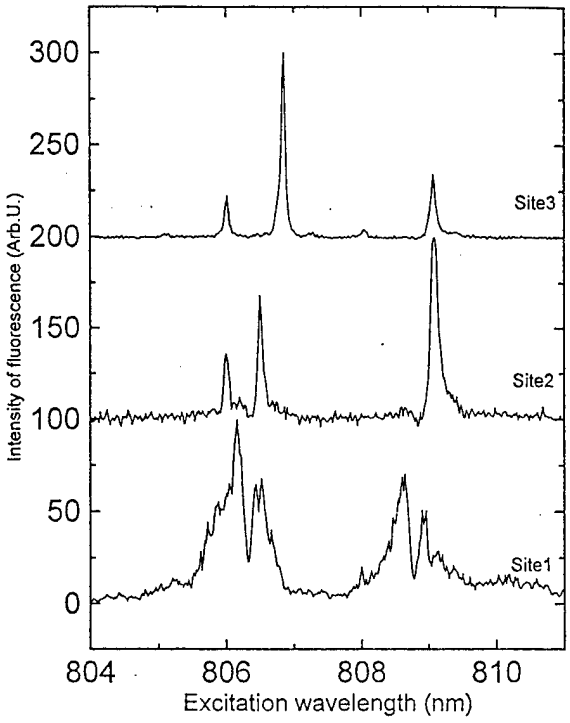

Fig 1-a

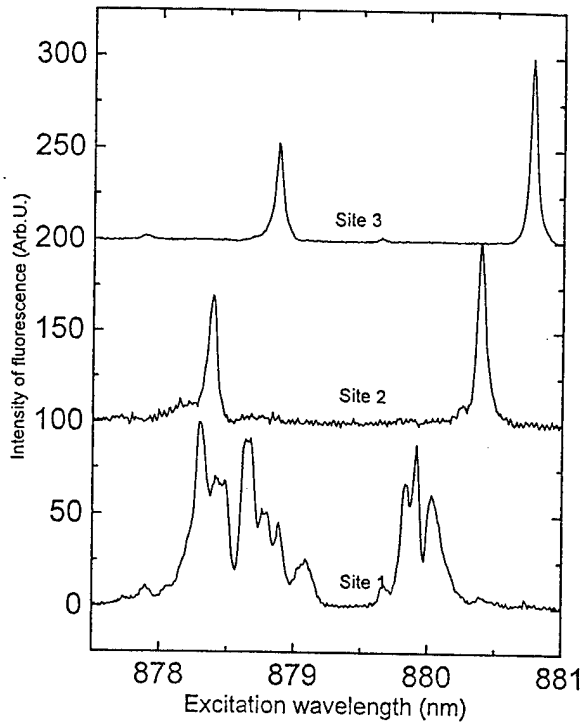

Fig 1-b

Fig. 1: Low temperature site selective excitation spectra of Nd^{3+} around a) 800 and b) 880 nm

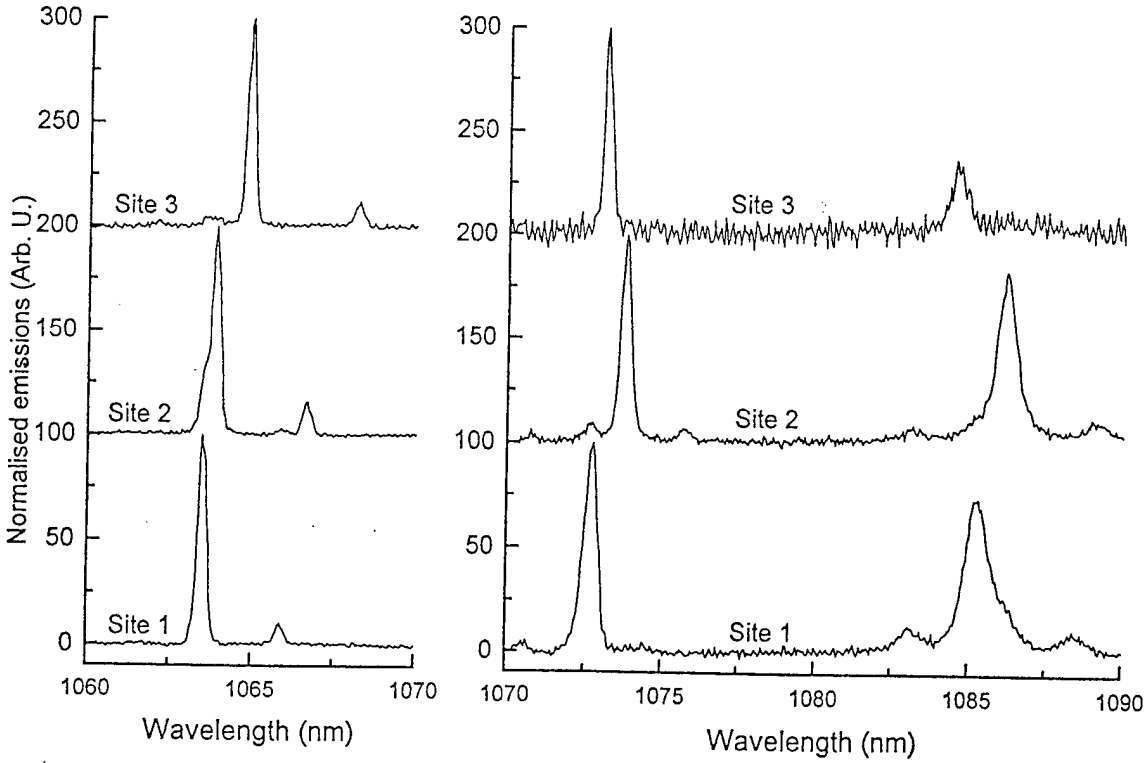

Fig. 2: Low temperature site selective emission spectra of Nd^{3+} in YVO_4 around 1.06 μm

Ultrafast Dynamics of Excited-State Absorption in V^{3+}:YAG Saturable Absorber

V.P. Mikhailov, K.V. Yumashev, N.V. Kuleshov, P.V. Prokoshin, N.N. Posnov
International Laser Center, Kurchatov str. 7, Minsk 220064, Belarus
Tel/Fax: 375-172-785 726, E-mail: user1@mikhai.bsu.minsk.by

Recently, the saturation of the optical absorption of tetrahedrally coordinated V^{3+} ion in YAG was investigated at 1.06 μm [1]. V^{3+}-doped YAG was shown to be efficient saturable absorber for passive mode-locking and Q-switching of solid-state lasers in the far red and near infrared spectral range. One of the key parameter of the saturable absorber is excited-state absorption (ESA), which can strongly affect saturable absorption and restrict the spectral range of operation. In a present paper the results of ESA spectra measurements on V^{3+}:YAG with picosecond temporal resolution in the 450-950 nm range are reported.

ESA spectra measurements were performed at room temperature using pump-and-probe laser technique. Ultrashort pulses of second harmonic of mode-locked Nd:$YAlO_3$-laser at 540 nm and a broad-band picosecond continuum generated from a D_2O cell were used as pump and probe beams, respectively. The spectrum of transmitted probe beam was analyzed with a spectrometer and detected with an optical multichanel analyzer.

Two bleaching bands at about 590 nm and 820 nm as well as two pump-induced absorption bands at 720 nm and 870 nm were observed in the ESA spectrum at zero delay time between pump and probe beams (Fig. 1). Bleaching bands had a lifetime of a few nanoseconds and were attributed to the saturation of the ground state absorption (GSA) of tetrahedral V^{3+}. Pump-induced absorption bands at 720 nm and 870 nm decay rapidly with increasing of the delay time. The decay time of these absorption bands was measured to be approximately 150 ps. These bands were assigned to the excited-state absorption of V^{3+}.

Bleaching band at 820 nm observed in the ESA spectra coinside completely with the $^3A_2$-$^3T_1(^3F)$ band in the GSA spectrum. According to the energy level structure of the V^{3+} ion with a $3d^2$ electronic configuration in a site with a local T_d symmetry the bleaching band at 590 nm is associated with the $^3A_2$-$^3T_1(^3P)$ transition. This band was not observed in the GSA spectrum of tetrahedral V^{3+} at room temperature due to overlaping with strong broad absortion band of octahedral V^{3+}.

Both pump-induced absorption bands at 870 nm and 720 nm in ESA spectra with the lifetime of 150 ps can not be assigned to transitions from the $^3T_2(^3F)$ excited state, since the lifetime of this state (5 ns) is much longer. Moreover,

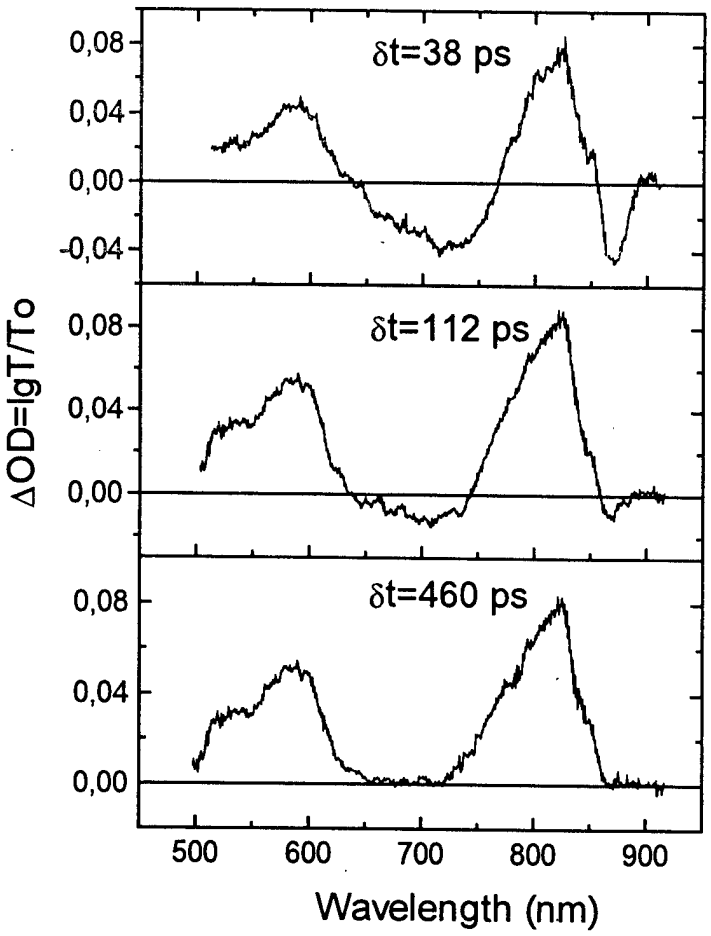

Fig. 1. ESA spectra of V^{3+}:YAG at different delay times.

higherst spin-triplet state of tetrahedral V^{3+} is $^3T_1(^3P)$ state and the energy gap between $^3T_1(^3P)$ and $^3T_2(^3F)$ states determined from GSA absorption spectrum at 77 K is of about 9000 cm^{-1} . Thus, no spin allowed transitions can be observed from the $^3T_2(^3F)$ state in the 870 nm and 720 nm spectral regions. Induced absorption can not be associated also with octahedral V^{3+} , because the lowest excited states of this ion $^1T_2$ and $^1E(^1D)$ have higher energy (approximmately 10250 cm^{-1} [2]) than energy of pump photons. We suppose, that pump-induced absorption is associated with ESA from the $^1E(^1D)$ excited state of tetrahedral V^{3+}. From the Tanabe-Sugano diagram the possible transitions from the $^1E(^1D)$ state are transitions to the $^1T_1(^1G)$ state for the 870 nm band and to the ^1E, $^1T_2$ (^1D) states for the 720 nm band. The energy level scheme for the tetrahedral V^{3+} in YAG was calculated from crystal field theory in T_d approximation using experimental data from GSA and ESA measurements (Fig. 2). The best fit to the experimental data was obtained for the parameters Dq=750 cm^{-1}, B=427 cm^{-1} and C=2780 cm^{-1}.

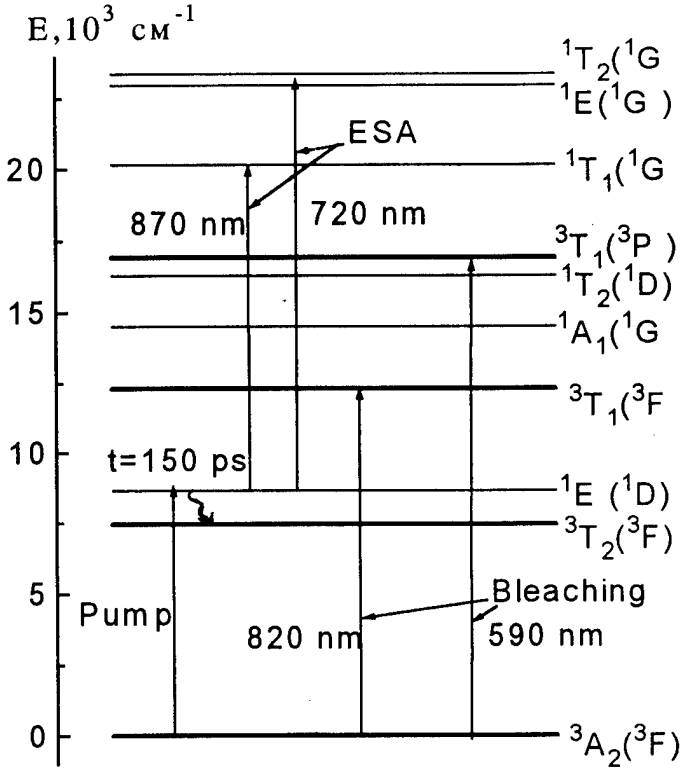

Fig. 2. Energy level scheme of tetrahedral V^{3+} in YAG.

An rms of approximately 850 cm^{-1} was associated, probably, with a symmetry distortion of impurity center.

According to the proposed scheme the decay time of ESA bands of 150 ps characterizes the lifetime of the $^1E(^1D)$ excited state. The energy gap between $^1E(^1D)$ state and zero-phonon level of the $^3T_2(^3F)$ state is equal to 1300 cm^{-1}. The $^1E(^1D)$ state exhibits weak coupling with phonons and an estimated rate of $6.6x10^{10}$ s^{-1} for the phonon assisted nonradiative electronic relaxation from the $^1E(^1D)$ to the $^3T_2(^3F)$ state seems to be reasonable. For comparison, the relaxation time between $^4T_2$ and ^1E states of the Cr^{3+} in emerald with energy gap of 400 cm^{-1} was measured to be 20 ps [3].

The absorption cross sections is determined for the both ESA transitions.

References

1. V.P. Mikhailov, N.V. Kuleshov, N.I. Zhavoronkov, P.V. Prokoshin, K.V. Yumashev, V.A. Sandulenko. Opical Materials 2 (1993) 267.
2. M.F. Weber and L.A. Riseberg. J. Chem. Phys. 55 (1971) 2032.
3. S.K. Gayen, W.B. Wang, V. Petricevic. et. al. J. Lumin. 47 (1991) 181.

Small signal gain in chromium forsterite amplifiers

Iain T. McKinnie

Department of Physics, University of Otago, PO Box 56, Dunedin, New Zealand
Tel. 64 3 479 7749 Fax 64 3 479 0964

Terrence A. King

Department of Physics and Astronomy, University of Manchester, Manchester, UK.

Since the first report of laser action in chromium forsterite in 1988[1], a number of studies of laser performance (see eg. [2]) and material optical properties (see eg. [3]) have been carried out. However, as far as we are aware no investigations of chromium forsterite amplifiers have been conducted. Here we present small signal gain measurements using a CW diode laser at 1300nm. The influence of material characteristics on amplifier performance is studied using four different crystals. Of particular interest is the performance of a new high dopant level crystal.

The 1130 - 1370nm operating wavelength range of chromium forsterite is attractive for a wide range of potential and actual applications. However, oscillators do not provide sufficient power for applications such as remote sensing and laser isotope separation. As the maximum useful energy which can be extracted from a single solid state oscillator is limited by considerations of damage and amplified spontaneous emission, these applications use master oscillator/ power amplifier (MOPA) chains to achieve required levels of energy (see eg.[4]). Small signal CW gain measurements provide a means to assess the potential amplifier performance, as well as monitoring temporal and polarisation effects through direct probing of the upper laser level.

Figure 1 shows the experimental configuration used to measure the small signal gain in forsterite. Each amplifier was pumped with a 1064nm Q-switched Nd:YAG laser, polarised along the b-axis of the crystal. The probe signal was provided by a counter-propagating 5mW InGaAsP diode laser. Pump and probe beams were focused to spot sizes of 750μm and 200μm respectively.

Table 1 presents physical and optical characteristics of the laser amplifier crystals. In a previous investigation[5] we studied the influence of crystal characteristics on oscillator performance. In that case crystal figure of merit (FOM) emerged as a critical parameter, and crystals of widely differing dopant level, but similar FOM, gave comparable laser performance.

Small signal gain for each crystal has been measured for a range of probe intensities, and for pump pulse energy of between 10 and 50mJ. Small signal power gain G is defined in terms of incident and transmitted probe intensity I_{in} and I_{trans} as

$$I_{trans} = G\, I_{in}$$

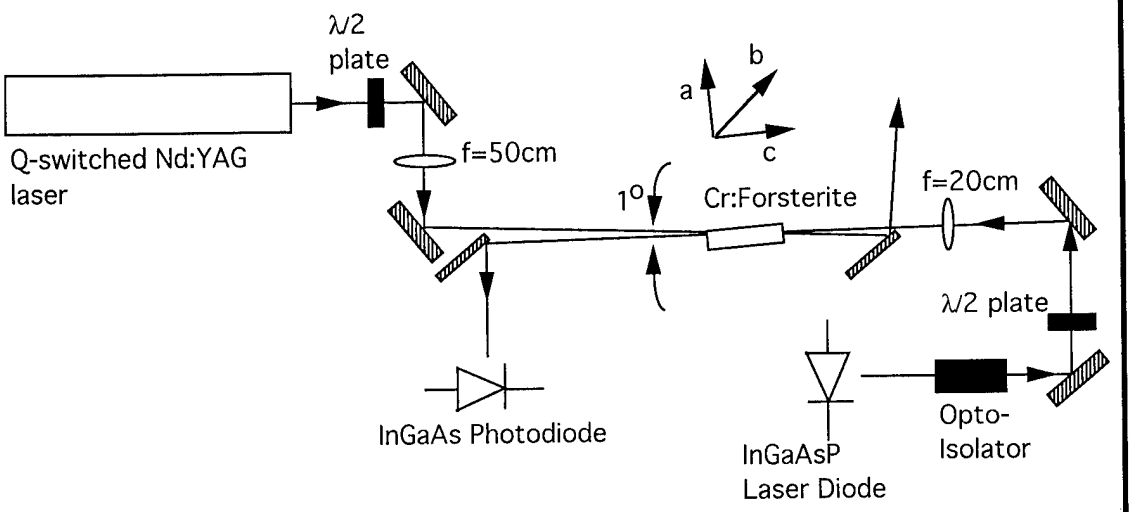

Figure 1. Experimental arrangement for small signal gain measurement.

Crystal dimensions (mm)	5x5x15	5x5x17	5x5x20	5x5x8
End Faces	Broad-band antireflection coated	Parallel Brewster cut	Parallel Brewster cut	Parallel Brewster cut
Cr(IV) dopant level no. density ($x10^{18}cm^{-3}$)	5.0	7.0	10	21.0
Cr(IV) dopant level (atomic %)	0.03	0.04	0.06	0.12
Figure of merit	24	17	17	23

Table 1 Characteristics of chromium forsterite amplifier crystals

At the maximum pump energy, small signal power gain of between 7 and 19 was measured for the different crystals. The results indicate that high chromium (IV) content does not lead to any degradation of amplifier performance. One typical result for a 0.04 atomic% intermediate dopant level crystal is shown in figure 2. Small signal power gain G is plotted as a function of pump energy for a probe power of 5mW.

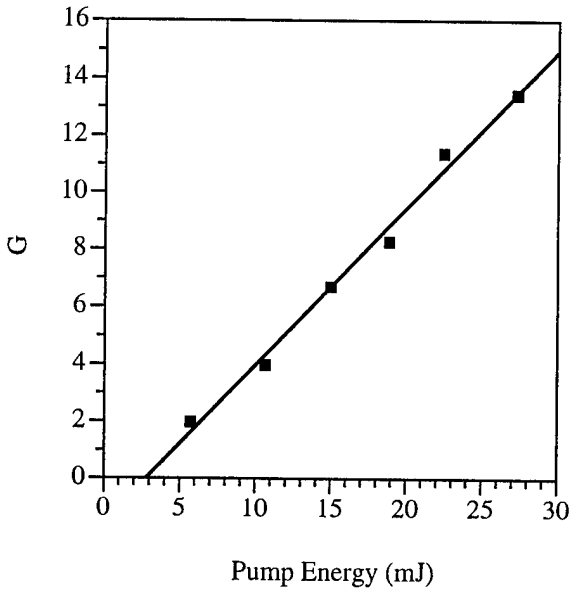

Figure 2. Small signal power gain G as a function of amplifier pump energy for the 0.04 atomic % crystal.

The temporal decay of the amplified signal has been measured to ascertain the duration of the amplified signal. A clear trend of decreasing duration with increasing pump energy is observed, and attributed to the effect of stimulated transitions. For each crystal gain anisotropy between polarisation states has been studied by varying probe polarisation. A polarisation dependence of the temporal shape of the pulse was observed. It is thought that this may indicate a multiphoton depopulation scheme in the excited chromium (IV).

Limits on amplifier performance have been assessed by measuring amplified spontaneous emission (ASE) and damage threshold. Significant variation in ASE with crystal parameters is observed, with high ASE levels measured for high dopant level crystals.

References

1. V. Petricevic, S.K. Gayen and R.R. Alfano Appl. Phys. Lett. **52** 1040 (1988).
2. T.J. Carrig and C.R. Pollock IEEE J. Quantum Electron. **29** 2835 (1993).
3. R. Moncorgé, G. Cormier, D.J. Simkin and J.A. Capobianco IEEE J. Quantum Electron. **27** 114 (1991).
4. J.C. Barnes, N.P. Barnes and G.E. Miller IEEE J. Quantum Electron. **24** 1029 (1988).
5. I.T. McKinnie, L.A.W. Gloster, Z.X. Jiang and T.A. King *Conference on Lasers and Electro-Optics* Vol. 8, OSA Technical Digest Series (Optical Society of America, Washington DC, 1994), paper CTuE4.

COMPOSITIONALLY TUNED Nd LASERS

Norman P. Barnes
Elka B. Ertur
NASA Langley Research Center
Hampton, VA 23681

Brian M. Walsh
Boston College
Chestnut Hill, MA 02167

Ralph L. Hutcheson
Scientific Materials Corporation
Bozeman, MT 59715

A Nd laser material was found which allows continuously compositional tuning, extending the utility of Nd lasers by allowing a match between the peak emission wavelength and the desired operating wavelength. Nd garnet laser materials are often regarded as stoichiometrically determined and capable of tuning only over a fraction of a relatively narrow linewidth. However, a garnet laser material was found where continuous compositional tuning is possible. In particular, Nd:YGAG, or $Y_3Ga_xAl_{(1-x)}O_{12}$, has been grown in six different compositions ranging from pure $Y_3Al_5O_{12}$ to pure $Y_3Ga_5O_{12}$ and four compositions in between. To the best of the authors knowledge, potential laser wavelengths of Nd:YGAG have not been measured at intermediate compositions [1]. Absorption and emission spectra have been taken to determine the range of compositional tuning as well as the variation in linewidth.

Nd:YGAG permits continous compositional tuning since Ga and Al can be used in any desired ratio. Garnets usually follow stoichiometrically dictated ratios, that is $A_IB_2C_{(6-I)}O_{12}$ where I is an interger. Only integer values of I are possible since the dodecahedral A site is much larger than the tetrahedral C site. Consequently, because of the site size difference, atoms which fill the A site will not be able to fit on the C site. While the position of energy levels, and therefore the possible laser wavelengths, do not depend strongly on the particular laser material, compositional tuning allows considerably greater wavelength flexability than tuning over the natural linewidth. However, if stoichiometry dictates the composition, only discrete tuning is possible. On the other hand, YGAG allows complete freedom in selecting the ratio of Ga to Al, thereby allowing continuous compositional tuning of the laser wavelengths.

Different possible laser transitions display substantially different behaviors and compositional tuning ranges. Emission data were taken on four different YGAG compostions ranging from a Ga concentration of 1.0, that is a x value of 1.0, to a Ga concentration of 2.0. Literature data were used for Nd:YAG [2], Ga concentration of 0.0, and Nd:YGG [3], Ga concentration of 5.0. $YGaO_3$ has been characterized spectroscopically previously [3].

Measured positions of the peak of various emission lines can then be determined as a function of Ga concentration. Typical data for the 0.94 μm region appears in Figure 1. Compositional tuning rates for the 0.939 and 0.946 μm lines vary by more than a factor of 4.0.

A compositional tuning range of 0.008 μm and 0.003 μm can be obtained for the 0.946 μm line and 1.064 μm lines, respectively. In the former case, compostional tuning yields a tuning range which is a factor of 0.009 of the center wavelength. In contrast, the linewidth, full width at half maximum, of this transition in Nd:YAG is an order of magnitude less than this, 0.0008 of the center wavelength. Compositional tuning is found to be well described by a linear relationship between the Ga concentration and the peak of the center wavelength. At this point, there appears to be no discrete steps in the compositional tuning range. Data is presently being taken on a Ga concentration of 3.0 to further confirm this.

Different compositional tuning behaviors indicate the possibility of multiple sites for the Nd. Comparing the various emission spectra for different composition reveals that the position of some of the lines appear to vary smoothly as the Ga concentration is varied. However, other lines appear to develop a shoulder in the emission spectra, the peak of which varies also as a function of the Ga concentration. A typical example is shown in Figure 2 for a Ga concentration of 1.27. While the 0.939 μm line appears as a single line but the 0.946 μm line appears to consist of two lines. Since there are only two transitions in this spectral region, contributions from different sites are suspected.

To test this supposition, the lifetime of the suspected features was measured using a frequency doubled Nd:YAG laser as a pump source. Preliminary measurements of the apparent lifetimes at 0.9447 and 0.9436 μm were 0.239±21 and 0.291±24 μsec, respectively. As expected the longer wavlength produced a lifetime nearly that of Nd:YAG while the shorter wavelength produced a longer lifetime, more like Nd:YGG. Laser performance of Nd:YAG and Nd:YGAG under similar circumstances is currently being evaluated.

1. M. Zodai, R. C. Powell, G. F. Imbusch, and B. DiBartolo, "Time Resolved Site Selection Spectroscopy Investigation Of $Y_3(Al_{1-x}Ga_x)_5O_{12}$:Nd Crystals," J. Appl. Phys., 50 5930-5936 (1979)

2. S. Singh, R. G. Smith, and L. G. Van Uitert, "Stimulated Emission Cross Section And Fluorescent Quantum Efficiency Of Nd^{3+} In Yttrium Aluminium Garnet At Room Temperature," Phys. Rev., 10, 2266-2572 (1974)

3. A. A. Kaminskii, G. A. Bogomolova, D. N. Vylegzhanin, Kh. S. Bagdasarov, A. M. Kevorkov, and M. M. Gritsenko, "Spectroscopic Properties Of Nd^{3+} Ions In Garnet Compounds Forming In the Y_2O_3-Ga_2O_3 System," Phys, Stat. Sol. 38, 409-422 (1976)

Wavelength Versus Ga Concentration

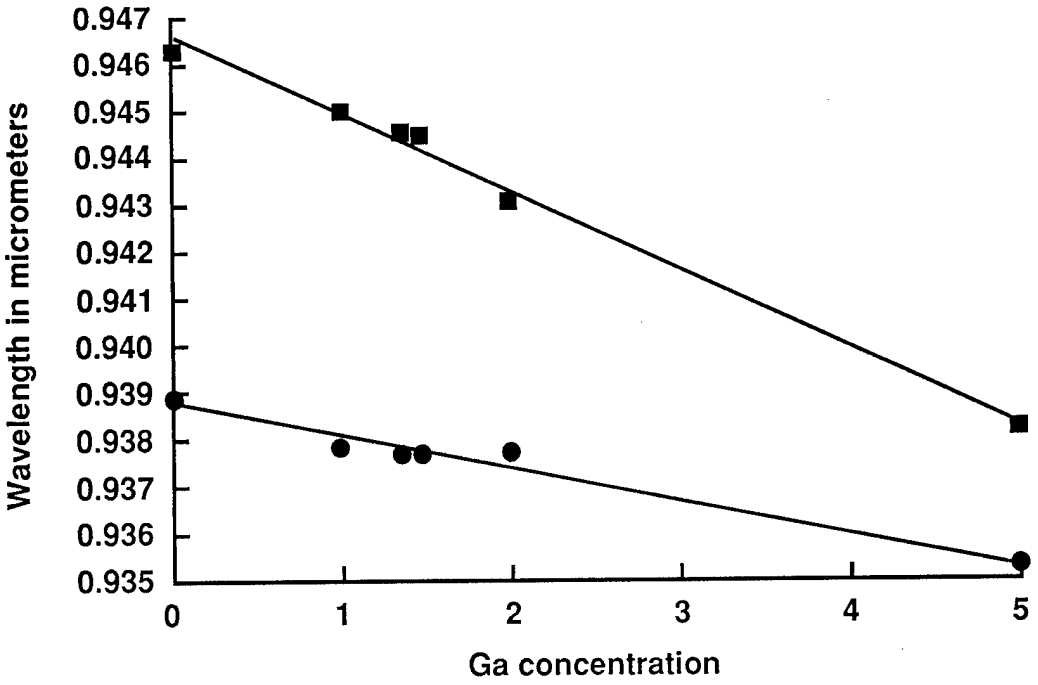

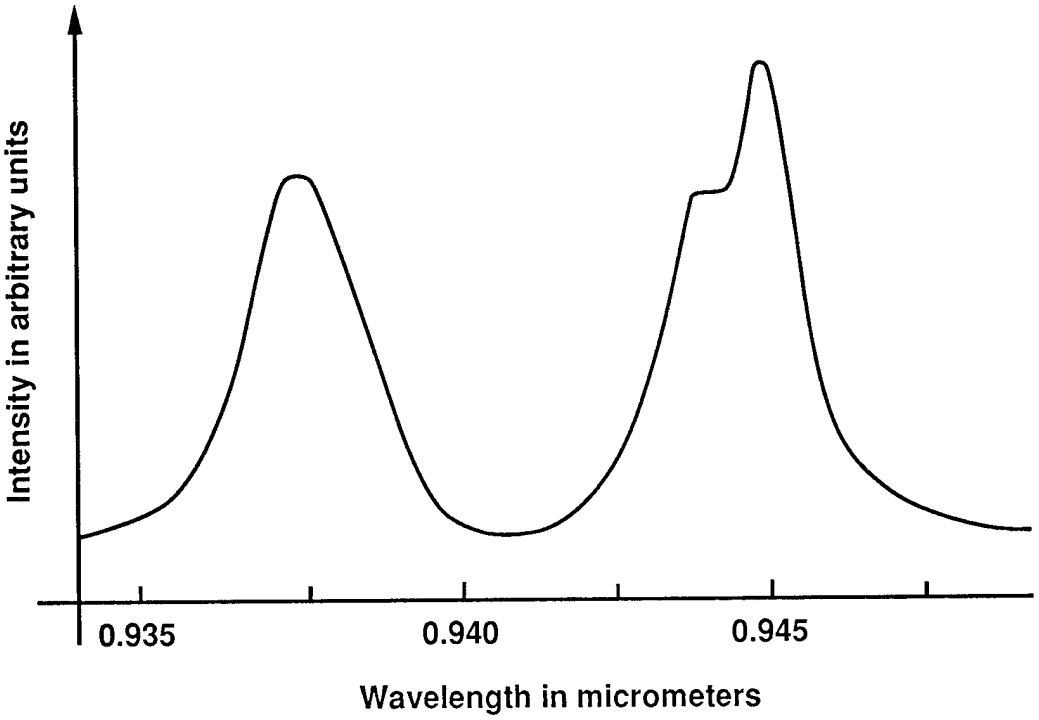

Thursday, February 1, 1996

Mid Infrared Lasers

ThE 10:45 am-12:30 pm
Gold Room

Norman Barnes, *Presider*
NASA Langley Research Center

Recent developments in Cr^{2+}-doped II-VI compound lasers

Ralph H. Page, Laura D. DeLoach, Kathleen I. Schaffers,
Falgun D. Patel, Stephen A. Payne, and William F. Krupke

Lawrence Livermore National Laboratory
Mailcode L-493
P.O. Box 808
Livermore CA 94550
(510) 422 2774
(510) 422 1930 facsimile
RPAGE@LLNL.GOV

Arnold Burger

Center for Photonic Materials and Devices
Department of Physics
Fisk University
1000 18th Ave. N.
Nashville TN 37208-3051

Many potential applications motivate the development of compact, rugged medium-average-power lasers widely tunable around 2000 - 5000 nm. Presently-available sources of coherent mid-IR light include difference-frequency mixers, parametric oscillators, Raman cells, lead-salt diode lasers, and various rare-earth lasers. Unfortunately, the nonlinear-optical schemes are complex and often give poor beam quality, the diode lasers involve cryogenic techniques, and the rare-earth lasers offer limited tunability. As reported last year,[1] we have demonstrated lasing in a new class of materials, Cr^{2+}-doped II-VI compounds. Their tuning ranges should eventually cover at least the 2100 - 3000 nm region, and efficient pumping with diode lasers is anticipated. We have embarked on a program to enhance the crystal quality, slope efficiency, and tuning range, and construct a small-package diode-pumped laser.

Absorption and emission properties of divalent transition-metal ions (TM^{2+}) in II-VI hosts have been studied for a few decades.[2] In the zinc chalcogenides, dopant ions substitute Zn^{2+} ions in sites of tetrahedral coordination (instead of the octahedral sites in more traditional laser hosts.) The tetrahedral sites lack inversion symmetry, greatly intensifying intra-shell transitions in the dopant ions. Furthermore, the even-parity components of the crystal field are weak enough to give mid-IR transitions. On the basis of the spectroscopic properties[3] of Co^{2+}, Cr^{2+}, and Ni^{2+} in ZnS, ZnSe, and ZnTe, Cr^{2+} was determined to be a prime laser candidate. Absorption and emission spectra and temperature-dependent emission lifetimes are shown in Figure 1. The ~1800 nm $^5T_2$ - ^5E absorption transition, the longest-wavelength band expected for Cr^{2+}, is seen to be quite intense, and accessible with available high-power InGaAsP diode lasers. The accompanying luminescence band extends all the way from 1800 to 3000 nm, with obvious potential for wide laser tunability. Figure 1(b) shows that the emission lifetime gradually increases until well above room temperature, so the room-temperature emission is only

slightly quenched by thermally-activated radiationless decay processes. The Cr^{2+}-doped II-VI compounds are special in this regard.

Table 1 should help to place the ZnSe:Cr^{2+} series of lasers in a familiar context. As far as the spectroscopic properties are concerned, Ti^{3+}:Al_2O_3 shows many similarities--a short emission lifetime, and very broad fluorescence linewidth. Qualitatively, mode-locking, ultra-short pulse generation, high repetition rate, and CW operation are predictable regimes for ZnSe:Cr^{2+}, but the short fluorescence lifetime precludes "energy-storage" operation to produce high-energy pulses. The saturation intensity ($h\nu / \sigma\tau$) for this system is ~15 kW cm^{-2}, a value low enough to facilitate efficient pumping with the focused output of diode laser arrays.

Our first laser tests[4] were done with thin, uncoated crystals in a 20-cm confocal resonator with up to 7.5% out-coupling. A Schwartz Electro-Optics model 1725 MgF_2:Co^{2+} laser operating around 1860 - 1895 nm furnished 40-μsec pump pulses that were partially absorbed in the test samples. The ~0.1 mj pump threshold predicted for these conditions was actually observed for the ZnS:Cr^{2+} laser, validating our spectroscopic analysis. The ZnSe:Cr^{2+} laser had a slightly higher threshold and exhibited a slope efficiency of ~23%, reflecting sub-optimum output coupling. Crystal losses in ZnS and ZnSe were ~10% per pass, apparently from residual absorption. Tunability from 2280 to 2530 nm was obtained (Fig. 2) with an intracavity quartz birefringent filter, which could easily be inserted in the laser cavity. This filter, which supported lasing in multiple orders, exhibited "mode hops" at the extremes of the tuning range. Wider coverage will occur with a more-selective tuning element (e.g. grating.)

In the course of reducing the crystal parasitic absorption losses so as to improve the laser slope efficiency, we have explored several means of producing Cr-doped ZnSe crystals. The first crystals were produced via melt growth with a modified Bridgman technique, but we have since found that seeded physical vapor transport (SPVT) can produce much lower-loss material. Also, the low melting temperatures and high mobilities of divalent transition-metal ions in the zinc chalcogenides make diffusion-doping of pure ZnSe an attractive technique for producing laser material.[5] A wide variety of crystals grown and doped by various techniques have now exhibited laser action.

Medium-average-power (1 - 10 Watt) diode-pumped laser designs for ZnSe:Cr must take into account the host material properties, which differ significantly from those of hard, refractory oxide hosts. ZnSe is well-known as a high-power window material for CO_2 lasers; it has a high thermal conductivity and low Young's modulus, making its fracture toughness suitable for high-power designs. As a semiconductor with a temperature-dependent band-edge position, its refractive index derivative (dn / dT) is comparatively large, making thermal lensing a prime consideration. Our laser design thus incorporates a zig-zag slab architecture, with the slab dissipating several tens of watts pump power from a laser diode array.

This work was performed under the auspices of the U. S. Department of Energy by Lawrence Livermore National Laboratory under Contract W-7405-ENG-48.

References

1. L. D. DeLoach, R. H. Page, G. D. Wilke, S. A. Payne, and W. F. Krupke, "Spectral properties of transition metal-doped zinc chalcogenide crystals evaluated for tunable IR radiation," ASSL '95 paper WE1.

2. R. Renz and H. - J. Schulz, "The decay of infrared luminescence in II-VI compound semiconductors doped by 3d transition elements," J. Phys. C **16**, 4917 - 4932 (1983).

3. L. D. DeLoach, R. H. Page, G. D. Wilke, S. A. Payne, and W. F. Krupke, "Transition metal-doped zinc chalcogenides: spectroscopy and laser demonstration of a new class of gain media," IEEE J. Quantum Electron., to be published.

4. R. H. Page, L. D. DeLoach, G. D. Wilke, S. A. Payne, and W. F. Krupke, "A new class of tunbable mid-IR lasers based on Cr^{2+}-doped II-VI compounds," CLEO '95 paper CWH5.

5. K.-T. Chen et al., "Diffusion of chromium and its solubility in zinc selenide crystals for Cr^{2+}:ZnSe tunable laser application," ACCG / east -95, 17 Oct 95, Atlantic City NJ.

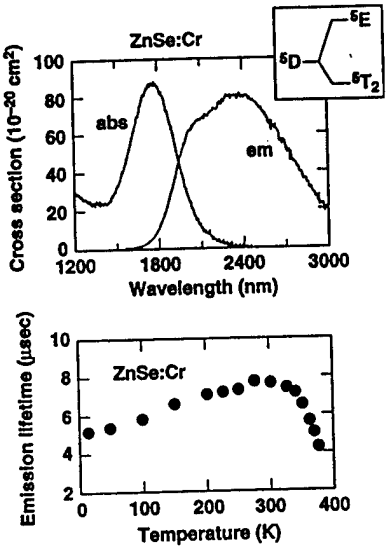

Fig. 1. (a) Cr^{2+} energy level structure and absorption / emission cross sections for ZnSe:Cr. The 1800-nm absorption is suitable for laser-diode pumping, and the broad fluorescence band gives wide laser tunability. (b) Temperature-dependent Cr^{2+} emission lifetime, suggesting high room-temperature quantum yield.

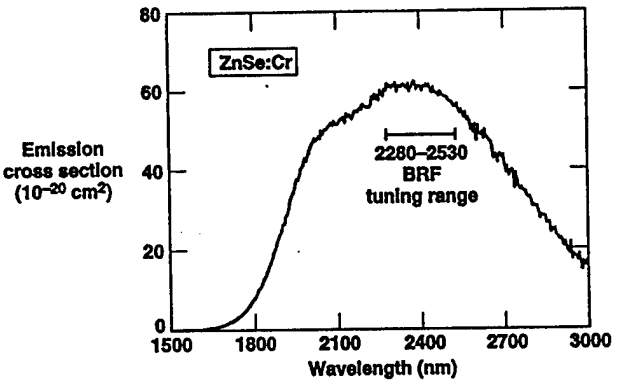

Fig. 2. Tuning range demonstrated in ZnSe:Cr with a quartz-plate birefringent filter. Use of a diffraction grating will enlarge the 250-nm tuning range.

Table 1. Spectroscopic similiarities of Ti^{3+} in Al_2O_3 and Cr^{2+} in II-VI hosts.

		$Ti^{3+}:Al_2O_3$	$ZnSe:Cr^{2+}$
Transition		$^2E \rightarrow {}^2T_2$	$^5E \rightarrow {}^5T_2$
Upper-level lifetime	τ_{em} (μsec)	3	9
Peak fluorescence wavelength	λ_{max} (nm)	800	2300
Fluorescence linewidth (RT)	$\Delta\upsilon$ (cm^{-1})	4300	1700
	$\Delta\lambda$ (nm)	300	1000

High power 2 μm wing-pumped Tm:YAG laser

R.J. Beach, S.B. Sutton, J.A. Skidmore, and M.A. Emanuel

Lawrence Livermore National Laboratory
P.O. Box 808, L-493, Livermore, CA 94550
TEL (510) 423-8986
FAX (510) 422-3358

The 2 μm radiation produced by the $^3F_4$-$^3H_6$ transition of Tm^{3+} has many practical applications because it is strongly absorbed by water and also because it is an 'eye-safe' wavelength. The strong absorption of 2 μm radiation by water makes this transition a very attractive candidate for performing laser surgical procedures as most tissue types are predominately composed of liquid water. The fact that 2 μm radiation is considered 'eye-safe' makes this transition attractive for laser range finding and remote sensing applications where other laser wavelengths could pose a safety hazard. At sufficiently high doping densities Tm^{3+} exhibits a beneficial two-for-one quantum pump efficiency enabling well developed AlGaAs laser diode arrays to be used as efficient excitation sources. Many applications requiring 2 μm laser radiation such as remote sensing, laser radar, anti sensor, sensor spoofing, and OPO pumping have driven the development of diode pumped all solid state Tm^{3+} laser systems because of their potential for efficiency, compactness, and ruggedness. In this presentation we focus on Tm^{3+}:YAG and the scalable diode end-pumping technology developed at LLNL which we believe will enable higher average power operation of diode pumped Tm^{3+} laser systems than has previously been possible.

Figure 1 shows a layout of our cw Tm:YAG laser. To date we have demonstrated cw operation of this laser at power levels of 26 W. The end-pumping technology used is the same as was previously used to demonstrate a 100 mJ Q-switched Nd:YLF laser[1]. A microlens conditioned stack of laser diode arrays having an overall aperture of 2.5 cm x 1 cm and consisting of 25 silicon microchannel cooled modules, each carrying a 1 cm long laser diode bar and microlens as shown in Fig. 2, has its output radiation delivered to the end of a Tm:YAG laser rod that is 2.5 mm in diameter and 5 cm long and doped with 4% Tm. The purpose of the microlenses is to collimate the fast axis radiation from the laser diode arrays. By expanding and collimating the fast axis radiation from individual bars, but not increasing the overall aperture area, the effective radiance of the diode arrays (where effective means the radiance referenced to the overall aperture area), can be increased without violating the conservation of radiance. Once the pump radiation is conditioned it can then be delivered to the end of the laser rod with very high efficiency by the lens duct that works by both lensing the conditioned pump light at its curved input face and then ducting the pump light down to the rod aperture by total internal reflection off its canted planar sides. The laser rod itself is held in a cooling jacket that permits water to be flowed along its length during laser operation.

To allow average power scaling of this laser it is not possible to pump at the peak of the absorption feature located at 785 nm as is conventionally done in end-pumped Tm^{3+}:YAG lasers. This is because in the heavily doped that give two-for-one pump quantum efficiencies, the resulting absorption length of the pump in the rod is too short to allow for effective thermal management in the rod. These short absorption lengths in turn lead to high intensity thermal generation near the pump input face of the laser which results in unacceptable temperature rises in the rod there negatively impacting the systems performance. Our analysis and experimental results demonstrate that wing pumping the Tm^{3+} off the peak of the main absorption feature can still be effective at creating sufficient inversions to overcome ground state reabsorption and allow for efficient laser operation while at the same time allowing the pump to penetrate deeply enough into the sample that the resulting thermal load becomes manageable. The laser rod itself has a barrel finish

over its entire length allowing the pump light that enters the rod at the pump input end to be efficiently ducted down the rod due to TIR confinement. The pump input end of the rod is dichroically coated to be transmissive at the pump wavelength and reflective at the 2.01 μm laser wavelength. The other end of the laser rod is AR coated at the laser wavelength and 90% reflective at the pump wavelength. This allows the pump light to be effectively double passed up and back down the laser rod. The wavelength of our pump laser diodes was 805 nm which corresponds to a 1/e pump absorption distance of 2.2 cm in the 4% doped rod used here. To date we have demonstrated optical-to-optical slope efficiencies of 20% and cw optical output powers up to 26 W as displayed in Fig. 3. In this figure the cw optical output power is plotted against total pump power measured at the diode array so that the quoted efficiency includes the collection efficiency of the cylindrical microlenses used to condition the diode output radiation as well as the delivery efficiency of the lens duct. In the present system the combined efficiency of the cylindrical microlenses and the lens duct delivery is 0.7.

One of the key technical developments that has enabled the level of performance we have achieved to date with the system was the use of a laser rod having an undoped end-cap fusion bonded to the pump input end of the laser rod. This end cap was 3 mm in length and effectively isolated the pump input face of the rod from the thermal generation source comprised by the doped portion of the laser rod. We have found the use of such laser rods with undoped end-caps to be critical to the performance of the laser. As a point of comparison, using the same laser with a laser rod not having an undoped end-cap, but in other ways identical to the one with the undoped end-cap, the maximum cw output power we could obtain from the system was 6 W at which point the laser output began to roll over because of the heat generated at the pump input face. An additional benefit of the undoped end-cap is that the dichroic coatings see a nearly uniform temperature profile at the pump input end of the laser rod.

In summary we have demonstrated a Tm^{3+}:YAG laser with an output power capability of 26 W cw. This level of performance was demonstrated on a system using a number of new developments and innovations such as the scalable diode end-pumping technology that has been developed at LLNL, wing-pumping the Tm^{3+} off to the side of its main absorption feature at 785 nm to give a manageable thermal load, and the inclusion of laser rods incorporating undoped end-caps fusion bonded to the doped portion of the laser rod at the pump input end of the rod to isolate the pump input end of the rod from the thermally loaded portion of the rod.

We gratefully acknowledge the expert technical assistance provided by Helmuth and Oliver Meissner at Onyx Optics in Dublin CA who fabricated the laser rods with the undoped diffusion bonded end-caps that were used in our system and Ralph Hutchinson of Scientific Materials in Bozeman, MT for the Tm:YAG and undopded YAG that was used in fabricating these laser rods. We also gratefully acknowledge many useful conversations with Steve Payne, Bill Krupke, and Rich Solarz all of Lawrence Livermore National Laboratory.

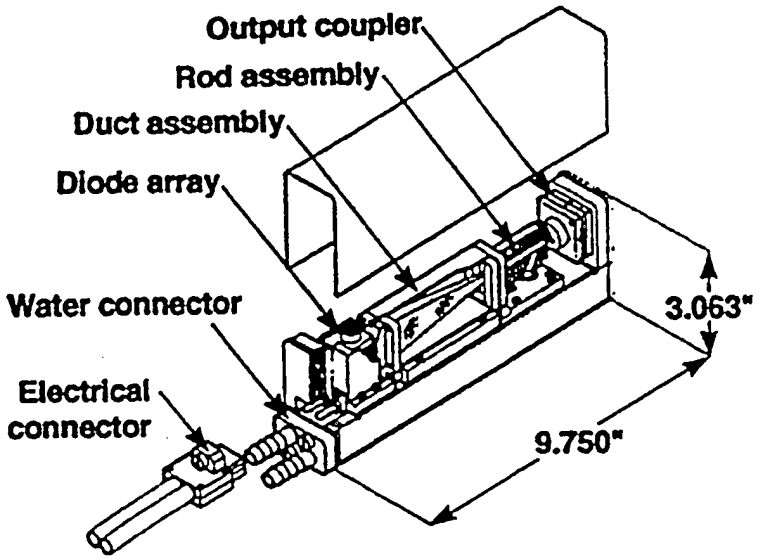

Fig. 1. Exploded diagram showing the layout of the Tm^{3+}:YAG laser.

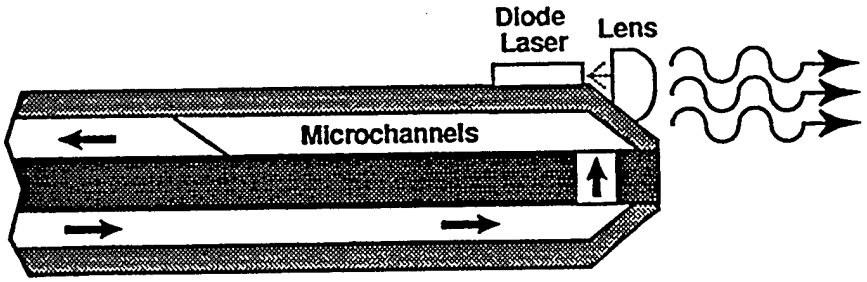

Fig. 2. Cross-sectional view of LLNL silicon microchannel cooler diode package with cylindrical microlens attached.

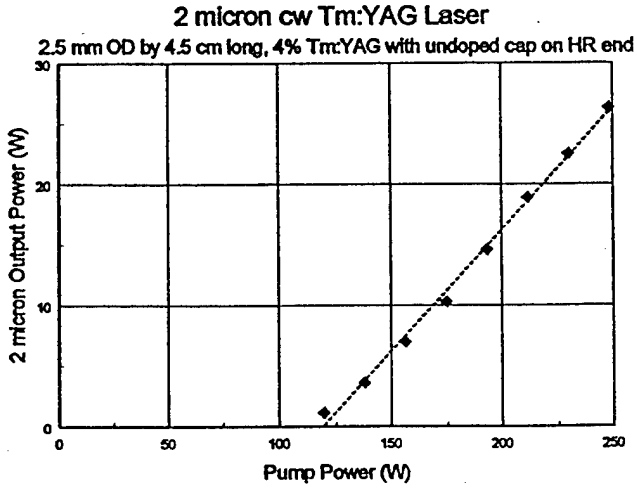

Fig. 3. Measured cw performance of the Tm^{3+}:YAG laser.

---

[1] R. Beach, R. Reichert, W. Benett, B. Freitas, S. Mitchell, S. Velsko, J. Davin, and R. Solarz, "Scalable diode-end-pumping technology applied to a 100-mJ Q-switched Nd^{3+}:YLF laser oscillator," Optics Letters, V 18, pp1326-1328 (1993).

2-Watt single-frequency CW Tm,Ho:YLF ring laser.

Andrew Finch and John H. Flint

Schwartz Electro-Optics Inc.,

45 Winthrop St., Concord MA 01742

Tel: 508 371 2299

Fax: 508 371 1265

Tm,Ho:YLF lasers are proving to be effective sources for a variety of coherent wind sensing applications. The majority of long range systems (>5 km) rely on pulsed i.e. Q-switched sources operating at 10 - 200 Hz repetition rates. However for short range applications single-frequency CW sources are useful and in some cases preferred. This paper details the performance of a breadboard Tm,Ho:YLF ring laser which will eventually be packaged for use in field measurements. To date the system has produced 2.1 W single frequency output which we believe represents the highest single-longitudinal mode power obtained from a Tm,Ho:YLF laser. Previous workers have reported the performance of single-frequency standing wave cavities, but output powers have been limited to 1.2 W [1]. The design used here, as shown in Figure 1, is a modification of a diode pumped Q-switched ring laser previously reported for use in clear-air-turbulence detection [2].

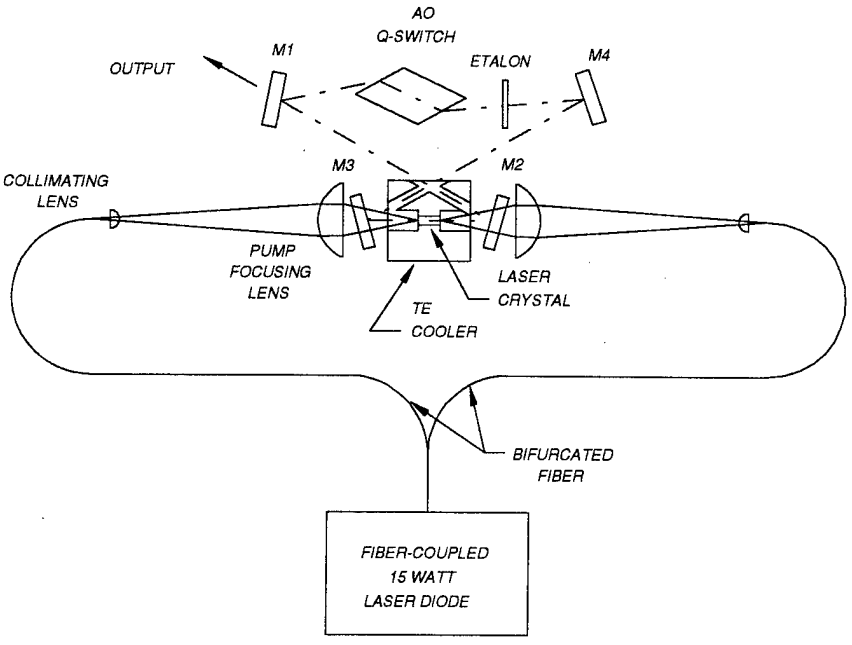

Figure 1. Schematic of the single frequency Tm,Ho:YLF ring laser

The 2-μm laser cavity contains a 10-mm long, 4-mm diameter 6% Tm, 0.5% Ho:YLF crystal mounted in a TE-cooled heat sink inside a purgeable enclosure. The hot sides of the TE-cooler are cooled to 5°C using a Neslab chiller, allowing the YLF crystal block to be cooled to as low as 235 K (-35°C). A single 20-W laser bar is used as the pump source, whose output is coupled to a bifurcated fiber bundle, i.e. the bundle was split into two separate smaller bundles each of which were imaged into either end of the YLF rod through HR/HT flat mirrors. The remainder of the ring resonator is a flat output coupler and a 50-cm curved high reflector. A Brewster-angled acousto-optic Q-switch is inserted in one leg of the cavity.

In previous work the ring laser, when operated in CW mode, was made to lase unidirectionally by employing an external mirror next to the output coupler to retroreflect one output back into the cavity. This acted to suppress that direction of lasing to a very low fluence level and the laser was effectively unidirectional. Its output was not single frequency, however, and typically suffered sporadic amplitude noise. This was due to phase fluctuations of the retroreflected light relative to the cavity field, since the outside mirror was not interferometrically matched to the cavity.

Achieving truly unidirectional (and hence single-frequency) operation requires the insertion of a unidirectional device inside the laser ring cavity. One possibility is to use an optical diode based on the Faraday material YIG. Unfortunately, the available samples of this material apparently had too small a through aperture. Based on recent work performed at the University of Southampton (U.K.) [3,4], an alternative approach is to use an acousto-optical modulator. Operating such a device slightly away from the Bragg angle sets up a differential loss between the two lasing directions in the ring cavity. The device is operated with RF applied just sufficient to suppress the one (back) direction, since the forward direction still sees loss due to the RF applied. Use of these devices may present a larger insertion loss to the cavity compared to an optical diode, however they provide the advantage of having variable control of differential loss. This is useful when optimizing the laser for different operating points and accommodating feedback effects from optics external to the cavity.

In these initial CW experiments, while maintaining constant RF power to the Q-switch, we adjusted it away from its Bragg angle while monitoring the power levels of each lasing direction. Optimum alignment (i.e. maximum differential loss for minimum RF applied -hence minimum insertion/forward loss) was achieved by additional vertical alignment adjustments of the two turning mirrors. Once aligned properly, unidirectional operation was reliably achieved and the output amplitude fluctuations were extremely small (<0.1% rms.). Over 2 W of single frequency output power was achieved (Figure 2), interestingly without any etalons in the cavity. Single frequency operation was verified using two Burleigh scanning interferometers with free spectral ranges of 8 GHz and 150 MHz. We suspect that the AR surface of the crystal and/or the windows around the purged enclosure are acting as etalons. We inserted a 100 μm etalon into the cavity and tuned the laser from 2.0671 to 2.0537 μm. A tuning curve is shown in Figure 3. The tuning was not continuous but separated by ~0.3 nm skips which is indicative of additional etalon elements inside the cavity. A variety of output couplers were tried; the optimum coupling seems to be in the 2.5 - 4% range.

These experiments suggest that it may be possible to design a generic ring cavity which can operate as either a multi-milli Joule Q-switched or a multi-Watt, single-frequency CW source without the inclusion or removal of any additional optics.

References

[1] C.P. Hale, S.W. Henderson, and P.J.M. Suni, Proc. on Advanced Solid-State Lasers **15**, 407 (1993).
[2] A. Finch, John Flint, CLEO'95, Tech. Digest Series 15, Paper CWH2 232 (1995).
[3] W.A. Clarkson, A.B. Nielson, and D.C. Hanna, Opt. Lett. **17** 601 (1992).
[4] M. K. Reed, W. K. Bischel, Opt. Lett. **17** 691 (1992).

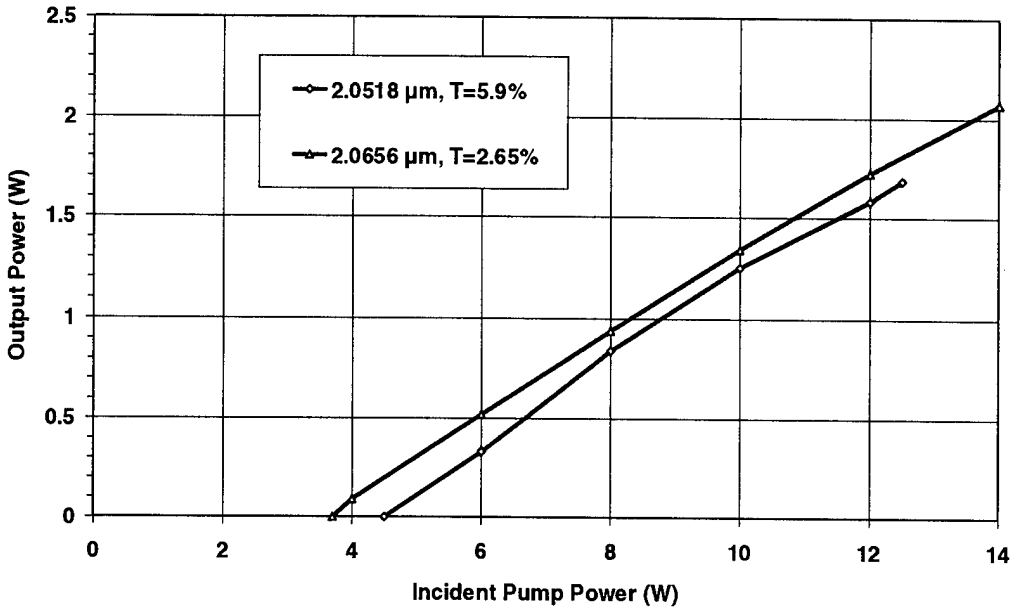

Figure 2. Input/ output data of single frequency ring laser. (Crystal block temperature = 238 K).

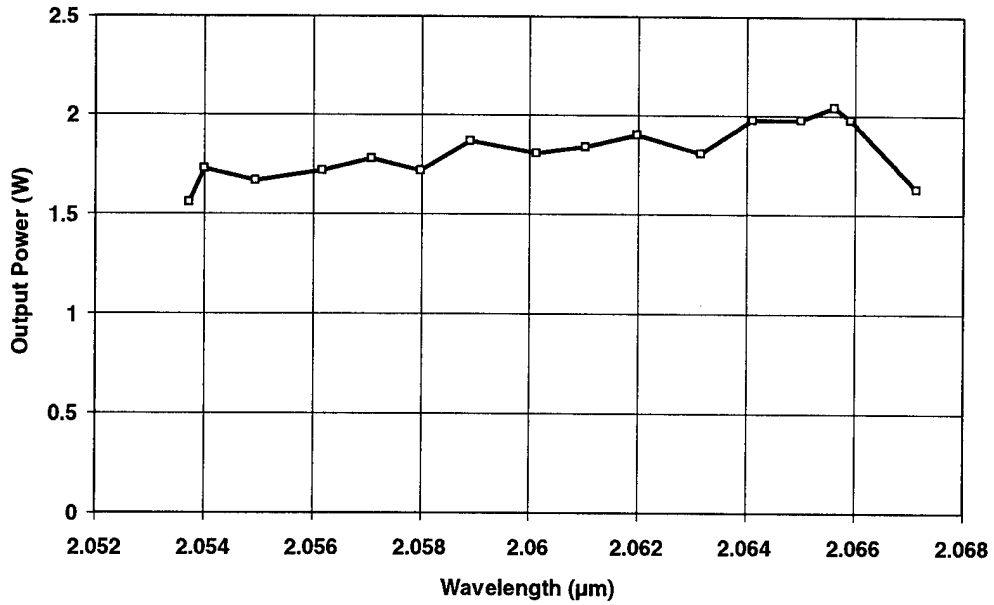

Figure 3. Tuning curve of single frequency ring laser (Pump power =14 W, crystal block temperature = 238 K)

1.55 µm-wavelength CW microchip lasers.

Philippe THONY, Engin MOLVA

LETI - CEA (Technologies Avancées)- Dépt Optronique
CENG, 17, rue des Martyrs, 38054 Grenoble, France

A reliable and compact laser source emitting near 1.55 µm is of great interest for a lot of applications[1]. Such a laser, operating in a pulsed or modulated emission regime, can be used to build a lidar, a range finder,... with free-space propagating beams. So we investigate on the development a microchip laser made of erbium and ytterbium codoped glass, keeping in mind that it has to stay very simple to use and to manufacture.

The most important feature in a continuous wave microchip laser is its simplicity. The device itself and the fabrication process have to remain simple, in order to get good reliability and low cost. The microchip laser is made of a laser material wafer, which is polished on both sides flat and parallel. The plates are one inch in diameter and the thickness vary from 0.3 to 1 mm. Both sides are directly coated with multi-layer dielectric films, in order to make the two mirrors of the laser resonator. The resonator is a flat/flat Fabry-Perot cavity. The wafer is then sawed in little square chips of 1 mm in side. Each chip is a laser and can be succesfully pumped to obtain laser operation. These lasers are mounted in special housings, which can be directly connected to the end of a fiber-coupled laser diode.

The input mirror is highly reflective for the 1.5 µm wavelength and presents a good transmission at the pump wavelength (94 %). The output coupler has a 1 % transmission at the laser wavelength and is highly reflective at the pump wavelength.

The gain medium is erbium and ytterbium codoped phosphate glass (Kigre QX/Er). The dopant concentrations have been calculated in order to minimize the laser threshold. A theoretical model of the er,yb:glass system, based on rate equations, allows us to optimize the material[2]. We have carried out some spectroscopic characterization on this glass. The figure 1 shows the emission spectra of a 0.4 mm thick sample, when it is pumped with a Ti-Sapphire laser emitting at 980 nm. The lifetime of the excited energy level $^4I_{13/2}$ is 6.5 ms with our special concentration.

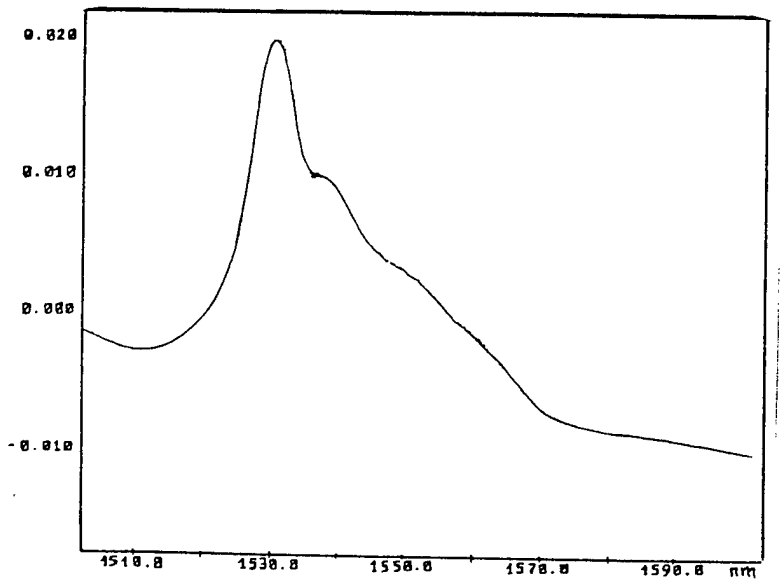

fig. 1 : fluorescence spectrum of er,yb:glass.

The microchip lasers have been pumped before sawing with a fiber-coupled laser diode (from SDL). The fiber has a 50 µm diameter core. The laser diode is tuned to 973 nm. The laser characteristics appear to be very homogeneous throughout the full plates. Threshold as low as 18 mW and slope efficiency of 33 % have been measured. This threshold is twice lower than Laporta's reported value[1]. The pump power has been increased up to 500 mW without any damage on the glass microchip lasers. Figure 2 shows the laser output versus input power for four different thicknesses of microchip laser. The absorption coefficient of the erbium and ytterbium codoped glass, which has been measured with the laser diode : is 13 cm^{-1}. Thresholds and slope efficiencies are summarized in table 1.

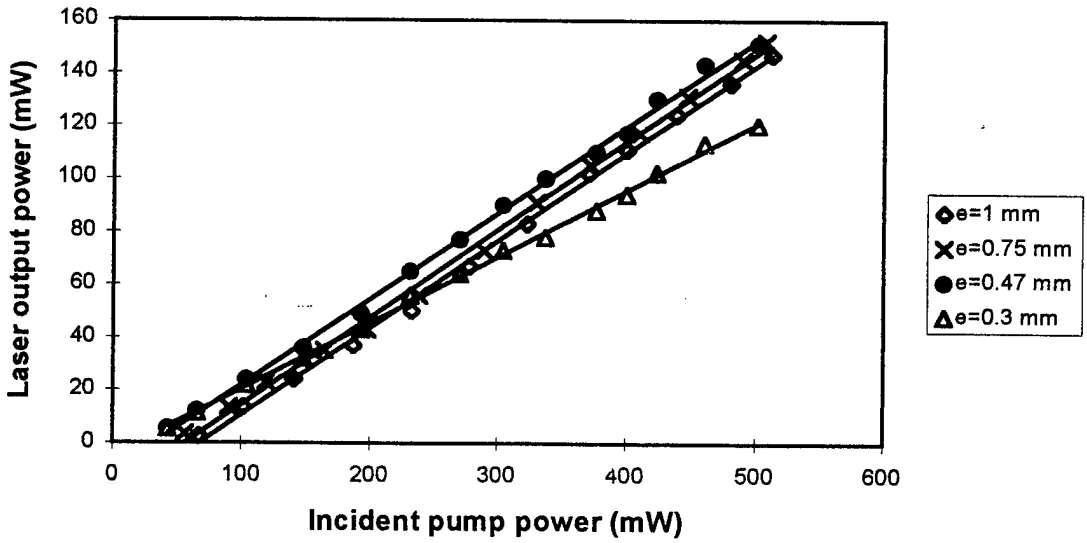

fig. 2 : output power versus incident input power for er,yb:glass microchip lasers

sample thickness	incident pump power threshold	absorbed pump power threshold	slope efficiency (incident pump)	slope efficiency (absorbed pump)
0.3 mm	18 mW	9 mW	25 %	48 %
0.47 mm	31 mW	21 mW	33 %	49 %
0.75 mm	57 mW	45 mW	33 %	41 %
1 mm	68 mW	59 mW	33 %	38 %

tab. 1 : threshold an slope efficiency of er,yb:glass microchip lasers

Spectral measurements have been carried out with a monochromator, which has a scanning output mirror (SPEX 500). With a 0.3 mm thick laser, single-frequency operation is observed up to an output power of 20 mW at a wavelenght near 1.530 µm. With a 0.47 mm thick sample, single-frequency is observed up to 10 mW at the same wavelength.

When the pump power is increased, the emission spectrum is varying in two ways : more and more peaks appears and each peak is shifted toward higher wavelength. The shift has been measured for the 0.3 mm thick laser : a rate of 1 nm for 100 mW of incident pump power is obtained. A simple thermo-mechanical analysis shows that in a phosphate glass host, the main effect is the thermal expansion, which increases the cavity length.

Full pump power spectra have been recorded too (at a power of 500 mW). For the 0.3 mm thick sample, 3 peaks near 1.535 µm are observed. These peaks are located at the maximum of gain in the laser material. For the 0.47 mm thick sample, 4 peaks near 1.535 µm and 3 peaks near 1.55 µm. For the 0.75 mm thick sample, 7 peaks are observed near 1.55 µm and for the 1 mm thick sample, up to 12 peaks can be observed between 1.55 µm and 1.56 µm. We see that the center wavelength changes when the thickness of the laser increases. Because the erbium laser is a three level system, the losses increase with the thickness of the laser cavity. This is also proved by considering the linear evolution of the threshold as a function of thickness in table 1. At low thickness, the low losses allow the laser to operate at its maximum gain level. At a higher thickness, the losses are greater and the laser operates at a maximum net gain, which correspond to a higher wavelength.

Conclusion

We have designed and built er,yb:glass microchip lasers with a collective fabrication process. Lasers of different cavity length have been operated under fiber-coupled laser diode pumping. The threshold can be as low as 18 mW in incident pump power and the slope efficiency as high as 33 %. Spectral measurements shows the shift of the wavelength as the pump power is increased, which allow the laser to be modulated (1.3 GHz/mW). A single-frequency power of 20 mW has been measured for a laser thickness of 0.3 mm.

This work is supported by the DRET (Direction des Recherches et Etudes Techniques) under contract 94-429. Thanks to ENSCP for lifetime measurements.

---

[1] "Diode-pumped microchip Er-Yb:glass laser", Laporta, Taccheo, Longhi, Svelto, Optics Letters, vol. 18, n°15, p. 1232, 1993.

[2] "Analysis and modelling of the erbium-ytterbium glass laser", Laporta, Longhi, Taccheo, Svelto, *Optics Communications*, vol. 100, p. 311, 1993.

Continuous Wave Fiber Laser Operation at a Wavelength of 3.9 Micrometers

J. Schneider, C. Carbonnier, U. B. Unrau

Institut für Hochfrequenztechnik, Technische Universität Braunschweig
Schleinitzstr. 22, D-38106 Braunschweig, Germany
Phone: +49 531 391-2458; Fax: +49 531 391-5841
e-mail: U.Unrau@tu-bs.de

Introduction

After introducing the first 3.9 μm laser in a Ho^{3+}-doped fluoride fiber [1], this paper presents efficient CW emission of the $^5I_5 \rightarrow {}^5I_6$ transition for the first time. Furthermore, laser operation was achieved using two different pump wavelengths, the previously reported 640 nm region and 890 nm.

Results and Discussion

In order to enhance the properties of the transition $^5I_5 \rightarrow {}^5I_6$, several mechanisms within the Ho^{3+}-ion had to be considered to enable laser oscillation around 3.9 μm. The pump wavelength around 640 nm was chosen because Ho^{3+} has a strong absorption in this pump range. This pump range lead to laser action, first. The cascade laser scheme 3.9/1.2 μm was chosen to deplete the lower laser level $^5I_6$ of the 3.9 μm transition to the ground state.

A fluorozirconate fiber fabricated by Le Verre Fluoré was used for the experiments. The fiber was doped with 2000 ppm Ho^{3+}. Previous results were obtained using a Fabry-Perot resonator with an input mirror of high reflectivity at 3.9 μm and 40 % reflectivity at 1.2 μm. The output coupler had a reflectivity of 96 % for both laser wavelengths. During the laser measurements the fiber was cooled with liquid nitrogen. Output powers of approximately 1 mW were achieved in [1], the laser at 3.9 μm was not entirely in CW mode.

The availability of higher pump power around 640 nm and improvements of the Fabry-Perot resonator resulted in an output power of 6.8 mW for the 3.9 μm laser. The mirror reflectivities were changed to high reflectivity for both laser wavelengths for the input mirror and 95 % and 88 % for the transitions at 1.2 and 3.9 μm, respectively. Laser action could still be observed up to 145 K, as shown in Fig. 1.

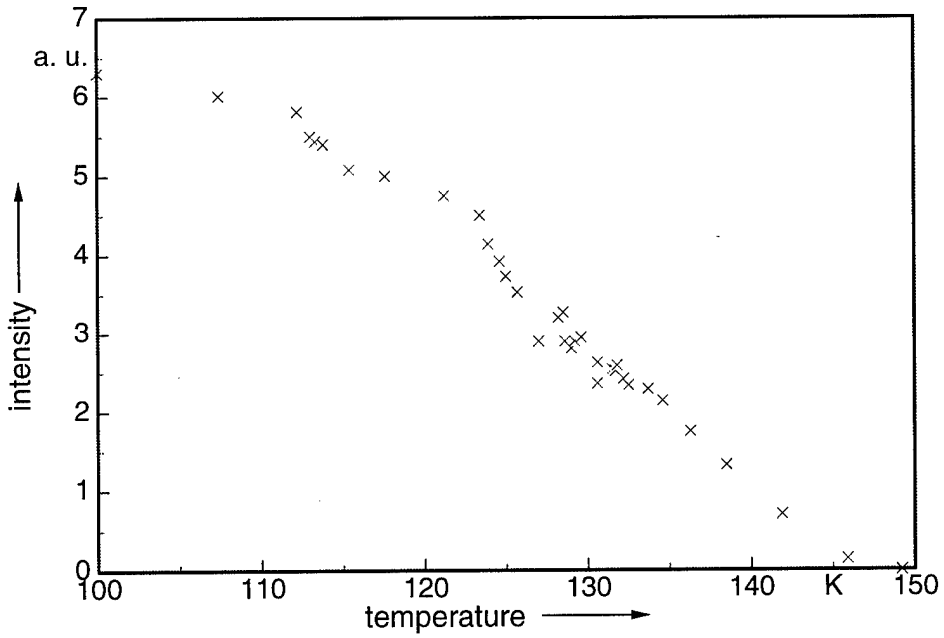

Figure 1: Behavior of the 3.9 μm laser pumped around 640 nm with increasing temperature

Using a pump wavelength of 890 nm from a Ti:Sapphire laser, even higher output powers were achieved. The laser characteristic is shown in Fig. 2. With support of the cascade laser process, the 3.9 μm laser had a maximum CW laser output power of 11 mW. A calculated efficiency of 1.7 % results with an estimated launching efficiency of 50 %. The 1.2 μm transition had a slope efficiency of 6.9 % with a CW maximum output power of approximately 70 mW. The results were obtained at 1.7 W launched pump power.

Conclusion

We reported for the first time 3.9 μm CW fiber laser action in Ho^{3+}-doped ZBLAN fibers taking advantage of the cascade lasing scheme, where the 1.2 μm transition supports laser action at the desired wavelength. With the output powers obtained, practical applications of the attenuation minimum in the atmospheric window 3–5 μm should become possible.

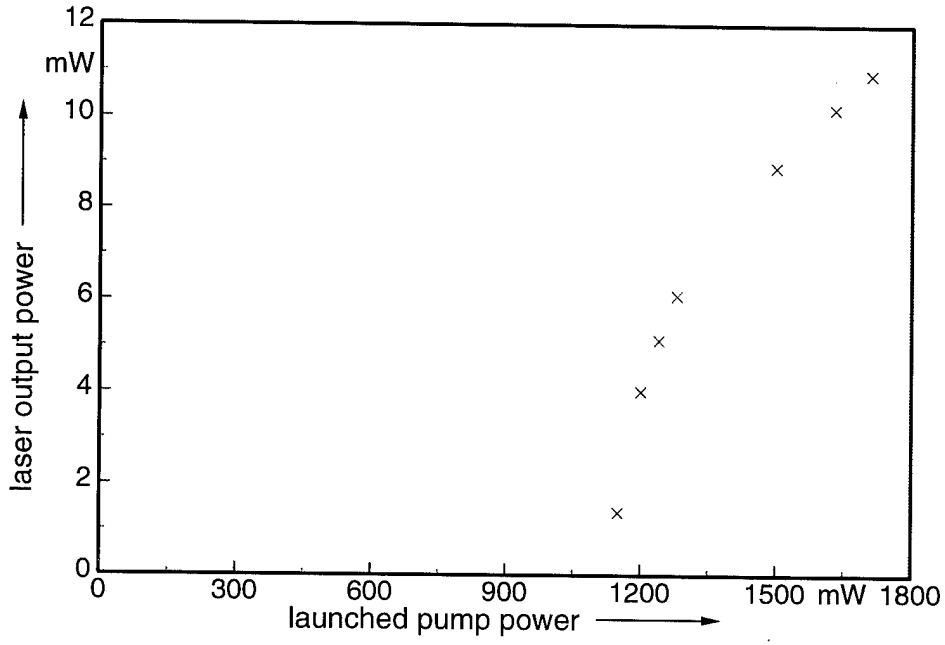

Figure 2: Laser characteristic of the laser at 3.9 μm pumped around 890 nm

References

[1] J. Schneider: 'Fluoride fibre laser operating at 3.9 μm', *Electronics Letters*, Vol. 31, No. 15, 1995, pp. 1250–1251.

[2] J. Schneider: 'Superfluorescent fiber source at 3.9 μm in the attenuation minimum of the atmospheric window 3 – 5 μm', *International Journal of Infrared and Millimeter Waves*, Vol. 16, No. 1, 1995, pp. 75–82.

Slope Efficiency of a Pulsed 2.8-μm Er^{3+}:$LiYF_4$ Laser

R. Spring, M. Pollnau, S. Wittwer, W. Lüthy, and H.P. Weber
Institute of Applied Physics, University of Bern,
Sidlerstrasse 5, CH - 3012 Bern, Switzerland
Phone +41-31-631 89 41, Fax +41-31-631 37 65, e-mail spring@iap.unibe.ch

In recent years there has been increased interest in lasers emitting at 3 μm mainly because of their potential applications in laser surgery. Due to the high absorption of 3 μm radiation in water, highly precise cutting or ablation of biological tissue with minimal thermal damage to adjacent tissue can be performed. Long pulses (300 μs) operating in aqueous media, e.g. in orthopedic surgery, lead to an optimum in ablation efficiency [1]. They can generated either by pulsed modulation of the cw output or by pulsed excitation of the laser.

However, pulsed excitation of an Erbium 3-μm laser affects the efficiency of the laser output. In this contribution the dependence of the slope efficiency of an Er^{3+}:$LiYF_4$ crystal (15 at. % with respect to Y^{3+} site, 4 mm length) at 2.8 μm on pump-pulse duration is investigated. The dopant concentration of 15 at. % in $LiYF_4$ is proven to be optimal for 3-μm emission [2].

The laser crystal was direct resonantly pumped with an Ar^+-laser-pumped Ti:sapphire laser at 973 nm into the $^4I_{11/2}$ upper laser level. The 970-nm pump band has been shown to be more efficient than other pump wavelengths used for this laser transition [3]. The pump beam was focused with 65 mm focal length onto the crystal front face with a beam waist of 40 μm. The pump absorption reached almost 100 %. The crystal was cooled with a heat exchanger and positioned close to the input mirror inside of a nearly hemiconcentric resonator. Both mirrors, the plane input and the concave (75-mm radius) output mirror had a non-optimized transmission of 1.2 % at 2.8 μm. The laser power was measured to be transmitted in equal parts on both sides of the resonator. The laser crystal was quasi-cw pumped with 20-ms pulses of a chopped (17 Hz, duty cycle 33 %) Ti:sapphire laser (TEM_{00} mode). The output power as function of the input pump power is shown in Fig. 1. The laser threshold was 13 mW. A maximum output power of 77 mW was reached with an input power of 250 mW which was limited by the available pump laser. A slope efficiency of 40 % was obtained, to our knowledge the highest value so far for any Er^{3+} laser. Thus the slope efficiency clearly exceeds the Stokes limit $\eta_{st} = \lambda_{pump} / \lambda_{laser}$ = 35 % due to energy recycling into the upper laser level via interionic upconversion ($^4I_{13/2}$, $^4I_{13/2}$ —> $^4I_{15/2}$, $^4I_{9/2}$) [3,4,5].

In a second experiment (c.f. Figs.2 and 3) the duty cycle of the chopper was varied between 33 % and 5.6 % while the chopper frequency (33.3 Hz) was kept unchanged. Thus the pump-pulse duration was reduced from 10 ms down to 1.67 ms, with dramatical consequences on slope efficiency. The experimental results (squares) are presented in Fig. 2 . The slope efficiency drops from 36 % (10 ms pump-pulse duration) to 21 % (1.67 ms pump-pulse

duration). With the help of a computer simulation considering all important processes (ground-state absorption (GSA), excited-state absorption (ESA), interionic processes and their inverse processes, stimulated emission and the experimental data of crystal and resonator) time-resolved rate equations similar to those presented in Ref. [4] were solved in order to reproduce (circles) the experimentally obtained data (squares) (c.f. Fig.2).

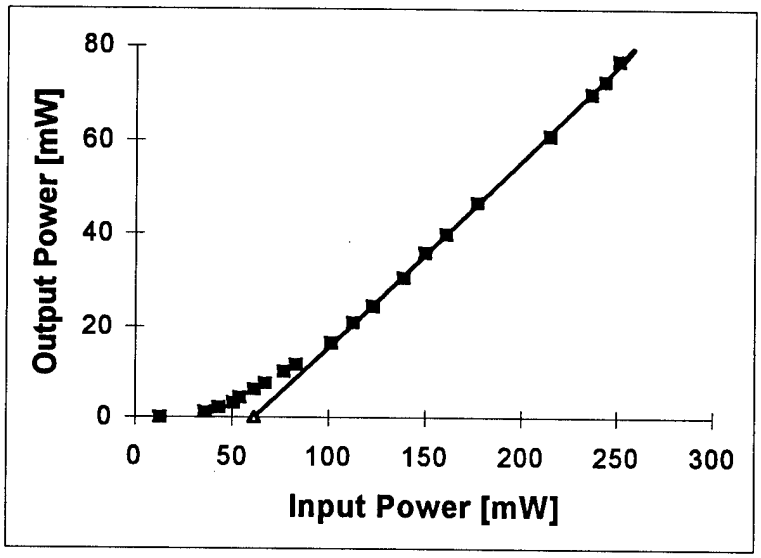

Fig. 1. : The output versus the input power of a pulsed Er^{3+}:$LiYF_4$ laser under quasi-cw Ti:sapphire laser excitation (20-ms pump pulses) is presented. A maximum slope efficiency of 40 % has been experimentally demonstated. The threshold of the laser is 13 mW and the slope threshold, is 60 mW (triangle).

In Fig.3 the slope threshold $P_{slope,thr}$, defined as the zero point of the progression line of the linear input-output slope, is presented as a function of pump-pulse duration. With the experimentally obtained values for slope efficiency $\eta(10\ ms)$ = 36 % (c.f. Fig.2) and slope threshold $P_{slope,thr}(10\ ms)$ = 60 mW (c.f. Fig.3) and values for the resonator losses of 0.8 % and the emission cross section of σ_{em} = 1.5 x 10^{-20} cm^2, the computer simulation gave good agreement with the experiment.

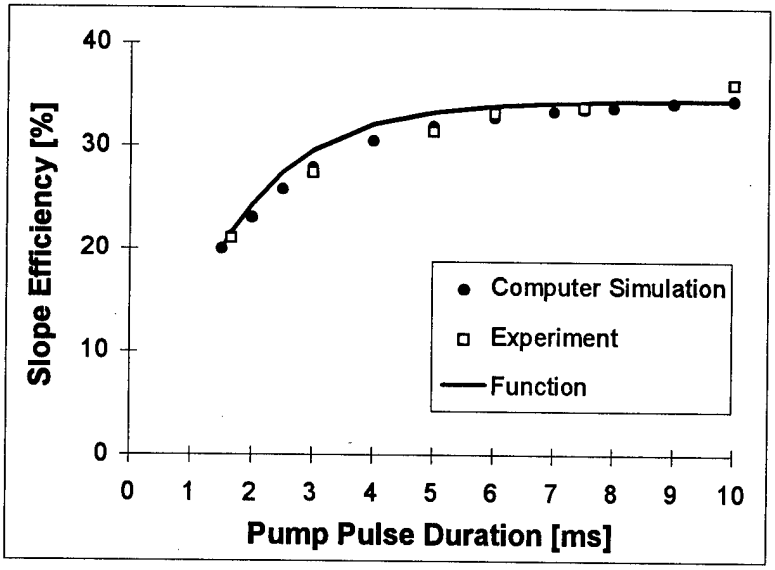

Fig. 2. : The dependence of the slope efficiency on the pump-pulse duration is shown. Data from the experiment (squares) and from the computer simulation (circles) are approximated by a function (line) which depends on the storage time of the upper laser level.

The dependence of the slope efficiency $\eta(T)$ on pump-pulse duration T can be approximated by a function (c.f. Fig.2) :

$$\eta(T) = \eta(cw)\ \{1 - \exp[-(T - E_{thr} / P_{in}) / \tau_{store}]\} \qquad (1)$$

with slope efficiency for quasi-cw pumping $\eta(cw) \cong \eta(10\ ms)$, threshold energy E_{thr} = 60 µJ and input power P_{in} = 180 mW (derived from experiment). The storage time of the upper laser level τ_{store} , the characteristic time constant of the system, can be expressed as

$$1/\tau_{store} = 1/\tau_2 + W_{22} \cdot N_2 \qquad (2)$$

with intrinsic lifetime of the upper laser level τ_2 = 4 ms, upconversion parameter W_{22} = 1.8 x 10^{-17} $cm^3 s^{-1}$ [5], and upper laser level population N_2 = 2.6 x 10^{19} cm^{-3} (derived from simulation). A storage time of τ_{store} = 1.4 ms is determined from formula (2).

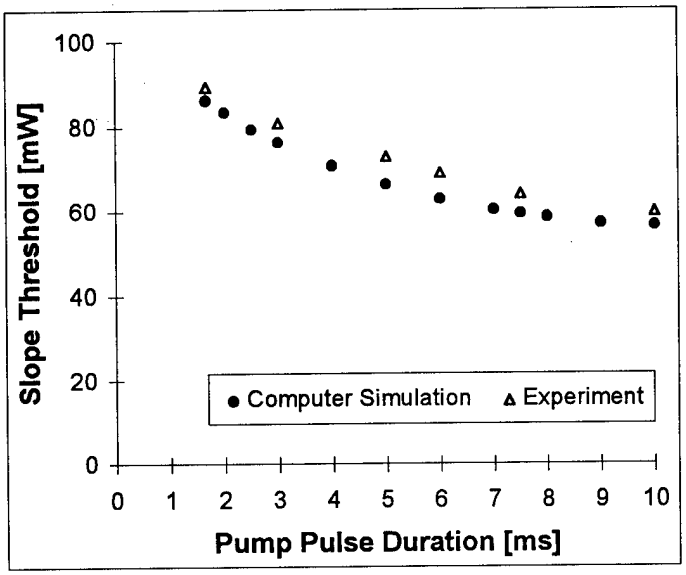

Fig. 3. : The slope threshold, defined as the zero point of the progression line of the linear input-output slope, is presented as a function of pump-pulse duration. The data experimentally obtained (triangles) are reproduced by the computer simulation (circles).

In conclusion a slope efficiency of 40 % from an Er^{3+}(15 % at.):$LiYF_4$ 2.8 µm laser is demonstrated. This value clearly exceeds the Stokes limit of 35 % due to energy recycling from lower to upper laser level. A decrease of the slope efficiency with reduced pump-pulse duration is experimentally observed and reproduced by a computer simulation.

This work was supported in part by the Swiss Priority Program "Optique".

References

[1] M. Ith, H. Pratisto, H.J. Altermatt, M. Frenz, and H.P. Weber, Appl. Phys B **59**, 621 (1994).
[2] T. Jensen, A. Diening, and G. Huber, in Conference of Lasers and Electro-Optics, Vol. **15**, 1995 OSA Technical Digest Series (Optical Society of America, Washington DC, 1995), postdeadline paper CPD29.
[3] R. C. Stoneman and L. Esterowitz, Opt. Lett. **17**, 816 (1992).
[4] M. Pollnau, W. Lüthy, and H. P. Weber, Phys. Rev. A **49**, 3990 (1994).
[5] H. Chou and H.P. Jenssen, in Tunable Solid State Lasers, Vol. **5** of the OSA Proceeding Series, M.L. Shand and H.P. Jenssen, eds. (Optical Society of America, Washington, DC, 1989), pp. 167 - 174.

Quasi-cw Diode Pumped 2.8 μm Laser Operation of Er^{3+}-doped Garnets

T. Jensen, G. Huber, and K. Petermann

Institut für Laser-Physik, Jungiusstr. 11, 20355 Hamburg, Fed. Rep. Germany

Recent laser experiments demonstrated cw laser performances between the upper $^4I_{11/2}$ and lower $^4I_{13/2}$ laser level in several Er^{3+}-doped crystals with efficiencies near to or equal to the quantum defect [1-4]. For pump wavelengths around 970 nm the quantum defect is about 35%. These results are remarkable, because, taking a straight laser theory into account, one expects a self terminating laser behavior, due to a much longer lifetime of the lower laser level in comparison to the upper laser level.

Upconversion processes starting from the lower laser level efficiently recycle population to the upper laser level, so that cw laser action becomes possible. Beyond that, the upconversion process is so strong, that the slope efficiency of the laser can reach the quantum defect, what is normally inaccessible for a typical four-level laser. Obviously the upconversion process lifts the pump efficiency above one. For a laser system operating near to the quantum defect in cw mode at 2.8 μm, we estimate a pump efficiency between 1.2 and 1.5.

In quasi-cw diode pumped operation these high slope efficiencies should be attainable as well, but reported output powers and efficiencies are still very low. Pulse energies of 7 mJ for Er:YAG [5] and of 3.4 mJ for Er:YSGG [6] were achieved.

The damage threshold of the semiconductor facets limit the output intensity of diode lasers very strongly [7]. The increase of intensity, when operating the diodes in a quasi-cw mode instead of the normal cw mode, is quite small. To reach output powers of several hundred watts the emitting dimensions have to be enlarged. Due to heatsink layers between the arrays the brightness of the whole emitting area becomes relatively low. Therewith the pump threshold of the Er^{3+}-laser increases strongly.

A pump geometry with special imagining properties has to be chosen to guaranty a good matching between the pump area and the laser mode inside the laser crystal. We decided to use a lens duct [8] for collecting the diode laser beams and imagining them longitudinally into the laser crystal (Fig.1). The lens duct is introduced here in an InGaAs semiconductor pumped Er^{3+} laser system at 2.8 μm for the first time. This optical transmittance system provides a very easy handling and a setup, which can be extended for an increasing number of diodes with an appropriate lens duct design.

We coupled two water cooled diode stacks into the lens duct, each consisting of five 1 μm x 10 mm arrays emitting at 970 nm and being supplied with micro cylindrical lenses for the fast divergence direction. In the horizontal plane the light is focused to the exit face of the lens duct by the refraction of the entrance face. The light propagating in the horizontal plane is guided to the exit face of the lens duct by total reflections at the side faces.

The ten diode arrays emit 500 W output power behind the microlenses. The transfer efficiency of the lens duct with 970 nm AR coated entrance and exit face is 93%. The crystals were coated as monolithic laser resonators with a total transmission of about 1% at 2.8 μm.

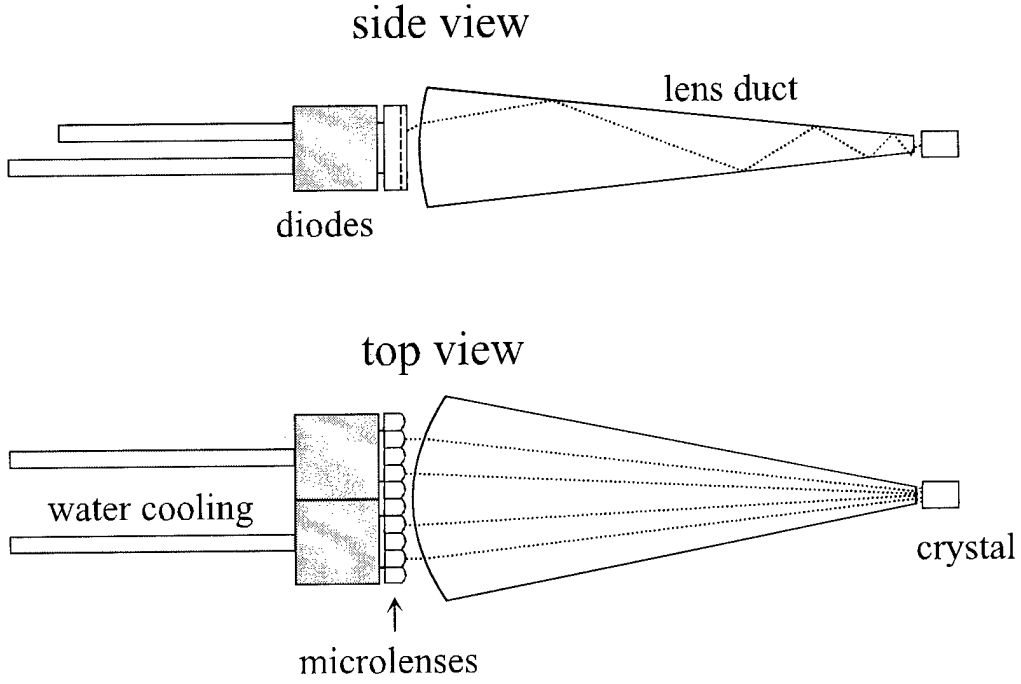

Fig.1: Experimental setup for quasi-cw diode-end-pumping of Er^{3+} doped garnets.

Fig.2 shows the results of first experiments with Er:YSGG at two doping levels. The difference in the efficiency of the 28% and 50% Er^{3+} doped crystals is obvious. The 28% Er^{3+} doped crystal has a 50% higher slope efficiency than the higher doped YSGG crystal, while the pump threshold for the 50% doped crystal is twice as big as for the lower doped one. With the Er(28%):YSGG crystal we achieved 11% slope efficiency at a pump threshold of 13 mJ at 600 μs pulse duration.

This concentration dependence of the efficiency is in very good agreement with our previous laser experiments, operated in cw mode [2]. To exclude an influence of the crystal quality on the determined efficiencies, we performed Findlay-Clay measurements [9] in cw operation with different output couplings for the 28% and 50% Er^{3+} doped YSGG crystals. The determined crystal losses are very small and about 0.1% for both crystals.

Fig. 3 shows experimental results measured with an Er(30%):GGG crystal. Efficient cw laser experiments confirmed the high optical quality of this crystal already [4]. The results for different pump lengths are given in Fig.3. A maximum output energy of 19 mJ at 2.8 μm was achieved at 600 μs pulse duration. Increasing the pulse duration is followed by a slight increase in pump threshold, which yield the difference of the curves at high pump powers. Mounted in a copper plate the crystal did not suffer from thermal influences. The repetition rate was about 20 Hz. A slightly different behavior is observed in comparison to the Er(28%):YSGG crystal.

Although the pump threshold of the Er(30):GGG crystal is higher, the slope efficiency of 13% is also higher. Different upconversion rates might be responsible for this behavior.

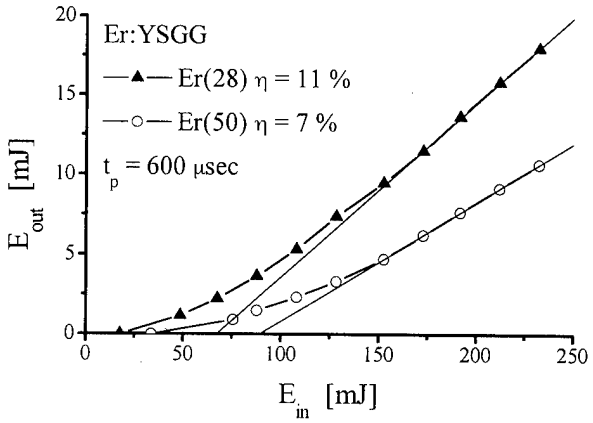

Fig.2: Concentration dependent results for Er:YSGG at 600 µs pulse length

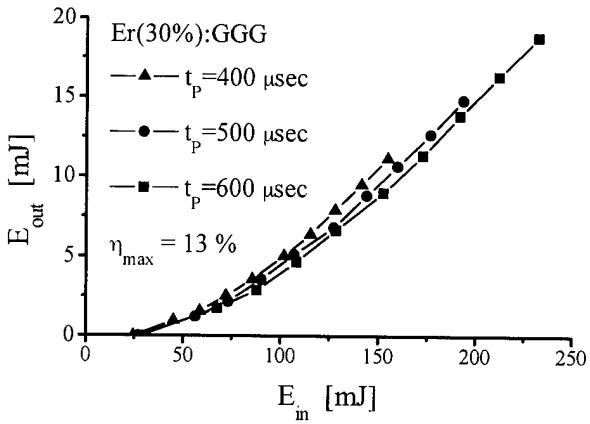

Fig.3: Experiments with Er(30%):GGG at different pump durations

In conclusion we increased the pulse energy at 2.8 µm by coupling several diode arrays longitudinally into the laser crystal using a lens duct transmittance system. We obtained to our knowledge the highest reported output power for diode pumped setups of 19 mJ at 2.8 µm so far.

Experiments are still in progress and an improvement of the lens duct design in connection with appropriate crystal dimensions should improve the output energy further.

The Er:YSGG crystals were placed to our disposal by O.V. Kuzmin, FIRN Krasnodar (Russia). The work was supported by the BMFT (minister for research and technology) within the contract 13N6165.

References

1. R.C. Stoneman and L. Esterowitz, "Efficient resonatly pumped 2.8 µm Er^{3+}:GSGG laser", Opt. Lett. **17** (11), 816 (1992)
2. T. Jensen, V.G. Ostroumov, and G. Huber,"Upconversion processes in Er^{3+}:YSGG and diode pumped laser experiments at 2.8 µm", OSA Proceedings on Advanced Solid-State Lasers, B.H.T. Chai and S.A. Payne (eds.), (1995)
3. B.J. Dinerman and P.F. Moulton, "3-µm cw laser operation in erbium-doped YSGG, GGG, and YAG", Opt. Lett. **19** (15), 1143 (1994)
4. T. Jensen, A. Diening, and G. Huber, "A diode pumped 1.1 W cw Er:YLF laser at 2.8 µm", in Conference on Lasers and Electro-Optics, OSA Technical Digest Series Vol. **15,** postdeadline paper CPD29 (1995)
5. C.E. Hamilton, R.J. Beach, S.B. Sutton, L.H. Furu and B. Krupke,"900 mW average power and tunability from a diode-pumped 2.94 µm Er:YAG laser", in Conference on Lasers and Electro-Optics, OSA Technical Digest Series Vol. **8** , paper CTuE2, 65 (1994)
6. B.J. Dinerman, J. Harrison, and P.F. Moulton, "Continuous wave and pulsed laser operation at 3 µm in Er^{3+}-doped crystals", OSA Proceedings on Advanced Solid-State Lasers Vol. **20**, T.Y. Fan and B.H.T. Chai (eds.), 168 (1994)
7. J.S. Yoo, S.H. Lee, G.T. Park, Y.T. Ko, and T. Kim, "Peculiarities of catastrophic optical damage in single quantum well InGaAsP/InGaP buried-heterostructure lasers", J. Appl. Phys. **75** (3), 1840 (1994)
8. R. Beach, P. Reichert, W. Benett, B. Freitas, S. Mitchell, A. Velsko, J. Davin, and R. Solarz, "Scalable diode-end-pumping technology applied to a 100-mJ Q-switched Nd^{3+}:YLF laser oscillator", Opt. Lett. **18** (16), 1326 (1993)
9. D. Findlay and R.A. Clay, "The measurement of internal losses in 4-level lasers", Phys. Lett. 20 (3), 277 (1966)

Friday, February 2, 1996

Plenary IV

FA 8:00 am-8:30 am
Gold Room

Hagop Injeyan, *Presider*
TRW

The Challenge of Solid-State Lasers for Inertial Confinement Fusion

Howard T. Powell
Lawrence Livermore National Laboratory
P.O. Box 808, L-488
Livermore, California 94551
Telephone: (510) 422-6149
Fax: (510) 423-6212

The U.S. is now embarked on the grand challenge of building a National Ignition Facility (NIF) to demonstrate energy break-even and gain in the laboratory by laser-driven inertial confinement fusion (ICF) for near-term defense applications and long-term energy applications. Break-even is defined as fusion energy out equal to the laser energy impinging on the target. Fusion ignition occurs when the alpha particles produced by the fusion reaction sufficiently heat the compressed fuel to produce a fusion chain reaction. The NIF laser driver[1] is based on low-repetition-rate, flashlamp-pumped, Nd:glass technology which is frequency converted to its third harmonic to produce an output of nearly 2 MJ (see Fig. 1). Despite its enormous scale, the NIF laser will incorporate new technologies described here to provide both precision beam control and flexibility in order to optimize the conditions for fusion ignition. Following and building on NIF laser technology, one can envision a several-Hertz repetition rate, diode-pumped, solid-state laser system[2] which produces a single-pulse output of approximately 5 MJ and provides the high efficiency and long lifetime needed for an inertial fusion energy power plant. Developing and building these large-scale, solid-state laser systems which have the unique and demanding performance characteristics required for these important applications is a major challenge to the laser community which will provide technology spin-offs to many other applications.

The NIF is designed primarily for indirect-drive ICF in which the laser pulse is converted in a high-Z hohlraum (a cylindrical metal can) to soft x-rays which uniformly bathe and compress a plastic capsule positioned at the center of the hohlraum and containing the fusion fuel, a mixture of deuterium and tritium (Fig. 2). The top-level requirements of the NIF are 1.8 MJ at 0.35 μm in 192 beams which are precisely tailored over a 20-ns temporally-shaped pulse having a main 3-ns drive component at the end. The temporal pulse shaping is chosen (and can be adjusted) to produce the temperature and density conditions in the compressed fuel which produce ignition at minimum laser energy. The individual beams must be adequately power balanced, precisely pointed, and spatially profiled at the hohlraum wall to control the symmetry of the x-ray drive to suppress the growth of hydrodynamic instabilities. Prescribed amounts of laser bandwidth and spatial incoherence of the NIF beams are required to prevent nonlinear scattering processes (stimulated Raman and Brillouin scattering) both in the output laser optics and the long scale-length plasmas present in the target.

The NIF laser system is an advanced solid-state laser system which is specifically designed to meet the target requirements. We are developing fiber-optic-based oscillators and amplifiers (using laser-diode-pumped, Yb-doped silica fibers) and fiber modulators to provide temporal and spectral control of the individual beams. Their output is then amplified in very stable, diode-pumped, Nd:glass regenerative amplifiers and flashlamp-pumped, multipass rod amplifiers in order to provide precisely controlled, multi-joule inputs to each of the 192 beamlines. The large aperture (40 cm) power amplifiers in each of the beamlines are used in four passes to minimize the large hardware required for amplification and thereby reduce the system cost. Spatial incoherence on target is controlled by using small gratings at the front end of each chain to spectrally disperse the 2-3 angstrom bandwidth provided by the fiber modulators using the technique of smoothing by spectral dispersion (SSD).[3] A simplified view

of this form of coherence control is that the grating causes the focused beam to "wiggle" in time as its frequency is varied, thereby smoothing the focal spot in a time-averaged sense. The overall spatial envelope of intensity on target (after frequency conversion to the third harmonic) is controlled by using special diffractive optics at the output, so-called kinoform phases plates.[4] We are designing these phase plates using a recently developed algorithm and constructing them in pure fused silica using wet chemical etching to provide high damage resistance at 0.35 μm.

Although the NIF design is based on the requirements for indirect drive ICF, it offers sufficient flexibility to be adapted for direct drive. With the direct drive ICF, the laser beams impinge directly on the capsule to cause implosion rather than using an incoherent source of x-rays. Since in this approach the laser beams must come equally from all directions, rearrangement of the NIF beam focusing apertures is required from the indirect drive geometry. The engineering aspects of this rearrangement are now being considered. A fundamental difficulty of direct drive is that nonuniformity (laser speckle) inherent in coherent laser beams can imprint acceleration differences potentially leading to capsule break-up. Beam smoothing and precise beam balance described above are essential and must be substantially enhanced over indirect drive to produce the required drive uniformity (approximately 1% over the surface of the capsule) necessary to counter hydrodynamic instability.

The ultimate challenge of lasers for ICF is to provide NIF-like capability at 5 Hz, 10% efficiency, and with a 30-year lifetime as needed for production of commercial electrical power by inertial fusion energy (IFE). The development of such capability is currently a very small effort in the national ICF program and is at the invention and conceptualization stage rather than at the engineering stage. Nonetheless, substantial progress has been made in the past several years in showing the potential of a diode-pumped, solid-state laser (DPSSL) system as an alternative to a heavy ion, KrF laser, or light ion drivers which have been proposed by others for this application. We have identified solutions for several key problems associated with a DPSSL-based IFE system. First we have identified a near-optimum laser material, Yb-doped fluoroapatite, which has the requisite energy storage characteristics (1 ms storage time), gain properties, and crystal growth characteristics. We have evaluated and have been encouraged by the potential of laser diode pumps to reach the necessary cost and performance goals. We have also recently shown experimentally the potential for face cooling of the crystal faces using helium gas to reach the large apertures sizes and meet the high beam quality requirements for such a system. Finally, we have obtained very encouraging experimental results on the optical performance of heated fused silica final optics under the radiation dose conditions of a fusion power plant. All of these results have been put together in an overall system model which finds that electricity could potentially be produced at a competitive price using the DPSSL approach to IFE.[2] Most importantly, much of the required development can proceed with modest investments and can ride heavily on the technology developments and experience of the NIF Project.

The author is pleased and grateful to report on the work of many dedicated individuals in the ICF Program and NIF Project at Lawrence Livermore National Laboratory (LLNL). He is particularly indebted to Mike Campbell, Associate Director for Laser Programs; to Jeff Paisner, the NIF Project Manager; and to John Lindl and Joe Kilkenny, the scientific director and target physics leader of the LLNL ICF Program. This work was performed under the auspices of the U.S. Department of Energy by Lawrence Livermore National Laboratory under contract W-7405-Eng-48.

References

1. *National Ignition Facility Conceptual Design Report*, Lawrence Livermore National Laboratory, Livermore, CA, UCRL-PROP-117093 (1994).

2. C. D. Orth, S. A. Payne, and W. F. Krupke, "A Diode-Pumped Solid-State Laser Driver for Inertial Fusion Energy," *Nuclear Fusion*, **35** (11) (1995) in press.

3. S. Skupsky, R. W. Short, T. Kessler, R. S. Craxton, S. Letzring, and J. M. Soures, "Improved laser-beam uniformity using the angular dispersion of frequency-modulated light," *J. Appl. Phys.* **66** (8), 3456 (1989).

4. S. N. Dixit, J. K. Lawson, K. R. Manes, H. T. Powell, and K. A. Nugent, "Kinoform phase plates for focal plane irradiance profile control," *Opt. Lett.* **19** (6), 417 (1994).

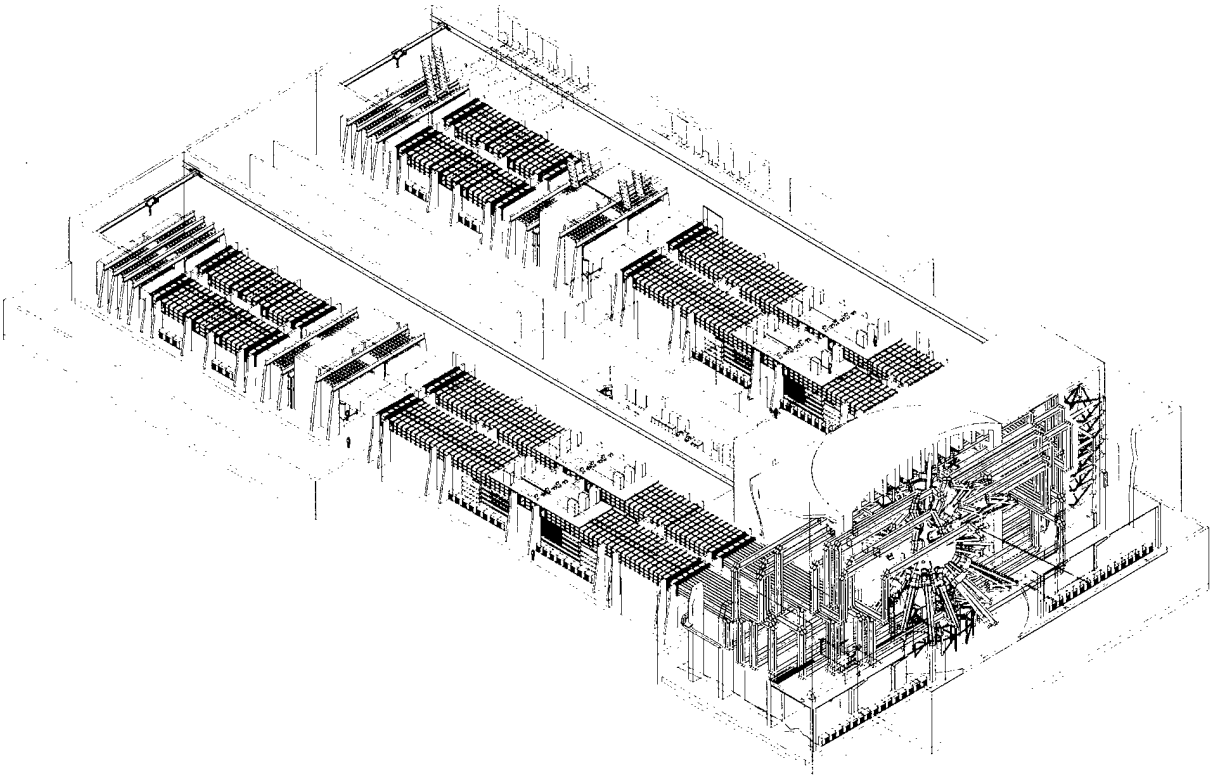

Figure 1. Schematic drawing of the NIF laser facility. The overall building length is 550 feet.

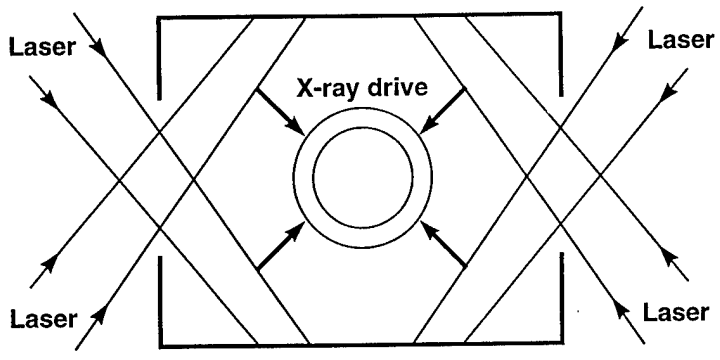

Figure 2. Schematic drawing of an indirect drive ICF target. The NIF target has a 10-mm long hohlraum and a 2 mm diameter capsule.

Friday, February 2, 1996

Spectroscopy and Characterization

FB 8:30 am-9:45 pm
Gold Room

Richard Moncorgé, *Presider*
University of Lyon, France

Excited state absorption and stimulated emission measurements of Cr^{4+}-doped $Y_3Al_5O_{12}$, $Y_3Sc_{0.9}Al_{4.1}O_{12}$, and $CaY_2Mg_2Ge_3O_{12}$

S. Kück[1], K. L. Schepler[1], K. Petermann[2], and G. Huber[2]
[1] USAF Wright Lab, WL/ELOS
2700 D Street Suite 2, WPAFB, OH 45433-7405, USA
Tel.: ++1 (513) 255-3804-x331
Fax: ++1 (513) 255-7312
Email:KUECK@physnet.uni-hamburg.de
[2] Institut für Laser-Physik, Universität Hamburg
Jungiusstraße 11, D 20355 Hamburg, Germany

Cr^{4+}-doped crystals are known for many years as room temperature tunable solid-state lasers in the infrared spectral range. They exhibit emission between 1μm and 2μm, which is quenched to some extend by nonradiative decay processes. However, the observed laser tuning ranges are smaller than expected based on the emission spectra. In this paper detailed excited state absorption and stimulated emission measurements of three Cr^{4+}-doped garnets are presented and discussed.

$Y_3Al_5O_{12}$ (YAG), $Y_3Sc_{0.9}Al_{4.1}O_{12}$ (YSAG), and $CaY_2Mg_2Ge_3O_{12}$ (CAMGAR) belong to the garnet family of crystals. They crystallize in the cubic space group Ia3d (O_h^{10}). The Cr^{4+} ion is incorporated into the tetrahedrally coordinated lattice site with D_{2d} site symmetry. The splitting of the Cr^{4+} energy levels in a tetrahedral field with T_d (regular tetrahedron) and D_{2d} (tetragonally distorted tetrahedron) symmetry is schematically shown in Figure 1. The splitting decreases in the order YAG, YSAG, CAMGAR, because of the decreasing crystal field strength.

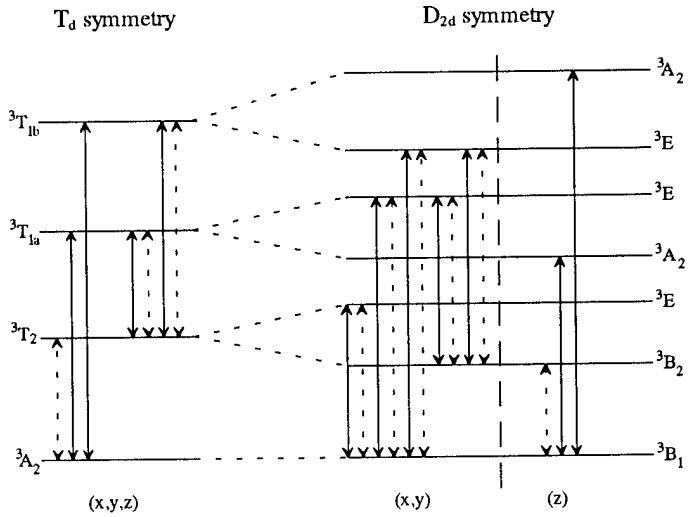

Figure 1. Basic energy level scheme of the Cr^{4+} ion in T_d and D_{2d} symmetry. Electric (magnetic) - dipole allowed transitions are indicated with a solid (dashed) arrow-line. Note that singlet levels are omitted.

The crystals were grown by the Czochralski method using an iridium crucible and oxidizing growth atmosphere. For YAG and YSAG, an additional codoping with calcium was necessary for charge compensation.
The excited state absorption measurements were performed with a pump and probe technique by measuring the difference in the transmission of the pumped and unpumped crystal. The technique is described in detail in Refs. [1, 2]. The pump source was a polarized Nd:YAG laser (for Cr^{4+}:YAG) or an argon-ion laser (for Cr^{4+}:YSAG and Cr^{4+}:CAMGAR). The transmitted intensity of a tungsten-halogen lamp was measured with a liquid nitrogen cooled InSb-detector or a PbS-detector. In the case of Cr^{4+}:YAG, the probe beam of the lamp was polarized parallel to the pump beam polarization. The Cr^{4+}:YAG crystal was cut along the crystallographic axis and placed in the beam, so that the beam propagations were parallel to one axis and the beam polarizations parallel to another axis. For Cr^{4+}:YSAG and Cr^{4+}:CAMGAR unpolarized measurements were performed.

The difference of the transmissions in the pumped and unpumped case (ΔT) normalized with the simultaneously measured transmission (T) is given by,

$$\frac{\Delta T}{T} = \frac{\left(I_p - I_u\right)}{I_p} \propto \sigma_{GSA} + \sigma_{SE} - \sigma_{ESA}.$$

I_p and I_u are the transmitted intensities in the pumped and unpumped case, respectively and σ_{GSA}, σ_{SE}, and σ_{ESA} are the ground state absorption, excited state absorption, and stimulated emission cross section, respectively. This expression is valid for $I_p \approx I_u$.
In Figure 2, the $\Delta T/T$-spectra for the investigated crystals are shown. The spectrum of YAG was normalized with an absorption cross section of $6 \cdot 10^{-18}$ cm^2 at 1020nm, assuming no significant excited state absorption at this wavelength [3]. For CAMGAR, the same absorption cross section as for YAG was assumed as a first estimation. The YSAG spectrum was normalized with an emission cross section of $1.4 \cdot 10^{-19}$ cm^2 at 1750nm [4]. In all spectra, the ground state absorption bleaching is clearly observed for the absorption bands around 650nm and 1000nm which correspond to the transitions between the $^3B_1(^3A_2)$ ground state and the $^3E(^3T_{1a})$ and $^3A_2(^3T_{1a})$ excited states, respectively (see Figure 1). Excited state absorption is observed between 600nm and 900nm and between 1100nm and 1600nm, due to the transitions between the $^3B_2(^3T_2)$ metastable upper laser level and the ^3E components of the $^3T_1$ levels. Both transitions are electric-dipole allowed.
Stimulated emission was only observed for YAG and YSAG. The stimulated emission cross section is an order of magnitude smaller compared to the absorption around 1000nm. This is due to the fact that the electronic transition is magnetic-dipole allowed and the transition becomes only partially electric-dipole allowed due to the coupling of non-totally symmetric phonons. In Figures 3 and 4, the spectral range of the stimulated emission is shown in more detail. Laser action up to 1750nm (for YAG) and 1950nm (for YSAG) should be possible. This would extend the tuning range further into the infrared compared to earlier published results [5]. However, the laser efficiency on the short wavelength side - especially for YSAG - is affected by excited state absorption, as can be seen from the comparison with the emission spectrum.
Laser experiments in the spectral range above 1600nm are in progress. A more detailed analysis of the excited state transitions and the cross sections will also be presented.

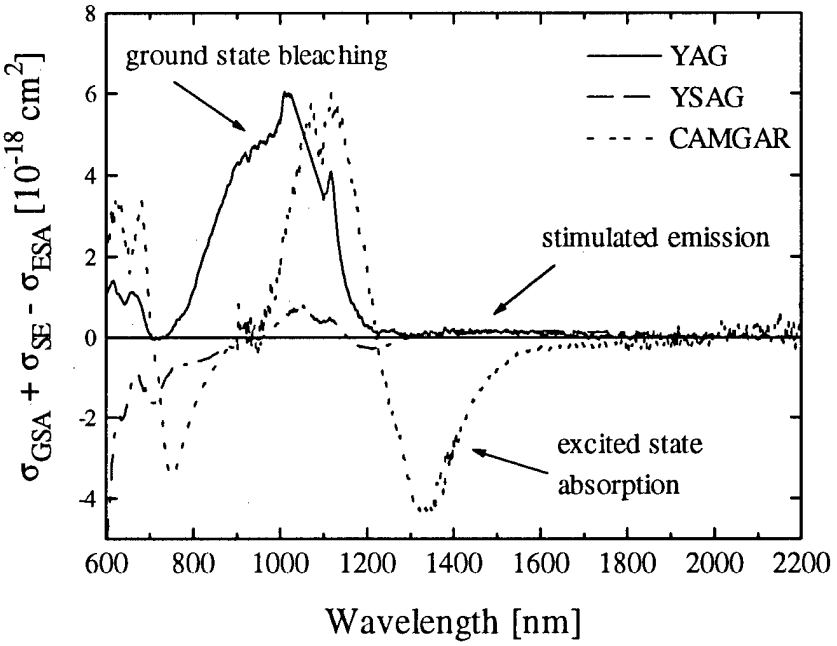

Figure 2. ΔT/T-spectrum of Cr^{4+}:YAG, Cr^{4+}:YSAG, and Cr^{4+}:CAMGAR.

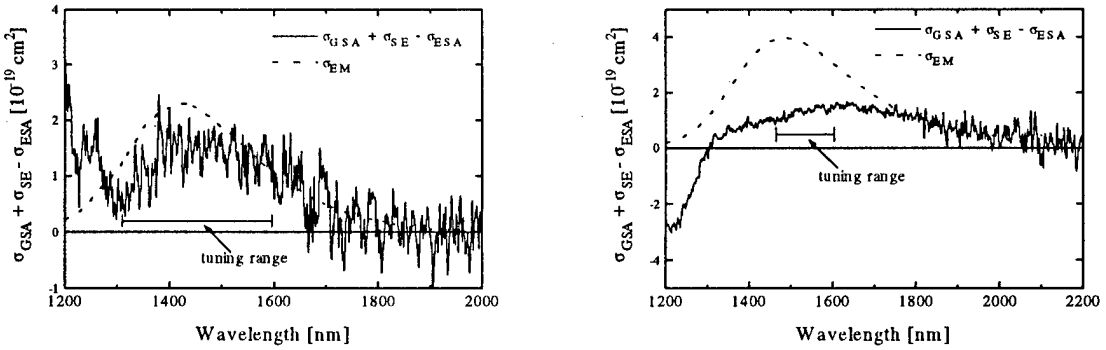

Figure 3 and 4. Comparison of the emission cross section and stimulated emission cross section of Cr^{4+}-doped YAG (left) and YSAG (right). The maximum tuning range achieved until now is indicated in the figures [5].

References

1. S. Zemon, G. Lambert, W. J. Miniscalco, R. W. Davies, B. T. Hall, R. C. Folweiler, T. Wei, L. J. Andrews, and M. P. Singh, SPIE Vol. 1373 Fiber Laser Sources and Amplifiers 2, 21 (1990).
2. J. Koetke, G. Huber, Appl. Phys. B61, 151 (1995).
3. H. Eilers, K. R. Hoffman, W. M. Dennis, S. M. Jacobsen, and W. M. Yen, Appl. Phys. Lett. 61, 2958 (1992).
4. S. Kück, K. Petermann, U. Pohlmann, and G. Huber, Phys. Rev. B, 51, 17323 (1995).
5. S. Kück, K. Petermann, U. Pohlmann, U. Schönhoff, and G. Huber, Appl. Phys. B58, 153 (1994).

Spectroscopic Studies of Potential Mid-IR Laser Materials

S. R. Bowman, L. B. Shaw, J. A. Moon, B. B. Harbison

Optical Sciences Division

Naval Research Laboratory, Washington, D.C. 20375-5320

Phone (202) 767-9418

and Joseph Ganem

Department of Physics, Loyola College in Maryland,

4501 N. Charles Street, Baltimore, MD 21210

There are many applications for simple, rugged sources of mid-infrared radiation. Currently the only practical sources of mid-IR radiation (3 to 12 μm) are thermal sources, gas lasers and nonlinear parametric down converters. Blackbodies are relatively weak sources in the mid-IR while gas lasers and OPOs suffer from problems of complexity and reliability. Recently, we have investigated the possibility of generating high brightness mid-IR sources using direct emission from rare earths doped into low phonon energy solid state materials. The recent demonstration of efficient room temperature operation of a 7 μm praseodymium laser confirms the potential of this approach. [1] Continuing with this line of investigation, we report initial studies into several other potential mid-IR laser materials.

The host materials for these studies include trichloride and tribromide crystals as well as chalcogenide glasses. Each of these materials has both potential advantages and problems as a mid-IR laser host. The trichloride and tribromide crystals exhibit strong absorption and emission bands for the rare earth. They have very low phonon energies (170 - 260 cm^{-1}) which maintains the rare earth optical activity even for very low energy gap transitions. These crystals however are quite hygroscopic which makes their preparation and handling somewhat involved. The

chalcogenide glasses, on the other hand, are much more durable, non-hygroscopic and can be pulled into fibers. They typically exhibit somewhat higher phonon energies (250 - 300 cm^{-1}) and broader emission lines. However, the transmission range of these glasses is limited by the low bandgap energy (2.3 eV) as well as extrinsic absorption features.

Our recent studies have focused on the mid-IR transitions in trivalent erbium and terbium. The laser lines of interest in erbium are the $^4F_{9/2}$ => $^4I_{9/2}$ transition which emits at 3.5 μm and the $^4I_{9/2}$ => $^4I_{11/2}$ transition which emits at 4.5 μm. These are promising laser lines since laser diode arrays can access the pump bands for both of these transitions, 670 and 800 nm. Laser operation has been previously demonstrated for both of these erbium transitions. [2-4] However, all of these demonstration suffered from very low efficiency due to rapid multi-phonon quenching of the upper states. In an attempt to solve this problem, we have studied Er^{+3} doped into $LaCl_3$ crystals and BaGeGaS glasses. We have also examined pure $ErCl_3$ crystals. Table 1 shows the erbium lifetimes measured using a nanosecond 805 nm pump pulse. While all the upper state lifetimes are significantly improved in these materials, the millisecond lifetime of the $^4I_{9/2}$ level in pure $ErCl_3$ crystals is quiet remarkable. With its combination of strong pump absorption and long lifetimes, $ErCl_3$ looks like a very promising material for both the 3.5 and 4.5 μm lasers. Efforts to grow laser quality crystals of this material are ongoing.

Table 1.

Material	Energy level	Transition	Fluorescence Lifetime
0.2% Er:LaCl3	4I9/2	4.5 μm	2.6 msec
ErCl3	4I9/2	4.5 μm	1.2 msec
ErCl3	4F9/2	3.5 μm	0.15 msec
BaGeGaS with 0.1% Er	4I9/2	4.5 μm	0.35 msec

Investigations of potential terbium lasers have concentrated on the $^7F_4$ => $^7F_5$ transition. This transition fluoresces in the 7.2 to 9.4 μm range, although it does not appear to have been

reported previously. Lifetimes of the terbium ^7F levels were measured in samples of doped $LaCl_3$ and $LaBr_3$ crystals. As shown in Table 2, the first excited state, $^7F_5$, is metastable in both materials. However the upper laser level, $^7F_4$, is metastable only in the bromide. Indeed, with a 2 msec upper state lifetime and strong pump bands at 1.9, 2.0 and 2.3 μm terbium doped $LaBr_3$ appears to be a good candidate for the first solid state laser in the 8 to 9 μm spectral region. More details will be presented at the meeting.

These studies are supported by the Office of Naval Research. Dr. Shaw's work is supported by a National Research Council - NRL Research Associateship. Dr. Ganem's work is supported by Research Corporation.

Table 2.

Material	Energy level	Transition	Fluorescence Lifetime
1% Tb:LaCl3	7F5	5 μm	10 msec
1% Tb:LaCl3	7F4	9 μm	0.005 msec
1% Tb:LaBr3	7F5	5 μm	22 msec
1% Tb:LaBr3	7F4	9 μm	2.2 msec
1% Tb:LaBr3	7F3	11 μm	0.05 msec

[1] S. R. Bowman, L. B. Shaw, B. J. Feldman and Joseph Ganem, "A Room Temperature Seven Micron Solid State Laser," paper CPD-26 at Conference on Lasers and Electro-Optics, Baltimore, MD, May 1995.

[2] A.A. Kaminskii, "Modern Tendencies in the Development of the Physics and Spectroscopy of Laser Crystals," Izv. Akad. Nauk SSSR Ser. Fiz. vol. 45, no. 2, pp. 106 - 114, 1981.

[3] J. F. Pinto, L. Esterowitz and G. H. Rosenblatt, "Continuous Wave 3.4 μm Er:LiFY4 Laser," OSA Proceedings on Advanced Solid State Lasers, 1994, Vol. 20. pp. 174 - 177.

[4] H. Tobben, "Room Temperature CW Fibre Laser at 3.5 μm in Er^{3+} - Doped ZBLAN Glass," Electronic. Lett. vol. 28. no. 14. pp 1361 - 1362, 1992.

Gain Measurements in Dy^{3+}-doped $LaCl_3$: A potential 1.3μm optical amplifier for telecommunications

K. I. Schaffers, R. H. Page, R. J. Beach, S. A. Payne, and W. F. Krupke
Lawrence Livermore National Laboratory, L-Code 493, Livermore, CA 94550, (510)422-5084

The recent development and deployment of laser diode-pumped Er^{3+}-doped silica fibers as optical repeaters to amplify signals at the 1.55 μm wavelength has been a tremendous advance for the telecommunications industry. [1] Some of the attractive features of these amplifiers are their wide bandwidth, high gain, reliability, compactness, and low power consumption. However, there is currently no efficient amplifier that can be integrated into the existing infrastructure of the fiber optic-based telecommunications network which operates near the 1.31 μm wavelength. At this time electronic repeaters are used to amplify the information signal after it has traveled through several tens of kilometers of optical fiber. [2] Diode-pumped, Pr^{3+}-doped ZBLAN fluoride glass fibers [3] are the most promising candidates for an amplifier with sufficient gain at 1.3 μm, but the Pr^{3+} ion has a relatively short emission lifetime, ~100 μs, in this host which requires a high pump power. To increase the lifetime, a new series of Pr-host media based on chlorides has previously been studied and order of magnitude increases in the emission lifetime have been seen. [4] One drawback to this system is that Pr^{3+} ions are difficult to pump directly so we are now also considering Dy^{3+}-doped chlorides which have several strong pump transitions available. A number of Dy^{3+}-doped chlorides have been studied to date and spectroscopic data indicate that several possess useful 1.3 μm emission bands as well as emission lifetimes on the order of a millisecond. Here, we report on the growth, spectroscopy, and gain properties of $LaCl_3$:Dy^{3+} which shows promise for providing the properties necessary for a 1.3 μm amplifier for telecommunications, owing to the combination of large emission lifetime and strong pump absorption bands.

Great care must be taken to obtain crystals of $LaCl_3$:Dy^{3+} with the appropriate optical quality to ensure efficient operation. Oxide impurities and exposure to moisture can inhibit crystal growth. Therefore, a multiple step process based on vaporizing the molten $LaCl_3$ and $DyCl_3$ is employed to ensure the purity of the starting materials before the crystal growth is pursued. This purification process has led to marked improvements in crystal quality.

Spectroscopic results reveal that the emission band of $LaCl_3:Dy^{3+}$ is centered around 1.3 μm; the absorption and emission spectra are shown in Figure 1. The radiative lifetime is greater than 1 msec which is consistent with a quantum yield above 70% (compared to 3% for Pr:ZBLAN). As is the case with the Er^{3+} silica amplifier, Dy^{3+} exhibits significant ground-state absorption which must be bleached before net gain can be achieved.

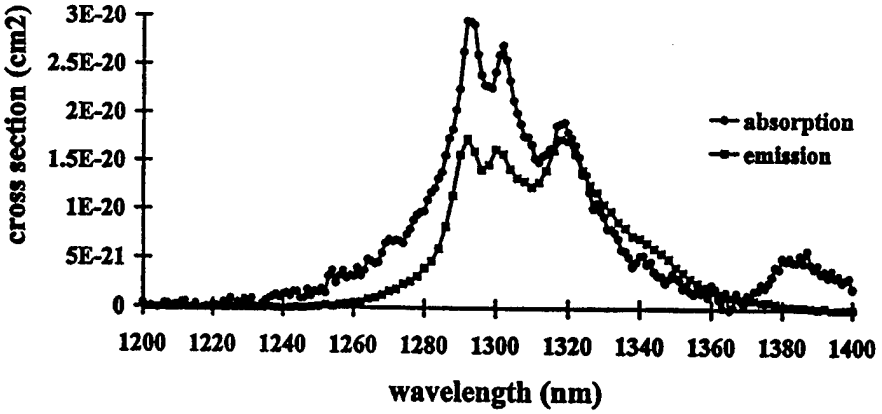

Figure 1. Absorption and emission spectra for $LaCl_3:Dy^{3+}$.

Gain measurements were made on crystals ~2 mm thick, with a Cr:LiSAF laser providing 0.2 msec pump pulses at 917 nm, and a CW Nd:YAG laser probing with 1319 and 1338 nm lines. A transient digitizer recorded the time-dependent gain signals, and allowed subtraction of background fluorescence by recording signals with the probe blocked. Gain results for the two different probe wavelengths are shown in Figures 2 and 3. The unpumped sample's transmission (T) at 1319 nm is 0.79; therefore, a signal increase above 1/T = 1.27 results in net gain in the crystal. With the available pump fluence, the overall probe signal increase of 40% corresponds to a net gain of (40-27) = 13%. At 1338 nm, the emission cross section is larger with respect to the absorption cross section, and a smaller inversion fraction gives transparency; here the net gain is ~14% above the ground-state absorption of 8%.

These data show great promise for the development of a 1.3 μm optical amplifier with high quantum efficiencies based on Dy^{3+}-doped chlorides, although many issues concerning crystal growth, waveguide fabrication, and device optimization remain.

This work was performed under the auspices of the U.S. Department of Energy by Lawrence Livermore National Laboratory under Contract No. W-7405-Eng-48.

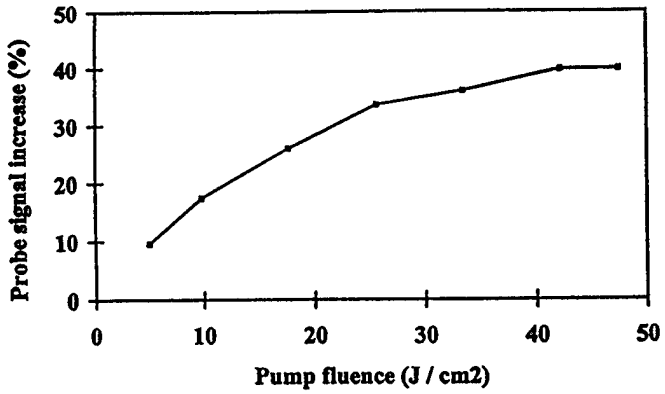

Figure 2. Gain versus pump fluence for $LaCl_3:Dy^{3+}$ at 1319 nm.

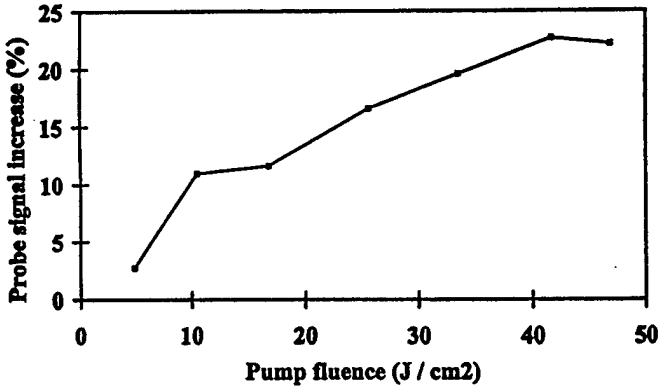

Figure 3. Gain versus pump fluence for $LaCl_3:Dy^{3+}$ at 1338 nm.

Acknowledgments. I'd like to thank J. Tassano, G. Wilke, and P. Waide for their technical contributions to this effort.

1. E. Desurvire, "The Golden Age of Optical Amplifiers," *Physics Today*, 20-27 (January 1994).
2. N. Edagawa, "Applications of fiber amplifiers to telecommunication systems," in Rare Earth Doped Fiber Lasers and Amplifiers, Michel J. F. Digonnet, ed. (Marcel Dekker, Inc., New York, 1993).
3. US Patent No. 5,309,452; Shimizu, et. al., "28.3 dB Gain 1.3 μm-based Pr-doped Fluoride Fiber Amplifier Module Pumped by 1.017 μm InGaAs-LD's," *IEEE Photonic Technology Letters,* **5**, 654-657 (1993).
4. R. H. Page, K. I. Schaffers, G. D. Wilke, J. B. Tassano, S. A. Payne, and W. F. Krupke, "Spectroscopy and decay kinetics of Pr^{3+}-doped chloride crystals for 1300-nm optical amplifiers," *ASSL 95*, 29 Jan. - 2 Feb. 95, paper TuD3.

Investigation of Luminescent Properties of Sc:CaF_2 and Sc,Ce:CaF_2 Crystals as Promising New Media for UV Tunable Solid State Lasers

S. B.Mirov, A.Yu.Dergachev, W.A.Sibley
Physics Department, University of Alabama at Birmingham, Birmingham, Alabama 35216
Tel.: (205) 934-8088, FAX: (205) 934-8042

L.Esterowitz
Naval Research Labarotary, Code 5605, Washington D.C. 20375-5000
Tel.: (202) 767-3535, FAX: (202) 404-8613

V.B.Sigachev, A.G. Papashvili
General Physics Institute, Moscow, Russia 117942
Tel.: (095) 135-0318, FAX: (095) 135-0267

Condensed media having strong vibronic transitions are of considerable interest in quantum electronics. Such media usually feature very wide and homogeneously broadened spectral bands in absorption and luminescence, as well as high stimulated transition probabilities. Here we report on the results of luminescent studies in γ-irradiated CaF_2 and Ce:CaF_2 crystals codoped with Scandium. Sc^{3+} ion substitutes for divalent cation (Ca^{2+}) and the excess positive charge is compensated by some defect or impurity. It was shown that the additional treatment of Sc:CaF_2 crystals, such as by X-ray or γ-irradiation, additive and electrolytic coloration allows Sc^{3+} ions to transform into Sc^{2+} at cubic sites of the crystal lattice [1,2]. Because Sc^{2+}, as well as Ti^{3+}, ions have a simple and unique $3d^1$ electronic configuration, Sc^{2+} is certain to be of great interest as a luminescent and/or laser active ion.

In our experiments we used two sets of Sc doped fluoride crystals: 1) Sc:CaF_2 crystals grown in vacuum by Optovac, Inc. with ScF_3 concentration in the melt up to 1 mol.%, and 2) Sc,Ce:CaF_2 crystals grown at the General Physics Institute (Moscow, Russia) with concentration of ScF_3 in the melt up to 0.3 mol.% (Ce concentration in all samples was about 0.001 mol.%). Both sets of crystals were γ-irradiated at 77 K or 300 K with a dosage 10^3 - $2x10^6$ rad.

Absorption spectra in the 190-850 nm range for CaF_2 crystals (Optovac) with different concentration of ScF_3 γ-irradiated with a $2x10^5$ rad dosage at 77 K are shown in Fig.1a. We observed several absorption bands peaked at 310, 450 and 600 nm. Absorption properties of γ-irradiated CaF_2:Sc crystals after ionizing treatment were briefly investigated in earlier studies [3-5], however, no luminescence was detected.

Typical example of luminescence spectra in Sc:CaF_2 crystals (> 0.3 mol.% of ScF_3) γ-irradiated with the dose of $2x10^5$ rad at 77 K under 280 nm laser excitation is shown in Fig. 2a (curve 1). We observed a broad band luminescence with the maximum at 380 nm with the decay time equal to 17.4 μs at 300 K. The intensity of this luminescence band depends linearly upon the intensity of laser beam what confirms one step mechanism of excitation. The excitation spectrum of 380 nm luminescence band in γ-irradiated 1%ScF_3:CaF_2 crystal is shown in Fig. 2a(curve 2). Comparison of excitation and absorption spectra of the crystal shows that the position of the excitation band maxima does not correlate with that of the absorption band at 310 nm. Therefore, we can state that the absorption band at 310 nm, induced after γ-irradiation of Sc:CaF_2 crystals, is

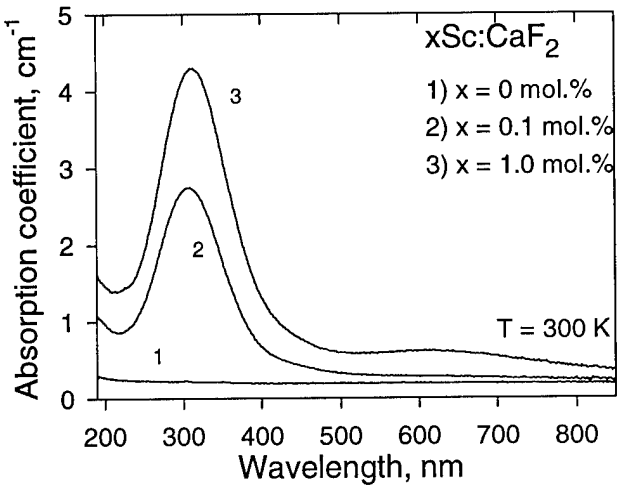

Fig.1a Absorption spectra of $xSc:CaF_2$ crystals γ-irradiated with $2x10^5$ at 77 K

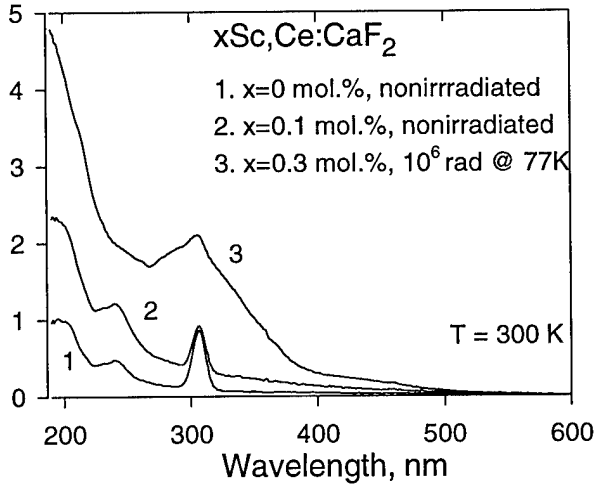

Fig.1b Absorption spectra of $xSc:Ce:CaF_2$ crystals

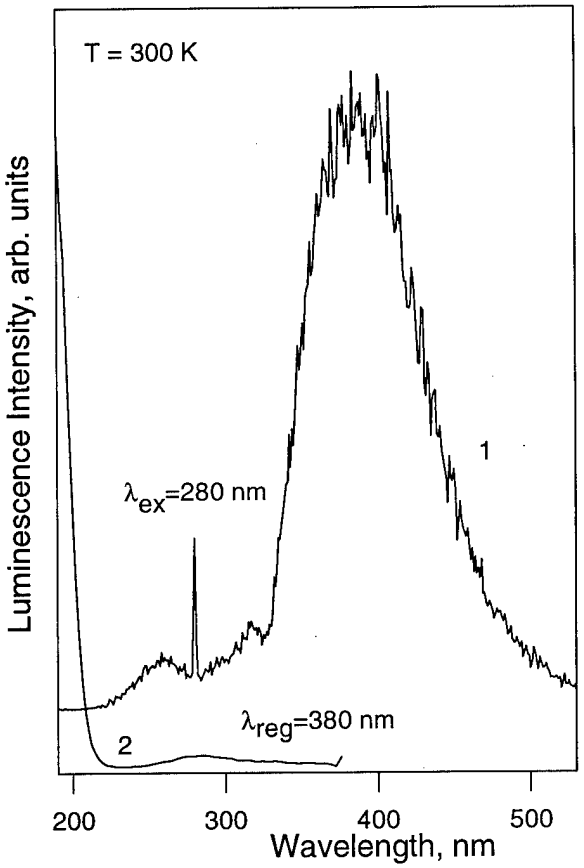

Fig.2a Luminescence (1) and excitation (2) spectra of $1\%Sc:CaF_2$ crystal γ-irradiated with $2x10^5$ rad at 77 K

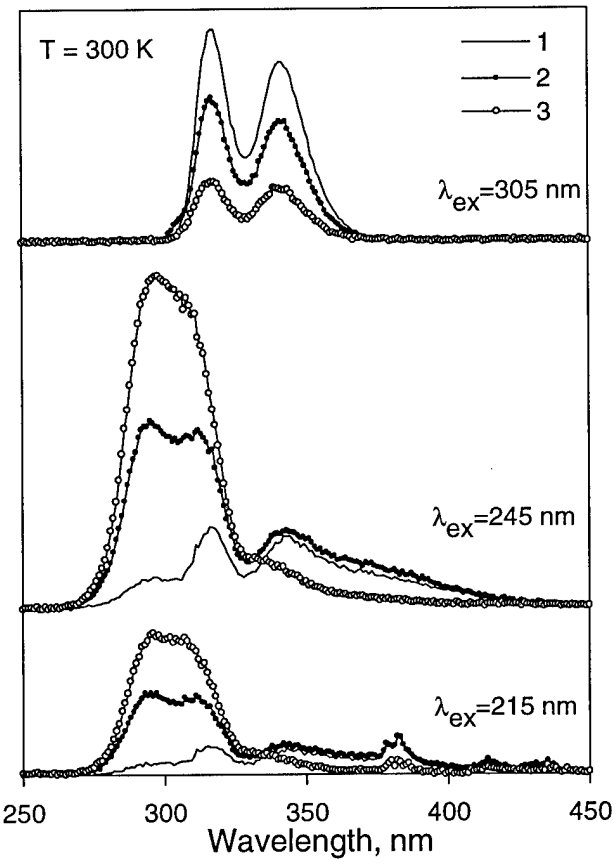

Fig.2b Luminescence spectra of $xSc,Ce:CaF_2$ crystals: 1. x=0 mol.%, nonirrad.
2. x=0.1mol.%, nonirrad.
3. x=0.3 mol.%, 10^6 rad at 77K

not responsible for the luminescence band at 380 nm. So the 310 nm absorption band masks another weaker band that gives rise to the studied luminescence. This weak absorption band responsible for the 380 nm luminescence is lying at about 190 nm and becomes detectable at ScF_3 contents exceeding 0.3 mol.%. Taking into account the broadband character of observed luminescence and its relatively long lifetime (~17 μs) we can attribute this luminescence to Sc^{2+} ions.

In order to evaluate possible effects of chemical stabilization we investigated properties of γ-irradiated Sc:CaF_2 crystals additionally doped with: a) oxygen ions and b) low concentration of Ce^{3+} ions. Sc:CaF_2 crystals codoped with oxygen feature much better photo- and thermostability of Sc^{2+}-like optical centers. Co-doping of Sc:CaF_2 crystals with O^{2-} seems to be very promising for stabilization of Sc^{2+} centers. Addition of Ce impurity (which is good donor of electrons) is interesting from two points of view. First, Ce dopant can increase the efficiency of Sc^{3+} reduction under ionizing, additive or electrochemical treatment. Similar effects were reported for RE ions [6,7]. Second, Ce^{3+}-like centers perturbed by Sc impurity may serve by themselves as promising luminescent and active optical centers.

Introduction of Sc results in considerable changes in luminescent properties Ce:CaF_2 crystal. In γ-irradiated Ce:CaF_2 crystals with concentration of ScF_3 exceeding 0.3 mol.%, we observed the same luminescence band at 380 nm with 17 μs lifetime as for Sc:CaF_2 crystals (Optovac) described above. In addition, a much more intense luminescent band around 300 nm, featuring extremely high photostability, was observed in Ce:CaF_2 crystals doped with high, as well as low, concentrations of Sc. We attributed this band to Ce^{3+}-like centers.

Absorption and luminescence spectra of Ce:Sc:CaF_2 and γ-irradiated Ce:Sc:CaF_2 crystals in comparison with the spectra for Ce:CaF_2 crystal are shown in Fig.1b and Fig.2b. All spectra were measured under the same experimental conditions. The increase of Sc concentration in Ce:CaF_2 and subsequent γ-irradiation of the crystal results in increase of concentration of new Ce^{3+}-centers emitting near 300 nm and decrease of concentration of centers with well known luminescence at 318, 342 [8] and another new band at 382 nm. As a result, the strongest luminescence in γ-irradiated Ce:Sc:CaF_2 crystal occurs at 300 nm. The decay time of the different Ce^{3+}centers is in the range of several tenths of nanoseconds, but is shorter for 300 nm luminescence (about 40 ns), and longer for 382 nm luminescence (about 130 ns).

This work was supported by the National Science Foundation grants OSR-9450570 and DMR 9404712.

References

1. U.T. Hochli, Phys.Rev. **162**, 262 (1967)
2. J.R.Herington et al., Phys.Rev.B **10**, 833 (1974)
3. J.R.O'Connor, J.H.Chen, Phys.Chem.Solids **24**, 1382 (1963)
4. L.V.Krotova, P.G.Mikaelyan, V.V.Osiko, Izv.Akad.Nauk SSSR, Neorg.Mater. **3**, 1123 (1967)
5. G. Kotitz et al., Phys.Stat.Sol.(a) **31**, 371 (1975).
6. V.A.Arkhangelskaya, L.A.Alekseeva, Opt.Spectrosc. **21**, 50 (1966))
7. J.L.Merz, P.S.Pershan, Phys.Rev. **162**, 217 (1967)
8. P.P.Feofilov, Opt. i Spektrosk. **6**, 234 (1959) (in Russian)

CrO_4^{3-} and MnO_4^{2-}: Broadband Emitters in the NIR and Potential Laser Systems

Thomas C. BRUNOLD, Menno F. HAZENKAMP, and Hans U. GÜDEL

Institut für anorganische und physikalische Chemie, Freiestrasse 3, Universität Bern, CH–3000 Bern 9, Switzerland.

Ti^{3+} doped sapphire is the most prominent laser material with a $(3d)^1$ activator ion. Recently we reported the first photoluminescence studies of the $(3d)^1$ ions Cr^{5+} and Mn^{6+} in a tetrahedral oxo coordination [1, 2]. CrO_4^{3-} can be incorporated into various phosphate(V), vanadate(V), and arsenate(V) host lattices. The CrO_4^{3-} doped Li_3PO_4 crystals used for the present study were grown from a LiCl/CsCl flux. MnO_4^{2-} can be doped into sulfate(VI), chromate(VI), selenate(VI), and molybdate(VI) host lattices. Crystals can be grown both from aqueous solution and from KCl/NaCl fluxes. The latter always contain Mn^{5+} besides Mn^{6+} [3].

Figure 1 shows the 15 K luminescence spectrum of nominally 3 mol% Cr^{5+} doped Li_3PO_4 excited at 674.1 nm. The sharp lines due to a Mn^{5+} impurity are indicated. The inset shows the temperature dependence of the relative luminescence intensity. At 300 K it is only reduced to 25% of its 10 K value. Figure 2 shows the 10 K luminescence spectrum of K_2CrO_4: 0.1% Mn^{6+} upon broadband photoexcitation in the VIS. In this material the temperature quenching is more pronounced, the intensity at 300 K is reduced to about 6% with respect to 10 K.

As shown schematically in the inset of Figure 2, the luminescence is due to a $d \rightarrow d$ transition between the $^2T_2$ excited state and the ^2E ground state. This is in the idealized tetrahedral MO_4 symmetry. In reality, the symmetry of the CrO_4^{3-} and MnO_4^{2-} ions is lower than T_d in all the host lattices reported here [4]. This leads to a splitting of the electronic states. In both the spectra of Figures 1 and 2 the origins of the two transitions I and II corresponding to the orbital components of the ^2E ground state are readily identified. The ^2E splitting of Cr^{5+} in Li_3PO_4 is only 19 cm^{-1} reflecting the small deviation of the PO_4^{3-} units from tetrahedral symmetry. This is in contrast to the large splitting of 984 cm^{-1} for Mn^{6+} in

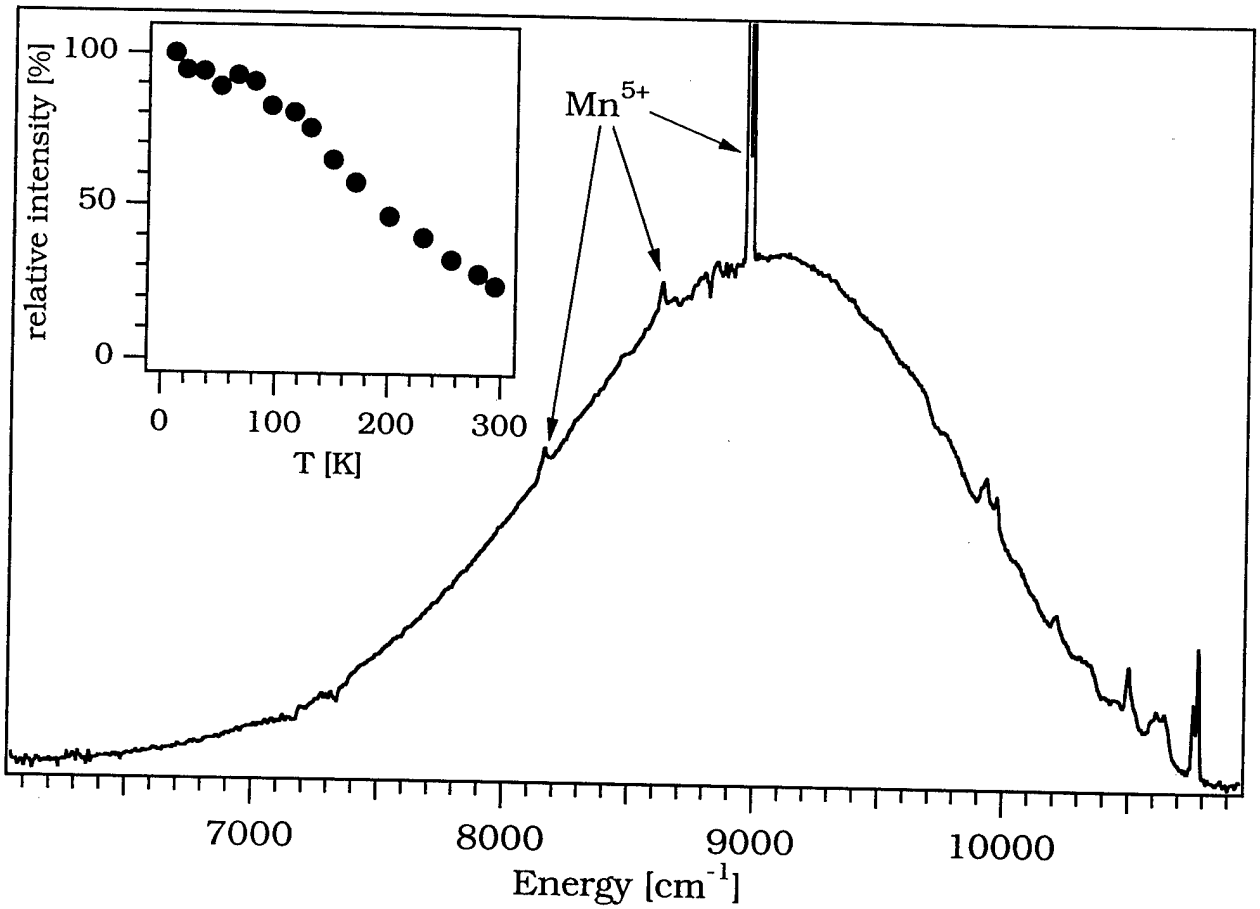

Figure 1: 15 K luminescence spectrum of Li_3PO_4: Cr^{5+} excited at 674.1 nm. The inset shows the temperature dependence of the relative luminescence intensity.

the K_2CrO_4 host lattice (I and II in Figure 2) due to a much stronger C_s site perturbation. The luminescence bands are broad for both systems, with bandwidths at 10 K of the order of 4000 cm^{-1} for all the lattices studied so far. The bandshapes vary considerably, some host lattices such as K_2CrO_4 in Figure 2 exhibiting an extremely rich fine structure at 10 K. The band positions are very similar for CrO_4^{3-} and MnO_4^{2-}.

The temperature quenching of the MnO_4^{2-} systems studied so far can be correlated with the ionic radius of the M^{6+} ion for which Mn^{6+} substitutes in the lattice. For a given crystal–structure type it is weakest in sulfates, in which Mn^{6+} is squeezed into a site which is too small, and strongest in molybdates, in which there is too much space available for MnO_4^{2-}.

For $BaSO_4$: Mn^{6+}, which is a potential candidate for a laser material, we find a radiative lifetime $\tau_{rad} = 2.75\ \mu s$ and calculate a peak stimulated emission cross section $\sigma_{se} = 9.4 \times 10^{-19}$ cm^2 at 9260 cm^{-1} [5]. This is five times larger than for Cr^{4+} doped forsterite [6]. In addition the width of the luminescence found in $BaSO_4$: Mn^{6+} exceeds the width of the Cr^{4+}: forsterite luminescence. We feel, therefore, that CrO_4^{3-} and MnO_4^{2-} doped crystals have a potential as tunable NIR solid state laser materials.

This work was financially supported by the Swiss National Science Foundation.

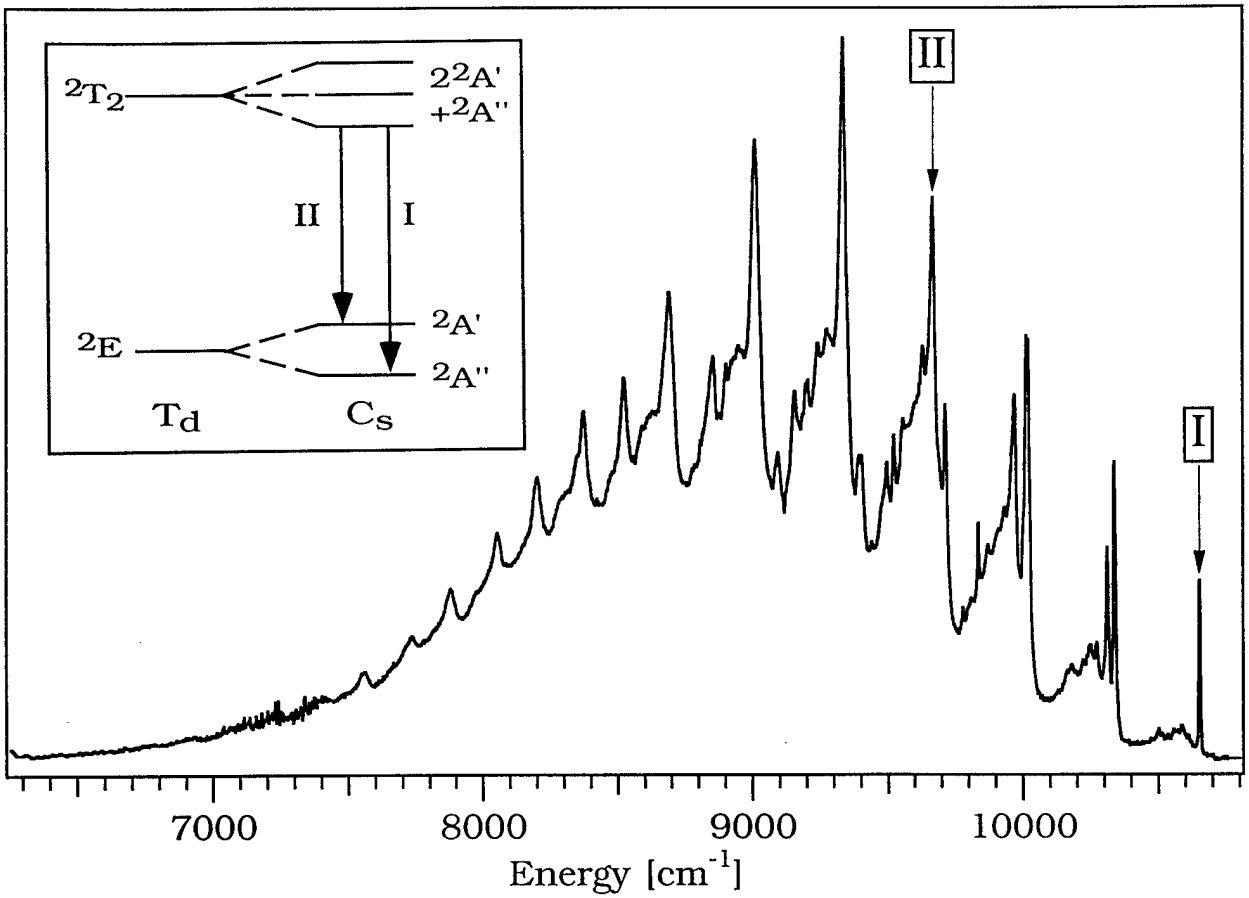

Figure 2: 10 K luminescence spectrum of K_2CrO_4: Mn^{6+} upon broadband excitation. The inset shows the effect of the $T_d \rightarrow C_s$ site perturbation on the energy levels of a $(3d)^1$ system.

References

[1] M.F. Hazenkamp and H.U. Güdel, submitted for publication in Chem. Phys. Lett.

[2] T.C. Brunold, M.F. Hazenkamp, and H.U. Güdel, J. Am. Chem. Soc. **117**, 5598 (1995).

[3] T.C. Brunold and H.U. Güdel, manuscript in preparation.

[4] R.W.G. Wyckoff, Crystal Structures, Vol. 3 (Interscience, New York, 1965; 2nd ed.).

[5] T.C. Brunold and H.U. Güdel, submitted for publication in Appl. Phys. Lett.

[6] R. Moncorgé, H. Manaa, and G. Boulon, Optical Materials **4**, 139 (1994).

Friday, February 2, 1996

Spectroscopy Poster Session

FC 9:45 am-10:45 am
Terrace Room

Spectroscopy and Optical Amplification in Cr doped $LiNbO_3$

J.M. Almeida, A.P. Leite

Centro de Física do Porto
Faculdade de Ciências
Universidade do Porto
P. Gomes Teixeira
4000 Porto, Portugal
Fax 351.2.319 267
Tel 351.2.200 1653

R.M. De La Rue
C.N. Ironside

Dept. of Elec. and Elec. Eng.
University of Glasgow
Glasgow G12 8QQ
Scotland
Fax 44.41.330 4907
Tel 44.41.339 8855

J. Amin, M. Hempstead
J.S. Wilkinson

Optoelectronics Research Centre
Dept. of Elec. and Comp. Science
University of Southampton
United Kingdom
Fax 44.1703.593149
Tel 44.1703.592792

Introduction

Recent efforts in the development of planar waveguide lasers and amplifiers have resulted in the demonstration of sophisticated rare-earth-doped waveguide devices in $LiNbO_3$, taking advantage of the host material electro- and acousto-optic properties [1-3]. However, RE^{3+} ions in $LiNbO_3$ typically exhibit a short tuneability range. Transition metal ions, such as chromium, have on the other hand been used extensively in the past few years to demonstrate broad tuneability in various crystalline host materials [4], other than $LiNbO_3$.

The absorption spectrum of Cr-doped lithium niobate shows two bands with peaks at 480 nm and 660 nm, approximately [5]. The fluorescence spectrum consists of a broad band with a peak at around 900 nm and half-width of about 200 nm [5]. Gain in proton-exchanged waveguides in chromium bulk-doped lithium niobate has been reported [6]. Using Ti-indiffused waveguides fabricated in Cr diffusion doped substrates internal gain was observed [7].

These results, if confirmed, indicate a significant potential for an integrated, broad-band tuneable laser in the 750-1150 nm spectral range, with the additional prospect of diode laser pumping, using Cr-doped $LiNbO_3$ substrates. However, attempts to repeat these measurements, combined with the new measurements of polarised cross-sections, cast doubt upon the accuracy of the earlier results.

Previous calculations of the gain behaviour [8] were based on published values for the cross sections and lifetimes and showed that reasonable gain could be expected in waveguides on Cr-doped lithium niobate substrates. We present here the measured absorption and emission cross sections and the resulting theoretically predicted amplification in Cr-doped lithium niobate waveguides.

Spectroscopy of Cr-Doped $LiNbO_3$

The spectroscopy of Cr^{3+} ions in octahedral crystal fields is usually discussed using the Tanabe-Sugano diagram [9]. This is a plot of the energy eigenvalues of the crystal field Hamiltonian of the d^3 configuration as a function of Dq, the strength of the octahedral field. The free ion states relevant for the optical properties are, in order of increasing energy, ^4F, ^4P and ^2G. The crystal field splits level ^4F into a ground state orbital singlet $^4A_2$ and excited state orbital triplets $^4T_2$ and $^4T_1$. The broad absorption bands are due to transitions from level $^4A_2$ to the level $^4T_2$ (band centered at 650 nm) and $^4T_1$ (band centered at 480 nm). Also, due to the crystal field, splitting of the free ion excited state ^2G gives rise to level ^2E. Transitions from the ground state $^4A_2$ to level ^2E lead to the narrow absorption band overlapping the wing of the broad absorption band due to the transition from $^4A_2$ to $^4T_2$. Depending upon whether level ^2E lies below or above level $^4T_2$, the fluorescence spectrum shows sharp R lines or a broad fluorescence band.

In the case of lithium niobate, these levels are almost degenerate and the fluorescence spectrum shows both features. The broad fluorescence band is due to the transition from level $^4T_2$ to level $^4A_2$. Transitions from level ^2E to ground state $^4A_2$ give rise to sharp R lines near 725 nm [9]. These can only be seen at low temperatures because the transition from level $^4T_2$ is vibronically broadened. The Stokes shift between absorption and fluorescence in the $^4T_2$-$^4A_2$ transition provides a possible 4-level optical amplification system.

Absorption and emission spectra

Four samples of Cr-doped LiNbO3 were used to measure absorption and emission cross sections. The concentrations for three samples, grown by the University of Tianjin (UT)-China, were supplied as 0.5, 0.9 and 1.3 ($x10^{19}$ cm^{-3}) of Cr^{3+}. The fourth sample was grown by Union Carbide (UC) and its concentration was $0.4x10^{19}$ cm^{-3}.

For sample UC, the absorption cross section is shown in fig. 1, for both σ and π polarisations together with the labelling of the corresponding transitions. The spectra were measured on a Perkin-Elmer Lambda 9 spectrophotometer. A peak value of $8.3x10^{-19}$ cm^2 at 657 nm was measured for σ polarisation. The shape of the polarised absorption spectra compares well with the published uncalibrated plots [10].

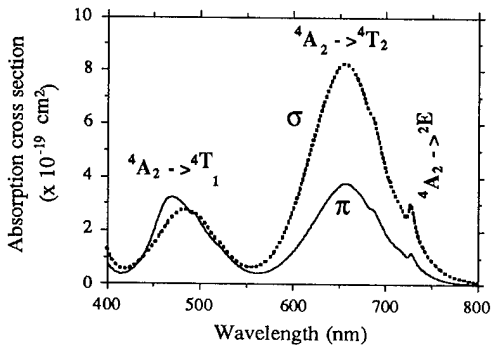

Fig. 1: *Polarised absorption cross sections for sample UC doped with $0.4x10^{19}$ cm^{-3}*

The polarised fluorescence spectra measured for sample UC are shown in fig. 2, and are typical of the $^4T_2$-$^4A_2$ transition. An argon ion laser at 488 nm was used to populate level $^4T_1$, from which a fast decay to level $^4T_2$ occurs.

In order to calculate the emission cross section we used the Fuchtbauer-Ladenburg relation [11]. The peak emission cross section is given by:

$$\sigma_e^{peak} = \frac{\lambda_{peak}^4}{8\pi c n^2 \tau_{rad} \Delta\lambda_{eff}}$$

where λ_{peak} is the wavelength at the peak of fluorescence , c is the light velocity in vacuum, n is the refractive index of the medium at the peak wavelength, τ_{rad} is the radiative lifetime and $\Delta\lambda_{eff}$ is the fluorescence effective linewidth, defined as:

$$\Delta\lambda_{eff} = \frac{\int I_{FLR}(\lambda)d\lambda}{I_{Peak}}$$

where I_{FLR} (λ) is the fluorescence intensity spectrum measured in arbitrary units and I_{peak} its peak value.

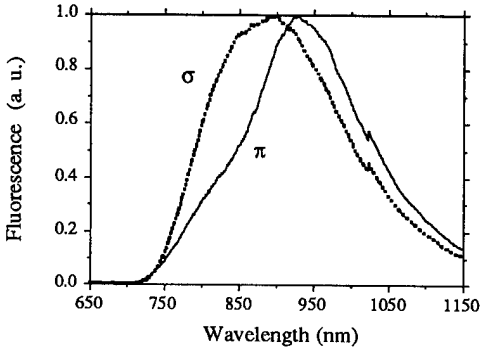

Fig. 2: *Polarised fuorescence spectra for sample UC doped with $0.4x10^{19}$ cm^{-3} showing the $^4T_2$->$^4A_2$ transition.*

The fluorescence lifetime was previously measured as a function of temperature in the same UC sample [7]. We measured a constant value of approximately 9 μs at temperatures below 100 K and 1 μs at room temperature. We assume that the radiative lifetime is 9 μs, and that the room temperature lifetime is due to multiphonon nonradiative decay, indicating the room temperature fluorescence quantum efficiency to be ≈ 0.11.

Using the above relation and the measured data, we calculated, for the σ polarised emission- cross section, $8.4x10^{-20}$ cm^2 at 898 nm, and $1.1x10^{-19}$ cm^2 at 927 nm for the π polarised emission cross section. In [12] Babadjanyan et al presented a value of $2x10^{-19}$ cm^2 , but did not mention a specific polarisation.

Cr:$LiNbO_3$ waveguide amplifiers

A simple model of laser amplification was applied to estimate the behaviour of Cr:LiNbO3 channel waveguides in both bulk- and diffusion-doped structures [5], using the measured cross-sections as above and reasonable estimates for the scattering losses and waveguide modal profiles for pump and signal. The rate equations for a 4-level laser system in the steady state were used, as in [13], for the cases of bulk- and diffusion-doped amplifiers.

Due to the high peak value of the absorption cross section we chose a pump wavelength of 750 nm, for which we measured an absorption cross section of

8.9×10^{-20} cm^2 in σ polarization. We assumed a signal wavelength of 927 nm, which is the peak of the emission cross section. A surface Cr concentration of 5.0×10^{20} cm^{-3}, which can be readily achieved in diffusion-doped samples [5], was used. We assume scattering losses to be on the order of 0.4 dB/cm, an effective pump area of 20 μm^2 and a lifetime of 1 μs (at room temperature).

The gain evolution as a function of cavity length is shown in fig.3 for three values of launched pump power. It was found that, for a launched pump power of 100 mW, a theoretical maximum net gain of 0.85 dB can be obtained for a waveguide length of around 1 mm.

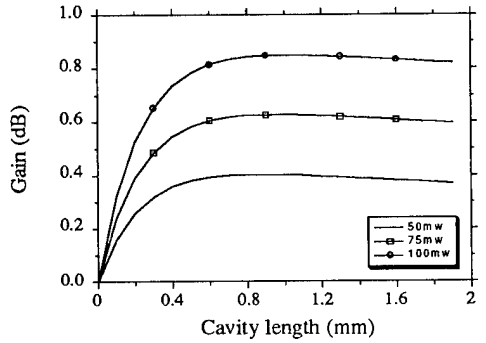

Fig. 3: *Simulated gain evolution in a waveguide on Cr:LiNbO$_3$.*

As it is difficult to fabricate a device as short as 1 mm, further detuning of the pump absorption is desirable, along with a decrease in the Cr concentration. If a pump wavelength of 800 nm is used, an optimum cavity length of 4.5 mm was calculated, for which a maximum gain of 0.68 dB could be achieved for 100 mW of launched pump power. A decrease in the Cr concentration has not been considered, because it would also reduce the gain.

Based on the above calculation we can conclude that Cr:LiNbO$_3$ is, at best, a low gain material, yielding a gain below 1dB for a 1 mm sample, when a reasonably high pump power is launched, thus requiring waveguides with very low loss. Moreover, the short wavelengths that have to be used to excite the Cr^{3+} ions are known to induce photorefractive damage in LiNbO$_3$, increasing the losses and further reducing the gain. Proton-exchange in conjunction with MgO doped LiNbO$_3$ may potentially overcome the problems associated with optical damage.

Conclusions

The polarised absorption and emission cross sections of Cr doped LiNbO$_3$ were measured for the first time. Using this accurate spectroscopic data, an estimate of the gain behaviour of a waveguide amplifier has been carried out using a simple model. The combination of a relatively small emission cross section with a short lifetime shows that this material exhibits low gain for high pump power density in contrast to previous expectations.

Acknowledgements

A.P. Leite and J.M. Almeida acknowledge the financial support of JNICT and PRAXIS XXI. The Optoelectronics Research Centre is partially funded by the UK EPSRC.

References

[1] H. Suche, in Proceedings of the European Conference on Integrated Optics (ECIO) 565, Delft, April 1995

[2] E. Lallier, D. Papillon, J. P. Pocholle, M. Papuchon, M. De Micheli, D. B. Ostrowsky, Electron. Lett. **29**, 175 (1993)

[3] J. Amin, M. Hempstead, J.E. Román, J.S. Wilkinson, Opt. Lett., **19**, 1541 (1994)

[4] L.K. Smith, S.A. Payne, W.L. Kway, L.L. Chase, B.H.T. Chai, IEEE J. Quant. Elect. **QE-28**, 2612 (1992)

[5] J.M. Almeida, G. Boyle, A.P. Leite, R.M. De La Rue, C.N. Ironside, F. Caccavale, P. Chakraborty, I. Mansour, J. Appl. Phys., **78**, 2193 (1995)

[6] F. Zhou, R.M. De La Rue, C.N. Ironside, T.P.J. Han, B. Henderson, A.I. Ferguson, Electron. Lett. **28**, 2041 (1992)

[7] J.M. Almeida, A.P. Leite, R.M. De La Rue, C.N. Ironside, F. Caccavale, P. Mazzoldi, in Proceedings of the European Conference on Integrated Optics (ECIO) 237, Delft, April 1995

[8] J.M. Almeida, R.M. De La Rue, C.N. Ironside, F. Caccavale, A.P. Leite, 1994 International Workshop on Ferroelectric Integrated Optics, Breckenridge, CO (1994)

[9] J.F.H. Nicholls, T.P.J. Han, B. Henderson, F. Jaqué, Chem. Phys. Lett., **202**, 560 (1993)

[10] A. M. Glass, J. Chem. Phys. **50**, 1501 (1969)

[11] E. Desurvire, *Erbium-Doped Fiber Amplifiers* (John Wiley & Sons, New York, 1994)

[12] V. G. Babadjanyan, E. P. Kokanyan, R. B. Kostanyan, V. R. Nikogosyan, Opt. Commun. **78**, 257 (1990)

[13] W. Sohler, in *Proceedings of the NATO ASI on Waveguide Optoelectronics*, edited by J.H. Marsh and R.M. De La Rue (Kluwer Academic Publishers, Dordrecht, Series E-vol. 226, 1992)

High Excited Ion Density Effects on the Effective Fluorescence Lifetime in Q-Switched Solid State Lasers

Brian W. Baird
Electro Scientific Industries
13900 NW Science Park Drive
Portland, OR 97229
(503) 671-5423
FAX (503) 671-5651

Richard K. DeFreez
Linfield Research Institute
900 S. Baker Street
McMinnville, OR 97128
(503) 434-2473
FAX (503) 648-9606

Eric M. Freden
Utah State University
987 E. Lagoon Street
Roosevelt, UT 84066
(801) 722-2294
FAX (801) 722-5678

The use of diode-pumped Q-switched solid state lasers is increasing in industrial applications, including laser repair of semiconductor memory devices and laser trimming of discrete components. In laser repair of semiconductor memory devices, a single laser pulse is typically employed to blow a microscopic fuse in order to disconnect the address line to a memory cell. This process can be highly sensitive to pulse-to-pulse energy variations on the order of a few percent. Commonly, the laser memory repair process will utilize interpulse periods which vary from a millisecond to several tens of milliseconds between pulses to accommodate the random pitch at which fuses must be blown on devices. As a consequence, the laser memory repair process can be sensitive to the roll-off in pulse energy which occurs with increasing pulse repetition frequency (PRF) in q-switched solid state lasers. As is well understood[1], this roll-off is dependent on the fluorescence lifetime of the material chosen as the active medium.

Diode-pumped Q-switched Nd:YLF lasers operating at 1047 nm with pulsewidths ranging from 3 ns to 30 ns and with pulse energies ranging from 20 μJ to 150 μJ are standard in advanced laser memory repair processes. It has been commonly observed that the roll-off in pulse energy with increasing PRF in these lasers is less than expected when calculated using

$$E_1 = E_0 [1 - \exp(-t/\tau_f)]$$

and where $\tau_f \approx 500$ μs based on the work of Harmer[2].

Fan and co-workers[3] observed yellow emission from Nd:YLF under 791 nm diode excitation and Malinowski and co-workers[4] have reported on laser induced up-conversion processes in Nd:YLF. Otsuka and Kubodera[5] presented a simplified rate equation for the number of excited states assuming excited state absorption and suggested that Nd stoichiometric lasers could be subject to lifetime shortening for high excitation rates.

We have extended this work to derive an expression for the pulse energy of a Q-switched solid state laser for the case with high pumping rate and significant excited state absorption. The simplified rate equation for this case, ignoring the effect of finite lower level lifetime described by Fan[6], is

$$dN_2/dt = W_pN_0 - N_2/\tau_f - qN_2^2/\tau_f$$

which can be solved to give for the energy dependence on interpulse time t

$$E_1 = \frac{E_0\{1 - \exp[-t((W_p + 1/\tau_f)^2 + \chi)^{1/2}]\}}{\{1-(1/\beta)\exp[-t((W_p + 1/\tau_f)^2 + \chi)^{1/2}]\}}$$

where

$$\chi = 4qW_pN_{tot}/\tau_f$$

and where $1/\beta \rightarrow 0$ for $q \rightarrow 0$. Note that the term $((W_p + 1/\tau_f)^2 + \chi)^{1/2}$ yields an effective fluorescence lifetime which explicitly depends on the pumping rate W_p and the excited state absorption parameter q. For the simple case of q=0, this expression shows the importance of the pumping rate term as it becomes of comparable order to the inverse of the single-ion fluorescence lifetime value τ_f.

In an effort to experimentally determine if fluorescence lifetime shortening could be observed in Nd:YLF under intense laser diode pumping, 3.0 mm diameter discs of 1.0% atomic and 1.8% atomic Nd:YLF were obtained from Lightning Optical and AR-coated for diode pumping. For the 1.0% doping level, disc thicknesses of 0.25, 0.50, and 1.0 mm were used. For the 1.8% doping level, disc thicknesses of 0.1, 0.25, 0.50, and 1.0 mm were used. A Sony 305YT 3.0 W laser diode with an emission width of 500 μm was used as the diode source. The laser diode was operated in pulsed mode with 1 ms pulsewidth using a SDL 820 Diode Driver. It was coupled into a sapphire nonimaging concentrator with 700 μm input aperture diameter and 200 μm output diameter which was then closely end-coupled to the sample discs of Nd:YLF under test. The fluorescence was imaged onto an RCA 31034 photomultiplier tube at the exit port of a Spex 1269 1.26 m spectrometer incorporating a 600 gr/mm grating. Figure 1 shows the measured fluorescence lifetime vs sample thickness for a diode current of 5.0 A. The data shows a decrease in measured fluorescence lifetime with smaller disc thickness corresponding to a higher excited ion density.

References

1. W. Koechner, Solid-State Laser Engineering, Springer-Verlag, 2nd Ed., 402, (1988).
2. A.L. Harmer, A. Linz, and D.R. Gabbe, J. Phys. Chem. Solids, **30,** 1483, (1969).
3. T.Y. Fan, G.J. Dixon, and R. L. Byer, Opt. Lett., **11**, No. 4, 204, (1986).
4. M. Malinowski, B. Jacquier, M. Bouazaoui, M.F. Joubert, and C. Linares, Phys. Rev. B., **41**, No. 1, 31, (1990).
5. K. Otsuka and K. Kubodera, IEEE J. Quant. Elect., **QE-16**, No. 5, 538, (1980).
6. T. Y. Fan, IEEE J. Quant. Elect., **QE-24**, No. 12, 2345, (1988).

Fig. 1: Fluorescence Lifetime vs Sample Thickness

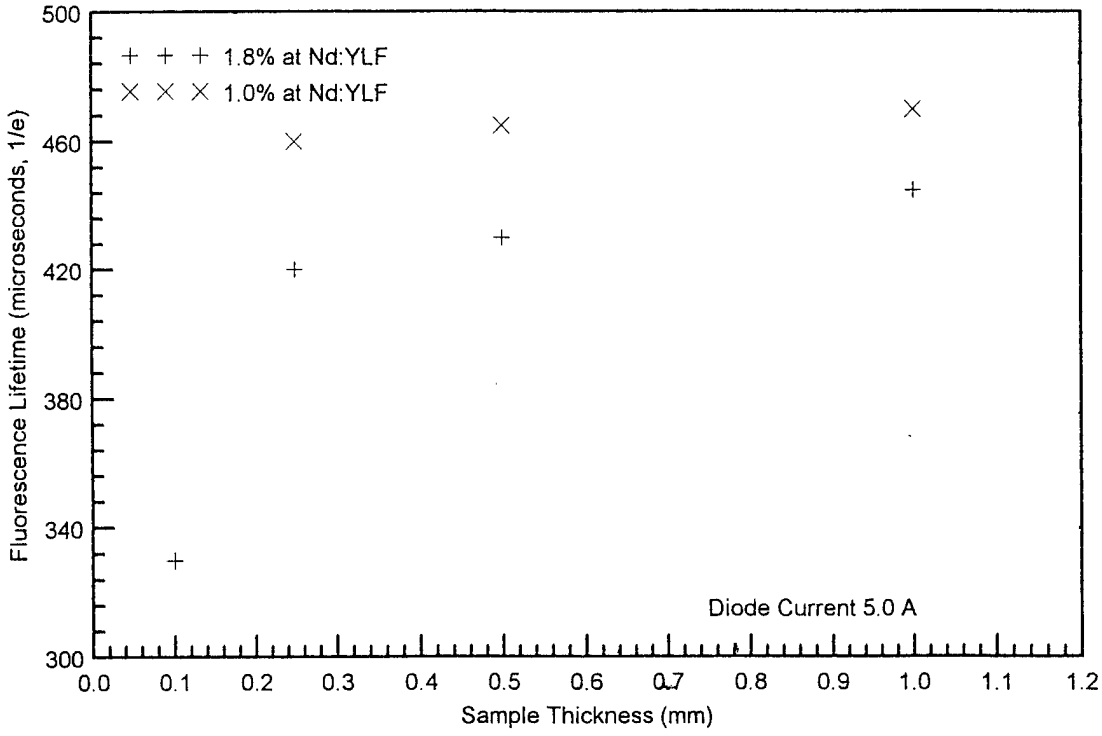

SELF QUENCHING OF THE Nd $^4F_{3/2}$ MANIFOLD

Norman P. Barnes
NASA Langley Research Center
Hampton, VA 23681

Elizabeth D. Filer
Norfolk State University
Norfolk, VA 23504

Clyde A. Morrison
Army Research Laboratories
Adelphi, MD 20783

An alternate approach, using computed energy transfer parameters, to describe self quenching of the Nd $^4F_{3/2}$ manifold is developed and found to agree with experimental results. Self quenching shortens the apparent lifetime of the upper laser level which detracts from the efficiency. An optimum Nd concentration therefore is a compromise between absorption efficiency, which increases with Nd concentration, and storage efficiency. Data on Nd:$LaSc_3(BO_3)_4$ provides a good test for this approach since upper laser level lifetime data are available over a wide range of Nd concentrations [1]. While computed results agree very well with measured data for both Nd:YAG and Nd:YLF, the ranges of concentrations are limited

An extension of a quantum mechanical model was used to calculate self quenching and diffusion parameters, beginning with the measured energy levels in the laser materials. While other approaches have utilized both self quenching and diffusion to describe the shortening of the $^4F_{3/2}$ manifold lifetime, often the inverse of the lifetime was described in terms of either a linear or a quadratic dependence on the concentration. An alternate approach is proposed here which describes the inverse of the lifetime as essentially independent of the concentration for low concentrations and linearly related to the concentration for higher concentrations. Since many functions can be made to fit data with only a few sets of points, having extensive lifetime data agree with the predicted behavior is highly encouraging.

Another distinction of this approach compared with other existing approaches arises from the discrete nature of a crystal lattice. A classical approach to calculating the energy transfer parameters essentially integrated over all possible orientations and distances between interacting atoms [2]. Since the energy transfer parameter depends on the separation of the interacting atoms to the inverse sixth power, the selection of the closest possible separation assumes extreme importance. In this approach, the closest possible separation of nearest similar neighbors is set by the crystal lattice. Energy transfer parameters, that is self quenching and diffusion, are calculated in this approach using a summation over orientations and separations set by the crystal

lattice. As a consequence, for laser materials such as Nd:YLF self quenching is less probable than diffusion.

Comparisons of the predictions of this model with the lifetime measurements of Nd:YLF and Nd:YAG yield good agreement. In the case of Nd:YLF, diffusion is fast compared with the inverse of the fluorescent lifetime of the $^4F_{3/2}$ manifold so that a linear relationship is expected between the inverse of the lifetime and the concentration. In fact, a linear relationship is observed, as shown in Figure 1, and the slope agrees well with the calculated slope. In the case of Nd:YAG, diffusion is not fast compared with the inverse of the fluorescent lifetime for all concentrations. As such, for low concentrations, the inverse of the lifetime should be nearly independent of the concentration while for higher concentrations the inverse of the lifetime should increase linearly with concentration. In fact, measured lifetime as a function of concentration is in agreement with these calculated predictions. In addition, the transition between the nearly independent regime to the linear regime is also in agreement with the energy transfer parameters derived from the quantum mechanical model.

Nd:$LaSc_3(BO_3)_4$ has displays behavior similar to Nd:YAG but data is available for concentrations ranging from 0.001 to 0.50. At the suggestion of one of the authors [1], the datum at unity concentration was not utilized. In this laser material, the upper laser level lifetime is independent of Nd concentration up to a Nd concentration of approximately 0.1. However, above this concentration, the inverse lifetime increases linearly with the concentration. Note that if the datum at a concentration of 0.5 were not available, the inverse lifetime could be made to fit either a linear or a quadratic dependence on the Nd concentration reasonably well.

In summary, an alternative approach to model the dependence of the upper laser level of the Nd $^4F_{3/2}$ manifold on the Nd concentration has been calculated and found to agree with experimental data. Upper laser level lifetime depends on both the diffusion and self quenching parameters, both of which can be calculated given the energy levels of the laser material. Good agreement is found for Nd:YAG and Nd:YLF where the extensive energy level data is available. Nd:$LaSc_3(BO_3)_4$ has more limited energy level data available. However, the wide range of upper laser level lifetime versus Nd concentration data supports the proposed approach well.

1. V. Ostromov, T. Jensen, J.-P. Meyn, G. Huber, and M. A. Noginov, "Concentration Quenching And Up-Conversion Of Neodymium Ions In $LaSc_3(BO_3)_4$ and $GdVO_4$ Crystals," Technical Digest Of The Advanced Solid State Laser Conference, Memphis TN (1995)

2. D. L. Dexter, "A Theory Of Sensitized Luminescence In Solids," J. Chem. Phys., 21 836-850 (1953)

Nd:YLF Upper Level Lifetime Versus Nd Concentration

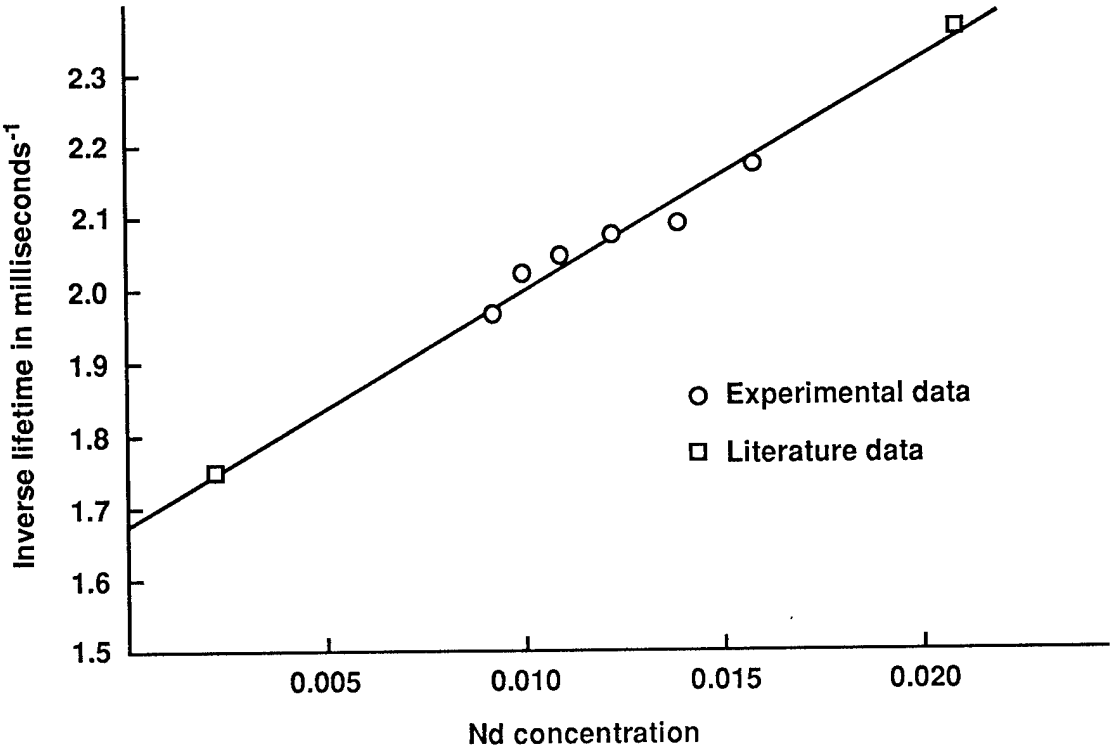

Inverse Lifetime of Nd:$LaSc_3$ $(BO)_4$ Versus Concentration

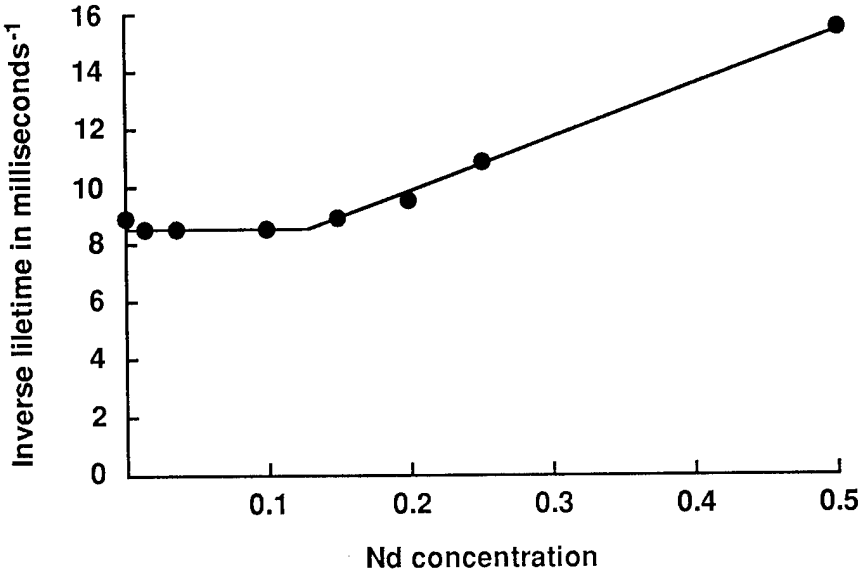

Multiphonon relaxation in the rare-earth ions doped laser crystals.

T.T.Basiev, Yu.V.Orlovskii, K.K.Pukhov,
V.B. Sigachev, M.E. Doroshenko, I.N. Vorob'ev
General Physics Institute, 38 Vavilov st., 117942, GSP-1,
Moscow, Russia, phone:(095) 135-0267, fax:(095) 135-0270
e-mail: basiev@ftt.gpi.msk.su

For the direct measurements of fluorescence kinetics decay from different multiplets of Tm^{3+} and Ho^{3+} ions in $Y_3Al_5O_{12}$, $Lu_3Al_5O_{12}$ and $LiYF_4$ laser crystals the direct laser excitation of the multiplet in study has been used. In the case when direct excitation was not available the first upper lying multiplet with the smaller energy gap ΔE to the multiplet of interest was excited. The following various laser types has been used: 1)the pulsed tunable (1.08-1.28μm) LiF:F_2^- color centers laser "MALSAN" pumped by the Q- switched flash lamp pumped the YAG:Nd laser (t_p=10ns, f=12.5-25Hz) - $^3F_4$, $^3H_5$ of Tm^{3+}, $^5I_7$, $^5I_6$ of Ho^{3+}, 2)780nm of a Ti:Al_2O_3 crystal laser pumped by the 531 nm of frequency doubled nanosecond Q- switched Ce:Nd:GGG crystal laser- $^3H_4$ of Tm^{3+} ion, 3)the 531 nm of frequency doubled nanosecond Q-switched Ce:Nd:GGG crystal laser- $^5S_2$ of Ho^{3+}, 4)the tunable (0.84-1.09 μm) LiF:F_2^+ color center laser "Malsan" pumped by 657 nm nanosecond pulses of frequency doubled 1.34 μm Q-switched Nd:$YAlO_3$ laser - $^5I_5$ of Ho^{3+} in YLF, YAG and LuAG, 5)the pulsed tunable Oksazin-17 dye laser ($t_p \approx$ 5ns, λ_{gen}=632-670nm) pumped with the copper vapor laser (t_p=10ns, f=10kHz) - $^5F_5$ of Ho^{3+}in YAG and LuAG, $^3F_3$ of Tm^{3+} in YLF, 6)the pulsed Oksazin-17 dye laser (639-641nm) pumped by the 531nm of frequency doubled Q-switched Ce:Nd:GGG crystal laser - $^5F_5$ of Ho^{3+} in YLF.

For the measurements of the strongly quenched fluorescence kinetics decay the time-correlated photon-counting technique was used whereas for the others the 20 MHz or 200 MHz digital transient recorders along with appropriate photo multiplier (S1 or S20 type) or PbS photo-resistor were employed.

The measured lifetimes for YLF, YAG, and LuAG Tm^{3+} and Ho^{3+} doped crystals at T=77 and 300 K are presented in Table 1.

The analysis of these and earlier measured multiphonon relaxation (MR) rates [1-3] for the transitions with n<5 shows that every so often the good correlation between the MR rates and the reduced matrix element $U^{(2)}$ is observed. This is in an agreement with the non-linear (NL) theory of multiphonon relaxation [4-6] for n<5 when the contribution of $U^{(4)}$ and $U^{(6)}$ is negligible for the case when the ion and the lattice types are the same and for the transitions with the equal number of phonons involved. For example, for the 2 phonon transitions in the YAG:Nd^{3+} crystal the six times increase of the low rank matrix element $\langle U^{(2)} \rangle^2$ for the $^4G_{7/2}+^2K_{13/2} \rightarrow ^4G_{5/2}+^2G_{7/2}$

transition ($\langle U^{(2)}\rangle^2$=0.06, τ=0.37ns) comparing to the $^4D_{3/2}\rightarrow{}^2P_{3/2}$ transition ($\langle U^{(2)}\rangle^2$=0.01, τ=2.2ns) also causes 6 times increases of the MR rate. Also, for the 4 phonon transition in the YAG:Ho^{3+} crystal the six times increase of the $\langle U^{(2)}\rangle^2$ for the $^5S_2+{}^5F_4\rightarrow{}^5F_5$ transition ($\langle U^{(2)}\rangle^2$=0.1944, τ=4μs) in comparison with the $^5I_6\rightarrow{}^5I_7$ one ($\langle U^{(2)}\rangle^2$=0.0319, τ=44.3 μs) gives fairly good agreement with approximately one order decrease of the life time and corresponding increase of the multiphonon relaxation rate.

It was observed that the MR rate strongly depends on crystal and R.E. dopant type. For the same crystals but different rare-earth ions some specific regularity has been observed for the first time, i.e. the larger the radius of R.E. ion the faster the multiphonon relaxation in the same hosts when the number of phonons involved and reduced matrix elements $U^{(k)}$ are equal which is also in an agreement with NL theory. For example, the radius of the Nd^{3+} ion is larger than for the Er^{3+} one and for the 4 phonon $^4G_{7/2}\rightarrow{}^4G_{5/2}+{}^2G_{7/2}$ transition in Nd^{3+} ($(U^{(2)})^2\approx$0.06, τ=110.5ns) and $^4F_{5/2}\rightarrow{}^4F_{7/2}$ one in Er^{3+} ($(U^{(2)})^2\approx$0.07, τ=53.2ns) in the LaF_3 crystal when the reduced matrix elements $U^{(2)}$ for both transitions are approximately equal the MR is 6 times faster for Nd^{3+} than for Er^{3+}. The main reason of this enhancement is the increase of the contribution of the Coulomb and non-Coulomb interactions to the multiphonon relaxation for the 4-phonon transition in the LaF_3:Nd^{3+} in comparison with the LaF_3:Er^{3+}.

Another dependence of multiphonon relaxation rates versus the crystal type is also discussed. The example of the latter dependence is ~ 15-th times faster relaxation for the 4 phonon $^4F_{5/2}\rightarrow{}^4F_{7/2}$ transition (τ=658ns, $(U^{(2)})^2\approx$0.08) in LaF_3:Er^{3+} than for 4 phonon $^3H_5\rightarrow{}^3F_4$ transition ($\tau\approx$10μs, $(U^{(2)})^2\approx$0.09) in YLF:Tm^{3+} which is for close values of ionic radii mainly deals with the larger electron-phonon coupling in LaF_3 than in YLF. It is found that when all other factors being approximately the same in most cases the larger maximum phonon frequency in a crystal correlates with the less strength of electron- phonon coupling in R.E. doped laser crystals.

For most of the transitions the temperature dependencies of relaxation rates in the range of 77-700K were measured and analyzed using Bose-Einstein distribution function and single and double frequency models of phonon spectrum.

References:

[1] T.T. Basiev, A.Yu. Dergachev, Yu.V. Orlovskii, A.M. Prokhorov J of Lum., v. 3/1-6, 19-23, 1992.

[2] T.T. Basiev, A.Yu. Dergachev, Yu.V. Orlovskii, A.M. Prokhorov, Proceedings of General Physics Institute, Moscow, Nauka, V. 46, 1994, 3-64 (in Russian).

[3] Yu.V.Orlovskii, R.J.Reeves, R.C.Powell, T.T.Basiev, K.K.Pukhov, Phys. Rev. B, v. 49 (1994) 3821.

[4] K.K.Pukhov, V.P.Sakun, Phys. Stat. Sol. (b), 95 (1979) 391.

[5] K.K.Pukhov, Fiz.Tverd.Tela 31 (1989) 144 [Sov. Phys. Solid State, v. 31 (1989) 1557].

[6] Yu.V.Orlovskii, T.T.Basiev, K.K. Pukhov, T. Tsuboi, Opt.materials, v. 4 (1995) 583.

Table 1. The measured lifetimes $\tau_{meas.}$ for the transitions of some multiplets of Ho^{3+} and Tm^{3+} ions in YLF, YAG and LuAG laser crystals. (ΔE is the minimal energy "gap" to the nearest multiplet below; n is the minimal number of the phonons involved in the transitions ($n=\Delta E/\hbar\omega_{max}$ and $\hbar\omega_{max}$ is the maximal phonon frequency in laser host, $\hbar\omega_{max}\approx 560cm^{-1}$ for YLF and $850cm^{-1}$ for YAG and LuAG).

Crystal	Transition	$\Delta E, cm^{-1}$	n	τ_{meas} 77K	τ_{meas} 300K
YLF:Tm^{3+}	$^3F_3\rightarrow{}^3H_4$	1700	3	78 ± 0.7 ns	54 ±0.4ns
	$^3H_5\rightarrow{}^3F_4$	2301	4		5.0±0.2μs
	$^3H_4\rightarrow{}^3H_5$	4070	8	2.89±0.04ms	2.15±0.02ms
	$^3F_4\rightarrow{}^3H_6$	5185	9(10)	18.05±0.07ms	15.2±0.1 ms
YLF:Ho^{3+}	$^5F_5\rightarrow{}^5I_4$	1953	4	57.2 ±0.5 μs	28.1±0.2 μs
	$^5I_5\rightarrow{}^5I_6$	2443	5	36.1 ±1.8 μs	19.2±1 μs
	$^5S_2+{}^5F_4\rightarrow{}\rightarrow{}^5F_5$	2824	5	147.4±1.4 μs	59.3±0.4 μs
	$^5I_6\rightarrow{}^5I_7$	3378	6	3.52±0.03ms	3.32±0.03ms
	$^5I_7\rightarrow{}^5I_8$	4978	9	14.32±0.1 ms	14.74±0.11ms
YAG:Tm^{3+}	$^3F_3\rightarrow{}^3H_4$	1500	2		< 2 ns
	$^3H_5\rightarrow{}^3F_4$	2278	3		54.3±1.2ns
	$^3H_4\rightarrow{}^3H_5$	3900	5	622±5μs	548 ±5 μs
	$^3F_4\rightarrow{}^3H_6$	4947	6	15.33±0.17ms	10.9±0.1ms
YAG:Ho^{3+}	$^5F_5\rightarrow{}^5I_4$	1894	2(3)	388.5±5.0ns	373.4±3.8ns
	$^5I_5\rightarrow{}^5I_6$	2369	3		436±41 ns
	$^5S_2+{}^5F_4\rightarrow{}\rightarrow{}^5F_5$	2707	4	4.0±0.1μs	3.8 ±0.2μs
	$^5I_6\rightarrow{}^5I_7$	3278	4	44.3±1.3μs	44.7±2.6μs
	$^5I_7\rightarrow{}^5I_8$	4693	6	6.54±0.08ms	7.16±0.06ms
LuAG:Tm^{3+}	$^3H_5\rightarrow{}^3F_4$		3		50±5 ns
	$^3H_4\rightarrow{}^3H_5$		5	551.9±4.9μs	479.9±5.1μs
	$^3F_4\rightarrow{}^3H_6$		6	14.38±0.09ms	10.4±0.1ms
LuAG:Ho^{3+}	$^5F_5\rightarrow{}^5I_4$		2(3)	347.9± 2.8ns	342.5±1.3ns
	$^5I_5\rightarrow{}^5I_6$		3		364±21 ns
	$^5S_2+{}^5F_4\rightarrow{}\rightarrow{}^5F_5$		4	3.64±0.05μs	3.24±0.06μs
	$^5I_6\rightarrow{}^5I_7$		4	39.6±1.7μs	38.6±1.3μs
	$^5I\rightarrow{}^5I$		6	6.18±0.03ms	6.87±0.04ms

Lack of Correlation Between Tm, Ho Upconversion Measurements

Kenneth M. Dinndorf
LADAR Development and Evaluation Research Facility
Wright Laboratory, Armament Directorate, (WL/MNGS), Eglin AFB, FL 32542
VOICE (904) 882-1726 / FAX (904) 882-1717

Hans P. Jenssen
Center for Research and Education in Optics and Lasers (CREOL)
University of Central Florida, Orlando, FL 32826
VOICE (407) 658-3900 / FAX (407) 658-6880

Introduction

When modeling the behavior of solid state lasers, it is common practice to model energy transfer processes by using an "average" energy transfer parameter[1,2]. Although rigorous analytical treatments of energy transfer theory do not support the use of average transfer parameters[3], their use can often be justified under certain conditions and can greatly simplify the solution of the dynamic equations.

Accurate measurement of the average transfer parameter for many of these processes is not simple; extraction of the parameter from experimental data often involves complex analysis and is susceptible to any assumptions made in the analysis process. In this paper, we examine measurements of the $^5I_5$ upconversion process in Tm, Ho: YLF and show that different analysis techniques applied to simultaneously measured data produce values for the $^5I_5$ upconversion parameter that do not agree within experimental uncertainties.

Model

In Fig. 1, the dynamic processes in the Tm, Ho system are diagrammed. Here we model the energy transfer processes between manifolds with average transfer parameters, αs.

Here W_p is the pumping rate of the $^3H_4$ manifold while N_x and N_x' are respectively the x's manifold population in Tm and Ho. α_T and α_T' are the average parameters for transfer and back-transfer from Tm($^3F_4$) to Ho($^5I_7$), while α_1 and α_1' are transfer parameters for $^3H_4$-$^3F_4$ upconversion and cross-relaxation. α_2 is the parameter for $^5I_7$-$^5I_5$, $^3F_4$-$^3H_6$ upconversion, and α_2' the parameter for the corresponding

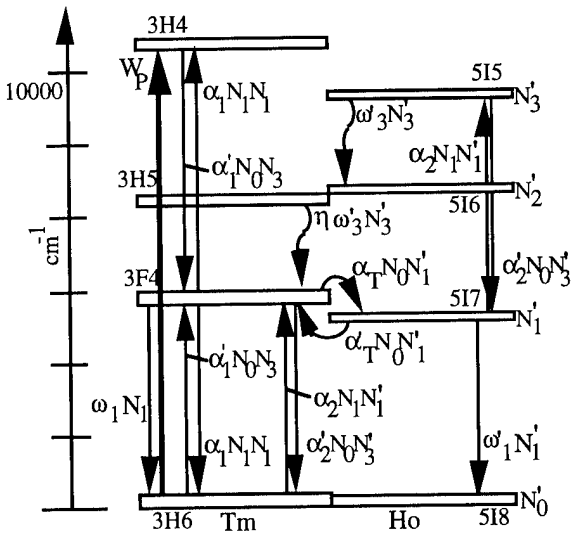

Figure 1. The Tm-Ho system. Spontaneous emission processes from some levels have been omitted.

cross-relaxation. ω_1, ω_1', and ω_3' are the single-ion relaxation probabilities in singly-doped crystals. The dominant contributions to ω_1 and ω_1' come from radiative relaxation, while the primary process contributing to ω_3' is multi-phonon relaxation to the $^5I_6$ manifold. We assume that any excitation lost from the $^5I_5$ manifold by this relaxation transfers to the $^3H_5$ and non-radiatively relaxes to the $^3F_4$ manifold with efficiency η. η depends on unassessed processes affecting the $^5I_6$ but should be close to unity. Many of the inter-manifold radiative relaxation processes are not included as their effects are small in comparison to those of the non-radiative and energy transfer processes. We do not consider additional processes which may occur at extremely high excitation densities. Rate equations can be developed from this

diagram and will be used in fitting to experimental data.

Experiment and Analysis

The upconversion parameter α_2 can be determined by fitting the rate equations to measured data. Our method is to measure the transient response of the Tm-Ho system to square pulse pumping [4]. We simultaneously measure the $^3F_4$, $^3H_6$, $^5I_7$, and $^5I_5$ fluorescence transients with the system described in [5] using 30 ms long square pulses with a duty cycle of roughly 25%. Rate equations are then fit to the shapes of the fluorescence transients. This technique depends only on the transient shapes and not the scale of the signals.

It is important in this fitting procedure to correctly account for the differing excitation densities in the material. Both the Gaussian nature of the pump and the exponential absorption must be modeled. For this fitting procedure, we have divided the pumped volume (0.2 mm x 1.3 mm) into 150 radially symmetric regions of excitation.

It is also important to minimize the adjustable parameters in the rate equations. The pump rate (W_p) is determined by measuring the absorbed power. We have previously measured manifold lifetimes and the cross-relaxation parameters for these materials [5, 6] and have shown that the $^3F_4$-$^3H_4$ upconversion parameter is negligible at most pump intensities. Thus, only 3 unknowns are left: the $^3F_4$-$^5I_7$ transfer and back-transfer parameters, and the $^5I_5$ upconversion parameter.

We first concentrate on the transfer and back-transfer parameters. Within our experimental temporal resolution (~40 μs), there is no measurable difference between the $^3F_4$ and $^5I_7$ dynamics, implying that the manifolds are in equilibrium for this time scale. This is consistent with earlier measurements which place the equilibration time between 10-100 μs [7, 8] and sets a conservative lower limit on the value of the $^3F_4$->$^5I_7$ transfer parameter of $5x10^{-17}$ cm^3s^{-1} in YLF. For the purposes of our modeling, it is sufficient to know only the ratio of the transfer parameters as this ratio determines the excitation distribution between these manifolds. We have measured this ratio in the steady state [9]; therefore, the only remaining unknown is the $^5I_5$ upconversion parameter. In Fig. 2 the $^5I_7$ fluorescence transient as well as fits to this transient are shown.

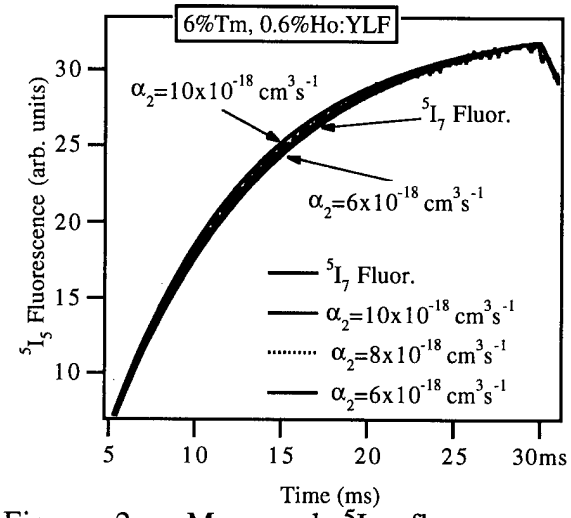

Figure 2. Measured $^5I_7$ fluorescence transient for 6% Tm, 0.6% Ho:YLF with fits for varying values of α_2. The transients resulting from different values of the upconversion parameter have been normalized to overlay the experimental data. Note how the fits for the values of α_2= $10x10^{-18}$ cm^3s^{-1} and α_2=$6x10^{-18}$ cm^3s^{-1} bracket the measured $^5I_7$ fluorescence transient.

From fitting to the above transient, the value of α_2 was determined to be $(8.0\pm1.5)x10^{-18}$ cm^3s^{-1}. The uncertainty estimate was obtained by varying the all measured parameters within their experimental uncertainties. The value of α_2 obtained by fitting showed a slight dependence on pump power, which was varied by ±10% in the fitting procedure. The measured absorbed power implies an absorption coefficient of 3.2 cm^{-1}, within 3% of the value previously measured for this sample.

In Fig. 3, the measured $^5I_5$ fluorescence as well as the predictions of the rate equations are displayed.

Note how the best fit to the $^5I_5$ fluorescence produces an α_2 of (13.5 ± 1.5) $x10^{-18}$ cm^3s^{-1}, in contrast to the value of $(8\pm1.5)x10^{-18}$ cm^3s^{-1} for α_2 obtained when fitting to the $^5I_7$ fluorescence. These two

measurements of α_2 **do not agree** within their experimental uncertainties.

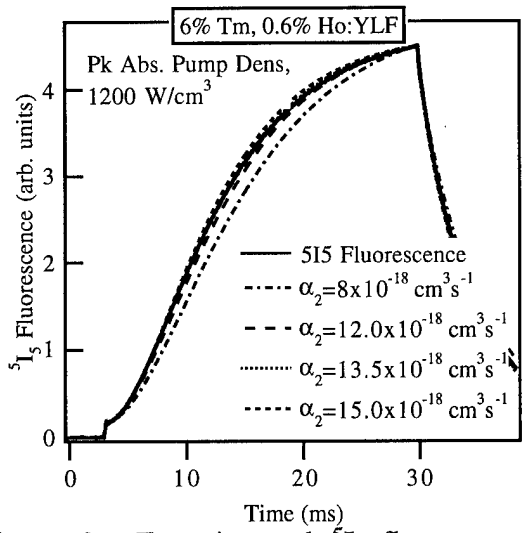

Figure 3. Experimental $^5I_5$ fluorescence transient and fits for 6% Tm, 0.6% Ho:YLF. The best fit was obtained with α_2=13.5x10^{-18} cm^{3}s^{-1}. The small initial step in the signal results from a direct feeding process that feeds the $^5I_7$ manifold with ≈1.5% efficiency when the $^3H_4$ manifold is pumped at 793 nm.

Uncertainty estimates for both of these values were obtained in the manner described above; additionally, the value of α_2 produced by varying the transfer parameters changed in the same manner for fits to both the $^5I_7$ and the $^5I_5$ transients; therefore, it is unlikely that the difference between these two values can be explained as a result of larger than assumed measurement uncertainties. Values of the upconversion parameter from these and other measurements are tabulated in Table 1.

Meas.	α_2x10^{-18}	α_2/α_2'
$^5I_5$ Cr-rel	15.0 ± 2.0[10]	0.116[10]
$^5I_7$ Fit	8.0±1.5	0.06±0.01
$^5I_5$ Fit	13.5±1.5	0.10±0.01
Others($^5I_7$)	5[4]	0.06[4]

Table 1. Values of the upconversion coefficient α_2 and ratios between α_2/α_2'. Values in the Cr-rel row are theoretical expectations from [10].

Also included in Table 1 is the ratio of the upconversion parameter to the cross-relaxation parameter α_2/α_2'. As the $^5I_5$ cross-relaxation rate is much larger than the relaxation rate for the $^5I_7$ manifold the fitting technique used actually measures this ratio. Note how the ratios obtained from measurements on the same manifold are in rough agreement.

Summary

The average $^5I_5$ upconversion parameter has been obtained from simultaneously measured data in two different manners. These two measurement do not agree within their experimental uncertainties. These results indicate that the model used to describe the Tm-Ho system is inadequate. We will discuss the implications of these measurements and possible reasons for these deviations in our presentation.

1 T. Y. Fan, G. Huber, R. L. Byer, and P. Mitzscherlich, IEEE J. Quant. Elect., V24, N6, (1988), P924.
2 G. Armagan, B. M. Walsh, N. P. Barnes, E. A. Modlin, and A. M. Buoncristiani, OSA Proc. of the Adv. Sol. State Laser Conf, V20, ed T.Y. Fan and B.H. Chai, Salt Lake City, (1994), P. 141.
3 D. L. Dexter, J. Chem. Phys., V21, N5, (1953), P836.
4 G. Hansson, A. Callenas, and C. Nelsson, OSA Proc. of the Adv. Sol. State Laser Conf, V16, ed A.A. Pinto and T.Y. Fan, New Orleans, (1993), P446.
5 K. M. Dinndorf, PhD dissertation, Mass. Inst. of Tech., Cambridge, MA (1993).
6 K.M. Dinndorf, M. Tonelli, A. Cassanho, Y. Yamaguchi, and H.P. Jenssen, OSA Proc. of the Adv. Sol. State Laser Conf, V16, ed A.A. Pinto and T.Y. Fan, New Orleans, (1993), P202.
7 A. Brenier, J. Rubin, R. Moncorge and C. Pedrini, J. Phys. France, V50, (1989), P1463.
8 G. Armagan, A. M. Buoncristiani, A. T. Inge, and B. DiBartolo, OSA Proc. on Adv. Sol. State Lasers, V10, Ed. G. Dube and L. Chase, Hilton Head, (1991), P222.
9 K.M. Dinndorf and H.P. Jenssen, OSA Proc. of the Adv. Sol. State Laser Conf, V20, ed T.Y. Fan and B.H. Chai, Salt Lake City, (1994), P. 131.
10 K.M. Dinndorf and H.P. Jenssen, "Relation-ships between upconversion and cross-relaxation parameters.," CLEO, Anaheim, (1994).

Crystal Growth and Luminescence properties of Er^{3+} doped YVO_4 single crystals.

F.S. Ermeneux[¤], R. Moncorge[¤], P. Kabro[*], J.A. Capobianco[*†], M. Bettinelli[§], E. Cavalli[◊]

* Department of Chemistry and Biochemistry, Concordia University
1455 de Maisonneuve Boluevard West, Montreal, Quebec, Canada, H3G 1M8
¤ Université de Lyon I, URA 442 CNRS, 6922 Villeurbanne, France
§ Università Degli Studi Di Verona, Ca' Vignal, Strada Le Grazie, 37134 Verona, Italy
◊ Dipartimento di Chimica Generale ed Inorganica, Chimica Analitica, Chimica Fisica
Universita' di Parma, Italy.
† To whom correspondance should be addressed.

Yttrium vanadate single crystals doped with Er^{3+} ions were grown using the flux method. This method is based on the same techniques used for the synthesis and growth of rare-earth orthophosphate (RPO_4) and orthoarsenate ($RAsO_4$) single crystals from molten salt solutions[1,2]. The procedure in both cases involves dissolution of a rare earth oxide in melted lead pyrophosphate ($Pb_2P_2O_7$) or lead pyroarsenate ($Pb_2As_2O_7$) at high temperature, with spontaneous nucleation and crystal growth of RPO_4 and $RAsO_4$ respectively, achieved by slow cooling of the solution.

The $Pb_2V_2O_7$ flux is a satisfactory solvent for growing the vanadate crystals, because of its ease of preparation and extremely low vapor pressure. The crystals grew in the form of long clear pink rods about 7.5 mm x 2 mm x 2 mm or clear pink plates of dimensions 5 mm x 3 mm x 1 mm.

Oxide crystals doped with rare earth ions have received an increasing amount of attention due to their wide range of novel optoelectronic applications. Interest in the Er^{3+} ion has been heightened since many Er^{3+} doped crystals show upconversion and can be efficiently pumped with laser diodes. The YVO_4 single crystals, doped with Er^{3+} ions, are suitable for laser pumping with argon and krypton ions lasers around 500 and 650 nm as well as Ti:Sapphire and diode lasers around 800 nm and 1.48 μm. Crystals codoped with Yb^{3+}, Er^{3+} ions, can also be pumped with diodes around 980 nm. In this paper a systematic spectroscopic investigation of Er^{3+} in YVO_4 is presented.

Polarized absorption and emission spectra were recorded to determine the Stark components of the ground state and of the excited states of Er^{3+} in the vanadate crystal. Fluoresecence lifetimes and emissions spectra in the visible and in the infrared regions were also registered at room temperature, 77K and 6K for the crystals doped with 0.1, 1, 2.5 and 10% Er^{3+}.

A phenomenological approach using the Judd-Ofelt formalism[3,4] can be used to evaluate the radiative transition probabilities. Negligible J mixing and equal population of all the Stark components of each multiplet are assumed. The calculations are based on measured absorption line strengths at room temperature. For an electric dipole transition, the matrix elements $U^{(t)}$ for a given trivalent rare-earth ion vary slightly from host to host and may be considered unchanged[5,6].The host dependent part of the line strengths is contained in the Judd-Ofelt intensity parameters Ω_t (t=2,4, and 6).

The average refractive index of 2.02[7] for YVO_4, over the σ and π polarizations, was used . The measured electric dipole line strengths were used to calculate the Judd-Ofelt parameters (Ω_t) (Table 1).

Table 1: Calculated Judd-Ofelt intensity parameters Ω_t

	Ω_2 ($10^{-19}cm^2$)	Ω_4 ($10^{-20}cm^2$)	Ω_6 ($10^{-20}cm^2$)
YVO_4: Er^{3+}	1.055	1.83	1.233

From the above Ω_t parameters the radiative transition probabilities were calculated.

Table 2 lists these results in addition to the branching ratio β of each transition as well as the total radiative lifetime τ_R of the various excited levels .

Table 2: Calculated radiative transition probabilities (A_{ed}, A_{md}) and branching ratios β for Er^{3+}:YVO_4

Transition	λ (nm)	A_{ed} (s^{-1})	A_{md} (s^{-1})	τ_R (ms)	β
$^4I_{13/2} \rightarrow {}^4I_{15/2}$	6553	263.8	82.4	2.88	1
$^4I_{11/2} \rightarrow {}^4I_{15/2}$	10121	403.8	0	2.14	0.87
$\rightarrow {}^4I_{13/2}$	3568	45.6	16.5		0.13
$^4I_{9/2} \rightarrow {}^4I_{15/2}$	12453	347	0	2.16	0.75
$\rightarrow {}^4I_{13/2}$	5900	110.3	0		0.24
$\rightarrow {}^4I_{11/2}$	2331	2.55	2.88		.01
$^4F_{9/2} \rightarrow {}^4I_{15/2}$	15197	3326	0	0.27	0.89
$\rightarrow {}^4I_{13/2}$	8644.5	193			0.05
$\rightarrow {}^4I_{11/2}$	5076.1	183.3			0.05
$^4S_{3/2} \rightarrow {}^4I_{15/2}$	18315	2529.6	0	0.26	0.67
$\rightarrow {}^4I_{13/2}$	117618	1029.5			0.27
$\rightarrow {}^4I_{11/2}$	8193.5	85.6			0.02
$\rightarrow {}^4I_{9/2}$	5861.7	138			0.03
$^2H_{11/2} \rightarrow {}^4I_{15/2}$	19084	29289	0	0.033	0.96
$\rightarrow {}^4I_{13/2}$	12531	16.8			0.01
$^4F_{7/2} \rightarrow {}^4I_{15/2}$	20367	6602.4	0	0.11	0.75
$\rightarrow {}^4I_{13/2}$	13813	1228.4			0.14
$\rightarrow {}^4I_{11/2}$	10245	572.7			0.06
$\rightarrow {}^4I_{9/2}$	7913.3	323.3			0.03
$^4F_{5/2} \rightarrow {}^4I_{15/2}$	22124	2967.2	0	0.15	0.44
$\rightarrow {}^4I_{13/2}$	15571	2832.5			0.42
$\rightarrow {}^4I_{11/2}$	12004	317.5			0.05
$\rightarrow {}^4I_{9/2}$	9670.6	326.5			0.05
$\rightarrow {}^4F_{9/2}$	6926.3	287.5			0.04
$^4F_{3/2} \rightarrow {}^4I_{15/2}$	24752	3522.1	0	0.11	0.38
$\rightarrow {}^4I_{13/2}$	18199	387			0.04
$\rightarrow {}^4I_{11/2}$	14631	3585.5			0.39
$\rightarrow {}^4I_{9/2}$	12299	1382.3			0.15
$\rightarrow {}^4F_{9/2}$	9554.9	104.7			0.01
$\rightarrow {}^4S_{3/2}$	6437	112.3			0.01
$^2H_{9/2} \rightarrow {}^4I_{15/2}$	24752	2815	0	0.11	0.31
$\rightarrow {}^4I_{13/2}$	18199	4529.5			0.50
$\rightarrow {}^4I_{11/2}$	14631	1257.6			0.14
$\rightarrow {}^4I_{9/2}$	12299	180.5			0.02
$\rightarrow {}^4F_{9/2}$	9554.9	96.7			0.01

The fluorescence lifetimes of the different energy levels were measured by exciting each of these levels directly. The results obtained for a 0.1% Er^{3+} crystal are given in table 3.

Table 3: Fluorescence lifetimes of the different levels in 0.1% Er^{3+} doped YVO_4.

Level	Lifetime
$^4S_{3/2}$	~ 10 µS
$^4F_{9/2}$	≤ 0.5 µS
$^4I_{9/2}$	≤ 0.5 µS
$^4I_{11/2}$	27 µS
$^4I_{13/2}$	~ 2.5 mS

The measured fluorescence lifetimes of the $^4I_{13/2}$ and $^4I_{11/2}$ were found to be about 2.5 ms and 27 µs respectively. The lifetime of the $^4I_{11/2}$ manifold is comparable to the value obtained for Er^{3+} in Y_2SiO_5[8]. This fast decay is due to an efficient multiphonon relaxation process. Thus the relaxation from the $^4I_{11/2}$ state is very effective in feeding the $^4I_{13/2}$ state. Excitation of the $^4I_{11/2}$ state of Er^{3+} via the $^4F_{5/2}$ state of Yb in the co-doped system(Yb,Er)

may be used to efficiently populate the $^4I_{13/2}$ state. The dynamics of the excitation of the codoped YVO_4 (Yb, Er) has been also studied in crystals doped with 1%, 3%, and 5% Yb^{3+} and 0.1% Er^{3+}.

A comparison of the experimental fluorescence lifetimes and the calculated radiative transition rates of all the excited states, led us to conclude that the non-radiative multiphonon relaxations dominate the deexcitation mechanisms. Other factors such as up-conversion energy transfer and cross-relaxation cannot be neglected depending upon dopant concentrations. Strong reabsorption (radiative energy transfer) could affect the fluorescence decay measurements of the transitions $^4I_{11/2}$, $^4I_{13/2} \rightarrow {}^4I_{15/2}$.

Other points such as fluorescence pathways excited state absorption, up-conversion energy transfer and cross relaxation will be described more extensively at the conference.

Acknowledgments

The authors would like to acknowledge the Natural Science and Engineering Research Council of Canada (J.A.C), and the Fonds pour la Formations de chercheurs et l'Aide a la Recherche (P.K.) for their financial support. Thanks are expressed to the Thomson Soceity for its interest in this work and financial support of one of us (F.S.E.).

References

(1) P. Sueptitz and J. Teltow "Transport of Matter in Simple Ionic Crystals (Cubic Halides)", Phys. Status Solidi 23 (1), 9-56 (1967).
(2) R. W. Dreyfus and A. S. Nowick "Ionic Conductivity of Doped NaCl Crystals", Phys. Rev. 126 (4), 1367-77 (1962).
(3)B. R. Judd, Phys. Rev. 127, 750 (1962).
(4) G. S. Ofelt, J. Chem. Phys. 37, 511 (1962).
(5) W. T. Carnall, P.R. Fields, K. Rajnale, "Electronic energy levels in the trivalent lanthanide aquo ions. I. Pr^{3+}, Nd^{3+}, Pm^{3+}, Dy^{3+}, Ho^{3+}, Er^{3+}, Tm^{3+}" J. Chem. Phys. 49 4424-4442 (1968).
(6) M. J. Weber, Phys. Rev. 157, 262 (1967).
(7) McKnight, H. G. and L. R. Rothrock, 1973, U. S. Army ECOM Technical Report ECOM 0022F (NTIS # 761 094).
(8) C. Li, C. Wyon, R. Moncorgé, IEEE, Quantum Electronics, 28, (4) 1209 (1992).

ESA-measurements of Cr^{4+} doped crystals with wurtzite-like structure

S. Hartung, S. Kück, K. Petermann, and G. Huber
Institut für Laser-Physik, Universität Hamburg
Jungiusstr. 9a, 20355 Hamburg
Phone: ##49-40-4123-5243, Fax: ##49-40-4123-6281

Excited state absorption (ESA) of ions in crystals is of both scientific and practical significance. On the one hand it provides information about the electronic and vibrational properties of the system and on the other hand it is an important loss mechanism for lasers. In case of ESA at the pump or at the lasing wavelength it affects the lasing threshold and the slope efficiency. This paper deals with ESA of Cr^{4+} doped $LiAlO_2$ and $LiGaO_2$, two promising candidates for tunable lasers in the IR spectral range.

Tunable solid state lasers in the IR spectral region are needed for scientific research, atmospheric measurements and optical communication. Until now best laser results were obtained with Cr^{4+} doped forsterite, YAG, and YSO [1 - 4]. The disadvantage is, that strong nonradiative processes yield very low quantum efficiencies and lifetimes shorter than 5µs.

Presently there is significant interest in Cr^{4+} doped $LiAlO_2$ and $LiGaO_2$ [5 - 7] due to its broad band fluorescence between 1 and 1.8µm with maximum at 1290nm and 1250nm, respectively, and due to the high fluorescence lifetime of 29µs for Cr^{4+}:$LiAlO_2$, which is the longest lifetime observed for Cr^{4+} systems.

$LiAlO_2$ and $LiGaO_2$ have a wurtzite-like structure and crystallize in the tetragonal space group $P4_12_12$ and in the orthorhombic space group $Pna2_1$, respectively. The investigated crystals of 0.5%Cr, 0.5%Mg:$LiAlO_2$ and 0.5%Cr:$LiGaO_2$ were grown at our institute by the Czochralski-method under oxidizing conditions.

The experimental setup of the excited state absorption (ESA) measurement is described in [8] in great detail. The measurements were performed with the pump and probe technique, using double lock-in technique in order to improve the signal to noise ratio. The pump beam was a Nd:YAG laser operating at 1064nm and a Titanium-Sapphire laser at 930nm.

It can be shown that the change of the transmitted probe beam intensity $\Delta T/T$ is proportional to the ground state absorption, excited state absorption and stimulated emission cross sections:

$$\frac{\Delta T}{T} = c \cdot (\sigma_{GSA} + \sigma_{EM} - \sigma_{ESA}).$$

In Fig. 1 the ΔT/T spectra together with the ground state absorption spectra of Cr: $LiAlO_2$ and $LiGaO_2$ are shown for the visible spectral region. The positive feature in the ΔT/T spectra corresponds to the bleaching of the ground state absorption from the $^3A_2$ level to the crystal field split components of the $^3T_1(t_2e)$. Calibration of the ΔT/T spectra with this bleaching signal reveals two ESA bands around 650nm and 800nm indicated with small arrows. These bands belong to the ESA transition from the $^3T_2(t_2e)$ to the crystal field split components of the $^3T_1(t_2^2)$. Since these states have different electron configurations, the ESA bands are expected to be broad. This is experimentally observed.

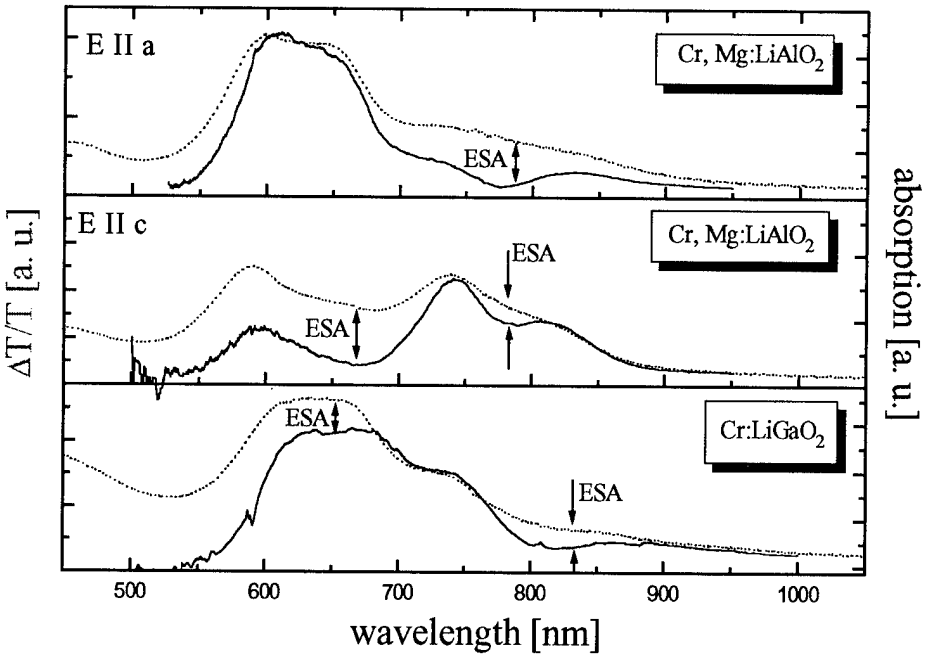

Fig. 1: ΔT/T (solid line) and absorption spectra (dotted line) of Cr:$LiAlO_2$ and Cr:LiGaO2 at room temperature

The ΔT/T spectra from 500nm to 2.2μm are depicted in Fig. 2. In both crystal systems a broad ESA-band covering the whole IR is revealed. This band is attributed to the $^3T_2(t_2e) \rightarrow {}^3T_1(t_2e)$ transition. Since both states derive from the same t_2e configuration this transition is expected to be narrow. This discrepancy between theory and experiment may be due to a Jahn-Teller effect in the $^3T_2$ and $^3T_1$ states.

By comparison of the fluorescence and the ΔT/T spectra laser action may occur in $LiAlO_2$ only at the short wavelength tail in E II a polarization at most up to 1130nm and in E II c polarization up to 1220nm. In comparison in $LiGaO_2$ laser action will occur up to 1150nm.

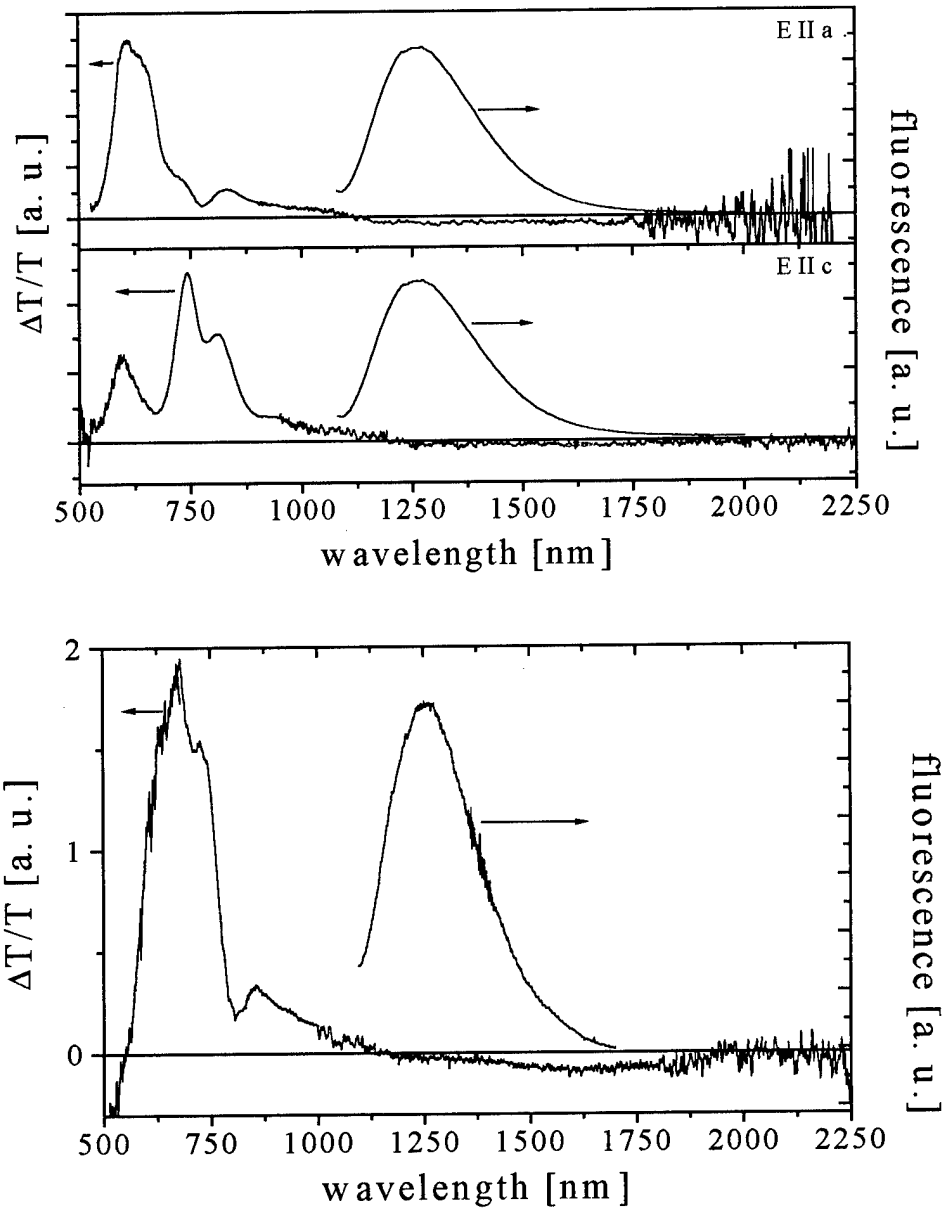

Fig. 2: Polarized ΔT/T spectra and fluorescence of Cr, Mg: $LiAlO_2$ (top) and ΔT/T spectrum and fluorescence of Cr:$LiGaO_2$ (bottom)

References:

1Petricevic, V., S. K. Gayen, and R. R. Alfano, Appl. Phys. Lett 53 (26), 2590 (1988)

2Verdun, H. R., L. M. Thomas, D. M. Andrauskas, T. McCollum, and A. Pinto, Appl. Phys. Lett 53 (26), 2593 (1988)

3Shkadarevich, A. P., OSA Proceedings on Tunable Solid State Lasers, M. L. Shand and M. P. Jenssen eds. (Optical Society of America, North Falmouth 1989), Vol. 5, pp. 60-65

4Koetke, J., S. Kück, K. Petermann, G. Huber, G. Cerullo, M. Danailov, V. Magni, L. F. Qian, and O. Svelto, Opt. Comm. 101, 195 (1993)

5Kück, S., S. Hartung, K. Petermann, and G. Huber, Advanced Solid State Lasers, OSA Technical Digest TuC8-1, 177 (1995)

6Kück, S., S. Hartung, K. Petermann, and G. Huber, Appl. Phys. B 61, 33 (1995)

7Chai, B. H. T., and X. X. Zhang, Advanced Solid State Lasers, OSA Technical Digest WE2-1, 289 (1995)

8Koetke, J., Ph.D. Thesis, Universität Hamburg (1995)

Effects of Radiation Trapping on Measured Excited-State Lifetimes

Markus P. Hehlen
Chemical Science and Technology Division, Los Alamos National Laboratory, Mailstop E535, Los Alamos, NM 87545.

Excited-state lifetimes are one key factor determining the performance of a solid state laser material. It is well known that the measured excited-state lifetime may be severely affected by reabsorption processes in the material. After the initial emission occurred within the sample each subsequent reabsorption event acts as a time "reset" on the relaxation of this excitation and, after a series of reabsorption/reemission processes, the result is an overall lengthening of the observed excited-state decay. Overestimates of intrinsic excited-state lifetimes and subsequent errors in derived quantities such as stimulated emission cross sections, threshold powers, or slope efficiencies are particularly pronounced for states with a unity branching ratio such as $^2F_{5/2}$ of Yb^{3+} or $^4I_{13/2}$ of Er^{3+}. In these cases, the radiative relaxation of the excited-state population can only take place by a transition to the ground state, and due to the high thermal population of the latter this relaxation pathway may be subject to considerable reabsorption. At room temperature, a regime of particular importance to solid-state laser design, the effects of radiation trapping on the measured excited-state lifetimes should be considered. One of the factors determining the probability of a reabsorption/reemission event is the average distance d the emitted light has to travel in the sample. The size of the sample, the spatial emission distribution, and the sample refractive index n_S all contribute to d. Shurcliff et al. have shown that by successive total internal reflections (TIR) at the sample/air interface a considerable fraction of the light generated within an ideal sample of high symmetry can be trapped.[1] Radiation trapping is very pronounced for high refractive index materials such as inorganic insulating crystals since the critical angle for TIR decreases with increasing n_S. In a real crystal however, even light emitted in a direction subject to indefinite TIR will eventually be scattered or reabsorbed/reemitted in a new direction and leave the sample. As a result, excessive TIR strongly increases d and subsequently enhances reabsorption effects.

Recently, Sumida et al. investigated the effects of radiation trapping on the measured excited-state lifetime in YAG:Yb^{3+}.[2] Motivated by the wide spread of values published for the $^2F_{5/2}$ lifetime of Yb^{3+} (Table 1) they proposed a refractive-index-matched experimental arrangement in an attempt to eliminate radiation trapping. A thin YAG:Yb^{3+} sample was optically contacted between two larger undoped YAG crystals forming a sandwich structure. The elimination of TIR at the YAG:Yb^{3+}/YAG interface allowed emitted light to pass into the undoped crystals, and axial luminescence was subsequently imaged onto the detector. Using this experimental geometry, Sumida et al. measured a $^2F_{5/2}$ room-temperature lifetime of 951±15 μs for YAG:1%Yb^{3+}, significantly improving over previously reported values. There remain, however, two unsolved problems with this experimental arrangement. First, although the low measured lifetime value suggests efficient suppression of TIR, there is, in principle, still the possibility for radiation trapping in the highly symmetric sandwich structure.[1] Hence it is uncertain if the measured 951 μs lifetime indeed corresponds to the intrinsic single-ion lifetime, or if it is still artificially lengthened by reabsorption processes. Second, the proposed geometry requires a doped and two undoped crystals, an approach which is therefore not universally convenient.

To completely eliminate reabsorption one would require an indefinitely small sample spherically surrounded by transparent material of identical refractive index. In this ideal case, emission would occur in the center of a sphere, pass into the index-matched material, and consequently encounter the sphere/air (n/n_0) interface at normal incidence. There still occurs internal Fresnel reflection at this interface, however it is not possible to trap light by TIR in this point-source arrangement. When realizing this geometry with a real sample, *e.g.* a cube with refractive index n_s and dimension a^3, the radius r of the sphere has to be greater than $an_s/2n_0$ in order to avoid TIR at the sphere/air interface. Based on this condition, a glass sphere has been fabricated which contains a stage to position samples in the center and planar windows for optical excitation and detection (Figure 1). Both the sample and the refractive-index-matching liquid were inserted through the top port which can be sealed to avoid evaporation of liquid. The performance of this index-matched sphere was studied by means of room temperature lifetime measurements in YAG:1%Yb^{3+}. A single crystal of dimensions $(2.8)^3$ mm^3 and optically polished on all faces was centered in the index-matched sphere and excited (~500 μJ/pulse at 968 nm) by grazing the focused laser beam along the front surface of the sample, thus minimizing the distance d the light has to travel through the sample. The excited area was imaged onto the detection system. The high refractive index of YAG of ~1.82 (Ref. 5) prevented a perfect index match of the crystal, due to the very high toxicity of the arsenic-containing index-matching liquids of refractive index above 1.8. Radiation trapping exhibits a threshold behavior in the sense that a minimum difference between the sample and surrounding medium refractive indices is required for indefinite TIR to occur.[1] For YAG, in particular, it can be shown that radiation trapping is not possible if $(n_s - n) \leq 0.18$. For this reason, a low-toxic chemically stable index-matching liquid (Cargille Laboratories) of n=1.640 was used in the experiments. Figure 2 shows two transients recorded in this experimental geometry along with their single-exponential fits. Without index-matching liquid a $^2F_{5/2}$ lifetime of 1242±0.7 μs is observed. By subsequently immersing the crystal in n=1.640 index-matching liquid the observed lifetime drops by almost 25%, and a value of 948.9±0.6 μs is measured. Table 1 compares these values with results reported earlier in the literature.

Table 1: Compilation of $^2F_{5/2}$ lifetimes of YAG:Yb^{3+} (300 K) reported in the literature. All non index-matched experiments overestimate the lifetime by at least 14%.

Reference	τ [μs]	Type of refractive-index matching
G.A. Bogomolova et al.[4]	1300	unmatched
This work	1242	unmatched
P. Lacovara et al.[6]	1160	unmatched
L.D. DeLoach et al.[3]	1080	unmatched
D.S. Sumida et al.[2]	951	YAG/YAG:Yb^{3+}/YAG sandwich
This work	948.9	n=1.640 index-matched sphere

It is evident that all unmatched experiments overestimate the $^2F_{5/2}$ lifetime by at least 14%, in one case by 37%. This wide spread of experimental lifetimes reflects the strong dependence of reabsorption on spatial factors such as sample size and excitation geometry. The lifetime measured in the index-matched sphere only very slightly improves over the one obtained from the YAG sandwich structure (Ref. 2), hence confirming the results reported by Sumida et al. The value of 948.9±0.6 μs is most likely only slightly contaminated with reabsorption arising from

the non-perfect index match (n_s≈1.82 vs. n=1.64) and the finite sample size, and it is expected to be very close to the intrinsic single-ion lifetime.

In conclusion, efficient elimination of reabsorption effects in YAG:Yb^{3+} was achieved by applying a refractive-index matched sphere, yielding the lowest $^2F_{5/2}$ lifetime value reported so far. A drop of 25% in the measured lifetime was observed upon index matching the crystal. This, along with lifetime values from other non-index-matched experiments, suggests that many lifetimes reported in the literature for a variety of materials might be significantly overestimated. This is particularly true for excited states with a strong transition to the ground-state multiplet. In contrast to other index-matched arrangements, the index-matched sphere presented here is easily realizable and offers the flexibility for convenient application to a wide variety of materials and experiments.

1 W.A. Shurcliff and R.C. Jones, J. Opt. Soc. Am. **39**, 912 (1949).
2 D.S. Sumida and T.Y. Fan, Opt. Lett. **19**, 1343 (1994).
3 L.D. DeLoach, S.A. Payne, L.L. Chase, L.K. Smith, W.L. Kway, and W.F. Krupke, IEEE J. Quantum Electron. **29**, 1179 (1993).
4 G.A. Bogomolova, D.N. Vylegzhanin, and A.A. Kaminskii, Sov. Phys. JETP **42**, 440 (1976).
5 A.A. Kaminskii, *Laser Crystals*, Springer, Berlin, 1990.
6 P. Lacovara, H.K. Choi, C.A. Wang, R.L. Aggarwal, and T.Y. Fan, Opt. Lett. **16**, 1089 (1991).

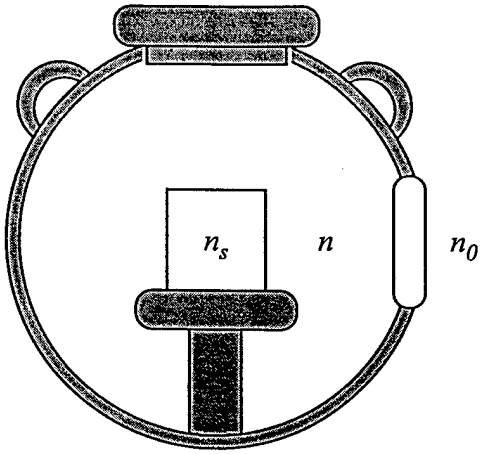

Figure 1: Design of the refractive-index matched (n_s=n) glass sphere (r=18 mm) used in the experiments. The crystal, immersed in refractive-index liquid, is centered on a stage and optically accessible through planar windows. As described in the text a minimum sphere radius of $an_s/2n_0$ is required.

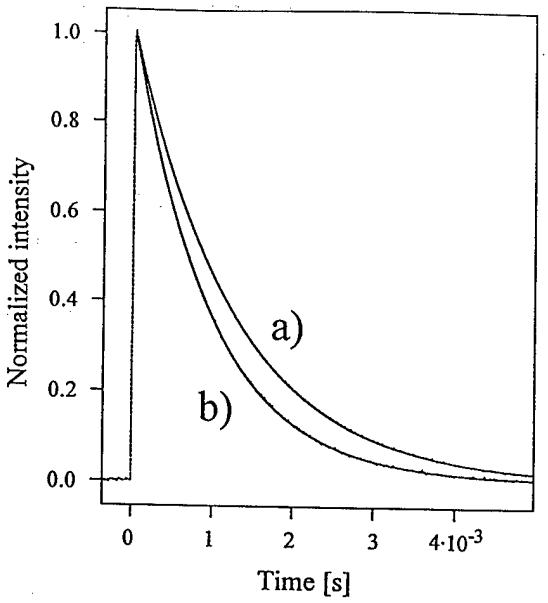

Figure 2: $^2F_{5/2} \rightarrow {}^2F_{7/2}$ relaxation in YAG:1%Yb^{3+} at room temperature (dashed) and respective fits to a single exponential (solid). The measured lifetimes were a) 1242±0.7 µs from an unmatched setup, and b) 948.9±0.6 µs from the (n=1.640) index-matched sphere.

Far-Infrared Spectra of Ultrahigh Purity III-V and II-VI Nonlinear Crystals

Gregory S. Herman
University of Arizona
Science Applications International Corporation
NASA-LaRC M/S 468, Hampton, VA 23681
Tel. (804) 864-8616
FAX (804) 864-8828

Gianluigi Bertelli
Old Dominion University
Science Applications International Corporation
NASA-LaRC M/S 468, Hampton, VA 23681
Tel. (804) 864-8772
FAX (804) 864-8828

Derrick Whitehurst
Norfolk State University
NASA-LaRC M/S 468, Hampton, VA 23681
Tel. (804) 864-7571
FAX (804) 864-8828

Sudhir Trivedi
Brimrose Corporation of America
7720 Bel Air Road, Baltimore, MD 21236
Tel. (410)668-5800
FAX (410)668-4835

Atmospheric scientists, radio astronomers and communications engineers all are in need of heterodyne receiver technology in the frequency range 1 - 30 TeraHertz (300 to 10 micrometers). To develop the local oscillator of the receiver, the traditional microelectronics approach uses upconversion techniques employing Gunn oscillators, electronic multipliers and varactors. Difference frequency generation (DFG) of frequency-stabilized, diode-pumped, solid-state lasers in nonlinear optical mixing devices has been proposed as an alternative technical approach to develop the local oscillator. For such an all-optical scheme, proposed nonlinear optical mixing devices include fast metal-semiconductor-metal (MSM) photoconductors, multiple quantum wells (MQWs) and bulk nonlinear crystals. Of these potential devices, only the latter has the potential to handle the large incident pump intensities needed to efficiently generate the Far-Infrared (FIR) radiation. In this investigation, the FIR transmission spectra of many bulk nonlinear optical crystals were measured to determine which crystals were suitable candidates for frequency conversion to the FIR. FIR transmission spectra were measured for GaP, GaAs, CdTe, ZnTe, CdMnTe, BBO, LBO, KTP, $LiNbO_3$ and $LiIO_3$.

It is shown that ultrahigh purity III-V and II-VI nonlinear crystals are the best candidate crystals for the generation of Far-Infrared (FIR) radiation via difference frequency generation (DFG) from the Near-Infrared (NIR) or Mid-Infrared (MIR). FIR transmission spectra were measured with a Fourier Transform Spectrometer that can operate from the ultraviolet to the FIR.

In general, it is shown that for FIR wavelengths greater than 100 micrometers, ultrahigh purity III-V 43m crystals such as GaP and GaAs may be useful for DFG from the Near-Infrared (NIR) or Mid-Infrared (MIR) to the FIR. Because the Restrahlen band for these crystals is in between the pump frequency and the FIR frequency that is to be generated, the coherence length of the interaction is on the order of millimeters due to the jump in the real refractive index across the band. This long coherence length allows a quasi-phasematched crystal to be fabricated mechanically via optical bonding the first-order length pieces together. For FIR wavelengths from 10 to 50 micrometers, II-VI 43m crystals such as CdTe, ZnTe, and CdMnTe may be useful for frequency conversion from the NIR or MIR to the FIR. However, in these crystals the coherence length of the interaction is much shorter because all of the frequencies of the interaction are in the same transmission window. To produce a first-order quasi-phasematched device, modulating the nonlinear coefficient by controlled twinning along the 111 plane during growth is a possible technique that may be more effective than optical bonding.

In all crystals, the FIR transmittance is highly dependent on the conductivity of the samples as free carrier absorption will deleteriously affect FIR transmission. Corroborating measurements include FIR (CO_2-pumped methanol) laser transmittance, sample conductivity, and the temperature dependance of the NIR transmission up to extremely high temperatures.

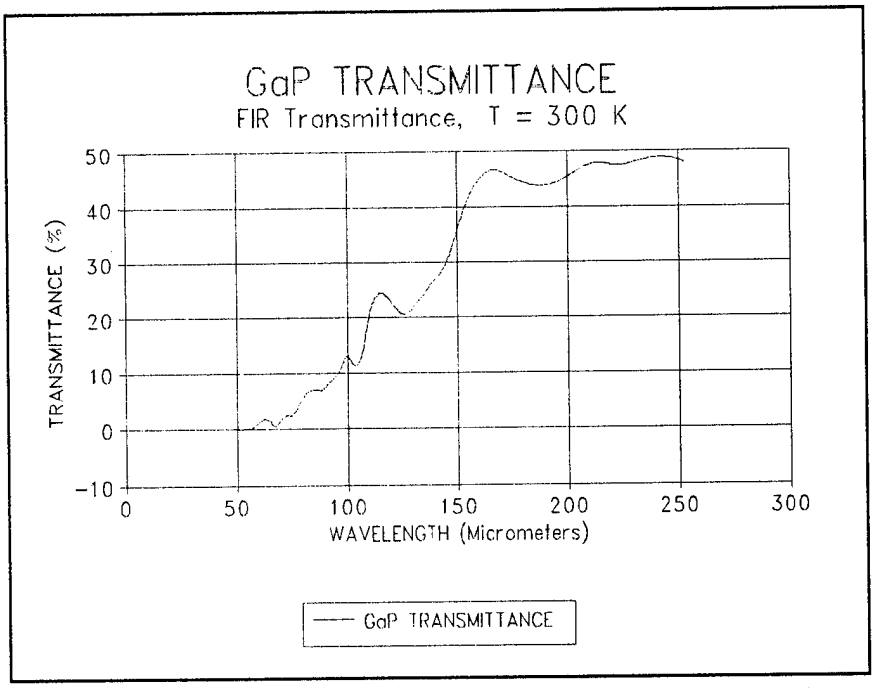

Figure 1. FIR Transmittance of GaP, length = 4.0 mm, n ~ 3.35

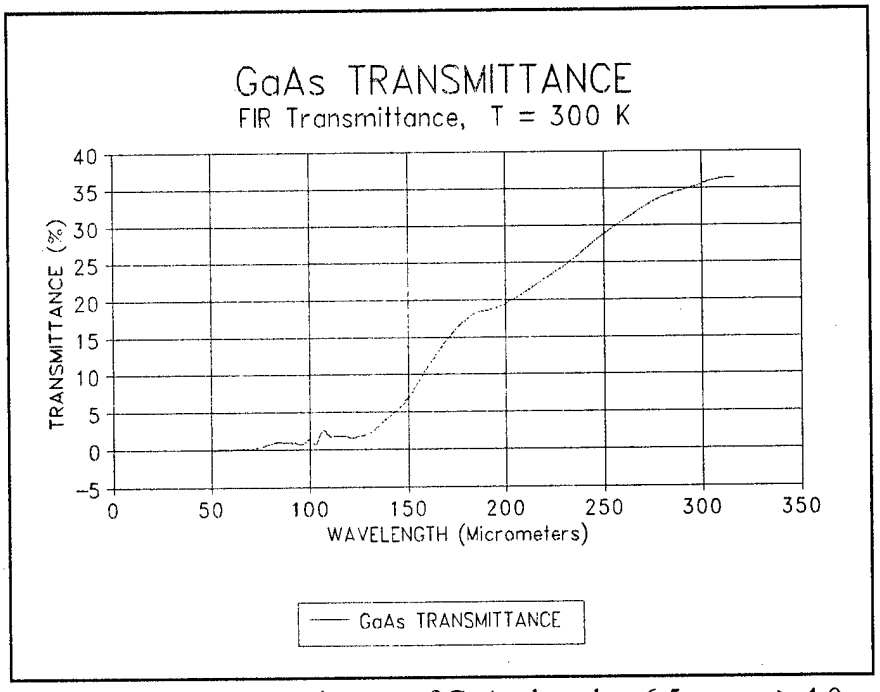

Figures 2. FIR Transmittance of GaAs, length = 6.5 mm, n > 4.0

Time-Resolved Excited-State Absorption Measurements in Cr^{4+}-Doped Mg_2SiO_4 and Y_2SiO_5 Laser Materials

N.V. Kuleshov, V.G. Shcherbitsky, V.P. Mikhailov
International Laser Center, Kurchatov str. 7, Minsk 220064, Belarus
Tel/Fax: (0172)-785-726, e-mail: user1@mikhai.bsu.minsk.by

S. Kuck, K. Petermann, G. Huber
Institut fur Laser-Physik, Universitat Hamburg, Jungiusstr. 11, 20355 Hamburg, Germany
Phone: +49-40-4123-5256, Fax: +49-40-4123-6281

Recently, saturation of Cr^{4+}-absorption was investigated in the 800-900 nm region in Y_2SiO_5 and $Ca_2Al_2SiO_7$ [1] and at 694 nm wavelength of ruby laser in Mg_2SiO_4, Y_2SiO_5 and Gd_2SiO_5 [2]. Cr^{4+}-doped silicates were shown to be promising solid state saturable absorber Q-switches for ruby and Cr-LiSAF lasers. Q-switched laser pulses as short as 80 ns with energy up to 250 mJ were obtained from ruby laser using Cr^{4+}:Mg_2SiO_4 as a saturable absorber [2]. Residual absorption observed in Cr^{4+}-doped silicates was attributed to an excited state absorption (ESA). In this paper time-resolved ESA spectra measurements have been performed on Cr^{4+}-doped Mg_2SiO_4 and Y_2SiO_5 in the 200-900 nm spectral range using pump-and-probe technique.

The experimental setup used in these measurements was described in Ref. [3]. The samples were excited by 50 ns pulses from an excimer laser pumped dye laser at 570-600 nm wavelengths. A probe beam of a Xe flash lamp was detected with an optical multichannel analyzer attached to a spectrometer.

Ground state absorption spectrum of Cr^{4+}:forsterite exhibits three strong broad bands in the spectral range of measurements with peaks at 570 nm (Ella), 650 nm (Ellc) and 740 nm (Ellb), which are attributed to the $^3A_2$ - $^3T_1(^3F)$ transition of tetrahedral Cr^{4+}, split due to symmetry distortion [4]. Polarized ESA spectra of the Cr^{4+}:Mg_2SiO_4 for the two delay times between pump and probe beams are shown in Fig 1. The features of these spectra are bleaching bands in the visible and near infrared which are attributed to the saturation of the $^3A_2$ - $^3T_1(^3F)$ ground state absorption, as well as strong pump-induced absorption bands in the UV-violet (200-400 nm), which exhibit strong polarization dependence. From the temporal behavior of the ESA spectra the lifetime of bleaching bands and pump-induced absorption bands was measured to be of about 3 μs, which strongly correlates with the lifetime of the luminescence from the $^3T_2$ level of the Cr^{4+} at

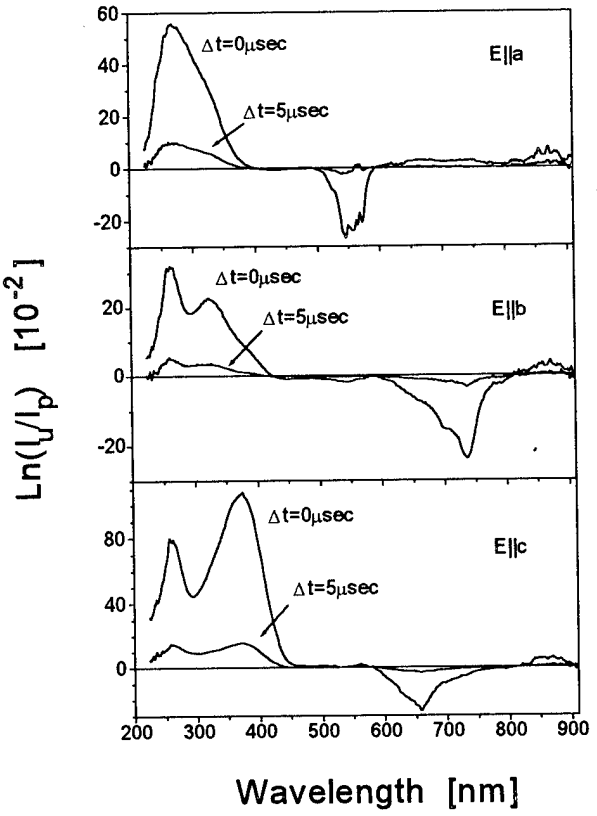

Fig. 1. Time-resolved polarized ESA spectra of Cr^{4+}:Mg_2SiO_4 at room temperature.

at room temperature. Pump-induced absorption was attributed to the ESA from the $^3T_2(^3F)$ storage level of the Cr^{4+}. Peak excited-state absorption cross sections for different polarizations were estimated to be $(2\text{-}5)\times10^{-18}$ cm^2.

Similar behaviour of the ground state absorption saturation and pump-induced absorption was observed in Cr^{4+}:Y_2SiO_5 (Fig.2). Bleaching bands observed in the ESA spectra for all three polarizations and centered at 590 nm and 720 nm are assigned to the saturation of $^3A_2$ - $^3T_1(^3F)$ ground state absorption of tetrahedral Cr^{4+}, which was described in Refs. [5-7], while strong pump-induced absorption in the 200-400 nm range is associated with excited-state absorption from the $^3T_2(^3F)$ level.

In conclusion, strong excited state absorption in Cr^{4+}-doped Mg_2SiO_4 and Y_2SiO_5 is observed in the 200-400 nm region and does not affect the saturable

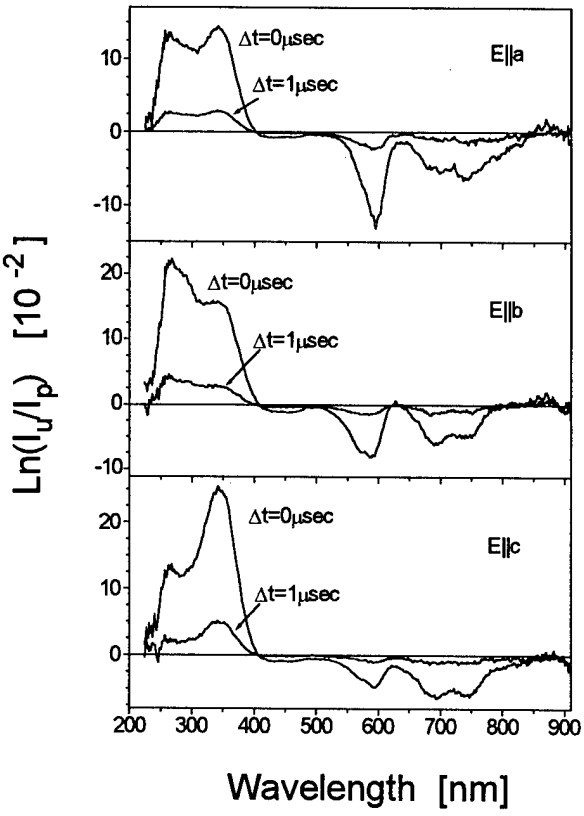

Fig. 2. Excited state absorption spectra of Cr^{4+}:Y_2SiO_5.

absorption of the $^3A_2$ - $^3T_1(^3F)$ transition. These materials can be used as solid state passive Q-switches for lasers with wavelengths from 550 nm to 800 nm.

References

1. E. Munin, A.B. Villaverde, M. Bass and X.X. Zang. Appl. Phys. Letts. **63** (1993) 1739.

2. V.P. Mikhailov, N.I. Zhavoronkov, N.V. Kuleshov et.al. Opt. and Quant. Electron (accepted for publication).

3. T. Danger, A. Bleckmann, G. Huber. Appl. Phys. B. **58** (1994) 413.

4. V. Petricevic, Dissertation , The City University of New-York (1990).

5. C. Deka, M. Bass, B.H.T. Chai, Y. Shimony J. Opt. Soc. Am B. **10** (1993) 1499.

6. U. Hommerich, H. Eilers, S.M. Jacobsen, W.M. Yen, and W. Jia, J. Lumin. **55** (1993) 293.

7. N.V. Kuleshov, V.P. Mikhailov, V.G. Shcherbitsky, B.I. Minkov, T.J. Glynn, R. Sherlock, Opt. Mater. **4** (1995) 488.

Spectroscopic Evaluation of Visible Laser Potential of Several Pr^{3+} and Tm^{3+} Doped Crystals

Larry D. Merkle and Bahram Zandi
IR OPTICS TECHNOLOGY OFC
ARMY RESEARCH LABORATORY
10235 BURBECK RD STE 110
FT BELVOIR VA 22060-5838
phone 703-704-1701
fax 703-704-1752

and Bruce H. T. Chai
University of Central Florida
Center for Research and Education in Optics and Lasers
12424 Research Parkway
Orlando, FL 32836
phone 407-658-3990
fax 407-658-6880

With the appearance of short-wavelength laser diodes, one can consider development of visible solid-state lasers pumped directly in the visible, removing the fragility of flashlamps and the complexities of frequency conversion processes. It would be especially valuable to find diode pumpable materials with long upper state lifetimes to produce Q-switched pulses. We report here recent results in our investigation of candidate materials. We focus particularly on Pr^{3+}, of interest for its strong transitions, and Tm^{3+}, attractive for its long $^1G_4$ lifetime.

We recently reported the spectroscopy and laser action of Pr,Mg:$SrAl_{12}O_{19}$ (Pr,Mg:SAM).[1] Its $^3P_0$ lifetime is about three times that of Pr:$Y_3Al_5O_{12}$ (Pr:YAG), and the short wavelength of its first 4f5d absorption band reduces the danger of excited state absorption (ESA) at pump and emission wavelengths. Since it is also important to obtain good thermal and mechanical properties, we have now investigated the garnets. To determine the best garnet for study, we have used a simple model for estimating the host dependence of the energy separation between the $4f^2$ and 4f5d configurations.[2] Large energy separation as predicted by this model correlates with weak crystal field at the dopant site. Thus, it can help us select hosts that not only minimize ESA problems but also maximize upper state lifetime, by reducing mixing of $4f^2$ with opposite parity states. The calculation requires one parameter not independently known, which we have fixed by fitting the lowest energy 4f5d absorption peak in Pr,Mg:SAM, Pr:YAG and Pr:$Ca_5(PO_4)_3F$ (Pr:FAP), then assuming it to be constant for other hosts.[1] In this way we have estimated the $4f^2$ to 4f5d energy separation for ten oxide garnets. Of the ten, the smallest energy separation was predicted for Pr:YAG and the largest for Pr:$La_3Lu_2Ga_3O_{12}$ (Pr:LLGG). The predicted energy of the lowest 4f5d band in the latter is 43,200 cm^{-1}, substantially larger than the 35,500 cm^{-1} observed in Pr:YAG and not too much less than the 47,000 cm^{-1} in Pr,Mg:SAM.[1]

For this reason, samples of Pr:LLGG have been grown at CREOL by the Czochralski technique. Samples have been grown with nominal Pr concentrations of 0.1 and 1 % atomic, with chemical analysis yielding the actual concentrations given in Table I.

The room temperature absorption of Pr:LLGG is shown in Figure 1. The solid curve represents data taken on a 1 % sample, while the dashed curve shows the ultraviolet absorption divided by five, taken on a 0.1 % sample. Disappointingly, the strong ultraviolet peak is at 35,100 cm^{-1}, about the same as in Pr:YAG. It is not known whether this peak is due in fact to the 4f5d configuration or to charge transfer. The absorption by the $^3P_{0,1,2}$ and $^1I_6$ manifolds is usefully strong with 1 % doping.

The weak crystal field of LLGG results in a longer $^3P_0$ lifetime than in Pr:YAG, as expected. As shown in Table I, the fluorescence decay is single exponential with a

nearly 30 μs lifetime in the 0.1 % sample, and suffers negligible quenching in the 1 % sample. Fluorescence upon excitation into the ^3P_J levels is shown in Figure 2, and is attributable to $^3P_0$ and/or $^1I_6$ emission, except for peaks at 605.8 and 609.6 nm and a few weaker features nearby, all due to $^1D_2 \rightarrow {}^3H_4$. The emission $^3P_0, {}^1I_6 \rightarrow {}^1G_4$ is much weaker, as shown by the branching ratios given in Table II. A 0.1 % sample was used to minimize reabsorption of the $^3P_J \rightarrow {}^3H_4$ emission. Assuming the 0.1 % fluorescence lifetime to be purely radiative, stimulated emission cross sections can be estimated for the strongest peaks. The results are 5.0×10^{-20} cm^2 at 484 nm, 4.3×10^{-20} cm^2 at 487 nm, 1.2×10^{-20} cm^2 at 496 nm, 1.4×10^{-20} cm^2 at 546 nm and 4.0×10^{-20} cm^2 at 620 nm. The last, particularly, should be quite sufficient for laser operation.

Table I. Fluorescence lifetimes of visible-emitting manifolds in several materials. When the decay is not single exponential, the effective lifetime is given (time integral of fluorescence decay, divided by initial fluorescence signal.) Also given is maximum absorption coefficient in the pump band.

Material	Actual Dopant Concentration (cm^{-3})	Initial State	Temperature (K)	Peak Abs. Coeff. (cm^{-1})	Dominant Lifetime (μs)	Effective Lifetime (μs)
Pr:LLGG, 0.1%	1.3×10^{19}	$^3P_0, {}^1I_6$	T ≤ 295		29	single exp
		$^1D_2$	T ≤ 295		210	single exp
Pr:LLGG, 1%	9.8×10^{19}	$^3P_0, {}^1I_6$	295	3.1	27	single exp
		$^1D_2$	295		150	90
Tm:SFAP, 1%	1.8×10^{19}	$^1G_4$	16		340	single exp
			295	0.31	310	280
Tm:FAP, 2.5%	unknown	$^1G_4$	295	2.7	165	80
Tm:$CaYAlO_4$, 1%	1.2×10^{20}	$^1G_4$	295		145	90
Tm:$CaYAlO_4$, 3%	4.1×10^{20}	$^1G_4$	295	1.4	70	25
Tm:CaYSOAP, 1%	1.5×10^{20}	$^1G_4$	16		330	185
			295	0.46	210	110
Tm:CaYSOAP, 6%	9.4×10^{20}	$^1G_4$	295		22	5

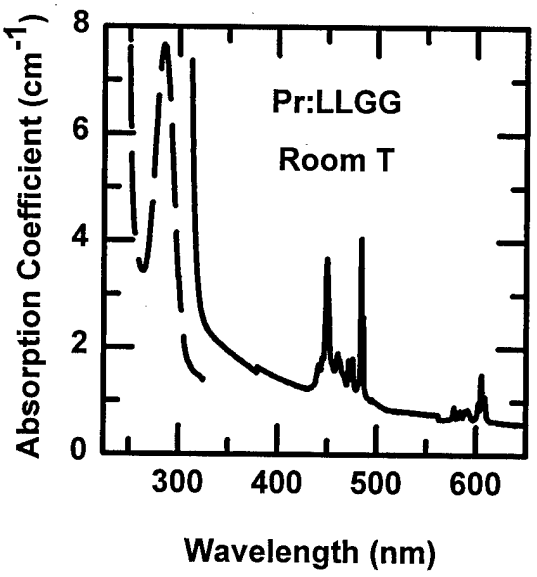

Figure 1. Room temperature absorption of Pr:$La_3Lu_2Ga_3O_{12}$.

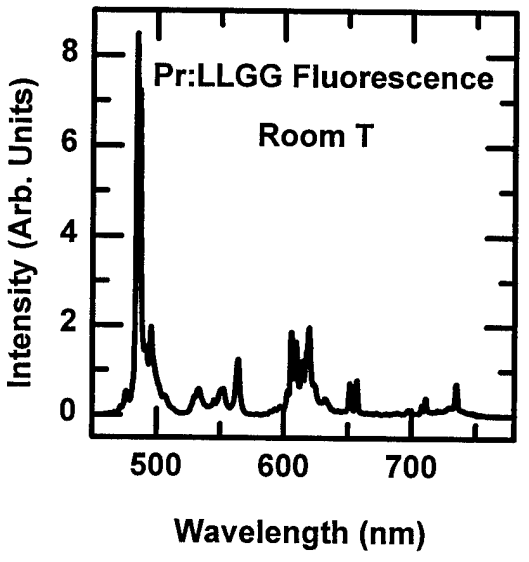

Figure 2. Room temperature $^3P_0, {}^1I_6$ emission of Pr:$La_3Lu_2Ga_3O_{12}$.

The challenge for use of Tm^{3+} as a visibly-pumped visible laser material is to obtain strong enough $^1G_4$ absorption for pumping without concentration quenching. Table I shows that for Tm:$CaYAlO_4$ and Tm:$CaY_4(SiO_4)_3O$ (Tm:CaYSOAP) serious quenching occurs at concentrations sufficient to produce satisfactory pump absorption (at least 1 cm^{-1}, preferrably higher). The long, virtually exponential $^1G_4$ in 1 % Tm:SFAP is

attractive, and its absorption and emission spectra are given in Figures 3 and 4, respectively. In Fig. 3 the dashed curve gives unpolarized data divided by 100. The strongly polarized emission helps to maximize the product of cross section and lifetime, and if the observed 310 μs lifetime is radiative, the stimulated emission cross sections for π polarization are estimated to be 6.1×10^{-21} cm^2 at 482 nm, 3.3×10^{-21} cm^2 at 492 nm and 1.2×10^{-20} cm^2 at 652 nm. These values are small, but not out of line with cross sections employed successfully in 1.5 μm and 2 μm lasers, and may be worth working with to obtain the very long energy storage time of this material.

However, it has proven very difficult to grow more concentrated Tm:SFAP, as needed to obtain sufficient $^1G_4$ absorption. Table I shows that Tm:FAP may be more interesting, particularly if a modest reduction in concentration reduces the quenching. This possibility will be pursued, as will laser experiments. Based on these data, we believe that a visibly-pumped visible laser with usable cross sections and good storage times is indeed possible based on Tm^{3+}.

References

1. L. D. Merkle, B. Zandi, Y. Guyot, R. Moncorgé, H. R. Verdun, B. McIntosh, M. D. Seltzer, C. A. Morrison, B. H. T. Chai, and J. B. Gruber, OSA Proceedings on Advanced Solid-State Laser, Tso Yee Fan and Bruce H. T. Chai, eds. (Optical Society of America, Washington, DC 1994), Vol. 20, pp. 361-366.
2. C. A. Morrison, J. Chem. Phys. 72, 1001-1002 (1980).

Table II. Observed room temperature branching ratios of fluorescence from the Pr:LLGG $^3P_0$,$^1I_6$ and Tm:SFAP $^1G_4$ manifolds.

Pr:LLGG Final Manifold	Average Wavelength (nm)	Branching Ratio	Tm:SFAP Final Manifold	Average Wavelength (nm)	Branching Ratio
$^3H_4$	490	0.49	$^3H_6$	475	0.70
$^3H_5$	550	0.15	$^3F_4$	652	0.11
$^3H_6$	619	0.20	$^3H_5$	780	0.09
$^3F_2$	654	0.03	$^3H_4$	1200	0.09
$^3F_3$+$^3F_4$	727	0.11	$^3F_2$+$^3F_3$	1510	0.01
$^1G_4$	920	0.02			
$^1D_2$	~2500	assumed ~0			

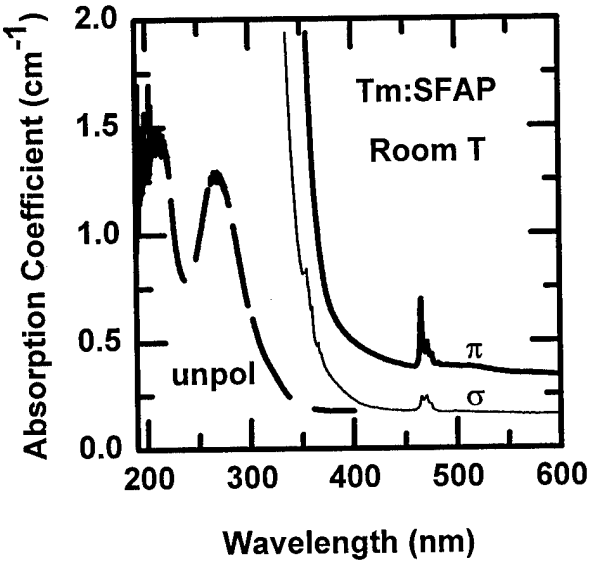

Figure 3. Room temperature absorption of $Tm:Sr_5(PO_4)_3F$.

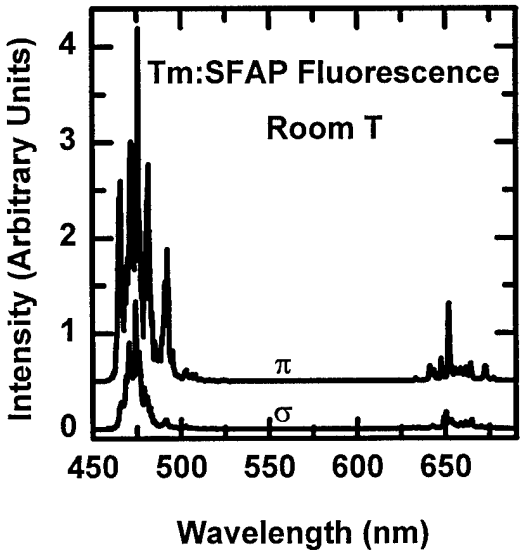

Figure 4. Room temperature $^1G_4$ emission of $Tm:Sr_5(PO_4)_3F$.

Photoconductivity and Electro-Motive Force Study of Rare Earth Doped YSGG Laser Crystals

M. A. Noginov*, N. Kukhtarev**, N. E. Noginova, H. J. Caulfield**,
P. Venkateswarlu*, M. Mahdi

*Center for Nonlinear Optics and Materials
**Center for Applied Optical Studies
Department of Physics, Alabama A&M University, P. O. Box 1268, Normal, Al 35762
e-mail: freenet.scri.fsu.edu, phone: (205) 851-5305

Energy transfer and energy migration are very important processes in the laser crystals. In the majority of experimental situations energy transfer is well described in terms of incoherent Förster-Dexter[1,2] multipolar or exchange interaction. However, in some cases (see for example Refs. [3-6]) the experimentally determined transfer rates are so high that they require difficult to prove assumption of very efficient interaction or alternative models and explanations.

It was recognized that 4f→4f transitions can borrow intensity from 4f→5f transitions or from the ligand 2p (O^{2-}) wavefunctions [7-9]; 4f electrons can exchange energy with ligands *via* empty 5d shells or filled 5p shells [10-12]. In rare earth (RE) doped garnets the overlapping 5d-6s band forms the conduction subband close the bottom of the conduction band [13]; 4f electrons contribute to the conduction 5d-6s subband *via* indirect interaction with ligands [11,12]. According to Ref. [13], photocurrent properties of RE doped garnets are determined by RE ions and their interactions *via* an intermediate link – oxygen ions.

There are two questions arise: 1) whether photocurrent and/or indirect interaction of 4f electrons with ligands can accelerate 4f→4f energy transfer, and 2) whether it is possible to control the efficiency of 4f-4f energy transfer by influencing the carriers concentration, electric field distribution, *etc.* In this paper we present our first experimental results of photocurrent (PC) and electro-motive force (EMF) studies of Cr, Er, Tm, and Ho doped YSGG laser crystals, the observed correlations between photocurrent and excited state concentrations of the particular 4f energy levels, and the theoretical model describing photocarriers motion.

The photoconductivity measurements with silver painted electrodes mounted on the same or opposite faces of the crystal were carried out using the scheme shown in Fig. 1. The scheme for the EMF experiments is shown in Fig. 2. The idea behind non-steady-state photoinduced EMF measurements is as follows [14]: Two mutually coherent beams form in the crystal the grating of photoinduced carriers and 90° shifted distributed electric field grating. If one of the mirrors (# 3, Fig. 2) is moved periodically with a small amplitude and a frequency, ω, greater than the inverse life-time of the distributed electric field grating, $\tau_M=\varepsilon/\sigma$ (σ - average photoconductivity and ε - dielectric constant), and smaller than the inverse life-time of photocurrent carriers, τ,

then the carriers grating will periodically move *versus* electric field grating causing an alternative EMF [14]. The dependence of EMF *versus* frequency, angle between pumping beams, and external bias, contains information on τ_M and τ times, carriers diffusion length, *etc.* [14].

The main features of photoconductivity common for all the crystals studied, *e.g.* Er doped YSGG, are the following:

1) The photoconductivity can be excited with visible or infrared (IR) light. At IR pumping the excitation spectrum of photocurrent in Er doped YSGG was shown to be identical to the absorption spectrum at the transition $^4I_{15/2} \rightarrow {}^4I_{9/2}$.

2) The photoconductivity is linearly proportional to the external bias.

3) The photocurrent is linearly proportional to the pump intensity (in opposite to Refs. [15,16]),

4) The photoconductivity is linearly proportional to the excited state concentration of the mostly populated metastable level ($^4I_{13/2}$). Under pulsed excitation photocurrent kinetics followed $^4I_{13/2}$ luminescence kinetics, showing the same build-up and decay times, Fig. 3.

5) The ratio of photoconductivity to dark conductivity varied from sample to sample, possibly depending on crystal growth conditions.

6) Redistribution of electric charge in the crystal screening the external electric field was found. The recharging of the sample occurred in the seconds-to-minutes time range.

An alternative EMF was found in the set up shown in Fig. 2. This proves the presence of photoinduced electric field grating in the crystal. The dependencies of EMF signal *vs.* frequency, ω, angle, Θ, and external bias, V, are shown in Figs. 4-6 (λ_{pump}=488 nm). The last dependence (Fig. 6) implies the possibility to influence the charge and carriers distribution in the crystal by external force.

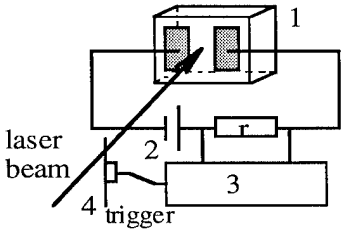

Fig. 1. Photoconductivity set up: 1) crystal, 2) voltage supply, 3) lock in amplifier or oscilloscope, 4) chopper.

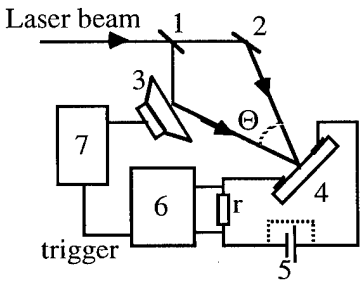

Fig. 2. EMF set up. 1) beamsplitter, 2) mirror, 3) mirror on the speaker, 4) crystal with electrodes, 5) external bias, 6) lock in amplifier, 7) wavefunction generator.

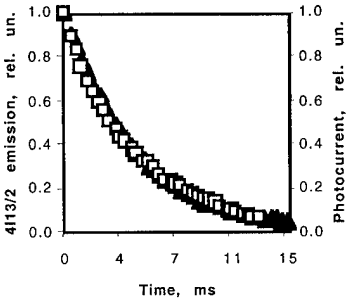

Fig. 3. Decay of $^4I_{13/2}$ emission (triangles) and photocurrent (squares) in Er($4x10^{21}cm^{-3}$) doped YSGG after long-pulse excitation.

Our working model is close to that of Refs. [10-13] and accounts for 2p (O^{2-}) valence band, electronic transitions in 4f shell, 5p shell, 5d+6s conduction subband, trap levels supporting dark current, and conduction band, Fig. 7. We describe the EMF signal under periodically moving light grating excitation with the rate equations for carriers concentration, population of 4f excited levels, equation for the electric field, and equation for

the current density (accounting for diffusion and drift of carriers), close to those conventionally used for description of charge transfer in photorefractive crystals and different in some details from equations used in Ref. [14].

The exact solution for the current caused by EMF was obtained. According to the theory, as $\omega \to 0$, the current (j) is proportional to $\tau_M \omega$; as $\omega \to \infty$, $j \propto (\tau\omega)^{-1}$; and the maximum of the dependence of EMF on speaker frequency corresponds to $\omega_o = (\tau_M \tau)^{-1/2}$. We determined in Er doped YSGG $\tau_M \approx 1.2$ s and $\tau \approx 5$-7 ms (Fig. 4). The last value is close to $^4I_{13/2}$ life-time and carriers life-time determined in the photoconductivity experiment (Fig. 3). The maximum of the dependence of EMF *vs.* grating wave vector, **K**, corresponds to the inverse diffusion length of carriers, L_D^{-1}. We determined in Er doped YSGG $L_D \approx 1$ μm (Fig. 5), which is close to the diffusion length for the $^4I_{13/2}$ excitation migration at $\rho_{Er} = 4 \times 10^{21}$ cm^{-3} [6]. However, at this point we are not sure, whether this coincidence is accidental or not.

The more detailed account of the experimental observations and the model of holographic current in laser crystals will be presented at the conference.

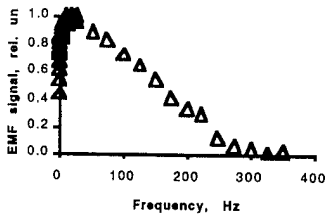

Fig. 4. Frequency dependence of EMF signal in Er(4×10^{21} cm^{-3}) doped YSGG. Θ=0.17

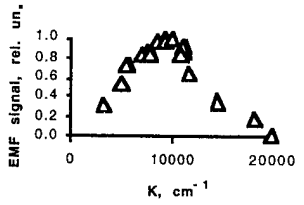

Fig. 5. Dependence of EMF signal in Er(4×10^{21} cm^{-3}) doped YSGG on grating vector, **K**.

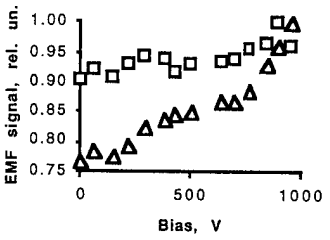

Fig. 6. Dependence of EMF signal in Er(4×10^{21} cm^{-3}) doped YSGG on external voltage, V. Θ=0.17 rad, ω=20 Hz (squares) and ω=70 Hz (triangles).

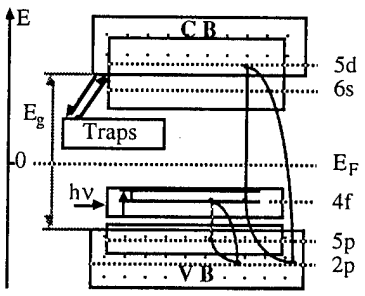

Fig. 7. Band structure and energy transfer in RE doped garnets (according to [12,14] and our measurements). E_g - gap width, E_F - Fermi level, CB - conduction band, VB - valence band.

1) Th. Förster, Ann. Phys, **2**, 55 (1948).
2) D. L. Dexter, J Chem. Phys., **21**, p. 836 (1953).
3) C. M. Lawson, *et al.*, Phys. Rev. B, **26**, p. 4836 (1982).
4) V. A. French, R. C. Powell, Opt. Lett., **16**, p. 666 (1991).
5) F. M. Hashmi, *et al.*, Opt. Materials, 1, p. **281** (1992).
6) M. A. Noginov, *et al.*, OSA Ann. Meeting, 1995, paper # MLL3.
7) B. R. Judd, Phys. Rev., **127**, p. 750 (1962).
8) R. C. Powell, *et al.*, Phys. Rev. B, **41**, p. 8593 (1990)
9) G. Huber, in Current Topics in Materials Science, **4**, p. 1 (1980).
10) M. V. Eremin, *et al.*, Sov. Phys. Solid State, **24**, p. 1049 (1982).
11) A. A. Kaminskii, *et al.*, Sov. Phys. Solid State, **27**, p. 279 (1985).
12) M. V. Eremin, *et al.*, Sov. Phys. Solid State, **27**, p. 339 (1985).
13) A. E. Nosenko *et al.*, J Appl. Spectroscopy, **46**, p. 89 (1987).
14) M. P. Petrov, *et al.*, J. Appl. Phys., **68**, p. 2216 (1990).
15) S. A. Basun *et al.*, *OSA Proceedings on Advanced Solid-State Lasers*, **13**, p. 333 (1992).
16) S. A. Basun *et al.*, *OSA Proceedings on Advanced Solid-State Lasers*, **15**, p. 339 (1993).

Excited-state dynamics in the low-phonon materials Er^{3+}:BaY_2F_8 and $Cs_3Er_2Br_9$

M. Pollnau, W. Lüthy, and H. P. Weber
Institute of Applied Physics, University of Bern,
Sidlerstrasse 5, CH-3012 Bern, Switzerland
Tel. +41-31-631 89 37, Fax +41-31-631 37 65, e-mail pollnau@iap.unibe.ch

K. Krämer and H. U. Güdel
Institute of Inorganic Chemistry, University of Bern,
Freiestrasse 3, CH-3009 Bern, Switzerland

R. A. McFarlane
Hughes Research Laboratories,
3011 Malibu Canyon Road, Malibu, California 90265

The development of compact blue and green emitting crystal lasers pumped by infrared diodes has become interesting for applications in the fields of data storage and display. The BaY_2F_8 and $Cs_3Er_2Br_9$ crystals which are investigated in this paper are candidates as host materials for green laser emission. Phonon energies of 415 cm^{-1} in BaY_2F_8 [1] and 190 cm^{-1} in $Cs_3Er_2Br_9$ [2] lead to a long lifetime of the $^4S_{3/2}$ upper laser level in erbium. The measurement of excited-state absorption (ESA) and fluorescence provides important information on the population dynamics in Er:BaY_2F_8 and $Cs_3Er_2Br_9$. Owing to different size and weight of the ligands the excitation mechanisms, fluorescence properties, ESA and stimulated-emission (SE) dynamics are completely different in the bromide compared to the fluoride material. Systematic changes are discussed.

A pump- and probe-beam technique is used for the measurement of quasi-cw-pumped ESA spectra. The broadband probe light is transmitted through the sample, spectrally analyzed with a monochromator (resolution 0.2 nm), and detected by an optical photodiode. The difference of the transmitted probe-beam intensities I_p and I_u with and without 800-nm excitation of the sample is measured in double-lock-in technique [3]. With dopant concentration n_0, excitation density n_e, sample thickness d, and ground-state-absorption (GSA) cross section σ_{GSA}, the cross section $\sigma_{ESA} - \sigma_{SE}$ originating from level i at wavelength λ is calculated using the equation [4]

$$\Sigma_i [(n_i / n_e) (\sigma_{ESA,\,i} - \sigma_{SE,\,i})] = \ln (I_u / I_p) / (n_e\, d) + \sigma_{GSA}. \qquad (1)$$

The fluorescence spectra are also measured with this arrangement and the same spectral resolution with a normal lock-in technique.

The energy level scheme of erbium, the intrinsic lifetimes of the various metastable levels in the different host materials, the excitation mechanisms under 800-nm radiation, and the investigated transitions are indicated in Fig. 1. Lifetimes were measured in $Er^{3+}(1\%):BaY_2F_8$ [1] and $Er^{3+}(1\%):Cs_3Lu_2Br_9$ [2].

The erbium ions are excited into the $^4I_{9/2}$ level. In BaY_2F_8 multiphonon relaxations populate the $^4I_{11/2}$ and $^4I_{13/2}$ levels. Interionic upconversion and multiphonon relaxations populate the $^4S_{3/2}$ level which leads to emission $^4S_{3/2} \rightarrow {}^4I_{15/2}$ at 550 nm (Fig. 2). In BaY_2F_8 the green emission has a spectral overlap with parasitic ESA $^4I_{13/2} \rightarrow {}^2H_{9/2}$. This ESA may limit green laser operation $^4S_{3/2} \rightarrow {}^4I_{15/2}$ to cryogenic temperatures [5]. The strong ESA $^4I_{11/2} \rightarrow {}^2K_{15/2} + {}^2G_{9/2}$ at 560-570 nm has no overlap with green emission. The originating levels of the different ESA transitions are known from time-resolved ESA measurements in $Er^{3+}:YAlO_3$ [4].

Differences between $Cs_3Er_2Br_9$ and BaY_2F_8 are mainly induced by the larger size and higher atomic weight of the bromide ions compared to the fluoride ions. The larger size widens the lattice and weakens the electric crystal field that is induced at the rare-earth site by the Br^- ligands. Thus the Stark splitting of every level is reduced. The high atomic weight limits the energetic spectrum of the lattice vibrations which results in the almost complete absence of multiphonon transitions even at room temperature. The close proximity of two erbium ions in the $Cs_3Er_2Br_9$ lattice [2], the high erbium concentration of 3.8×10^{21} cm^{-3}, and the long lifetimes of otherwise multiphonon-quenched levels lead to the occurrence of ion-ion interactions that are not observed in BaY_2F_8. The population mechanisms are, therefore, dominated by fluorescence decay as well as specific interionic upconversion and cross-relaxation processes.

In $Cs_3Er_2Br_9$ pumping the $^4I_{9/2}$ level does not lead to the population of the $^4I_{11/2}$ level via multiphonon relaxation. Instead, a considerable population is created in the pump level itself which is then subject to interionic energy transfer (Fig. 1). Cross-relaxation and upconversion processes populate the $^4I_{13/2}$ level. Upconversion processes populate the $^4S_{3/2}$ and $^2H_{9/2}$ levels.

The reabsorption of fluorescence $^4S_{3/2} \rightarrow {}^4I_{15/2}$ by parasitic ESA $^4I_{13/2} \rightarrow {}^2H_{9/2}$ is systematically avoided. Owing to the smaller Stark splitting there is no spectral overlap (Fig. 2). Also the inverse process of the ESA, the green fluorescence $^2H_{9/2} \rightarrow {}^4I_{13/2}$, is observed (Fig 2), because the $^2H_{9/2}$ level is not quenched by multiphonon relaxation. The $^4I_{13/2}$ level is more highly populated than the $^2H_{9/2}$ level. The $^4I_{13/2} \leftrightarrow {}^2H_{9/2}$ transition is, therefore, detected as an ESA process in the ESA/SE spectrum (Fig. 2). The strong ESA $^4I_{11/2} \rightarrow {}^2K_{15/2} + {}^2G_{9/2}$ observed at wavelengths longer than 560 nm in BaY_2F_8 is completely missing in $Cs_3Er_2Br_9$ (Fig. 2).

This work was supported in part by the Swiss Priority Program "Optique" and by the U.S. Air Force Office of Scientific Research under Contract No. F49620-94-C-0018.

[1] D. S. Knowles and H. P. Jenssen, IEEE J. Quantum Electron. **28**, 1197 (1992).
[2] M. P. Hehlen, K. Krämer, H. U. Güdel, R. A. McFarlane, and R. H. Schwartz, Phys. Rev. B **49**, 12475 (1994).
[3] J. Koetke and G. Huber, Appl. Phys. B **61**, 151 (1995).
[4] M. Pollnau, E. Heumann, and G. Huber, Appl. Phys. A **54**, 404 (1992).
[5] M. Pollnau, E. Heumann, and G. Huber, J. Lumin. **60+61**, 842 (1994).

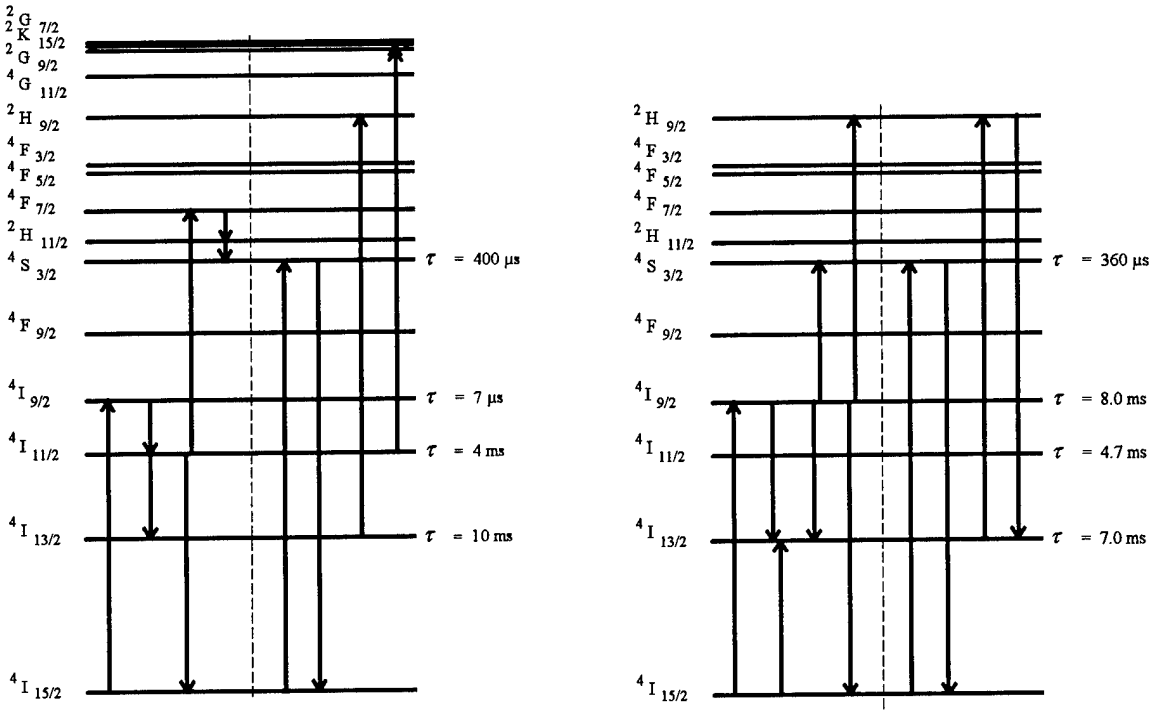

FIG. 1. Energy level diagram indicating the excitation mechanisms and the detected transitions in $Er^{3+}(7.5\%):BaY_2F_8$ (left-hand side) and $Cs_3Er_2Br_9$. Whereas multiphonon relaxations and the population of the $^4I_{13/2}$, $^4I_{11/2}$, and $^4S_{3/2}$ levels are dominant in BaY_2F_8, interionic processes lead to the excitation of the $^4I_{13/2}$, $^4S_{3/2}$, and $^2H_{9/2}$ levels in $Cs_3Er_2Br_9$ under 800-nm pumping.

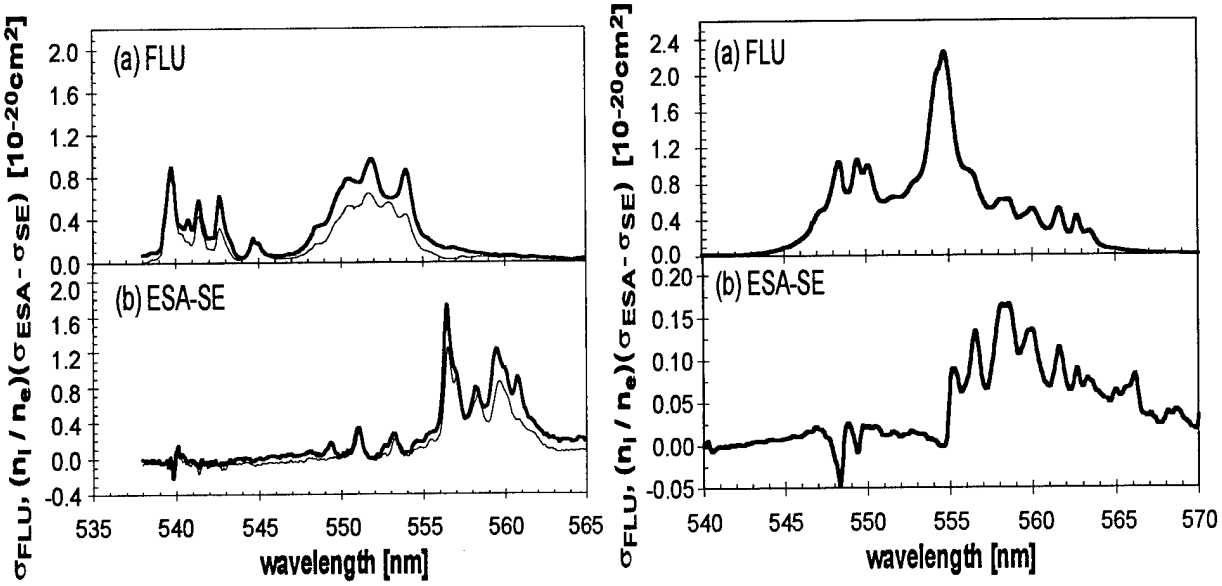

FIG. 2. Left-hand side: (a) Fluorescence and (b) ESA spectra of $Er^{3+}(7.5\%):BaY_2F_8$ with E||y (thick line) and E||z (thin line). Right-hand side: (a) Fluorescence and (b) ESA spectra of $Cs_3Er_2Br_9$ in arbitrary polarization.

Time resolved Fourier spectroscopy of energy transfer in multisite (Yb,Ho)KYF_4.

C. J. Schwindt, H. Weidner, and R. E. Peale
Department of Physics
University of Central Florida
Orlando, FL 32816
407/823-3076(V), 407/823-5112(F), rep@physics.ucf.edu

(Yb,Ho):KYF_4 is a demonstrated IR pumped green-lasing crystal[1]. The 1 μm absorption band of Yb^{3+} ions is laser pumped, and energy is transferred in two sequential steps to Ho^{3+} ions, leaving them in the green-emitting $^5S_2$, $^5F_4$ levels. Thermally activated back-transfer has been shown to limit high temperature upconversion efficiency[2]. Modeling of the phonon-assisted back-transfer[3] has considered only a single pathway, namely $Ho(^5S_2, ^5F_4) + Yb(^2F_{7/2}) \rightarrow Ho(^5I_6) + Yb(^2F_{5/2})$. The neglect of other back-transfer pathways is shown in this work to be a poor assumption. An additional purpose of this work is to demonstrate the power of time-resolved Fourier transform spectroscopy (TRFTS), a new technique applied by us to laser crystals for the first time. A detailed description of this technique is presented separately[4].

Figure 1 presents an energy level spectrum of Ho^{3+} and Yb^{3+}. We use a pulsed Nd:YAG-pumped dye laser to pump the $^5F_5$ levels of Ho^{3+}. The $^5F_5$ absorption spectrum of Ho^{3+}:KYF_4 at 1.7 K is presented in Fig. 2. The lines pumped in this work are indicated by arrowheads on the bottom axis. Pumping the low frequency line has been shown[5] to produce luminescence lines from three similar doping sites (Class II) out of six sites available in KYF_4. Pumping the high frequency line results in signal from Ho ions in the other three sites (Class I).

Fig. 3 presents the results of TRFTS for a sample with 20% Yb and 0.1% Ho at a temperature of 80 K. Photoluminescence spectra were collected at 1 cm^{-1} resolution over a frequency range of 8,500 to 13,000 cm^{-1} at 11 μs intervals from 6 to 500 μs. All data were collected for each pump wavelength in less than 1 hour. No averaging was performed. The signal to noise ratio is nevertheless quite good, and there is no evidence of artifacts[4]. Only the first two time delays are shown in Fig. 3 for a limited range of frequencies corresponding to the $Yb(^2F_{5/2}) \rightarrow Yb(^2F_{7/2})$ and $Ho(^5F_5) \rightarrow Ho(^5I_7)$ luminescence transitions. When pumping the Ho^{3+} Class I line, Ho^{3+} Class I emission is observed in the 6 μs spectrum but is already gone by 17 μs. Similarly, the Class II pump produces a quickly decaying Ho^{3+} Class II spectrum. While the Ho^{3+} signal decays, the Yb^{3+} emission grows, indicating the presence of Ho $\rightarrow$ Yb energy transfer. Since Ho^{3+} is excited in the red, the green emitting levels are not populated (except perhaps weakly via high order processes). Hence we have identified another back transfer pathway than that exclusively considered in Ref. 3: Excited Ho ions in the $^5S_2$, $^5F_4$ levels may relax non-radiatively first to the $^5F_5$ level, where back transfer to Yb can occur. A likely pathway is $Ho(^5F_5) + Yb(^2F_{7/2}) \rightarrow Ho(^5I_7) + Yb(^2F_{5/2})$.

An additional observation is that the relative line strengths within each Yb luminescence spectrum are essentially identical regardless of whether Ho Class I or II is pumped. The most likely explanation is that at an Yb concentration of 20% energy transfer on the Yb lattice is much faster than the time scale of this experiment. To test the possibility that energy transfer is site selective requires a sample of lower Yb doping. Indications that Ho → Yb transfer proceeds at different rates for the two Ho classes is found in these preliminary data.

References

[1]. R. J. Thrash, R. H. Jarman, B. H. T. Chai, and A. Pham, "Upconversion Green Laser operation of Yb,Ho:KYF4," in Compact Blue-Green Lasers, 1994 Technical Digest Series, Vol. 1 (Optical Society of America, Washington, DC, 1994). pp. 73-75.

[2]. X. X. Zhang, P. Hong, M, Bass, "Ho^{3+} to Yb^{3+} back transfer and thermal quenching of upconversion green emission in fluoride crystals," Appl. Phys. Lett. 63, 2606 (1993).

[3]. X. X. Zhang, P. Hong, M. Bass, R. E. Peale, H. Weidner, and B. H. T. Chai, "Temperature and concentration dependences of Ho3+ to Yb3+ energy transfer in Yb3+, Ho3+ codoped KYF_4," J. Lumin. 60&61 (1994).

[4]. H. Weidner and R. E. Peale, "Time resolved Fourier-transform spectroscopy of laser crystals," this conference.

[5]. R. E. Peale, H. Weidner, P. L. Summers, and B. H. T. Chai, "Site-selective spectroscopy of Ho^{3+}:KYF_4," J. Appl. Phys. **75**, 502 (1994).

Figure Captions

Fig. 1. Energy level spectrum of Yb^{3+} and Ho^{3+} ions. The absorption pumped and the luminescence transitions observed are indicated.

Fig. 2. Ho^{3+} $^5F_5$ absorption band at 1.7 K. Arrowheads indicate pump frequencies. Lines belonging to Ho ions in each of the two classes of doping sites are indicated.

Fig. 3. Portion of the time-resolved Fourier spectroscopy data for the two pump frequencies. The vertical and horizontal scales are the same for each plot.

Fig. 3 →

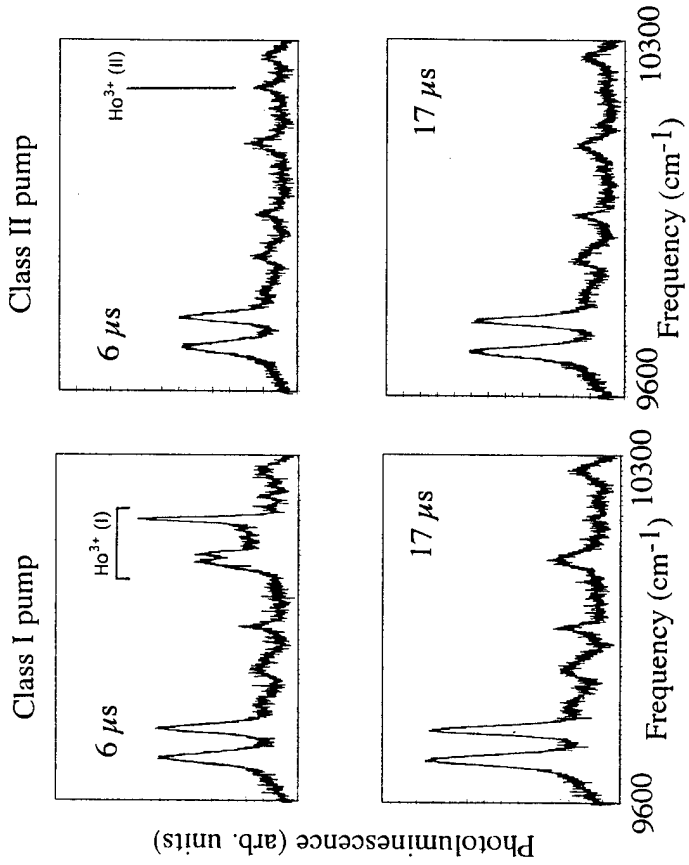

Fig. 1 ↓

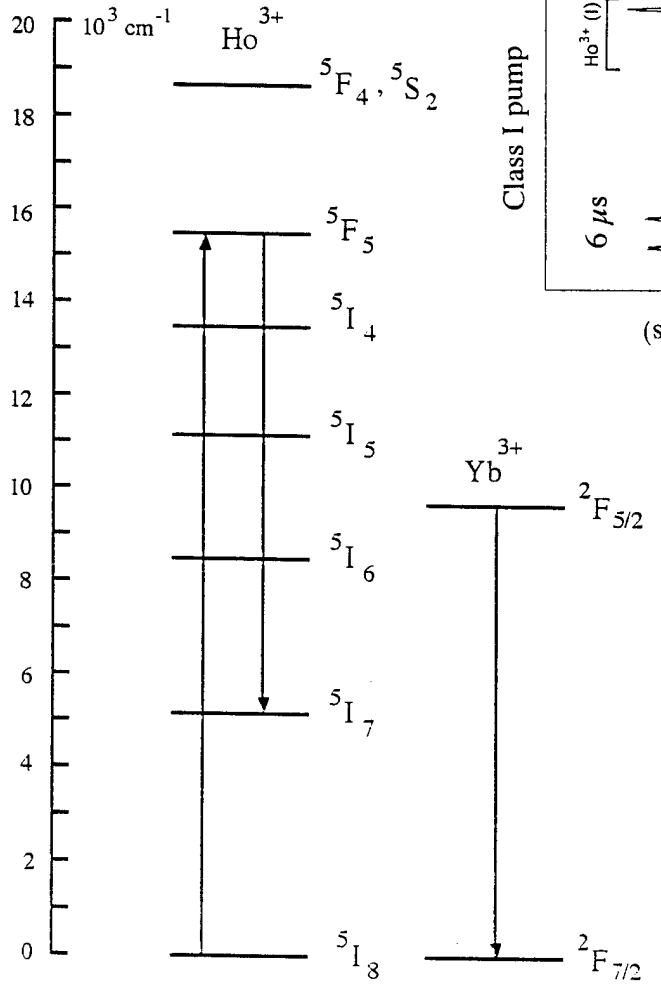

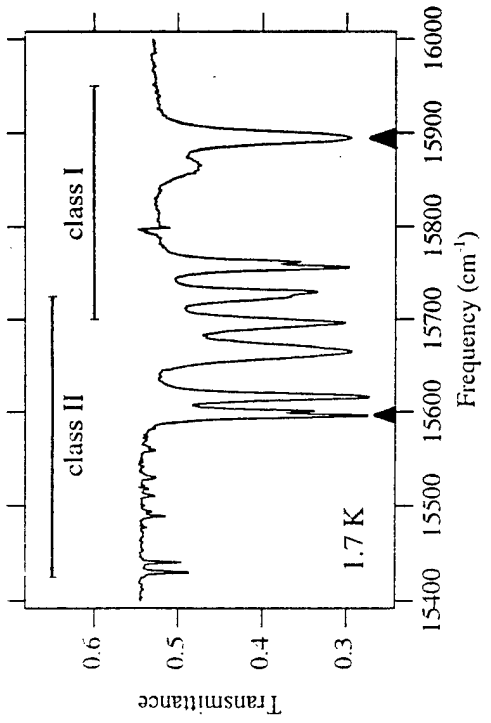

Fig. 2 →

Radiative and Nonradiative Transition Rates of Pr^{3+} in $LaCl_3$

L.B. Shaw, S.R. Bowman, and B.J. Feldman
Laser Physics Branch, Code 5640
Naval Research Laboratory, Washington, DC 20375-5320
Phone (202)767-9418
and
Joseph Ganem
Department of Physics, Loyola College in Maryland
4501 N. Charles Street, Baltimore, MD 21210
Phone (410)617-2048

The recent success of lasing at 5.2 μm [1] and 7.2 μm [2,3] in Pr:$LaCl_3$ has prompted investigations to quantify the radiative and nonradiative mechanisms which influence lasing at these wavelengths. The Judd-Ofelt (JO) model [4,5] and the theory of multiphonon emission rates developed by Moos [6] are very useful tools in this analysis. In addition, the spectroscopic parameters obtained from this methodology are useful for determining potential laser transitions in this host material. We will report the results of this methodology to both known and potential laser transitions of Pr^{3+} in $LaCl_3$.

Polarized absorption spectra were recorded at room temperature in a 0.7% sample of Pr:$LaCl_3$. The crystal was grown by a vertical Bridgman-Stockbarger technique and its concentration was verified by wet chemical analysis to within ±10%. Spectra were recorded for the $^3H_4$ to $^3H_5$,$^3H_6$,$^3F_2$,$^3F_3$,$^3F_4$, and $^1G_4$ transitions . The polarized spectra of these transitions are shown in Figure 1. These integrated absorbance of each band was averaged and weighted by polarization. In cases where the absorption spectra of different bands overlapped, the individual interstark transitions between bands were fit with Lorentzian lineshape functions in order to separate the bands.

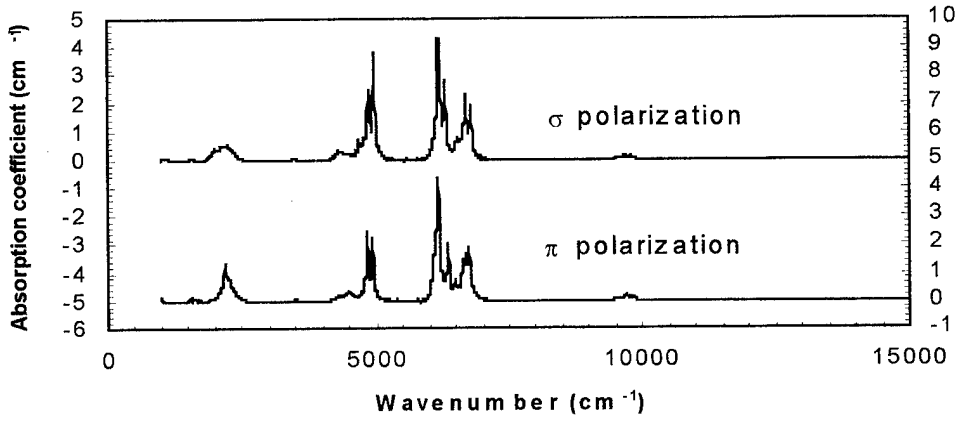

Figure 1. Room temperature polarized absorption spectra of Pr:$LaCl_3$

Line strengths for electric dipole transitions from the ground state were calculated using the absorption coefficients above and index of refraction calculated from dispersion

equations for $LaCl_3$. The magnetic dipole contribution to the absorption intensity was calculated and found to negligible and thus not considered in the calculation of the electric dipole line strengths. These line strengths were used to calculate the JO parameters utilizing a least squares fit. The calculated parameters are

$$\Omega_2 = 9.5 \times 10^{-20}\ cm^2 \quad \Omega_4 = 4.4 \times 10^{-20}\ cm^2 \quad \Omega_6 = 11.3 \times 10^{-20}\ cm^2$$

These parameters were utilized to calculate radiative rates, branching ratios, and integrated emission coefficients for all transitions from the lower lying manifolds as shown in Table 1. We note, by comparison, that the JO parmeters calculated by German, Kiel, and Guggenheim [7] from the visible transitions of $^3P_0$ in Pr:$LaCl_3$ are substantially different from those listed above. Use of their parameters for the IR transitons result in transition probabilities which are, in general, smaller than those we have determined from our JO parameters.

Table 1. Calculated electric dipole transition probabilities (A_{ed}), branching ratios (β) and integrated emission cross section (Σ). Shaded transitions have been successfully lased in Pr:$LaCl_3$.

Transition	λ (μm)	A_{ed} (s^{-1})	β	Σ (x 10^{-18} cm^2)
$^3H_5$->$^3H_4$	4.7	26.7	1	2.3
$^3H_6$->$^3H_5$	4.8	22.3	0.39	2.0
->$^3H_4$	2.4	34.5	0.61	0.76
$^3F_2$->$^3H_6$	10	0.80	0.001	0.66
->$^3H_5$	3.6	129.2	0.166	6.6
->$^3H_4$	2.0	647.5	0.833	10.5
$^3F_3$->$^3F_2$	7.3	0.53	0.0004	0.11
->$^3H_6$	4.8	46.8	0.031	4.4
->$^3H_5$	2.4	229.8	0.152	5.3
->$^3H_4$	1.6	1230.0	0.816	12.2
$^3F_4$->$^3F_3$	20	0.02	0.00002	0.04
->$^3F_2$	5.5	2.4	0.002	0.29
->$^3H_6$	4.0	87.2	0.082	5.1
->$^3H_5$	2.2	286.1	0.269	5.4
->$^3H_4$	1.5	688.5	0.647	6.0
$^1G_4$->$^3F_4$	3.4	42.1	0.037	1.9
->$^3F_3$	3.0	8.0	0.007	0.28
->$^3F_2$	2.1	4.0	0.004	0.07
->$^3H_6$	1.8	291.0	0.260	3.9
->$^3H_5$	1.3	715.5	0.639	5.0
->$^3H_4$	1.0	59.6	0.053	6.0

Multiphonon rates were calculated and utilized to calculate fluorescence lifetimes and quantum efficiencies of the transitions. In the case of the $^3H_6$ and $^3F_2$ levels and the

$^3F_3$ and $^3F_4$ levels, it was found that these levels were essentially coupled whereby the ions in these levels rapidly thermalize through interaction with the lattice. Consequently the fluorescent lifetimes of these levels are calculated as a sum of the rates of these two levels weighted by their Boltzman factors. The results of these calculations along with experimentally measured decay rates from these states are shown in Table 2. As we see, the agreement between the calculated and measured fluorescence lifetimes is quite good. Discussion of these results as they relate to mid-IR lasers already demonstrated in Pr:$LaCl_3$ as well as to new mid-IR lasers in Pr:$LaCl_3$ will be given at the conference.

This work was supported by the Office of Naval Research. The work of L.B. Shaw was supported by the National Research Council Postdoctoral Fellowship Program. The work of Joseph Ganem was supported by Research Corporation.

Table 2. Calculated radiative lifetimes (τ_{rad}), multiphonon relaxation lifetimes (τ_{mp}), fluorescence lifetimes (τ_{fluor}) and quantum efficiencies (η) with experimentally measured lifetimes (τ_{exp}).

Upper State	τ_{rad} (msec)	τ_{mp} (msec)	τ_{fluor} (msec)	τ_{exp} (sec)	η
$^3H_5$	37	500	34	22	0.92
$^3H_6$,$^3F_2$	14	1.2×10^3	14	8	1.0
$^3F_3$,$^3F_4$	0.69	0.38	0.24	0.20	0.35
$^1G_4$	0.89	1.1×10^7	0.89	---	1.0

References

[1] S.R. Bowman, J. Ganem, B.J. Feldman, and A.W. Kueny IEEE J. Quantum Electron. QE-30, 2925 (1994)

[2] S.R. Bowman, L.B. Shaw, B.J. Feldman, and J. Ganem, "A room temperature seven micron solid state laser," delivered as postdeadline paper CPD 26 at the Conference on Lasers and Electro Optics (CLEO), Baltimore, Maryland, May 21-26, 1995.

[3] S.R. Bowman, L.B. Shaw, B.J. Feldman, and J. Ganem, "A seven micron solid state laser," delivered as postdeadline paper PD 5 at the Advanced Solid State Lasers Topical Meeting, Memphis, Tennessee, January 30 - February 2, 1995.

[4] B.R. Judd, Phys. Rev. 127, 750 (1962)

[5] G.S. Ofelt, J. Chem. Phys. 37, 511 (1962)

[6] L.A. Riseberg and H.W. Moos, Phys. Rev. 174, 429 (1968)

[7] K.R. German, A. Kiel, and H. Guggenheim, Phys. Rev. B 11, 2436 (1975)

A Multi-Dimensional Spectroscopic Facility for the Characterization of Laser Materials

Lee H. Spangler
The Optical Technology Center
Department of Chemistry
Montana State University
Bozeman, MT 59717
FAX (406) 994-5407

and

Ralph Hutcheson
Scientific Materials Corp.
Ice Pond Road
Bozeman, MT 59715

The performance of rare-earth based solid state laser materials is dependent on photophysical processes that can be quite complicated owing to processes such as energy transfer, cross - relaxation, and upconversion. It is desirable to track these processes and determine which levels get populated in what time scale and how these dynamics are affected by pump wavelength, duration, and crystal temperature. To this end a multi-dimensional spectroscopic facility utilizing a Bruker 66 step-scan interferometer has been constructed which is capable of simultaneous high spectral and temporal resolution in both excitation and emission. This system is capable of measuring rise and fall times of multiple lines and multiple manifolds over a 10,000 cm^{-1} range simultaneously following narrowband 5 ns pulsed excitation.

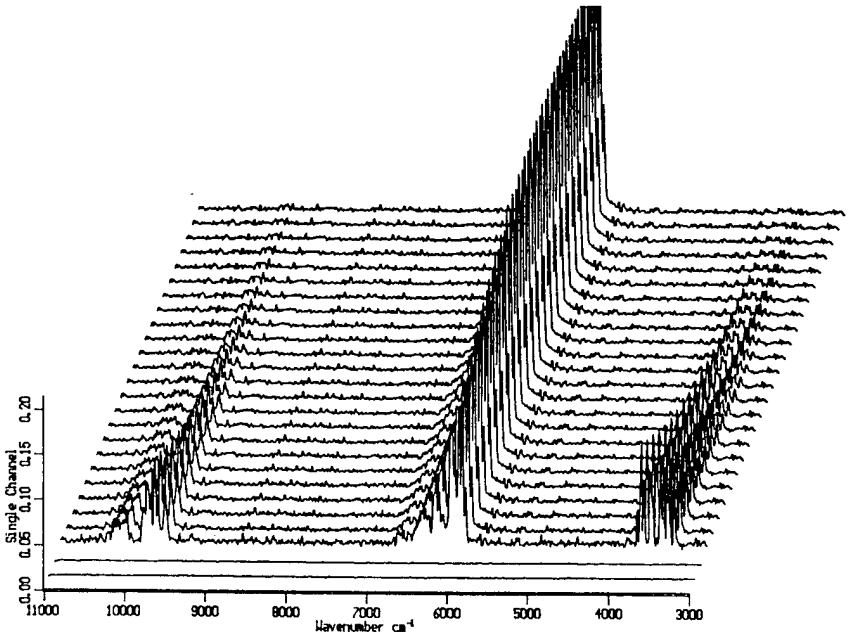

Figure 1. The time and frequency resolved IR emission from Er:YAG following a 10 ns 532 nm excitation pulse. Each trace is 10 μs apart in time.

Emission studies on rare - earth doped crystals illustrate some of the systems capabilities. Figure 1 shows the near IR emission from 4% Er:YAG following a 10 ns 532 nm pulse. The emission from higher excited states centered at 10,000 cm^{-1} and 3500 cm^{-1} both decay rapidly compared to the $^4I_{13/2}$ - $^4I_{15/2}$ at 6000 cm^{-1} which displays a long risetime.

Figure 2 shows the time and frequency resolved emission spectra of Tm in two different hosts following a 1 ms diode laser pulse at 782 nm. As can be seen, both the emission frequencies and decay times show significant lattice effects.

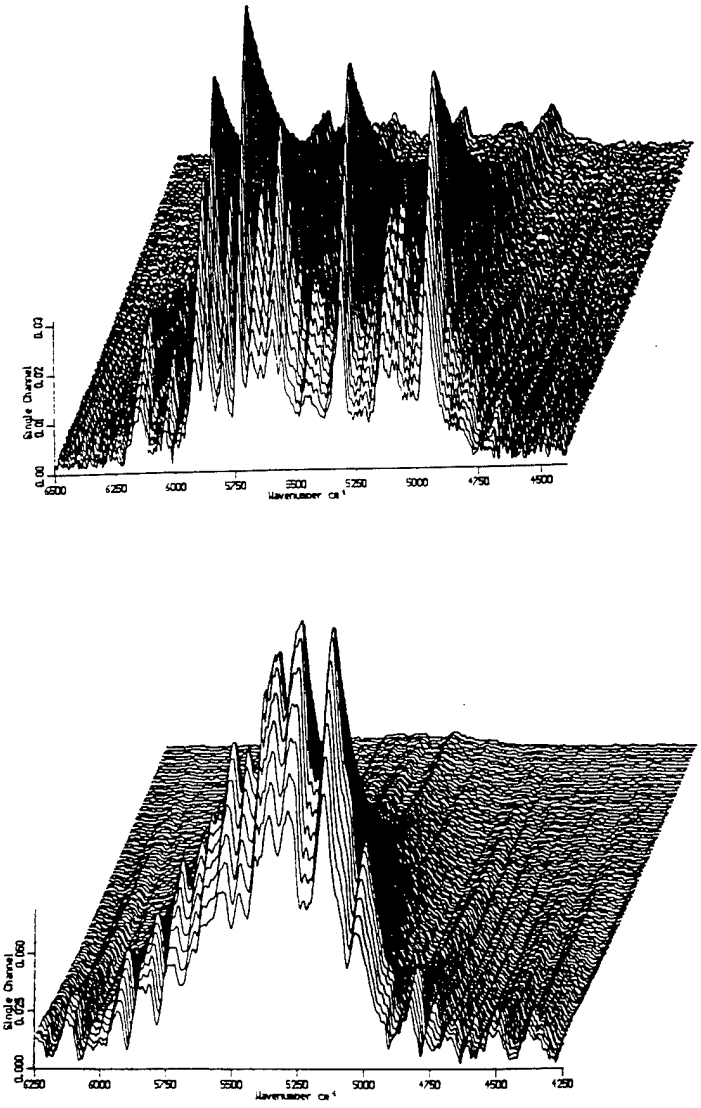

Figure 2. The time and frequency resolved emission of 6% Tm:YAG (top) and 3% Tm:YALO (bottom) following a 1 ms 782 nm diode laser pulse. The time scale is 100 μs per trace.

Using this system, the data acquisition time for conventional absorption and emission profiles can be as short as a few seconds. The complete absorption - emission - temporal profile requires approximately two hours data acquisition time. From this data set absorption cross sections, emission cross sections, branching ratios, fluoresescence lifetimes, Stark splittings, energy transfer, and upconversion processes can be determined.

OPTICAL PROPERTIES OF Tm^{3+} IN LANTHANUM BERYLLATE

V. Sudesh, J. A. Piper
Centre for Lasers and Applications,
School of Maths, Physics, Computing and Electronics
Macquarie University, Sydney, NSW 2109, Australia.
email : vikas@mpce.mq.edu.au fax: 61-2-8508983

D. S. Knowles
Naval Command , Control and Ocean Surveillance Centre
53475 Strothe Ave, San Diego, CA 92152-6325

and
R. S. Seymour
Defence Science Technology Organisation
Salisbury, P. O. Box 1500, Adelaide , SA
Australia

Introduction

Mid infrared tunable solid state lasers based on the thulium (Tm^{3+}) ion have become well established for various applications in medicine and industry[1]. Lanthanum Beryllate (BeL) as a laser host has been reported for the neodymium ion for the first time by Morris et al.[2] and its optical, spectroscopic and laser properties have been described in detail since then [3,4]. YAG has been an established preferred laser host for rare earth dopants including thulium for its high thermal conductivity and mechanical strength. Ease of crystal growth, good mechanical and optical properties of BeL and sharp absorption bands of Tm^{3+} ions at diode wavelengths of 680 nm and 785 nm suggest that BeL may be a desirable alternative host for thulium.

Several large Tm:BeL crystal boules with varying Tm^{3+} concentrations have been grown by the Czochralski crystal-growth method. We have investigated the optical properties of this material to assess its potential as a mid infrared solid state laser medium. Absorption and emission spectra have been measured, together with the temperature dependence of the lifetime of the $^3F_4$ level.

Crystal growth and sample preparation

Single crystals of Tm:BeL were grown by the Czochralski method using computer controlled pullers. Starting materials La_2O_3, BeO and Tm_2O_3 were supplied by Cerac Chemicals Ltd and were of 99.99% purity or higher. All oxides were fired at 1000°C for 24 hours to eliminate moisture. Stoichiometrically mixed powders were then melted in a Pt- 10% Ir crucible at about 1400°C. A flowing dry argon atmosphere were used for growth. The rate was 1mm/hr and the seed rotation rate was 40 rotations per minute.

Initial crystal attempts at growing Tm:BeL revealed some difficulties. Electron microscopy studies of the samples showed traces of platinum metal in the boule, indicating the crucible was breaking down at 1400°C contaminating the mix. The thulium ion concentration was found to vary across the sample cross section. However, optimising the flow of dry argon gas and rate of pull of the crystal boule has resulted in progressive improvement of the crystal quality. Several Tm:BeL single crystals of different sizes and dopant concentration were grown. The thulium ion concentrations in the mix were 0.1%, 0.3%, 0.5%, 1% and 2%. At present, the segregation coefficient of Tm in BeL is not known, however there is evidence that the segregation coefficient is significantly less than unity

(about 30-40%). All crystals were grown to sizes between 8-15 mm in diameter and 10-120 mm in length. Small pieces of Tm:BeL for spectroscopic analysis were prepared with faces polished and oriented in the x, y, z directions.

Optical properties

Absorption data were measured with a Varian Cary 5 spectrophotometer. The emission data were taken with a 0.5 metre single spectrometer of Czerny-Turner design. The emission signal was detected by a liquid nitrogen cooled InSb detector in combination with a lock-in -amplifier. The pump source was a 785 nm temperature tuned cw or pulsed laser diode, device type SDL 2362-P1. The emission signal was observed perpendicular to the direction of excitation and was filtered using a Si filter. The output from the lock-in-amplifier was digitised and stored on a PC. The lifetime was measured by exciting the crystal with a pulsed diode laser at 785 nm.

The absorption coefficients as a function of diode pump wavelengths in the vicinity of 785 nm ($^3H_6$-$^3H_4$) transition for 1% Tm:BeL along x, y, z directions are shown in fig (1). As is evident from the figure, the absorption is maximum in the z direction and is minimum in the x direction. Similar measurements show that the absorption on the 680 nm ($^3H_6$-$^3F_3$) transition is 50% higher than at 780 nm suggesting the strong possibility of diode pumping the crystal at 680 nm wavelength in the future.

The unpolarised measured emission spectra near 1.9 μm on the $^3F_4$-$^3H_6$ laser transition and near 1.5 μm on the $^3H_4$-$^3F_4$ for Tm:BeL at various temperatures are shown in fig.(2). At lower temperatures, fewer transitions are seen because of reduced Boltzman population in the upper level of the multiplet. Broad room temperature spectra probably indicate strong phonon coupling in Tm:BeL compared to Tm:YAG. Tm:BeL emission is much broader than Tm:YAG, hence the tunable range in Tm:BeL may be wider than for Tm:YAG. Tm:BeL emission is blue shifted with respect to Tm:YAG, perhaps allowing laser operation over shorter wavelengths. The polarised emission spectra of Tm:BeL at room temperature is shown in fig.(3).

Variation of lifetime of the $^3F_4$ level with temperature is shown in fig.(4). The room temperature lifetime is 435 μs compared to 10 ms for Tm:YAG. This indicates that either Tm:BeL has higher effective emission cross section than Tm:YAG or in Tm:BeL the $^3F_4$ level is depopulated nonradiatevely. The Tm site in BeL is expected to be more distorted than in YAG, which is consistent with a higher emission cross section in Tm:BeL.

Further work is underway to determine the oscillator strength for 1.9 μm transition and to investigate the various energy transfer processes (such as cross relaxation etc) known to occur in Tm:YAG.

Conclusion

The present results indicate that Tm:BeL has considerable promise as a mid infrared solid state laser material. Current efforts are directed at growth of laser quality Tm:BeL with a higher concentration of Tm.

References

[1] R. C. Stoneman and L. Esterowitz, "Efficient, broadly tunable, laser-pumped Tm:YAG and Tm:YSGG cw lasers," Opt. Lett., vol. 15, pp. 486-488, 1990.

[2] R. C. Morris, C.F. Cline, R.F.Begley, M. Dutoit, P.J.Harget, H.P.Jenssen, T.S.LaFrance, and R.Webb, "Lanthanum Berryllate: A new rare-earth ion laser host," Appl.Phys. Lett., 27(8), pp. 444-445, 1975.

[3] H. P. Jenssen, R. F. Begley, R. Webb, and R. C. Morris, " Spectroscopic properties and laser performance of Nd^{3+} in lanthanum beryllate," Journal of Applied Physics, Vol. 47, No. 4, pp. 1496-1500, 1976

[4] J. Richards, K. Fueloep, R. S. Seymour, D. Cashmore, P. J. Picone, and M. A. Horsburgh, " Nd:BeL Laser at 1365nm," Proceeding of the OSA Topical Meeting On Tunable Solid State Lasers, pp. 119-123, 1989 .

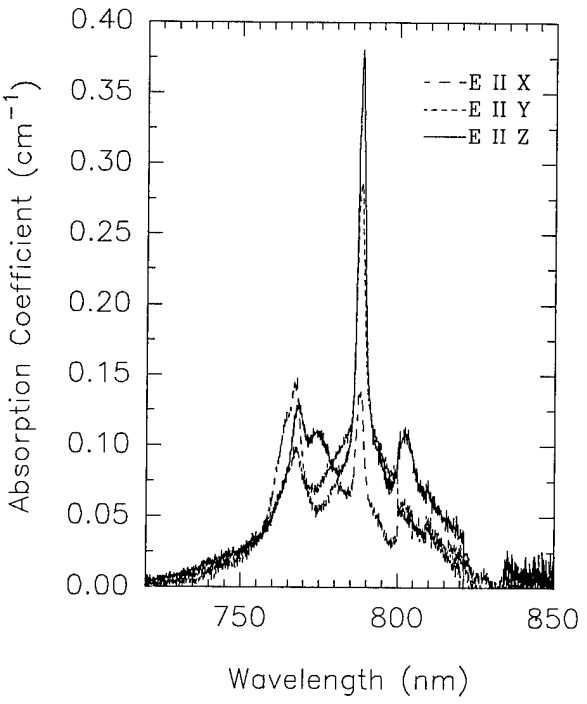

Fig.(1) Absorption coefficient of !% Tm:BeL along x, y, z directions

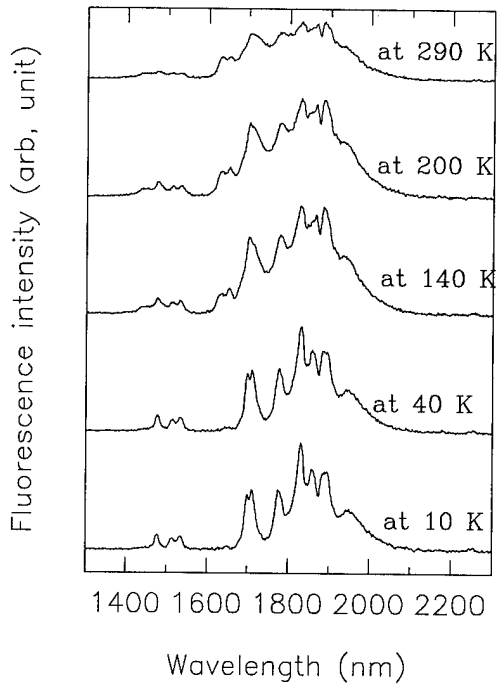

Fig (2) Unpolarized fluorescence spectra of Tm:BeL at different temperatures

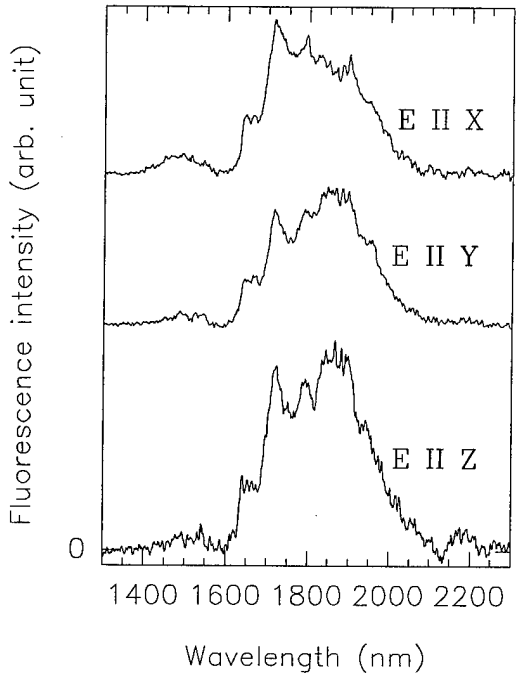

Fig (3) Polarized fluorescence spectra of Tm:BeL at room temperature

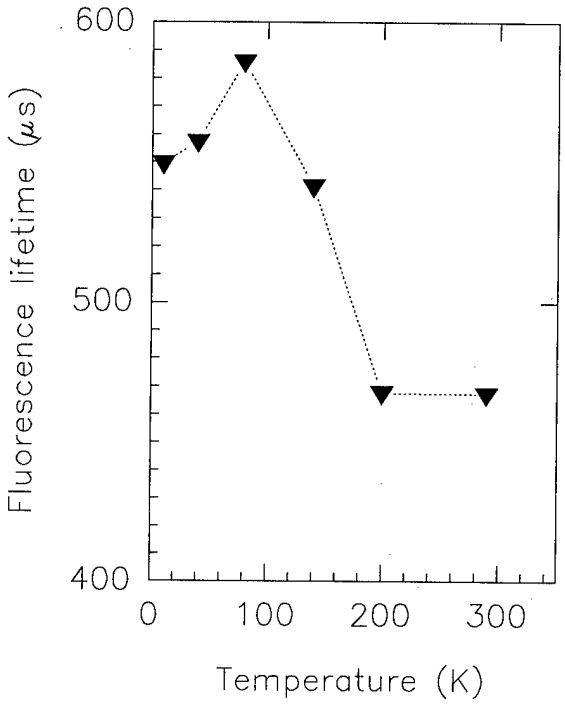

Fig (4) Variation of 3F4 level lifetime with temperature

A powerful new technique for laser crystals: Time-resolved Fourier spectroscopy

H. Weidner and R. E. Peale
Department of Physics
University of Central Florida
Orlando, FL 32816
(407)823-3076(V), (407)823-5112(F), rep@physics.ucf.edu

Time-resolved spectroscopy is useful for characterizing energy transfer in laser crystals. Fourier transform spectroscopy (FTS) has demonstrated advantages for frequency accurate, high resolution, broad band absorption and site-selective photoluminescence spectroscopy [1,2]. The combination, time-resolved Fourier-transform spectroscopy (TRFTS), has never been applied to laser crystals - until now. Our spectrometer is of the common continuously-scanning type which means one interferometer mirror is in continuous motion while the interferogram data are being collected. While this allows cost effective dynamic alignment with spectral coverage to UV frequencies, it also complicates the acquisition of time-resolved data and can be the source of artifacts. We have developed a new method of acquiring and analyzing the interferogram that overcomes the complications and sources of artifacts, making TRFTS useful for high resolution IR -> vis spectroscopy of luminescence dynamics in the μs to ms range. We have applied this technique to the problem of energy transfer in laser crystals for the first time. Since the technique is uniquely powerful, but is also quite complicated and new to the solid-state-laser community, we feel a presentation on the technique alone is justified for this conference. A detailed application to a frequency converting multisite crystal will be presented separately [3].

Previous approaches to TRFTS with continuously-scanning interferometers were based on the requirement to acquire interferogram data at fixed positions of the moving mirror, which arises from the desire to use a fast Fourier transform algorithm (FFT) to obtain the spectra. Those positions are determined by the interference pattern of a HeNe laser. The spatial separation of the sample locations translates into a temporal spacing depending on the speed of the mirror. This can be extremely demanding on the scanning hardware if one chooses to adjust the speed to achieve the desired time step size without compromises. Furthermore, any variation in the mirror speed leads to timing errors. These create uncertainties in the time delay of the spectral information and cause variations in the magnitude of the recorded (decaying) signal, which in turn can be the source of strong artifacts.

Our new approach is to sample the spectral information using fixed time intervals. Now, the sampling rate and the timing uncertainty are only limited by the analog to digital converter (ADC) . Mirror speed variations lead now to unequal spatial separations of the samples. The actual location of samples can be calculated from measured mirror speed information and the times when the samples were taken. But regular FFT relies on equal data spacing and cannot be used here to obtain the spectra. We see two ways to deal with the unequal spacing. The most direct approach would be an interpolation to find the signal at points of equal spatial separation followed by an FFT. If the mirror speed

variations are small, calculated data points would always lie close to measured points and a low order interpolation (less sensitive to experimental glitches than higher order) can be sufficient. A second way of dealing with the unequal spacing are so called periodograms [4] which are least square fits of harmonic functions to the interferogram. By fitting a series of frequencies, one can obtain a power spectrum. This second method is numerically more demanding than the first (it actually utilizes FFT to evaluate its formulae) but its fitting nature appears to make it less susceptible to artifacts.

We have successfully implemented the hardware necessary to acquire the interferogram information, data from a reference detector, and mirror speed measurements. The reference detector allows the correction of shot-to-shot variations of the pump laser energy, which significantly improves the S/N ratio [5]. The implementation is based on a personal computer (486DX2, 66 MHz, ISA bus) which contains the ADC (Keithley DAS1800HR) and a timer card. Some (low cost) external electronics is necessary to collect the signals from the interferometer and the detectors, to measure the mirror speed, and to form the signals that trigger the pump laser (Nd:YAG GCR150-30 from Spectra Physics + dye laser from Laser Photonics). We also implemented two pieces of software: one that controls the hardware and collects the experimental data and the second to descramble the information and to calculate the periodograms.

To test the performance of our hardware and software, we used the well studied laser crystal Nd:$KLiYF_5$ [1] grown by a modified Czochralski method. The crystal provides two similar sites A and B for Nd ions. The corresponding two sets of emission lines can be distinguished at low temperatures (100 K). The sample was excited by pumping a line at 15988 cm^{-1} in the $^2H_{11/2}$ manifold. This should lead to excitation of mostly ions in site A (there is some B absorption from the neighboring line at 15983 cm^{-1}). The excited ions relax rapidly to the $^4F_{3/2}$ manifold from which emission is observed. The Si-detector and filter (RG780) allow simultaneous observation of frequencies in the range from 8500 cm^{-1} to 13000 cm^{-1} . A resolution of 1 cm^{-1} was chosen. Without averaging, the acquisition of spectra for 30 different time delays takes about 35 minutes. A narrow section of the measured spectra is presented in Fig. 1. It shows the time dependent intensities of two lines at 9536 cm^{-1} and 9545 cm^{-1} originating in sites A and B, respectively. The A line shows strong initial intensity with a very short (<10 μs) rising part which is caused by the relaxation towards the emitting level. The B line shows a slow rise (40 μs) and a subsequent decay. At long times, the B line is stronger than the A line which is expected from non-selective experiments with continuous excitation.

The broad range covered (4500 cm^{-1}), the high resolution (1 cm^{-1}), the high S/N ratio without averaging, the absence of artifacts, and the short collection time demonstrate the potential of the technique for studying energy transfer in rare-earth activated materials. With our instrument, frequencies from FIR to UV can be covered at resolutions up to 0.02 cm^{-1}. Our current time resolution is limited by the speed of our detectors and ADC. With appropriate detectors and available fast 12 bits-ADCs, time resolutions of 30 ns are possible. Hence, the technique has even more potential than demonstrated here.

[1] P. L. Summers, H. Weidner, R. E. Peale, B. H. T. Chai, "Spectroscopy of Nd^{3+} in $KLiYF_5$ and $KLiGdF_5$", J. Appl. Phys. **75**, 2148 (1994).

[2] R. E. Peale, H. Weidner, P. L. Summers, and B. H. T. Chai, J. Appl. Phys. **75**, 502-505 (1994).

[3] C. J. Schwindt, H. Weidner, R. E. Peale, "Time resolved Fourier spectroscopy of energy transfer in multisite (Yb, Ho) KYF_4", technical digest of this conference

[4] N. R. Lomb, "Least-Squares Frequency Analysis of Unequally Spaced Data", Astrophys. and Space Science **39**, 447-462 (1976).

[5] S. A. Rogers and S. R. Leone, "Pulsed Laser Photolysis Time-Resolved FT-IR Emission Studies of Molecular Dynamics", Appl. Spectr. **48**, 1430 (1993).

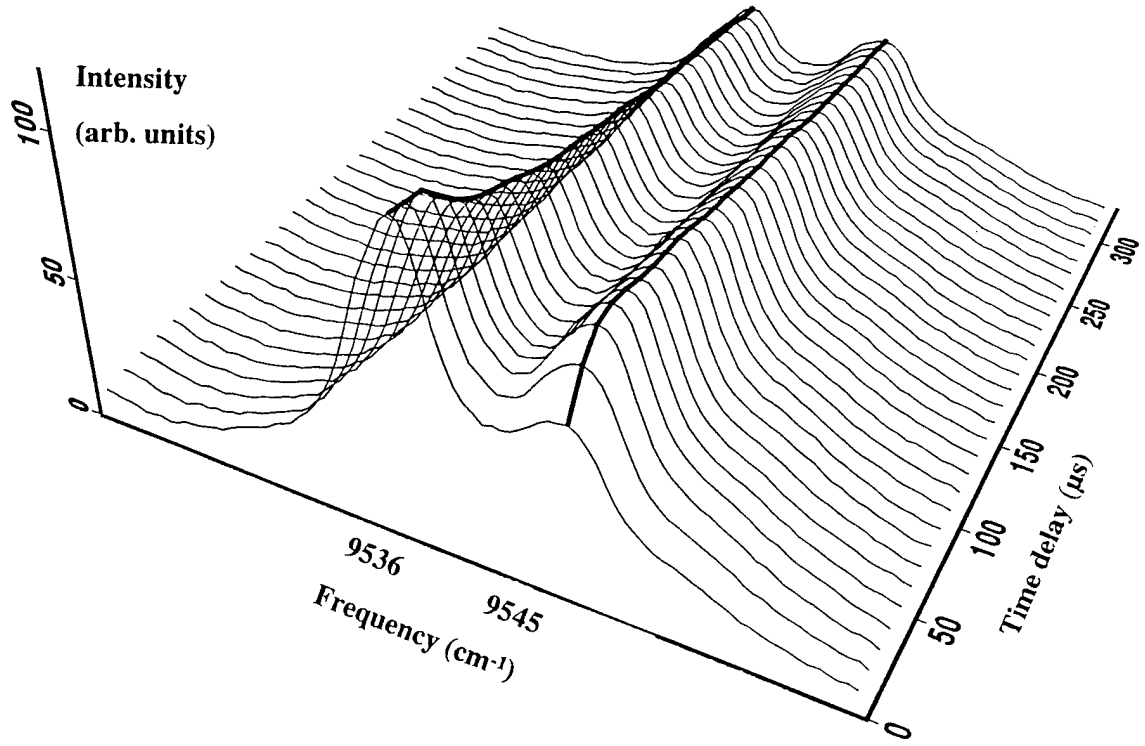

Figure 1. Observation of time-dependent line intensities arising from site-selective excitation of Nd3+:KLiYF5 and subsequent energy transfer demonstrates potential of time-resolved Fourier transform spectroscopy with continuously scanning interferometers.

Friday, February 2, 1996

Novel Architecture

FD 10:45 am-12:30 pm
Gold Room

Douglas Anthon, *Presider*
ATx-Telecom Systems

Deformable-Membrane Frequency Tuning of Microchip Lasers

J. A. Keszenheimer, A. Mooradian , J. Prince
Micracor, Inc., 43 Nagog Park, Acton, MA 01720
Tel: (508) 263-1080, e-mail: Lasers2u@tiac.net

S. Humphrey
Rome Laboratory/OCPC, 25 Electronics Parkway, Griffiss AFB, NY 13441-4515
Tel: (315) 330-1818, e-mail: HumphreyS@ocp.rl.af.mil

An electrostatically deformable mirror has been used to vary the cavity length of a single frequency microchip laser, thereby continuously tuning its optical frequency. Frequency tuning of 6 GHz and tuning rates up to 20 kHz have been initially demonstrated at a lasing wavelength of 1.3 μm. Tuning across the gain bandwidth of Nd:YAG should be possible with <100V using this technique. Silicon nitride micromachining has been previously used to produce deformable mirrors for use in Fabry-Perot interferometers.[1] Vertical cavity microinterferometers have also been constructed using similar techniques, but for use with GaAs semiconductor systems.[2] We believe this is the first demonstration of a deformable mirror used to tune the wavelength of a diode-pumped solid-state laser.[3]

The microchip cavity configuration is shown in Figure 1. The Nd:YAG microchips were polished flat and parallel to ~1-mm thickness. The surfaces were coated for high reflectivity at 1.3 μm on the first surface and low reflectivity on the second surface. The deformable membrane was fabricated from a single crystal silicon wafer. A thin, ~1-μm layer of silicon nitride was deposited on the surface of the silicon. Regions varying in diameter from 2 to 10 mm were lithographically defined on the silicon for KOH etching, which stop-etched at the silicon nitride interface. The etch left the thin layer of silicon nitride in the form of an edge-supported, nearly circular membrane. Gold (+) electrodes were deposited in an annular quadrant pattern on the membrane leaving a 1-mm clear aperture in the center, as shown in Figure 2. A dielectric coating of 2% transmission at 1.3 μm was deposited in this central region, forming the output coupler for the laser. Individual membrane elements were diced from the wafer. A single 5-mm-diameter element was held within 100 μm of the Nd:YAG microchip using insulating spacers. A thin, copper (-) electrode with a 1-mm clear aperture was mounted against the Nd:YAG surface. When pumped with a fiber pigtailed laser diode, the cavity was aligned for optimum output power resulting in a circular, diffraction-limited beam. CW output power at 1.3 μm was ~50 mW.

The output spectra was monitored on a Fabry-Perot spectrum analyzer. A sinusoidal voltage was applied across the electrodes resulting in a modulation of the frequency spectrum. Figure 3 shows a modulation width of 6 GHz for an applied voltage of 200 V at an arbitrary modulation rate of 4 kHz. The spectrum deviates slightly from the classical Bessel FM spectrum due to thermal and acoustic drift of the unpackaged laser assembly, which limited the accuracy of this measurement method at lower frequencies. Tuning was observed at rates from d.c. up to 20 kHz at which point the measurements were limited by the voltage source.

A separate set of measurements were made using an unequal path Michelson interferometer and a He-Ne laser in order to verify the displacement of the membrane as a function of voltage. One path of the interferometer had a reference mirror that was adjusted to maintain a nearly quadrature phase shift. The other path had a deformable membrane for a mirror. The center of the interference pattern formed at the output of the interferometer was monitored through a pinhole with a silicon photodetector. A sinusoidal voltage was applied to the deformable membrane, inducing a path length change in the interferometer. The resulting intensity modulation from the interferometer was monitored on an oscilloscope and a spectrum analyzer. The output spectrum exhibited a Bessel series consisting of a number of components, dependent on the magnitude of the phase shift. The ratios of the Bessel component amplitudes were used to determine the phase shift and from Equation 1, the path length difference, hence, membrane displacement were inferred.

$$\Delta\phi = \frac{2\pi \cdot \Delta L}{\lambda} \tag{1}$$

$\Delta\phi$ is the phase difference in radians, ΔL is the path length change (equal to the membrane displacement), and λ is the wavelength of the source. At 4 kHz, the measured displacement corresponded to a laser frequency modulation of 6 GHz, which was in agreement with the actual measured modulation from the membrane-tuned microchip laser.

In conclusion, we have demonstrated a deformable-membrane-tuned microchip laser that may be used in coherent sensor and communications systems. The laser was frequency tuned 6 GHz, which was also verified by measuring membrane displacement through the use of an unequal path interferometer.

We would like to gratefully acknowledge the contributions Robert W. Sprague for the optical coatings. This work was supported by Rome Laboratory of the Air Force Materiel Command.

References

1. J. H. Jerman, D. J. Clift, S. R. Mallinson, Sensors and Actuators A, **29**, 151, (1991).
2. M. C. Larson, B. Pezeshki, J. S. Harris, Jr., *IEEE Photon. Technol, Lett.*, **7**, 382, (1995).
3. J. J. Zayhowski, A. Mooradian, US Patent #5,022,745.

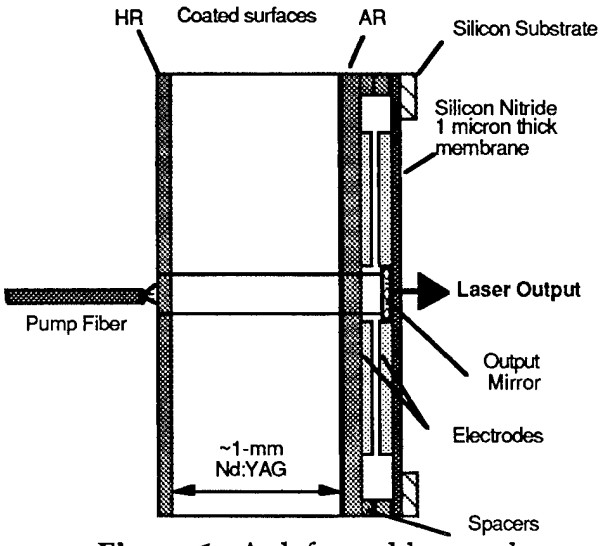

Figure 1: A deformable membrane attached to the output face of a Nd:YAG microchip laser. Tuning is accomplished via an applied electrostatic field.

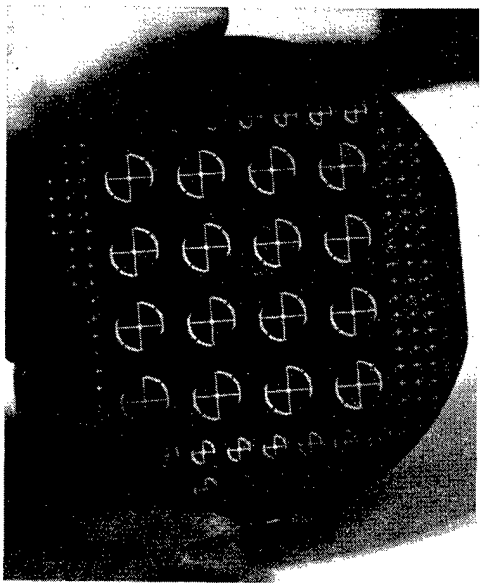

Figure 2: An etched silicon wafer with silicon nitride membranes and gold electrode quadrants.

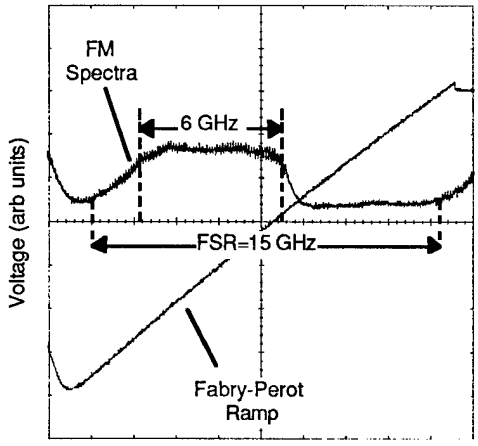

Figure 3: Fabry-Perot spectrum showing 6 GHz of modulation width at 4 kHz repetition frequency. The applied voltage was ~200 V.

Single Axial-Mode Oscillation of a Coupled Cavity Yb:YAG Laser

Takunori TAIRA and Takao KOBAYASHI

Faculty of Engineering, Fukui University, 3-9-1 Bunkyo, Fukui 910, JAPAN

***William M. TULLOCH and *Robert L. BYER**

*Edward L. Ginzton Laboratory, Stanford University, Stanford, CA 94305, U.S.A.

(Tel. +81-776-23-0500)
(Fax. +81-776-27-8749)
E-mail; taira@optele.fuee.fukui-u.ac.jp

Trivalent Yb ion doped solid-state materials are attractive as high efficiency, high stability, high energy laser. Diode-pumped Yb:YAG laser has several advantages relative to Nd:YAG lasers; i.e., low thermal load, long upperstate life time and large absorption width around the InGaAs laser emission range. In addition, Yb:YAG has no excited state absorption and upconversion loss[1]. A great deal of effort has been made toward high efficiency and high power operation with diode-pumped Yb:YAG lasers[2, 3]. What seems to be lacking, however, is about a single-axial mode operation. Although a Yb:YAG laser has a relatively wide fluorescence bandwidth, ~2.66 THz, that is a disadvantage for single-axial mode oscillation. In this paper, we report our recent results for single axial-mode oscillation of Yb:YAG with using a coupled-cavity configuration.

Figure 1 shows the schematic of the coupled cavity Yb:YAG laser geometry. In this configuration, we must take account into three mirror effects[4]. For a three mirror cavity, the transmitted electric field from output mirror is given by

$$E_T = \frac{t_2 t_3 \sqrt{\tilde{g}_1 \tilde{g}_2}}{1 - r_2\left(r_1 \tilde{g}_1 - r_3 \tilde{g}_2\right) - r_1 r_3 \tilde{g}_1 \tilde{g}_2} E_s \qquad (1)$$

where r_1, r_2, r_3 are the reflectivity for the electric field amplitude of the surface of 1, 2 and 3, respectively, $\tilde{g}_1 = \exp(\gamma_1 - j\phi_1)$, $\tilde{g}_2 = \exp(\gamma_2 - j\phi_2)$ are the round-trip gains which include the laser gain or loss, γ_1 and γ_2, and the phases, ϕ_1 and ϕ_2. We find a threshold condition from the denominator of Eq. (1). With the gain coefficient g_1 and the loss coefficient α_1, it is possible to represent the laser gain or loss as $\gamma_1 = (g_1 - \alpha_1)L_1$, where L_1 is the length of region 1. From the three mirror model, a threshold gain coefficient are given by

$$g_{th} = \alpha_1 - \frac{1}{L_1} \ell n \frac{r_1\left(r_3 e^{\gamma_2} \cos(\phi_1 + \phi_2) + r_2 \cos\phi_1\right)}{1 + r_2 r_3 e^{\gamma_2} \cos\phi_2} \qquad (2)$$

From this model, a threshold of the resonant cavity and non-resonant cavity mode are given by $\cos\phi_1 = \cos\phi_2 = \cos(\phi_1 + \phi_2) = 1$ and $\cos\phi_1 = \cos\phi_2 = -\cos(\phi_1 + \phi_2) = -1$, respectively. The threshold ratio of the resonant mode with three mirror cavity compare to a conventional two mirror cavity

with a AR-coated crystal is given by $R_2 = 0$. As R_2 of Eq. (2) increases, it is evident that the threshold ratio of the non-resonant mode to resonant mode ($g_{th,NR}/g_{th,R}$) becomes large so that the multi-longitudinal mode operation is suppressed. The internal face of the crystal for conventional laser cavity is AR-coated at laser wavelength to avoid the reflectivity loss. Following conventional concept a laser which has uncoated crystal has a higher threshold than the anti-reflection coated crystal and it is difficult to oscillate because it has the Fresnel loss for lasing wavelength. However, it is expected that single longitudinal mode oscillation using an uncoated crystal should have a low threshold. From Eq. (2), we obtain ($g_{th,NR}/g_{th,R}$) = 3.31 and ($g_{th,R}/g_{th,AR}$) = 0.55.

A Yb:YAG crystal with 10-at.-% Yb^{3+} doping (Scientific materials Co.), with dimensions a diameter of 4 mm and thickness of 1.1mm was used for this experiments. Typically longitudinally pumped configurations require an interface coated for high reflectivity (>99.9 %) at the lasing wavelength and high transmission (>80 %) at the pumping wavelength to couple the pump light into the laser cavity. The Yb:YAG crystal has high transmission from 920 nm to shorter wavelength, therefore these experiments were conducted using a Ti:Al_2O_3 pump laser tuned to 913 nm which is third absorption peak of the Yb:YAG crystal. An oposite side of the Yb:YAG crystal has the Fresnel loss, ~8.45%. The external mirror was a 10 mm radius of curvature mirror, coated for a reflectivity of 95 % at 1030 nm and > 99 % at the pump wavelength. The position of this external mirror was separated 7.5~8.0 mm from the crystal and adjusted by a piezo-electric-device (PZT). A 50 mm focal length mode matching lens was used to focus the pump beam to a diameter of 58 μm in the laser crystal. The temperature of the laser holder was controlled by using a thermo-electric cooler set at 20 °C. In our case, the free spectral range (FSR) of the Yb:YAG crystal and a total cavity length are ~75 GHz and ~17 GHz, respectively.

The Yb:YAG output power vs. Ti:Al_2O_3 absorbed pump power for the laser operating in a single axial mode is shown in Figure 2. The threshold was measured to be 27.1 ~ 33.9 mW and the slope efficiency was η_s = 32 % in single axial mode relative to the absorbed power at 913 nm. The maximum output power for the microchip laser was 41.6 mW for single axial mode oscillation at 198 mW of absorbed pump power. The maximum output power reached 50.4 mW for multi axial mode operation. On other hand, with an AR-coated crystal the threshold power was 41.8 mW and the maximum output power was 91.2 mW in multi axial mode operation. Therefore, the threshold power using uncoated crystal is 20 ~ 35 % lower than using AR-coated crystal, which is in good agreement with the theoretical results.

In conclusion, single-axial-mode oscillation of Yb:YAG laser has been demonstrated with a the wide FWHM fluorescence width of Yb:YAG at 1030 nm of 9.4 nm, or 2.66 THz. An uncoated Yb:YAG crystal was used to operate as a coupled cavity laser configuration. This technique not only achieve the single axial mode operation but also decrease the threshold power. These effects are consistent with our theoretical and experimental results. Single axial mode Yb:YAG may find applications as stable master oscillator for higher power Yb:YAG lasers.

References

[1] P. Lacovara, H. K. Choi, C. A. Wang, R. L. Aggarwal, and T. Y. Fan, Opt. Lett., vol. 16, no. 14, pp.1089-1091, 1991.

[2] D. Sumida and T. Y. Fan, LEOS Annual Meeting, PaperSS3.2, 1994.

[3] U. Brauch, A. Giesen, M. Karszewski, C. Stewen, and A. Voss, Opt. Lett., vol. 20, no. 7, pp. 713-715, 1995.

[4] T. Taira, W. M. Tulloch,R. L. Byer, and T. Kobayashi, Extended Abstracts (The 42 th Spring Meeting, 1995) the Japan Society of Applied Physics of Applied Physics, Tokyo, Japan, Paper 18pA12.

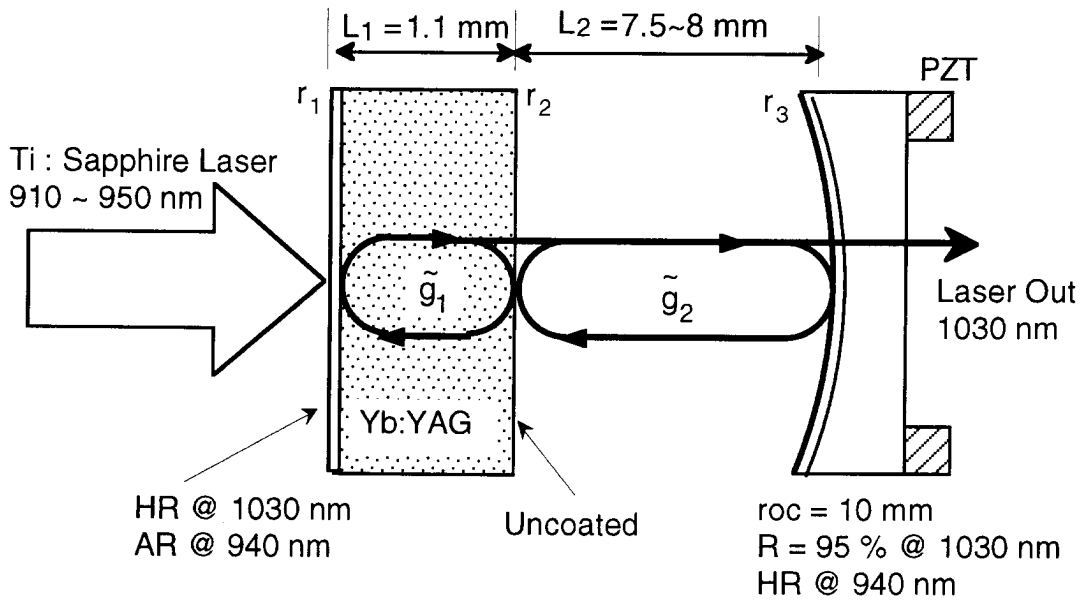

Fig. 1 Schematic of the coupled cavity Yb:YAG laser. The internal surface of Yb:YAG crystal is uncoated.

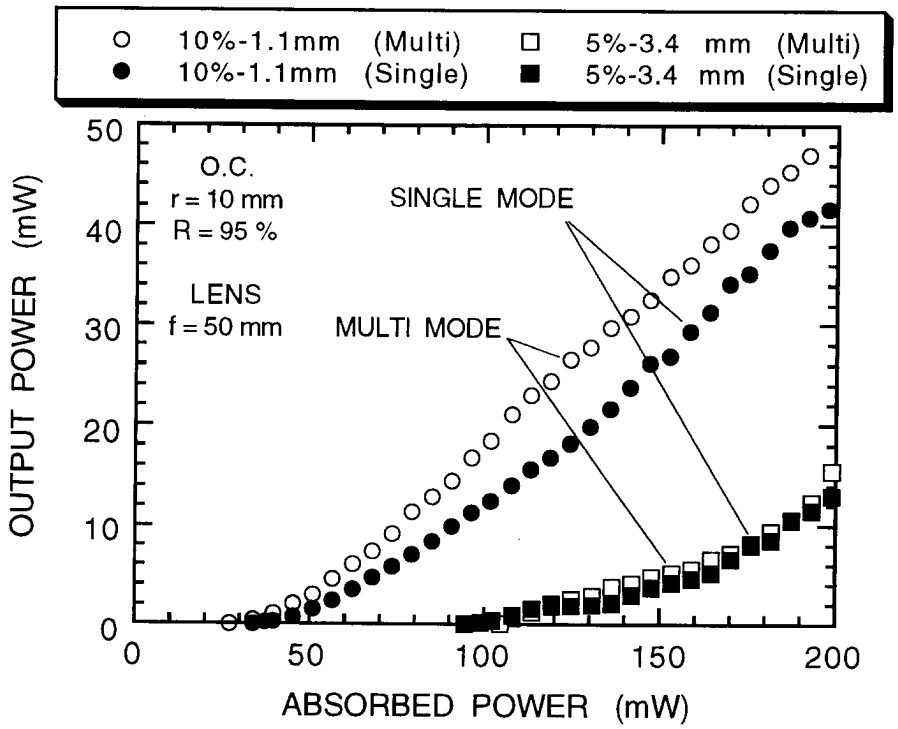

Fig. 2 Input-output power characteristics of the coupled cavity Yb:YAG laser pumped by a Ti:sapphire laser. Up to 42 mW power of single frequency output has been obtained without any intracavity elements.

1 W CW 2.12 μm Lamp Pumped Room Temperature YAG:Yb-Ho Laser

A.A.Nikitichev, V.A.Pis'mennyi

Institute for Laser Physics, SC"Vavilov State Optical Institute"
199034, St.Petersburg, Russia

ABSTRACT

CW 2.12 μm YAG:Yb-Ho lamp pumped room temperature laser with the output power of 1 W is reported for the first time. The processes of energy transfer, creating the operating scheme of the laser, are studied.

INTRODUCTION

The sensitization of the Ho-ion lasing transition by Tm ions is the most usual operating scheme of the diode-pumped Ho laser. The first CW room temperature diode-pumped YAG:Tm-Ho laser was realized in 1987 [1,2]. Nearly double quantum yeld of the absorbed energy to the storage levels and the coincidence of the sensitizer absorption spectrum with the emission spectrum of AlGaAs laser diodes make this sensitization scheme the most efficient for the diode-pumped Ho-lasers both for the oxide and for fluoride crystals.

However, some features of Tm-Ho system spectroscopy, as well as low intensity and width of Tm-ions absorption line, prevent the use of the lamp pump of the CW Tm-Ho laser. First, stored energy distribution between the manifolds of Tm and Ho-ions, caused by the reversible character of the energy transfer process, results in the increase of the pump power threshold. Second, up-conversion of the stored energy, caused by the nonlinear interaction of Tm and Ho-ions, diminishes significantly the lifetime of the upper laser manifold and enlarges the heat deposition [3,4]. For example, in the crystal YAG:Tm-Ho the up-conversion rate exceeds the spontaneous decay rate 3-4 times already at the threshold level. So the threshold absorbed power is somewhat 350 W/cm^3 - practically impossible to be provided under the non-selective excitation.

Yb ion is another efficient sensitizer of Ho ion. The ions of Yb reveal the strong electron - phonon interaction in comparison with other rare earths, providing thus the developed character of the absorption spectrum and high probability of the nonresonant energy transfer. The absorption band of Yb ion coincides with Xe arc emission spectrum.

In this paper we propose the new active medium for the CW lamp-pumped Ho-laser: the YAG:Yb-Ho crystal. Energy transfer processes, laying in the lasing scheme basis, are studied.

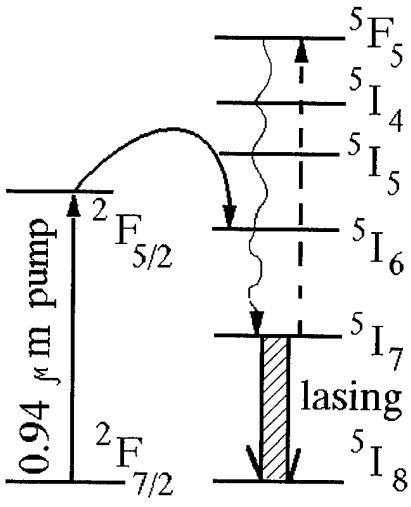

Fig.1. YAG:Yb-Ho operating scheme

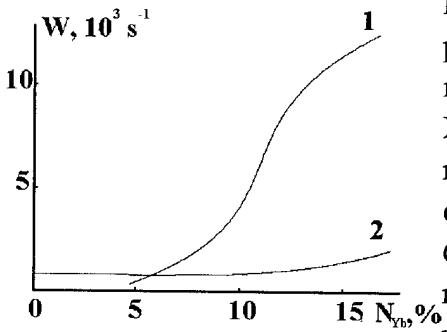

Fig.2. Yb-Ho energy transfer (1) and concentration quenching (2)

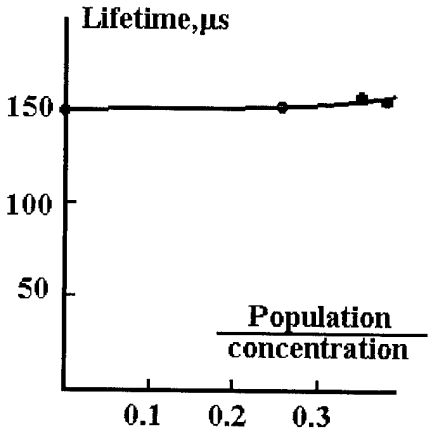

Fig.3. Dependence of the Yb ion manifold $^2F_{5/2}$ lifetime vs. invertion factor

1.SPECTROSCOPY

The working scheme of the medium YAG:Yb-Ho is shown in the Fig.1.

(1) The energy, absorbed on the transition $^2F_{7/2}$-$^2F_{5/2}$, via the inter-center transfer $|^2F_{5/2}(Yb); {}^5I_8(Ho)\rangle$ - $|^2F_{7/2}(Yb); {}^5I_6(Ho)\rangle$ and the consequent radiation-less relaxation $^5I_6$-$^5I_7$, comes to the upper laser manifold.

(2) The process of up-conversion $|^2F_{5/2}(Yb); {}^5I_7(Ho)\rangle$ - $|^2F_{7/2}(Yb); {}^5I_5(Ho)\rangle$ with the consequent radiation-less relaxation of the $^5F_5$-manifold of Ho back to the upper laser manifold results in the loss of one of the absorbed pump energy quantum in each summation act.

Experimental measurement of Yb-ion decay kinetic provided evaluation of the parameters of the processes (1) and (2). Optically thin samples were mounted in the pumping system and excited by the Xe-lamp flash with the duration 10 μs. Up-conversion rate parameter was measured using the pre-excitation of the specimen by the high energy pulse (duration 600 μs), providing the sufficient rate of laser manifolds' inversion. The absolute value of population of $^5I_7$ (i.e., calibration of the luminiscence intensity) was measured as follows. The increase of the luminiscence signal and the corresponding increase in the heat release were detected in the YAG:Ho crystal at broadening of spectrum of crystal excitation from 620 to 680 nm (it corresponds to including of the $^5F_5$ absorption band). As the level $^5F_5$ in YAG:Ho undergoes nonradiative decay to $^5I_7$, an increase in population depends on the temperature increase: $\Delta N = C_V \Delta T/\varepsilon_{ext}$, here C_V=2.86 J/cm^{3}K, ε_{ext}=2.16x10^{-19} J - heat release quantum. The heating of the crystal was measured using the thermocouple.

The parameter of the Yb-Ho energy transfer, determined from the static decay in the crystal with the low Yb-ion concentration, is C_{DA}=1.2x10^{-40}cm^{6}s^{-1}. In the Fig.2 are shown the dependencies of energy transfer probability from Yb to Ho and of concentration quenching of Yb vs. Yb concentration (Ho concentration was 0.3 at.%). One can see, that for Yb concentration of 15 at.% and

more the sensitization efficiency is as high as 0.9. The parameter of the excitation migration across the Yb ions, measured for the linear region of the curve, equals $C_{DD}=3.5x10^{-37}cm^6s^{-1}$.

The time constant of the energy transfer Yb - Ho was measured for various relations of the laser manifolds ($^5I_6$ and $^5I_7$) populations with the purpose to determine the up-conversion parameter (Fig.3).

These results showed, that the up-conversion parameter equals to that of energy transfer process, i.e. $C_{DA}^{up}=1.2x10^{-40}cm^6s^{-1}$. Hence, for the threshold population inversion, which equals 0.15, only 15% of quanta absorbed is lost in the up-conversion channel.

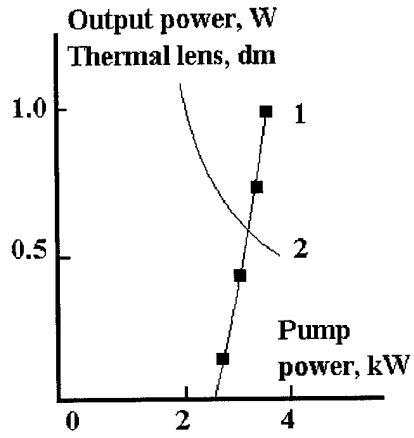

Fig.4. CW output (1) and thermal lens focal length (2) in Yb-Ho laser

2. LASER CHARACTERISTICS

Lasing experiment was carried out using the active element with the 3 mm diameter and 80 mm length. It was mounted in the elliptic Eu-doped fused silica monolith reflector. Xe lamp (discharge gap diameter 7 mm, length 80 mm) was used for the crystal pumping; water solution of the potassium bichromate was used as the cooling agent. The plane mirrors formed the cavity; output mirror reflectivity was equal 96%.

Generation with the wavelength 2.12 and 2.128 μm was observed. In the Fig.4 are shown the dependencies of the output power and focal length of the thermooptical lens in the active element vs. pumping power.

The rate of heat deposition, measured on the generation threshold using the thermooptical lens parameters correspond to the value, predicted from the spectroskopy analysis. In the active element with the diameter 3 mm the thermal gradient was 25°, i.e., three times lower than the maximal possible value. Consequently, the laser can work with the double threshold ratio, providing the output power of 1.5 W per 1 cm of the active element length.

So, for the first time was realized the CW room-temperature generation in the lamp-pumped 2-μm laser. Generation of 1 W was realized for the pump power of 3.6 kW. The processes of energy transfer, creating the operating scheme of the laser, were studied.

REFERENCES

1. T.Y.Fan, G.Huber, R.L.Byer, P.Mitzsherich. Opt.Lett., v.12, p.678 (1987)
2. G.J.Kintz, L.Esterovitz, R.Allen. Electron.Lett., v.23, p.616 (1987)
3. B.M.Antipenko, V.A.Buchencov, A.S.Glebov, T.I.Kiseleva, A.A.Nikitichev, V.A.Pis'mennyi. Opt.Spectrosc. (USSR), v.64, p.772 (1988)
4. A.A.Nikitichev. Sov.J.Quantum Electron., v.18, n.7, p.918 (1988)

Diode-pumped gas-cooled-slab laser performance

C. D. Marshall, L. K. Smith, S. Sutton, M. A. Emanuel,
K. I. Schaffers, S. Mills, S. A. Payne, and W. F. Krupke
Lawrence Livermore National Laboratory, L-493, Livermore, CA 94551

B. H. T. Chai
Center for Research and Education in Optics and Lasers
University of Central Florida, Orlando, FL

The conceptual characteristics of a solid-state laser architecture that promises to provide appropriate characteristics for high average power (MW scale) solid-state lasers, such as those desired for Inertial Fusion Energy (IFE) applications, was first outlined in the early 1980's by J. Emmett, B. Krupke, and J. Trenholme.[1] This design employed a solid-state gain medium that was optically pumped and extracted as well as gas-cooled through the two large apertures of the slab. Experimental work was then pursued several years later, when Albrecht, Sutton and co-workers explored this new strategy for cooling solid-state amplifier-slabs with resistive-electrical surface heaters.[2] Yb:$Sr_5(PO_4)_3F$ (Yb:S-FAP) was discovered and found to be an efficient energy storage gain media and to posess other properties well-suited to a high efficiency rep-rated operation.[3] The emergence of high power diode arrays provided the final ingredient needed to build an efficient gas-cooled-slab (GCS) DPSSL. Orth and co-workers assembled these advances to describe the performance of a MJ scale GCS DPSSL within the laser-driven fusion-energy context.[4] A Yb:S-FAP DPSSL was previously demonstrated that had 12% electrical to optical slope efficiencies without the complications of active cooling.[5] We report here the first results for a gas-cooled-slab laser device.

This laser was constructed to provide enhanced credibility for this type of novel cooling technology and to demonstrate that solid-state lasers can be extended to high repetition rates and average powers in the MW range. The GCS cooling technology is unique, as compared to more conventional transverse water cooled rod or zigzag slab designs, in that the cooling and optical extraction will simultaneously occur across the two large faces of the slab.

The basic structure of a gas cooled laser consists of the gain medium slab over which gas flows across the two large faces of the slab through narrow (~1 mm thick) channels. In addition, a laser diode array is utilized to longitudinally pump the slab through access windows on either side of the slab. A schematic of the system is shown in Figure 1. A laser-diode array with 192 bars with an aperture of 3.5x10 cm was utilized that had a 43% electrical efficiency at 900 nm with a 5.5 nm FWHM including the thermal-induced spectral-chirp within the ms pulse length. The output of this array which was ~20 J in 1 ms at a peak current of 140 A. The diode light was concentrated with a lensing duct down to a 2x2 cm aperture with an 85% efficiency. A f2 relay lens was utilized to transfer the diode energy from the lensing duct to the Yb:S-FAP laser slab in the gas flow channel.

Helium was chosen as the coolant gas due to its uniquely low scatter properties (low index) and good thermal conductivity (for a gas). The gas flow is separated into two broad channels at the bottom of the stack in a diffuser to homogenize the flow as shown in Fig. 1. The flow is then accelerated at 4 atm pressure to Mach 0.1 in a nozzle section specifically designed to prevent flow instabilities and directed to flow across both faces of the laser slab in 1 mm thick by 22 mm wide rectangular channels. For our operating conditions of 80 standard liters of He per minute, the flow was characterized to be well into the turbulent rather than laminar or

intermittent flow regime. Turbulent flow is critical because it minimizes the thermal impedance between the gas and the slab by minimizing the effects of the thermal boundary layer. The flow is then gently decelerated in a tapered channel and exhausted as denoted with an arrow in Fig. 1 through an additional diffuser.

Figure 2 presents the laser output efficiency which was observed to be 51% with respect to the absorbed pump power. When the measured cavity losses of 4.3% are backed out an intrinsic laser slope efficiency of 67% is obtained. Figure 3 shows the results of operating the GCS-DPSSL from 2 to 25 Hz. Up to 50W of optical power was achieved in this configuration. The Yb:S-FAP slab was observed to fracture above 25 Hz. This is not unexpected since the laser was operating a significant fraction of the thermal fracture limit. It is relevant to note that the maximum repetition rate before fracture is 2-5X higher than that proposed for MW scale IFE laser facilities[4] (typically 5-10 Hz). These experiments were also conducted at a thermal flux out of each face of the slab up to 3.2 W/cm^2. This again is several times greater than that required for a large IFE driver operating at moderate rep-rates.

1. J. L. Emmett, W. F. Krupke, J. B. Trenholme, "Future development of high-power solid-state laser systems," Sov. J. Quantum Electron., vol. 13, 1983, pp. 1.
2. S. B. Sutton, G. F. Albrecht, "Optimum performance considerations for a large-aperture average power solid-state laser amplifier," J. Appl. Phys., vol. 69, 1991, pp. 1183, and references therein.
3. L. D. Deloach, S. A. Payne, L. K. Smith, W. L. Kway, W. F. Krupke, "Laser and spectroscopic properties of $Sr_5(PO_4)_3F$:Yb," J. Opt. Soc. Am. B, vol. 11, 1994, pp. 269, and references therein.
4. C. D. Orth, S. A. Payne, W. F. Krupke, "A diode pumped solid state laser driver for inertial fusion energy," Nuclear Fusion, in press 1995, ibid. 1994 ASSL Conference Proceedings.
5. C. D. Marshall, L. K. Smith, R. J. Beach, M. A. Emanuel, K. I. Schaffers, and S. A. Payne, "Diode pumped ytterbium-doped Yb:$Sr_5(PO_4)_3F$ laser performance", submitted to IEEE J. Quantum Electronics, 1995., and ibid. 1995 ASSL Conference Proceedings.

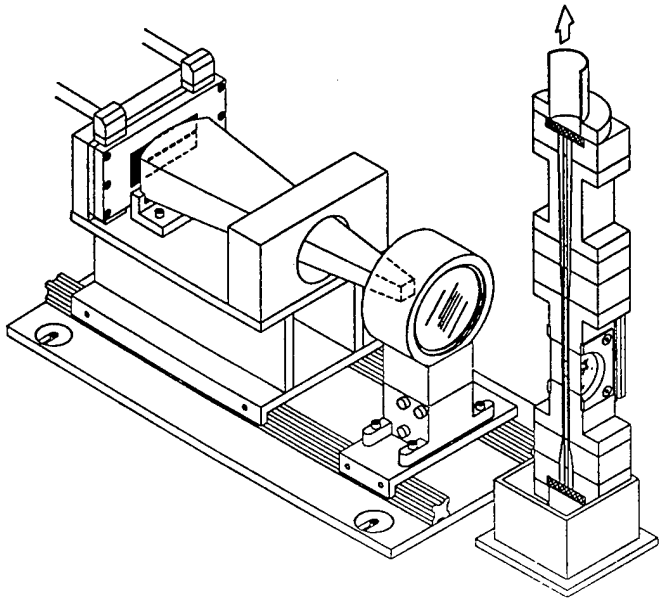

Figure 1. Sketch of diode-pumped gas-cooled slab laser. Cutaway view on the right hand side shows the He-gas coolant-nozzles that accelerate the flow to Mach 0.1 at 4 atm.

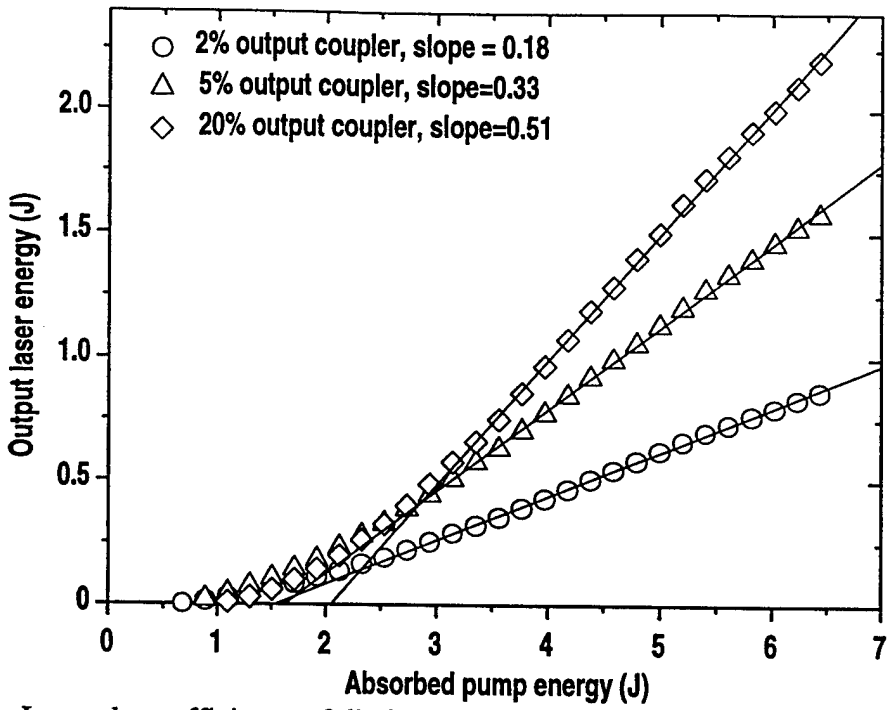

Figure 2. Laser slope efficiency of diode-pumped gas-cooled slab laser for several different output couplers. A 2x2x0.5 cm Yb:S-FAP slab gain element was utilized.

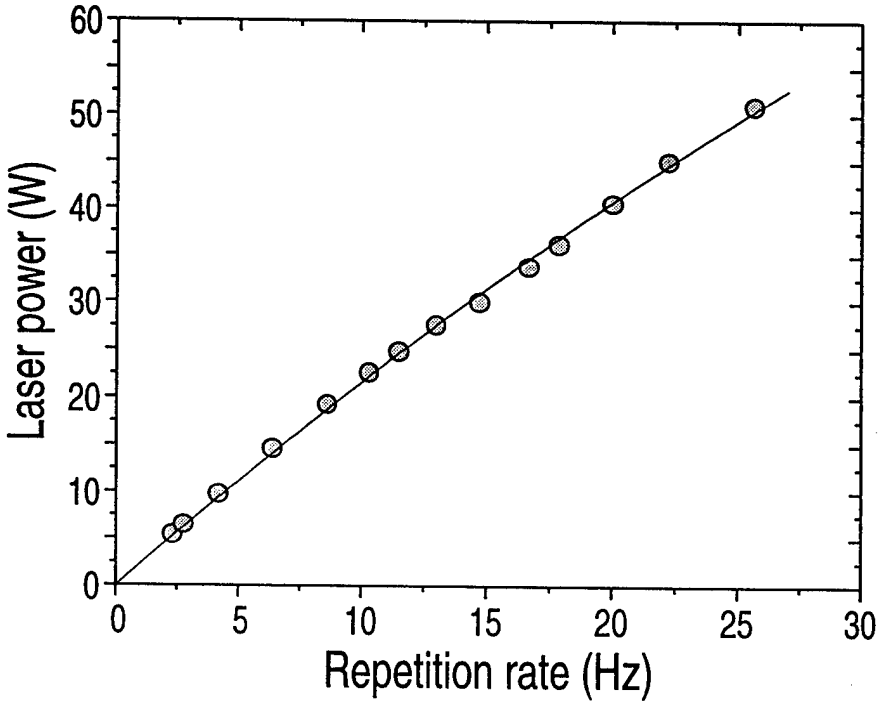

Figure 3. Rep-rated performance of diode-pumped gas-cooled slab laser.

This work was performed under the auspices of the U.S. Department of Energy by Lawrence Livermore National Laboratory under Contract No. W-7405-Eng-48.

Near-Diffraction-Limited Output From a High-Power Diode-Pumped Laser Via Phase Correction With Aspheric Diamond-Turned Optics

Jeffrey J. Kasinski and Ralph L. Burnham

Fibertek, Inc., 510 Herndon Pkwy, Herndon, VA, 22070

Abstract

Output with 1.3X diffraction-limited beam quality in 0.76 J at 60 Hz (46 W) at 1.064 μm from a diode-pumped Nd:YAG rod laser was achieved using a diamond-turned aspheric optic to compensate thermally-induced phase distortion. The output was frequency doubled to 30 W, 2.4X diffraction-limited at 532 nm.

Introduction

High far-field irradiance from diode-pumped lasers necessarily requires high beam quality simultaneously with high pulse energy and average power. Phase conjugation has been shown to provide good beam quality in an injection-seeded diode-pumped laser.[1] This approach, however, imposes some limitations on the laser system design in that generally a narrow bandwidth, double pass geometry, and short pulse are required for satisfactory operation. Other disadvantages include the use of a fluid-filled or high pressure gas cell, lifetime and thermal concerns for higher power scaling.

An alternative method is to directly correct any system phase aberrations with a suitably shaped optic designed to cancel the distortions present.[2,3] In this paper, we present a high-power diode-pumped pulsed Nd:YAG laser in which near-diffraction-limited output is obtained by correcting the thermal aberration of the YAG rods with a diamond-turned CaF_2 aspheric lens. This approach allows for laser designs over a wide range of bandwidths, pulsewidths, and amplifier geometries, and maintains the all-solid-state attribute of diode-pumping in a robust, scalable device.

Experimental

A militarized high-power diode-pumped Nd:YAG rod laser for space-based laser radar applications was constructed in a MOPA configuration, as illustrated in Figure 1. The laser diodes were quasi-cw 5-bar arrays (Spectra Diode Labs) operated at 60 W/bar at 200 μsec at 60 Hz; the oscillator head consisted of a 5 mm diameter rod pumped by 80 bars and each amplifier head contained a 9 mm diameter rod pumped by 160 bars, for a total of 400 bars. An AR coated CaF_2 diamond-turned aspheric lens (Interoptics, Canada) was placed between the two heads of the double pass amplifier chain to correct for the thermal aberration of the amplifier rods. The amplifier output was frequency doubled with a 7 mm long KTP crystal.

Results

The output energy of the diode-pumped MOPA was 0.76 J (46 W) at 1.064 μm with a 25 nsec FWHM at a repetition rate of 60 Hz. The laser unit required 930 W of prime power and the associated cooling unit operated on 240 W of power, resulting in a true wallplug efficiency of 3.9% at 1 μm. The laser was operated with a broad bandwidth with a coherence length measured in the green of 0.9 cm (required for certain imaging applications and greatly simplifying the master oscillator

design). The shot-to-shot pulse energy was stable to ≤ 2%, and the beam pointing jitter was ≤ 19 μrad.

Near-diffraction-limited output was obtained by placing one CaF_2 aspheric compensating lens between the two amp heads in order to correct the higher order thermal distortion in the rod. The resulting output beam quality was 1.3X diffraction-limited, with $\theta d = 2.3$ mm-mrad (86% energy diameter and full angle), as shown in Table 1; (the original uncorrected output was 2.0X diffraction-limited). The near field beam profile was in between a tophat and a Gaussian; the far field profile is given in Figure 2. The profile of the diamond-turned optic, which was designed from interferometric measurements, was a plano-concave shape as shown in Figure 3; the major correction was for induced high-order spherical aberration on the order of 0.4 waves in the center 2.5 mm of the 8 mm diameter beam.

The output was frequency doubled in KTP with a resulting output energy of 0.5 J (30 W) at 532 nm, for a conversion efficiency of 65%; the laser true wallplug efficiency in the green was 2.6%. The beam quality in the green was 2.4X diffraction-limited, with $\theta d =$ 2.06 mm-mrad (Table 1); the far field is shown in Figure 2. The green beam quality is presently limited by thermal aberration in the doubling crystal, as KTP has a noticeable absorption at 532 nm (typically 1-5 %/cm for large crystals, dependent on vendor and process) and a low thermal conductivity; higher absorption crystals were found to produce a degradation in both beam quality and conversion efficiency.

Conclusion

A high-power diode-pumped pulsed Nd:YAG laser with 1.3X diffraction-limited 1 μm output of 0.76 J, 46 W was demonstrated using a diamond-turned aspheric optic to correct the thermally-induced phase distortion of the lasing medium. Also demonstrated was diode-pumped output at 532 nm of 0.5 J, 30 W, and 2.4X diffraction-limited. Our approach was shown to have the advantages of greater simplicity and a wide applicability to laser designs. Work is continuing on scalability to higher power and adaptability to other systems and nonlinear devices. Efforts on future improvement in the green output will include the use of lower absorption crystals such as LBO and applications of phase correction methods to the SHG output.

Acknowledgements

This work was sponsored by the U. S. Airforce, Wright Research and Development Center (WRDC/ELOS) and Phillips Laboratory (PL/LIDA).

References

1. R. J. St. Pierre, H. Injeyan, R. C. Hilyard, M. E. Weber, J. G. Berg, M G. Wickham, C. S. Hoefer, and J. P. Machan, **OSA Proceedings on Advanced Solid-State Lasers, Vol. 15,** (ASSL Conference, Feb. 1993, New Orleans, Louisiana), pp. 2-8.

2. S. C. Tidwell, J. F. Seamans, and D. D. Lowenthal, **OSA Proceedings on Advanced Solid-State Lasers, Vol. 15,** (ASSL Conference, Feb. 1993, New Orleans, Louisiana), pp. 150-153.

3. J. R. Leger, D. Chen, and Z. Wang, **Opt. Lett., Vol. 19,** (1994), pg. 108-110.

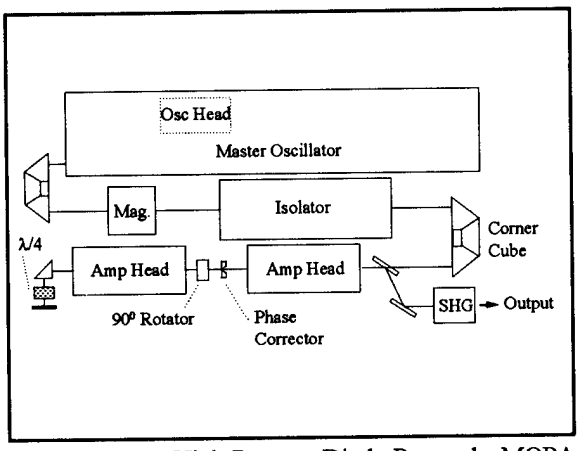

Figure 1. High-Power Diode-Pumped MOPA Schematic. Osc Head = 5 mm Nd:YAG rod pumped by 80 SDL diode bars, Amp Head = 9 mm Nd:YAG rod pumped by 160 diode bars. Total bars = 400 bars at 60 W/bar and 200 μsec. CaF_2 phase corrector placed in double pass amp chain. SHG = KTP frequency doubler.

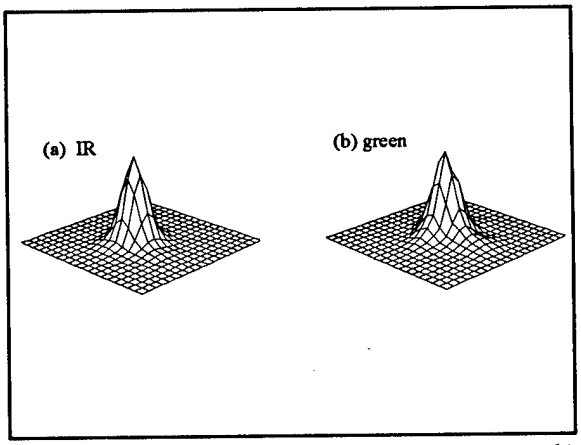

Figure 2. Far Field Profile of Output. (a) = 1.06 μm, (b) = 532 nm.

Table 1. Measured Output Beam Quality.

Output	θd	X diff.-ltd.
1.06 μm, 0.76 J, 46 W	2.30 mm-mrad	1.3
532 nm, 0.5 J, 30 W	2.06 mm-mrad	2.4

θd = the divergence - spot size product, where d is the diameter of 86% of the energy of the beam and θ is the full angle (86% energy diameter) divergence of the beam. X diff.-ltd. = times diffraction limited as compared to the calculated θd of the ideal near field profile with no phase error.

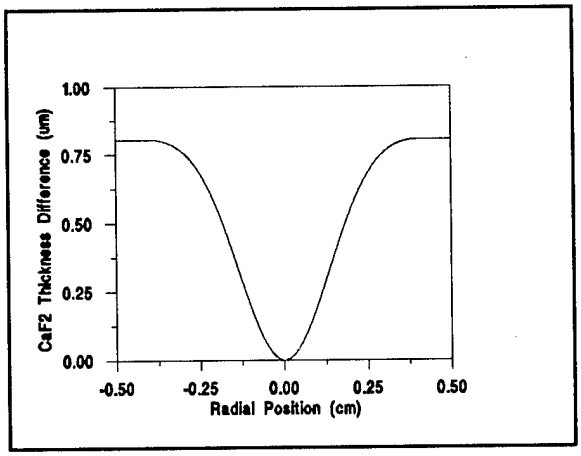

Figure 3. Phase Corrector Profile. Material = CaF_2, nominal diameter = 12 mm, nominal thickness = 3 mm. Shape = plano-concave, concave profile = diamond-turned aspherical.

A NOVEL DESIGN FOR HIGH BRIGHTNESS FIBER LASERS PUMPED BY HIGH POWER DIODES

P. Glas, M. Naumann, I. Reng, A. Schirrmacher and J. Townsend*

Max-Born-Institut für Nichtlineare Optik und Kurzzeitspektroskopie,
Rudower Chausse 6, D-12489 Berlin, Germany
Tel.: +49 30 6392 1448
Fax : +49 30 6392 1459
E-mail : glas@mbi.fta-berlin.de

**University Southampton, Southampton SO17 1BJ, UK*

This work was motivated by ideas to improve existing fiber laser geometries to accomplish a miniaturized high power, short pulse laser source with special emphasis on the realization of a coupled fiber array.
The requirements to reach this goal are the following:
Effective optical pumping with a high power diode laser (array) necessitates both a high numerical aperture and a large entrance area of the fiber. A high brightness source, however, is characterized by a low numerical aperture. Furthermore, a high as possible saturation power is desirable for the laser. The design of the M-profile fiber is plotted schematically in Fig.1.

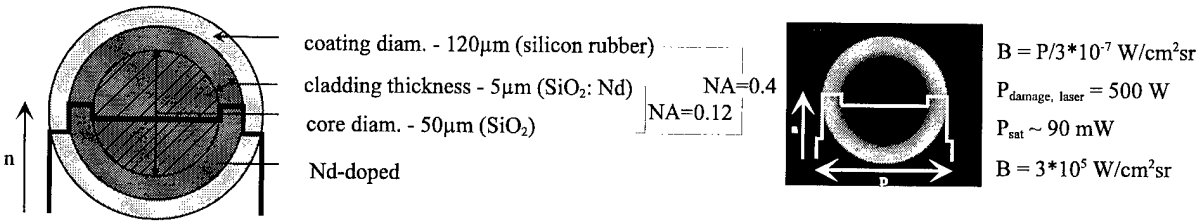

Fig.1 Design of the M-profile fiber

In contrast to conventional fibers, the MPF resembles a tube waveguide being firstly described theoretically by STOLEN /1/ in 1975 as a passive light guide. We have modified the structure to get a lasing one by surrounding the undoped low index core with a concentric ring of high index glass, being doped with Nd_2O_3.
The first properly working fiber laser with a M-refractive index/doping profile was made from phosphate glass doped with Nd_2O_3. Better results were obtained using silica instead of phosphate glass. The silica fiber was manufactured in collaboration with the University of Southampton. The Nd_2O_3 doping concentration is about 1000 ppm. The characteristic parameters of the silica fiber have been determined as follows: small signal gain $g_o \sim 0.006$ cm^{-1}; absorption loss of the pump radiation at λ=804nm $\alpha_{l,p} \sim 0.026$ cm^{-1}, fiber loss for the laser radiation guided in the ring $\alpha_{l,l} \sim 2*10^{-4}$ cm^{-1}. The laser emits at a wavelength of λ=1060nm.

The spectral bandwidth amounts to about 10nm. The laser set-up is conceivably simple. The mirrors are butt-coupled possessing a reflectivity of R_1=99% and R_2=70%, resp. The output mirror is a dichroic one. The radiation of the pump diode is focused with an optics onto the fiber front surface facing a mirror, that is AR-coated at 804nm and HR-coated at 1054nm. The output beam is analysed with a CCD-camera (near-, far field), a spectrograph and a calibrated power meter. Fig.2 shows the distribution of the pump light and the ASE within the silica M-profile fiber. Absorption occurs mainly within the doped ring. Obviously, the structure is not optimised, because a large amount of pump light is contained in the second cladding bordering on the doped ring. This cladding will be thinned or completely removed in the next improved design.
Optimum results concerning the conversion efficiency were obtained for the case

$$NA_{pump} \leq NA_{MPF}^{core,coat}$$

The near and far field pattern of the radiation emitted by the MPF laser are shown in Fig.3a, 3b.

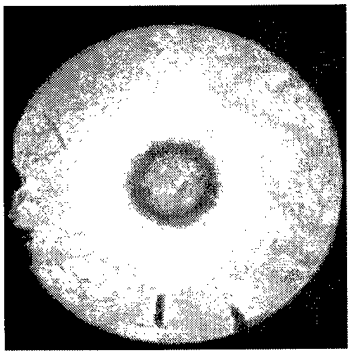

Fig.2a

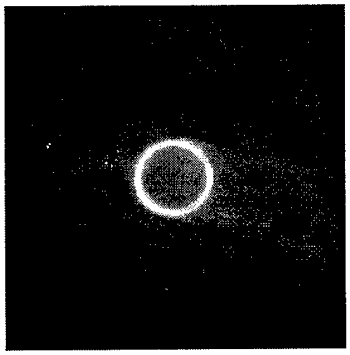

Fig.2b

Fig.2 Near field intensity distribution of the pump radiation at 804nm (Fig.2a) and the fluorescence at 1060nm (Fig.2b)

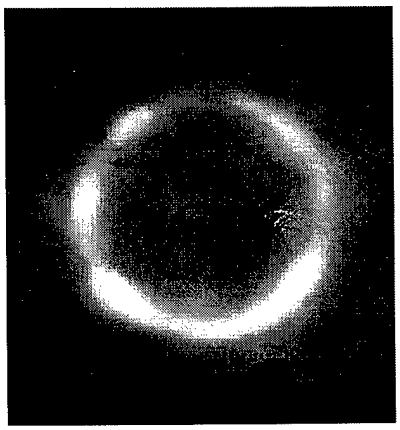

Fig.3a

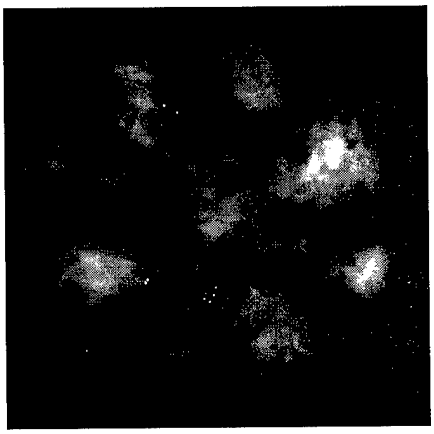

Fig.3b

Fig.3 Near field intensity distribution of the M-fiber laser above threshold (Fig.3a) and the corresponding far field pattern (Fig.3b)

The output power is shown as a function of diode pump power in Fig.4.

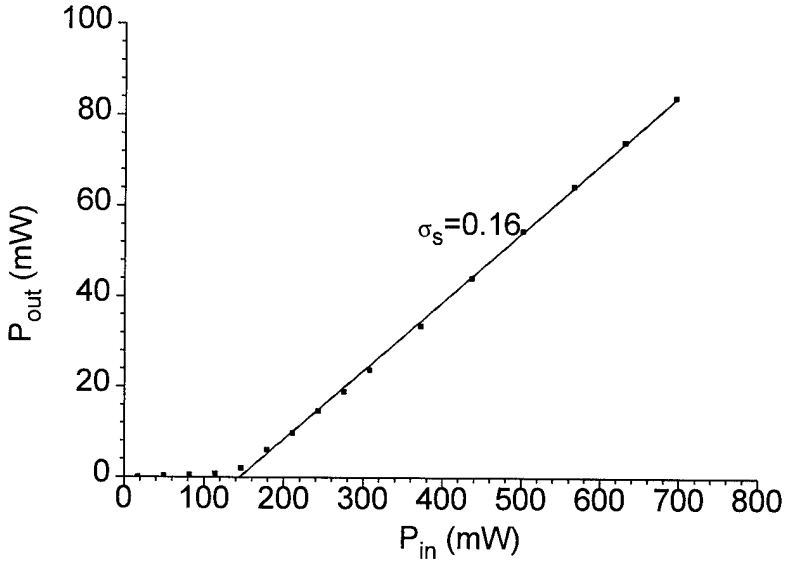

Fig.4 M-fiber laser output power vs. absorbed pump power (R_1=1, R_2=0.7)

In summary, we have proposed and tested a new design for a fiber laser which promises comparable performances related to the double clad fiber. The MPF may serve as a potential candidate for a high power, high brightness fiber laser source. MPFs are light guides with a near-surface guiding structure being advantageous related to fiber coupling, modulation and distributed reflection.

This work is sponsored by BMFT under contract 13N 6363.

The phosphate glass fiber has been manufactured by FIBERWARE GmbH, Berlin, the silica glass fiber by Opt.El. Res. Cent., Univ. Southampton.

References

/1/ R.H.Stolen
Appl. Opt. 14(7)1975, 1533

Distributed-Feedback Ring All-Fiber Laser

D. Yu. Stepanov, J. Canning, I. M. Bassett, and G. J. Cowle

Optical Fibre Technology Centre
Building GO5, Maze Crescent
The University of Sydney
NSW 2006, Australia
tel: +61 (02) 335 0925
fax: +61 (02) 335 0910
e-mail: D.Stepanov@oftc.usyd.edu.au

Using fiber Bragg gratings to provide feedback in fiber lasers permits all-fiber devices, repeatability of parameters, and tunability over wide wavelength range. Bragg gratings directly written into active fiber make it possible to build distributed-feedback (DFB) all-fiber lasers [1]. The use of short pieces of heavily doped fiber, as required for a fiber DFB, has a natural disadvantage of low slope efficiency and large linewidth compared to optimized single-frequency ring fiber lasers [2] using long low doped fiber lengths. However, single-frequency operation of ring lasers reported to date has been achieved mostly with pigtailed non-fiber intracavity elements.

We report here a novel all-fiber ring DFB laser configuration consisting of a grating written into an active fiber, which is pumped through a WDM, and an output coupler (Fig.1). The fiber coupler provides the output coupling as well as additional feedback from the portion of the lasing signal retained in the ring. The reduction in effective resonator losses causes a decrease in the lasing threshold. To determine the efficiency arising from the feedback, the predicted lasing threshold of the $\Lambda/4$-shifted DFB structure within the ring as a function of output coupling is plotted in Figure 2 for a grating strength, $\kappa L = 2\pi/3$, assuming uniform gain along the grating. As can be seen, a considerable reduction in the threshold can be achieved with only half of the

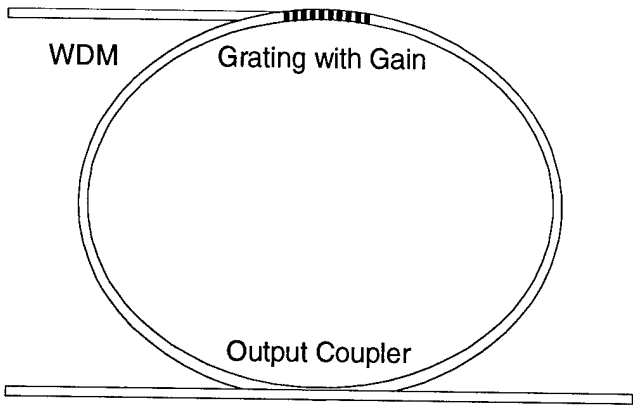

Figure 1: Schematic of distributed-feedback ring laser configuration.

DFB structure output re-injected via the ring. We have considered the $\Lambda/4$-shifted DFB case since it is known to provide lowest thresholds, especially for high grating strengths [1].

Further advantage of the ring configuration arises from self-injection of the lasing mode due to partial coupling of the output from one end of the DFB structure to another end. The feedback through the loop can be considered as an extended cavity, which is a known means of achieving

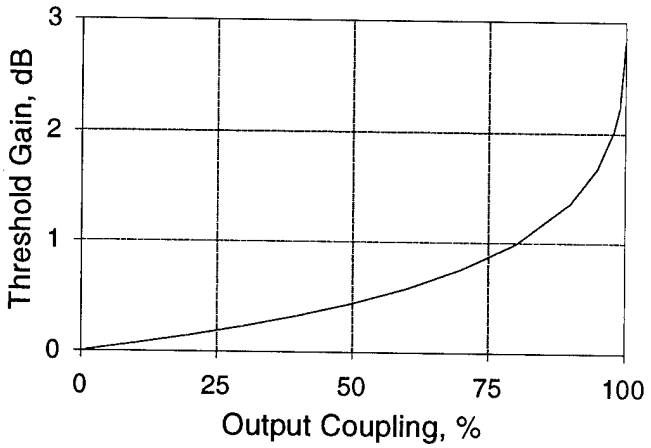

Figure 2: Single-pass gain threshold vs output coupling for grating strength $\kappa L = 2\pi/3$ and uniform gain.

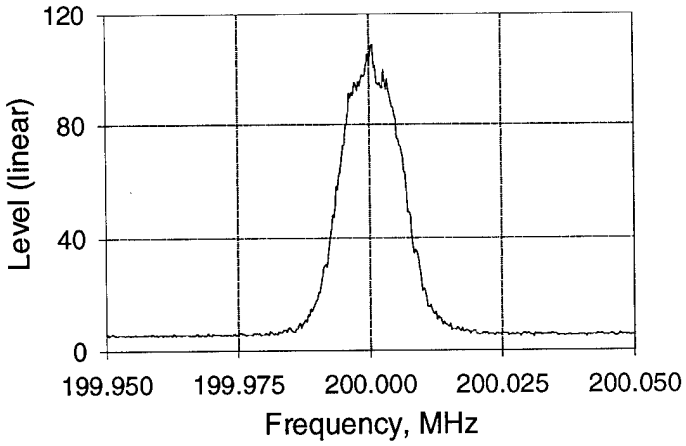

Figure 3: Spectral linewidth of the DFB ring laser.

laser linewidth narrowing [3].

To demonstrate the concept, a 3-cm long grating with R >99%, holographically written with 193 nm light in an Er^{3+}/Yb^{3+}-doped phosphosilicate fiber, was pumped with a 980-nm pump laser diode. When pumping the grating, its center wavelength shifted to longer wavelengths with the simultaneous appearance of a transmission peak within the photonic bandgap that can be attributed to an induced phaseshift due to nonuniformity of pumping along the grating. Splicing the DFB structure within the ring led to lasing at the transmission peak wavelength. Lasing was robustly single longitudinal mode, confirmed using a scanning Fabry-Perot interferometer. The linewidth of the ring DFB laser was measured to be 6.5 kHz (Fig.3) using a conventional self-heterodyne technique with a 20-km delay line. This linewidth is an order of magnitude narrower than has been reported for a conventional DFB [1]. Slope efficiency and accurate threshold measurements are the subject of future work. The obtained results clearly demonstrate the advantages of the ring DFB configuration over the conventional DFB.

[1] J. T. Kringlebotn, J.-L. Archambault, L. Reekie, and D. N. Payne, Opt. Lett., **19**, 2101 (1994).

[2] G. J. Cowle, D. N. Payne, and D. Reid, Electron. Lett., **27**, 229 (1991).

[3] R. Wyatt and W. J. Devlin, Electron. Lett., **19**, 110 (1983).

Friday, February 2, 1996

Short Pulse Lasers II

FE 1:30 pm-3:15 pm
Gold Room

Richard Wallenstein, *Presider*
Kaiserslautern University, Germany

Broadband Tuning of a Femtosecond Neodymium Fiber Laser

M. H. Ober, M. Hofer, R. Hofer, and G. A. Reider
Technische Univerität Wien, Abteilung Quantenelektronik und Lasertechnik
A-1040 Vienna, Austria, Gusshausstr. 27/359-4, Phone : 43-1-58801-3948

G. D. Sucha, M. E. Fermann, and D. Harter
IMRA America Inc., 1044 Woodridge Ave., Ann Arbor, MI-48105, USA

C. A. C. Mendonca and T. H. Chiu
AT&T Bell Laboratories, Crawfords Corner Rd., Holmdel, NJ 07701, USA

The closed outer shell electron configuration of rare earth elements usually entails relatively small spectral gain bandwidths even if strong inhomogeneous broadening is present such as in glass hosts; typical values for the FWHM bandwidth of Nd:glass are $\approx$ 30 nm as compared to 200 nm of Ti:Sapphire. This deficiency of rare earth doped glasses is partially compensated by the fact that silicate glasses lend themselves to easy fabrication of high quality low loss active optical wave guides [1]. The enormous gain interaction length provided by active glass fibers produces considerable gain, sufficient for laser operation even from the very wings of the spectrum. In fact, tuning of a cw Nd-glass fiber laser was reported [2] soon after the realization of doped fibers.

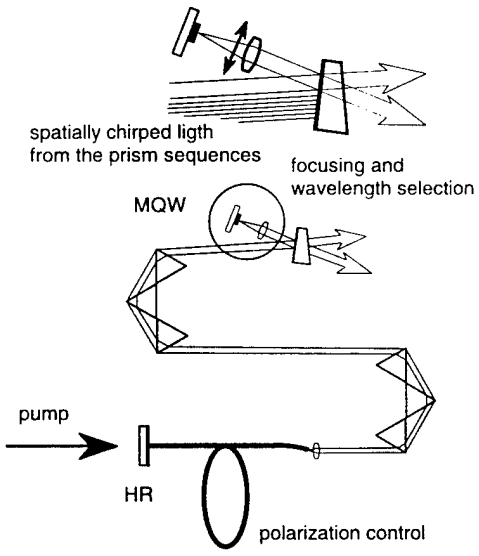

Figure 1: cavity design for a broadband tunable Nd-fiber laser. The insert shows the details of the wavelength selection via the focusing lens.

In the present paper, we report femtosecond mode-locked operation of a Nd^{3+} doped fiber laser from 1054 to 1128 nm, delivering pulses of 300-400 fs duration at a repetition rate of 70 MHz and with an output power of 8 mW. Apart from the extraordinary width of the tuning range, it should be noted that it is precisely adjoining the tuning range of commercial Ti:Sapphire lasers. Given the low pump power requirements of 250 mW, which can be provided even by a moderate size semiconductor laser, this laser may be a very attractive complement to the Ti:Sapphire laser for spectroscopic studies.

Since the laser presented in this paper is

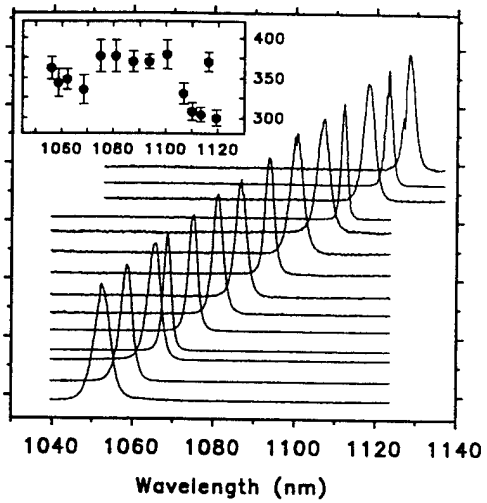

Figure 2: Ouput spectra from the laser as a function of wavelength; the insert shows the corresponding pulse durations.

to be operated far off the main emission peak of the gain spectrum (Fig. 3), our efforts had to focus on an optimized design of the multi-quantum-well (MQW) saturable absorber unit. It consists of a carefully designed Bragg mirror on top of which the actual MQW is grown. The semiconductor saturable absorber design follows the rules given by Keller [3]. The low-power reflectivity had a bandwidth of $\approx$ 95 nm with a peak of $\approx$ 80 % at 1080 nm (Fig. 3).

The basic setup of the laser is shown in Fig. 1. Tuning was achieved by moving the lens laterally with respect to the resonator axis. Since the mode is spatially chirped in this section of the cavity, the position of the lens aperture effectively determines the part of the laser spectrum. In order to provide sufficient spatial chirp we choose a prism separation of 87 cm. Thus the overall dispersion was strongly negative (~ -44000 fs^2); this had, however, no effect on the achievable pulse width [4]. The laser was self-starting over the full tuning range. In cw operation (with the saturable absorber replaced by a high reflector), the tuning range of the laser was as wide as 80 nm (see Fig. 3), which is somewhat larger than the value for mode-locked operation (75 nm). While the tuning range is

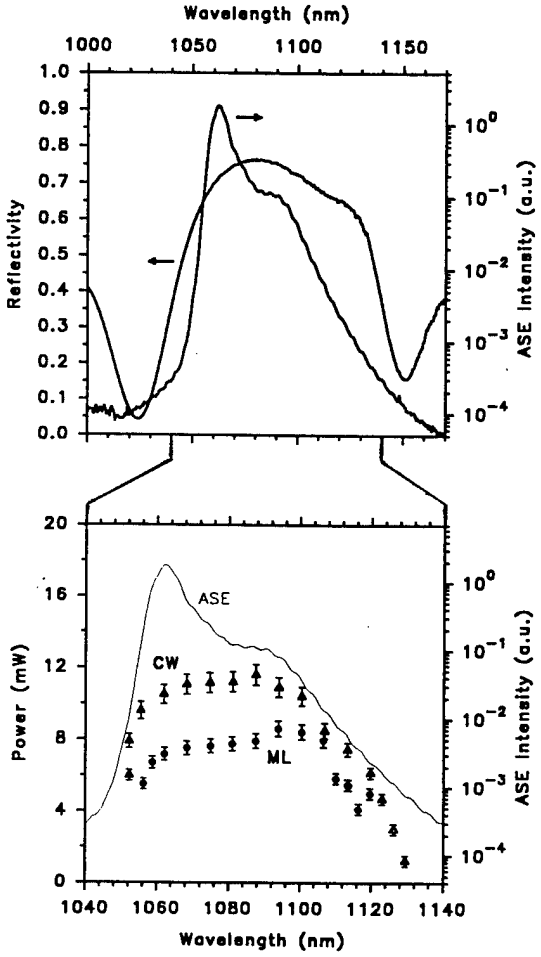

Figure 3: *Top:* low-power reflectivity of the MQW and spectrum the amplified spontaneous emission. *Bottom:* output power *vs* wavelength; (• mode-locked; △ free running laser).

obviously limited by the gain spectrum (see Fig. 3), one should note that at the cut-off of mode-locked operation the corresponding

ASE has dropped to as little as 10^{-3} of its peak value. Pulse widths varied between 300 and 400 fs as displayed in Fig. 2 (insert) when tuning over the 75 nm tuning range. From the time-bandwidth products which varied between 0.29 and 0.36 we conclude the pulses to be nearly bandwidth limited. The output power (7-8 mW) was flat over most of the tuning range with maximum values around 1.1 μm. Similar to previously reported results [4, 5, 6], we observed a slight tendency to pulse bunching and multiple pulsing, however, this could be suppressed by a proper alignment of the focusing lens and a careful setting of the cavity loss [5].

In conclusion we have demonstrated tuning of a femtosecond Nd:fiber laser over a range more than twice as large as the FWHM gain bandwidth. Femtosecond pulses were readily generated over a wavelength range from 1054 nm to 1128 nm. Optimal matching of the reflection characteristics and the band gap energy of a MQW semiconductor absorber to the spectral characteristics of the Nd fiber allows 75 nm tuning of the mode-locked fiber laser. The pulse widths routinely achieved are 300-400 femtoseconds over the full tuning range.

This work was supported in part by the Fonds zur Förderung der wissenschaftlichen Forschung in Österreich, grant No. P10515-PHY and the Österreichische Nationalbank, grant No. P5530.

References

[1] S. B. Poole, D. N. Payne, and M. E. Fermann, Electron. Lett., **21**, 737 (1985).

[2] L. Reekie, R. J. Mears, S. B. Poole, and D. N. Payne, J. Light. Tech. **LT-4**, 956, (1986)

[3] U. Keller, Appl. Phys. B **58**, 347 (1994).

[4] M. H. Ober, M. Hofer, U. Keller, and T. H. Chiu, Opt. Lett., **18**, 1533, (1993).

[5] B. C. Barnett, L. Rahman, M. N. Islam, Y. C. Chen, P. Bhattacharya, W. Riha, K. V. Reddy, A. T. Howe, K. A. Stair, H. Iwamura, S. R. Freberg and T. Mukai, Opt. Lett. **20**, 471 (1995).

[6] A. B. Grudinin, D. J. Richardson and N. D. Payne, Electron. Lett., **28**, 67 (1992).

Femtosecond mode-locked Yb:YAG lasers

C. Hönninger, F. X. Kärtner, G. Zhang, and U. Keller
Ultrafast Laser Physics Laboratory, Institute of Quantum Electronics, Swiss Federal Institute of Technology, ETH Hönggerberg, HPT, CH-8093 Zürich, Switzerland
Tel: [011] 41 1 633 21 81, Fax: [011] 41 1 633 10 59, e-mail: clemens@iqe.phys.ethz.ch

A. Giesen
Institut für Strahlwerkzeuge, Universität Stuttgart, Pfaffenwaldring 43,
D-70569 Stuttgart, Germany

We have passively modelocked a Yb:YAG for the first time, generating pulses as short as 540 fs with typical average powers of 150 mW. We achieved modelocking at either 1.03 μm or 1.05 μm, controlled by the design of the bandgap and antiresonance wavelength of the antiresonant Fabry-Perot saturable absorber (A-FPSA [1, 2]). Without dispersion compensation in the laser, we obtained pulses as short as 1.7 ps. Previously, only active modelocking in Yb:YAG has been demonstrated with a pulse duration of 80 ps [3].

Yb:YAG is interesting as a high power diode-pumped laser source due to its low thermal loading and its wide absorption band at 940 nm [4, 5], and a power-scalable concept using these features has been recently demonstrated [6]. Yb:YAG can also support femtosecond pulses due to its broad emission spectrum. We have previously demonstrated simple, passive femtosecond modelocking using the A-FPSA and have shown that power-scalability of this device is also feasible by adjusting both the incident laser spot size on the absorber and the top reflectivity with respect to the intracavity power [7]. Thermal problems in the A-FPSA device could also be addressed by face cooling similar to the thin disc concept [6]. Therefore an A-FPSA mode-locked Yb:YAG laser is a potentially promising approach to ultimately obtain high peak powers with high average power.

In our experiments, we used two different design regimes of the A-FPSA, a low-finesse [8] and high-finesse [1] A-FPSA (Fig. 1). The low-finesse design is scaled such that only the Fresnel reflection from the semiconductor / air interface as its top reflector is necessary, resulting in simpler fabrication. Both saturable absorbers provided a maximum modulation depth of ≈ 0.5%, however, the saturation fluence of the high-finesse A-FPSA is 4.5 mJ/cm^2 and of the low-finesse A-FPSA 120 μJ/cm^2 (i.e. 40 times smaller). This means that with the limited available pump power in our experiment, we can more easily saturate the low-finesse device and benefit from its maximum modulation depth. In contrast, if the device is operated far below saturation the lower modulation depth results in longer pulses or even poor modelocking. The saturation intensity was adjusted to prevent self-Q-switching [9] and is determined by both the top reflector (≈95% for the high-finesse and 30% for the low-finesse) and the carrier lifetime [7], which was measured to be 3.8 ps for the high-finesse and 6 ps for the low-finesse A-FPSA. Both saturable absorbers also exhibit a bitemporal impulse response with a fast component of ≈200 fs [2].

Figure 2 shows the schematic of the laser cavity. The spot diameter on the A-FPSA is 24 μm for the high-finesse device or 160 μm for the low-finesse device, adjusting for their different saturation fluence given the available intracavity power. Without dispersion compensation, we obtained pulses as short as 1.7 ps at 1.03 μm (Fig. 3) at 110 MHz repetition rate with average powers between 125 mW to 190 mW at an absorbed pump power of 1.2 W using the high-finesse A-FPSA. Shorter soliton-like pulses are obtained with dispersion compensation (Fig. 2) [10]. Using the low-finesse A-FPSA we obtained soliton-like pulses of 570 fs at 1.05 μm at 80 MHz repetition rate and an output power of 170 mW at 900 mW absorbed pump power (Fig. 4). We also designed a thin absorber to favor 1.03 μm over 1.05 μm (Fig. 1a), and achieved self-starting mode-locked pulses of 540 fs duration (Fig. 5) and 100 mW average power at an absorbed pump power of 750 mW. With the high-finesse A-FPSA, we obtained subpicosecond pulses of 900 fs duration at 1.05 μm and output powers of 150 mW at 1 W absorbed pump power. In all cases the time-bandwidth-product was typically 0.35 indicating that the pulses were nearly transform-limited assuming a sech^2 pulse shape. The available intracavity power was insufficient to more strongly bleach the high-finesse A-FPSA, reducing the achievable modulation depth and therefore increasing the pulse duration. Generally, a higher modulation depth should allow to use a broader fraction of the emission bandwidth and thus lead to shorter pulse generation.

1. U. Keller, D. A. B. Miller, G. D. Boyd, T. H. Chiu, J. F. Ferguson, M. T. Asom, *Optics Letters* **17**, 505 (1992)
2. U. Keller, *Applied Phys. B* **58**, 347 (1994)
3. S. R. Henion, P. A. Schulz, CLEO 1992, paper CThQ2 p. 540
4. P. Lacovara, H. K. Choi, C. A. Wang, R. L. Aggarwal, T. Y. Fan, *Optics Letters* **16**, 1089 (1991)
5. T. Y. Fan, *IEEE Journal of Quantum Electronics* **29**, 1457 (1993)
6. A. Giesen, H. Hügel, A. Voss, K. Wittig, U. Brauch, H. Opower, *Applied Phys. B* **58**, 363 (1994)
7. L. R. Brovelli, U. Keller, T. H. Chiu, *Journal of the Optical Society of America B* **12**, 311 (1995)
8. I. D. Jung, L. R. Brovelli, M. Kamp, U. Keller, M. Moser, *Optics Letters* **20**, 1559 (1995)
9. F. X. Kärtner, L. R. Brovelli, D. Kopf, M. Kamp, I. Calasso, U. Keller, *Optical Engineering* **34**, 2024 (1995)
10. R. L. Fork, O. E. Martinez, J. P. Gordon, *Optics Letters* **9**, 150 (1984)

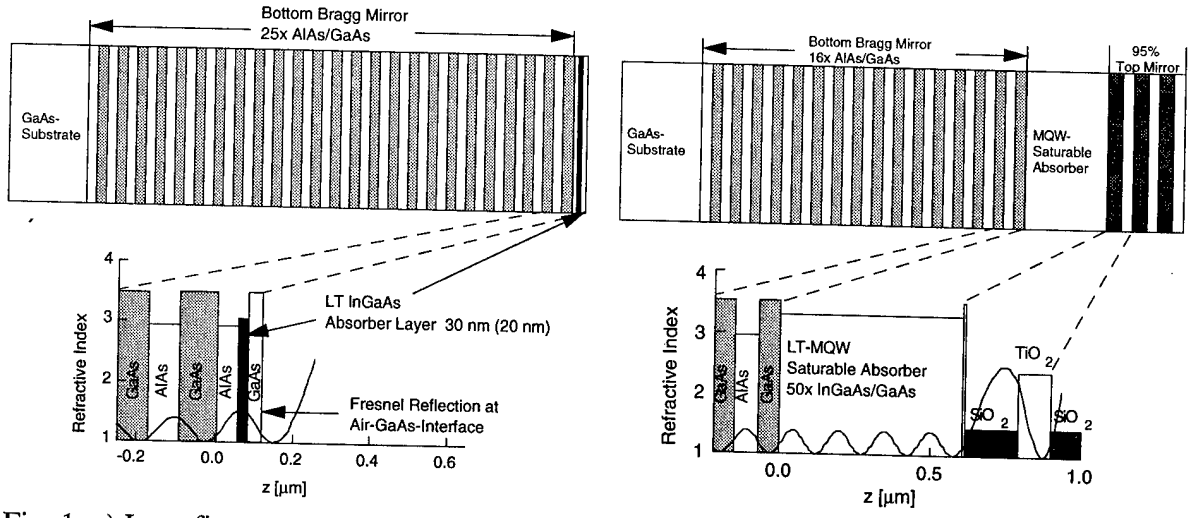

Fig. 1: a) Low-finesse and b) High-finesse A-FPSA with refractive index profile and standing-wave intensity distribution.

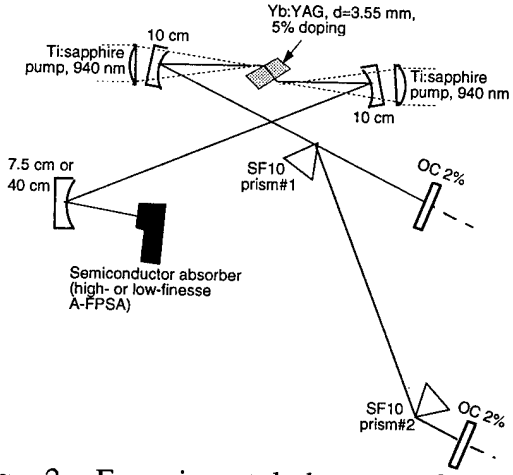

Fig. 2: Experimental layout of the modelocked Yb:YAG laser.

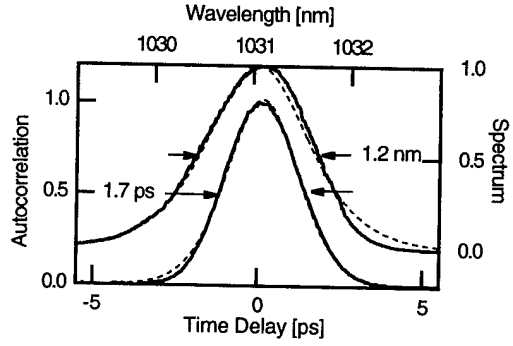

Fig. 3: Mode-locked pulse obtained without dispersion compensation and using the high-finesse A-FPSA ($\Delta\nu\,\Delta\tau \approx 0.6$ to 1.3).

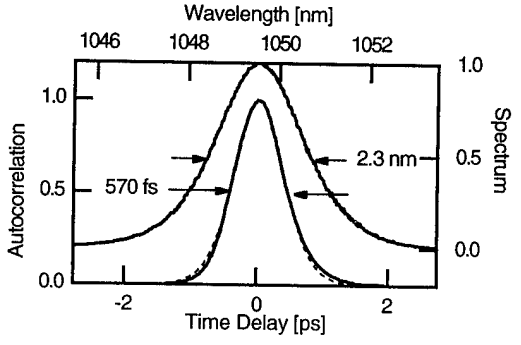

Fig. 4: Pulse obtained with dispersion compensation and focusing onto the 30 nm thin low-finesse A-FPSA ($\Delta\nu\,\Delta\tau = 0.36$).

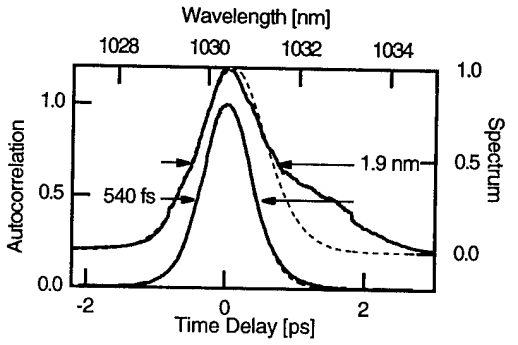

Fig. 5: Pulse obtained with dispersion compensation and the low-finesse A-FPSA designed for 1.03 µm.

Femtosecond Visible Kerr Lens Mode-Locked Pr:YLF Laser

J. M. Sutherland, P. M. W. French and J. R. Taylor

Femtosecond Optics Group, Physics Department,
Imperial College, London SW7 2BZ, U.K.
Tel. : 44-171-594 7706 Fax. : 44-171-589 9463 email: paul.french@ic.ac.uk

B. H. T. Chai

Center for Research in Electro-Optics and Lasers (CREOL)
University of Central Florida, 12424 Research Parkway, Orlando,
FL 32826, United States of America

Solid-state lasers operating at room temperature provide a convenient source of c.w. radiation. Over the past few years considerable materials research has been undertaken in order to extend the wavelength versatility and efficiency of room temperature solid-state lasers and, to date, the majority have been operated in the near infra-red region of the spectrum. Limited spectral coverage in the visible is provided by the recently demonstrated c.w. Pr:YLF laser [1]. Previously pulsed Pr^{3+}:YLF lasers had been demonstrated [2 3]. A visible c.w. laser has potential applications including display technology, printing and spectroscopic diagnostics. In our previous work [4], we demonstrated the operation of a c.w. Pr:YLF laser at 607 nm and 639 nm simultaneously. We now report simultaneous operation of the Pr:YLF laser at 522 nm and 604 nm. Thus, a blue pump laser at 476 nm, together with the outputs in the green and red, could constitute a compact "RGB" laser system.

For many applications, including two photon microscopy and low coherence interferometry, it is desirable to generate pulses and a mode-locked Pr:YLF laser could be an attractive replacement for synchronously pumped dye lasers in many applications. We previously demonstrated a Kerr Lens Mode-locked (KLM) Pr:YLF laser which was initiated using either a saturable absorber dye or cadmium selenide colloidally coloured glass filter [4]. This yielded picosecond pulses at 607 nm and 639 nm, the shortest being of 8 - 10 ps duration. We also demonstrated self-starting KLM operation at 607 nm, following the prescriptions of Cerullo et al. [5] For these transitions, the spectral linewidths precluded the generation of pulses shorter than ~ 1 ps. We have recently observed what we believe to be 14 new laser transitions in Pr:YLF, pumping c.w. with 476 nm radiation. Two of these transitions have sufficiently broad linewidths to support subpicosecond pulses. We have now successfully generated femtosecond pulses for the first time from a visible solid-state laser.

Initially we investigated c.w. laser action in a cavity similar to those described in reference [4]. The Pr^{3+}:YLF crystal was grown at the Center for Research in Electro-Optics and Lasers (CREOL) and had an active doping of 0.8 atomic %. It was cut into a 9 mm long rod of 6 mm diameter and had Brewster angled faces polished on each end such that the electric field vector was perpendicular to the crystal c axis, initially for examination of the $^3P_0$ - $^3F_2$ and $^3P_0$ - $^3H_6$ transitions at 639 nm and 607 nm respectively. For investigations with the $^3P_1$ - $^3H_5$ transition at 522 nm a similarly sized rod was used but cut with the c axis parallel to the electric field vector. The rod was clad in indium and held in a water cooled copper jacket, although for the average pump powers required for mode locked laser action a compact thermo-electric (Peltier) cooler directly contacted to the copper housing of the rod is adequate. For each crystal

orientation, we used an optical spectrum analyser to study the various laser transitions. An argon ion laser provided a pump power of up to 3.6 W at 476 nm, of which at maximum 1.7W was absorbed in the crystal. Throughout the work, 476 nm pumping was employed although the 457 nm, 465 nm and 472 nm lines of the Ar^+ laser can also be used, as well as other pumping schemes. The pump radiation was focused using a 10 cm focal length lens L, through a 10 cm radius of curvature folding mirror into the active medium. Figure 1 shows the fluorescence profile of the Pr:YLF crystal (recorded for Ellc) and the various laser transitions observed. All of the transitions have been identified, using the data from reference [6], except the transitions at 699 nm and 722 nm. Laser action was achieved for each of these transitions with thresholds varying from 40 mW absorbed pump power for the 639 nm transition to 370 mW for the 522 nm transition. Typical slope efficiencies ranged from 5 - 10 % for unoptimised cavities with output couplers of ~ 1 %. Note that the transitions at 613 nm, 620 nm and 721 nm have linewidths of ~ 1 nm, 0.5 nm and 0.5 nm respectively, sufficient to support subpicosecond pulses.

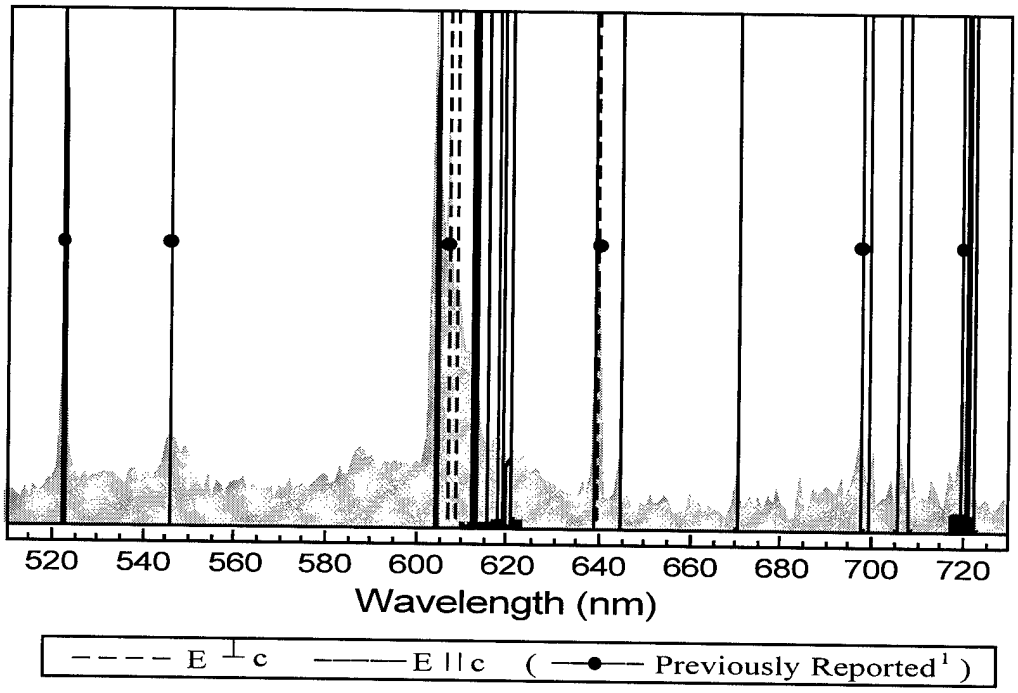

Figure 1. Schematic of laser emission and fluorescence profile of Pr:YLF laser

In order to demonstrate an RGB laser, the crystal was orientated Ellc and laser action was obtained simultaneously at 522 nm and 604 nm. The cavity employed all high reflectors which typically resulted in output powers of ~ 10 mW per beam for a total absorbed pump power of 1.6 W. An optimised resonator, together with a more absorbing Pr:YLF laser rod, should yield considerably higher output powers with lower laser thresholds. We note that if this pump power could be obtained from an all-solid-state diode-pumped laser, perhaps a frequency-doubled Cr:LiSAF laser, then a compact RGB laser system could be demonstrated.

Femtosecond pulse generation was achieved at 613 nm using KLM in the symmetrical cavity shown in Figure 2. The rod was pumped from both sides and a maximum of 1.5 W pump power was absorbed. KLM was initiated by simply tapping an end mirror. The laser provided stable operation for a few minutes at a time but was easily perturbed due to the extremely critical alignment. The two intracavity F2 glass prisms provided compensation of the intracavity GVD. Transform-limited pulses as short as 400 fs were obtained from the 613 nm transition. The

bandwidth of these pulses is as much as can be supported by this transition. Figures 3 and 4 show the autocorrelation and spectral profile of these pulses.

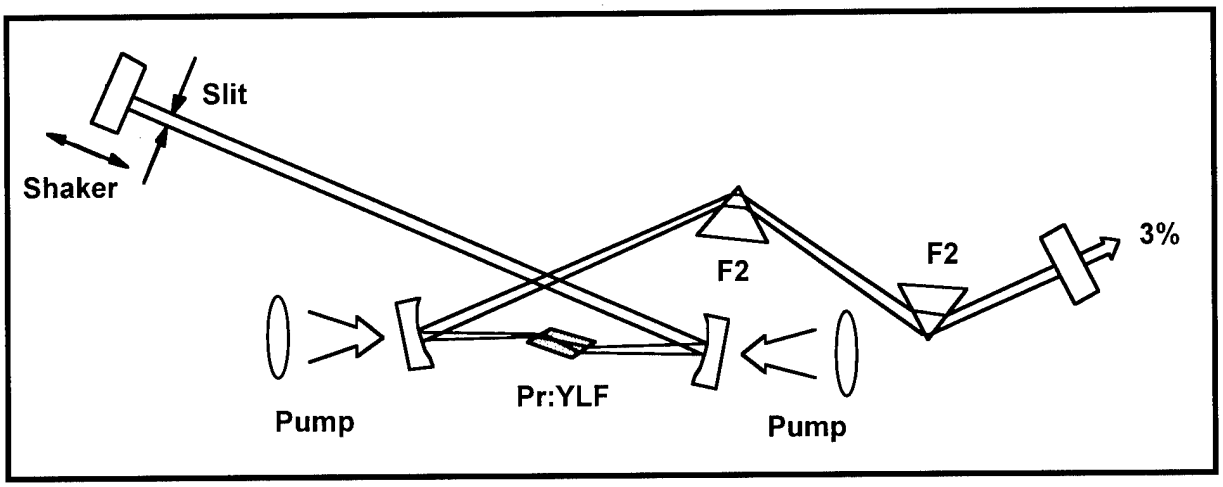

Figure 2. Cavity configuration for the femtosecond KLM Pr:YLF laser operating at 613 nm

In conclusion, we have demonstrated 14 new laser transitions in a c.w. Pr:YLF laser pumped at 476 nm. We have demonstrated simultaneously laser action in the green and red using a blue pump laser and we have achieved femtosecond pulse generation from a visible solid-state laser for the first time. This laser may find application in display and printing technologies and can certainly be used in place of some ultrafast dye lasers. Clearly the spectral coverage is limited, compared to dye lasers, and it is hoped that this will be improved by doping the Pr^{3+} into alternative laser hosts. This is the subject of active investigation.

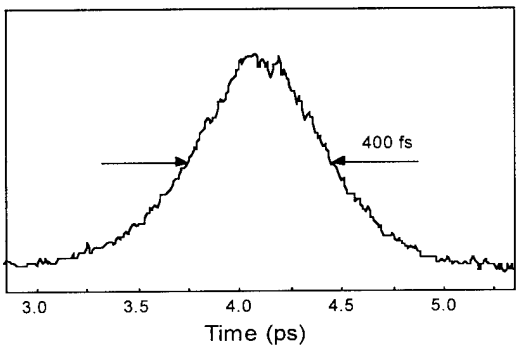

Figure 3. Autocorrelation trace of pulses from KLM Pr:YLF laser at 613 nm

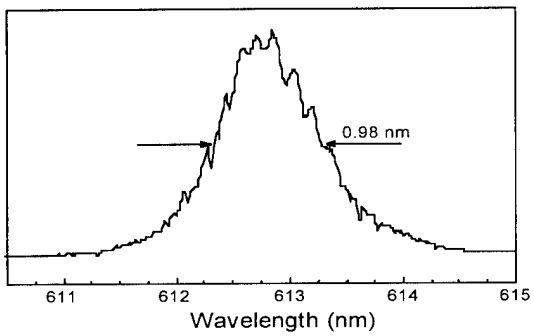

Figure 4. Spectral profile of pulses from KLM Pr:YLF laser

References

[1] T. Sandrock, T. Danger, E. Heumann, G. Huber and B. H. T. Chai, *Appl. Phys B*, **58**, 149 (1994)
[2] L. Esterowitz, R. Allen, M. Kruer, F. Bartoli, L. S. Goldberg, H. P. Jenssen, A. Linz, and V. O. Nicolai, *J. Appl. Phys.* **48**, 650 (1977).
[3] A. A. Kaminskii, *Sov. Phys. Dokl.* **28**, 668 (1983).
[4] S. Ruan, J. M. Sutherland, P. M. W. French, J. R. Taylor and B. H. T. Chai, *Opt. Lett*, **20**, 1041 (1995)
[5] G. Cerullo, S. De Silvestri and V. Magni, *Opt. Lett.* **19**, 1040 (1994)
[6] J. Adam et. al. *J. Luminescence*, **33**, 391 (1985)

Diode-pumped passively mode-locked 1.3 μm Nd:YVO_4 and Nd:YLF lasers using semiconductor saturable absorbers

R. Fluck, K. J. Weingarten, G. Zhang and U. Keller
Ultrafast Laser Physics Laboratory, Institute of Quantum Electronics, Swiss Federal Institute of Technology, ETH Hönggerberg, HPT, CH-8093 Zürich, Switzerland,
Tel: [011] 41 1 633 68 15, Fax: [011] 41 1 633 10 59, e-mail: rfluck@iqe.phys.ethz.ch,
WWW: http://iqe.ethz.ch/~kopf/ULP.html

M. Moser
Paul Scherrer Institute, CH-8048 Zurich, Switzerland

Motivated by the need for simple and compact picosecond sources at 1.3 μm for applications such as telecommunications and fiber-sensing, we have demonstrated self-starting passively mode-locked Nd:YLF at 1313 nm and 1321 nm and Nd:YVO_4 at 1342 nm using semiconductor saturable absorbers. Pulses as short as 4.6 ps durations were achieved with Nd:YVO_4 and 5.7 ps with Nd:YLF. Passive modelocking was achieved using either a high-finesse [1] or low-finesse [2] anti-resonant Fabry-Perot saturable absorber (A-FPSA) design, with lattice-mismatched InGaAs (≈40% In concentration) to provide the 1.3 μm saturable absorber. This is the first demonstration of passive modelocking with an A-FPSA device at 1.3 μm.

Modelocking at 1.3 μm in Nd:YLF has been previously achieved both actively [3] and passively in a coupled cavity system (APM) [4]. Nd:YVO_4 has been recently mode-locked at 1 μm [5] but has not been mode-locked at 1.3 μm to our knowledge. Nd:YAG is another possible candidate for mode-locking at 1.3 μm but usually lases at two closely spaced lines there, making clean modelocking difficult.

Figure 1 shows a schematic view of the laser cavity. We used two 1-W, 100 μm stripe-width pump diodes spatially coupled parallel to their fast axes [6]. Using two high-brightness diodes allows for relatively high end-pumped gains, which improves the passive modelocking build-up time and helps prevent self-Q-switching. This is a concern due to the low gain cross-sections of typical 1.3 μm laser transitions. The spot size on the high-finesse A-FPSA was set to approximately 30 μm radius with a 7.5 cm curved mirror, or approximately 100 μm radius with a 30 cm curved mirror for the low-finesse A-FPSA. The output coupler was at a fold mirror, resulting in two output beams.

We initially mode-locked Nd:YLF at both 1313 nm and 1321 nm using a high-finesse (top reflector ≈94%) A-FPSA. We achieved a pulsewidth of 5.7 ps (Fig. 2a) at an average power of 130 mW (one beam) and a repetition rate of 98 MHz (peak power ≈230 W). However, clean pulses were only achieved after we purged the laser cavity with dry nitrogen to eliminate spurious water absorption lines which overlapped the laser spectrum. This extra absorption was unexpectedly strong enough to modulate the mode-locked spectrum, resulting in pulses that were longer and with significant pedestals or wings. The observed spectral holes

corresponded to published values for water vapor absorption [7]. When purged with nitrogen, the spectral modulation disappeared and the pulses were short and clean.

We chose Nd:YVO_4 as a promising alternative crystal for passive modelocking at 1.3 μm due to its large stimulated emission cross section and its relatively short upper state lifetime. Additionally, its large absorption coefficient at 808 nm is attractive for diode-pumping and further increases the small-signal gain when end-pumped. We modelocked this laser with a low-finesse saturable absorber, which uses just the semiconductor-air interface as a top reflector (≈30%). This design is simpler to fabricate (no dielectric coating on top) and has a larger nonlinear modulation depth, at a given available intracavity power, due to its smaller saturation fluence. This allows us to more fully saturate the device and achieve a larger modulation depth then a high-finesse A-FPSA which is not well-saturated by the given available intracavity power. However these specific devices also have a higher insertion loss (several percent). We achieved 4.6 ps pulses (Fig. 2b) with an average power of 50 mW (one beam) at 93 MHz and a corresponding peak power of ≈120 W. This laser did not require N_2 purging for clean pulseshapes, possibly due to the larger modulation depth which overcame the residual water absorption lines in the spectrum.

Figure 3 shows the design of both saturable absorbers. To achieve saturable absorption at 1.3 μm, the Indium concentration must be approximately 40%, which results in a significant lattice mismatch to the GaAs substrate. Low-temperature growth partially relieves this mismatch but these devices still exhibit more defects than a 1 μm A-FPSA. However we were able to achieve devices with good saturable absorption properties and nonsaturable (fixed) losses of a few percent. The pump-probe measured nonlinear reflectivity of both samples indicate a carrier lifetime of 9.5 ps for the high-finesse and 4.1 ps for the low-finesse A-FPSA (Fig. 4).

1. U. Keller, D. A. B. Miller, G. D. Boyd, T. H. Chiu, J. F. Ferguson, M. T. Asom, *Optics Letters* **17**, 505 (1992)
2. I. D. Jung, L. R. Brovelli, M. Kamp, U. Keller, M. Moser, *Optics Letters* **20**, 1559 (1995)
3. F. Zhou, G. P. A. Malcolm, A. I. Ferguson, *Optics Letters* **16**, 1101 (1991)
4. D. A. Armstrong, A. Robertson, N. Langford, A. I. Ferguson, CLEO 1995, paper CThM2 p. 344
5. J. D. Kafka, CLEO 1995, paper CThH3 p. 286
6. T. Y. Fan, A. Sanchez, *IEEE J.Quantum Electron.* **26**, 311 (1990)
7. HITRAN program for atmospheric transmission, National Climatic Data Center of NOAA

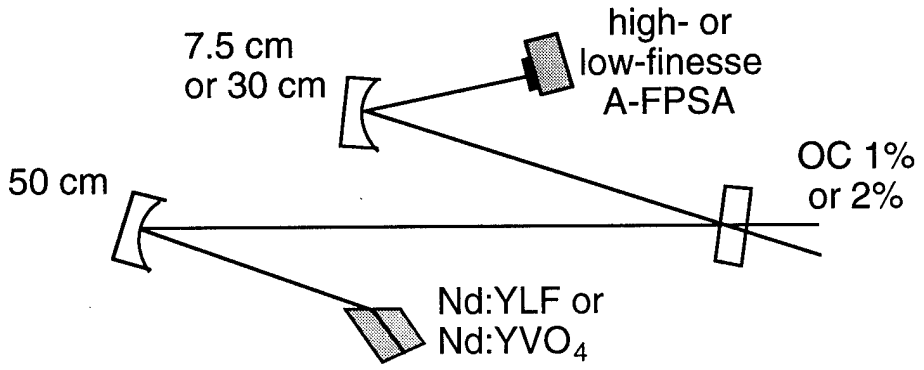

Fig. 1: Experimental laser set-up for the mode-locked Nd:YLF and Nd:YVO_4 laser.

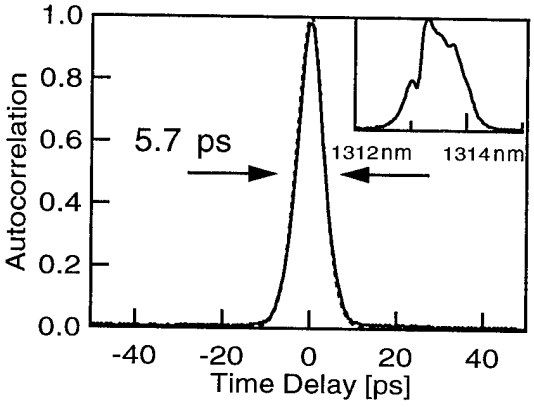

Fig. 2a: Autocorrelation and spectrum (inset) of Nd:YLF using high-finesse A-FPSA.

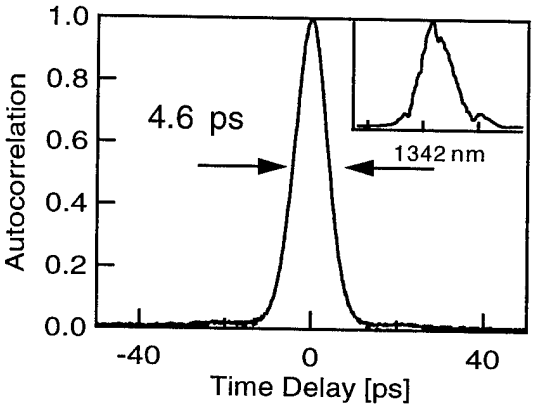

Fig. 2b: Autocorrelation and spectrum (inset) of Nd:YVO_4 using low-finesse A-FPSA.

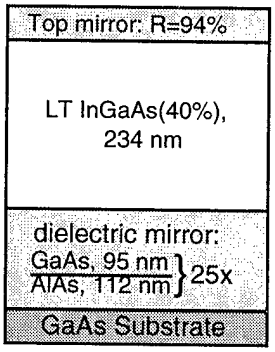

Fig. 3a: High-finesse A-FPSA cross-section.

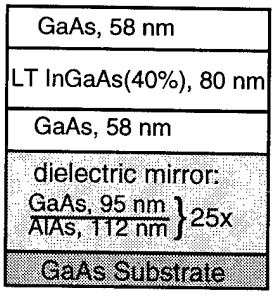

Fig. 3b: Low-finesse A-FPSA cross-section.

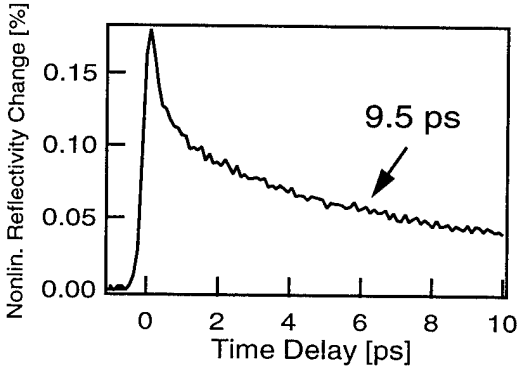

Fig. 4a: Pump-probe measurement of the high-finesse A-FPSA response measured at 1322 nm.

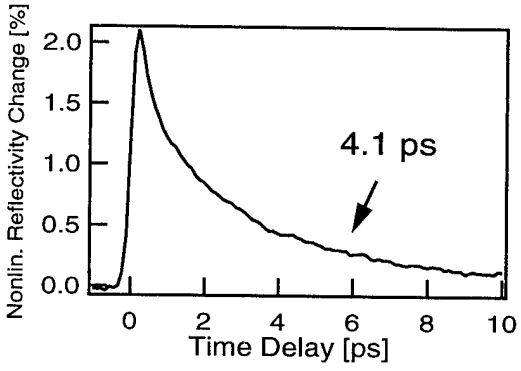

Fig. 4b: Pump-probe measurement of the low-finesse A-FPSA response measured at 1322 nm.

Self-Mode-Locked Solid State Intracavity Raman Lasers

J. T. Murray, P. T. Guerreiro, L. K. Calmes, R. C. Powell, N. Peyghambarian
Optical Sciences Center, University of Arizona
Tucson, AZ 85721, ph:(520) 621-2747,fax:(520) 621-9613

W. Austin
Lite Cycles, Inc.
6540 N. Camino Libby,
Tucson, AZ 85718, ph:(520) 742 - 5680, fax: (520) 297 - 4199

Development of intracavity solid state Raman lasers is currently an active area of research because they offer a very efficient means of producing high power diffraction limited optical radiation at useful wavelengths [1,2]. We further extend this research by demonstrating, for the first time to our knowledge, the utility of solid state stimulated Raman scattering (SSRS) as a means to passively mode-locking a cw laser and self-mode-locking an intracavity Raman laser. The elegance and simplicity of this method should enable the development of inexpensive, high power, ultra-short laser radiation at alternative wavelengths.

Spontaneous mode-locking of the first Stokes radiation, induced by an intracavity stimulated Raman scattering medium, was first predicted by T. I. Kuznetsova [3] and demonstrated by N. V. Kravtsov and N. I. Naumkin [4] in a Q-switched ruby laser utilizing a high pressure hydrogen cell as the intracavity Raman media. Self-mode-locking in Raman lasers is accomplished by the acute discrimination between noise spikes in the temporal structure of the oscillating Stokes field, as a result of the strong nonlinear Raman gain. Because the temporal structure of the Stokes and pump fields will repeat every round trip, discriminating features in both fields will be preferentially amplified, resulting in the development of a stable train of mode-locked pulses in both fields.

Two laser systems have been built that demonstrate this phenomenology: (1) A cw mode-locked arc-lamp pumped Nd:YAG laser operating at 1.338 μm; and (2) a repetitive acoustooptic Q-switched self mode-locked coupled cavity Raman laser [1] operating at repetition rates from 0 to 10 kHz with an output wavelength at 1.556 μm. Both lasers utilized a sol-gel coated 10x10x50 mm barium nitrate crystal (Crystal Associates) which was centered at the beam waist of the pump cavity. Figure 1 shows the optical layout for both systems.

Laser cavity (1) utilized a 3 % output coupler and yielded a maximum output of 3.5 W at an input of 2.2 kW to the arc lamp. At this same input power level to the arc lamp, a maximum of 25 W is obtained when the Raman crystal is removed and the cavity dimensions re-optimized. The discrepancy in output powers is attributed to the poor optical quality of the Raman crystal.

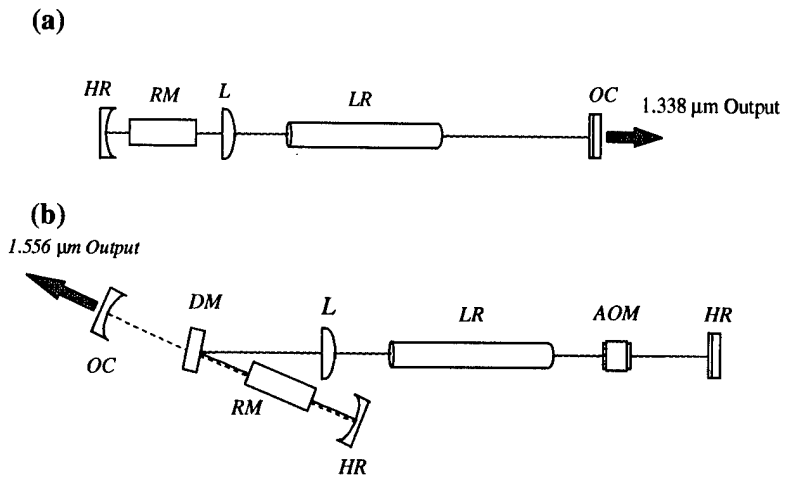

Figure 1. Optical layout for (a) cw mode-locked 1.338 μm laser and (b) repetitively Q-switched self mode-locked 1.556 μm Raman laser. HR, high reflector; OC, output coupler; RM, Raman medium which is $Ba(NO_3)_2$; L, lens; LR, laser rod; AOM, acoustooptic modulator; DM, dichroic mirror.

Similarly, 500 mW of 1.556 μm radiation at 2 kHz was obtained from laser cavity (2) where a 2 % output coupler at 1.556 μm was employed in the Raman cavity. All mirrors in the pump cavity were highly reflective. This system would not operate cw (i.e. with the Q-switch off) because the insertion loss of the Raman crystal was too high for the Stokes cavity to be over oscillation threshold.

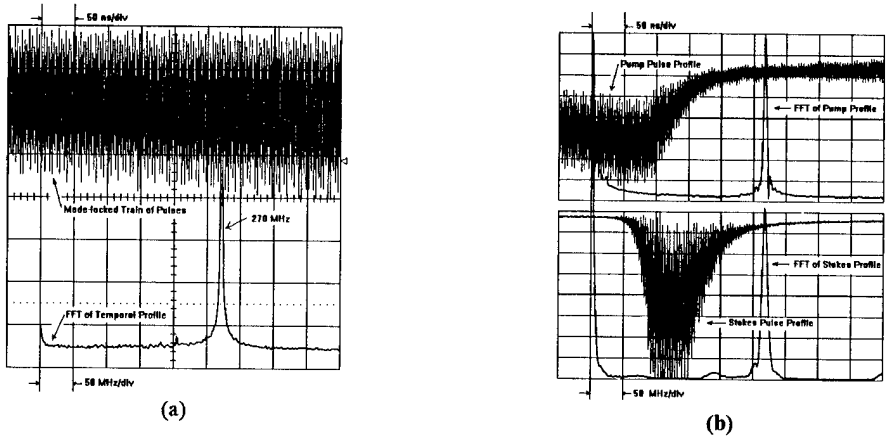

Figure 2. Temporal profiles of the (a) cw mode-locked 1.338 μm laser and (b) repetitively Q-switched self mode-locked 1.556 μm Raman laser. The top trace in (a) is the output pulse train of the laser and the bottom trace is the FFT of that trace which has a peak at 270 MHz, which is the free spectral range of the cavity. The top box in (b) displays a pump pulse train along with it's FFT and the bottom box shows the corresponding Stokes pulse train along with its FFT. In this case the pump and Raman laser cavities were matched.

Figure 2(a) displays a typical temporal output structure from the cw mode-locked 1.338 μm laser along with the fast Fourier transform (FFT) of the oscillogram. The peak in the output spectrum agrees well with the calculated axial mode spacing of 270 MHz. Likewise, Figure 2(b) shows the

output pulse profiles of the pump and Stokes emissions from the repetitively Q-switched Raman laser along with the FFT's of the respective profiles. Mode-locked pulse trains are evident within the Q-switched envelope of both the pump and Stokes temporal profiles. At higher pumping power levels multiple pulses in the envelope function are evident in the Stokes and pump profiles. This complex dynamical behavior can be attributed to gain switching and has been observed by others [5]. Careful cavity design can be implemented to eliminate this behavior. The anatomy of the output pulse profiles have been studied [6,7] and shown to exhibit signatures of dynamical chaos.

Both laser systems prefer to spontaneously lock on two separate axial mode spacings depending on the initial conditions. The most prevalent spacing is defined by the free spectral range of the resonator cavities c/(2 L), where L is the optical cavity length. The other, a more intermittent spacing, is given by c/(2 L'), where L' is the optical cavity length defined between the center of the Raman crystal and the end mirror. This implies that the Raman medium is acting, intermittently, as a feedback element and may suggest that backwards SRS plays a significant role in determining the overall cavity dynamics of the system. This presumption is under investigation.

We have demonstrated SSRS induced passive mode-locking in two laser cavity configurations. The work presented is novel in that, to our knowledge, SRS induced mode-locking has not been previously demonstrated employing a solid state Raman medium and SRS has not been utilized to mode-lock a cw pumped laser. Because SRS is not an absorptive phenomena, this technique can be used to mode-lock other laser systems where passive mode-locking elements have not yet been identified or where the currently used elements are cumbersome to use.

1. J. T. Murray, R. C. Powell, N. Peyghambarian, D. D. Smith and W. Austin, Opt. Lett. **20**(9), 1017 (1995); J.T. Murray, R.C. Powell, N. Peyghambarian, D.D. Smith and W. Austin, Proc. Advanced Solid State Lasers Conference '95, Memphis, TN, Tech. Digest, 371; J.T. Murray, R.C. Powell, N. Peyghambarian, D.D. Smith and W. Austin, Proc. Nonlinear Optics '94 Conference, Postdeadline, July, 1994, Kona Hawaii; J.T. Murray, R.C. Powell, R.J. Reeves, P.G. Zverev, T.T. Basiev, Conference on Lasers and Electro-optics '93, vol. 11, CThD3, Baltimore, MD (1993); J.T. Murray, R.C. Powell, R.J. Reeves, P.G. Zverev, T.T. Basiev, Proc. Advanced Solid State Lasers Conference '93, vol. 15, 156 (1993); P.G. Zverev, J.T. Murray, R.C. Powell, R.J. Reeves, T. T. Basiev, Opt. Comm. 97, 59-64 (1993)
2. P. G. Zverev and T. T. Basiev, Proc. Advanced Solid State Lasers Conference '95, Memphis, TN, Tech. Digest, 380
3. T. I. Kuznetsova, JETP Lett. **10**, 98 (1969)
4. N. V. Kravtzov and N. I. Naumkin, Sov. J. Quant. Electron., **9**, 223 (1979)
5. Y. B. Band, J. R. Ackerhalt, J. S. Krasinski and D. F. Heller, IEEE J. Quant. Electron., **25**, 208, (1989)
6. R. G. Harrison, I. A. Al-Saidi and D. J. Biswas, IEEE J. Quant. Electron., **21**, 1491, (1985)
7. V. N. Chizhevsky, D. E. Gakhovich, A. S. Grabchikov, S. Ya. Kilin, V. A. Orlovich and L .L. Tomilchik, Opt. Comm., **84**, 47 (1991)

Diode-pumped high-average power femtosecond fiber laser systems

M. E. Fermann, A. Galvanauskas, D. Harter
IMRA America, Inc., 1044 Woodridge Ave., Ann Arbor, MI 48105
J. D. Minelly, J. E. Caplen, Z. J. Chen and D. N. Payne
ORC, University of Southampton, Southampton SO17 1BJ, U.K.

The recent progress in femtosecond laser technology is currently driven by the prospect of fully diode pumped systems, which promise the eventual replacement of the well-established Ti:sapphire laser in the field of ultrafast optics. Apart from more traditional diode-pumped solid-state lasers, fiber-based systems have received an increasing amount of attention due to the uniquely compact assemblies possible with fiber lasers. However, to date fiber lasers have replaced Ti:sapphire- based systems only in areas, were low power levels are required, such as the injection seeding of regenerative amplifiers[1]. Here, we show that fiber lasers can also produce power levels and pulse widths that are sufficient for the pumping of optical parametric oscillators (OPOs) and amplifiers (OPAs).

The key to generating high average powers from fiber laser based systems is to employ double-clad fibers as amplifiers[2], as double-clad fibers allow a uniquely simple method for brightness conversion from high-power multi-stripe diode arrays. Self-phase modulation in the amplifiers is then minimized by employing an all-fiber chirped pulse amplification technique based on chirped fiber Bragg gratings (FBGs)[3].

Femtosecond amplifier systems need to be seeded with ultra-fast oscillators; preferred are erbium oscillators, where one typically has two options. Either passively modelocked systems operating at their fundamental cavity round-trip time in short lengths of fibers or passive harmonically modelocked systems in long lengths of fibers[4] can be employed. Fundamentally modelocked oscillators allow the generation of pulses at repetition rates between $\approx 1 - 50$ MHz with pulse widths between 1 psec - 100 fsec and pulse energies between $\approx 6 - 300$ pJ, giving average seed powers between $\approx 0.006 - 15$ mW. At a seed power level of 15 mW, a single fiber power amplifier can in principle be used to generate a power level of about 2 W.

In this work, however, for experimental convenience we preferred employing harmonically modelocked fiber lasers, as they allow the construction of femtosecond oscillators with adjustable repetition rates anywhere between 25 and 500 MHz (with the present state of the art). However, due to the intrinsic jitter ($\approx$100 psec) of passive harmonically modelocked oscillators they are at present not suitable for the pumping of OPOs. In Fig. 1 we show the optical spectrum (30 nm FWHM) of a harmonically modelocked laser operating at 150 MHz, which produced 200 fsec (1.8×bandwidth-limited) pulses with a pulse energy of 30 pJ. Nearly the full bandwidth of the oscillator pulses can be preserved in an amplification process, as also shown in Fig. 1, where we used an Er/Yb co-doped double-clad amplifier[5] pumped by a 1 W diode array (operating at 980 nm). By a careful selection of the oscillator and amplifier gain spectrum 300 pJ pulses with a bandwidth of 28 nm were generated, where the average output power was 50 mW. Currently we are developing a system pumped by an array of

1 W diode lasers pig-tailed to a fiber bundle, which should allow an increase in the pulse energies by a further order of magnitude.

We have demonstrated that self-phase modulation in the amplifiers can be minimized by employing an all-fiber chirped pulse amplification system. The experimental set-up of such a system is shown in Fig. 2. For pulse stretching and compression we employed a 5 mm long positively chirped FBG with a bandwidth of ≈ 15 nm centered at ≈1.555 μm, a dispersion of +3.40 ps^2 and a reflectivity of ≈ 90%. Here the oscillator was similar to the one described above and operated at 50 MHz and thus the first chirped FBG stretched the oscillator pulses to a width of about 50 psec. Due to coupling losses and some residual reflections in the system we had to employ a pre-amplifier between the oscillator and the power amplifier. The power amplifier was a singly-doped double-clad Er fiber (Er^{3+} doping level = 1000 ppm)[6], which has ≈1.7 times the optical bandwidth (≈43 nm) of an Er/Yb co-doped fiber. Using a pump power of 1.15 W delivered from two MOPA diode lasers, an output power of 420 mW was generated before compression in the second chirped FBG. After recompression an average output power of 260 mW was obtained and thus the pulse energy is 5.2 nJ.

The autocorrelation trace and the corresponding pulse spectrum are shown in Fig. 3. The FWHM pulse width is 380 fsec assuming a $sech^2$ pulse shape. The corresponding time-bandwidth product is ≈0.5. Some spectral re-shaping is evident, which in fact is caused by grating non-uniformities and the onset of nonlinear spectral re-shaping at this pulse energy. We calculated the nonlinear phase delay of the pulses in the present system to be around π by solving the rate equations of the power amplifier for the signal-power distribution along the fiber. A further reduction in the nonlinearity of the amplifier is possible by simply reversing the direction of the pump light. The present system is capable of generating 400 fsec pulses with pulse energies of 20 nJ with an average power of about 1 W. Power levels well in excess of 1 W and even shorter pulses should be possible by employing longer and more uniform chirped FBGs.

In conclusion we have described some of the fundamental design principles and performance limitations of high-average power femtosecond fiber laser systems. We believe that these systems are competitive with conventional femtosecond solid-state lasers.

References

1. A. Hariharan et al., 'Alexandrite-pumped Alexandrite regenerative amplifier for femtosecond pulse amplifications', subm. to Opt. Lett.
2. E. Snitzer et al., Digest of Conference on Optical Fiber Sensors (Optical Society of America, Washington, D.C.), paper PD5 (1988)
3. A. Galvanauskas et al., Appl. Phys. Lett., **66**, 1053 (1995)
4. S. Gray et al., Electron. Lett., **29**, 1860 (1993)
5. J. D. Minelly et al., IEEE Photonics Techn. Lett., 5, 301 (1993)
6. J. D. Minelly et al., European, Conference on Optical Communication, ECOC, Brussels, 1995

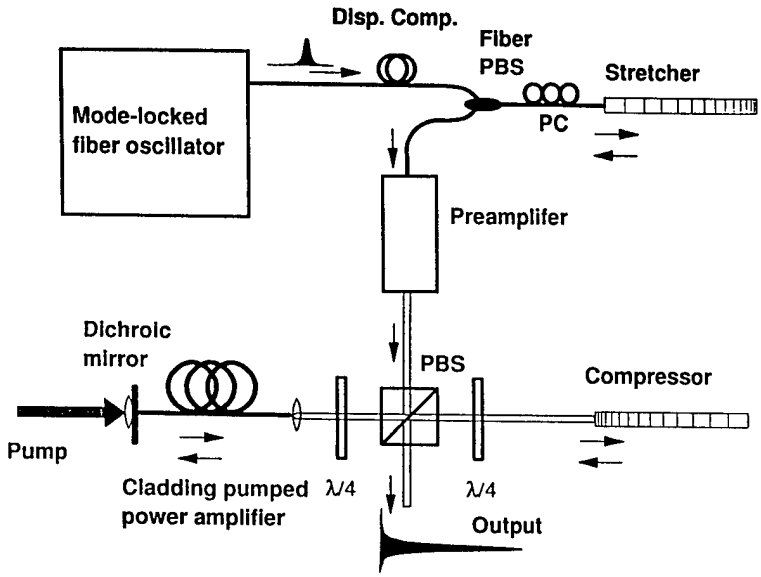

Fig.2) Experimental set-up for an all-fiber chirped-pulse amplification system employing chirped fiber gratings and cladding-pumped fiber amplifiers.

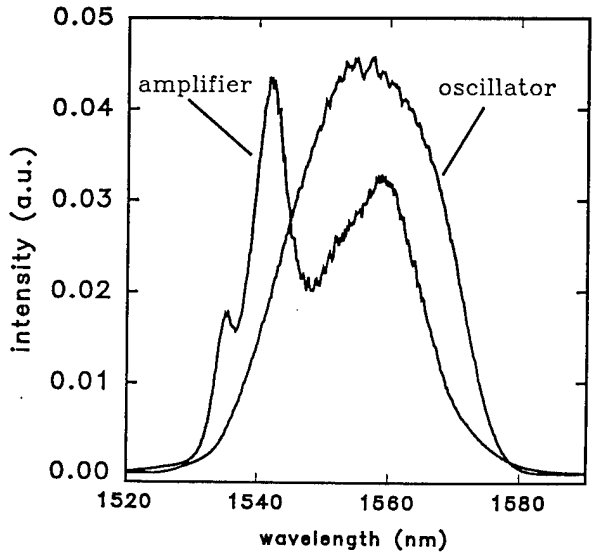

Fig. 1) Spectrum of a passive harmonically modelocked Er-fiber oscillator amplified in a cladding-pumped Er/Yb fiber amplifier.

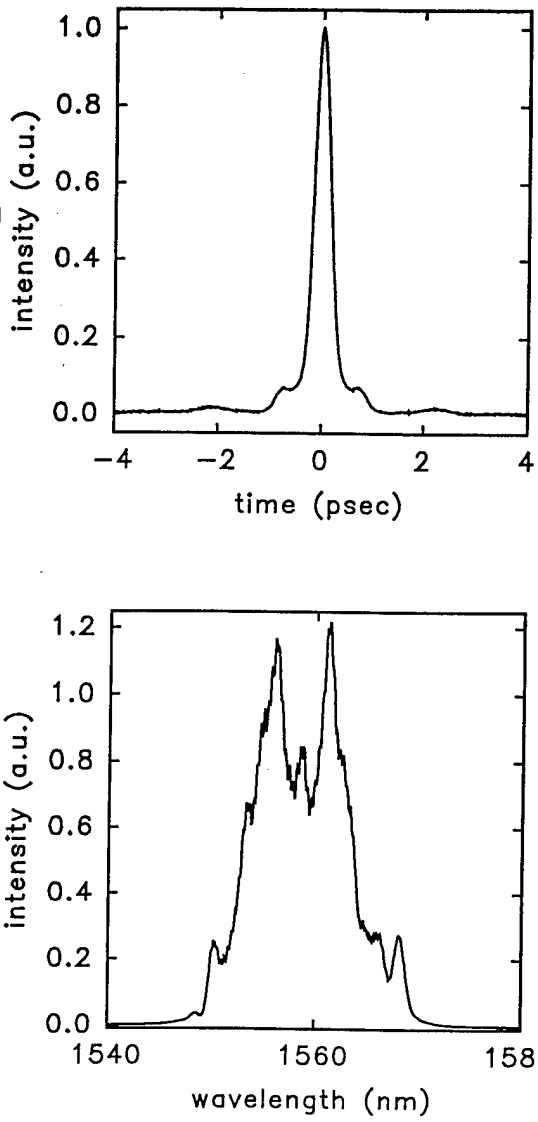

Fig. 3) Autocorrelation and spectrum of 5.2 nJ, 380 fsec pulses generated with the all-fiber chirped pulse amplifications system. The average systems output power is 260 mW.

Passively Q-switched 180 ps Nd:LSB microchip laser

B. Braun, F. X. Kärtner, and U. Keller
Ultrafast Laser Physics Laboratory, Institute of Quantum Electronics, Swiss Federal Institute of Technology, ETH Hönggerberg, HPT, CH-8093 Zürich, Switzerland,
Tel: [011] 41 1 633 21 39, Fax: [011] 41 1 633 10 59, e-mail: braun@iqe.phys.ethz.ch,
WWW: http://iqe.ethz.ch/~kopf/ULP.html

J.-P. Meyn* and G. Huber
Institute of Laser-Physics, University of Hamburg, Jungiusstr. 9 - 11, D-20355 Hamburg, FR Germany

We demonstrate a Nd:$LaSc_3(BO_3)_4$ (Nd:LSB) microchip laser passively Q-switched by an antiresonant Fabry-Perot saturable absorber (A-FPSA) [1, 2], and have achieved the shortest reported pulses from a passively Q-switched solid-state laser (Fig. 1). We measured single-frequency, TEM_{00}, 180 ps FWHM pulses with 0.1 μJ pulse energy at a repetition rate of 110 kHz, resulting in a peak power of approximately 500 W at an average power of 11 mW. In addition, we can vary the pulsewidths from 180 ps to 30 ns and the repetition rates from 50 kHz up to 7 MHz by varying the design of the A-FPSA and the pump power.

Q-switched microchip lasers are compact, robust solid-state lasers that can provide high peak power with a single-frequency diffraction limited output beam. The short cavity, typically less than 1 mm, allows for single-frequency Q-switched operation with very short pulsewidths. Previously, pulse durations as short as 218 ps have been reported with a passively Q-switched microchip laser consisting of a composite structure of Nd:YAG bonded to a thin piece of Cr^{4+}:YAG [3, 4]. With a monolithic Cr:Nd:YAG laser, pulses of 290 ps have been demonstrated [5].

Nd:LSB is an very interesting material for a microchip laser, because of the short absorption length (110 μm at 25% doping) and the broad absorption bandwidth of 3 nm, centered around 808 nm, which allows for efficient single-frequency operation and diode-pumping [7]. For Q-switched pulses, the short cavity length of the microchip offers the potential to decrease the pulsewidth into the picosecond range.

In our experiment, a 220 μm thick Neodymium-Lanthanum-Scandium-Borate (Nd:LSB) laser crystal [6, 7, 8] is sandwiched between a 10% output coupler and an A-FPSA coated for high reflection at the pump wavelength of 808 nm and design reflectivity (typically 80%) at the laser wavelength of 1.062 μm (Fig. 2). The crystal is pumped by a Ti:Sapphire laser at 808 nm through a dichroic beamsplitter which transmits the pump light and reflects the output beam at 1.062 μm. The pump radius was measured to be 40 μm. Single-frequency output was achieved up to an incident pump power of about 550 mW.

The A-FPSA is a low temperature grown InGaAs/GaAs multi-quantum-well absorber (growth temperature T=350 °C and a carrier recombination time of 24 ps) placed between an AlAs/GaAs bottom mirror and a dichroic top reflector (Fig. 2). The top reflector and

operation of the Fabry-Perot at anti-resonance increase the saturation fluence of the multiple quantum well absorber from 50 $\mu J/cm^2$ for an antireflection coated sample to practically any desired higher value [9].

The use of an A-FPSA as saturable absorber device allows us to control the most important Q-switching parameters for a specific laser crystal [9, 10]. The independently-variable design parameters are the thickness of the absorber, the reflectivity of the top reflector and the growth temperature of the MBE grown material. These parameters determine the amount of saturable loss of the absorber, the saturation intensity, and the recovery time of the absorber. Even if the mode size is fixed, which is the case in most microchip lasers, there are sufficient free parameters to independently optimize the saturable losses and the effective saturation intensity, which are the most important parameters for Q-switching. In addition, because the A-FPSA is used as an end mirror and has an effective penetration depth of less than one micron, we can add a saturable absorber to our laser with only a negligible increase in the cavity length. This allows us to maintain a shorter cavity length and therefore shorter Q-switched pulsewidths compared to other approaches which require larger bulk modulation elements.

Depending on the saturation fluence and the amount of saturable losses, which can be adjusted by changing the reflectivity R_t of the top reflector, and the pump power, the pulsewidth can be varied from 180 ps to 30 ns and the repetition rate from 50 kHz up to 7 MHz (Fig. 3a, 3b). The highest peak power we achieved was 1.6 kW from 360 ps, single-frequency, 0.6 μJ pulses at 86 kHz, using an 80% top reflector on the A-FPSA and a 10% output coupler at an incident pump power of 450 mW.

To accurately measure the picosecond pulses, we used a 50 GHz sampling oscilloscope (Tektronix CSA 803) with a 40 GHz photodetector. We verified that the overall time resolution was less than 20 ps by measuring its impulse response with a 4 ps pulse from a modelocked Nd:YLF laser.

In conclusion, we have demonstrated that the A-FPSA device is a new and interesting way to passively Q-switch microchip lasers. The device characteristics allow us to tailor the saturation behavior to achieve a wide range of pulsewidth and repetition rates. Because of the properties of Nd:LSB, which allows for very short microchip laser, and the A-FPSA, which provides saturable absorption without significantly increasing the cavity length, we were able to generate the shortest reported passively Q-switched pulses from a solid-state laser. With available semiconductor technology, we can extend these devices to many other laser crystals at different wavelengths, in contrast to Cr^{4+}:YAG, which is limited to specific spectral regions.

Acknowledgments: We would like to thank T. H. Chiu from AT&T Bell Laboratories for growing some of the semiconductor saturable absorbers. This research was supported by the Swiss priority program in optics.

*Present address, Edward L. Ginzton Laboratory, Stanford University, Stanford, California 94305

1. U. Keller, D. A. B. Miller, G. D. Boyd, T. H. Chiu, J. F. Ferguson, M. T. Asom, *Optics Letters* **17**, 505 (1992)
2. U. Keller, *Applied Phys. B* **58**, 347 (1994)
3. J. J. Zayhowski, C. Dill, *Optics Letters* **19**, 1427 (1994)
4. J. J. Zayhowski, J. Ochoa, C. Dill, CLEO 1995, paper CTuM2 p. 139
5. P. Wang, S.-H. Zhou, K. K. Lee, Y. C. Chen, *Optics Communications* **114**, 439 (1995)
6. S. A. Kutovoi, V. V. Laptev, S. Y. Matsnev, *Sov. J. Quantum Electr.* **21**, 131 (1991)
7. B. Beier, J.-P. Meyn, R. Knappe, K.-J. Boller, G. Huber, R. Wallenstein, *Applied Physics B* **58**, 381 (1994)
8. J.-P. Meyn, T. Jensen, G. Huber, *IEEE Journal of Quantum Electronics* **30**, 913 (1994)
9. L. R. Brovelli, U. Keller, T. H. Chiu, *Journal of the Optical Society of America B* **12**, 311 (1995)
10. F. X. Kärtner, L. R. Brovelli, D. Kopf, M. Kamp, I. Calasso, U. Keller, *Optical Engineering* **34**, 2024 (1995)

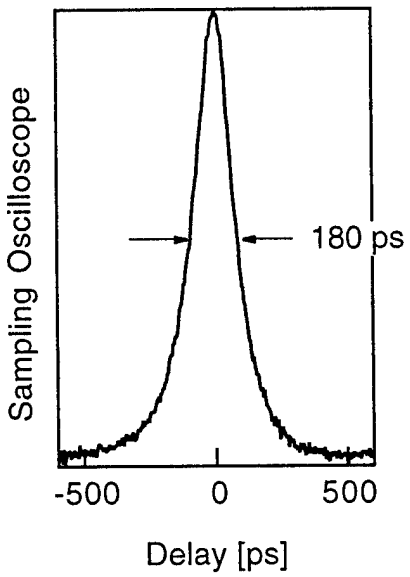

Fig. 1: Oscilloscope trace of the single-frequency 180 ps long Q-switched pulse (≈20 ps measurement resolution)

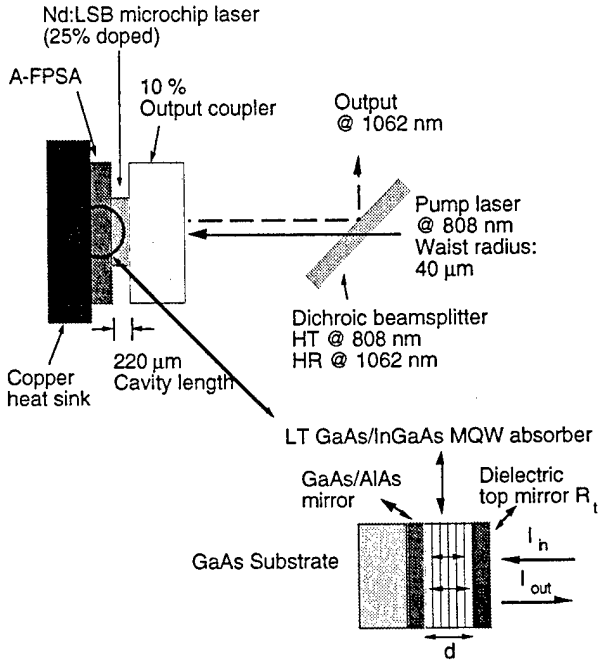

Fig. 2: Layout of the Q-switched Nd:LSB laser with an A-FPSA directly attached to the crystal

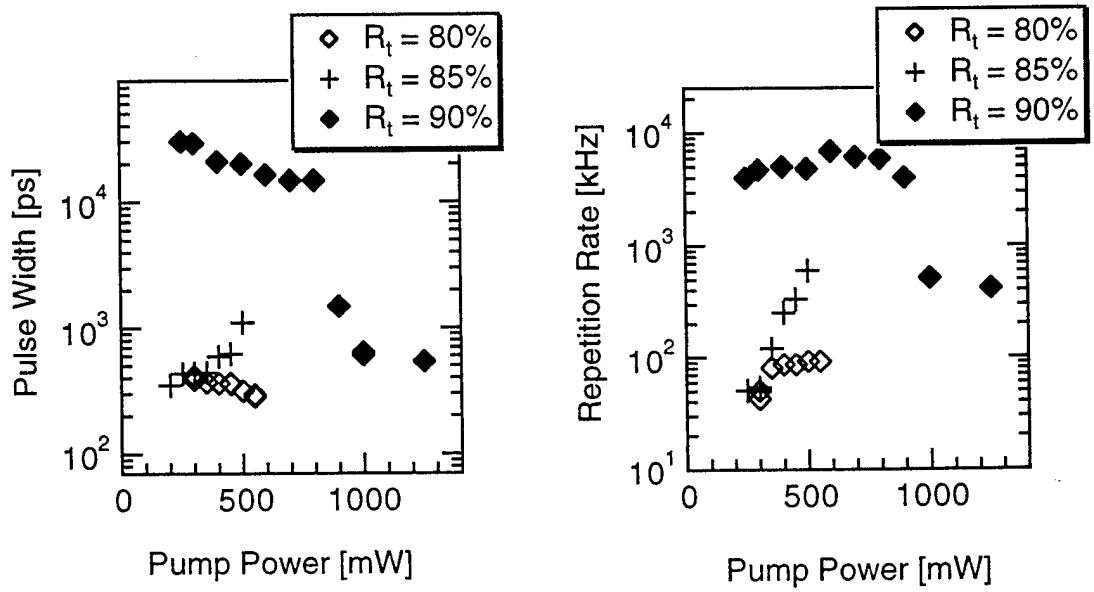

Fig. 3: Pulsewidth and repetition rate of the Q-switched Nd:LSB laser versus pump power

Friday, February 2, 1996

IR Lasers II
Poster Session

FF 3:15 pm-4:15 pm
Terrace Room

Picosecond diode-pumped Cr:LiSAF laser seeded Ti:Sapphire laser amplifiers

Franck Falcoz, Frederic Estable*, Luc Vigroux*, Patrick Georges, and Alain Brun

Institut d'Optique Théorique et Appliquée
Unité de Recherche Associée au CNRS N°14
Université Paris-Sud
BP 147
91403 Orsay Cedex, France
Ph: 33-1-69 41 68 56
Fax: 33-1- 69 41 31 92

* B. M. Industries
CE 2901, 91029 Evry Cedex, France

Since its first demonstration [1], Ti:Sapphire has proved to be powerful solid state laser material and is used in a great number of laser systems from the cw to the fs regime [2,3]. It has a large fluorescence bandwidth in the near IR (670 - 1080 nm) that permits the development of tunable solid state laser. The possibility to produce and amplify femtosecond pulses with Ti:Sapphire crystal in combination with a new technique of mode-locking [4] has revolutionized the world of ultrafast laser. However, due to its absorption band in the blue-green, Ti:Sapphire can not be directly pumped by a laser diode. On the other hand, Cr^{3+}:$LiSrAlF_6$ (Cr:LiSAF) is a new solid state laser [5] material that exhibits also a large fluorescence bandwidth in the near IR (750 - 1000 nm) but with an absorption in the red, between 600 and 700 nm. Although its thermal properties are poor compared to that of Ti:Sapphire, this crystal remains interesting since it can be directly diode-pumped by GaAlInP high power laser diode. Recently, picosecond and femtosecond pulses have already been produced in diode-pumped LiSAF lasers [6,7].

In our work presented here, we have tried to combine the advantages of the two laser materials and we present a picosecond laser system based on the use of a diode-pumped LiSAF actively mode-locked oscillator followed by Ti:Sapphire amplifiers that boosts the energy of the pulses from one tenth of nanojoule to hundred millijoules.

The purpose of our work was to develop a tunable picosecond laser source in the near infrared. We followed the classical scheme which consists first to produce the short pulses, whatever their energy, and than to amplify the pulses to the energy required in different stages of amplification.

The oscillator was an actively mode-locked diode-pumped LiSAF laser (Fig.1). We used a single stripe GaAlInP laser diode that produced 400 mW cw at around 670 nm with an emitting area of 100 µm per 1 µm. After reshaping, the beam is focused in a 5 mm long Brewster angle cut crystal of LiSAF with a doping level of 1.5 % corresponding to an absorption of 90 % at 670 nm. The cavity consisted of four mirrors, two concave mirrors (150 mm radius of curvature) around the crystal, a plane high reflector end mirror and a plane output coupler with 1% transmission between 800 and 900 nm. To adjust the cavity wavelength and also to reduce the spectrum width, we used a three plate birefringent filter. An acousto-optic modulator, placed near the output coupler, is used to produce the picosecond pulses. In this case, pulses as short as 18 ps with a bandwidth of 0.06 nm at around 850 nm have been obtained indicating that the pulses are

transform limited. By reducing the RF power in the acousto-optic modulator or slightly disaligning it, one can increase the pulse duration to 100 ps or more. The average output power was around 15 mW at 125 MHz repetition rate corresponding to an energy per pulse of 0.1 nJ.

To amplify the picosecond pulses, we used Ti:Sapphire because of its large saturation fluence and its high thermal properties. First we used a regenerative amplifier (Fig.1) pumped at 10 Hz by the second harmonic of a flashlamp pumped Q:Switched Nd:YAG. To simplify the experiment we avoided to use the classical Chirped Pulse Amplification Technic (CPA) [8]. So, in order to reduce the peak power in the amplifier we kept the pulses duration at 100 ps. The regenerative cavity consisted of two high reflective plane mirrors. The gain guiding in the Ti:Sapphire crystal stabilized the cavity and the output beam was gaussian. A Pockels cell and a polarizer were used to inject and dump the pulses. An intracavity prism was used to reduce the width of the spectrum and to adjust the central wavelength to that of the oscillator. The build up time was around 200 ns corresponding to 13 round trips. The pump energy was around 50 mJ and the output energy at 846 nm was 4 mJ. No mode matching was used to adjust the input beam and the beam of the regenerative amplifier. Nevertheless, the injection was very easy despite the relative low input energy.

Then we used a multipass amplifier to increase the pulse energy. We expand the beam in an afocal to avoid non linear effect in the amplifier. The Ti:Sapphire crystal was both sides pumped in order to keep the pump fluence under 1.5 J/cm^2. Total pump energy was around 350 mJ and after 4 passes the output energy was 50 mJ. Finally, after another beam expander, we used a second multipass amplifier to reach 100 mJ energy per pulse. The pump energy was again in the order of 400 mJ in the last amplifier. As pump lasers, we used two Q:switched Nd:YAG lasers producing each 400 mJ in 12 ns pulses at 10 Hz. The first laser pumped the regenerative and the first multipass amplifier, while the second was used for the last amplifier. The use of two lasers permitted us to adjust the delay between the two lasers and optimize the pump arrival time in the second amplifier and so to take into account the build up time of the gain in the regenerative amplifier.

In conclusion, we reported a new picosecond laser system based on the used of a diode pumped LiSAF laser followed by Ti:Sapphire amplifiers. This system produces tunable narrow band 100 ps pulses with an energy of 100 mJ. This system may find a lot of applications in time resolved spectroscopy and remote sensing. Furthermore, with the recent development of femtosecond diode pumped LiSAF laser, one can think about a high peak power femtosecond laser chain based on this scheme in combination with the CPA technique.

References :

[1] P. F. Moulton, JOSA B**3**, 125 (1986).
[2] P. Albers, E. Stark, and G. Huber, JOSA B**3**, 134 (1986).
[3] F. Salin, J. Squier, G. Mourou and D. Harter, Opt. Lett. **16** 324 (1991).
[4] D.E. Spence, P.N. Kean and W. Sibett, Opt. Lett. **16**, 42 (1991).
[5] S.A. Payne, W.F. Krupke, L.K. Smith, W.L. Kway, L. Davis DeLoach, and J.B. Tassano, IEEE J. Quantum Electron. **28**, 1188 (1992).
[6] P.M.W. French, R. Mellish, J.R. Taylor, P. Delfeytt and L.T. Florez, Opt. Lett. **18**, 1934, (1993)
[7] M.J. Deymott, and A.I. Ferguson, Opt. Lett. **19**, 1988 (1994).
[8] D. Strickland and G. Mourou, Opt. Comm., **56**, 219 (1985).

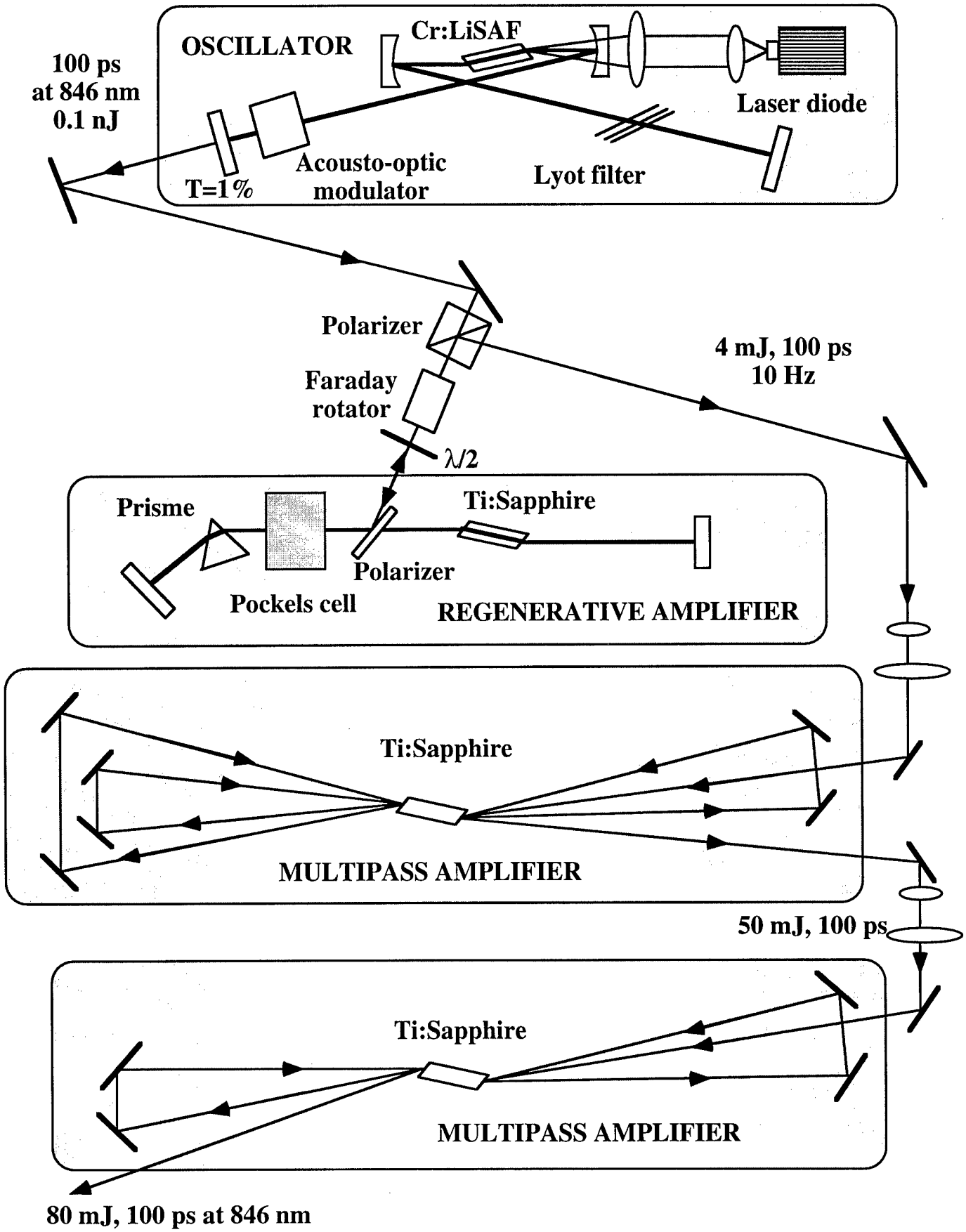

Figure 1: experimental set-up

High-repetition-rate mode-locked Ti:sapphire laser using a saturable Bragg reflector

Taro ITATANI, Takeyoshi SUGAYA,
Tadashi NAKAGAWA, Yoshinobu SUGIYAMA
Electrotechnical Laboratory (ETL)
Umezono 1-1-4, Tukuba, Ibaraki, 305 JAPAN
Zhenlin LIU, Chengyou LIU, Shinji IZUMIDA,
Nobuhiko SARUKURA, Tomoyuki HIKITA, and Yusaburo SEGAWA
Photodynamics Research Center,
The Institute of Physical and Chemical Research (RIKEN),
Nagamachi Koeji 19-1399, Aoba-ku, Sendai, Miyagi 980, Japan
Telephone: +81 22 228 2012 Facsimile: +81 22 228 2010

There has been a break-through in mode-locking techniques for solid-state lasers. [1,2] Applying these techniques utilizing Kerr type nonlinearity, most solid-state lasers can be mode-locked down to the femtosecond region. These ultrashort-pulse lasers are extremely powerful tools for scientific applications. However, these alignment-critical and bulky lasers are still far from turn-key systems, which can serve as compact black boxes for more general use in real-world applications. [3] To develop lasers which meet such requirements, we need to find some devices to mode-lock laser-diode-pumped solid-state lasers robustly and stably. Anti resonant Fabry-Perot saturable absorbers (A-FPSA) [4] and saturable Bragg reflectors (SBR) [5] are candidates for this. Both of them are nonlinear mirrors utilizing thin-film semiconductors. High-repetition capability is one of the most of desired features for real world applications. [6] In this paper, we investigated high-repetition rate mode-locked operation of Ti:sapphire laser with SBR.

The saturable Bragg reflector was grown on a (100)-oriented semi-insulating GaAs substrate by molecular beam epitaxy. After a 500-nm-thick buffer layer was grown on the substrate, a Bragg reflector including a single quantum well was formed. The Bragg reflector consists of 24 pairs of AlGaAs/AlAs quarter-wave layers and a top quarter-wave layer of AlGaAs including a single quantum well of 10 nm. The AlAs layer thickness is 72.6 nm, and that of the AlGaAs layer is 63.2 nm.

The mode-locked laser setup using a saturable Bragg reflector as a saturable absorber is shown in Figs. 1 and 2. The cavity geometry is designed for high repetition-rate, mode-locking pulse generation. The laser cavity consists of a 1.0% transmittance output coupler, a pair of folding mirrors with 10-cm curvature, an AR-coating lens with focal length of 5-cm, and a saturable Bragg reflector at the focus of the lens. The pump source is an all line Ar laser. The pumping beam is focused onto the Ti:sapphire crystal longitudinally with a 10-cm focal-length lens.

We obtained self-starting 2.4 psec pulses at a 540 MHz repetition rate (Fig. 4) with 200 mW output power. Figure 3 shows a typical autocorrelation trace and the corresponding mode-locked spectrum. The time-bandwidth product is 0.82. Shorter-cavity length resulted in Q-switched, mode-locked operation.

In conclusion, passive mode-locking at a repetition rate of 540 MHz has been achieved for a Ti:sapphire laser with a semiconductor saturable absorber using a Bragg reflector. The pulsewidth as short as 2.4 psec has been obtained for self-starting operation at high repetition frequency. Further optimization will increase the repetition rate and reduce the pulse duration.

References:

1. D. E. Spence, P. N. Kean, and W. Sibbett, Opt. Lett. 16, 42 (1991).
2. N. Sarukura, Y. Ishida, and H. Nakano, Opt. Lett. 16, 153 (1991).
3. W. H. Knox, Conference on Lasers and Electro-Optics, Vol. 15, 1995 OSA Technical Digest Series, (Optical Society of America, Washington, D.C., 1995), paper JMA1.
4. U. Keller, D. A. B. Miller, G. B. Boyd, T. H. Chiu, J. F. Ferguson, and M. T. Asom, Opt. Lett, 17, 505 (1992).
5. S. Tsuda, W. H. Knox, E. A. de Souza, W. Y. Jan, and J. E. Cunningham, Opt. Lett. 20, 1406 (1995).
6. B. Bouma, and J. G. Fujimoto, Conference on Lasers and Electro-Optics, Vol. 15, 1995 OSA Technical Digest Series, (Optical Society of America, Washington, D.C., 1995), paper CWM3.

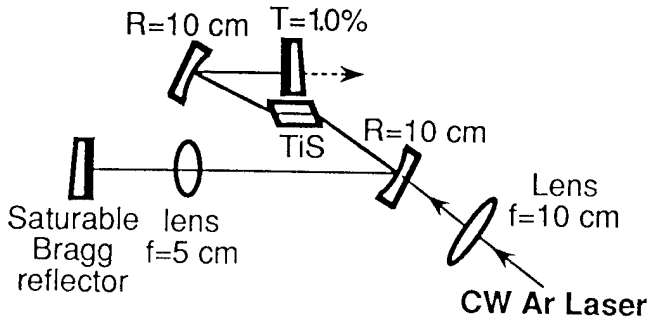

Fig. 1 Experiment setup of the high repetition rate mode-locked Ti:sapphire laser using a saturable Bragg reflector as a saturable absorber

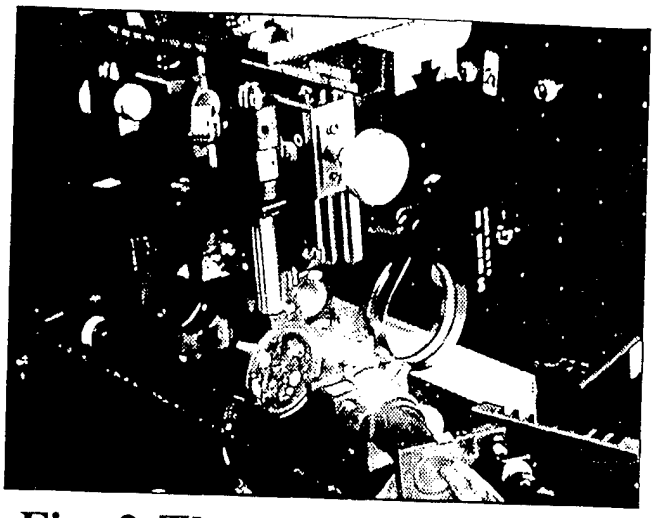

Fig. 2 The photograph of the experiment setup of the high repetition rate mode-locked Ti:sapphire laser

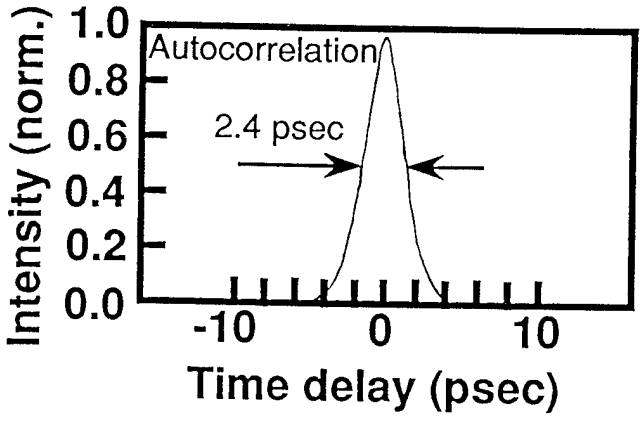

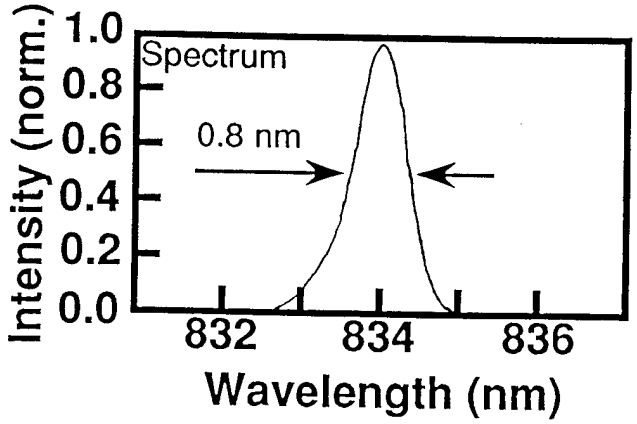

Fig. 3 Autocorrelation trace and corresponding spectrum of the resulting pulses. The time-bandwidth is 0.82.

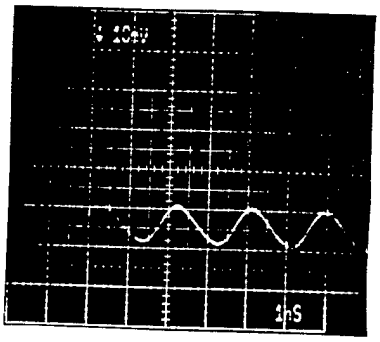

Fig. 4 Oscilloscope trace of the 540MHz repetition rate mode-locked Ti:sapphire laser pulse

Measurements of operation parameters and nonlinearity of a Nd^{3+}-doped fiber laser by relaxation oscillations

R.Böhm, V.M.Baev and P.E.Toschek.

Institut für Laser-Physik, Universität Hamburg,
Jungiusstr.9, D-20355 Hamburg, Germany
Tel.: (040)-41232380
Fax: (040)-41236571

1. Introduction

Fiber laser oscillators and amplifiers are compact and inexpensive systems, which are successfully used for many practical applications, as for a spectroscopic light source, for light amplification in optical telecommunication, and for intracavity absorption spectroscopy [1]. In comparison with bulk lasers, fiber lasers show higher nonlinearities, which cause, e.g., doubling of the laser frequency [2]. This leaves current laser models inapplicable to fiber lasers. However, an adequate laser model for the determination of operating parameters is important for the estimation of the ultimate performance of fiber lasers, as referring to linearity and dynamical range of gain, sensitivity limit of the detection of absorption [3], slope efficiency, and the stability of cw laser operation [4].

Several parameters of Nd^{3+}-doped silicate fiber laser have been measured so far, using various techniques. The fluorescent decay time of the upper laser level $^4F_{3/2}$, has been found 460±15 μs by monitoring the fluorescent intensity vs. time [5]. The lifetime of the terminal laser level ($^4I_{11/2}$) has been measured less reliably because the radiation, at 5 μm wavelength, and corresponding to transition $^4I_{11/2} \rightarrow {}^4I_{9/2}$, is absorbed by the glass host. The reported values range from 350 ps to 100 ns [6]. The cavity loss has been measured by monitoring relaxation oscillations induced by a small variation of the pump power [7]. However, the fluorescent decay time of the upper laser level derived from this measurement (300 - 400 μs [4,7]), disagrees with reported values. These discrepancies result from the oversimplified 4-level model [8] used for the evaluation of the experimental results.

We develop an extended model for a 4-level laser and test it experimentally by application to relaxation oscillations in a Nd^{3+}-doped silicate fiber laser at various levels of cavity loss and pump rate. From the experimental data we derive the cavity loss, gain coefficient, the total number of excited atoms, the lifetimes of the upper and lower laser levels, the efficiency of frequency doubling, and the number of oscillating modes. The measurements have been performed for four types of fibers.

2. Laser model

A Nd^{3+}-doped fiber laser is pumped by a diode laser at $\lambda \cong 810$ nm. The emission wavelength is $\lambda = 1{,}09$ μm. We extend the current model [8] by taking into account a decay rate A_4 of the population of the lower laser level, frequency doubling in the fiber, and spontaneous emission into the laser modes. In the following, N_i and A_i are population of atomic level i and its rate of relaxation, respectively. The photon numbers in the laser cavity at

the fundamental (ν) and at the second harmonic (2ν) are M and M_2, and N_i^0 and M_i^0 are corresponding stationary solutions. Since the decay rate A_4 and the loss rate of the cavity γ_2 at the second harmonic are much larger than the loss rate γ of the cavity for the fundamental frequency and than the decay rate A_3, we use the adiabatic approximation $\dot{N}_4 = 0$ and $\dot{M}_2 = 0$. Appropriate rate equations for the 4-level laser are

$$\dot{N}_3 = A_3 N_3^0 \eta - A_3 N_3 - B N_3 M \frac{A_4 - A_3}{A_4 + BM} \tag{1}$$

$$\dot{M} = -\gamma M + B N_3 M \frac{A_4 - A_3}{A_4 + BM} - \alpha M^2 + B N_3 R \ , \tag{2}$$

where R is the number of oscillating laser modes, $\eta = P/A_3 N_3^0$ is the relative pump rate and α is the rate of frequency doubling

Solutions of Eqs (1) and (2) are damped oscillations with practically the same frequency as for an ideal 4-level laser $\omega \cong \sqrt{\gamma A_3(\eta - 1)}$. The damping rate is different, however. It depends on the relaxation rate of the lower laser level, on the efficiency of frequency doubling, and on the rate of spontaneous emission:

$$\Gamma \cong \frac{A_3 \eta}{2} + \frac{A_3(\eta - 1)\gamma}{2A_4} + \frac{A_3(\eta - 1)\alpha}{2B} + \frac{\gamma B R}{2A_3(\eta - 1)} \ . \tag{3}$$

3. Experiment

Two of the four specimens are SiO_2/GeO_2 fibers with attenuation 19 dB and 9.5 dB at 810 nm and core diameter 2.7 μm and 3.7 μm, respectively; they have been manufactured by Lycom. The third fiber of similar composition with 9.5 dB attenuation and core diameter 5.5 μm was produced by IAV (Germany). The fourth specimen is a ZBLAN fiber with 2000 ppm Nd^{3+} concentration, (Le Verre Fluore, France). One end of each fiber has been coated with a set of dielectric layers that provides 99.5% reflectivity at 1.1 μm and serves as the cavity end mirror. The transmission of this mirror for the pump wavelength is about 90%. Two aspheric lenses are used for focusing the pump beam and for collimating the fiber-laser emission. Various dielectric mirrors with transmission values extending from 3 to 30% at 1.1 μm have been used as the external output mirror. A glass prism, whose surfaces subtend Brewster's angle with the laser axis, is placed in the open part of the cavity for spectral selection and tuning the laser output. The laser is pumped through the end mirror. A pulse generator is used for switching the pump power above threshold at time zero.

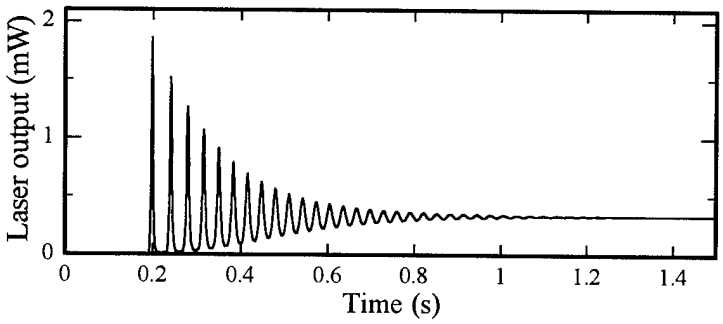

Fig.1. Output power of the fiber laser after the pump has been switched above threshold at time zero.

Fig. 1 shows the output power of the Lycom fiber (attenuation 9.5 db) after starting the pump, characterized by relaxation oscillations with frequency ω and damping rate Γ. The dependence of the damping rates upon the pumping rate η for this laser at different levels of the cavity loss rate is shown in Fig.2.

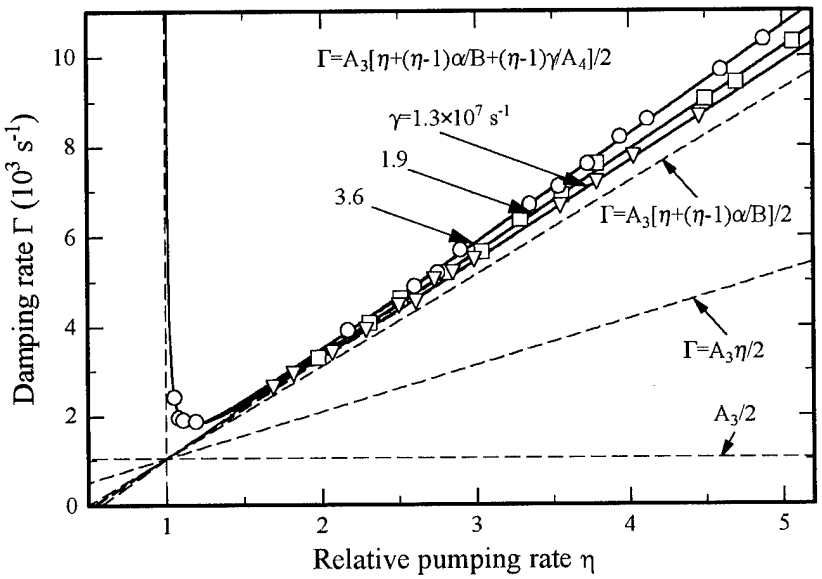

Fig.2. Damping rate of relaxation oscillations of a fiber laser versus relative pumping rate η at different levels of the cavity loss rate γ. Solid lines are fitted by Eq.(3). Dashed lines show calculated data (R=0) for $\alpha = 0$, $A_4 = \infty$ $\Gamma = A_3\eta/2$ [8], $\alpha \neq 0$, $A_4 = \infty$ and $\alpha \neq 0$, $A_4 \neq \infty$ (from below).

The fitting, by Eq.(3), of the experimental data of damping rates for different values of the cavity loss rate at large pumping rates, and measuring the frequency of relaxation oscillations provides us with the values A_3, A_4, α, and γ. Data fitting at small pump rates gives the number of oscillating modes R. For the Lycom fiber (9.5 db) we found the values A_3=2084 s^{-1}, A_4=1.05×10^8 s^{-1}, α=9×10^{-6} s^{-1}, and R=66. From the rate of frequency doubling α one derives the nonlinear susceptibility of the fiber, $\chi^{(2)} \cong n^2\sqrt{\gamma_2\varepsilon_0 V\alpha/h\nu^3}/2\pi$. Here, n is the refractive index of the fiber, h is Planck's constant, ε_0 is the dielectric permeability of free space, and V is the volume of the laser mode. We observe $\chi^{(2)} = 5\times10^{-15}$ m/V.

In conclusion, we have developed an extended model of a 4-level laser for application with fiber lasers and demonstrated a simple way for precise measurement of various laser parameters including nonlinearity, which are important for optimizing the operational characteristics of these lasers.

1. R.Böhm, A.Stephani, V.M.Baev, P.E.Toschek, Optics Lett. 18, 1955-1957 (1993)
2. U.Österberg, W.Margulis, Optics Lett. 12, 57-59 (1987).
3. V.M.Baev, P.E.Toschek, "Sensitivity limits of intracavity laser spectroscopy", in *Optical Methods in Atmospheric Chemistry*, H.I.Schiff, U.Platt, Eds, Proc. SPIE 1715, 381-392 (1993).
4. S.Bielawski, D.Derozier, P.Glorieux, Phys. Rev. A46, 2811-2822 (1992).
5. W.L.Barnes, P.R.Morkel, J.E.Townsend, Optics Comm. 82, 282-288 (1991).
6. W.Koechner, *Solid-state laser engineering*, p.56, Springer, Berlin, Heidelberg (1992)
7. D.C.Hanna, R.G.Smart, P.J.Suni, A.I.Ferguson, M.W.Phillips, Optics. Comm. 68, 128-132 (1988).
8. A.E.Siegman, *Lasers*, University Science Books, Mill Valley, CA (1986).

Tuning and stability properties of single-frequency diode-pumped coupled cavity Nd:YVO_4 laser

Peter Lichtenberg Hansen, Christian Pedersen, Torben Skettrup and Preben Buchhave.

Technical University of Denmark, Department of Physics, 2800 Lyngby, Denmark,

Phone: (+45) 45 93 12 22, ext. 3289, Fax (+45) 45 93 16 69, E-mail plh@mips.fys.dtu.dk

Frequency tuning of a coupled cavity solid-state Nd:YVO_4 laser has been investigated both theoretically and experimentally. The frequency tuning curve was calculated from equations describing the normalized circulating field (enhancement) of a coupled cavity introducing a Lorentzian gain profile into one of the cavities. The equations describing the coupled cavity have been derived by substituting the passive cavity by a mirror, with a frequency dependent reflection coefficient and phase shift [1, 2, 3]. Using a 1 mm long Nd:YVO_4 crystal (cavity C_{12}) coupled to a 30 mm long hemisperical resonator (cavity C_{23}) the enhancement factor of the cavity is shown in *Figure 1*. Introducing a Lorentzian gain into cavity C_{12} a temperature dependent frequency tuning curve as shown in *Figure 2* is be obtained. The laser experiences large mode-hops of about 60 GHz coincident with the mode spacing of cavity C_{12} as the temperature of the laser crystal is changed. In addition smaller mode-hops of about 5 GHz coincident with the mode spacing of cavity C_{23} occur. The calculation shows that the threshold varies substantially as the laser is tuned; this was also seen in a measurement of the emitted power.

The frequency stability of the laser has also been measured. The stability measurement was performed by temperature tuning the coupled cavity Nd:YVO_4 laser to make its oscillation frequency coincident with the oscillation frequency of a nonplanar monolithic Nd:YAG ring laser. The difference frequency between the two lasers was measured by a heterodyne beat experiment. The result is shown in *Figure 3*. The stability of the measured beat frequency was compared to the stability of a similar measurement on two identical reference lasers. From the measured time dependent frequency fluctuations the stability was then described through the square root of the so-called Allan variance as shown in *Figure 4*. For comparison the Allan variance of a single-frequency Nd:YAG laser using a linear cavity with an intra cavity etalon was also measured. The relationship between the Allan variance and the power spectral density is calculated according to the following equation:

$$\sigma_y^2(\tau) = 2\int_0^\infty S_y(f)\frac{\sin^4(\pi f\tau)}{(\pi f\tau)^2}df$$

From the power spectral density the laser linewidth can be calculated for a given time period.

1. C. Pedersen, P. L. Hansen, T. Skettrup and P. Buchhave, Opt. Lett. **20**, 1389 (1995).
2. C. Pedersen, Ph.D. dissertation (Department of Physics, Technical University of Denmark, Lyngby, Denmark, 1994).
3. C. Pedersen and Torben Skettrup, Submitted to JOSA B.
4. D. W. Allan, Proceedings of the IEEE, **54**, 221 (1966).
5. M. Ohtsu, H. Fukada, T. Tako and H. Tsuchida, Jpn. J. Appl. Phys. **22**, 1157 (1983).

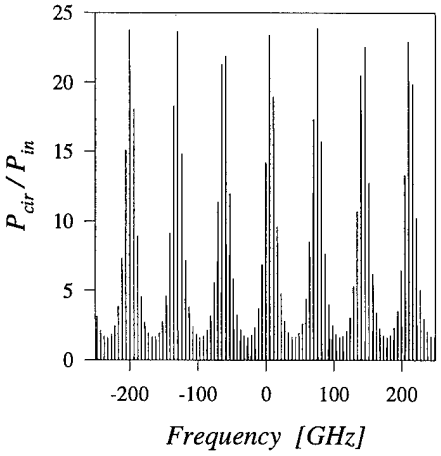

Figure 1: The calculated enhancement factor of the coupled cavity: L_{12} = 1 mm, L_{23} = 30 mm using published temperature dependent parameters of Nd:YVO_4.

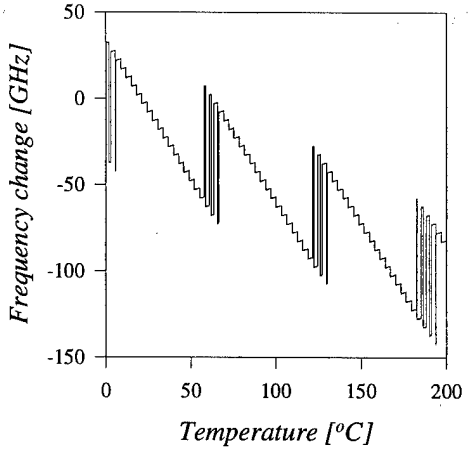

Figure 2: The calculated temperature dependent frequency tuning of the coupled cavity: L_{12} = 1 mm, L_{23} = 30 mm using published temperature dependent parameters of Nd:YVO_4.

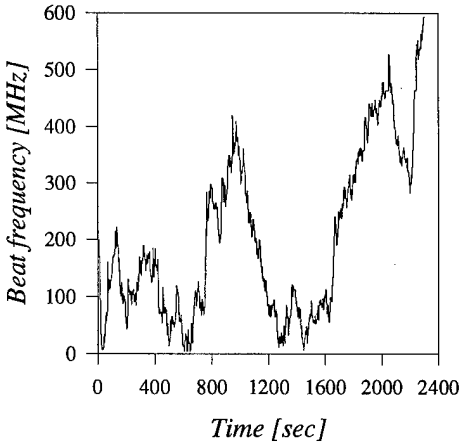

Figure 3: Beat frequency between a coupled cavity Nd:YVO_4 laser and a monolithic Nd:YAG laser

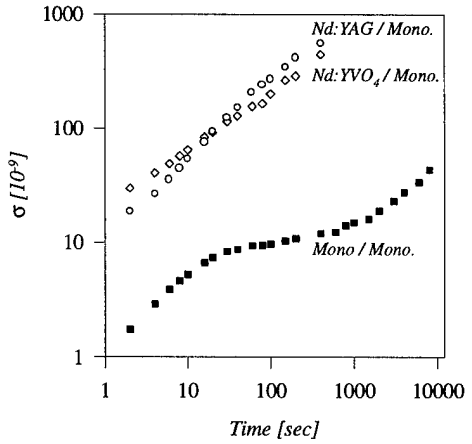

Figure 4: Square root of Allan variance measured for: coupled cavity laser, linear cavity with intra cavity etalon, and as reference a monolithic ring laser.

Investigation of frequency stability and design criterion of ring lasers

Christian Pedersen, Peter Lichtenberg Hansen, Preben Buchhave and Torben Skettrup

Technical University of Denmark, Department of Physics, 2800 Lyngby, Denmark,

Phone: (+45) 45 93 12 22, ext. 3289, Fax (+45) 45 93 16 69, E-mail plh@mips.fys.dtu.dk

We present a comprehensive Jones matrix analysis[1,2] of two commonly used ring laser resonators. Different aspects on how to obtain low loss eigenmodes and/or a high loss difference between the two directions of the cavity, and thus high frequency stability, are investigated. Also different approximations are evaluated. Since the theory has been kept general, the derived results can be applied to a large class of ring laser designs. Finally the influence of backscattered light on the stability is considered. Experimental results on two ring lasers are discussed.

In Fig.1 the "prism laser" design is shown. This is a further development and considerably more versatile version of the ring laser described in Ref. 3. The prism laser design includes an optical diode consisting of a 0.53° reciprocal polarization rotation θ_{res} coming from a 2° tilt on the output face of the Nd:YAG crystal and Faraday rotation θ_{Far} of 1.3° from a 1 Tesla magnet surrounding the Nd:YAG rod. Finally a quartz Brewster's prism with polarization strength T= 0.76 is used as a polarization discriminator. T is defined as the ratio of the transmission coefficient for s- and p-polarization for the 4 Brewster faces. Graphs of the azimuth α, the ellipticity ε, frequency shifts and losses are found as a function of the polarization strength T. From the general analysis it is found that the approximation

$$\Delta Loss = \sin^2(\theta_{res} + \theta_{Far}) + \sin^2(\theta_{res} - \theta_{Far})$$

where $\Delta Loss$ is the loss difference (corresponding to the case where T=0) should be avoided except for T-values close to 0. An exact equation for determination of the losses for arbitrary T is given. If T is chosen to be close to the optimal value (for maximum loss difference) it is found that the exact cancellation of the reciprocal rotation and nonreciprocal rotation is important even for the small rotation angles considered here. Otherwise a considerable loss can occur for the oscillating mode.

When we experimentally compare the prism laser (operating in a linearly polarized eigenstate with a loss difference of $\approx$ 0.6%) to a monolithic nonplanar ring oscillator operating in an elliptical polarization eigenstate[4], we have observed that the NPRO design has far better resistance to optical feedback although a loss difference of less than 0.01% is calculated for this laser. We suggest that the frequency shift accompanying an elliptical eigenstate is responsible for this. When light from the lasing direction is reflected back into the NPRO cavity it is frequency shifted

with respect to the resonance frequency of the original direction. The result is that back reflected ligth is undergoing destructive interference and hence inhibited. This effect has been noted in the litterature[4], but here we calculate the effect based on the frequency shift and the cavity parameters. For the prism laser this can lead to more than 8% loss for $T \approx 0.95$, using the mentioned parameters.

Fig.2 shows the Allan variance of the frequency fluctuations of two monolithic lasers (temperature stabilized), and of a monolithic laser and the prism laser (not temperature stabilized), measured from a beat experiment. It is observed that for τ-values in the second range the prism laser is more stable than the NPRO. The reason for this we attribute to the temperature drift, which affect the monolithic lasers more on this time scale. The general conclusion from Fig. 2 is that stable diode-pumped single-frequency ring lasers can be constructed using discrete components as demonstrated for the prism laser.

In this particular beat experiment the prism, shown in Fig. 1. has been rotated 180° so that an increased angle of incidence on the Nd:YAG rod can be obtained (from 10.6° to 30° angle of incidence). Consequently a considerably smaller overlap region between the incident and reflected wave is obtained at the input face of the Nd:YAG crystal, thus leading to reduced residual holeburning. This leads to single-frequency operation at significantly higher output powers. An optimized version with reduced residual holeburning are currently being implemented.

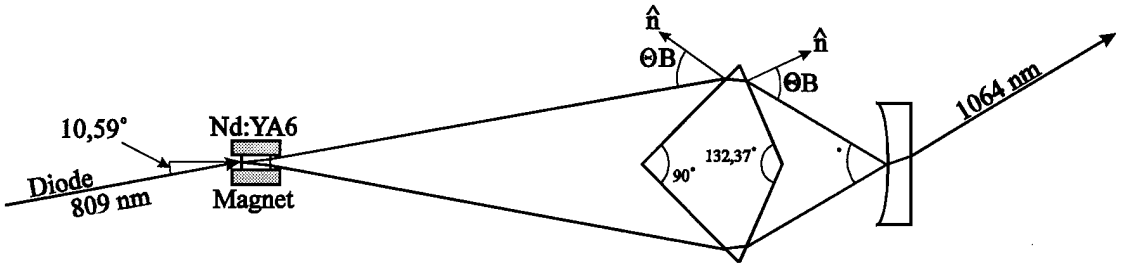

Fig. 1. Prism laser design.

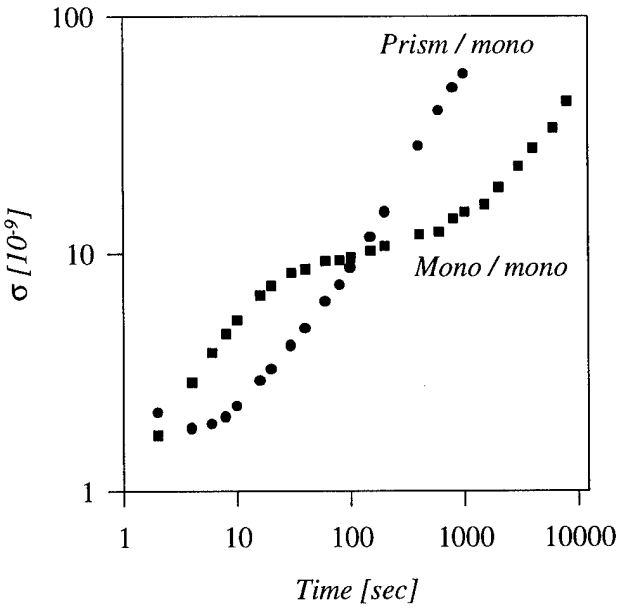

Fig. 2. Square root of Allan variance

1. V. Ya. Molchanov and G.V. Skrotskii. Soviet Journal of Quantum Electronics, Vol. 1, No. 4.

2. S.V. Kruzhalov and N.M. Kozhevnikov. Soviet Physics-Technical Physics, Vol. 17, No. 7.

3. W.A. Clarkson and D.C. Hanna. Optics Communication, Vol.73, No. 6, 15 November 1989.

4. Alan C. Nilsson, Eric K. Gustafson, and Robert L. Byer. IEEE Journal of Quantum Electronics, Vol. 25, No. 4, April 1989.

Single frequency coupled-cavity gain-switched chromium forsterite laser

Iain T. McKinnie, Andrew Tiffany and Donald M. Warrington

Department of Physics, University of Otago, PO Box 56, Dunedin, New Zealand

Tel. 64 3 479 7749 Fax 64 3 479 0964

We report (for the first time, to our knowledge) successful single axial mode operation in chromium forsterite, based upon an innovative dual cavity configuration. Near transform-limited bandwidth pulses are emitted in stable gain-switched operation. Single frequency operation in this important spectral region is not currently provided by other solid state laser systems. It is also anticipated that this laser cavity will be widely applicable to other laser media.

Laser operation of chromium (IV) doped lasers was first reported independently in 1988 by a number of groups[1,2,3]. Since then the potential of chromium forsterite and chromium YAG has been exploited in gain-switched, continuous wave, flashlamp pumped and mode-locked operation. However, although a broadly tunable pulsed ultra-narrow linewidth infrared laser source has potential applications in spectroscopy, nonlinear optics and remote sensing, spectral-narrowing in chromium (IV) systems has not been investigated to date. This may have been due to limitations in crystal quality. However, recent results with short, high dopant level, low loss chromium forsterite crystals[4,5] indicate considerable potential for these media in lossy, dispersive cavities. We have accordingly extended our preliminary investigation[5] to develop a pulsed narrow bandwidth laser.

We chose to use passive line-narrowing in preference to an injection seeding technique. Injection seeding with a narrow bandwidth CW source can yield low threshold, narrow bandwidth operation[6], but the tuning range is limited by the operating range of the seed source. In applications where the full wavelength range of the solid state laser is required, a passive cavity may be more versatile. Our geometry is based on the dye laser cavity originally reported by Hänsch[7]. This configuration was selected in preference to other passive cavities such as the grazing incidence laser. Our previous work with dye lasers[8] indicates that a significantly lower threshold can be obtained with the Hänsch-type laser. This is a critical factor in solid state lasers where pump induced crystal damage occurs at high pump pulse energy.

The single frequency chromium forsterite cavity is depicted in figure 1. The cavity was bounded by a high reflector and Littrow grating. The high reflector was coated for high reflectivity over the range 1150 — 1350nm, with high transmission and high damage threshold at the pump wavelength of 1064nm. The grating was blazed for Littrow operation in 6th order at 1250nm, close to the anticipated peak laser wavelength in forsterite. Coarse wavelength tuning was achieved by rotation of the grating, and the 4th diffraction order escaping the cavity was designated as the laser output. In order to maximise grating resolution. an achromatic four-prism beam expander was incorporated. Prisms were coated for antireflection at an incident angle of 55°. An etalon was inserted between the beam expander and diffraction grating. The etalon free spectral range of 30GHz, and finesse of 12 at the emission wavelength range were selected to isolate a single cavity mode. However the free-running bandwidth of the Littrow cavity without the etalon was sufficiently broad to allow the oscillation of more than one etalon mode. The final intracavity

element was the dichroic filter, which acted in a dual role. A reflectivity of > 99% at 1064nm ensured that the depleted pump was reflected back into the crystal, maximising pump absorption, and protecting the grating and etalon from damage. In addition, a reflectivity of around 5% between 1200 and 1300nm, allowed the dichroic filter to act as a reflector for a low finesse slave cavity within the dispersive resonator. It was the interplay of the coupled cavity modes which combined with the intracavity dispersive elements to ensure single frequency operation.

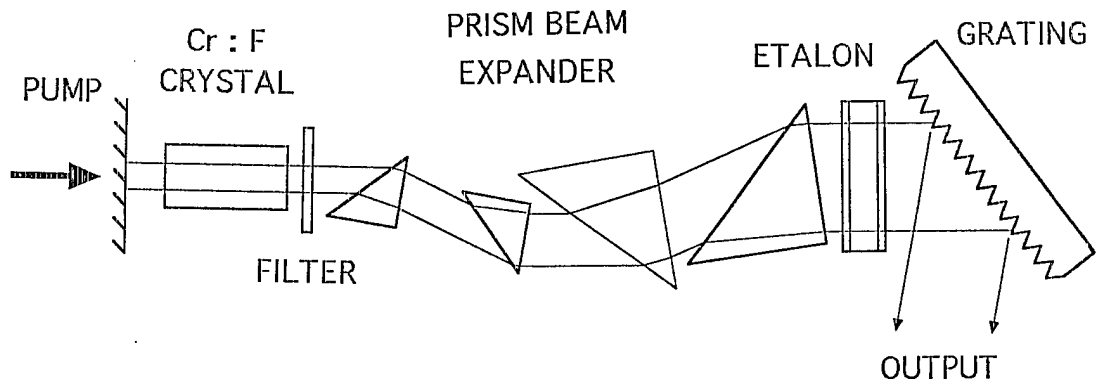

Figure 1. Schematic diagram of the coupled-cavity chromium forsterite laser

Excitation for the forsterite crystal is provided by a Q-switched Nd:YAG laser emitting 10ns pulses. The forsterite was doped with chromium (IV) to 0.1 atomic% by weight, and cut with a and b axes parallel to the end face edges. Pump polarisation was oriented parallel to the crystal b-axis for maximum conversion efficiency.

Evidence of the dual cavity operation of the laser is provided by analysis of the mode structure of the spectral output prior to insertion of the etalon. In this configuration the laser oscillates at up to 6 frequencies over a range of 100GHz. The total number of oscillating modes may be varied by fine adjustment of the dichroic filter, but single mode operation was not obtained. No attempt has been made to ascertain the linewidth of the modes of this cavity, but it was clearly below the 10GHz resolving limit of the analysing interferometer used in this case. An analysis of the mode structure will be carried out for an analogous Fox-Smith resonator[9].

Insertion of the etalon resulted in an increase of the laser threshold from 10.4 to 12.5mJ. Adjustment of filter and etalon led to a region of stable, single axial mode operation. Single frequency output was readily obtained at across the 100nm operating range of the laser. Figure 2 shows a measurement of the laser bandwidth using a 2.5GHz free spectral range interferometer. The measured linewidth of 150MHz was close to the measured instrument resolution of 120MHz, indicating that the 20ns pulses were close to transform-limited.

Both laser pulse duration and the delay between pump and gain-switched laser pulses were observed to vary with the pump intensity and the operating wavelength of the cavity. At the peak

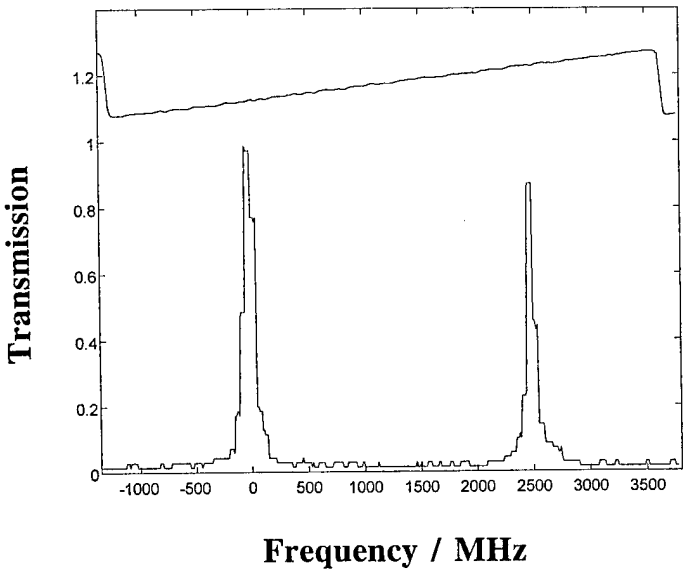

Figure 2. Interferometer transmission intensity as a function of frequency for the single mode chromium forsterite laser. The voltage ramp indicates interferometer scan duration.

emission wavelength of 1220nm, a pulse duration of 20ns, and delay of 110ns were measured. At 1180nm, the lower limit of the tuning range, pulse duration and delay increased to 80ns and 360ns respectively.

Although the laser routinely emits smooth pulses, in certain regions of operation strong temporal modulation was observed. This may indicate self-pulsing in the coupled cavity system.

The dual cavity single frequency laser described here is widely-applicable in other gain media. The relatively low threshold is particularly attractive for low gain or high loss materials. We have recently obtained stable, single frequency operation of titanium sapphire in this geometry.

References

1. V. Petricevic, S.K. Gayen and R.R. Alfano, Appl. Phys. Lett. **52** 1040 (1988).
2. H.R. Verdun, L.M. Thomas, D.M. Andrauskas and T. McCollum, Appl. Phys. Lett. **53** 2593 (1988).
3. N.B. Angert, N.I. Borodin, V.M. Garmash, V.A. Zhitnyuk, A.G. Okhrimchuk, O.G. Siyuchenko and A.V. Shestakov, Sov. J. Quantum Electron **18** 73 (1988).
4. G. Onishukov, W. Hodel, H.P Weber, V. Mikhailov and B. Minkov Opt. Comm. **100** 137 (1993).
5. I.T. McKinnie, L.A.W. Gloster, Z.X. Jiang and T.A. King *Conference on Lasers and Electro-Optics* Vol. 8, OSA Technical Digest Series (Optical Society of America, Washington DC, 1994), paper CTuE4.
6. C.H. Bair, P. Brockman, R.V. Hess and E.A. Modlin IEEE J. Quantum Electron **24**, 1045 (1988).
7. T.W. Hänsch Appl. Opt. **11**, 895 (1972).
8. I.T. McKinnie, H.B. Ahmad, A.J. Berry and T.A. King J. Phys D **25** 1687 (1992).
9. P.W. Smith Proc. IEEE **60** 422 (1972).

High-brightness cw-500-W Nd: YAG rod laser

Koji Yasui

Laser & Optics Technology Department
Advanced Technology R&D Center, Mitsubishi Electric Corporation
8-1-1 Tsukaguchi, Amagasaki 661, Japan

Phone: 81(Japan)-6-497-7110
Fax: 81(Japan)-6-497-7288
E-mail: yasui@lap.crl.melco.co.jp

The beam quality of commercial cw-based high-power solid-state lasers of over 400-W class is around $M^2 \approx 100$ or $\omega\theta$ (radius x - half angle of divergence) $\approx$ 33.7 mm-mrad and the focusing ability is approximately ten-times worse than that of commercial high-power CO_2 lasers even taking into consideration the short-wavelength advantage of solid-state lasers. Thermal distortion of the solid-state material is considered to be the main source of the beam quality degradation and there proposed are several solutions. Although laser diode-pumping [1] and slab-laser geometry [2] are considered to be promising methods to reduce the thermal distortions, diode-pumping requires expensive laser diodes with new, sometimes complicated, pumping configuration. Slab geometry also requires expensive slab-shaped materials and it is not adequate to generate symmetrical beam patterns for precious material processing applications. Therefore, we have set our goal to develop a high-brightness industrial solid-state laser based on a lamp-pumped rod-geometry design as can be operated in continuous-wave (cw) mode for high speed processing applications. Our independent analysis has shown that the polarization bifocusing compensation should play an important role in generating stable high-brightness laser beams. To prove this analysis in quantitative manner, we have developed an advanced laser configuration for a rod-geometry solid-state laser.

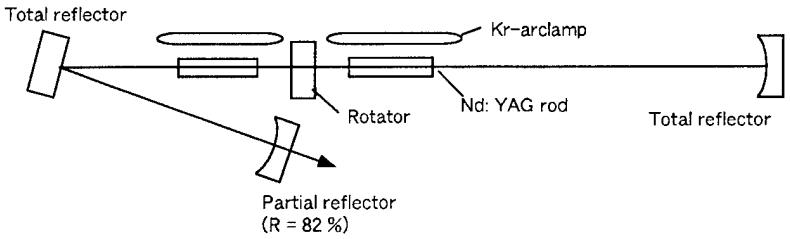

Fig. 1 Experimental setup.

Figure 1 shows the experimental setup. Two Nd: YAG rods with a quartz 90-degree polarization rotator between them are placed in a stable cavity. The Nd: YAG rod is 120 mm in length and 8 mm in diameter with Nd doping of 0.6 %. Each rod is pumped by a Kr-arc lamp. The resonator consists of a concave partial reflector (reflectance of 82 %), a total reflector, and a folding

mirror. Similar multi-rod configuration with a polarization rotator has been proposed but confirmed the operation only in low-power laser systems to generate linearly polarized TEM_{00} mode [3] or high power TEM_{00} mode reducing the depolarization loss [4]. Here the main purpose is to cancel out the bifocusing of the Nd: YAG rod for two polarization beams along the radial direction: r-polarization and the tangential direction: ϕ-polarization in the rod [5,6,7]. By introducing the bifocusing compensation, two stability zones for r- and ϕ-polarization became nearly identical as shown in Fig. 2 (a). Without the bifocusing compensation, the stability zones for r- and ϕ-polarization beams appeared on different positions as shown in Fig. 2 (b). For effective working of this bifocusing compensation, the thermal lensing uniformity in the rod is important. To generate uniform thermal lensing within the rod cross section, the pumping chamber is carefully engineered.

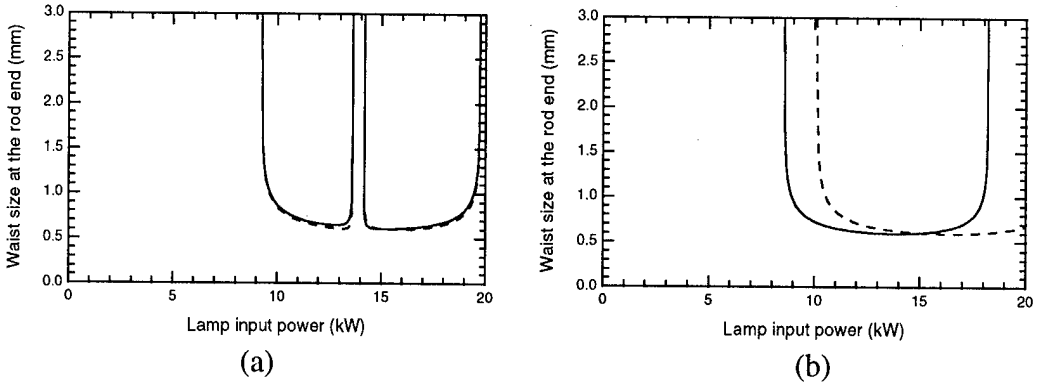

Fig. 2 Stability zone calculations for two polarization beams along the radial direction: r-polarization (solid lines) and the tangential direction: ϕ-polarization (broken lines) in the rod. The beam spot size for theoretical Gaussian beams at the end surface of the Nd: rod was calculated as a function of the lamp input power (a) with bifocusing compensation, and (b) without bifocusing compensation.

Figure 3 shows the lasing performance. By placing the polarization rotator between the Nd: YAG rods, the laser power increased in proportional to the lamp input power: P_{lamp} and reached 500 W at P_{lamp} = 18.4 kW. The power ratio against higher multi-transverse-mode operation at $M^2 \approx 100$ was approximately 80 %, which corresponds to the mode volume ratio in the rods. The beam mode shape was circular and the circular ratio defined by the minimum diameter divided by the maximum diameter was over 98 %. The beam quality slightly varied between M^2 = 19 - 30 and the best beam quality of M^2 = 19 or $\omega\theta$ = 6.4 mm-mrad was obtained at the laser power of cw-500W with the brightness of 126 MW / cm^2sr. This brightness is comparable with that of industrial CO_2 lasers. The beam quality measurement agreed well with theoretical calculations without considering the thermal lensing aberrations [7] of the Nd: YAG rods. When the polarization rotator was removed, the laser power decreased at least 20 % and saturated at P_{lamp} > 15 kW. At this saturating region, one circular polarized mode becomes dominant and this mode should be sensitive to the small depolarization loss variation in the rod [8]. In addition to the laser power enhancement, by introducing the bifocusing compensation, the laser power stability was improved. With the polarization rotator, the laser power was always stable with the power fluctuation of less than 1 % by a calorimetric power meter and the beam quality was easily measured by a Coherent's M^2 meter.

Without the polarization rotator, however, the laser power fluctuated at least 5 % and the alignment of resonator mirrors became very difficult. Because of this high fluctuation, beam quality measurement was impossible except a narrow region of $P_{lamp} \approx 15$ kW, where the two stability zone lines for r- and ϕ-polarization beams cross to each other as shown in Fig. 2 (b).

In conclusion, we achieved the enhancement of the lasing efficiency and the power stability of a high-brightness cw Nd: YAG rod laser by compensating the thermally induced bifocusing of the Nd: YAG rod. Maximum laser power of cw-500 W was obtained at the lamp input power of 18.4 kW with the beam quality $M^2 = 19$ or $\omega\theta$ (radius x - half angle of divergence) = 6.4 mm-mrad and the power fluctuation of less than 1 %. The maximum brightness: 126 MW/cm^{2}sr is comparable with that of industrial CO_2 lasers or solid-state slab-lasers. The beam quality results agreed well with calculations without consideration of the thermal lensing aberrations of the Nd: YAG rod. This indicates that further enhancement of the beam quality by modifying the resonator configuration and higher power generation by pumping harder or by laser diode pumping should be possible. At the conference, we are also going to talk about the Q-switching performance of this high-brightness laser and high power green beam generation using the laser.

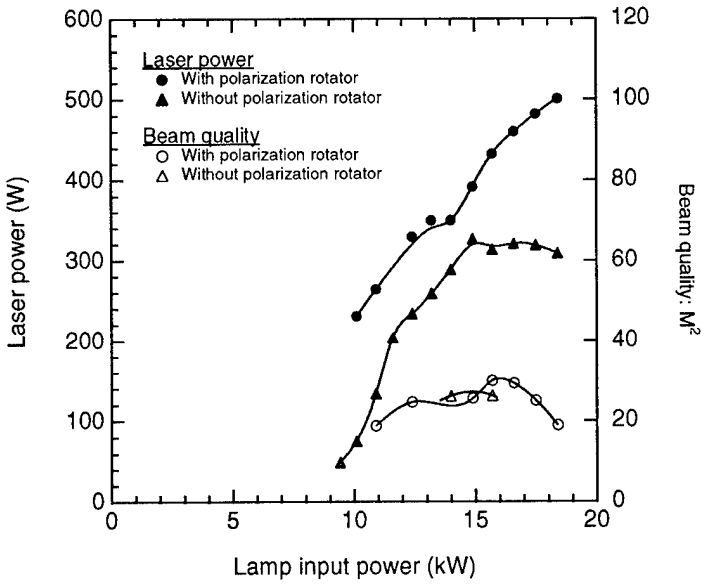

Fig. 3 Laser power and beam quality comparison between two cases: with and without bifocusing compensation.

References

1. R. L. Byer, Science 239, pp. 742, 1988.
2. W. S. Martin and J. P. Chernoch, "Multi internal reflection face pumped laser, " U.S. Patent 3,663,126 (January 4, 1972).
3. W. C. Scott and M. de Wit, "Birefringence compensation and TEM_{00} mode enhancement in a Nd: YAG laser, " Appl. Phys. Lett. vol. 18, pp. 3-4, 1971.
4. S. C. Tidwell, J. F. Seamans, and M. S. Bowers, "Highly efficient 60-W TEM_{00} cw diode-end-pumped Nd: YAG laser, " Opt. Lett. vol. 18, pp. 116-118, 1993.
5. N. U. Wetter, E. P. Maldonado, and N. D. Vieira Jr., "Enhanced efficiency of a continuous-wave mode-locked Nd: YAG laser by compensation of the thermally induced, polarization-dependent bifocal lens," Appl. Opt. vol. 32, pp. 5280-5284, 1993.
6. G. Cerullo, S. De Silvestri, V. Magni, and O. Svelto, " Output power limitations in CW single transverse mode Nd: YAG lasers with a rod of large cross-section, " Optical and Quantum Electron. vo. 25, pp. 489-500, 1993.
7. N. Hodgson and H. Weber, " Influence of spherical aberration of the active medium on the performance of Nd: YAG lasers, " IEEE J. Quantum. Electron. vol. 29, pp. 2497-2507, 1993.
8. K. Yasui and Jun-ichi Nishimae, "Beam-mode calculations of a strongly pumped solid-state rod laser with an unstable resonator, " Opt. Lett. vol. 19, pp. 560-562, 1994.

Q-switch and excited state absorption experiments with Cr^{4+}:LuAG single crystals

R. Moncorgé*, H. Manaa*, F. Deghoul*, Y.Guyot*,
Y. Kalisky†, S.A. Pollack#, E.V. Zharikov◊, M. Kokta△

*Université de Lyon I, URA 442 du CNRS, 69622 Villeurbanne, FRANCE
† Nuclear Research Centre-Negev, 84190 Beer-Sheva, ISRAEL
# Optitron Inc., 26340A S.W. ave, Lomita, CA 90717, USA
◊ General Phys. Inst., ul.Vavilova 38, Moscow 117942, RUSSIA
△ Union Carbide Corp., 750 S. 32nd st., Washougal, WA 98671, USA

As in Cr:YAG ($Y_3Al_5O_{12}$), tetrahedrally coordinated Cr^{4+} ions can be incorported in LuAG ($Lu_3Al_5O_{12}$) single crystals and give rise to similar optical and laser properties [1,2].

We report here on intracavity laser Q-switching of flash-lamp pumped Nd:YAG using Cr^{4+}:LuAG single crystals as saturable absorbers. We also report on a detailed investigation of saturable absorption of this system in connection with registration of fluorescence excitation and excited state absorption spectra made both in the visible and the infrared spectral domains.

In the intracavity laser Q-switching experiment we used a 40 cm long flash-lamp pumped Nd:YAG laser cavity with a Nd:YAG laser rod of 100 mm long and 7 mm in diameter and a 30 % transmittive output coupler at 1.064 μm. The Cr^{4+}:LuAG crystal was a disc of about 1 cm in diameter and 4 mm thick and its small signal absorption coefficient at 1.064 μm was about 2.5 cm^{-1}. Its faces were cut and polished flat and parallel without any antireflection coating . In the free-running regime the Nd:YAG laser delivers flash and laser pulses of about 50 μs duration at a repetition rate of 10 Hz. Intracavity laser Q-switching (Q.S.) was thus obtained at two pumping levels, first at a pumping level corresponding to a free-running (F.R.) laser pulse of about 100 mJ with the appearance of a single Q.S. pulse of about 25 ns and 35 mJ, then at a pumping level corresponding to a F.R. output of about 200 mJ with the appearance of two Q.S. pulses of about 35 ns each and a total energy of about 70 mJ. We show in Fig. 1 the profiles and the respective positions of the different pulses in the low pumping regime. The single Q.S. pulse appears 52 μs after pumping has started, whereas the first one of the two pulses obtained at high pumping level appears at about 42 μs, thus at shorter time. This behaviour can be easily explained by using a model such as the one used in Ref. 3.

The transmission measurements were made with the aid of a Q-switch Nd:YAG laser at 1.064 μm delivering pulses of 12 ns. We used the same Cr:LuAG crystal as above so that we had to correct the data from the reflection of the faces knowing that the refraction index of LuAG is about 1.81. We show in Fig. 2 the resulting curve for input pump fluences going up to about 3 J/cm^2. These data were fitted with an expression reported in Ref. 3:

$$\frac{dE}{dz} = -h\upsilon N_0 \left(1 - \frac{\sigma_{esa}}{\sigma_{gsa}}\right)\left[1 - \exp\left(-\frac{\sigma_{gsa}E}{h\upsilon}\right)\right] - N_0\sigma_{esa}E$$

in which we have assumed no nonsaturable losses, E is the energy fluence, hν the incident photon energy, N_0 the Cr^{4+} doping density and σ_{gsa} and σ_{esa} are the ground- and the excited-state absorption cross sections at 1.064 μm, respectively. With a value for $\sigma_{esa} < 3 \times 10^{-20}$ cm^2 it is concluded to negligible ESA around 1.064 μm, which is a very interesting result. For comparison, a value of $\sigma_{esa} \approx 2 \times 10^{-19}$ cm^2 (or 6×10^{-19} cm^2 under polarized laser conditions) was reported recently in Cr:YAG [4,5], thus limiting the transmission in the saturation regime to less than 90 %.

ESA and fluorescence excitation spectra were then registered, the former by using a standard pump-probe technique and the latter by monitoring the fluorescence of the crystal around 1400 nm. We used for that both the crystal described above and a smaller and thinner one. This was made first to deconvolute the absorption of the tetrahedrally coordinated Cr^{4+} ions from those with octahedral environments, about 90 % of the total dopant concentration according to previous works [5,6], then to use the resulting ground state absorption cross section spectrum to deduce the ESA cross section one in the same wavelength domain and to give an estimate of the maximum stimulated emission cross section. We show in Fig.3 a picture of the registered ESA difference spectrum given by

$$\ln(I_p / I_u) = (\sigma_{gsa} + \sigma_{em} - \sigma_{esa}) N^* l$$

where I_p and I_u stand for the transmitted intensities in the pump and unpumped regimes, σ_{em} for the emission cross section, N* is the density of excited ions and l the crystal thickness. If we consider each of the three sets of tetrahedrally coordinated Cr^{4+} ions separately [7], it is found around 1400 nm an effective stimulated emission cross section of about 2.8×10^{-19} cm^2, in perfect agreement with the value obtained from the laser experiments [1] and that derived from the emission bandshape and by using a fluorescence lifetime of 5.5 μs and a fluorescence quantum efficiency of 33 % [5].

In conclusion, Cr^{4+} doped LuAG, though having very similar general optical properties as Cr:YAG, may give rise to some more interesting characteristics such as reduced ESA at 1.064 μm. It was proved to lase CW; we also have already obtained pulsed laser action, but only for a short period of time, probably due to optical damage in the crystal.

Acknowledgments

Thanks are expressed to Prof. G. Boulon for his interest in this research and to Dr. T. Benyattou for his assistance in collecting the fluorescence excitation data.

References

1. J. Zhang, Y. Kalisky, G. Atkinson, M. Kokta, in Advanced Solid State Lasers Technical Digest, 1995 (Optical Society of America, Washington DC, 1995), paper TuC10, pp. 182
2. H. Eilers, U. Hömmerich, S.M. Jacobsen, W.M. Yen, M. Kokta, Opt. Lett. 18 (1993) 1928
3. Y.K. Kuo, M.F. Huang, M. Birnbaum, IEEE J. Quant. Elect. 31 (1995) 657
4. K. Spariosu, W. Chen, R. Shultz, M. Birbaum, A.V. Shestakov, Opt. Lett. 18 (1993), 814
5. S. Kück, Dostoral Dissertation, University of Hamburg, Germany (1994)
6. A.G. Okhrimchuk, A.V. Shestakov, Opt. Materials 3 (1994) 1
7. H. Eilers, K.R. Hoffman, W.M. Dennis, S.M. Jacobsen, W.M. Yen, Appl. Phys. Lett. 61 (1992) 2958

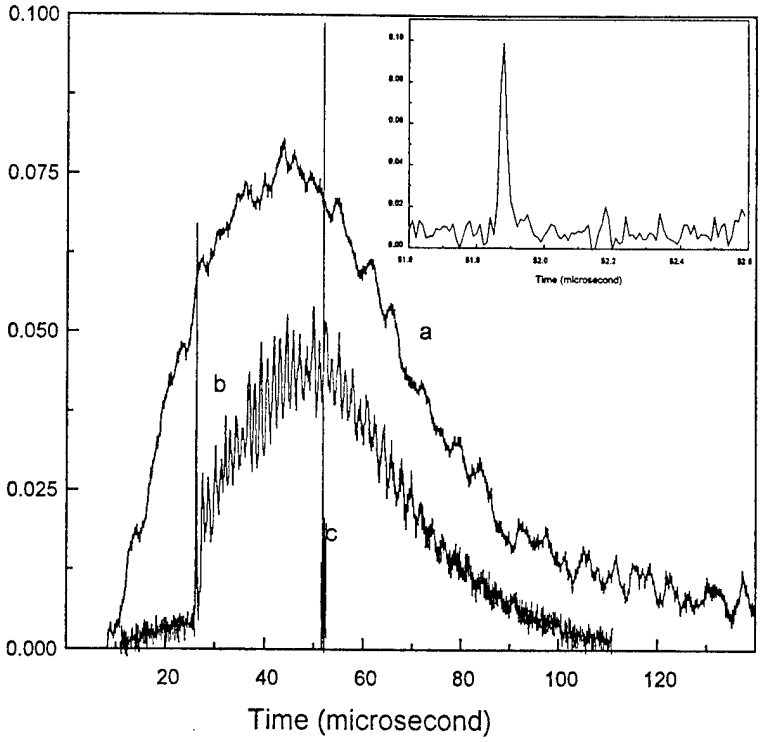

Figure 1: Flash-lamp (a), free-running (b) and Q-switch (c) laser pulses (insert: detail of Q-switch laser pulse) at low pump level

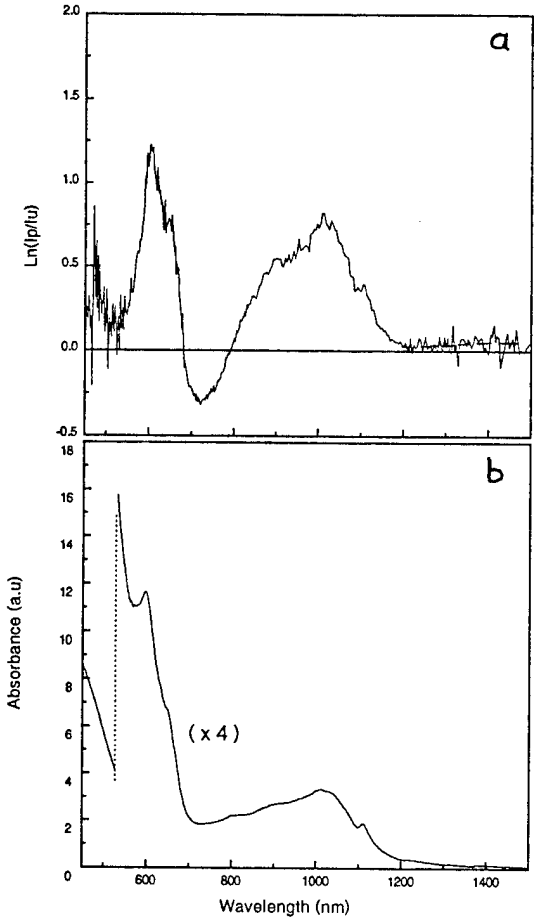

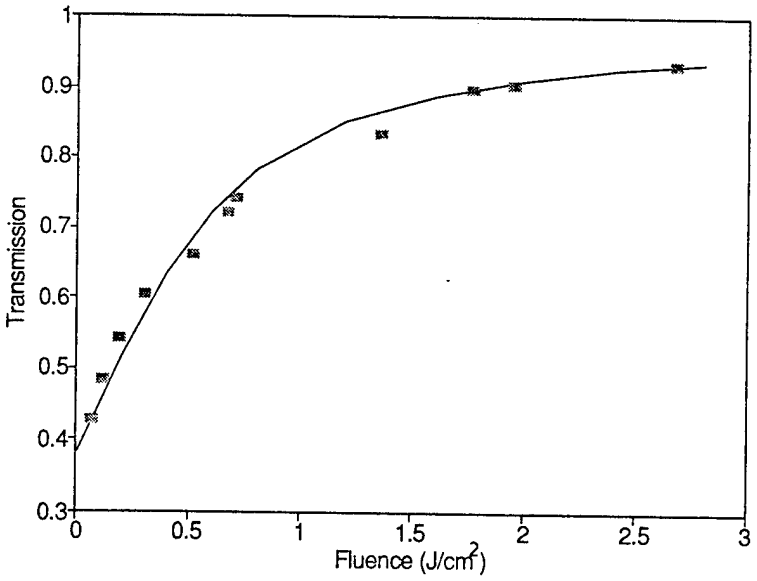

Figure 2: Transmission versus incident pump fluence in the case of LuAG:Cr (▣) (thickness e = 3.84 mm) and fits (——) to expression (2) in the text

Figure 3: Excited-state difference (a) and ground-state (b) absorption spectra of LuAG:Cr single crystal

HIGH AVERAGE POWER DIODE ARRAY PUMPED FREQUENCY DOUBLED YAG LASER.

B.J LE GARREC, G.J RAZÉ.
CEA/DCC/DPE/SPL, Centre d'études de Saclay
F-91191 Gif sur Yvette, FRANCE

1. INTRODUCTION.

In order to obtain high average power in the green, a diode pumped laser program is under development. High average power (tens of watts) and high repetition rate (tens of kilohertz) require: cw diode array pumping, high reprate Q-switching and intra-cavity second harmonic generation.
We report the demonstration of a transversely diode array pumped frequency doubled Nd:Yag. The 30 linear diode arrays are arranged radially around a single Nd:Yag rod providing up to 635 watts of pumping power around 808 nm.

2. DIODE PUMPED LASER MODULE.

The design of the diode pumped laser module follows very simple and specific rules: one single water cooling design, one single electrical supply.

Thirty 20 watts cw diode laser arrays supplied by Spectra Diode Labs (SDL-3470-S) are optically coupled to a Nd:YAG rod (6.2mm diameter, 105 mm long). It is not possible to mount each 1 cm long diode array on a water cooled brass submount like we did in our early experiments [1] .

The diode laser module is based on a 30 bars structure made of 5 water cooled submounts arranged in a fivefold symmetry around the laser rod. Each submount incudes 6 bars and 2 collimating cylindrical lens (anti-reflection coated cylindrical lens, diameter 6mm, length 90 mm). The collimating cylindrical lens holder is part of the water cooled submount. The thirty diode arrays are positioned at angles of 36° with respect to each other and arranged alternatively to pump the rod along 9 cm. To avoid suppliing the bars in parallel, we use a non conductive material for the cooling submount (Delrin). The cooling submount is provided with 6 square apertures (three on each side) . Each diode bar is mounted with a square flat joint and the water flows along the anode case of each bar throughout the cooling module. The Nd:Yag rod (diameter 6.2 mm, length 105 mm, 1% Nd doping) is polished and is mounted inside a glass sleeve for water cooling.

3. LASER RESONATOR FOR INTRA-CAVITY SHG.

The principle of the cavity has been proposed by Kuizenga and coworkers [2, 3]. In classical linear or L-shape cavities, the spotsize in the non-linear crystal decreases as the pump power is increased, and this can cause damage in the non-linear crystal. In the Z-shape resonator, an optical relay is formed by two concave mirrors between the laser medium and the non-linear crystal. The optical relay images the laser rod aperture into the non-linear crystal. Figure 1 illustrates this optical relay in the case of a magnification of 2 (mirrors curvatures: 200 and 100 mm) and a 4*4*6 mm^3 KTP crystal. The curved mirrors are tilted with an angle of 12° and the four cavity mirrors are high reflectors at 1064 nm.

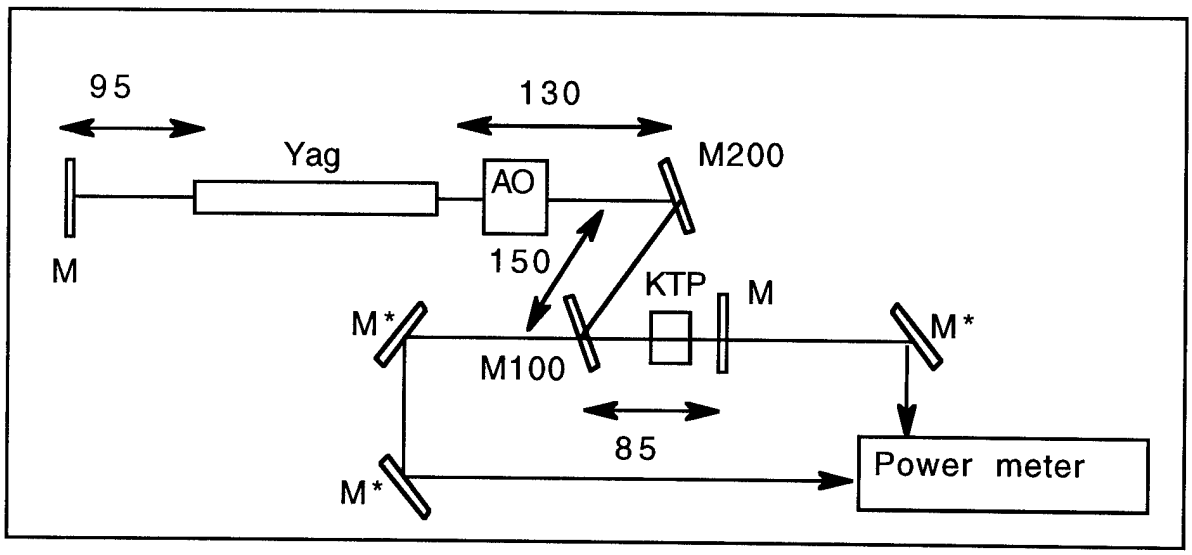

Fig.1. Z shape resonator for intra-cavity SHG: M: flat HR at 1064 nm, M200, M100 concave R=200 and R=100 mm HR at 1064 nm, M*: 45° HR at 532 nm.

The laser is repetitively Q-switched with an acousto-optic Q-switch at high repetition rate in the range of 5 to 25 kHz, and the the Q-switch off time and RF power are adjusted for maximum output power.

The laser resonator enables SHG along two opposite directions into the KTP crystal and the two main laser beams at 532 nm are extracted through the mirrors closest to the KTP crystal.

Between 30 and 32,5 amps diode drive current, the average green power is greater than 40 watts at 9 kHz in a 200 ns pulse (FWHM) leading to an optical to electrical efficiency greater than 2.1 %. At a maximum diode drive current of 32.5 A, we have obtained 46 Watts at 9 kHz in a 200 ns pulse (FWHM) leading to an optical to electrical efficiency of 2.3 %. Figure 4 shows the green average power and overall efficiency as functions of diode drive current.

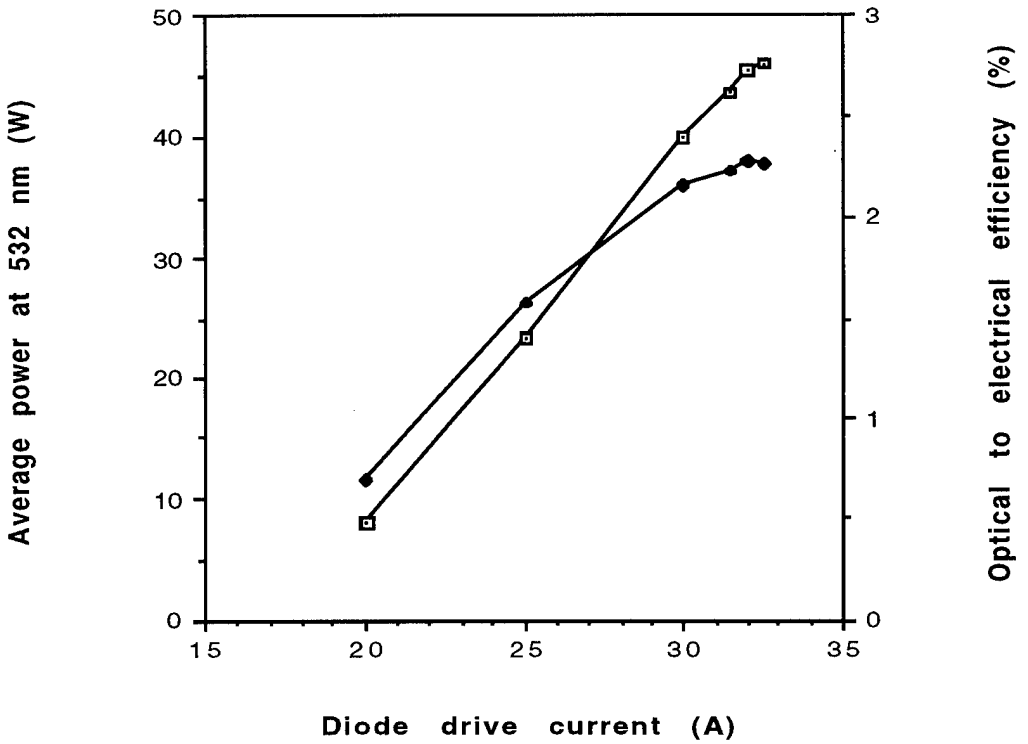

Figure 2: average output power at 532 nm and optical to electrical efficiency versus diode drive current at 9 kHz reprate.

4. CONCLUSION.

At 32.5 A diode drive current (585 watts pumping power), we have been able to obtain 46 watts average power at 532 nm in a Z shape cavity Q-switched at 9 kHz. The laser beam was intra-cavity doubled in a 6 mm long KTP crystal. The pulse to pulse stability is better than 0.5 % over several hours.

5. REFERENCES.

[1] B. Le Garrec, Ph. Féru: "High power diode-array-pumped frequency doubled Nd:Yag laser" Conference on lasers and electro-optics CLEO'94 Anaheim May 8-13, 1994 paper CTHC5 Volume 8 CLEO'94 Technical Digest p283-284.

[2] M. Ortiz, J. Fair, D. Kuizenga : " High average power second harmonic generation with KTiOPO4 ". OSA Proceedings on Advanced Solid State Lasers Vol.13, 1992, p361-365.

[3] D.J. Kuizenga: US Patent 4907235, 3-6-1990.

Precision Distance Measurements Using Frequency Stabilized Nd:YAG Lasers

V. Mahal, E. Inbar and A. Arie
Dept. of Physical Electronics, Faculty of Engineering, Tel Aviv University,
Ramat Aviv, Tel Aviv, Israel 69978
Tel: 972-3-6408047, Fax: 972-3-6423508

Accurate distance measurements are important in many industrial applications, such as position control, surface testing and integrated circuits profiling. For single wavelength interferometric distance measurements, the laser wavelength should be precisely known and kept fixed during the measurements in order to achieve sub-nanometer accuracy. However, single wavelength interferometric measurements are often limited by the short non-ambiguity range $\lambda/4$, which for Nd:YAG lasers is ~ 0.26 μm. Furthermore, the measured distance should be monitored continuously, otherwise small changes caused by air turbulence, mechanical vibrations, etc. may exceed the non-ambiguity range, thus rendering the data useless. The non-ambiguity range can be extended by using two different wavelengths (λ_1 and λ_2) to create a synthetic wavelength, Λ, where $1/\Lambda=1/\lambda_1-1/\lambda_2=\Delta\nu/c$, greater than the optical wavelength, hence having a longer non-ambiguity range. Precision dual wavelength interferometry requires calibration and control of the synthetic wavelength, i.e. of the frequency *difference* between the lasers, $\Delta\nu$.

Monolithic diode-pumped Nd:YAG lasers are attractive sources for interferometric measurements, owing to their excellent beam quality and long coherence length. Absolute frequency control of Nd:YAG lasers is now possible by locking the first harmonic to sub-Doppler lines of $^{133}Cs_2$ near 1064 nm [1] or the second harmonic frequency to sub-Doppler transitions of $^{127}I_2$ near 532 nm [2, 3]. These molecules have dense spectra within the tuning range of the Nd:YAG and doubled Nd:YAG lasers. The frequencies of several I_2 and Cs_2 transitions were recently measured with a high accuracy [1, 4]. These locked lasers can thus be directly utilized for precision single wavelength distance measurements. Moreover, locking the lasers to molecular transitions enables to determine not only the absolute frequencies but also their frequency difference $\Delta\nu$ with an accuracy of ~1 MHz. Hence, dual wavelength interferometry may be performed using two Nd:YAG lasers locked to sub-Doppler lines of Cs_2 or I_2. The independent stabilization of each laser saves the need for a high frequency offset control loop or a Fabry-Perot cavity for calibration. For example, the synthetic wavelength for $\Delta\nu\approx35$ GHz can be determined with a relative accuracy of $3\cdot10^{-5}$. Locking the lasers to different transitions of Cs_2 and I_2 allows for a wide selection of synthetic wavelengths, from a few millimeters to several meters.

For locking to I_2 transitions near 532 nm we have used a dual wavelength Nd:YAG laser (Lightwave Electronics 140 with modifications). An error signal was obtained by modulation transfer spectroscopy: The laser was split into a pump and probe beams which counter-propagated through a 15 cm I_2 cell held at 0 °C. The pump was phase modulated using an electro-optic modulator at 1 MHz, and the probe signal was detected and mixed with the modulating 1 MHz sine wave. This signal was then fed through a servo amplifier to the piezo electric actuator of the laser. The Allan variance of I_2-locked lasers was at a level of 10^{-13}. [2, 3] The maximum

excursion of the locked laser frequency was ~1 kHz in 1 hour [2]. The absolute frequency of one of the I_2 transitions near 532 nm was recently measured with an accuracy of $1.2 \cdot 10^{-10}$. [4] Absolute frequencies of many other I_2 transitions near 532 nm can be determined with an accuracy of ~ 250 kHz ($4.5 \cdot 10^{-10}$) using the heterodyne measurements of Ref. [2].

The second Nd:YAG laser (Lightwave Electronics 122) was locked to sub-Doppler lines of Cs_2 near 1064 nm using FM saturated absorption spectroscopy, see Fig. 1. The probe was phase modulated and the pump was chopped using a chopper and frequency shifted (to eliminate interferometric noise with probe) using an acousto-optic modulator. The 15 cm Cs_2 cell was held in a small oven which heated it to ~ 220 °C in order to increase to Cs_2 absorption. After passing through the cell the probe was detected and demodulated using a mixer and lock in amplifier, and the FM signal was then used to lock the laser frequency. The Cs_2-locked laser was characterized by measuring its beat frequency against the I_2-locked Nd:YAG laser. The Allan variance reached a minimum of $1.3 \cdot 10^{-11}$ for a measurement time of 20 s (beat frequency fluctuations of 3.65 kHz) [1]. The maximum excursion the locked frequency over a one hour period was ~100 kHz. The lower stability was due to the wider transition linewidth and the stronger dependence of the transition frequency on the cell temperature. However, the Cs_2-locked system was much simpler because second harmonic generation was not required. Additional improvement in stability may be achieved by placing the absorption cell inside a Fabry-Perot cavity [1], thus increasing the Cs_2 effective absorption length. By measuring the beat frequency between the I_2-locked laser and the Cs_2-locked laser we have determined the absolute frequencies of several Cs_2 lines with an accuracy of ~ $3 \cdot 10^{-9}$ (1 MHz) [1].

We have used the two-locked lasers as a source for synthetic wavelength interferometry. Two methods for measuring distance were tested, fringe contrast and phase shifting interferometry. In the fringe contrast measurements, the two interference signals were combined on a photodiode thus creating a beat signal whose amplitude is proportional to the fringe contrast, and consequently, to the synthetic phase. The optical path difference was then calculated by measuring the contrast. Typical rms error of a measurement covering a range of 2 mm in 0.2 mm increments with a synthetic wavelength of 17.540 ± 0.001 mm, was 68 μm. The main cause of error was interferometer misalignment which reduced the signal amplitude, thus inducing a shift in the measured phase. The measurement range was further limited since as the fringe contrast approaches maximum, a small error in the measured intensity corresponds to a large error in the calculated distance. For measuring longer distances we used phase-shifting interferometry: The optical phase was varied in 5 steps corresponding to $-\pi$, $-\pi/2$, 0, $\pi/2$, π by applying a 5 step voltage sequence from an arbitrary waveform generator to a PZT, attached to the reference mirror. We have measured the intensities of the two interference signals after each step. The optical phase of each signal was calculated using these intensities and the synthetic phase Φ (obtained by numeric subtraction of the optical phases) was used to determine the path difference. The results of two measurements obtained with synthetic wavelengths 19.675 ± 0.001 mm and 17.540 ± 0.001 mm, covering a range of 10 mm in 0.5 mm increments, are shown in Fig. 2. Typical rms error was 70 μm, i.e., $\Lambda/260$. This error was mainly due to variation in the optical path difference during the phase measurement, caused by air turbulence, thermal and mechanical vibrations of the table and mirror mounts etc.

The accuracy of our measurements was limited by fringe interpolation accuracy. However, if longer distances are measured, the accuracy will be eventually limited by the accuracy and stability of the synthetic wavelength. The independent locking of two Nd:YAG lasers to molecular absorption lines provides a feasible method of controlling the synthetic wavelength. This system can be simplified if both lasers are locked to Cs_2. Higher accuracy and stability can be achieved by locking both lasers to I_2. The advantages of large non-ambiguity range by using two-wavelength interferometry and high precision by using single wavelength interferometry may be combined if the two-wavelength measurement accuracy will exceed the optical non-ambiguity range of ~ 0.26 μm. In this case, a further improvement in accuracy to the sub-nanometer range may be achieved by repeating the measurement using a single wavelength. With the current fringe interpolation accuracy of $\Lambda/260$, the required two-wavelength interferometric accuracy may be reached using a Nd:YAG laser locked to Cs_2 or I_2 and an additional semiconductor laser or Nd:LNA laser locked to He or Cs_2 transition near 1083 nm [5].

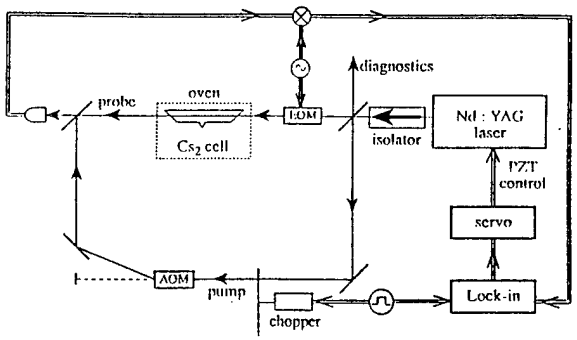

Fig. 1: Experimental setup for locking the Nd:YAG laser to Cs_2 using FM spectroscopy. EOM, electro-optic modulator; AOM, acousto-optic modulator; PZT, piezoelectric transducer.

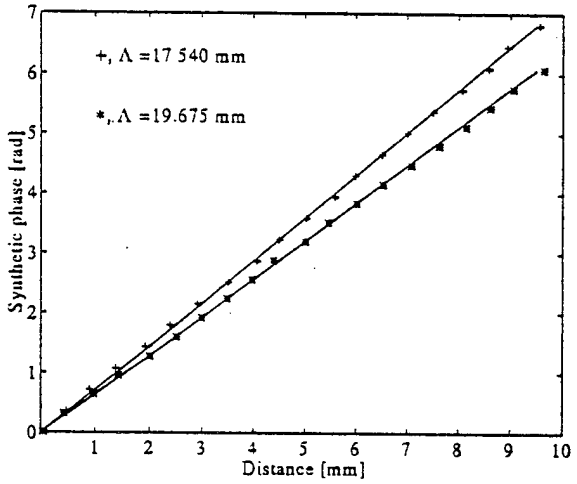

Fig. 2: Measured phase Φ for two synthetic wavelengths: Λ=19.675 denoted by (*) and Λ=17.540 mm denoted by (+). The distance is simply $\Lambda\Phi/4\pi$. Solid curves represent the theoretical phase.

This work was supported by the Israeli Science Foundation.

1. E. Inbar, V. Mahal and A. Arie, "Frequency stabilization of Nd:YAG lasers to $^{133}Cs_2$ sub-Doppler lines near 1064 nm", submitted for publication; A. Arie and E. Inbar, *Opt. Lett.* **20**, 88-90 (1995).

2. A. Arie and R. L. Byer, *J. Opt. Soc. Am. B* **10**, 1990-1997 (1993).

3. M. L. Eichoff and J. Hall, *IEEE Transaction Instrum. and Meas.* **44**, 155-158 (1995).

4. P. Jungner, S. Swartz, M. Eickhoff, J. Ye and J. L. Hall, *IEEE Transaction Instrum. and Meas.* **44**, 151-154 (1995).

5. A. Arie, P. C. Pastor, F. S. Pavone and M. Inguscio, *Opt. Comm.* **117**, 78-82 (1995).

LASER BEAM PROPAGATION IN A THERMALLY LOADED ABSORBER

Alphan Sennaroglu
Department of Physics, Koç University, Istinye, Istanbul 80860, Turkey
Phone: 90-212-277-6196; Fax 90-212-229-0680

Attila Askar and Fatihcan M. Atay
Department of Mathematics, Koç University, Istinye, Istanbul 80860, Turkey

In end-pumped solid-state laser crystals, absorbed pump power gives rise to thermal loading effects due to the temperature dependence of the refractive index and absorption coefficient. Hence, crystal transmission as well as the beam parameters are modified as a function of the incident pump power. Complete understanding of these effects is of paramount importance in designing efficient, well optimized laser systems. In this paper, the theory and results of a novel perturbative scheme to analyze this phenomenon is described. Numerical results clearly indicate the emergence of thermally induced, power-dependent lensing effects and show a decrease in crystal power transmission with increasing incident pump power.

Table 1 lists the key parameters of the model characterizing the optical and thermal properties of the solid-state absorber. The parameters z_0, ω_0, and z_f describe the unperturbed gaussian beam that would propagate, had there been no thermal gradients.

Neglecting absorption saturation, the temperature dependence of the refractive index n and the absorption coefficient α are assumed to be of the form

$$n = n_0 + n_T\left(T - T_r\right) \tag{1}$$

and

$$\alpha = \alpha_0 + \alpha_T\left(T - T_r\right). \tag{2}$$

Above, T is the temperature, T_r is the reference temperature at which n_0 and α_0 are measured and the other parameters are as described in Table 1. Furthermore, the electric field is assumed to propagate in the presence of a quadratic temperature distribution $T(r,\zeta)$ which can be expressed as

$$T(r,\zeta) - T_b = T_0(\zeta) - T_1(\zeta)r^2, \tag{3}$$

Name	Symbol	Units	Typical values
Differential absorption coefficient	α_0	cm^{-1}	1.5
Crystal thermal conductivity	κ	W/cm.K	0.13
Refractive index	n_0	1	1.8
Thermal index gradient	n_T	K^{-1}	9.8×10^{-6}
Thermal absorption gradient	α_T	$cm^{-1}K^{-1}$	5×10^{-5}
Incident pump power	P_i	W	0-5
Rayleigh range (unperturbed beam)	z_0	cm	1.3-133
Beam waist (unperturbed beam)	ω_0	μm	50-500
Focus location (unperturbed beam)	z_f	cm	0.5
Crystal radius	r_0	mm	2.5
Crystal length	L	cm	2
Pump wavelength	λ	μm	1.06

Table 1 Key parameters of the model

where r is the radial coordinate, $\zeta = \alpha_0 z$ is the dimensionless longitudinal coordinate, and T_b is the fixed temperature of the heat sink. The functions $T_0(\zeta)$ and $T_1(\zeta)$ are approximated from the exact solution for the heat equation with an attenuated gaussian beam as the heat source and by neglecting longitudinal heat conduction [1].

The treatment of beam propagation in a cylindrically symmetric medium in the absence of thermal effects is described by Yariv and Yeh [2]. For the thermal loading case, a similar functional form is assumed for the linearly polarized electric field $E_x(r,\zeta)$:

$$E_x(r,\zeta) = E_0 \exp\left(-i\left[p(\zeta) + \frac{k_c r^2}{2q(\zeta)}\right]\right)\exp\left(-ik_c\zeta/\alpha_0\right). \qquad (4)$$

In Eq. 4, $p(\zeta)$ and $q(\zeta)$ are the beam parameters and the wave number k_c expressed in terms of the vacuum wave number k_0 reads

$$k_c = k_0 n_0 - i\alpha_0/2. \qquad (5)$$

By substituting the electric field given by Eq. 4 into the scalar wave equation (see reference 2) and by making the change of variables

$$\frac{1}{q(\zeta)} = \frac{\alpha_0}{u(\zeta)}\frac{du}{d\zeta}, \qquad (6)$$

the modified beam parameter $u(\zeta)$ satisfies the equation

$$\frac{d^2u}{d\zeta^2} + \delta f(\zeta)u(\zeta) = 0, \qquad (7)$$

where

$$f(\zeta) = \frac{e^{-\zeta}}{1+\left(\zeta/a - z_f/z_0\right)^2} \qquad (8)$$

and

$$\delta = \frac{\left[2n_0 n_T k_0 - i(n_0\alpha_T + n_T\alpha_0)\right]k_0}{2k_c^2\alpha_0\kappa}\frac{P_i}{\pi\omega_0^2}, \qquad (9)$$

with $a = \alpha_0 z_0$. The dimensionless parameter δ expressed in terms of the parameters listed in Table 1 quantifies the extent of thermal effects and, in particular, is proportional to the incident pump intensity $P_i/\pi\omega_0^2$. Since Eq.7 does not have a closed-form analytical solution, a perturbative technique is employed to express the exact solution as a power series of the parameter δ in the form

$$u(\zeta) = u^{(0)}(\zeta) + \delta u^{(1)}(\zeta) + O(\delta^2), \qquad (10)$$

where $u^{(i)}$ is the ith-order solution. The zeroth-order solution $u^{(0)}(\zeta)$ given by

$$u^{(0)}(\zeta) = (\zeta - \alpha_0 z_f) + ia \qquad (11)$$

reproduces the well-known gaussian beam described in reference 2 for the non-thermal case. It can be shown using Eq.'s 7 and 10 that the first-order correction term $u^{(1)}(\zeta)$ can be computed from

$$u^{(1)}(\zeta) = -\int_0^{\zeta} d\zeta' \int_0^{\zeta'} d\zeta'' f(\zeta'') u^{(0)}(\zeta''). \qquad (12)$$

Once the first-order correction is evaluated through numerical integration, all of the other beam parameters such as the spot size and crystal transmission can be calculated in a straightforward fashion.

Fig. 1 shows the variation of beam spot size $\omega(\zeta)$ as a function of ζ for different levels of input pump power in a 2-cm-long absorber characterized by the parameters in Table 1. The beam waist in the absence of thermal loading is 50 μm. Note that the model successfully predicts the onset of thermally induced lensing with increasing incident

pump power. Furthermore, the expected result that the focal length of the induced thermal lens should decrease with increasing incident pump power is clearly evident.

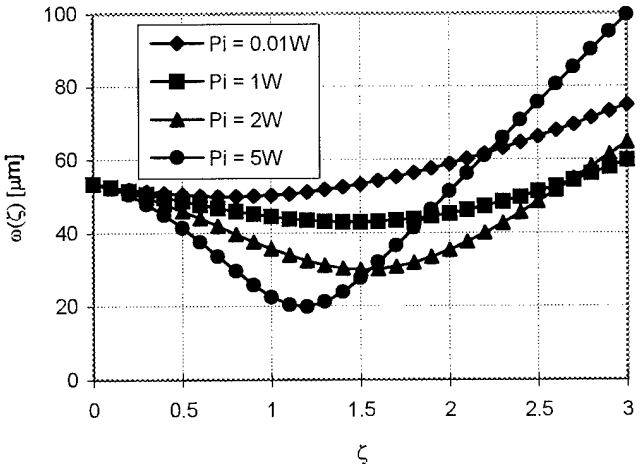

Fig. 1 Calculated variation of the beam spot size in μm as a function of the normalized distance ζ for different values of the incident power P_i.

Fig. 2 shows the variation of crystal power transmission τ as a function of the incident pump power P_i for different values of the unperturbed beam waist ω_0. The transmission, calculated at the end of a 2-cm-long crystal, is approximately 5% for $\alpha_0=1.5$ cm^{-1} in the absence of thermal loading. According to the present results, crystal transmission decreases with increasing incident pump power due to the presence of thermal loading effects. This is consistent with physical reasoning where higher temperatures at the crystal center would give rise to greater local absorption , since α_T and n_T are chosen to be positive .

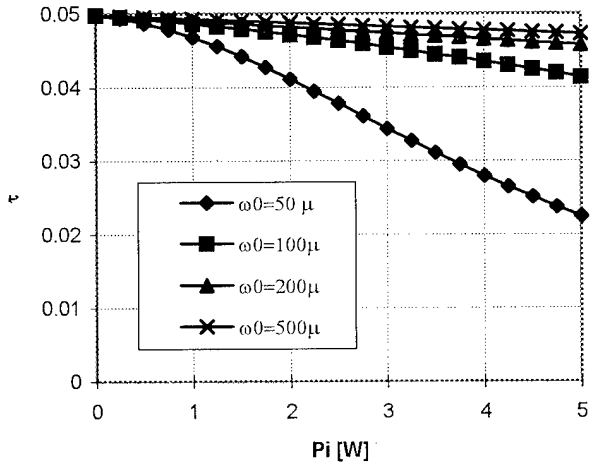

Fig. 2 Crystal power transmission τ as a function of input pump power P_i for different values of unperturbed beam waist ω_0.

References

[1] M. E. Innocenzi, H. T. Yura, C. L. Fincher, and R. A. Fields, *Appl. Phys. Lett.*, **56**, 1831 (1990).

[2] A. Yariv and P. Yeh, *Optical Waves in Crystals,* (John Wiley and Sons, New York, 1984), Chapter 2.

Analysis of Thermal Effects in Crystalline Media using a Dual-Interferometer

J. M. Laurenzano
USAF Phillips Laboratory
PL/LIDA; 3550 Aberdeen Ave SE; Kirtland AFB, NM 87117
(505) 846-4315 / FAX (505) 846-4313

B. W. Liby
Manhattan College
Physics Department; Riverdale, NY 10471
(718) 920-0899 / FAX (718) 920-0814

J. O. Grannis
USAF Phillips Laboratory
PL/LIDA; 3550 Aberdeen Ave SE; Kirtland AFB, NM 87117
(505) 846-4315 / FAX (505) 846-4313

Transient effects due to thermal loading are of particular interest in diode-pumped solid-state laser research and development. Michelson interferometers have been effectively used to measure surface aberrations.[1] This configuration, however, has been unable to accurately measure optical path difference (OPD) in a thermally loaded solid-state laser material; the aberrations incurred in the initial pass cannot be distinguished from those incurred on the return pass through the media. The Mach-Zehnder interferometer has been used in the measurement of OPD due to its single pass configuration[2], but is limited due to that same characteristic. A novel interferometric configuration incorporating both the Michelson and Mach-Zehnder interferometers can be used to make simultaneous measurements to provide an accurate diagnosis of transient and steady-state effects in solid-state laser materials due to thermal loading.

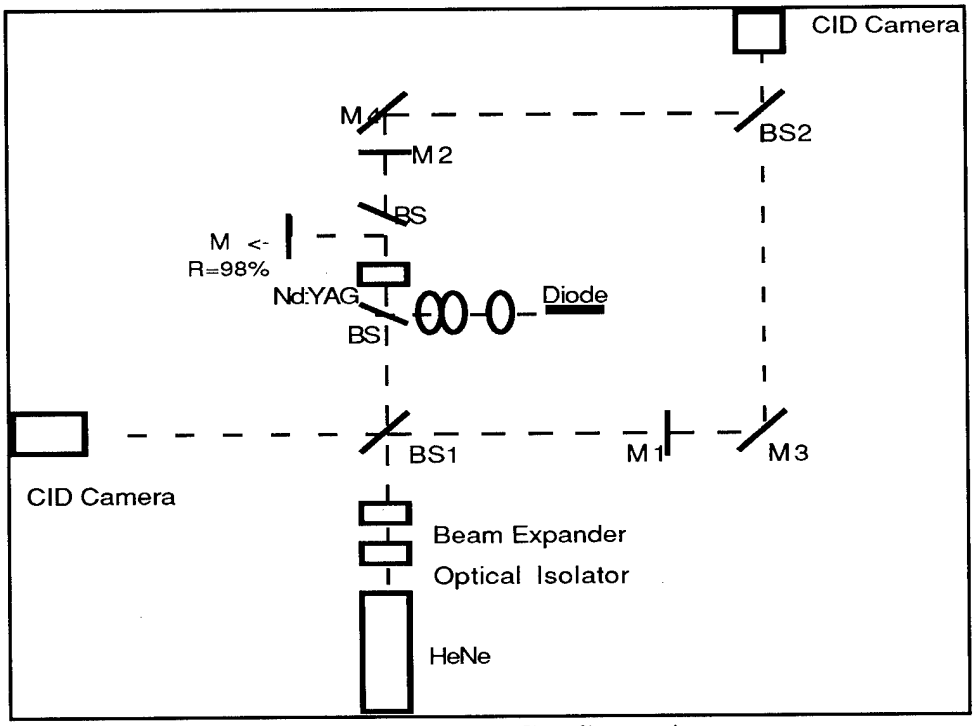

Figure 1: Double/Single Pass Configuration

The experimental arrangement used to correlate the double pass/single pass information is shown in Figure 1. A frequency stabilized, collimated HeNe laser was used as the interferometric source beam. The partially reflecting mirrors (M1 and M2) formed the end mirrors for the Michelson interferometer. A Nd:YAG crystal was pumped with 8.8W at 808nm to form the active resonator cavity with an output of 1.03W at 1064nm. The bent resonator configuration was designed to permit measurement of a lasing medium with minimal interference from additional optics. Both transient and steady-state fringe patterns were recorded for each interferometer output. Two separate CID cameras were used to allow simultaneous recording of the images. The camaera outputs were recorded on video tape and analyzed with frame-grabbing software on a PC. Initial fringe pattern analysis[3] indicates a direct correlation between the single pass and double pass results for both optical path difference and phase shift in the crystalline medium.

The two interferometers can be compared under slightly different conditions to investigate surface vs. bulk distortions in thermally loaded crystalline media. In this experiment, M2 as shown in Figure 1 was removed so that the front surface of a Nd:YAG crystal served as the end mirror for the sample leg of the Michelson interferometer. The Nd:YAG crystal was end pumped slightly off-axis to avoid interference with the interferometer. The same 8.8W, 808nm diode laser was used. In this configuration, the Michelson interferometer revealed surface distortions while the Mach-Zehnder provided information on bulk distortions as the crystal was thermally loaded. Fringe patterns were recorded using the CID cameras. Fringe analysis revealed substantially greater surface deformation than OPD for this pump configuration as expected. By using this technique, we will demonstrate the feasibility of extracting the aberration due to surface deformation from the total OPD.

References:

[1] Y. Xiang and C. Xiang, "Birefringent Common-Path Interferometer for Testing Large Convex Spherical Surfaces," Opt. Eng. 32, 1080-1082 (1993)

[2] D. Kopf, "Thermal Effects in End-Heated Laser Rods: A Time-Dependent Model and Diagnostic", USAF Phillips Laboratory, PL-TR--93-1079 (1994).

[3] M. Wickham and J. Munch, "CCD Holographic Phase and Intensity Measurement of Laser Wave Front," SPIE Vol. 1414, No. 9, 80-90 (1991)

Compensation of Polarization Distortion of a Laser Beam in a Four-pass Nd:glass Amplifier by using a Faraday Rotator

H. J. Kong, J. Y. Lee, H. S. Kim, K. Y. Um, and J. R. Park

Department of Physics, Korea Advanced Institute of Science and Technology,

373-1, Kusong-dong, Yusong-gu, Taejon 305-701, Korea

Phone : +82-42-869-2521

Fax : +82-42-861-1458

A four-pass Nd:glass laser amplifier, compensating the polarization distortion of a laser beam induced by thermal birefringence of optically pumped Nd:glass rod, has been designed and the characteristics have been investigated by experiments and computer simulations.

The polarization distortion is a serious problem in the use of four-pass amplifier since the state of polarization of a laser beam determines its path in the amplifier. In case that a quarter-wave plate was used as a polarization rotating element, unexpected multiple pulses instead of a single amplified pulse were obtained. When a Faraday rotator was used, the polarization distortion was considerably compensated and a single laser pulse was stably amplified with high gain. The gain of 10^4 - 10^5 was obtained for an input laser pulse with the energy of 1.5 μJ and the pulse width of 40 ps (FWHM).

Using Jones matrix formulation, the spatial intensity distribution of a depolarized beam in the amplifier was calculated and it was shown that a Faraday rotator effectively compensates the polarization distortion of a laser beam while a quarter-wave plate doesn't. Also the B-integral in this amplifier was calculated to be less than 1.

It can be concluded that the four-pass Nd:glass laser amplifier is suitable for high gain pre-amplifier in high-power laser systems followed by the multistage power amplifier.

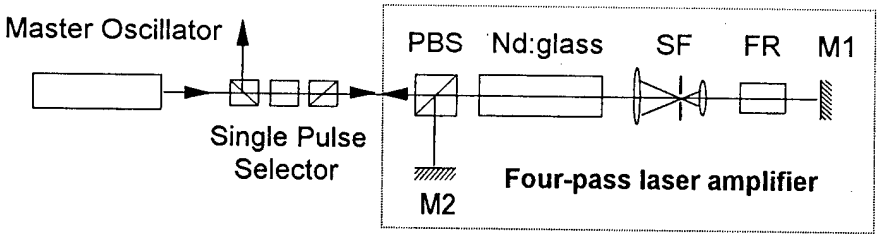

Fig. 1. Schematic diagram of four-pass Nd:glass laser amplifier. PBS, polarization beam splitter; SF, telescope with spatial filter; FR, Faraday rotator; M1 and M2, flat mirrors.

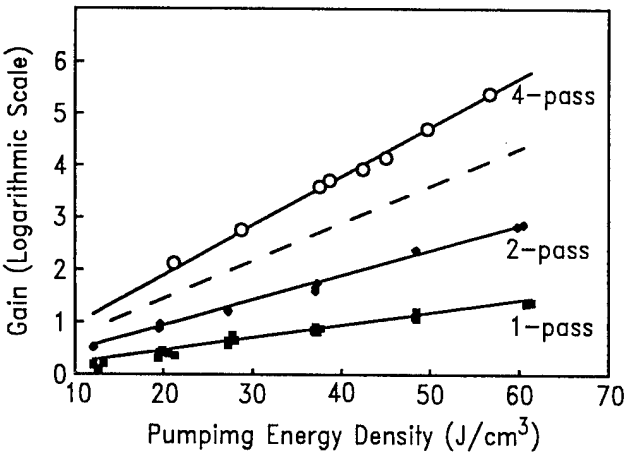

Fig. 2. Measured small-signal gain of the four-pass amplifier. 3-pass gain represented by the dashed-line was not measured.

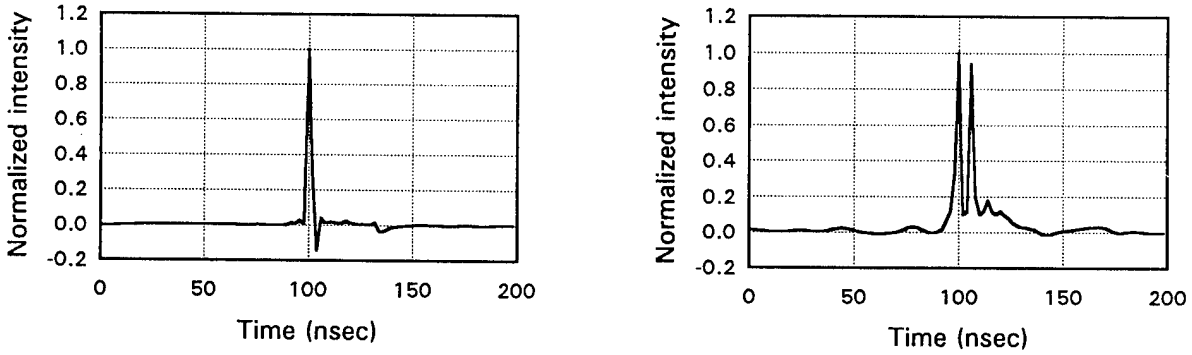

Fig. 3. Measured temporal profiles of amplified laser pulses through the four-pass amplifier using (a) a Faraday rotator and (b) a quarter-wave plate. The electrical pumping energy of the amplifier was 900 J and the input laser pulse had energy of 1.5 μJ and the pulse width of 40 ps (FWHM).

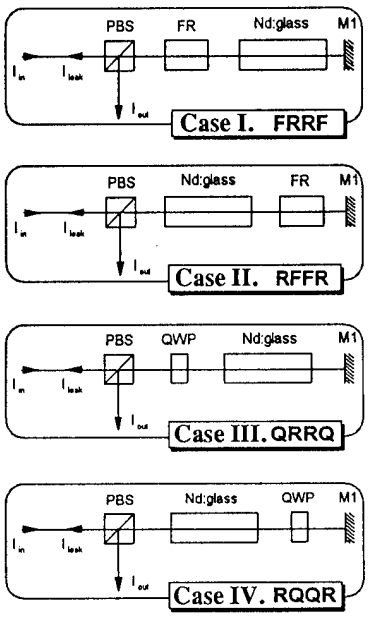

Fig. 4. Schematic diagrams of laser amplifiers with different polarization rotating elements and their positions. Numerical calculation of spatial intensity distribution of polarization distortion was performed for these schemes.

Table 1. Physical parameters of the laser amplifier used in the numerical calculation.

Physical parameters		*Value*
Temperature distribution		quadratic dependence on the radius
Incident laser beam		Top hat with diameter of 10 *mm*
Laser rod		Nd:glass (LHG-5 Hoya)
$2R$	Diameter	12 *mm*
L	Length	250 *mm*
α	Linear expansion coeff.	80 $[10^{-7}/^{\circ}C]$
E	Young's modulus	7.26 $[10^{5} kg/cm^{2}]$
ν	Poisson ratio	0.24
$\frac{\partial n}{\partial \sigma_{\parallel}}$	Photoelastic coeff.(parall.)	1.71 $[10^{-7}\,\mathrm{kg \cdot cm^{2}}]$
$\frac{\partial n}{\partial \sigma_{\perp}}$	Photoelastic coeff.(perp.)	3.91 $[10^{-7}/\mathrm{kg \cdot cm^{2}}]$

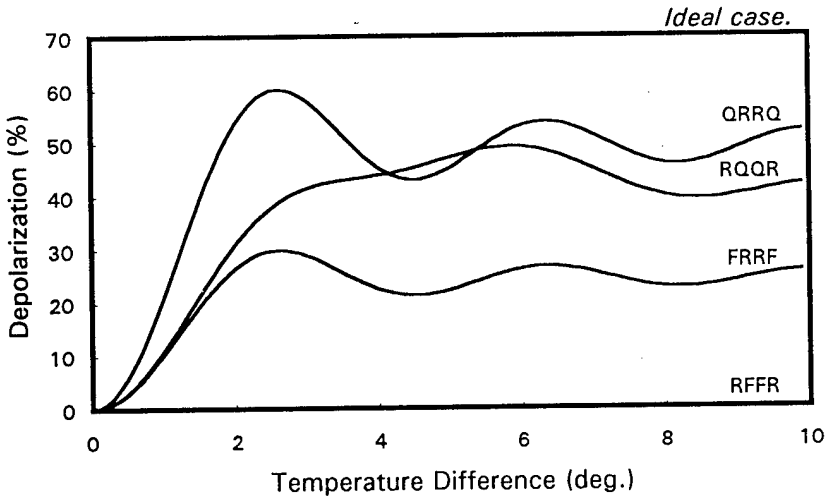

Fig. 5. Depolarization of a laser beam in the two passes in the amplifier. FRRF, RFFR, QRRQ, and RQQR denote schemes of amplifiers referred to Fig. 4.

Friday, February 2, 1996

Visible/Ultraviolet Lasers

FG 4:15 pm-6:00 pm
Gold Room

Martin Fejer, *Presider*
Stanford University

Highly-efficient second harmonic generation of green light from picosecond pulses in bulk quasi-phase-matched lithium niobate

V.Pruneri, S.D.Butterworth, P.G.Kazansky, W.A.Clarkson, N.Moore and D.C.Hanna

Optoelectronics Research Centre, Southampton University, Southampton SO17 1BJ, U.K.

fax.++44/1703/593142, tel.++44/1703/593136, email. vp3@orc.soton.ac.uk

Over the last few years quasi-phase-matching (QPM) has emerged as a reliable technique for efficient second-order nonlinear optical processes. QPM allows access to higher nonlinear coefficients and wider wavelength ranges compared to birefringent phase-matching. In lithium niobate (LN) QPM can be achieved by an appropriate periodic modulation of the sign of the nonlinear coefficient via periodic domain inversion, so that the phase-mismatch between interacting fields can be compensated. This nonlinear grating does not alter the linear properties of the material which are described by the dependence of the refractive index on the wavelength. Periodically poled LN (PPLN) has been demonstrated to give efficient operation for QPM frequency doubling [1,2] and QPM parametric oscillation [3,4] both in CW and Q-switched regimes. Recently 4.5 mW of average blue-light power with 13% conversion efficiency has been generated in a periodically domain-inverted $LiTaO_3$ waveguide by frequency doubling of ~20 ps pulses produced by a high-frequency superimposed laser diode [5].

When the nonlinear interaction involves pulses of a few picoseconds duration or less the linear dispersion of the material becomes important, since the temporal walk-off due to group-velocity mismatch (GVM) between interacting pulses having different frequencies can seriously limit the effective interaction length (l_{eff}). QPM is usually used in such a way that the largest component of the second-order nonlinear tensor can be exploited. In the case of PPLN this means that all the interacting waves should be extraordinary polarised, so that d_{33} (which has a value > 30 pm/V) can be accessed. Unfortunately for such a polarisation geometry the material is highly dispersive, e.g. in the case of frequency doubling of wavelengths around 1 μm, GVM is ~1 ps/mm. However, because of its high effective nonlinear coefficient d_{eff} ($=2/\pi * d_{33}$), PPLN can offer still a large product $d_{eff} * l_{eff}$ in the picosecond regime compared to other nonlinear materials.

Our experiments reported here have been aimed at confirming the suitability of PPLN for frequency doubling with picosecond pulses. Here we report on first-order QPM-frequency doubling of amplified picosecond pulses generated by an additive pulse mode-locked (APM) 1.047 μm Nd:YLF laser. The nonlinear material used in the experiment was a sample of PPLN, 3.2 mm long, suitable for frequency doubling of 2.6 ps pulses (l_{eff} ~ 2 mm). The periodic domain inversion, of pitch 6.4 μm, was obtained by applying high voltage pulses via liquid electrodes as described in refs. [1,2,4]. In these experiments we have scaled up the thickness of the sample from 0.2 mm to 0.3 mm and still find that it is possible to produce gratings of excellent quality.

Preliminary second harmonic (SH) measurements were carried out by using a CW diode-pumped Nd:YLF laser. The experimental temperature dependence of SH power on the crystal temperature (fig.1) agrees

well with the expected $sinc^2$ shape for a perfect grating 3.2 mm long. The estimated d_{eff} was $\sim$15 pm/V. This reduced value compared to the theoretical limit of $\sim$21 pm/V is probably mainly due to absence of periodic inversion in some regions of the sample as well as the duty cycle not being exactly 50/50, rather than due to random fluctuations in the position of the domain walls which would affect the shape of the phase-matching curve.

The APM configuration of the Nd:YLF laser gave transform-limited pulses at a repetition rate of 105 MHz. This CW mode-locked beam was pulse-sliced by an acousto-optic modulator and then the pulses were amplified in a diode-pumped bulk Nd:YLF amplifier used in a double pass configuration [6]. These amplified pulses of $\sim$2.6 ps duration were frequency doubled in the PPLN sample.

At the QPM temperature of 73.5 °C, CW-mode-locked pulses of average power 650 mW (peak intensity $\sim$110 MW/cm^2) were frequency doubled to $\sim$275 mW of green with an average conversion efficiency of $\sim$43%. All the powers given here are internal values in the uncoated sample. Assuming a $sech^2$ shape, the SH pulse duration was estimated to be $\sim$2.4 ps while the bandwidth of the corresponding frequency spectrum was $\sim$175 GHz. The time-bandwidth product was thus $\sim$0.42, indicating the presence of only a weak chirp.

The pulse train was then sliced before entering the amplifier, to produce an envelope of $\sim 10\mu s$ duration and repetition rate of 2 kHz. Fig.2 shows the dependence of the average SH power within each 10 μs envelope on the corresponding average fundamental power. For an average fundamental power of 2.14 W (peak intensity $\sim$360 MW/cm^2), the average SH power was 1.3 W, giving an average conversion efficiency $\sim$61%. Fig.3 shows the traces of the undepleted and depleted fundamental beam as well as of the SH beam.

At the highest conversion the measured M^2 beam quality factors for both SH and the exit fundamental beams were $\sim$1.1 in both planes indicating that photorefractive damage was not significant even though the average green power within the envelope was $>$1W and the peak intensities were $>$300 MW/cm^2. The absence of any roll-off at higher powers in fig.2 is further evidence for the lack of photorefractive damage.

In addition the long term stability of the green output was tested over several hours and there was no sign of any degradation in terms of power and beam quality.

Thus we have confirmed that PPLN can be very effective nonlinear medium for picosecond pulses, with further prospects for power scaling from the values we have reported here.

References

1. V.Pruneri, R.Koch, P.G.Kazansky, W.A.Clarkson, P.St.J.Russell and D.C.Hanna, to be published in Optics Lett.

2. J.Webjorn, V.Pruneri, P.St.J.Russell and D.C.Hanna, Elec.Lett.**31**, 669 (1995).

3. L.E.Myers, G.D.Miller, R.C.Eckardt, M.M.Fejer, R.L.Byer and W.R.Bosenberg, Opt.Lett. **20**, 52 (1995)

4. V.Pruneri, J.Webjörn, P.St.J.Russell and D.C.Hanna, to be published in Appl. Phys. Lett. (Oct.95)

5. K.Yamamoto, K.Mizuuchi, Y.Kitaoka and M.Kato, Opt. Lett. **20**, 273 (1995).

6. S.D.Butterworth, W.A.Clarkson, N.Moore, G.J.Friel and D.C. Hanna, to be submitted to Opt.Lett.

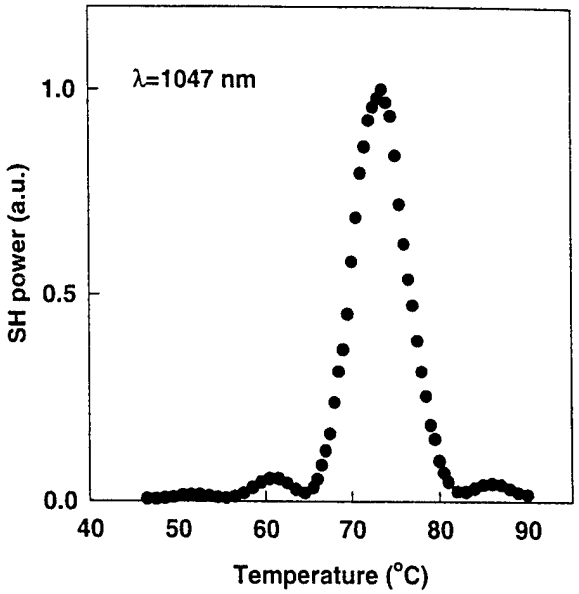

Fig.1 Dependence of generated second harmonic power on the temperature of the crystal.

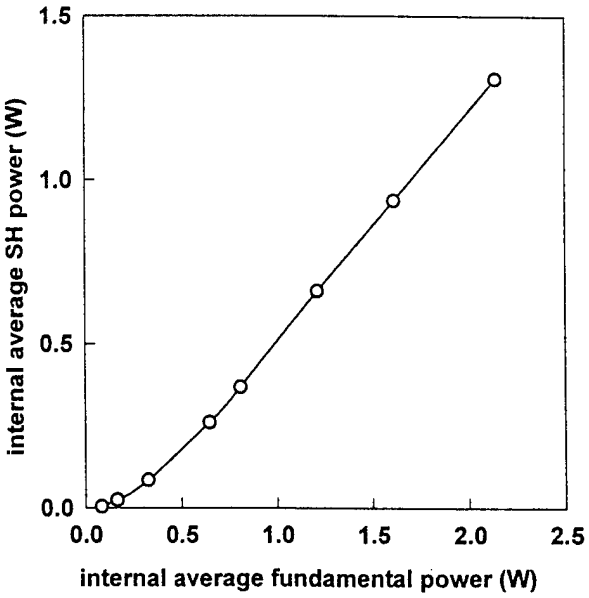

Fig.2 SH power as a function of the fundamental power in quasi-CW mode-locked regime. These powers are internal values in the uncoated crystal and average values over the 10 μs envelope.

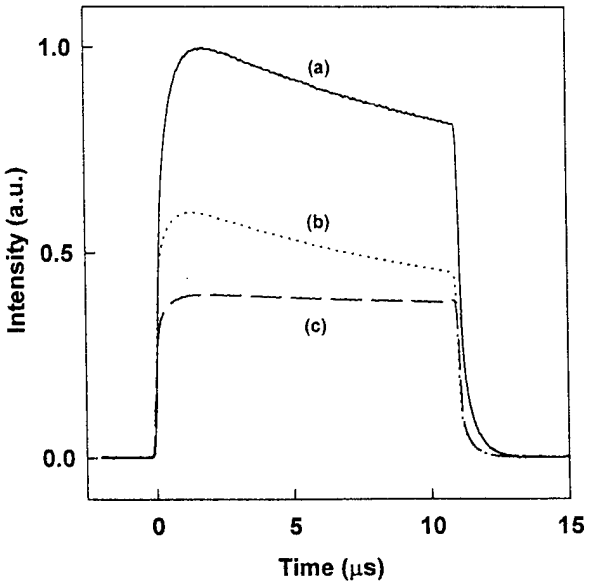

Fig.3 Temporal behaviour of: (a) undepleted pump, (b) second harmonic, (c) depleted pump.

Ultraviolet application of $Li_2B_4O_7$ crystals: Generation of the fifth and fourth harmonic of Nd:YAG lasers

Ryuichi KOMATSU, Tamotsu SUGAWARA, Koichi SASSA
Advanced Technology Research Laboratories,
Central Research Institute, Mitsubishi Materials Corporation,
1-297 Kitabukuro-cho, Omiya, Saitama 330, Japan
Nobuhiko SARUKURA, Zhenlin LIU, Shinji IZUMIDA, and Yusaburo SEGAWA
Photodynamics Research Center,
The Institute of Physical and Chemical Research (RIKEN),
Nagamachi Koeji 19-1399, Aoba-ku, Sendai, Miyagi 980, Japan
Telephone: +81 22 228 2012 Facsimile: +81 22 228 2010
Satoshi UDA, Tsuguo FUKUDA
Institute for Materials Research, Tohoku University,
Katahira 2-1-1, Aoba-ku, Sendai, Miyagi 980, Japan
Kazuhiko YAMANOUCHI
Research Institute for Electric Communication, Tohoku University\
Katahira 2-1-1, Aoba-ku, Sendai, Miyagi 980, Japan

With the rapid development of laser-diode pumped solid state lasers technology, high-power infrared light sources at around 1 μm, have been becoming more compact, more reliable, and less expensive. There have also been strong, continuous demands for a low-cost, high-power ultraviolet light source for various applications. Efficient nonlinear crystals are the key devices for developing such light sources. Already various borate crystals, including BBO[1], LiB_3O_5[2], CBO[3], SBBO[4], and the latest CLBO[5] have been reported for UV generation applications. None of these, however, can provide a unique solution for wide-spread frequency-conversion cases. Depending on the situations, the required characteristics and crystal size differ significantly. Therefore, further material research is still meaningful. $Li_2B_4O_7$ is a family of borate crystals, which is popular for SAW devices applications. However, its nonlinear optical properties in the UV region have not been studied yet, and it has a rather small optical nonlinear coefficient in the visible region [6]. In this paper, we will report an application of $Li_2B_4O_7$ crystals for ultraviolet frequency-conversion including the fourth and fifth harmonic generation of a Nd:YAG laser, and sum-frequency generation down to 209.3 nm.

Lithium tetraborate ($Li_2B_4O_7$) single crystals of 2 to 2.5 inch diameter were grown in air by the Czochralski (CZ) technique. Purified $Li_2B_4O_7$ polycrystalline powder with a molar ratio (B/Li) of 2.00 was used as the starting material. Figure 1 shows an as-grown $Li_2B_4O_7$ single crystal. The pulling direction is parallel to <110>. An X-ray topography photograph for a grown crystal is shown in Fig. 2. Only a few dislocations were observed

with a crystallographic symmetry. Etch pit density (EPD), exposed by acetic acid solution, is less than 10/cm^2. These results show that grown $Li_2B_4O_7$ is a high-quality single crystal. This high crystal quality and obtainable large crystal size are very attractive features for frequency conversion experiments. Compared with CLBO, the crystal is rather hard so cutting and polishing might be much easier. Using a 1-cm thick, 45-degree-cut crystal and a 4.2-cm thick, 90-degree-cut crystal, we evaluated the potential for UV frequency conversion applications.

To evaluate these crystals, We used an optical parameteric oscillator (Spectra Physics MOPO710) with BBO pumped by the third harmonic of a Q-sw Nd:YAG laser (440-1800 nm). $Li_2B_4O_7$ is known as a uniaxial negative crystal, and the phase-matching condition was type I. The shortest SHG wavelength was 243.8 nm for $\theta_m = 90$, and the SHG wavelength was 348.7 nm for $\theta_m = 45$. A conversion efficiency of 4.5% was recorded for a 495 nm, 42 mJ, 5-nsec incident pulse (spot size < 0.5 mm). As shown in Fig. 3, using a single 1-cm, 45 degree cut crystal, we demonstrated wide-range second harmonic generation for the fundamental light from 487.6 nm up to 1265 nm. This result shows that this crystal is usable for the fourth harmonic generation of Nd:YAG lasers. The fifth harmonic generation was also demonstrated using a 4.2-cm, 90 degree cut crystal in Type I SFG configuration. 6-mJ, 213-nm (the fifth harmonic of Nd:YAG laser) pulses were obtained for ~100 mJ, 266 nm and ~500 mJ, 1064 nm input pulses. The shortest SFG wavelength with 266 nm pulse mixed with idler pulse of OPO were 209.3 nm for $\theta_m = 90$. All the experimental SHG and SFG data are listed in Table. I. We are now trying to derive an accurate Sellmeier equation and nonlinear coefficient.

In conclusion, we have grown large size and high quality Lithium tetraborate ($Li_2B_4O_7$) crystals, and have found that $Li_2B_4O_7$ can be applied for ultraviolet frequency conversion including fifth harmonic generation of a Nd:YAG laser. These primitive results will strongly encourage further research of this crystal.

References

1. C. T. Chen, B. C. Wu, A. D. Jiang, G. M. You, Sci. sin. B18, 235 (1985).
2. C. T. Chen, Y. Wu, A. Jiang, G. You, R. Li, and S. Lin
   J. Opt. Soc. Am. B. 6, 616 (1989).
3. Y. Wu, T. Sasaki, S. Nakai, A. Yokotani, H. Tang, and C. Chen
   Appl. Phys. Lett. 62, 2614 (1993).
4. C. T. Chen, Y. Wang, B. Wu, K. Wu, W. Zeng, and L. Yu
   Nature, 373, 322 (1995).
5. Y. Mori, S. Nakajima, A. Taguchi, A. Miyamoto, M. Inagaki,
   W. Zhou, T. Sasaki, S. Nakai, Jpn. J. Appl. Phys. 34 L296 (1995).
6. T. Y. Kwon, J. J. Ju, J. W. Cha, J. N. Kim, S. I. Yun,
   Materials Lett. 20, 211 (1994).

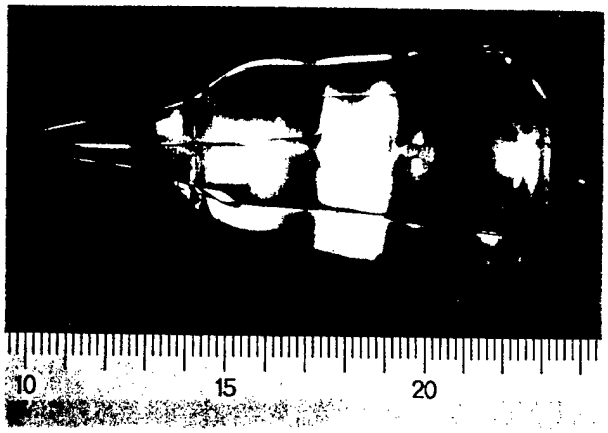

Fig. 1 $Li_2B_4O_7$ crystal boule grown by CZ method.

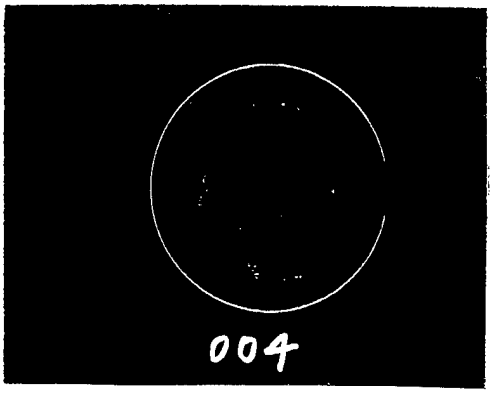

Fig. 2 X-ray topograph image showing excellent crystal quality.

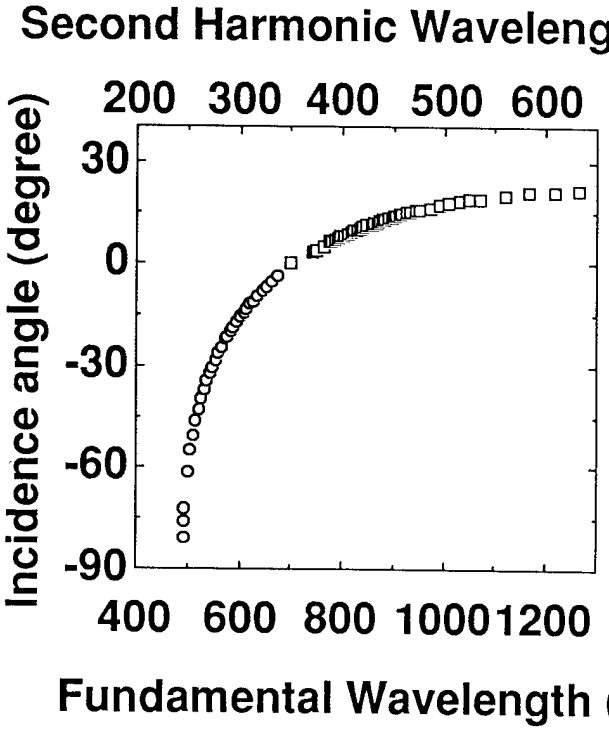

Fig. 3 wide range SHG and SFG data using 45-degree cut crystal.

Table I Various SHG and SFG data.

λ_1 (nm)	λ_2 (nm)	λ_3 (nm)	θ_m (deg)
487.6	487.6	243.8	90
697.3	697.3	348.7	45
266.0	1064.0	212.8	~70
266.0	981.0	209.3	90

where λ_1, λ_2 ; fundamental wavelength
λ_3 ; frequency mixed wavelength
θ_m ; phase matching angle

560 mW, Fifth Harmonic (213 nm), Flashlamp Pumped Nd:YAG Laser System

Ruikun Wu, Michael J. Myers, John D. Myers, Scott J. Hamlin

Kigre Inc.
100 Marshland Road
Hilton Head Island, SC 29926
Phone # (803) 681-5800
Fax # (803) 681-4559

INTRODUCTION:

Refractive Surgical Lasers (RSL) are used to correct the corneal refractive power of patients who are nearsighted, farsighted, or astigmatic in vision. There are several methods of accomplishing corneal correction. These methods are based upon different principals such as Intrastroma Photorefractive Keratectomy (IPK), using Nd:YLF and doubled YAG lasers and Laser Thermokeratoplasty (LTK), using Ho:YAG lasers. The popular RSL procedure known as Photorefractive Keratectomy (PRK) utilizes Argon Fluoride (ArF) excimer lasers at 193 nm and has been used for large area corneal surface ablation. PRK is recognized as having a high clinical success rate and predictable diopter corrections for most visual problems.

The UV laser beam introduces minimal thermal damage to tissue. This is primarily due to the short wavelength and the disruption of tissue bonds with high photon energy instead of thermal energy. In addition, because of the relatively short wavelength, the tissue ablation can be precisely controlled by modulating the laser energy density and manipulating the scanning pattern to achieve the optimum ablation profile.

Several different UV laser systems with slightly different wavelengths have been used to demonstrate PRK. In addition to the common excimer, R&D use of the fifth harmonic of Nd:YAG at 213 nm has become popular. The solid state, fifth harmonic, laser system is compact, lower in cost, offers a smaller foot print, utilizes no toxic gases, and is easier to maintain in comparison to argon fluoride excimer lasers.

Recently, we have demonstrated a flashlamp pumped, 200 Hz Q-switched TEM_{00} mode Nd:YAG laser system with 10 W of average output power, developed particularly for PRK type applications. Through the use of a three crystal nonlinear frequency conversion system, 560 mW of 213 nm output was demonstrated at 200 Hz.

LASER SYSTEM:

The laser system is basically a Master Oscillator Power Amplifier (MOPA) type system. A unique feature of the MOPA is that it utilizes a single flashlamp and Pulse Forming Network (PFN). The pump chamber is a newly developed FK series, housing two laser rods and the single flashlamp. Laser output is 50 mJ/per pulse with a 15 ns pulse width at 200 Hz. As required for efficient frequency conversion, the beam quality is quite good. 90 % of the beam profile fits a Gaussian distribution. The beam is 2.5 mm in diameter and the life of the flashlamp has reached 9×10^7 shots. The input average power

is less than 1.5 KW when operating at 200 Hz. The effective average pump power per unit length of the laser rod is less than 54 W/cm.

NONLINEAR FREQUENCY CONVERSION SYSTEM:

There are basically two approaches to obtain the fifth harmonic: mixing of second and third harmonic (the 2+3 approach), and mixing of the fundamental and fourth harmonic (the 1+4 approach). These two approaches are listed in Table 1 for both BBO and LBO non-linear crystals. If only the data in Table 1 is considered, it is very difficult to conclude which approach is optimum for generating 213 nm. Actually, the selection of the approach is not only decided by the performances of the crystal, but also by considerations of the whole system.

The data presented in Table 1 indicates that only BBO crystals can be used. The effective nonlinear coefficient, D_{eff}, of BBO for the 1+4 approach is nearly double that of the 2+3 approach; however, the acceptance angle for the 1+4 approach is only 62% of the 2+3 approach. Considering the absorption of the BBO crystal in the UV region and the associated damage thresholds, the 1+4 approach (1064 nm + 266 nm $\rightarrow$ 213 nm), which has two deep UV beams (266 nm and 213 nm) may have more damage problems than the 2+3 approach (532 nm + 355 nm $\rightarrow$ 213 nm) as the 2+3 approach has only one deep UV beam.

The damage threshold issue of the 1+4 method may be mitigated by using high quality BBO which has far less absorption in UV region[3]. On the other hand, the intense and high quality 1064 nm beam could be use to substantially enhance the conversion efficiency of 1+4 approach. The other key issues is how to deal with the very small acceptance angle which is about 0.21-0.13 mrad-cm.

In our experiments using the 2+3 approach, the first SHG crystal was oriented as a type I crystal. 90° non-critically phase matched LBO or 22° cut BBO could be used. The THG crystal was a 4X4X12 mm LBO (θ=41°) and (ϕ=90°). The final crystal was a 4X4X7 mm BBO (θ=51°). In order to obtain the required polarization, a waveplate was placed before the fifth harmonic generation crystal to rotate the plane of polarization of one of the beams 90°, without affecting the other.

Output energies of 40, 15, 7, and 2.8 mJ were obtained, corresponding to the fundamental, second, third, and fifth harmonics at 200Hz. A focusing lens was not used in the experiment; however, the laser beam was slightly focused in the non-linear crystals by the thermal lensing of the amplifier.

The 1+4 approach also has been tested in a simple experiment. The 4X4X7 mm type I BBO SHG crystal was the same as used in the 2+3 approach. The 532 nm beam was again doubled by a second 4X4X7 mm type I BBO crystal cut at 47.6°. The combined beam of the three wave lengths was incident upon the type I 51° cut BBO crystal. The fifth harmonic output measured about 1.8 mJ. No further attempts to date have been made to improve the fifth harmonic output using the 1+4 approach; although, the relatively lower output of the fifth harmonic using the 1+4 approach in comparison to the 2+3 approach doesn't mean this approach isn't as good. We feel our results were limited by our experimental arrangement and could be improved. Other researchers have reported good results utilizing the 1+4 approach[2,3,4].

REFERENCES:

1. J.T. Lin, "Critical Review on Refractive Surgical lasers", Optical Engineering, Vol. 34, No. 3, pp668-675 (1995).

2. C.E. Hamilton, F.D. Braun, C.I. Miyake, and D.D. Lowenthal, "High- Repetition-Rate, High-Average Power, Pulsed, Diode-Pumped Nd:YAG Oscillators", OSA Proceedings on Advanced Solid State Lasers, Vol. 15, pp17-19 (1993).

3. W. Wiechmann, L.Y. Liu, M. Oka, Y. Taguchi, H. Wada, Y. Minoya, T. Okamoto, and S. Kubota, "Efficient High-Repetition-Rate All-Solid-State Fifth Harmonic Generation from a Diode-pumped Q- Switched Nd:YAG Laser", CLEO '95 postdeadline paper CPD-19. (1995).

4. A B.Pertersen, W L.Nighan,Jr, "high-Repetition-Rate UV Generation with Diode-Pumped Nd:YVO4 Laser", CLEO'95 Paper CWG2(1995).

Table 1
BBO Performance for Fifth Harmonic

METHODS	TYPE	POLAR-IZATION	PHASE MATCHING ANGLE		WALK-OFF ANGLE	ACCEPTANCE ANGLE		D_{eff} ($\times 10^{-9}$ esu)
			($\theta°$)	($\phi°$)	($\theta°$)	($\theta°$)	($\phi°$)	
2+3	I	O+O⇒E	69.6		3.5	0.21 (mr-cm)		1.4
1+4	II	E+O⇒E	51.1		5.5	0.13 (mr-cm)		2.7
		O+E⇒E	57.2		5.0	0.16 (mr-cm)		1.4

Efficient intracavity frequency doubling of a room temperature cw 930nm Nd:$YAlO_3$ laser

T.Kellner, F.Heine, B.Struve, V.Ostroumov, K.Petermann, and G.Huber

Institut für Laser-Physik, Universität Hamburg, Jungiusstr.9a, 20355 Hamburg, Germany

Tel.: #49-40-41235241, FAX:#49-404123-6281
e-mail: kellner@physnet.uni-hamburg.de

Introduction

The development of efficient cw blue laser sources[1,2] is an urgent task to realize full color laser-displays and argon-laser replacements. Techniques like resonant external frequency doubling have shown high efficiencies[3], but they are inherently complicated.
Intracavity frequency doubling of lasers terminating into the ground-state (like the $^4F_{3/2} \rightarrow {}^4I_{9/2}$ transition) in the region of 910nm up to 946nm in Nd-doped crystals is less efficient in comparison to the four-level-case because of the reabsorption loss, limiting the available intracavity intensity. Therefore we made an systematic analysis of the intracavity SHG properties for different nonlinear crystals with Nd:$YAlO_3$.
The use of Nd:$YAlO_3$ offers several advantages in comparison to Nd:YAG:
1. The wavelength on the ground-state transition (930nm) is considerably shorter compared with the 946nm in Nd:YAG. This is an advantage for display-technology because the frequency doubled radiation yields a 'deeper' blue.
2. Because of the space-group symmetry (D^{16}_{2h}-Pbnm) of Nd:$YAlO_3$ the laser radiation is polarized so that in principal no additional intracavity polarizer is required.
3. Due to the large difference in the refractive indices[4] thermal induced depolarization is not an important issue in Nd:$YAlO_3$.
4. Nd:$YAlO_3$ possesses relative broad absorption bands with large absorption coefficients suitable for laser diode pumping.
5. Tunability of the laser wavelength over 2nm is possible.

Experimental setup

For the intracavity frequency doubling experiments a hemispherical resonator was used. The plan- and the 5cm-mirror were high-reflection coated at the fundamental wavelength (R>99.9%), and anti-reflection coated (R<2%) at the pump wavelength. They had a transmission higher than 95% in the blue region. The mirrors were also anti-reflection coated around 1070nm to suppress oscillation of the $^4F_{3/2} \rightarrow {}^4I_{11/2}$ transition. The pump radiation was focused with a lens of 50mm focal length into the laser crystal (pump beam waist ≈30µm). The nonlinear crystal was placed close to the laser crystal inside the resonator.

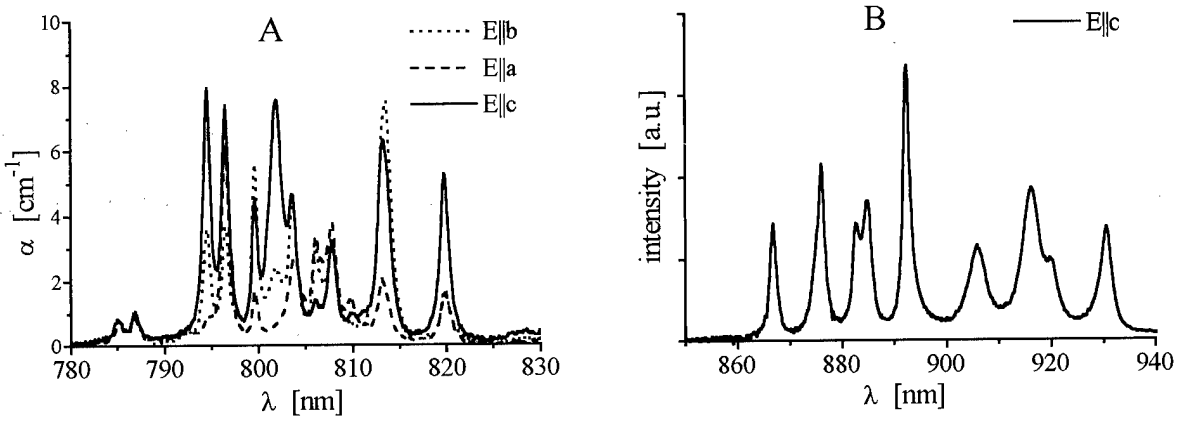

Fig. 1A/B. Absorption and fluorescence spectra of Nd:$YAlO_3$

Laser- and intracavity frequency doubling experiments:

An uncoated 1.4mm long Nd:$YAlO_3$ crystal with a dopant concentration of 0.8% neodymium was used. It was mounted on a water cooled copper heatsink. The absorption- and the fluorescence spectra of Fig. 1 were measured with a Fourier-transform-spectrometer. The fluorescence spectra were measured under unpolarized excitation with a fiber coupled argon ion laser. The laser crystal was pumped at 794.5nm with $\vec{E}||\vec{c}$. Laser emission was achieved at 930nm and at 915nm ($\vec{E}||\vec{c}$ see Fig. 1B). Because of the higher reabsorption losses at 915nm the performance at 930nm was superior. Discrimination ot the 915nm transition can easily be achieved by using propper mirror coatings. Experiments with several output transmissions were made. The best results were obtained with an output coupler with T=4.6% and nearly 80% reflection at the pump wavelength (see Fig. 3).

For the intracavity frequency doubling experiments BaB_2O_4 (BBO), LiB_3O_5 (LBO) and $LiJO_3$ crystals were used. They were 4mm long and anti-reflection coated at the fundamental and the second harmonic wavelength. All crystals were cut for angle-phasematching (type I). The best results were obtained with BBO and $LiJO_3$ because of their larger nonlinear coefficients. Figure 2 shows the difference in second harmonic output for the used nonlinear crystals. The conversion efficiency by using BBO as the nonlinear crystral from 930nm to 465nm is ≈20%.

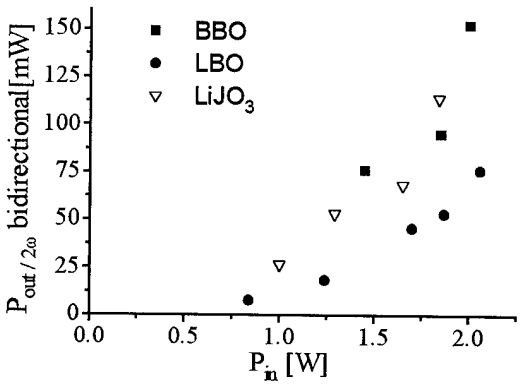

Fig. 2. Second harmonic output vs. pump power.

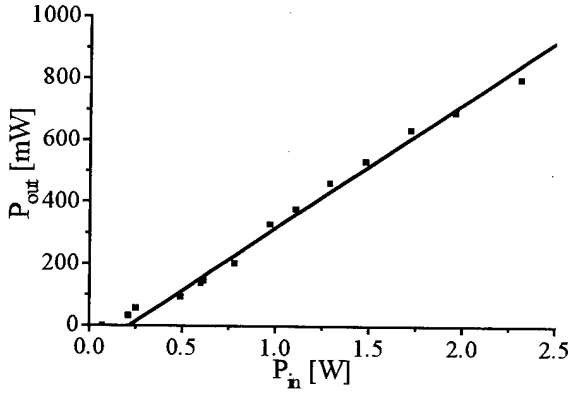

Fig. 3. Fundamental output with T=4.6%, slope efficiency 40%.

In contrast to the intracavity frequency doubling of a four-level-laser[5], resonator internal SHG of a quasi-three-level-laser requires a large single pass conversion efficiency in order to compete with the reabsorption losses. A strong nonlinear coupling i.e. a high nonlinear coefficient and relative long crystals must be used. For our setup it is not possible to determine analytically an optimum length. One can only determine an optimum focus for a given crystal length[6]. The optimum radius of the focus for BBO, $LiJO_3$, and LBO is about 20μm. The estimated beam diameter inside the nonlinear crystal was 50μm.

Conclusion

Efficient intracavity frequency doubling of a Ti:sapphire pumped 930nm Nd:$YAlO_3$ laser using nonlinear crystals LBO, BBO, and $LiJO_3$ was demonstrated. Total blue output power up to 150mW using 2W of incident pump power was achieved. Further improvement of intracavity frequency doubling should be possible by using $KNbO_3$ as the nonlinear crystal due to the combination of noncritical phasematching with a high nonlinear coefficient.

---

[1] W.P. Risk et al., Diode-laser blue light source at 473nm using intracavity frequency doubling of a 946nm Nd:YAG laser. Appl. Phys. Let., **54** (17), Sep. 1989.

[2] G.J. Dixon et al., Efficient blue emission from an intracavity-doubled 946-nm Nd:YAG laser, Opt. Lett., Vol.13 No.2, Feb. 1988.

[3] E.S. Polzik and H.J. Kimble, Frequency doubling with $KNbO_3$ in an external cavity, Opt. Lett., Vol.16 No.18, Sep. 1991.

[4] Y. Kuwano, Refractive indices of $YAlO_3$:Nd, J.Appl.Phys. **49**(7), July 1978.

[5] J.-P. Meyn and G. Huber, Intracavity frequency doubling of a continuous-wave, diode-laser-pumped neodymium lanthanum scandium borate laser, Opt. Lett., Vol. 19, No.18, Sep. 15, 1994.

[6] G.D. Boyd and D.A. Kleinman, Parametric interaction of focused gaussian light beams, J. Appl. Phys. / Vol.39, No.8 / July 1968

A quadrupled Nd:FAP laser at 1.126 μm for a Hg^+ optical frequency standard

F.C.Cruz
National Institute of Standards and Technology, Time and Frequency Division
325 Broadway
Boulder, CO, 80303
Phone: (303) 497 3794
FAX: (303) 497 7375
J.C.Bergquist
National Institute of Standards and Technology, Time and Frequency Division
325 Broadway
Boulder, CO, 80303
Phone: (303) 497 5459
FAX: (303) 497 7375

The better inherent frequency stability of solid-state lasers, compared to other types of lasers, makes them attractive for precision spectroscopy and metrology. In addition, an all-solid state laser is compact, efficient and reliable. In this paper we report on the development and performance of a single-frequency, solid-state Nd:FAP laser, at 1.126 μm, that will be used to realize an optical frequency standard based on the narrow $^2S_{1/2}$-$^2D_{5/2}$ quadrupole transition (λ=281.5 nm) of trapped and laser-cooled Hg ions (1). The fourth harmonic of the Nd:FAP laser oscillating at room temperature at 1.126 μm can be used to probe the narrow S-D transition of Hg^+ which has a natural linewidth of 2 Hz (1). Radiation at the fourth harmonic is generated by first doubling to 563 nm in an external cavity and then to 281.5 nm in a single-pass configuration.

Spectroscopic and lasing performances of Nd:FAP at 1.06 μm have been reported in refs. (2) and (3). The absorption spectrum of Nd:FAP, like Nd:YAG, has a strong peak near 807 nm which is well-matched to optical pumping with a diode laser. Our Nd:FAP crystal was cut and polished and oriented at Brewster's angle to avoid any AR coatings. The thickness of the crystal was 2 mm and, with a Nd doping of about 2%, about 95% of the light at 807 nm was absorbed. Thermal problems were largely eliminated by heat sinking the crystal into a tight fitting copper support piece. The optimum waist size of the pump laser and the mode size of the 1.126 μm cavity were determined empirically. Maximum output powers were achieved for waist sizes of about 80 μm to 100 μm.

The 1.126 μm laser was built as a ring cavity formed by two flat mirrors (input and output couplers) and two 15 cm curved mirrors (HR at 1.126 μm). This cavity produces a near optimum waist at the crystal of about 80 μm. The flat input coupler transmits 90% of the pump light at 807 nm and is highly reflecting at 1.126 μm. The output coupler was coated to transmit 1% of the radiation at 1.126 μm and 50% at 1.06 μm, which suppressed oscillation on the strong line at 1.06 μm. The pump beam was focused into the crystal to a spot size of about a 100 μm. The c-axis, which lays in the Brewster's cut surface, was oriented perpendicular to the laser polarization for optimum power. Because the crystal was positioned at Brewster's angle, the ring cavity is compensated for astigmatism. Unidirectional oscillation was enforced by an optical diode formed

by a Faraday rotator and a quartz compensating plate. Single-frequency operation at 1.126 μm in the TEM_{00} mode was achieved even without frequency selective elements inside the cavity, however, a thin etalon was used for mode stability and for tuning the wavelength to the desired color. The power performance for the 1.126 μm laser is illustrated in Fig.1. The input power was corrected for the 87% transmission of the lens and the input coupler. The slope efficiency is about 40%. For an input power of 778 mW, an output power of about 260 mW was achieved corresponding to an efficiency of 33%.

Frequency doubling to 563 nm was done in an external ring cavity using $KNb0_3$. Phase-matching is achieved by angle-tuning (critical phase-matching). The $KNb0_3$ crystal is 2 mm thick and oriented at Brewter's angle. The cavity is formed by two flat and two 5 cm mirrors. The crystal is positioned at the tight focus between the 5 cm mirrors and the fundamental beam is mode matched into the softer waist between the two flat mirrors. This cavity is also compensated for astigmatism and was locked to resonance by the Hansch-Couillaud method (4). With cavity power enhancement factors of about a hundred and the high doubling efficiency of $KNb0_3$, output power of about 50 mW at 563 nm are possible with 100 mW at 1.126 μm.

Doubling to 281.5 nm has been done by single passing a deuterated ADP crystal. Several μWatts of power at 281.5 nm is produced which is enough for application in our experiment with laser-cooled and trapped Hg ions.

We intend to study and caracterize the AM and FM noise spectrum of the Nd:FAP laser as well as measure its linewidth. The quadrupled laser scheme should also make simpler the implementation of a frequency chain from this Hg^+ clock transition to the methane frequency standard in the infrared and then to the Cs standard at 9.2 GHz..

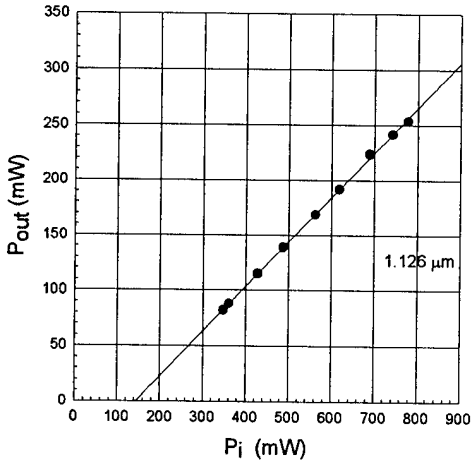

Fig.1 Output versus input power for the Nd:FAP laser at 1.126 μm. Input power was corrected by the transmissivity of the input lens and coupler (87%).

References

1. D.J.Wineland, J.C.Bergquist, W.M.Itano, F.Diedrich, C.S.Weimer, *The Hydrogen Atom*, G.F.Bassani, M.Inguscio and T.W.Hansch, Eds. (Springer-Verlag, Heidelberg, 1989) pp.123-133.
2. R.C.Ohlmann, K.B. Steinbruegge and R.Mazelsky, Appl.Opt. 7, 905 (1968).
3. X.X.Chang, A.B.Villaverde, M.Bass, G.Lutts and B.H.T Chai, SPIE Vol.1863, 35 (1993).
4. T.W.Hansch and B.Couillaud, Opt. Commun. 35, 441 (1980).

Ultraviolet picosecond pulses from an all-solid-state Ce:LiSAF master oscillator and Ce:LiCAF power amplifier system

Nobuhiko SARUKURA, Zhenlin LIU, Shinji IZUMIDA, and Yusaburo SEGAWA
Photodynamics Research Center,
The Institute of Physical and Chemical Research (RIKEN),
Nagamachi Koeji 19-1399, Aoba-ku, Sendai, Miyagi 980, Japan
Mark A. DUBINSKII
Laser Spectroscopy Laboratory, Department of Physics and Astronomy,
Howard University, Washington, DC 20059, USA
Vadim V. SEMASHKO, Alexander K. NAUMOV, Stella L. KORABLEVA, and Ravil Yu. ABDULSABIROV
Kazan State University, Lenin Street 18, 420008 Kazan, Russia

Ultrashort-pulse generation and amplification in the ultraviolet (UV) region has been receiving a great deal of interest for numerous applications. All known UV short-pulse master oscillator and power amplifier (MOPA) systems consist of mode-locked Ti:sapphire lasers or various dye-laser based oscillator stages, and excimer power amplifier stages. [1] The above systems are extremely complicated and bulky, and such drawbacks restrict their applications. However, solid-state tunable UV-laser materials such as Ce^{3+} ion activated $LuLiF_4$ (LLF) [2,3] $LiCaAlF_6$ (LiCAF), [4,5,6,8] and $LiSrAlF_6$ (LiSAF) [7,8] have recently been developed. With their broad gain-width, demonstrated reliability, and high efficiency, they are attractive for ultrashort pulse applications. To prove that, we have demonstrated UV picosecond-pulse amplification using Ce:LLF. [9] Furthermore, by employing a newly proposed passive self-injection-seeding scheme, we have directly generated UV picosecond pulse-trains from a Ce:LLF laser [10] and a Ce:LiCAF laser.[11] This presentation reports UV picosecond pulse generation and amplification in a compact, all-solid-state Ce:LiSAF/Ce:LiCAF MOPA system pumped by the fourth harmonic of a standard 10-nsec Q-switched Nd:YAG laser.

The Ce:LiCAF, which was first reported by Dubinskii et al in 1993, [4,5,6] is the first known all-solid-state tunable UV laser directly pumped by the fourth harmonic of a standard Nd:YAG laser. Ce:LiSAF is a structural analog (Colquiriite) of Ce:LiCAF with a similar spectroscopic properties. [7,8] Ce:LiSAF has slightly larger effective gain cross-section which is favorable for oscillators (Ce:LiSAF 6.8×10^{-18} cm^2 ; Ce:LiCAF 6.0×10^{-18} cm^2), and Ce:LiCAF has larger saturation fluence which is useful in power amplifiers (Ce:LiSAF 100 mJ/cm^2; Ce:LiCAF 115 mJ/cm^2).[8] The experimental setup of the Ce:LiSAF/Ce:LiCAF MOPA is shown in Fig. 1.

The Ce:LiSAF master oscillator with 12-mm cavity length was formed by a flat high-reflection mirror and a 70% transmission flat output coupler. A 1% doped Ce:LiSAF, 7-mm sample was used without any dielectric coatings on the polished surfaces. 3-mJ, 10-nsec, 1-Hz, 266-nm, horizontally polarized pumping pulses (the fourth harmonic of a conventional 10-nsec, Q-switched Nd:YAG laser) were focused longitudinally from the high-reflection mirror side by a 20-cm focal-length lens with a 300 mJ/cm^2 pumping fluence inside the active medium. The c-axis of the Ce:LiCAF

crystal was parallel to the direction of the pumping polarization. A single 3-μJ, horizontally polarized pulse at 290-nm was obtained at the sacrifice of the extracted energy from this master oscillator. The pulse did not have any satellite pulses because the pulse duration exceeded the cavity round trip time (80 psec). The pulse duration observed by a streak camera was 590-psec as shown in Fig. 2. A single short pulse can easily be generated from a low-Q, short-cavity Ce:LiSAF laser pumped by the fourth harmonic of a conventional 10-nsec Q-switched Nd:YAG laser.

Ce:LiCAF with higher saturation fluence was employed as the power amplifier stage. A 10-mm, 1% doped Ce:LiCAF sample with AR-coatings on each side was selected. The amplifier was designed with a confocal 4-pass configuration similar to the double-sided, coaxially-pumped, confocal-multipass configuration of a Ti:sapphire amplifier. [12] 266-nm pumping pulses with 10-mJ and 15-mJ energy from each side were weakly focused by a 40-cm focal-length lens up to about $1J/cm^2$. The amplifier consisted of a gain medium located at the beam waist of a confocal lens pair (30-cm focal-length) and two turning prisms for a small displacement of each pass (Fig. 3). The signal passes coincided with the pumped region with a small angular separation from the pumping beams (less than a few degrees). This configuration allowed the signal beams from different passes to overlap well in a small pumped region. The single-pass gain was over 5 times. The 4-pass differential gain was measured to be ~30 dB. The input 3-μJ pulse was amplified up to 300-μJ. The duration of the amplified pulse observed by a streak camera was 590 psec as shown in Fig. 4. There was no noticeable pulse-broadening accompanying amplification process. We believe this performance can be improved significantly after proper optimization.

In conclusion, we have demonstrated the simplest, all solid-state, UV short-pulse, MOPA system pumped by the fourth harmonics of a conventional Q-switched Nd:YAG laser.

References

1. For example; Y. Nabekawa, K. Kondo, N. Sarukura, K. Sajiki, S. Watanabe, Opt. Lett. 18, 1922 (1993).
2. M. A. Dubinskii, R. Y. Abdulsabirov, S. L. Korableva, A. K. Naumov, and V. V. Semashko, IQEC '92, Paper FrL2.
3. M. A. Dubinskii, R. Y. Abdulsabirov, S. L. Korableva, A. K. Naumov, and V. V. Semashko, Laser Phys. 4, 480, (1994).
4. M. A. Dubinskii, V. V. Semashko, A. K. Naumov, R. Y. Abdulsabirov, and S.L. Korableva, OSA Proceedings on Advanced Solid-State Lasers 1993, vol. 15, 195.
5. M. A. Dubinskii, V. V. Semashko, A. K. Naumov, R. Y. Abdulsabirov, and S.L. Korableva, Laser Phys., 3, 216, (1993).
6. M. A. Dubinskii, V. V. Semashko, A. K. Naumov, R. Y. Abdulsabirov, and S.L. Korableva, J. Mod. Opt., 40, 1, (1993).
7. J. F. Pinto, G. H. Rosenblatt, L. Esterowitz, and G. J. Quarles, Electron. Lett. 30, 240 (1994).
8. C. D. Marshall, S. A. Payne, J. A. Speth, W. F. Krupke, G. J. Quarles, V. Castillo, and B. H. T. Chai, J. Opt. Soc. Am. B. 11, 2054 (1994).
9. N. Sarukura, Z. Liu, Y. Segawa, K. Edamatsu, Y. Suzuki, T. Itoh, R. Y. Abdulsabirov, S. L. Korableva, A. K. Naumov, V. V. Semashko, and M. A. Dubinskii, Opt. Lett. 20, 294 (1995).
10. N. Sarukura, Z. Liu, Y. Segawa, R. Y. Abdulsabirov, S. L. Korableva, A. K. Naumov, V. V. Semashko, and M. A. Dubinskii, Opt. Lett. 20, 599 (1995).
11. N. Sarukura, Z. Liu, Y. Segawa, R. Y. Abdulsabirov, S. L. Korableva, A. K. Naumov, V. V. Semashko, and M. A. Dubinskii, Appl. Phys. Lett. 67, 602 (1995).
12. N. Sarukura and Y. Ishida, IEEE J. Quant. Electron. 28, 2134 (1992).

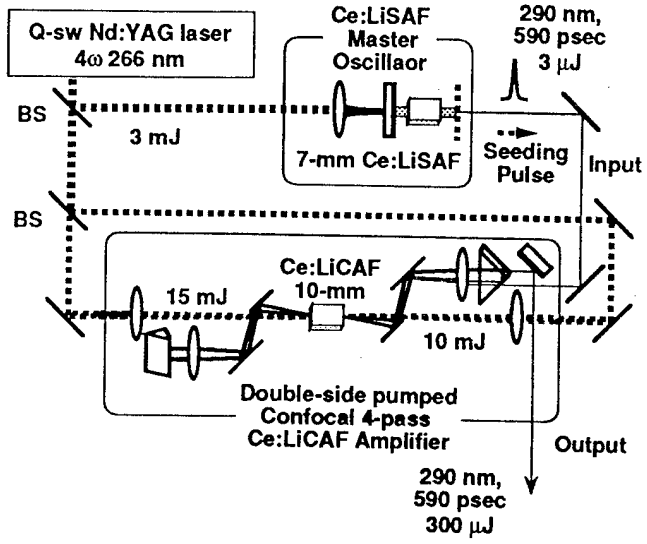

Fig. 1 The experimental setup of the Ce:LiSAF/Ce:LiCAF MOPA system.

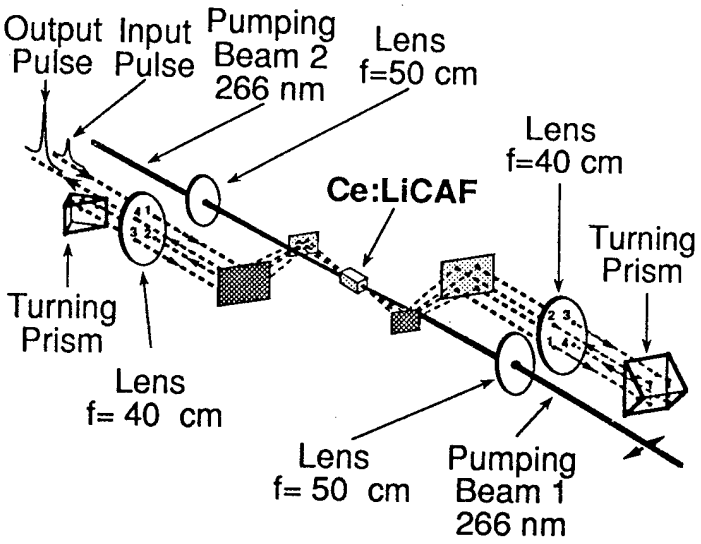

Fig. 3 The detailed optical geometry of Ce:LiCAF amplifier stage.

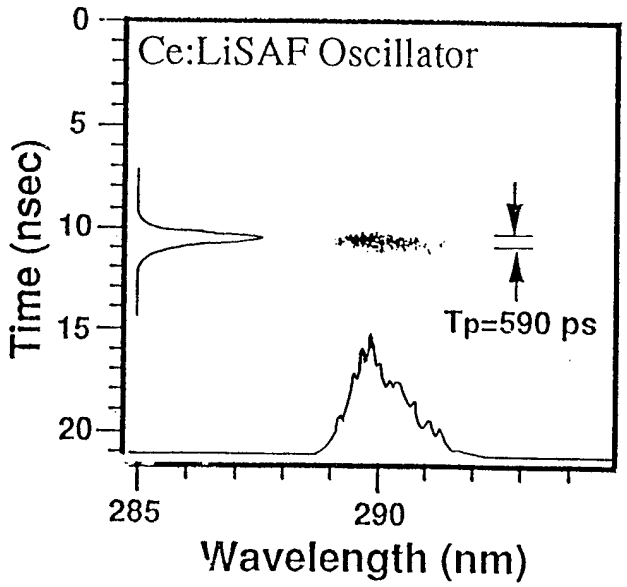

Fig. 2. Spectrally and temporally resolved streak camera image of the seeding pulse. The pulse duration in FWHM was 590 psec, and the center wavelength was 290 nm.

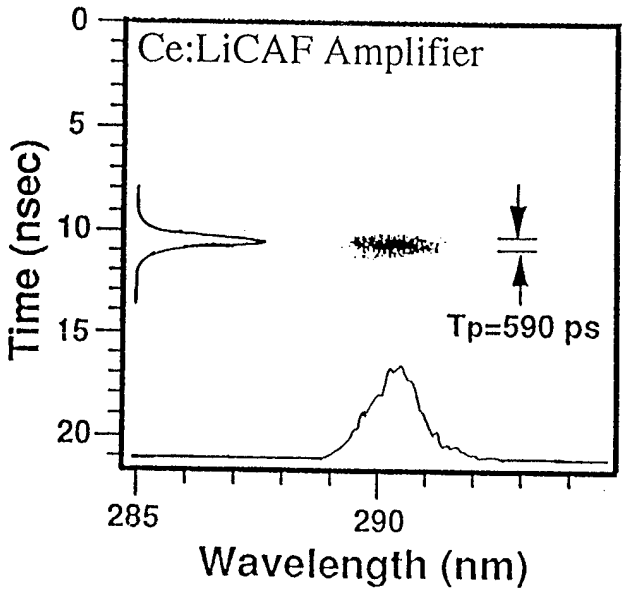

Fig. 4. Spectrally and temporally resolved streak camera image of the amplified pulse. The pulse duration in FWHM was 590 psec, and the center wavelength was 290 nm.

Ultra-broad-band continuum generation by a self-trapped ultra-short Ti:Al_2O_3 laser pulse

Hajime Nishioka, Wataru Odajima, Yoshimasa Sasaki, and Ken-ichi Ueda

Institute for Laser Science, University of Electro-communications
1-5-1 Chofugaoka, Chofu, Tokyo 182 JAPAN
Phone:+81-424-85-8960 FAX:+81-424-85-8960 e-mail:nishioka@ils.uec.ac.jp

Up to now, the frequency up-conversion to the VUV regions from IR or VIS lasers has quite low efficiency in the order of 10^{-4} even when the near resonant four-wave-mixing method is used. Moreover, effective wavelength regions are tightly limited by the tunability of the fundamental lasers and energy levels of the nonlinear materials.

In this paper, we report the generation of an intense and super-wide-band continuum ranging from the IR to 150 nm with a flat spectral intensity of greater than 10^8 W/nm. The method for the continuum generation is based on self-phase-modulation (SPM). Such a large spectra broadening using the SPM have never been demonstrated because extremely large laser intensity and interaction length in a Kerr media required. The spectra extending to the VUV region has been carried out by using a self-trapping technique. Intense laser light frequently produces self-focusing and self-trapping[1]. The trapped channels confine the laser beam over a long interaction length, thus it is an ideal situation to generate an ultra-broad spectrum. Here, we report the generation of an intense and flat frequency response continuum ranging from the IR to VUV regions by multi-self-trapping channels in atmospheric pressure rare

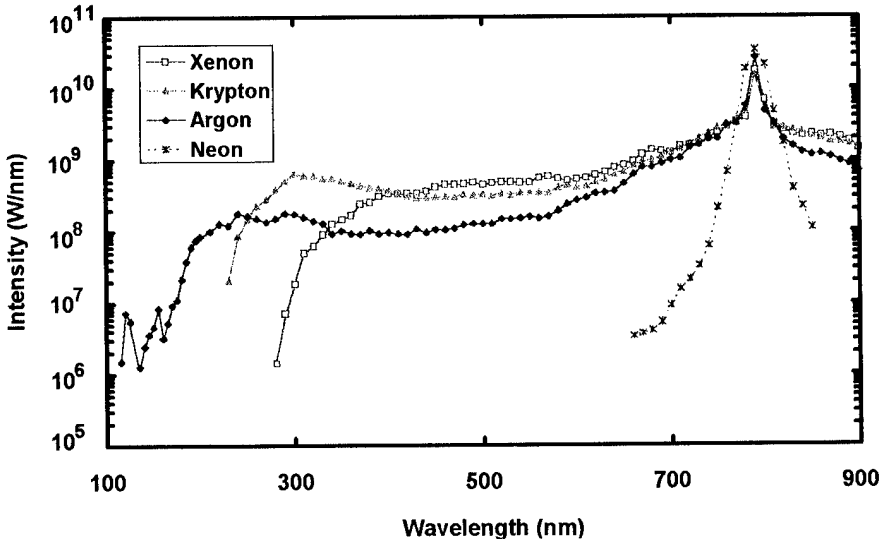

Fig.1 Spectral intensity of the hyper-continua generated in atmospheric pressure rare gases. The laser wavelength and laser power are 790 nm and 1.6 TW, respectively.

gases using a long focusing geometry.

A 2 TW Ti:Al_2O_3 laser was used as a short pulse generator. The laser produced a 125 fs pulse with 250 mJ energy at 790 nm operating at 10 Hz. The beam having multiple self-focusing spots was focused with a f=5 m lens into a traveling tube (length of 9 m) filled with atmospheric gases. The high F number configuration produces multi-channel self-trapped filaments behind the focal point. Spectral measurements have been carried out with a VUV monochromator (Acton VM-504). Spectral distribution of the continuum produced in noble gases are shown in Fig.1. An intense continuum from IR to near 150 nm was observed in Argon. This is the largest frequency coverage continuum to our knowledge. In comparison, the continuum in Neon, which has a small nonlinear refractive index, shows the conventional spectrum shape which is produced by the non-trapped laser beam. The spectral width for Neon, close to the laser frequency is much broader than the those of other gases. This is because except for in the Neon case, almost all of the laser beam is in the traps and strongly modulated. A residual non-trapped fraction, which has spatially a low intensity remains at the laser frequency. The spectral intensity in the visible region was almost constant. In Krypton and Xenon, stronger visible radiation was observed but the VUV component disappeared. The cutoff point of the plateau in Ar corresponds to the two photon ionization energy. Similarly in Kr and Xe, the cutoff is estimated to be three or four photon absorption. The maximum frequency deviation in the upper side-band in Ar corresponds to four times that of the laser frequency. We call them hyper-continua, which means the extended frequency (i.e. width of a side-band) exceeds the fundamental laser frequency.

The near and the far-field patterns of the continua were measured. In the air, the threshold energy for the trapping was 10 mJ, where a single channel was formed at the center of the expanding beam and a bright WHITE spot was observed in the channel, as shown in Fig.2(a). With increasing laser energy, the number of channels drastically increased. For a laser energy above 150 mJ, the expanding cone of the laser beam was closely filled with the fine trapping channels as shown in Fig.2(c). The diameter of the white-light spots was a function of laser intensity and nonlinear refractive index of the medium. No plasma formation was observed at the focal point except for the weak fluorescence which is excited by multi-photon absorption. A measured transmittance of the channels was 86 % in air for a laser energy of 167 mJ.

The far field spatial beam profile is shown in Fig. 3. The beam profile was performed by eliminating the spectrum components near the pump laser wavelength (longer than 740 nm) using a dichroic mirror. The beam divergence in Ar was measured to

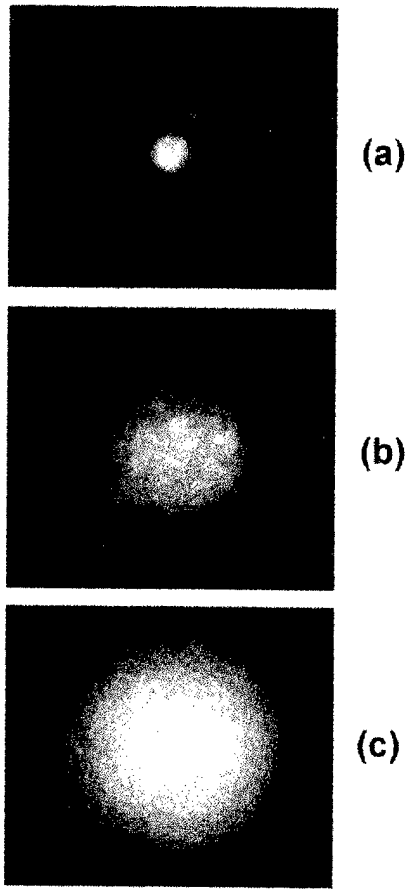

Fig.2 Near field beam profile taken at 5 m away from the focus. (a) at the threshold power of the self-trapping: 0.17 TW, (b) 0.52 TW, and (c)1.6 TW.

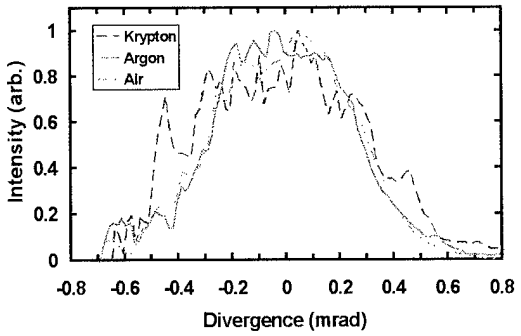

Fig. 3 Far-field beam profile of the hyper-continua generated in air, Ar, and Kr.

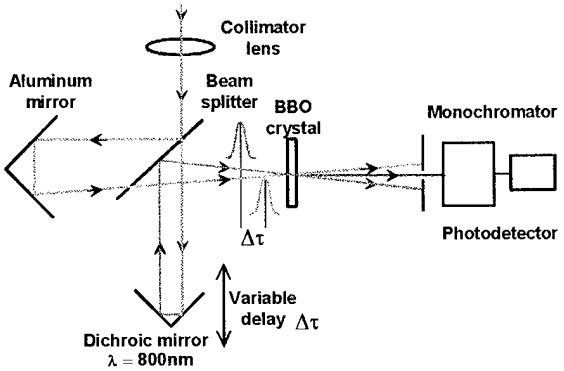

Fig. 4 Spectrum resolved pulse width measurements by the cross-correlation method.

be 0.9 mrad. For Kr, spatial structure due to strong self-focusing was observed. The beam divergence in Ar and air are almost equal to that of the primary laser beam.

Pulse duration of the continuum have been measured as a cross-correlation function between two spectral components of the continuum. The experimental setup is shown in Fig. 4. The white beam from the traveling tube was split into two beams. Dichroic mirrors which only reflect a laser component around 800 nm were used in one arm of the cross-correlator. The pump laser component and the white light coming from another arm were mixed in a BBO crystal having a thickness of 1 mm. Wavelength of a mixed component in the white light with the laser beam was monitored as a wavelength of the UV beam with a monochromator. Cross-

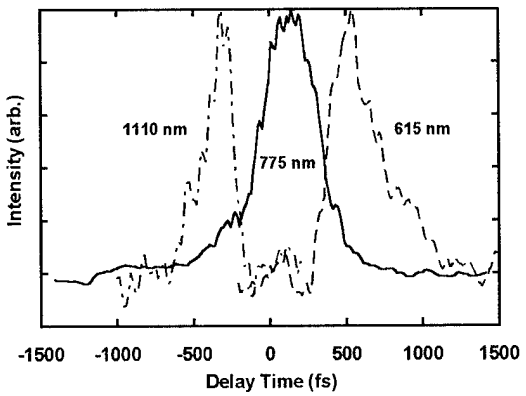

Fig. 5 Cross-correlation trace of the continuum in Kr.

correlation traces are shown in Fig. 5. The pulse duration of the continuum of around 250 fs has been measured assuming $sech^2$ pulse shape. Significant pulse delay was observed as a function of wavelength. The group delay is estimated to be dispersion in the trapping channels because the value of the delay is much longer than the pump pulse width of 125 fs.

It has been demonstrated that frequency extending to the VUV region from a femtosecond IR laser pulse is possible in atmospheric rare gases with a long focusing geometry. The high brightness and ultra-short pulse continuum in the whole light region is available for many applications including multi-frequency or multi-step pump-prove transient spectroscopy and multi-frequency nonlinear optics.

References

1 A. Braun, X. Liu, G. Korn, D. Du, J. Squier, and G. Mourou, Opt. Lett.**20**,73(1995).

ADVANCED SOLID-STATE LASERS
TECHNICAL PROGRAM COMMITTEE

Stephen Payne, *General Chair*
Lawrence Livermore National Laboratory

Clifford R. Pollock, *Program Chair*
Cornell University

Douglas Anthon
ATx-Telecom Systems

Norman P. Barnes
NASA Langley Research Center

Walter R. Bosenberg
Lightwave Electronics Corporation

Bruce H. Chai
University of Central Florida/CREOL

Christopher M. Clayton
Phillips Laboratory

Martin M. Fejer
Stanford University

Paul French
Imperial College of Science & Technology , UK

Hagop Injeyan
TRW

Richard Moncorgé
University of Lyon, France

Dave Nabors
Coherent Laser Group

Michio Oka
Sony Corporation, Japan

Joe Pinto
U.S. Naval Research Laboratory

C. Ward Trussell
U.S. Night Vision and Electronic Sensors Directorate

Richard Wallenstein
Kaiserslautern Unversity, Germany